FS SONNE

FAHRTBERICHT SO 108
CRUISE REPORT SO 108

ORWELL

OREGON AND WASHINGTON EXPLORATION OF THE LITHOSPHERE - A GEOPHYSICAL EXPERIMENT

San Francisco - Astoria
14.4 - 23.5. 1996

Edited by
Ernst R. Flueh and Michael A. Fisher
with contributions of cruise participants

GEOMAR
Forschungszentrum
für marine Geowissenschaften
der Christian-Albrechts-Universität
zu Kiel

Kiel 1996

GEOMAR REPORT 49

GEOMAR
Research Center
for Marine Geosciences
Christian Albrechts University
in Kiel

Redaktion der Serie: Gerhard Haass
Redaktion dieses Reports: Ernst R. Flueh, Michael A. Fisher
Umschlag: Kerstin Kreis, Harald Gross, GEOMAR Technologie GmbH

Managing Editor: Gerhard Haass
Editors of this issue: Ernst R. Flueh, Michael A. Fisher
Cover: Kerstin Kreis, Harald Gross, GEOMAR Technologie GmbH

GEOMAR REPORT
ISSN 0936 - 5788

GEOMAR REPORT
ISSN 0936 - 5788

GEOMAR
Forschungszentrum
für marine Geowissenschaften
D-24148 Kiel
Wischhofstr. 1-3
Telefon (0431) 600-2555, 600-2505

GEOMAR
Research Center
for Marine Geosciences
D-24148 Kiel / Germany
Wischhofstr. 1-3
Telephone (49) 431 / 600-2555, 600-2505

Table of contents

1.1 ZUSAMMENFASSUNG

Das Hauptziel der SONNE Ausfahrt SO108 war es, die großräumige Struktur der Cascadia Subduktionszone zu untersuchen, um das Erdbebenpotential, das diese Subduktionszone aufweist, besser zu verstehen. Die Ausfahrt wurde im April und Mai 1996 in Kooperation von Geomar mit dem USGS durchgeführt. Ozeanbodenseismometer (OBS) und -hydrophone (OBH) wurden auf 116 Stationen ausgesetzt. Damit wurden seismische Weitwinkelrefraktions- und -reflexionsdaten entlang von 12 Profilen senkrecht zum Streichen über den Kontinentalrand und im Streichen entlang des Kontinentalrandes vor Washington und Oregon sowie auf der angrenzenden Juan de Fuca Platte in einer Gesamtlänge von 1385 km aufgenommen. 1233 km Mehrkanal Reflexionsdaten (MCS) wurden entlang von 13 Profilen über den Kontinentalrand vor Washington geschossen, wobei zwei dieser Linien identisch mit Weitwinkellinien sind. Alle Weitwinkeldaten und zwei der MCS Linien wurden während der Ausfahrt prozessiert, geplottet und auf die Datenqualität hin getestet sowie vorläufig interpretiert.

Sowohl in den Weitwinkelreflexions- und -refraktionsdaten als auch den MCS Daten konnte die subduzierende ozeanische Kruste unter dem Kontinentalrand bis zu einer Entfernung von 20 km vor der Küste abgebildet werden. Es wurden drei wesentliche Unterschiede zwischen dem Kontinentalrand vor Washington und demjenigen vor Oregon entdeckt. Der Kontinentalrand vor Oregon ist wesentlich schmaler als derjenige vor Washington, jedoch ist die Tiefe der Basis der ozeanischen Kruste in Küstennähe in beiden Gebieten ähnlich (18-20 km). Daher ist das Abtauchen der ozeanischen Platte vor Oregon steiler als vor Washington. Der Abtauchwinkel der subduziereden Platte nimmt wahrscheinlich auch von Süd nach Nord im Bereich ds Kontinentalrandes vor Washington ab.

Der zweite große Unterschied liegt in der durchschnittlichen Geschwindigkeit der Sediment- und Krustengesteine, die die subduzierende Platte überlagern. Vor Washington wird die Geschwindigkeit selbst in Tiefen von 10-12 km nie größer als 5.3 kms^{-1}. Vor Oregon erreicht die Geschwindigkeit dagegen 6.5 kms^{-1} und beträgt 5 kms^{-1} oder mehr in Tiefen von mehr als 5 km. Diese Unterschiede repräsentieren Unterschiede in der Zusammensetzung der Kruste. Die Siletz River Basalte in Oregon reichen wahrscheinlich weiter seewärts. In Washington bestehen die Krustengesteine vermutlich aus bruchhaft verformten und geklüfteten Melangen aus dem Eozän und Miozän. Die Grenze zwischen diesen Krustenblöcken liegt möglicherweise südlich der Mündung des Columbia Rivers, wo die Struktur der Sedimente und der oberen Kruste sich dramatisch ändert.

Der dritte Unterschied liegt in der Mächtigkeit der Sedimente, die den kontinentalen Schelf unterlagern. Vor Oregon überschreitet die Mächtigkeit der Sedimente kaum 3 km, während vor Washington ein tiefes (3 bis 8 km), zum Teil tektonisch kontrolliertes, langgestrecktes Becken unterhalb des Schelfs liegt.

Die MCS Profile vor der Halbinsel Olympia und dem zentralen Washington zeigen, daß Aufschiebungen innerhalb des Akkretionskeils bis in die magmatische Kruste reichen. Demnach wird der gesamte, bis zu 3 km mächtige Sedimentstapel auf der ozeanischen Platte hier akkretiert. Die frontale Störung fällt landwärts ein und zeigt örtlich eine Reflexion mit hoher Amplitude, was wahrscheinlich auf fokussierten Fluidtransport zurückzuführen ist. Die Hauptstörungen in den äußeren 40 km des Keils fallen landwärts ein, und an ihrem landwärtigen Ende werden die Blöcke akkretierter Sedimente gegen einen Körper gelagert, der den Backstop aus älterem, festen Gestein darstellen könnte.

Die Refraktionsdaten von der Juan de Fuca Platte zeigen, daß die Kruste generell geringmächtiger ist als ozeanische Kruste im weltweiten Durchschnitt und daß sie von 1 bis 3 km Sedimenten mit geringer Geschwindigkeit überlagert ist. Klare S-Welleneinsätze vom Top der magmatischen Kruste sind weit verbreitet.

Weiteres Prozessing und die Analyse der Weitwinkel- und Mehrkanaldaten wird es ermöglichen, die Geologie der Cascadia Subduktionszone detailliert zu kartieren und mögliche Zonen der Erdbebenauslösung zu charakterisieren.

1.2 SUMMARY

The main goal of the R/V SONNE cruise SO108 was to investigate the large-scale structure of the Cascadia subduction zone to better assess the earthquake hazard it presents. The cruise was carried out in April and May of 1996 cooperatively by GEOMAR and the USGS. Ocean Bottom Seismometers (OBS) and Hydrophones (OBH) were deployed at 116 stations and collected wide-angle reflection and refraction seismic data along 12 profiles with a total length of 1385 km across and along the continental margin off Washington and Central Oregon and on the adjacent ocean floor of the Juan de Fuca plate. 1233 km of multichannel seismic reflection (MCS) data along 13 lines were collected over the Washington continental margin with two of the lines being coincident with wide-angle seismic profiles. All the wide-angle seismic data and two of the MCS lines have been processed, plotted, and analyzed during the cruise for quality control and for initial scientific interpretations.

Both wide-angle reflection and refraction data and the MCS data could detect the subducting oceanic crust under the continental margin to a distance of 20 km from shore. Three major differences between the continental margins of Washington and Oregon were discovered. The Oregon margin is much narrower than the Washington margin but the depth of the bottom of the subducting plate near the coast is similar in both areas (18-20 km), hence, the dip of the subducting plate is higher under the Oregon margin than under Washington. The dip of the subducting plate may also decrease from south to north under the Washington margin.

The second major difference is the average velocity of the sedimentary and crustal rocks overlying the subducting plate. Offshore Washington, the rock velocity never exceeds 5.3 km/s even at depths as deep as 10-12 km. Offshore Oregon, the rock velocity is up to 6.5 km/s and is 5 km/s or higher below 5 km depth. These differences represent differences in crustal composition. In Oregon, the Siletz River basalts are thought to extend offshore. In Washington, crustal rocks are probably broken and fractured Eocene to Middle Miocene melange. The boundary between these crustal domains is probably south of the mouth of the Columbia River where the sediment and upper crustal structure change dramatically.

The third difference is in the thickness of sediments underlying the continental shelves. Offshore Oregon sediment thickness does not exceed 3 km, whereas offshore Washington a deep (up to 8 km) partly fault-controlled elongate basin underlies the shelf.

MCS profiles off the Olympic Peninsula and central Washington show that thrust faults within the accretionary wedge extend downward to the level of the igneous oceanic crust, hence, the entire 3-km thickness of sedimentary rocks on the ocean plate is being accreted. The frontal thrust verges landward and locally returns a high amplitude reflection, which probably reveals focused flow of fluids. Major thrust faults in the outer 40 km of this wedge verge landward, and at their landward limit, they stack fault blocks of accreted sediment against what may be a backstop of older, indurated rock.

Refraction data from the Juan de Fuca plate show that the crust is generally thinner than the global average thickness of ocean crust and is overlain by 1-3 km of low-velocity sediments. Clear S-wave arrivals from the top of the igneous crust are common.

Further processing and analysis of the wide-angle and multichannel seismic data will enable us to map in detail the geology of the Cascadia subduction zone and to characterize the probable zone of earthquake nucleation.

2. INTRODUCTION
2.1 GENERAL BACKGROUND

(E. Flueh, M. Fisher, and D. Scholl)

Cascadia, which includes the Pacific Northwest of the United States and parts of adjacent British Columbia, Canada, is presently undergoing rapid urban growth. This region, like California to the south, is subject to a variety of geohazards, including great earthquakes, explosive volcanoes and tsunamis. These hazards exist in the Cascadia region because of its convergent margin setting along which the offshore Explorer, Juan de Fuca, and Gorda oceanic plates plunge or subduct eastward beneath the 1000-km-long coast that extends southward from Vancouver Island, B.C., to northern California (Figure 2.1.1).

Ten million people live along this subduction zone or convergent margin, in the cities and towns concentrated in the lowlands of Puget Sound of Washington and the Willamette Valley of Oregon, and on the Pacific coast. The rapidly growing urban corridor, which includes Portland, Seattle, and Vancouver, B.C., lies between the Cascade volcanic arc and, most threatening of all, the active subduction zone to the west.

In addition to the risk and consequences of catastrophic geologic events, the Cascadia margin is also the site of the production of large quantities of subduction zone methane and related hydrocarbons, and the sub-sea floor deposition of frozen methane, i.e., methane hydrate. The Cascadia margin is thus an important natural factory for the production and cycling of global-change gases, which, where they seep to the sea floor, somewhat paradoxically nurture the growth of large communities of benthic deep-water animals and microorganisms.

To gain a better understanding of the fundamental processes along active plate boundaries along continental margins, the Bundesministerium für Bildung, Wissenschaft, Forschung und Technologie (BMBF) of the Federal Republic of Germany provides the research vessel SONNE for such research projects. GEOMAR, Research Center for Marine Geosciences of the Christian Albrechts University in Kiel, and other German marine research institutions have a long tradition of research projects that are linked to GLOBAL CHANGE and IDNDR (International Decade of Natural Disaster Research) objectives. Such investigations recognize the worldwide necessity to study problems of global importance that have more than a local or regional impact on society. The ORWELL Project (from Oregon and Washington Exploration of the Lithosphere - A geophysical experiment) combines the research potentials of GEOMAR and the USGS to attack these problems on the Cascadia margin by geophysical studies. In subsequent legs of RV SONNE, geological and geochemical investigations along this margin will follow.

In recognition of the geohazardous setting of Cascadia, the US. National Research Council identified integrated field studies of active crustal deformation along the subduction zone setting of the Pacific Northwest (Cascadia) as a top priority (United States National Research Council, 1993). Similarly, the US Geological Survey National Earthquake Hazards Reduction and Deep Continental Studies Programs, in concert with the Interagency Coordinating Group for Continental Dynamics (NSF, DOE, USGS), identify Cascadia as a high priority region and are presently coordinating joint research efforts there. The Marine Sciences Program of the USGS similarly recognizes offshore and coastal studies of the Cascadia margin as an intergal part of a national-level effort in hazard mitigation investigations.

In recognition of the societal need for geohazard and geo-environmental studies of the Cascadia offshore, and the value of the science knowledge to be gained, efforts were begun in 1994 to combine German and US resources to initiate an investigation of the large-scale tectonic and structural fabric of the Cascadia margin. Within the USGS, the significance of hazard mitigation studies of Cascadia was the focus of a series of workshops held in 1993 and 1994. By early 1994, a comprehensive document was prepared that highlighted the key scientific problems to be addressed. An integrated approach to this work became the basis

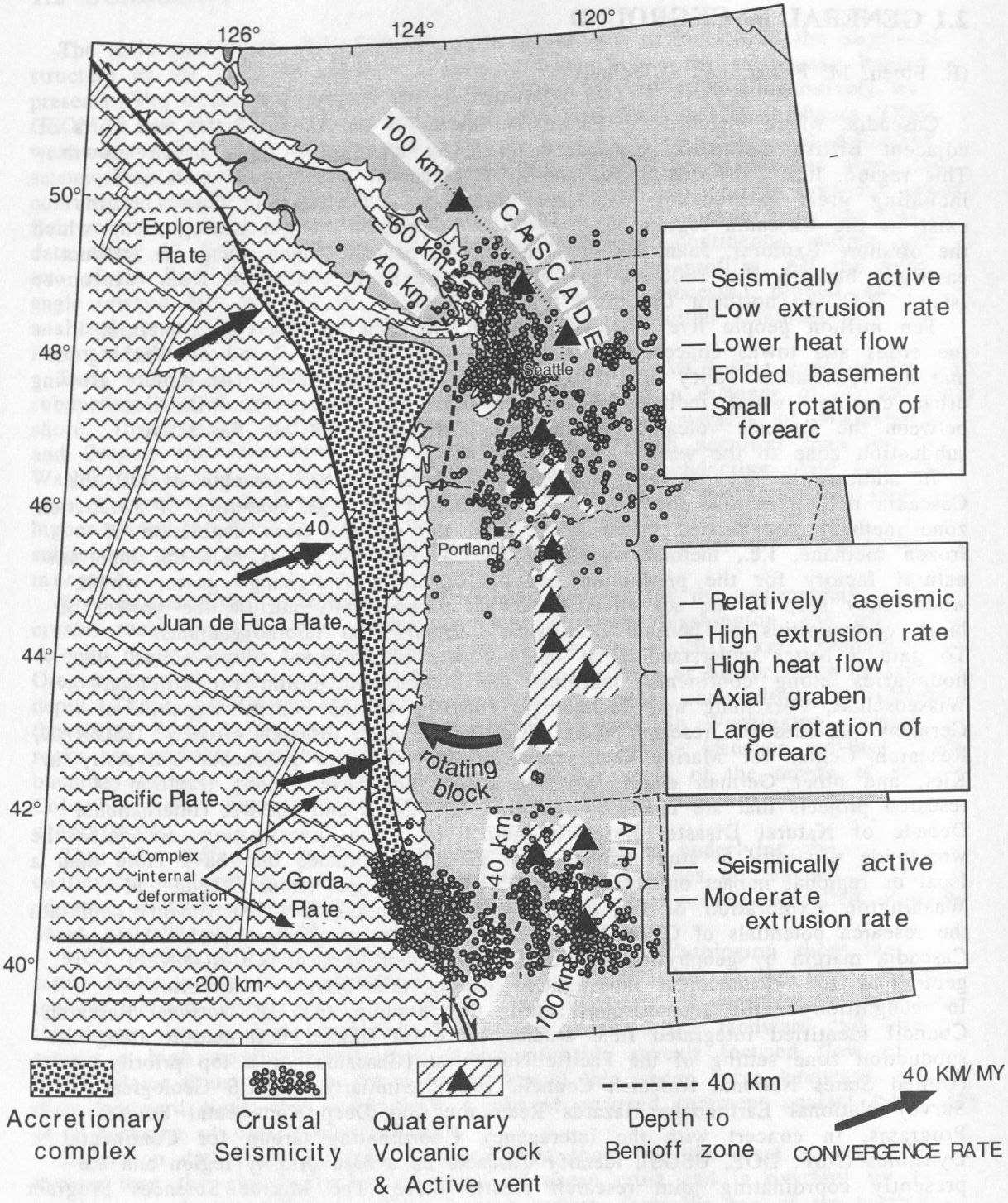

Figure 2.2.1: Major tectonic segments of the Cascadia margin with respect to crustal seismicity, regional style of active deformation, and voluminousness of arc magmatism. Along-strike tectonic segmentation is apparently linked to transpressively driven clockwise rotation of upper crustal blocks that extend landward at least to the volcanic arc. Adapted from illustration provided by Wells (1996). See also Wells and Heller (1988) and Wells (1989, 1990).

for a long-range plan of coastal and offshore investigations that was drafted and submitted for implementation in the summer of 1994.

Within a global context of the special societal and scientific merits of convergent margin studies, similar program-definition and related funding documents for Cascadia investigations were prepared at GEOMAR, Kiel. Meetings and communications between GEOMAR and the USGS scientists focused on the importance of addressing two high priority issues:

1) to distinguish and map in the subsurface the major elements and block boundaries of Cascadia's crustal structure and the interface with the subducting oceanic plate; the rationale for doing so is tied to the margin's potential for generating great earthquakes (>Mw 8) along the interplate surface, and also large shocks (>Mw 7-8) along faults bordering rotating and shifting upper crustal blocks, and
2) to more deeply track and map subsurface structures linked to processes of sediment accretion and sediment by-passing or subduction; the rationale for this work arises from the understanding that the flux of material in transport through the subduction zone may importantly influence the margin's potential for major interplate and upper plate shocks and processes of expulsion, storage and deep-crustal transport of pore fluids and global-change gases.

The ORWELL project, supported operationally by the R/V SONNE, during cruise SO-108, was designed to address the issues noted above through marine high-energy acoustic imaging of the major structural and mass-flux elements of the Cascadia margin. The ORWELL project involved the collection of wide-angle seismic reflection and refraction data from Ocean Bottom Hydrophone (OBH) and Seismograph (OBS) stations and onshore receiving locations. To this base of station data, underway multichannel seismic reflection profiles (24 fold, 48-channel data) were gathered over offshore Washington. Regional information implicates this sector of the Cascadia subduction zone may have been the nucleation area for great subduction zone ruptures. Scientific and technical personnel for shipboard work were supplied by GEOMAR and the USGS; onshore work was conducted by the USGS, Oregon State University, and the University of Washington.

2.2 REGIONAL BACKGROUND

2.2.1 SEISMIC SETTING OF THE CASCADIA MARGIN

(D. Scholl, adapted from documents largely written by Ray Wells, USGS)

The Cascadia subduction zone lacks historic thrust earthquakes on the interplate surface that are typical of most subduction zones. Heaton and Kanamori (1984) suggest that the Cascadia subduction zone may thus be locked and capable of generating magnitude 9 earthquakes, similar to the 1960 Chilean (the largest instrumentally recorded earthquake) and 1964 Alaskan (second largest) events. Limited geodetic data (Savage et al., 1991) and geologic studies of paleoseismic events suggest that great thrust earthquakes could occur along this margin (Atwater, 1987; Clarke and Carver, 1992). In the absence of a Wadati-Benioff zone of earthquake activity defining the interplate surface, the structure of the subduction interface and its potential for great earthquakes is one of the major scientific and societal problems in North America.

A combination of tectonic and geologic circumstances create the special setting for geologic hazards along the Cascadia margin. The most important of these conditions include:

1) an oblique or transpressively underthrust ocean margin to the northeast with respect to its north-south regional trend,
2) the existence beneath the margin of large blocks of early Tertiary basement rock that record a history of northward translation and clockwise rotation,
3) the accumulation of a thick sequence of ocean-floor sediment seaward of these blocks and the subduction zone underlying them, and

4) youthful oceanic plates underthrusting the Cascadia margin.

The unusually thick sequence of sediment that buries much of the oceanic plates (2-4 km at the base of the continental slope) has been supplied chiefly by the drainages of the Puget Sound region and the Columbia River. This blanket of water-rich sediment thermally insulates and covers relatively young (late Miocene and younger) oceanic crust generated at nearby segments of the Juan de Fuca spreading system (Figures 2.1.1 and 2.2.1). At a rate of approximately 40 km/my, the ocean crust and its overlying sedimentary column is swept tectonically into the Cascadia subduction zone at the base of the continental slope. Much of the sedimentary section is scraped off the subducting oceanic crust to form a large accretionary wedge or prism, in particular off Vancouver Island and northern Washington. Along with the oceanic crust, an unknown but potentially thick (> 1 km) section of the sedimentary pile may underthrust the bedrock framework of the Coastal Range to reach deep subcrustal and probably mantle depths. Fluid venting from the accretionary prism and underthrusting sediment occurs both diffusely and concentrated at faults, and probably also in association with mudstone diapirs. Entrained global-change gases (e.g., methane and other hydrocarbons) nourish the establishment and growth of cold-seep communities of benthic animals along the face of the margin and promote the deposition of carbonate minerals and thus cementation of accreted sediment (Carson et al., 1990; 1991).

Based on field measurement, theoretical considerations, and modelling results, the warmth of the underthrusting plate localizes potential nucleation sites of great subduction zone earthquakes beneath the Eocene framework rock of the submerged margin (Hyndman and Wang, 1993). This framework is broken into large crustal or basement blocks that extend well onshore and that are apparently driven northward and clockwise by transpressive plate-boundary coupling (Figures 2.1.1 and 2.2.1).

From a hazards point of view, the special circumstance of the Cascadia margin thus involves the underthrusting of a warm lithosphere, the mass input of sedimentary material to the subduction zone, the flux of some of this material to great depths, the expulsion of large volumes of pore fluids from accreted and underthrusting sediment, and the integrating effects of these conditions on interplate coupling and causing upper plate blocks to rotate and move northward. It is important to reemphasize that large earthquakes have not been recorded along Cascadia's interplate boundary. But geologic and observational evidence, and theoretical considerations strongly support the notion that catastrophic subduction zone earthquakes have nucleated between the two plates (see, for example, Atwater, 1987; Satake et al., 1996; Meyers et al., 1966). Although no *interplate* events have been recorded, *intraplate* earthquakes occur commonly within the subducting Juan de Fuca plate and within the overriding North American plate (Figures 2.2.1, 2.2.2, and 2.2.3). A number of these events have been significant shocks in that loss of life and property was substantial, particularly in the greater Seattle or Puget Sound region. Although coupling between the two plates is the underlying cause of recorded upper crustal seismicity and potential interplate or subduction zone ruptures, slab contraction caused by mineral phase transformation (basalt to eclogite) is evidently the source of lower plate seismicity (Steven Kirby, USGS, personal communications, 1996).

With respect to subduction zone ruptures, most earth scientists agree that the Cascadia subduction zone is an enormous geological hazard. Paleoseismologists who have examined evidence of rapid, episodic subsidence of coastal estuaries argue that many great earthquakes, some possibly as large as the devastating 1964 Alaska earthquake (Good Friday or Prince Williams Sound event) have occurred along the plate boundary over the past few thousand years. The last prehistoric earthquake in Cascadia of great magnitude occurred about 300 years ago, just prior to the establishment of European settlements in the region (Atwater, 1987; Meyers et al., 1996). Although no written record of the event exists, geologists along the Oregon coast have found firepits and woven cedar mats buried in the

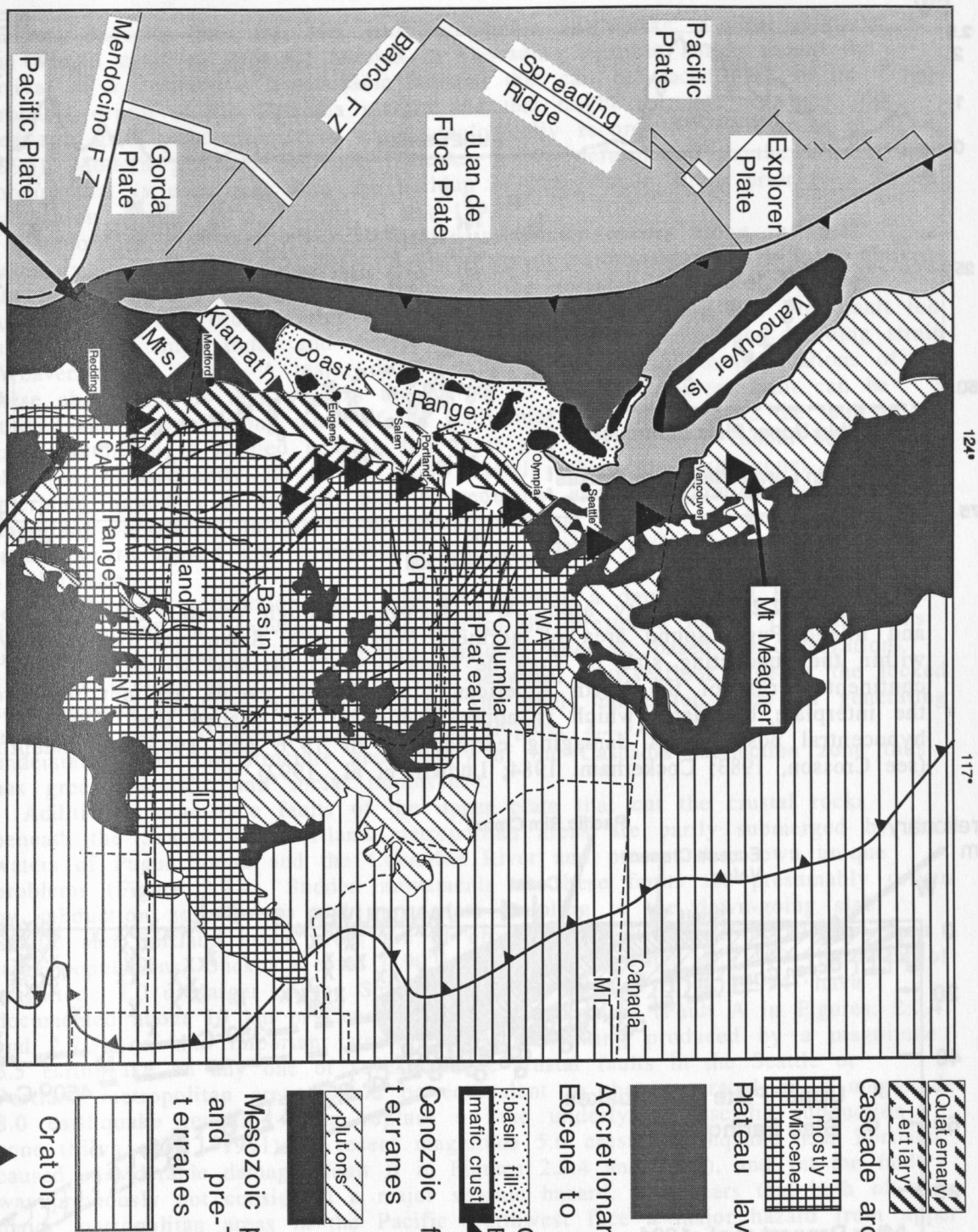

Figure 2.1.1: Major rock groups and plate-tectonic elements of the Cascadia subduction zone margin. Mt. Meagher and Lassen mark the northern and southern ends of the active centers of the arc volcanoes of the Cascade Range. The Columbia Plateau and Basin and Range are geomorphic provinces of the Cascadia backarc. Adapted from illustration provided by Wells (1996) and based on information and ideas provided in Wells and Heller (1988) and Wells (1989, 1990).

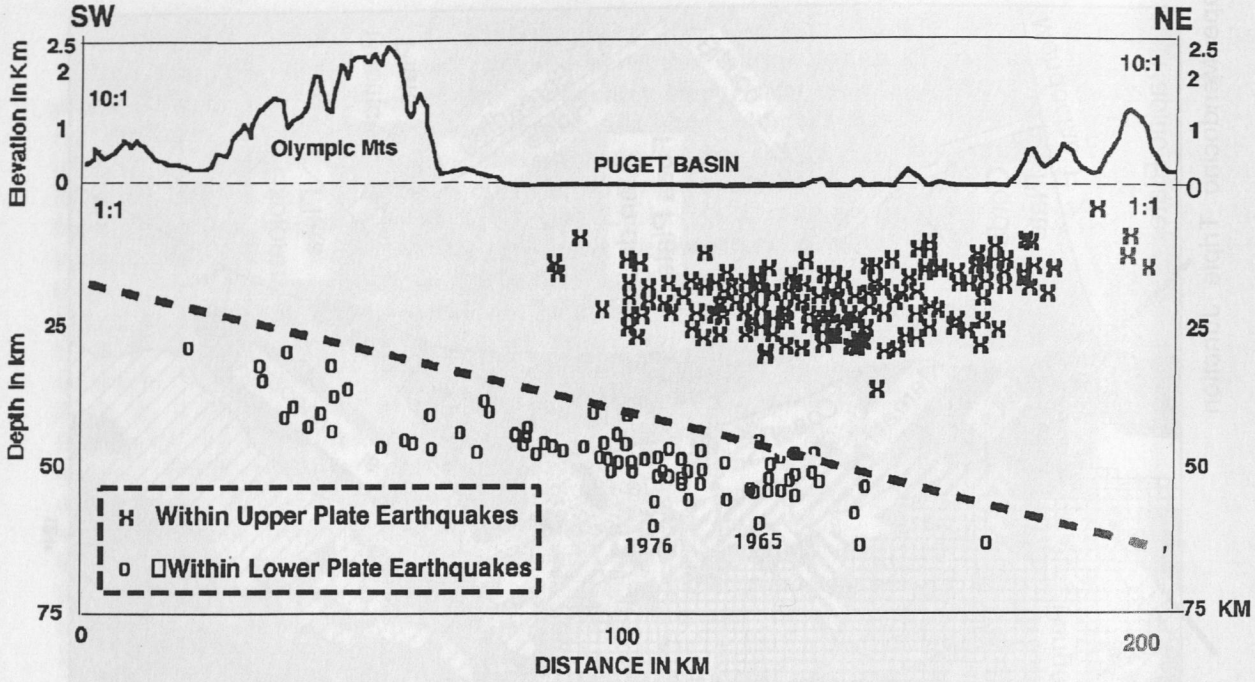

Figure 2.2.2: Seismicity along W-E transect through coastal Olympic Mountains and inland Puget sound area of northern Washington. Seismicity occurs only within the subducting slab of Juan de Fuca ocean crust and within the overlying continental crust of the North American plate. Thrust events are not recorded along the interplate boundary, which is approximated by the dashed line. The hypocentral positions of damaging earthquakes in 1976 and 1965 are indentified (see Crosson, 1983; Cockerham, 1984; Ludwin et al., 1992).

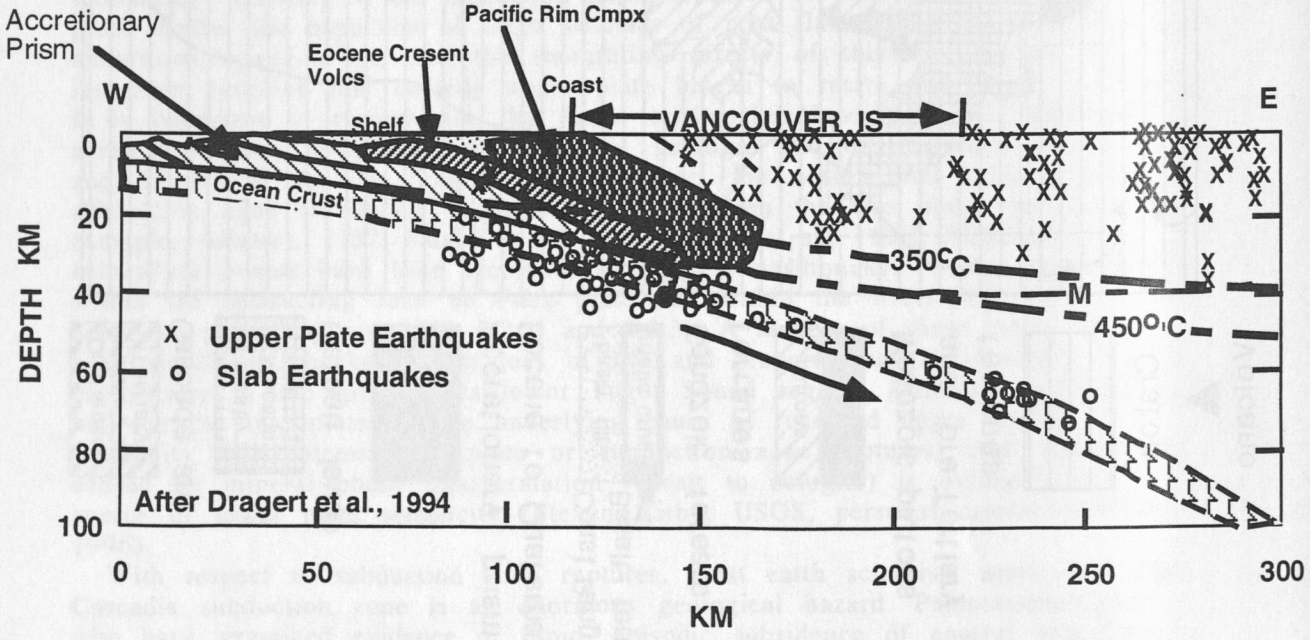

Figure 2.2.3: West-to-east cross-section of the Cascadia subduction zone of the Vancouver area of British Columbia, Canada. A large accretionary wedge of offscraped sediment is shown thrust beneath backstopping volcanic rocks of Coast Range basement basalt of Eocene age and structurally overlying pre-Tertiary units. Hypocenters of intraslab and upper crustal earthquakes are shown. Interplate or subduction zone earthquakes, if they occur, are presumably limited by rock rheology considerations to the segment of the interface above and below the 350 and 450°C isotherms. Adapted from Dragert et al (1994), see also Hyndman and Wang (1993).

tsunami deposits from this last great subduction earthquake, a clear reminder of the human costs of geologic hazards in Cascadia. Japanese annals record the arrival of a destructive transoceanic tsunami that can be traced back to its probable origin at the Cascadia margin and that might correlate with the 300-year-ago great subduction zone event geologically recorded there (Satake et al., 1996). Modern geodetic evidence indicates active deformation in the Washington forearc that is consistent with the buildup of interseismic strain prior to a future subduction zone rupture (Savage et al., 1991).

Paradoxically, although no present-day seismicity occurs along the plate boundary, the most likely source region of great earthquakes, the lack of activity has been compared to the circumstances of the northern section of the San Andreas fault that broke during the 1906 San Francisco earthquake. This fault too is seismically quiet today and therefore presumed to be locked and building strain (Weaver et al., 1988). A major difference in understanding the implications of these observation is that whereas the history of the San Andreas fault can be studied and mapped along much of the California coast, in Cascadia the fault of gravest concern is located beneath the coast and offshore and cannot be directly observed. Consequently, we do not know exactly where the fault (zone) of the interplate boundary is located, nor its geometry and configuration, which are important parameters in predicting ground shaking, nor do we know which segments are locked and consequently storing energy for a future great earthquake.

The Cascadia subduction zone interface presents a double-edged hazard in that the location of the landward, deeper part of the presumed locked fault threatens strong seismic shaking in the urban corridor, whereas, based on observations elsewhere (Pelayo and Wiens, 1992), the seaward, near-seafloor edge of the locked zone and its overlying folded rocks are the likely nucleation areas for generating regional as well as transoceanic tsunamis (Figure. 2.2.3). Gaining an understanding of the structure and history of the Cascadia subduction zone thus has great scientific and social importance.

Additional large-scale faults of the upper plate that cut the crustal rocks beneath the Seattle and Portland metropolitan areas are partly submerged by the waters of Puget Sound and the Columbia River and present their own unique problems (Figure 2.2.4). Sudden movements on these faults are presumably driven by subduction zone forces and upper-plate coupling to the down-going slab. Seattle and Portland urban areas are of obvious special concern because of their large populations. Bucknam et al (1992) recently documented a ~1100 ybp event of magnitude 7.0 or larger on the Seattle fault, and Johnson et al. (1994) have documented about 10 km of Cenozoic thrust displacement (Fault A in Figures. 2.2.4 and 2.2.5) on this important structure. Ground-shaking produced by a magnitude 6.5 earthquake on any one of several active crustal faults in the Seattle or Portland metropolitan areas would be equivalent to that generated by a magnitude 8.0 earthquake resulting from rupture on the underlying Cascadia subduction zone (Silva et al., 1991). A recent magnitude 5.6 crustal earthquake near Portland caused considerable damage (fault B in Figures 2.2.4 and 2.2.5), and yet the fault was previously not considered a major seismic hazard. It appears that both of the major metropolitan areas in the Pacific Northwest face a major hazard from upper plate crustal faults, but we still do not know where the faults are located, their connection at depth to the subduction zone boundary, much less understand their associated individual and cumulative seismic risk.

Offshore geological and geophysical investigative techniques can provide answers to major questions that must be address, these include:

WHERE ,IN THE SUBSURFACE, IS THE INTERPLATE BOUNDARY OR MEGATHRUST, THE SOURCE FOR GREAT SUBDUCTION ZONE EARTHQUAKES, EXACTLY LOCATED, AND WHAT IS ITS GEOMETRY AND CONFIGURATION?

Because of the lack of historic interplate seismicity, this critical information is presently seismologically *invisible* over much of the lateral and downdip extent of the interplate boundary, but this information is potentially

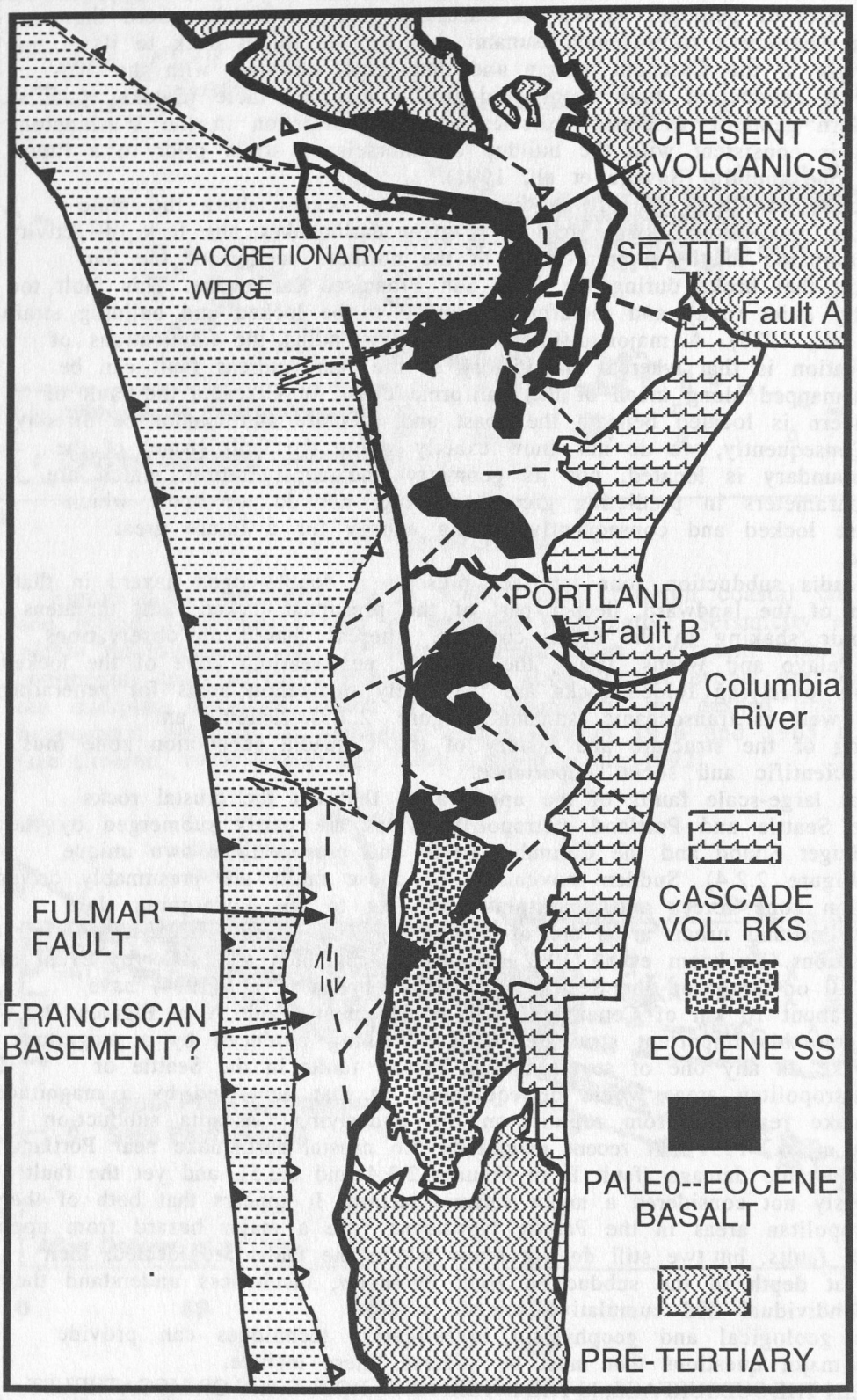

Figure 2.2.4: Generalized offshore and coastal geologic map of the Cascadia margin. Faults A and B are seismically active upper crustal fractures that pass close to the large urban centers of Seattle, and Portland, respectively. Adapted from Snavely (various publications, see in particular Snavely, 1987).

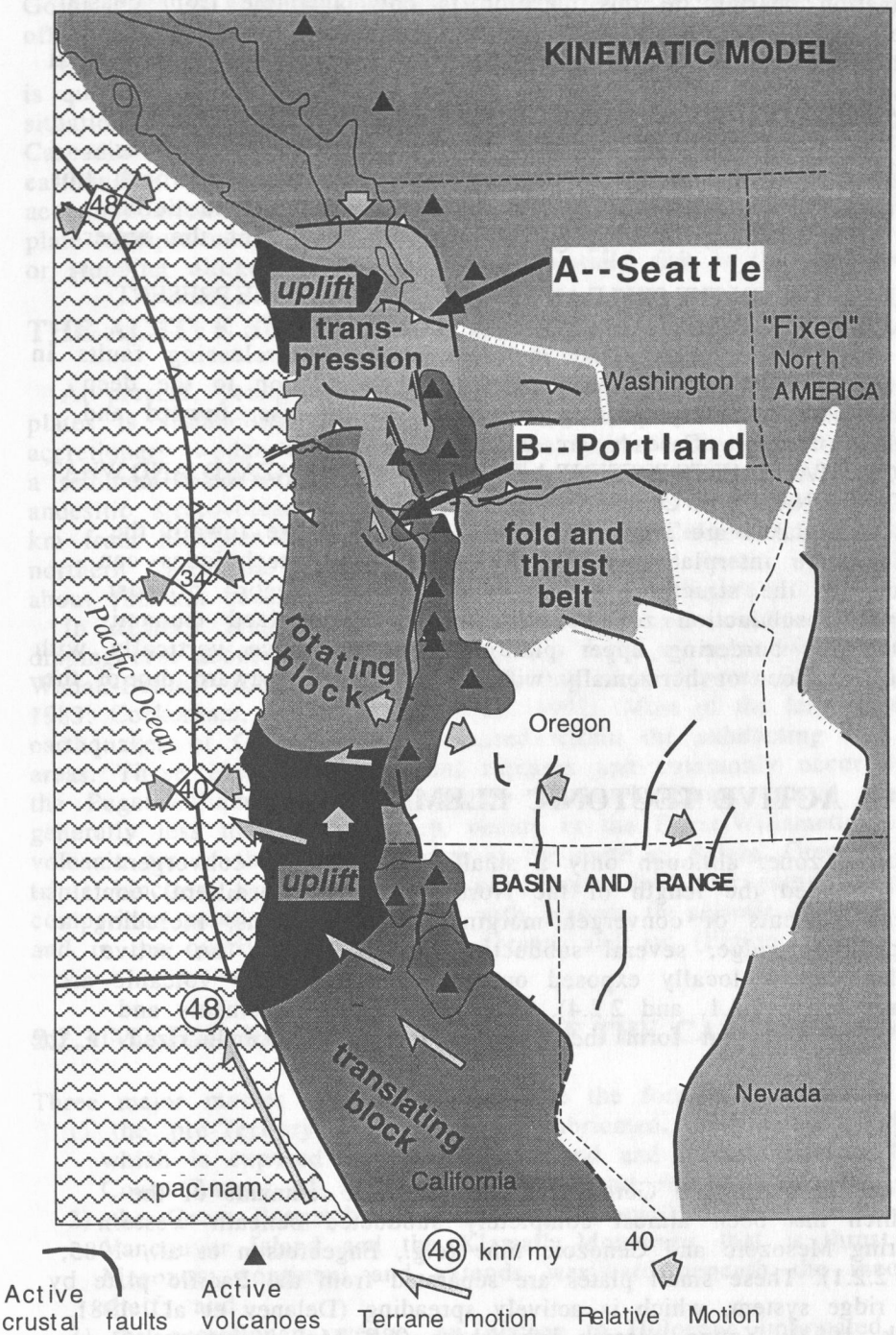

Figure 2.2.5: Genealized kinematic or block movement model of the Cascadia margin and adjacent regions of northern California and Basin and Range Province. Faults A and B are seismically active upper crustal fractures that pass close to the large urban centers of Seattle, and Portland, respectively. Adapted from illustration provided by Wells (1996) and based on information and ideas provided in Wells and Heller (1988) and Wells (1989, 1990).

available through high-energy marine seismic reflection and refraction techniques.

WHAT IS THE RECURRENCE RATE OF MAJOR SUBDUCTION ZONE EARTHQUAKES?

Presently, information bearing on this question is only available from coastal bays and inlets and sounds, and thus of limited time extent (about 6,000 years), but the continental margin potentially has a much longer structural and stratigraphic record of large strain-release earthquakes.

WHAT IS THE EXTENT OF THE HAZARD POSED BY GREAT EARTHQUAKES?

Marine seismic techniques through measuring the physical state of rocks along and adjacent to the interplate boundary can potentially approach this question by helping to identify locked and unlocked zones and to define lateral limits (segmentation) of slippage in overlying blocks of the upper plate

WHICH CRUSTAL FAULTS ON THE SHELF AND IN THE COASTAL ZONE PRESENT SUBSTANTIAL SEISMIC RISKS?

Marine seismic investigation can assist in identifying strain-releasing faults in urban areas and map, mainly in the subsurface, their relation to the deep underlying interplate boundary passing downward to the east toward and beneath the line of active Cascade arc volcanoes.

WHICH OF THE CRUSTAL FAULTS PRESENT A TSUNAMOGENIC HAZARD, AND WHAT IS THE RISK OF TSUNAMIS TO COASTAL POPULATIONS?

Many *tsunami* earthquakes are *slow earthquakes* that nucleate toward the seaward part of the interplate boundary. Marine seismic techniques can potentially identify the structural settings and structural record of past tsunami-generating subduction zone shocks, and also localized tsunami-generating fractures bordering upper plate blocks that move vertically with respect to the sea floor or horizontally with respect to the seaward dip of the continental slope

2.2.2 PRINCIPAL ACTIVE TECTONIC ELEMENTS

Cascadia subduction zone, although only a small remnant of a convergent margin that once extended the length of the North American Cordillera, contains all of the classical elements of convergent-margin tectonic systems, including a nearby oceanic spreading ridge, several subducting oceanic plates, an active accretionary complex that is locally exposed onshore, and an active volcanic arc and backarc (Figures 2.1.1, 2.2.1, and 2.2.4). The major tectonic elements and related rock units (terranes) that form the Cascadia margin are summarized in the sections below:

OCEANIC PLATES

The Explorer, Juan de Fuca, and Gorda plates are the last remnants of the Farallon plate, which has been almost completely subducted beneath western North America during Mesozoic and Cenozoic time (e.g., Engebretson et al., 1985; Figures 2.1.1 and 2.2.1). These small plates are separated from the Pacific plate by the Juan de Fuca ridge system, which is actively spreading (Delaney et al., 1981, Sinton and Detrick, 1992). Young oceanic lithosphere (4-8 Ma) is presently subducting beneath the Cascadia margin at about 4 cm/yr, and the ridge migrates northeastward toward the trench.

Complex triple junctions bound the Cascadia subduction zone to the north, and in particular to the south in the vicinity of Cape Mendocino (Figures 2.1.1 and 2.2.1). These junctions mark boundaries between dominantly transform and convergent relative motion. Deformation is introduced within the Gorda and Explorer plates (Bolt et al., 1968; Silver 1971; Masson et al.,1988; Wilson; 1989; Stoddard, 1991; Denlinger, 1992). Intraplate seismicity and distorted magnetic anomaly patterns indicate that the Gorda plate is deforming as a consequence of the transition from a subduction to a transform margin (Figure 2.2.1). Internal

deformation may be a key to understanding not only how the transition to a strike-slip continental boundary takes place but also the nature of the associated seismic hazards in the oceanic and continental plates. Active deformation of the Gorda plate is also demonstrated by relatively high-magnitude (Mw 6.0 to 7.3) offshore earthquakes (Lay et al., 1982; Velasco et al., 1993).

Unlike the Puget Sound and Mendocino areas, upper and lower plate seismicity is quite, as is the interplate surface, beneath central Oregon (Figure 2.2.1). If this situation indicates that the interplate surface is locked, then this sector of the Cascadia margin may also have the potential to spawn large interplate earthquakes. If, instead, the internal deformation of the Gorda plate indicates accommodation of the right-lateral shear component of North American-Pacific plate oblique convergence, then perhaps subduction of the Gorda plate is slowing or stopping altogether, and the related seismic risk is thus reduced.

THE ACTIVE SUBDUCTION ZONE

At present, young oceanic lithosphere of the Gorda, Juan de Fuca, and Explorer plates is subducting beneath North America, and a thick, actively-deforming accretionary wedge is forming along the base of the continental slope adjacent to a sediment-filled trench. The active Cascade arc, which consists of about 20 major andesitic stratovolcanoes and thousands of smaller volcanic vents, extends 1200 km from Meagher Mountain in southern British Columbia to Lassen Peak in northern California, consistent with the subsurface extent of a subducted slab at about 100 km beneath the full length of the arc (Figure 2.2.1).

In western Washington and northern California, localized planes of seismicity dipping east about 10° and extending to a depth of about 80 km are interpreted as a Wadati-Benioff zones within the subducting slab (Figures 2.2.2 and 2.2.3; Crosson, 1983; Cockerham, 1984; Ludwin et al., 1992). Most of the large historical earthquakes of Cascadia have occurred within the subducting slab in these two areas. These events are tensional ruptures and commonly occur 40-60 km beneath the Puget-Willamette lowland (Figure 2.2.2). Moderate crustal seismicity, generally less than 30 km deep, occurs in the Puget-Willamette lowland and the volcanic arc of the Cascade Range as far south as Salem, Oregon. At the Mendocino triple junction, crustal seismicity is intense. The intervening Oregon area is by comparison relatively quiet, both with respect to seismic activity within the slab and in the overlying crust of the forearc and arc (Figure 2.2.1).

2.2.3 MAJOR ROCK ELEMENTS OF THE CASCADIA FOREARC

Three major masses or terranes constitute the forearc of Cascadia (Figure 2.1.1):

1) the pre-Tertiary assemblage of imbricated, fault-bounded Mesozoic terranes, which is exposed on Vancouver Island and in the Klamath Mountains and Coast Ranges of northern California and southern Oregon;
2) the Coast Range basalt terrane of Eocene-Paleocene oceanic rocks between Vancouver Island and the Klamath Mountains that is thrust beneath the Mesozoic continent and extends westward beneath the inner continental shelf; and
3) the accretionary wedge, an Eocene to Holocene imbricated structural complex of offscraped and underplated sedimentary packages that largely makes up the continental slope and outer shelf.

The structure and arrangement of these coastal terranes varies substantially along strike. But, with respect to the seismicity of the central and northern sectors of the Cascadia margin, the two most important are the accretionary wedge and the Coastal Range basalt terrane. Seismicity at the southern end of the Cascadia margin is dominated by the complex tectonism underway in the area of the Cape Mendocino triple junction (Figure 2.1.1) where a thick accretionary prism has been elevated into the Coastal Ranges and thrust against, and partially beneath, a structural backstop of pre-Tertiary rocks.

COAST RANGE BASALT TERRANE

The oldest rocks of the Oregon and Washington Coast Ranges are tholeiitic pillow basalt and interbedded breccia and marine sedimentary rocks exposed in basement uplifts--the Coastal Range basalt terrane (Figure 2.1.1; Duncan, 1982; Bukry and Snavely, 1988). These exposures of oceanic basalt, capped in places by islands and seamounts edifices, include the Siletz River Volcanics in Oregon (Snavely et al., 1968), the Crescent Formation in Washington (Arnold, 1906; Brown et al., 1960; Cady, 1975) and the Metchosin Volcanics on southern Vancouver Island (Figures 2.1.1 and 2.2.4; Clapp, 1917; Muller, 1977). The most popular model for the origin of these basalts is one of tectonic accretion of hot spot-generated oceanic islands or aseismic ridges (for example, Snavely and Macleod, 1974, Simpson and Cox, 1977; Duncan, 1982; Wells et al., 1984). In an alternative model, rifting and in situ volcanism along the leading edge of the continental margin of western North America occurred as the continent encountered the Yellowstone hot spot during a period of rapid, highly oblique, northeast motion of the Kula plate that was initiated in the Paleocene (Wells et al., 1984; Snavely, 1987; Clowes et al., 1987).

On the outer continental shelf of Oregon the western boundary of the Coast Range basalt basement is delimited by the north-south-trending Fulmar fault (Figure 2.2.4).

On the basis of a linear aeromagnetic gradient (Bond and Zeitz, 1987) that Snavely et al. (1980b) interpreted to be the western edge of Coast Range basaltic basement, the offshore Fulmar fault may strike parallel to the coast for at least 200 km. Seismic-reflection profiles and offshore deep test wells confirm that the steeply-dipping Fulmar fault separates lower Eocene oceanic basalt on the east from lower Eocene quartzose lithic sandstone of continental source on the west (Snavely et al., 1982). The Fulmar fault is thus interpreted to be a major right-lateral fault of Eocene age that formed the western margin of an oblique pull-apart basin within which the Coast Range basalt erupted (Snavely, 1987; Wells et al., 1984). To the south, the fault intersects the coast south of Coos Bay and is inferred southward into northern California as the Graywhale fault. To the north multichannel seismic-reflection profiles indicate that the fault extends along the mid-shelf northward to about latitude 45°, where displacement may have been transferred inboard to a comparable fault bordering the eastern margin of the Coast Range basalt basement (Wells et al., 1984; Johnson, 1984; 1985). However, the eastern boundary of the Coast Range basement is covered by younger deposits of Puget Sound and the Cascade arc, and its location can only be inferred.

THE ACCRETIONARY WEDGE

A thick accretionary complex of offscraped sediments lies adjacent to the filled Cascadia Trench from the north end of Vancouver Island to Cape Mendocino, a distance of 1300 km (Figures 2.1.1, 2.2.1, and 2.2.4). Most of the accretionary complex lies offshore, except where it extends onshore in the Olympic Mountains and near Cape Mendocino. Geologic mapping in accretionary assemblages of the western Olympic Mountains (Rau, 1975; 1979; Snavely et al., 1986, 1989; Snavely and Kvenvolden, 1989) and interpretation of seismic profiles on the Vancouver Island margin (Clowes et al., 1987; Davis and Hyndman, 1989; Snavely and Wagner, 1981), on the Washington shelf (Snavely and Wagner, 1982), and on the Oregon continental slope (Snavely et al., 1985, 1987, 1993) indicate that strata as young as Miocene age have underplated older rocks along the convergent margin.

In the uplifted core of the Olympic Mountains of northern Washington accretionary material is thrust beneath the Coast Range basalt basement along a major thrust fault that juxtaposes middle Eocene mélange and broken formation to the west against coherent masses of basalt and overlying strata to the east (Tabor and Cady, 1978; Snavely et al., 1993; Brandon et al., 1988). On nearby southern Vancouver Island, reflection and refraction profiles from the Canadian Lithoprobe program indicate that Eocene accretionary strata underplate the lower

Eocene basalt of the Metchosin Formation and structurally overlying pre-Tertiary rocks (Clowes et al., 1987; Dragert et al., 1994; Figure 2.2.3).

To the south the extent of the accretionary wedge beneath the rest of the Coast Range is unknown. In a marine multichannel seismic survey and geologic profile across the continental shelf near Grays Harbor, Washington, Snavely and Wagner (1982) suggested that part of the accretionary wedge is thrust eastward beneath a thin upper plate of Coast Range basalt. Shelf and slope basin fill of Oligocene and younger age overlies the basalt basement offshore. Thrusting, fault-bend folding, and diapiric intrusion of mud matrix melange continued to deform the accretionary wedge and overlying basin fills to the present day. Although the upper levels of the subduction complex have been successfully imaged in several places, the deep structure of the accretionary wedge, its extent beneath the Coast Range basalt, its effect on the geometry of the subducting slab, and its physical properties at depth are poorly understood.

Farther to the south, off central Oregon, the accretionary wedge is narrower, and the Coast Range basalt extends farther offshore (Snavely, 1987), possibly forming a backstop for the subduction complex (Figure 2.1.1; Snavely et al., 1980b; Trehu et al., 1994). Most of the seismic profiles off Oregon show an accretionary complex of offscraped sediment and overlying slope basin deposits undergoing thrusting and folding landward from the deformation front to a pronounced outer-arc high along the shelf-slope break (e.g. Snavely et al., 1980b, Niem et al., 1990). In other subduction zones, this high commonly correlates with the seismic front (Byrne et al., 1988) and presumably the beginning of seismic coupling with the downgoing slab. However, in Oregon and Washington, there is little or no seismic activity along the coast. According to Byrne et al., high pore pressure in the accretionary wedge inhibits buildup of interplate shear stresses. In keeping with this observation, overpressured melange units have been found (downhole oil exploration data) on the Oregon shelf inboard of the outer-arc high (Snavely, 1991).

On the outer continental shelf of southern Oregon, a fault sliver of coastal Franciscan-equivalent terrane derived from southern Oregon and California forms the backstop for the accretionary complex (Snavely, 1987). The north-striking Fulmar fault described above forms the terrane boundary between the allochthonous sliver of lower Eocene graywacke on the west (Fulmar terrane) and Paleocene and lower Eocene oceanic basalt (Siletz terrane) on the east (Figure 2.2.4). The lower Eocene graywacke most likely overlies pre-Tertiary accreted rocks of Franciscan affinity.

The southernmost extent of the accretionary prism is 85-100 km wide and comprises at least two imbricate systems of north-northwest-trending, east-northeast-dipping thrust related anticlines and broad open synclines (Clarke, 1992). This structural domain is buttressed on the east by the Klamath Mountains and is underlain at depths as deep as about 20-22 km by the east-dipping oceanic slab of the subducting Gorda plate. (Figure. 2.1.1). Youthful tectonic activity related to Gorda-North American plate convergence indicates an active Cascadia subduction zone and strong partial interplate coupling (Clarke, 1992; Clarke and Carver, 1992).

MENDOCINO TRIPLE JUNCTION

The Mendocino triple junction at the southern end of the Cascadia margin has been migrating northward along the coast for 30 my as the Pacific plate moved northward with respect to North America. The coastal and offshore region of the triple junction region is structurally and dynamically the most complex sector of the Cascadia margin and it exhibits the highest rate of seismicity and tectonic uplift in the conterminous United States (Zandt and Furlong, 1982; Jachens and Griscom, 1983). As the triple junction moves northward, the small Gorda Plate remnant of the Farallon plate is being deformed between the shearing couple of the larger North American and Pacific plates (Wilson, 1989). Further tectonic complications attend the circumstance that to the south of the triple junction's

trailing edge an inferred slab window of ascending asthenoshpere is opening beneath the margin (Figure 2.2.1).

2.2.4 BLOCK ROTATION AND SEISMIC SEGMENTATION OF CASCADIA

Although the convergent margin of Cascadia shares most characteristics typical of subduction zones, in many ways it is a unique because the small oceanic plates of Cascadia are caught in the dextral shear couple between the encroaching Pacific and North American plates. The upper and lower plates thus appears to be tectonically segmenting as both the oceanic plate and that of the margin and magmatic arc break up into rotating blocks (Wells et al 1988, Wells,1989; 1990). As a result, along its strike the Cascadia margin exhibits dramatic north-south variations in exhibited seismicity, volcanism, and regional deformational pattern (Figure 2.2.1).

An inverse correlation between seismicity and Quaternary volcanic production rate along the arc appears to be a fundamental characteristic of Cascadia. A s displayed on Figure 2.2.1, the longitudinal distribution of earthquakes, volcanic activity, and styles of deformation divides the margins into three segments:

1) a northern, seismically active transpressional margin with a poorly developed volcanic arc (Washington and adjacent British Columbia);
2) a central aseismic segment with a robust volcanic arc (central Oregon) erupting within a widening graben; and
3) a seismically active southern segment in northern California with a well developed arc erupting in a transtensional environment.

This threefold segmentation also holds for other late Cenozoic geological elements, including:

1) in the outer forearc, variations in the width of the offshore accretionary wedge;
2) in the forearc generally, clockwise rotating blocks of basement rock and overlying sedimentary sequences.
3) in the backarc, major differences in elevation, magmatic history, and active deformational process (Figure 2.2.1).

The northern segment of Washington and adjacent parts of northern Oregon and southern British Columbia, the arc and forearc areas are seismically active, with a recognizable Wadati-Benioff zone of dipping *intraslab* earthquakes overlain by crustal events. The seismically active arc is undergoing dextral shear and is folded and uplifted, with isolated stratovolcanoes resting on the deformed arc platform of much older rocks (Figure 2.1.1). This segment is characterized by a broad accretionary prism that comes onshore in the Olympic Mountains and probably underplates the northward translating and rotating basalt basement blocks of the forearc. In the backarc is the topographically low, but seismically active, Columbia basin filled with flood basalt of the Miocene Columbia River basalt Group.

The central segment includes the subduction zone and upper plate of the central Oregon, this segment is relatively aseismic. It is characterized by a somewhat narrower accretionary prism than Washington and a monolithic forearc block of Coast Range basalt, which is rotating and translating northwestward in front of the volcanically robust extensional arc nested in its discontinuous axial graben (Figures 2.2.1 and 2.2.5). The Basin and Range Province of the backarc is volcanically active, topographically elevated, and seismically quiet (Figures 2.1.1 and 2.2.5). Pre-Tertiary crust may be missing in this area, which lies within the so-called Columbia embayment that is dominantly filled with Cenozoic volcanogenic and sedimentary rocks overlying an early Tertiary volcanic basement possibly equivalent to the Coast Range basalt. Recent and ongoing seismic and electromagnetic studies in the northern part of this corridor confirm an unusually thick mafic crust in the forearc, possibly in

contact with the subducting slab (Snavely et al., 1980; Wannamaker et al., 1989; Catchings and Mooney, 1988; Trehu et al., 1994; Luetgert et al., 1992).

The Mendocino or southernmost segment of the Cascadia margins includes the rapidly deforming, seismically active triple junction region, the southern terminus of the Cascade arc, and the seismically active arc--Basin and Range transition to the east. In this segment the accretionary prism comes onshore, and the uplifted pre-Tertiary orogenic belt of the Klamath Mountains forms the forearc backstop. The arc has a moderately high volcanic production rate, has well-developed graben structures, but is less rotated than the Oregon segment (Figures 2.1.1 and 2.2.1).

The large-scale tectonic segmentation of the Cascadia margin apparently reflects fundamental differences in the boundary forces and mechanisms of crustal strain acting along the margin. A critical question is whether this tectonic segmentation has any relation to possible *seismic segmentation* of the subduction zone thrust interface that underlies the submerged margin. Although the regional tectonic framework suggests that seismic coupling may vary along the subduction zone, not enough is known about the major framework fabric let along the detailed structure and history of the megathrust to determine if seismic segmentation is likely (Wells, 1989; 1990).

3. PARTICIPANTS

3.1. SCIENTISTS

Ernst R. Flüh, GEOMAR, Chief-Scientist
Jörg M.K. Bialas, GEOMAR
Robert Busby, USGS Woods Hole
Jonathan R. Childs, USGS Menlo Park
Janine Fest, GEOMAR
Michael A. Fisher, USGS Menlo Park, Co-Chief Scientist
David S. Foster, USGS Woods Hole
Kerstin Henneberg, GEOMAR
David Hogg, USGS Menlo Park
Katrin Huhn, GEOMAR
Stephan Husen, GEOMAR
Dirk Klaeschen, GEOMAR
Christian W. Kopp, GEOMAR
Nina Kukowski, GEOMAR
Dörte Mann, GEOMAR
Kevin O'Toole, USGS Menlo Park
Walter F. Olson jr., USGS Menlo Park
William Robinson, USGS Menlo Park
Thies Schillhorn, GEOMAR
David Scholl, Stanford/ USGS
Klaus-Peter Steffen, GTG
Uri S. ten Brink, USGS Woods Hole
Neus Vidal Martinez, GEOMAR
Harold D. Williams, USGS Menlo Park

3.2. CREW

Henning Papenhagen	Master
Heiner Lübbers	Chief-Officer
Norbert Ladewich	1st Officer
Wilfried Osterhues	Radio-Officer
Ingo F. Naeve	Surgeon
H. Andreas Martin	Chief-Engineer
Fritz H. Grund	2nd Engineer
Uwe H.C. Sandersfeld	2nd Engineer
Peter Neumann	2nd Engineer
Steffen Bekaan	Electrician Engineer
Rainer Duthel	Electronic Engineer
Rudolf Andermann	Electronic Engineer
Volkmar Gebhardt	System-Operator
Stefan Krause	System-Operator
Joachim F. Stenzler	Fitter
Hans Bethke	Motorman
Roland Teske	Motorman
Josef Kiefer	Motorman
Franz Gruen	Chief-Cook
Ralf Kegler	2nd Cook
Michael Both	Chief-Steward
Heinrich Schramme	2nd Steward
Klaus-Peter Hillmann	2nd Steward
Karl-Heinz Hartwig	Boatswain
Detlef Mahlmann	Able Bodied Seaman
Reiner Kaiser	Able Bodied Seaman
Andreas Schrapel	Able Bodied Seaman
Herbert Melsbach	Able Bodied Seaman
Günther Lude	Able Bodied Seaman
Günther Staengl	Able Bodied Seaman

3.3. ADDRESSES

GEOMAR: GEOMAR
Forschungszentrum für
marine Geowissenschaften der
Christian-Albrechts-Universität zu Kiel
Wischhofstraße 1-3
24148 Kiel
Germany
Tel. 0049 - 431 - 600 - 2972
Fax 0049 - 431 - 600 - 2922
e-mail nn@geomar.de

GTG: Geomar Technologie GmbH
Wischhofstraße 1-3
24148 Kiel
Germany
Tel. 0049- 431 - 7209610
Fax 0049- 431 - 7209699

USGS Menlo Park: U. S. Geological Survey
Marine and Coastal Geologic Surveys
345 Middlefield Road
Menlo Park, CA 94025, U.S.A.
Tel. 001 - 415 - 354 - 3147
Fax. 001 - 415 - 354 - 3191
e-mail mfisher@octopus.wr.usgs.gov

Stanford/ USGS: Stanford University and U.S. Geological Survey
Branch of Pacific Marine Geology, MS 999
345 Middlefield Road
Menlo Park, CA 94025, U.S.A.
Tel. 001 - 415 - 354 - 3127 (U. S. Geological Survey)
Tel. 001 - 415 - 354 - 4439 (Stanford Universtiy)
Fax. 001 - 415 - 354 - 3191
e-mail dscholl@octopus.wr.usgs.gov

USGS Woods Hole: U. S. Geological Survey
Marine and Coastal Geology, Northeastern Section
Quissett Campus
Woods Hole, MA 02543, U.S.A.
Tel. 001 - 508 - 457 - 2396
Fax. 001 - 508 - 457 - 2310
e-mail tenbrink@nobska.er.usgs.gov

4. AGENDA OF THE SONNE CRUISE SO108

(E. Flueh)

SONNE cruise SO108 started on April 15 in San Francisco, California, where she was docked at pier 94 and ended in Astoria, Washington, on May 23. 1996. In San Francisco, more than 40 t of geophysical equipment from the US Geological Survey was installed, including a large generator, two compressors, a reel containing a 2400 m streamer, a DFSV recording system, and Ocean Bottom Seismometers. Additional equipment needed by GEOMAR was already onboard from the previous cruise. Installing this equipment required carefull handling and planning, and the port regulations did not allow flexible operations.

On Wednesday, 17 April was the 90th anniversary of the 1906 San Francisco earthquake, and a COMAR reception (Cooperation in Ocean MArgin Research) was held onboard the SONNE in recognition of the long-standing cooperation in scientific research between Germany and the United States of America. At this meeting the asssembled group also took the opportunity to acknowledge Prof. Emeritus Magna Cum Laude Roland von Huene, who retired while at sea on the previous SONNE cruise SO107, and who initiated the ORWELL project. After four days all instruments were securely stored and SONNE left the pier on 19. 04. at 11:03 and passed beneath the Bay Bridge and Golden Gate Bridge with fresh winds. During the two day transit to the first experiment, the "Rosette" profiles on the Juan de Fuca Plate, several tests of the instruments (OBH release, airguns, and streamer) were made. Deployment of 20 OBS/OBH started late sunday night (21.04.). Deployment was finished at 13:00 the next day, and shooting started shortly thereafter. During the night with increasing wind and swell several guns failed, and at 23.04. 11:00 with the wind at force 9 the guns were retrieved. SONNE rode out the storm for 26 hours, and shooting started again in rather calm seas but was interrupted again at 11:00 24.04. because of rough seas (force 7 to 8). Only 5 of the profiles were completed, and instrument recovery had to start, since on some instruments the batteries were running short. OBS01 did not respond and despite several hours of searching and sending multiple release commands was finally given up as lost. Recovery of the instruments was completed on 26.04. at 10:30. The next experiment consisted of one E-W and two N-S transects across the Oregon margin. Twenty instruments were deployed along the 200 km long E-W line (profile 7). This deployment ended at 06:00 27.04., and shooting started soon after in rather calm seas. The profile was finished 09:00 28.04. All OBH and some OBS (other OBS remained at the bottom for the next lines) were recovered and then redeployed along two 60-mile-long N-S transects. Shooting along the two north-south profiles started at 17:00 29.04. and finished 0:00 01.05. While shooting, the ship was informed that a fisherman had picked up one of the OBH and took it to Newport, Oregon. Recovery of all other instruments was completed at 15:00 01.05., and SONNE headed northward to the SW-Washington margin.

The southwest Washington Transect started with the deployement of 21 OBH/OBS at 2:30 02.05. For the first time during SO108, the vertical array was deployed. A swimming line was attached to all OBS instruments for easier retrieval. Shooting along the E-W transect lasted from 17:00 02.05. to 21:00 03.05. in calm seas. The ships speed was reduced to 3.5 kn, and the trigger rate was set to 60 s, based on the preliminary results obtained during the Oregon dip line. At the end of the line, the 24 channel Mini Streamer was also deployed to minitor the guns signature and to obtain vertical-incidence data. The retrieval of the instruments was interrupted at midday 04.05., when a supply boat was met at the mouth of Columbia River. This boat also returned the OBH that was picked up by a Newport fisherman. The remaining six OBS/OBH were picked up after the first 7 instruments of the Washington N-S line were deployed in the southern part.

Deployment of the Washington N-S profile was completed by 12:00 05.05.; a total of 21 were recorders spaced at about a 7-mile interval. The vertical array was deployed again. Shooting started at 15:30, the ship's speed was 3.5 kn and the guns wre fired at a 60 s interval. Most important, the seas wre calm. The profile was finished at 10:00 07.05., and retrieval of the instruments was completed by 07:00 at 08.05.

The last OBH/OBS profile was located across the accretionary wedge west of the Olympic Mountains. Deployment of 21 instruments including the vertical array and one OBH on a 1500 m long anchor line started at 10:00 08.05. and was completed by 21:00 on the same day. Shooting took place from 00:00 09.05. to 06:30 10.05. at 3.5 kn and a 60 s shot interval. Seas were flat throughout the time. Pickup of the instruments was completed between 08:00 and 23:00. One OBH did not give reasonable ranges when released from the bottom, but minutes later a weak radio signal was detected. Following that radio signal, SONNE found the 4 miles from where it was deployed. It had apparently been dragged by a fishing vessel. We were fortunate that the OBH was still within the range of the release unit.

Following the wide-angle work the remaining time was devoted to collecting MCS data. After the first deployment and balancing of the 2400 m long streamer, the tail buoy was invisible and the last 6 sections sank to depth of more than 20 m. The remaining part of the streamer was well balanced at 12 m and quite, and the first line - profile 101 - was started at 11:23 11.05. in force 6 winds. With decreasing winds this line was finished at 02:00 12.05. During the turn to the next profile two broken airguns were fixed, and the front part of the streamer was checked, because a leakage problem on all the channels had became apparent. No damage was detected on the lead-in or the stretch section due to collision with the airguns. Profile 102 was started at 12:00 and finished at 4:30 13.05. Three guns failed during this profile and the leakage problem became more intense, but still not troublesome. After the end of this profile the streamer was checked again and the leakage was found at the first connector, which had not been properly sealed. After streamer and gun repair, profile 103, coincident with wide-angle profile 12 (Olympic transect) was started at 13:30 13.05. in calm seas. The end of line 103 was reached 09:30 on 14.05., and during the transit to line 104 the SONNE passed through many crab pots. Increased streamer tension clearly indicated that some crab pot buoys had been caught. For unexplained reasons this action caused the tail buoy to raise. Also. the calm sea state made it become visible and the end part of the streamer was at shallower depth of around 15 m. An attempt to untangle the fishing lines from the tail buoy by sending a crew in the Zodiak was only partly successful.

Profile 104 was started at 14:30 14.05. and terminated in absolutely calm seas at 08:30 15.05. After line 105 was finished the streamer was taken aboard for ballasting and to check the tailbuoy, which meanwhile had dropped all its additional gear. The gun array was modified again, since some of the larger airguns continued to fail.

Profile 105 was started at 17:00 15.05. and terminated short of its planned end around 06:30 16.05. In perfectly calm sea it was decided to do a 270° turn with the portside array just pulled astern of the vessel, without retrieving it to the deck. A short transit profile, profile 106 which runs coincident to a part of the wide-angle line Washington N-S (profile 11) was started around 09:00 and ended at 14:30. Profile 107, coincident with the wide-angle profile 10, was started in absolutely calm seas at 14:30 about 15 miles from shore, just crossing profile 106. It was finished at 07:30 17.05., and followed by a short north-south segment, profile 108, which was shot with one gun array only. The other array was taken aboard for preventive maintanence. Within a few hours gale winds forced us to terminate profile 108 at 10:00, the other array had two gun failures and was also taken aboard. After the wind died down, the sea state still did not permit us to start a new profile, instead we transited southward to the endpoint of the southernmost line, profile 109. Around 06:00 18.05. the sea state permitted the deployment of the airguns and profile 109 was started from west to east and terminated at 20:00 on the shelf.

Again some maintanence had to be done on the airgun arrays and on the transit north another short line, profile 110 was collected using one array only. This line was terminated at 03:00 19.05., and sea state was rough again, so several hours of waiting were required. Profile 111 was shot from east to west from 08:00 to 24:00, after retrieval of the airguns several hours had to be spend on repair. Another short line, profile 112 was shot between 09:00 and 12:30 20.05. The last MCS line, profile 113 was then shot from south to north from 13:00 20.05. to 15:00 21.05. After retrieval of the arrays and the streamer, some tests of the shipboard equipment was made and SONNE headed south to meet the pilot at the mouth of

Columbia River. She finally docked in Astoria at 13:15 22.05. after 34 days at sea, and the scientific equipment was unloaded. A complete trackchart of cruise SO108 is shown in Figure 4.1.

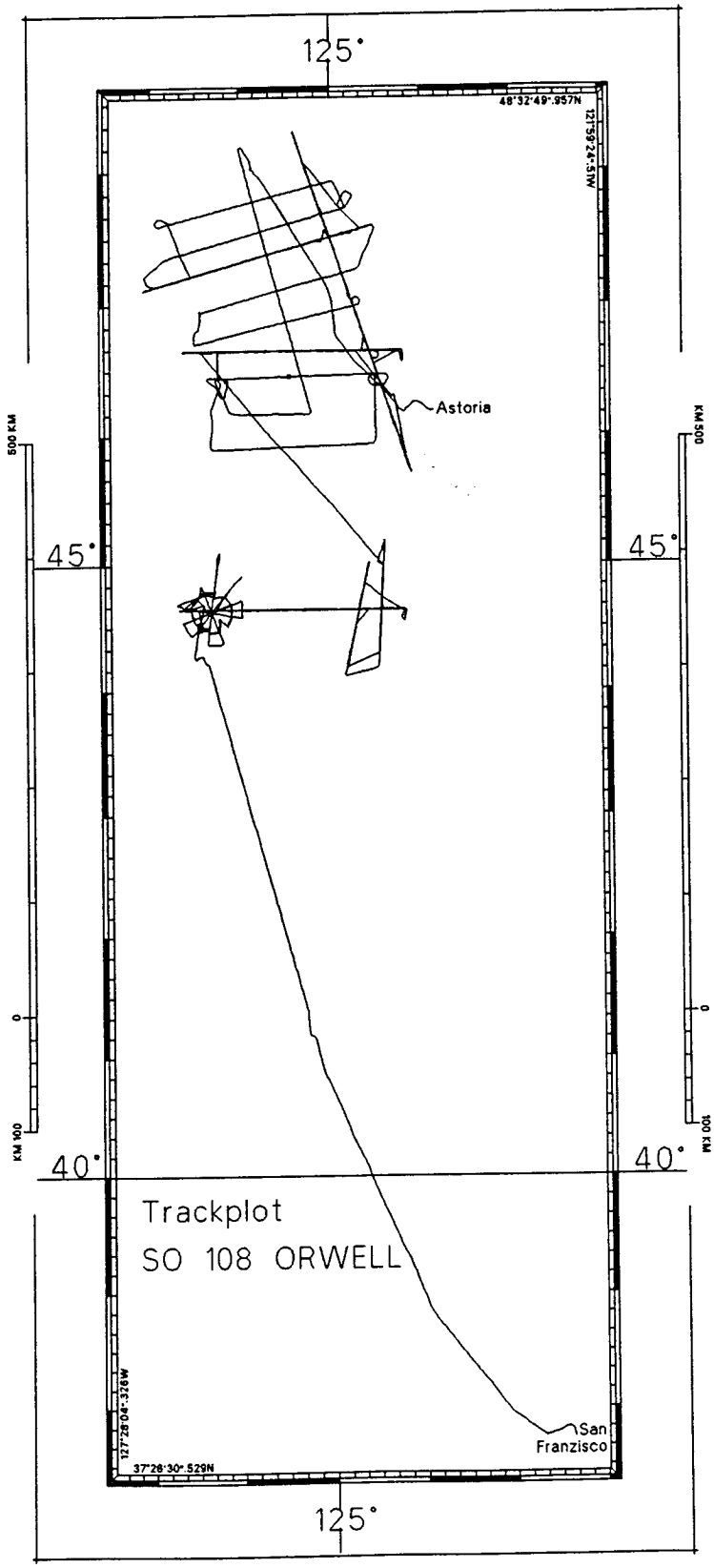

Figure 4.1: Trackchart of SO108

5. SCIENTIFIC EQUIPMENT
5.1 COMPUTER FACILTIES

(J. Bialas)

For data analysis and processing purposes GEOMAR installed the following hardware configuration:

a) Sun-IPC: 24 MB RAM, 4.5 GB disk, 17" color monitor
Methusalem SCSI (OBH playback)
HP-DAT drive, CD ROM
1/2" Storage Tek tape drive with long record driver

b) Sun-Lx: 32 MB RAM, 12.5 GB disk, 17" color monitor
Methusalem SCSI (OBH playback)
HP-DAT drive
OYO G612 thermal plotter

c) Sun-Sparc 10:
32 MB RAM, 12.5 GB disk, 17" color monitor
HP-DAT drive

d) HP 5900:
32 MB RAM, 4.5 GB disk, 19" color monitor
HP-DAT drive
CD-ROM

e) Macintosh PowerPC:
16 MB RAM, 500 MB disk, 17" color monitor

f) Macintosh IIfx:
8 MB RAM, 360 MB disk, 14" color monitor

g) HP LaserJet 4MP:
1 MB RAM, MIO (Ethernet, Local Talk)

h) 2 X-Terminals:
14" color monitor

In addition several portable labtops and PC were installed for word processing and dedicated tasks. The USGS group installed a Sun Sparc 2 workstation with 12 GB disk space, a DAT and Exabyte drive as well as a 1/2" tape drive.

The magnetik and clean laboratory were choosen for the set up of these units. All components were connected to the ship's thinwire ethernet. Setting up the YP services on the Sparc 10 computer all users could benefit from netwerk services like NFS, NIS and Automount. Easy access could be provided as only one network wide home account per user was established. Data access was simplified by remote mounting of data disks across the network. Besides the GEOMAR printer and plotter access could be provided to the ship's HP DesignJet. Using ftp and telnet the Sun workstation of the USGS and the ship's Vax computer could be contacted. Other than on previous cruises the ship's HP computers designated for Hydrosweep processing were not reachable. Unfortunately the WTD could not locate the problem.

The slow IPC workstation was dedicated to OBH-data playback and navigation file processing. The Sparc Lx system was used for the seismic processing of the OBH data. Using the software packages GEOSYS (GecoPrakla) and Seismic Unix (Colorado School of Mines) first processing steps and section display were done. The most powerful Sparc 10 workstation was used for reflection seismic processing using the GEOSYS software package. First raytracing models could be done using Rayinvr on the Sun workstations and MacRay on the Macintosh computers. During the cruise two 4 GB disk drives reported severly damaged blocks that could not be repaired and must be switched off. One of them could be replaced by a spare unit.

5.2 SEISMIC DATA AQUISITION
5.2.1 MULTICHANNEL RECORDING AND CONTROL SYSTEM

(J. Childs)

During the latter half of the program, vertical incidence reflection data were collected with the airgun source. Two hydrophones arrays were used: a 24-channel, 150-meter *mini-streamer* was deployed during the final three OBS/OBH deployments (lines 10-12); and a 48-channel, 2400-meter conventional streamer was deployed for the multichannel seismic (MCS) survey collected during the final ten days of the program. Both streamer arrays were recorded on a DFS-V recording instrument.

The mini-streamer, manufactured by Innovative Technologies, Inc (ITI), utilizes cylindrical *thin-film* hydrophones that are both highly sensitive and broadband (5 Hz to 5 kHz). Each channel consists of a single hydrophone, 6.25 m apart, resulting in an active length of 143.75 m. The near channel of the streamer was towed about 150 m astern - approximately 100 m aft of the far airgun. The mini-steamer was used only during the OBH/OBS deployments, during which a shot rate of 60 s and a speed of approximately 3.5 kn were maintained, resulting in a shot spacing of approximately 108 m. Coverage at the 3.125-meter base CDP interval was therefor only about 70% (100% coverage would require a shot interval one-half of the active length, or about 72 m.). However, even if simply summed into a single trace per shot, the resulting reflection profiles provide some detail of the geologic structure immediately beneath the OBH/OBS stations.

The MCS streamer is a conventional oil-filled (E-size) transformer-coupled, analog array build by Teledyne Corp. late in the 1980's. The array is programmable; for this project it was configured for 48 50-meter groups, with 40 Teledyne T-1 hydrophones per group. With the lead-in and initial strech sections, the near offset was 190 m and the far offset 2540 m from the middle of the source array (Figure 5.3.1.1). Streamer depth was monitored and maintained using a Digicourse 293A controller with 395/03 and 5010 depth control units, called *birds* attached to the streamer at 8 positions. A 12-meter target depth (+-1 m) was consistently maintained, except for the rear 600 m, which was always 6 to 8 m deeper .

Data from both streamer were recorded with a DFS-V multichannel seismic recorder and written in SEG-B (multiplexed) format to 1600 bpi nine-track tape at a 4 ms sample rate. Record length was 6-10 s for the mini-streamer, 16 s for the MCS data. Selected analog channels were reconstructed from true read-after-write off the magnetic tape and displayed on an SIE R10A oscillograph and a Raytheon LSR-1807 line scan recorder for quality control and monitoring. An optional SEG-B extended trace header contains shot count, gun fire times and GPS time at sequence start, derived from a dedicated GPS clock receiver. All times were recorded to 1 ms precision.

DFS-V tapes were read and demultiplexed off-line on a UNIX workstation running Advance Geophysical's ProMAX software. Data were written out in SEG-Y format to both Exabyte 8 mm and DAT 4 mm media.

The airgun array was synchronized with a Litton Industries LRS-100 16-gun controller. This unit individually delays the gun trigger signals to maintain better than 2 ms simultaneity. Individual gun fire times were recorded in the DFS-V extended head (see above). Gun firing was controlled by an USGS-designed master control unit. Firing sequence intervals were based strictly on time. For the OBH/OBS lines, a shot interval of 60 s was maintained (90 s for the portion of line 7 deeper than 200 m). The oscillator that controlled the shot rate lost about 180 ms per day (i.e. a shot instant synchronized to 00.000 s would drift to 00.180 s 24 hours later). For the MCS lines, the shot times were adjusted manually according to the ship speed over ground from 20 to 22 s as needed to maintain a shot interval of approximately 50 m.

5.2.2 THE USGS OCEAN BOTTOM SEISMOMETERS

(U. ten Brink, R. Busby, and D. Foster)

Nine US Geological Survey Ocean Bottom Seismometers (OBS) were used aboard the RV Sonne cruise SO108 offshore Oregon and Washington to record wide-angle seismic reflection and refraction information. Each OBS is housed in a 24-inch aluminum sphere (Figure 5.2.2.1) and contains data-acquisition system designed to record continuous data from a vertical geophone, 2 horizontal geophones, and a pressure compensated hydrophone. The OBS is designed to free-fall to the ocean bottom with an anchor plate attached and to stay at depths of up to 5000 meters for up to 10 days. An acoustic release is incorporated in the instrument to allow release from its anchor upon command from the surface, permitting the buoyant OBS sphere to ascend. Once on the surface, a light strobe and a radio beacon help locate the instrument.

The experiment included 5 deployments of 7-8 instruments each (see Tables 5.2.2.1 and 5.2.2.2 for details) or total of 36 deployments. Some of the instruments recorded more than one line (see Table 5.2.2.3) during the Rosette and the Oregon deployments, hence a total of 75 records were generated. All instruments recorded 4 channels on all the lines except for 6 instruments on the Oregon deployment, which were programmed to record only channels 1 and 4. Sadly, the first OBS deployed in this experiment has not been recovered, and this represents a real loss to the USGS OBS program. Another instrument did not record data on one deployment.

Data quality were good on at least one channel in each instrument in each deployment (see Table 5.2.2.4). Several sedimentary and crustal arrivals can be identified on all but 4 OBS records from shallow waters (<100 m). In general the data quality of the 24 records from shallow waters (< 150 m) was surprisingly good, owing probably to the calm seas during the recording period. The horizontal channels performed particularly well in shallow waters and generated records which were sometimes superior to the vertical geophone and the hydrophone records. They seemed to be less affected by the engine noise from fishing boats. In deep water, the horizontal channels recorded the pegleg multiples, but the first arrivals were worse than those on the vertical geophone and the hydrophone.

OPERATION

The instruments were brought into the seismic laboratory approximately 4 hours prior to deployment where the battery power was connected, all components of the system were tested, the data logger were programmed, and the spheres were sealed and vacuumed. Deployment was done through the starboard-side crane at mid-ship. A small stand was set on deck and the anchor was placed on top of it. The OBS was placed on top of the anchor and the two were bolted together. During later deployments, a floating ("swimming") line with an end-float was wrapped tightly around the base of the sphere, and the end of the floating line was tucked between the base of the sphere and the anchor. Once on location, the OBS and its anchor were lifted up by the crane and into the water where it was released using a slip knot and a pin.

Recovery was done using the same starboard-side crane which lifted the OBS on board. A tag line was attached to the OBS with a Happy Hooker or a lifting hook. In later deployments, the floating line was caught by throwing a rope with a hook, and dragging the floating line with the OBS closer to the side of the ship. The use of the floating line shortened considerably the time needed for the 3000-ton ship to maneuver alongside the OBS. The OBS was lifted to deck, was washed in fresh water, and carried back to the lab, where the post-deployment checks were done. The data logger was brought to the lower-deck lab, checked for time drift against the GPS clock, and attached to the computer. While the data, recorded on the data logger, were being downloaded, new batteries were installed into the OBS

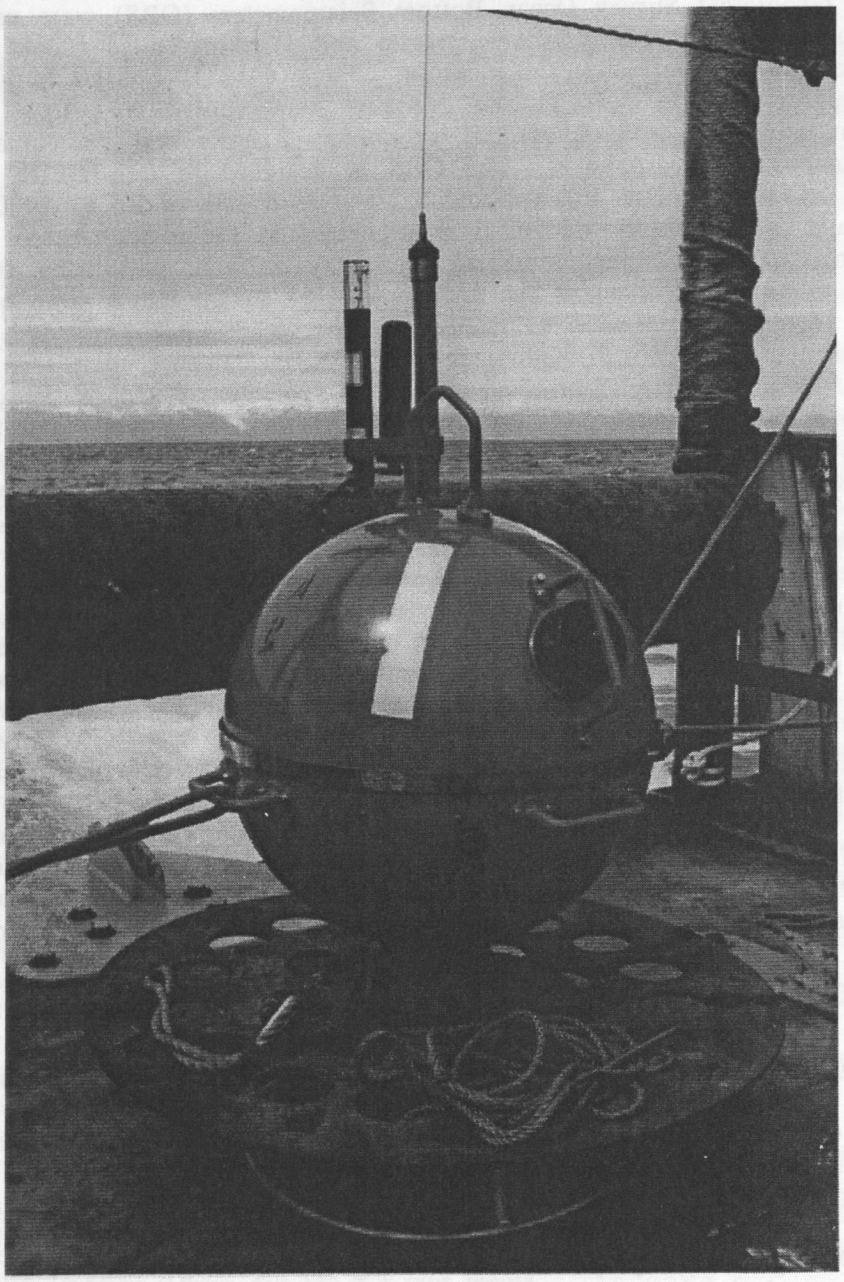

Figure 5.2.1.1: A USGS OBS on its anchor ready to be deployed offshore the Southern Alps of New Zealand (Photo by R. Busby).

in anticipation of redeployment at a later time. The sphere was then closed and tied down to the main deck. Once the data was recovered, the data logger was placed on a charging station to recharge the gelcell battery and to keep the oven-controlled oscillator at operating temperature. Some data loggers were programmed and immediately placed back into their sphere, because of the short time between recovery and the next deployment.

DATA REDUCTION AND PROCESSING

Step 1 - Data were down loaded from the data logger to a PC computer, one file per data logger. The raw data were written on one 8 mm Exabyte tape for each deployment, and a duplicate tape of the raw data was made.

Step 2 - Shot instance and navigation data, supplied by Geomar, were converted from UKOOA format to our format.

Step 3 - OBS location and depth from our log were entered to NAVD file, and *.src files with trace header information were created for each OBS for each seismic line.

Step 4 - *.src files were used in program OBSTOOLS to create SEGY files from the raw data. Specifically, the header file was edited to give the length of each trace, the project number and location, OBS name etc. The program uses shot instant from the *.src files to determine the start of each trace, and the difference between shot location and the OBS location to determine shot-receiver offset. SEGY files for each deployment were written as a SEGY binary tar tape.

Step 5 - The SEGY tapes were read into Promax processing software and processed. The processing sequence included:

1. tar tape into UNIX workstation hard disk.
2. Read SEGY disk input file.
3. Spiking deconvolution with an operator length of 80 ms.
4. Bandpass filter (Butterworth) - 4-7-18-32 Hz.
5. 2-D spatial filtering (not used in this cruise because of poor navigation).
6. Trace equalization (not used in this cruise).
7. Linear moveout correction (6 km/sec).
8. Automatic gain control with a window of 2000 msec.
9. Trace header math with the equation
   cdp = offset in meters + no. in meters; where no. > total length of line.
   Trace header math with Line no. and OBS no.
10. Plot data by cdp (effectively by offset).

Because a plotter was not connected to the SUN workstation with the Promax system during cruise SO108, data were written to a DAT tape in SEGY format, read by a different SUN workstation into Geomar's GEOSYS software and plotted by D. Klaeschen using this software.

Steps 1-4 were performed on a 386-PC. Step 5 was performed on a SUN Sparc-10 workstation on board.

NARRATIVE OF THE USGS OBS COMPONENT

Predeployment - In initial testing, an oscillator on one data logger failed, prohibiting one OBS from being deployed during each of the subsequent deployments. That OBS was used for spare parts during the experiment.

Deployment 1 - 8 OBS were deployed along 6 lines in a rosette shape. Only 5 lines were shot due to severe weather. The gun arrays were battered and we were forced to stop shooting twice. Guns operated at partial capacity for periods of time. One OBS (A2) could not be ranged and was never recovered and is either at the bottom or floating. 3 hours at night and 4 hours in daylight were spent looking for it. >40 release commands were sent from 4 azimuths and the ship searched in a ~4 x 4 n.m. area around the deployment location. It was the first OBS deployed in the experiment. Weather during shooting was stormy with winds of up to 50 knots and 8-12 ft. waves. Windy but calm seas during deployment and calm weather

during recovery.

Deployment 2 - Oregon lines - 6 OBS were deployed at intervals of 4 n.m. along the landward end of the E-W line (Line 7). Calm seas and light wind during deployment, shooting, and recovery. Guns fired at almost full capacity. Ship navigation froze during deployment as we approached shore and at the 3-mile limit we were 2.5 miles off, hence, we did not deploy the planned seventh instrument. Exact positions of instruments were found during recovery. 4 instruments were recovered, 2 instruments near the junction with Line 9 were left at the bottom after locating and ranging on them. The instrument, not deployed on the E-W line, was deployed at the crossing with Line 8. The remaining 3 OBS were recovered without incident after the shootings of Lines 8 and 9.

Deployment 3 - SW Washington line - 3 OBS were deployed in the lower continental slope and 4 instruments were deployed along the landward end of the line. The 3 instruments in the lower continental slope were recovered before we left the line to meet a supply boat. The remaining 4 OBS were recovered when the ship reached the area again after deploying some OBS and OBH along the N-S Washington line. All guns fired. Calm seas and light wind during deployment, shooting, and recovery.

Deployment 4 - From the meeting point with the supply boat off Astoria, we continued south to the southern end of the N-S line and deployed our 3 OBS already on board. The remaining OBS, picked from the SW Washington line during the deployment, were deployed at the northern end of the line. Deployment, shooting, and recovery was carried out amidst fishing boats and crab buoys. Two of the guns (a 580 and a 500 cu.in.) ceased shortly after beginning of shooting so we had only 5200 cu.in. of air for shooting. The northern end of the line was relocated slightly farther offshore at the shelf edge to avoid deploying in waters that are too shallow.

Deployment 5 - Olympic Line- Upon the recovery of the last OBS from Deployment 4, the ship sailed to the eastern end of the Olympic Line, and within 3 hours, the first OBS was deployed. 3 more OBS were deployed in shallow waters (67-171 m), and 3 OBS were deployed in a flat section of the continental slope. The line was shot at full gun capacity. Recovery of the OBS started from the eastern end of the line. The sea was very calm during deployment, shooting, and recovery.

TABLE 5.2.2.1. LOCATION, DEPTH, AND CLOCK DRIFT

Deployment 1 - Lines 1, 2, 4, 5, 6, 102, 506 - Rosette

#OBS	Latitude	Longitude	Depth	BTime	BShift	ETime	EShift	Drift	TT#
A2	44 30.036	126 28.655	2898	96:04:22:01:27	4.5				A4
A1	44 30.004	126 21.582	2889	96:04:22:01:56	6.0	96:04:26:06:48	0.9	-5.1	A1
C3	44 27.513	126 22.012	2901	96:04:22:01:47	2.2	96:04:26:07:55	-3.9	-6.1	C3
A3	44 28.187	126 14.666	2898	96:04:22:02:00	-0.3	96:04:26:09:10	-0.2	0.1	A3
C9	44 34.100	126 14.337	2871	96:04:22:01:32	-1.5	96:04:26:10:18	-5.8	-4.3	C9
C1	44 30.867	126 09.043	2895	96:04:22:01:54	3.1	96:04:26:12:23	1.5	-1.6	C1
C4	44 35.915	126 06.358	2892	96:04:22:01:59	3.9	96:04:26:13:42	2.3	-1.6	C4
A8	44 41.123	126 06.673	2871	96:04:22:01:41	8.7	96:04:26:14:28	20.8	12.1	A8

Deployment 2 - Lines 7, 8, and 9 - Oregon E-W, N-S coastal, N-S seaward

#OBS	Latitude	Longitude	Depth	BTime	BShift	ETime	EShift	Drift	TT#
A4	44 38.276	124 41.798	234	96:04:26:22:46	2.1	96:05:01:12:30	-2.1	-4.2	C4
C1	44 38.343	124 35.990	193	96:04:26:22:50	1.4	96:05:01:12:46	0.8	-0.6	C1
A3	44 38.353	124 30.195	127	96:04:26:23:02	-0.7	96:04:29:07:07	-1.1	-0.4	A3
A8	44 38.439	124 23.957	75	96:04:26:22:39	2.3	96:04:29:08:09	4.8	2.5	A8
A1	44 38.343	124 17.911	79	96:04:26:23:12	0.3	96:04:29:09:15	-2.4	-2.7	A1
C9	44 38.279	124 11.407	59	96:04:26:22:56	3.8	96:04:29:10:34	1.2	-2.6	C9
C4	44 38.302	124 27.129	100	96:04:29:00:21	2.7	96:05:01:19:59	-1.9	-4.7	C3

Deployment 3 - Line 10 - SW Washington

#OBS	Latitude	Longitude	Depth	BTime	BShift	ETime	EShift	Drift	TT#
A4	46 38.987	125 38.931	1989	96:05:02:02:28	5.4	96:05:04:11:18	5.8	0.4	C3
C1	46 38.987	125 31.588	2129	96:05:02:02:31	0.6	96:05:04:12:54	0.8	0.2	C1
C4	46 38.992	125 24.936	1913	96:05:02:02:34	-2.2	96:05:04:13:54	-1.3	0.9	C4
C9	46 38.981	124 29.004	108	96:05:02:02:40	1.3	96:05:05:08:28	0.9	-0.4	C9
A1	46 38.992	124 24.003	84	96:05:02:15:25	8.4	96:05:05:06:46	8.1	-0.3	A1
A8	46 38.984	124 18.995	68	96:05:02:15:30	8.1	96:05:05:07:24	14.1	6.0	A8
A3	46 38.996	124 14.028	48	96:05:02:15:36	-2.1	96:05:05:05:17	-2.7	-0.6	A3

Deployment 4 - Line 11 - Washington N-S

#OBS	Latitude	Longitude	Depth	BTime	BShift	ETime	EShift	Drift	TT#
A4	45 50.969	124 10.285	99	96:05:04:21:04	3.7	96:05:07:19:19	1.1	-2.6	C3
C1	45 56.586	124 13.036	105	96:05:04:21:08	0.8	96:05:07:20:08	1.1	0.3	C1
C4	46 03.282	124 16.698	105	96:05:04:21:14	-1.4	96:05:07:21:33	-0.9	-0.5	C4
C9	47 42.495	125 05.971	376	96:05:05:08:45	0.9	96:05:08:10:50	0.6	-0.3	C9
A8	47 49.939	125 09.787	353	96:05:05:07:52	0.5	96:05:08:12:03	14.4	13.9	A8
A1	47 56.335	125 13.045	176	96:05:05:07:01	8.2	96:05:08:13:08	7.6	-0.6	A1
A3	48 03.297	125 16.574	150	96:05:05:06:21	-2.7	96:05:08:14:06	-3.3	-0.6	A3

Deployment 5 - Line 12 - Olympic

#OBS	Latitude	Longitude	Depth	BTime	BShift	ETime	EShift	Drift	TT#
A1	47 34.343	124 39.949	67	96:05:08:13:25	7.6	96:05:10:16:07	7.1	-0.5	A1
A3	47 33.336	124 45.195	93	96:05:08:15:23	-3.3	96:05:10:16:15	(-3.0)	-0.3	A3
A8	47 32.463	124 49.746	121	96:05:08:12:33	4.5	96:05:10:16:58	1.7	-2.8	A8
C1	47 31.581	124 54.815	171	96:05:08:01:24	0.6	NO DATA			A2
C4	47 26.262	125 22.896	1492	96:05:07:21:52	-0.9	96:05:10:21:45	-0.5	0.4	C4
C9	47 25.271	125 28.287	1484	96:05:08:11:07	0.6	96:05:10:23:01	0.1	-0.5	C9
A4	47 24.247	125 33.942	1478	96:05:07:19:39	1.1	96:05:10:23:49	-1.8	-2.9	C3

GMT = Data logger_time + Shift ; A negative Shift means GPS clock pulse behind (is later than) Data logger Time in UTC (7 hours ahead of local time).

Drift = (EShift - BShift) in milliseconds.
Correction_Shift = BShift + [Drift * (Orig_Starttime - Btime)] in milliseconds.
Corrected_Trace_Starttime = Orig_Starttime + Correction_shift
The value of Correction_shift for each SEGY trace is (added to the value) stored in the trace header under Total_Static

TABLE 5.2.2.2. DEPLOYMENT, RECOVERY, AND RECORDING TIMES

(Recording ends upon recovery)

Deployment 1

Start of recording: 96:04:23:01:00

#OBS	deployment	on surface	on board
A2	4:22:06:20	----------	---------
A1	4:22:07:23	4:26:07:15	4:26:07:43
C3	4:22:07:38	4:26:05:18	4:26:05:32
A3	4:22:08:22	4:26:08:28	4:26:08:47
C9	4:22:09:19	4:26:09:30	4:26:09:56
C1	4:22:10:16	4:26:11:54	4:26:12:06
C4	4:22:11:06	4:26:13:04	4:26:13:19
A8	4:22:11:50	4:26:14:03	4:26:14:09

Deployment 2

96:04:27:13:00, 96:04:29:15:00 for C4

#OBS	deployment*	on surface	on board
A4	4:27:09:06	5:01:10:32	5:01:10:51
A1	4:27:11:35	4:30:08:30	4:30:08:45
C3			
A3	4:27:10:24	4:30:06:16	4:30:06:24
C9	4:27:12:25	4:30:09:39	4:30:10:20
C1	4:27:09:46	5:01:11:25	5:01:11:46
C4	4:29:06:49	5:01:17:32	5:01:17:43
A8	4:27:11:01	4:30:07:32	4:30:07:56

Deployment 3

Start of recording: 96:05:02:22:00 for A4, C1, C4
96:05:03:00:00 for A1, C9, A3, A8

#OBS	deployment	on surface	on board
A4	5:02:13:12	5:04:10:56	5:04:11:03
A1	5:02:19:00	5:05:06:23	5:05:06:32
A3	5:02:21:53	5:05:04:57	5:05:05:05
C9	5:02:18:31	5:05:07:08	5:05:07:20
C1	5:02:13:51	5:04:12:30	5:04:12:42
C4	5:02:14:29	5:04:13:28	5:04:13:40
A8	5:02:21:26	5:05:05:39	5:05:05:48

Deployment 4

96:05:05:19:00

#OBS	deployment	on surface	on board
A4	5:04:22:34	5:07:18:41	5:07:18:48
A1	5:05:18:38	5:08:12:40	5:08:12:48
A3	5:05:19:30	5:08:13:38	5:08:13:48
C9	5:05:16:56	5:08:10:25	5:08:10:38
C1	5:04:23:17	5:07:19:34	5:07:19:57
C4	5:05:00:04	5:07:20:45	5:07:20:58
A8	5:05:17:50	5:08:11:36	5:08:11:50

Deployment 5

Start of recording: 96:05:09:07:00

#OBS	deployment	on surface	on board
A4	5:08:22:44	5:10:23:25	5:10:23:33
A1	5:08:16:51	5:10:14:42	5:10:14:52
A3	5:08:19:20	5:10:15:23	5:10:15:35
C9	5:08:20:12	5:10:22:31	5:10:22:41
C1	5:08:18:17	5:10:17:09	5:10:17:16
C4	5:08:21:41	5:10:21:18	5:10:21:26
A8	5:08:19:45	5:10:16:34	5:10:16:42

Time in UTC (7 hours ahead of local time).

TABLE 5.2.2.3 SHOT LOG FOR OBS/OBH LINES

time (UTC)	Shot #	Gun Volume (cubic inch)	Comments	shot interval (seconds)	average speed (knots)
Line 1					
4:22:23:30	28	6348	start	45	~5
4:23:01:22	?	5798			
4:23:04:12	405	5218			
4:23:07:45	687	4638			
4:23:09:07	796	4638	end of line		
Line 102					
4:23:09:08	797	4638	start		
4:23:11:29	987	4638	end		
Line 2					
4:23:11:30	988	4638	start		
4:23:14:30	1260	4338			
4:23:16:24	1381	3788			
4:23:17:54	1500	3238	end		

Line 4

4:24:20:30	25	6348	start		
4:25:01:00	383	6348	end		

Line 5

4:25:03:54	616	6348	start		
4:25:04:10	638	5798			
4:25:09:15	?	4918			
4:25:09:53	1096	4918	end		

Line 6

4:25:11:26	1220	4918	start		
4:25:17:52	1733	4918	end		

Line 7

4:27:14:39	45	6348	start	60	~4
4:27:19:00	306	6348		90	
4:28:02:00	585	6154			
4:28:02:32	608	6154		60	
4:28:07:01	875	6154		90	
4:28:15:52	1230	6154	end	90	

Line 8

4:30:01:37	1	6348	start	60	~4
4:30:14:24	768	6348	end	60	

Line 809

4:30:14:56	800	6348	start	60	~4
4:30:15:33	837	5768			
4:30:17:09	933	5768	end		

Line 9

4:30:18:21	1005	5768	start	60	~4
4:30:18:40	1024	5218			
4:30:23:54	1337	0	guns off for whales		
5:01:00:06	1350	5218	guns back on		
5:01:22:06:44	1748	5218	end		

Line 10

5:03:00:00	1	6348	start	60	~3.7
5:03:20:26	1228	0	guns off to deploy ITI streamer		
5:03:20:41	1241	6348	guns back on		
5:04:04:05	1686	6348	end	60	

Line 11

5:05:22:15	1	5768	start	60	~3.5
5:06:05:37	443	5228			
5:07:16:10	2516	-540			
5:07:17:00	2566		end		

Line 12

5:09:07:38	1	6348	start	60	~3.5
5:09:07:57	6-20	various guns off for testing			
5:09:07:58	21	6348	real start		
5:09:20:09	752	6113			
5:10:13:26	1790	6113	end		

TABLE 5.2.2.4 SUMMARY OF DATA QUALITY

Channel Quality Indicator shown for each channel recorded in each deployment. The channels are shown in order; 1=vertical, 2=horizontal1, 3=horizontal2, and 4=hydrophone. Channel Quality Indicators; A=excellent, B=good, C=noisy, D=corrupted signal, F=failed, #=not checked, and – =channel not enabled.

OBS Sphere	Deploy1 Lines 1-6	Deploy2 Line 7	Line 8,9	Deploy3 Line 10	Deploy4 Line 11	Deploy5 Line 12
A1	BCBF+	C—F+		C##C+	BAAD+	BABD+
A2	1234					
A3	CBBC	B—B+		C##C+	CCCC+	CBAC+
A4		A—D+	B—C+	A##A+	BBBB+	ABBD+
A8	DBCB	CBBA+		D##A+	DBBB+	ABBA+
C1	BCBB	B—B	B—B	A##B+	DBBB+	FFFF+
C3	BBCF					
C4	BBCC		C##B	A##B+	BAAB+	BAAB+
C9	BBBB	C—B		B##B+	BCCB+	ABBB+

+=swimming line attached to sphere

TECHNICAL PROBLEMS AFFECTING OPERATIONS AND DATA QUALITY

Deployment 1
A2 not recovered. 3 hours at night and 4 hours in daylight spent looking for it. >40 release commands sent from 4 azimuths. No clear response from ranges or releases. It was the first OBS deployed in the experiment.
C4 strobe leaked, strobe damaged and replaced with fresh unit. This delayed sighting upon recovery.

Deployment 2
On recovery C4 geophone pack found to be knocked off gimbals, reassembled.
C9 vertical geophone wire broken in sensor pack, found and fixed after recovery. Channel known to be bad on deployment but no time to fix it. Data QC does not indicate a problem.
After recovery, A1 hydrophone found to be wired to RS-232 in upper sphere. Fixed.
A4 no signal from hydrophone at preamp board. Fixed, FM.
C3 could not be deployed during deployment 2-5 because of a bad oscillator.

Deployment 3
A8 vertical examined with scope for any noise problem. No problem found.
A1 low signal at data logger input for horizontal 1. No repair attempted.

Deployment 4
A8 vertical still bad. Swapping sensor pack with C3 during deployment 5 remedied the problem. Problem appears to be with geophone pack. Probably the vertical geophone has a damaged suspension and must be replaced.
A1 has weak hydro and low horz1.

Deployment 5
C1 with datalogger from A2 did not record anything. It was in acquisition mode but the time was way off and no tracks were recorded. Probably the clock was glitched installing datalogger into sphere.
A3 lost time reference at recovery or more likely during a frequency check. Estimate drift at +0.3 msecs on the basis of previous deployments.

SPECIFICATIONS OF THE USGS OBS

Bottom time - 10.5 days

Continuous recording time
with 200 Mbytes disk: 4 channels - 74 hours (3 days), 2 channels - 148 hours (6 days). Recording time increases proportionally with 500 (185 hours, 7.7 days for 4 channels) and 840 Mbytes (310 hours, 13 days for 4 channels)

Downloading and turnaround time for next deployment
40 min. to 1 hour When repair is not needed. Only one instrument can be downloaded and prepared at one time.

Dimensions	width	Height	Weight in air
Sphere and external sensors	0.69 m (27")	0.97 m (38")	92 kg (248 lb.)
at launch (with anchor)	1.02 m (40")	0.97 m (38")	119 kg (320 lb.)

Release
12.5 kHz Acoustic command with range capabilities.

Sensors
3 axis gimbaled 4.5 Hz geophones (Mark Product L-15B) hard mounted inside the sphere, 1 external hydrophone OAS E-2S.

Recording system
continuous digital recording at 100 samples/sec from a pre-programmed start time on up to 4 channels (3 geophones +1 hydrophone). Data logger - "Tattletale 6" with 1 Mbytes memory buffer and 200 Mbytes of hard disk in 7 instruments, 500 Mbytes in 1 instrument.

Dynamic range
72 dB (AD converter) + 30 dB step gain range for each data point.

Data handling
Binary with header information for each 1 Mbytes of data. Data is transferred from the hard disk to an Exabyte tape drive after each deployment via a 486 PC.

Clock
Oven crystal oscillator accurate to 10^{-8} (< 1 msec drift/day). Oscillators are interfaced with GPS clock for accurate calibration before and after deployment.

Power supply
72 Alkaline batteries providing +24 V, +12 V, and -12 V for 10 days deployment.

Shipping
~30 boxes, ~5000 lb. (2250 kg) plus palette of anchors at 72 lb. (32.5 kg)/anchor.

DATA FORMAT

Trace header format on SEGY files of all OBS files are as follows:
Byte position 1 = trace # (a number from 1 to the # traces in the file).
Byte position 5 = trace # as above.
Byte position 9 = channel # (1 = vertical geophone, 2 and 3 = horizontal geophones, and 4 = hydrophone).
Byte position 13 = shot # (from navigation data).
Byte position 29 = trace id code (1 for seismic data)
Byte position 31 = # of vertically stacked traces (1 for 1 trace)
Byte position 33 = # of horizontally stacked traces (1 for 1 trace)
Byte position 35 = data use (1 for production)

Byte position 37 = Shot-receiver offset (Offsets are negative for all shots occurring south/west of each OBS location and positive for all shots occurring north/east of each OBS location)
Byte position 41 = receiver elevation (negative value of the OBS depth)
Byte position 65 = water depth of receiver (OBS depth)
Byte position 73 = source longitude (in seconds)
Byte position 77 = source latitude (in seconds)
Byte position 81 = OBS longitude (in seconds)
Byte position 85 = OBS latitude (in seconds)
Byte position 89 = coordinate units (2 for seconds of arc)
Byte position 109 = delay recording time (0 in this case)
Byte position 115 = # samples in this trace
Byte position 117 = sample interval (in microsec, 10,000)
Byte position 119 = gain type (1 for fixed)
Byte position 125 = correlated (1 for not correlated)
Byte position 141 = alias filter frequency (in hertz)
Byte position 143 = alias filter slope (dB/octave)
Byte position 157 = year of shot
Byte position 159 = day of year (Julian)
Byte position 161 = hour of day
Byte position 163 = minute
Byte position 165 = second
Byte position 167 = time basis code (2 for GMT - GMT used for all time references)
Byte position 169 = trace weighting factor (data values are recorded with the least significant bit corresponding to 10's of microvolts for a weight factor of 14)
Byte position 181 = milliseconds of the shot time
User provided:
Byte position 221 = Line no. (4 Byte integer)
Byte position 225 = OBS no. (4 Byte integer), Examples: A8 = 18; C4 = 34.

5.2.3 THE GEOMAR OCEAN BOTTOM HYDROPHONE (OBH)

(E. Flueh, S. Husen, and C. Kopp)

THE INSTRUMENT

The first GEOMAR Ocean Bottom Hydrophone was built in 1991 and tested at sea in January 1992. A total of 14 instruments were available for SO108. This type of instrument has proved to have a high reliability; in fact during this cruise, the 500th successful deployment was made. Altogether 77 locations were occupied during the ORWELL cruise.

The principle design of the instrument is shown in Figure 5.2.3.1, and a photograph showing the instrument upon recovery is seen in Figure 5.2.3.2. The design is described in detail by Flueh et al. (1994).

The systems components are mounted on a steel pipe, which holds the buoyancy body on its top. The buoyancy is made of syntactic foam and is rated, as are all other components of the system, for a waterdepth of 6000 m. Attached to the buoyant body are a radio beacon, a flash light, a flag and a swimming line for retrieving from aboard the vessel. The hydrophone for the acoustic release is also mounted here. The release transponder is a model *RT661CE* made by *MORS Technology*. Communication with the instrument can be made through the ships transducer system, and even at maximum speed and ranges of 4 to 5 miles release and range commands are successful. For anchors, we used pieces of railway tracks that weighed about 40 kg each. The anchors are suspended 2 to 3 m below the instrument. The sensor is an *E-2PD* hydrophone from *OAS Inc.*, and the recording device is a *Methusalem* recorder of *DELTA t*, which is contained in its own pressure tube and mounted below the buoyant body opposite the release transponder (see Figure 5.2.3.1). The *Methusalem* consists of a preamplifier (26 dB), a highpass and antialias filter, a 13 bit A/D converter and a core memory of 0.768 MB. Signals are sampled at 800 Hz, and after FIR-decimation filtering, a resolution of 14 to 15 bits is achieved. Data are stored as 16 bit integers on a DAT-cassette, which is run in audio-mode to save power consumption and which can store about 1.1 GB of data. The power supply is from alkaline batteries for long term deployments or from rechargeble lead batteries for short term deployments (up to 3.5 days). The instrument can be programmed before deployment through an RS232 interface. Up to 4 channels with different amplifications and sampling rates can be recorded. A DTCXO (0.05 ppm accuracy) is checked against GPS time before and after deployment. The DAT-cassettes are read from a playback system, which simulates a SCSI-interface, to a workstation for data reduction and analysis (see Chapter 6.3.2).

DATA PROCESSING

The OBH data recorded on the *Methusalem* have to be converted into standard SEG-Y format for further processing. The necessary program structure was mainly taken from the existing REFTEK routines and modified for the OBH requirements and GEOMAR's hardware platforms. Because the GEOMAR OBH works in a continous mode, most of the modifications on the existing program package had to be done in the program parts handling continuous data streams.

A flow chart shown in Figure 5.2.3.3 illustrates the processing scheme applied to the raw data. A detailed description of the main programs follows below:

- **ref2segy**

Downloading the raw data from DAT tape on a harddisk of a SUN workstation is done by the program ref2segy. It will produce a pseudo SEG-Y trace consisting of one header and a continous data trace containing all samples. For each channel (different amplifications) one file will be created. The name of this file contains the start time, the serial number of the *Methusalem* and the channel number. In addition a log and an error file will produced protocolling the download process. The file size of the data is directly related to the recording time. For example a recording time of one hour sampled with 200 Hz will produce a file size of 1.44 MB

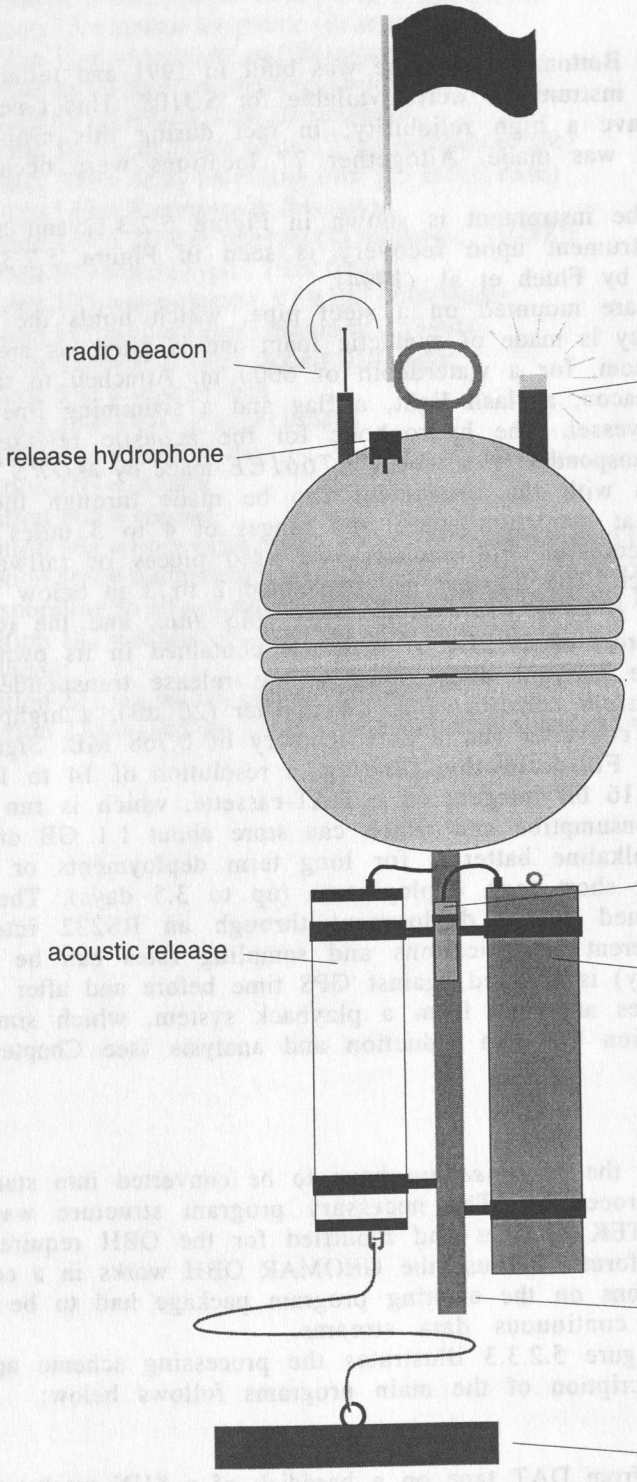

Figure 5.2.3.1: The design of the GEOMAR OBH.

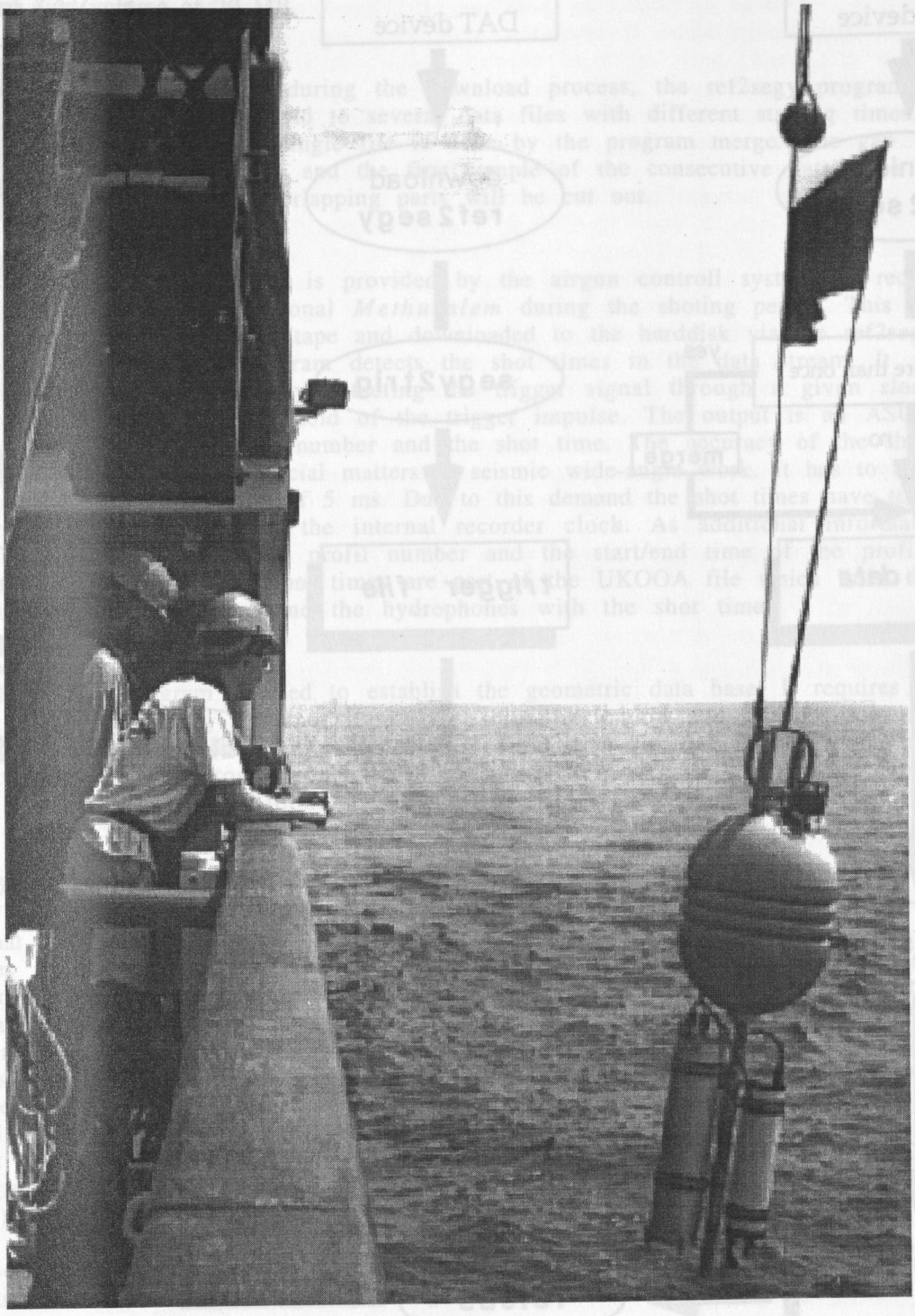

Figure 5.2.3.2: The GEOMAR OBH upon recovery.

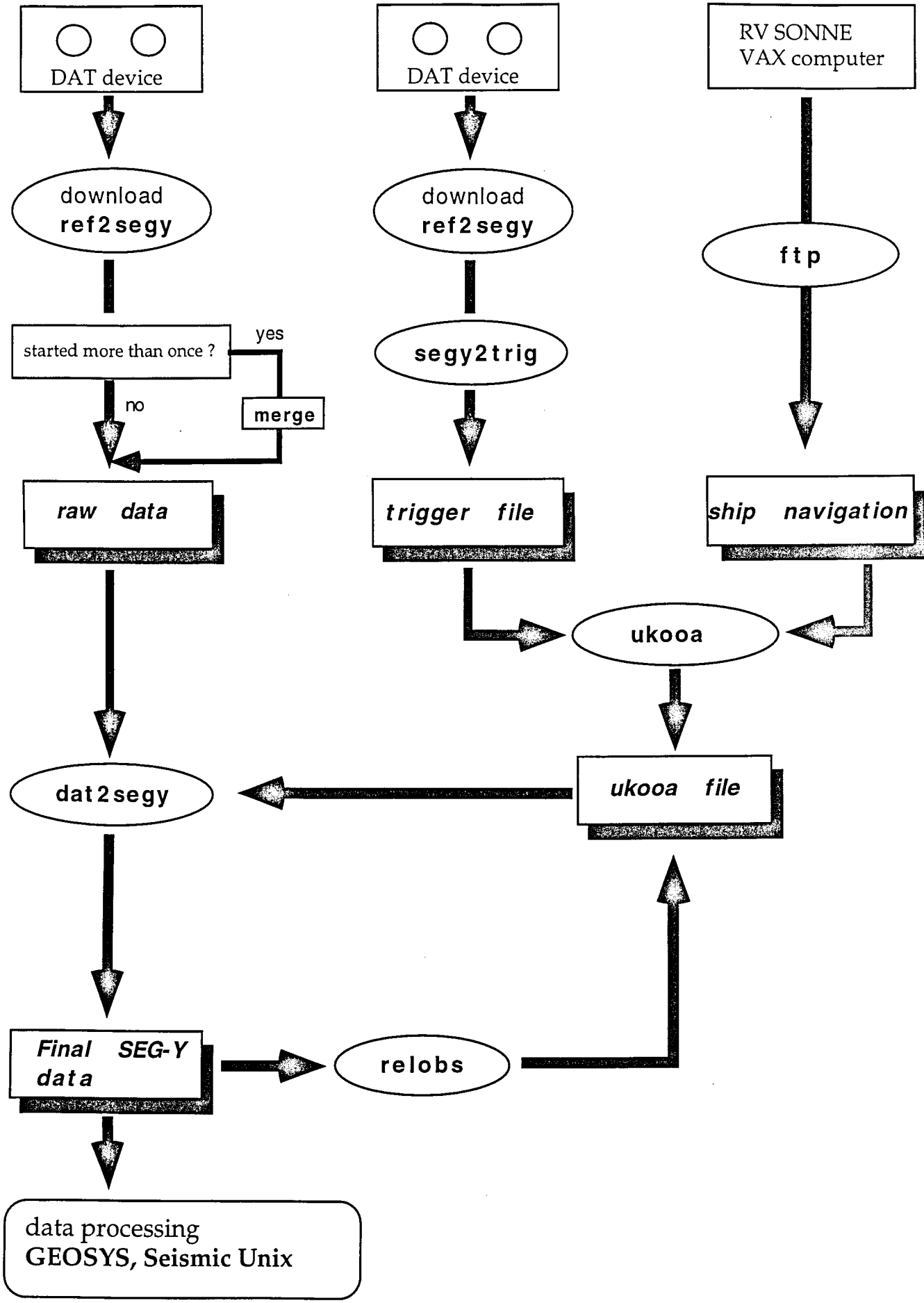

Figure 5.2.3.3: processing flow from raw data to SEG-Y records.

per channel. A record with two channels and a recording time of two days will get a total data volume of 70 MB.

- **merge**

If a tape error occured during the download process, the ref2segy program has to be restarted. This will lead to several data files with different starting times. Merging these files into a single file is done by the program merge. The gap between the last the sample and the first sample of the consecutive data trace will be filled up with zeros. Overlapping parts will be cut out.

- **segy2trig**

The trigger signal, which is provided by the airgun controll system, is recorded simultaneously on an additional *Methusalem* during the shoting period. This tape is treated as a regular data tape and downloaded to the harddisk via the ref2segy program. The segy2trig program detects the shot times in the data stream. It determines the shot times by detecting the trigger signal through a given sloop steepness, duration and threshold of the trigger impulse. The output is an ASCII table consisting of the shot number and the shot time. The accuracy of the shot time is one of the most crucial matters in seismic wide-angle work. It has to be reproduced with a precision of 5 ms. Due to this demand the shot times have to be corrected with the shift of the internal recorder clock. As additional information the trigger file contains the profil number and the start/end time of the profil and the trigger recording. The shot times are part of the UKOOA file which links the coordinates of the source and the hydrophones with the shot times.

- **ukooa**

The ukooa program is used to establish the geometric data base. It requires the trigger file containing the shot times, the ships navigation and the position of each OBH for input. The ship navigation is stored in a database about every 30s (see Chapter 5.4.3). The program calculates the coordinates of each shot and creates a file in the UKOOA-P84/1 format as output. This file will be used when creating a SEG-Y section via the dat2segy program.

- **dat2segy**

The dat2segy program produces standard SEG-Y records in a 16 bit integer format by cutting the single SEG-Y trace (from the merged ref2segy file) into traces with a certain time length. It reads both the ukooa file with the geometry informations and the downloaded raw data as produced with the ref2segy program. In addition the user can use several parameters for controlling the output. These parameters are informations about the profile and the receiver station, number of shots to be cutted out, trace length, time offset of the trace and reduction velocity (to determine the time of the first sample within a record (see Chapter 6.3.2)). The final SEG-Y format consists of the file header followed by the traces. Each trace is built up by a trace header followed by the data samples. The output of the dat2segy program can be used as input for further processing with GEOSYS or Seismic Unix (SU).

Beside these main programs for the regular processing sometimes additional features are needed for special handling of the raw data:

- **divide**

The program divide cuts the raw data stream in traces with a given length without offset and time informations. The output is stored as SEG-Y format. The routine is useful for a quick scan at the raw data or if a timing error has occured.

- **segyhdr**

The routine segyhdr prints all the header values of the raw data on the screen.

- **segyshift**

The program segyshift modifies the time of the first sample, which means that the whole raw data trace can shifted by a given value. This is very useful when

shifting the time base from Middle European Time to Greenwich Mean Time or any local time. Because of recording problems, the data sometimes shows a constant time shift, which can be corrected as well with segyshift.

- **castout**

The program castout allows you to cut out a specified time window of the raw data stream. When the shoting window is much smaller than the recording time, one can reduce the data volume by cutting out only the useful informations. This will reduce the demand on diskspace.

- **relobs**

Due to a drift of the OBH during deployment and errors of the ship's GPS-navigation system the OBH-positioning may have a mislocation of up to several 100 m. As this error leads to an asymmetry and wrong traveltime information in the record section it has to be corrected, which is done with the program relobs. As input the assumed OBH-location, shot-locations and the picked traveltimes of the direct wave near to its apex are needed. By shifting the OBH-position relobs minimizes the deviation between computed and real traveltimes using a least mean square fitting algorithm assuming a constant water velocity.

5.2.4 THE VERTICAL ARRAY

(J. Bialas)

Besides the hydrophone equipped OBH systems GEOMAR owns a vertical array. This array consists of 40 single Benthos AQ-1 type hydrophones which are grouped into 4 channels with one AQ-302 preamplifier each. The groups have an overall length of 25 m while each hydrophone is spaced 2 m apart. The overall system length is 110 m. The array has a total weight of 46 kg in air and 17.5 kg in water and is rated to a water depth of 6000 m. Ambient noise levels are expected to be smaller on a 10 hydrophone group compared to a single hydrophone. Vertical stacking of the four channels should also improve the signal to noise ratio and it could be expected to detect weak arrivals at larger offsets than from the single hydrophone. Stacking with differential delays should simulate a velocity filter. Tests show that during the seismic refraction work the main frequency of the USGS airgun array is in the range of 5-10 Hz (see Chapter 6.3.2). Therefore the length of the vertical array is close to half the wave length and suppression of multiples should benefit.

Prior to the first deployment the final check of the intrument failed. Supported by the WTD of RV SONNE a broken water proof connector could be replaced. During the following checks the internal DC/DC converter gave up. Again the WTD of RV SONNE could provide a spare solution and the array could finaly be deployed three times. Also the deployment of a 100 m long hydrophone cable with an floatation at the one end and a 40 kg heavy anchor at the other end is not as simple as with the standard OBH the routine and support of the ships crew enabled to savely complete the operation within 30 minutes.

As there were no previous experiences with the resolution of the AQ-1 hydrophones there was also one OAS hydrophone mounted on the floatation. Instead of channel 2 of the vertical array the single hydrophone was recorded to provide a comparative signal. Each channel of the array was recorded with a different amplification (1, 4 and 8) during the first deployment. It turned out that factor 2 should be the best while the single hydrophones are amplified by 8. All channels of the array were covered by a sinoidal ground noise of approx. 1 Hz (Figure 5.2.4.1.A). The clear sine waveform of the noise implies that it is generated by the slowly swinging array cable which might be induced by currents. The large amplitudes of this frequency cover almost the whole dynamic range of the instrument hence the moduled seismic events start to be clipped during recording also their absolut energy is within the sensitivity. The turn around time for the second deployment was too short to change the highpass filter of the analogue data input. Nevertheless reducing the amplification to 1, 2 and 2 for the three array

channels improved the data quality. Prior to the third deployment the resistors of the analogue input could be changed to increase the highpass cut off frequency. Testing with a sine wave generator the highpass cut off could be determined with 0.65 Hz while it has been 0.1 Hz before. Further increases need changes to the capacity in order to keep a high resistance at the input. Frequency spectra from the new highpass filtered array (Figure 5.2.4.1.B) show that the cut off frequency was high enough. Now the frequency of the airgun signals dominates the whole section which represents offsets from -10 km to 10 km. Therefore events can be detected with good data quality up to a distance of 60 km (Figure 5.2.4.2.A). Compared to the single hydrophone (Figure 5.2.4.2.A) very strong reverberation of the signals were observed on the array channels (Figure 5.2.4.2.B). Even a single spike causes a trail of 11 periods before the amplitudes decrease to the general noise level. This indicates that the preamplifiers need some special attention in order to increase the attenuation of the circuit. Evaluation of this problem includes the question if the attenuation can be done at the interface of the recording unit or if the preamplifiers included in the array need to be replaced. According to the stacked signal of four hydrophones per channel the amplitudes of the array seem to be much stronger than those from the single hydrophone (Figure 5.2.4.2.A & B). In addition one has to recognize that due to the chingling of the array signal the resolution decreases shingling remarkably.

Prior to stacking the array data some processing need to be applied in order to equalize the shape of the signals on the array channels otherwise stacking might result in a destructive process rather than constructive. Deconvolution tests show that a spike deconvolution with an operator length of 450 ms achieves the best suppression of the shingling (Figure 5.2.4.3). After deconvolution the data from channel three and four were shifted acording to their offset (50 and 75 m) using water velocity of 1.5 km/s prior to stacking channels one, two and three. The stacked section (Figure 5.2.4.2.C) shows clear arrivals up to a distance of more than 60 km. Due to the deconvolution the wave form of the event has been reduced to two periods instead of the four and more recognized on the single hydrophone and the single array channels. While on the single hydrophone the events are dying out at about 55 to 60 km the stacked arrivals are still displayed with a prominent amplitude. Even in the range from 65 to 75 km now some weak arrivals were observed. Neither the single hydrophone nor the single channel display can give a hint of these events. Just stacking of only three out of four channels improve the section by another 10-20 km offset. Stacking all four channels should at least improve the signal to noise ratio of the additional now weak arrivals. Hopefully the offset could again be enlarged by another 5-10 km.

This first data prove that the array is an availuable tool to improve the quality of marine wide-angle recordings. Although its use may not become the standard especially in areas with a poor signal-to-noise ratio or where larger offsets are required, it shall be used. Further test to use it for multiple surpression and as a velocity filter will have to be made.

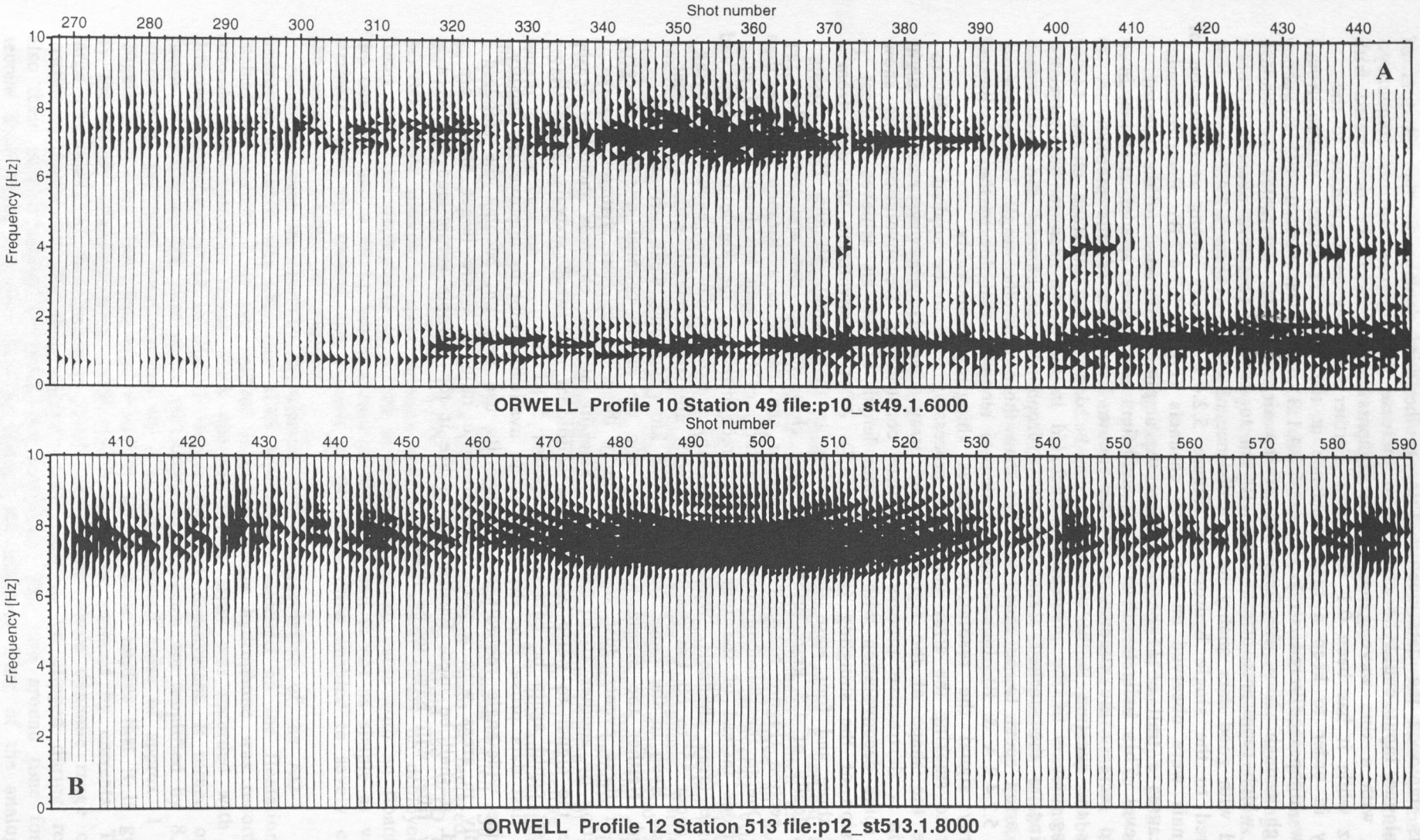

Figure 5.2.4.1: Frequency spectra of the vertical array; channel 1:
(A) original highpass cutoff at 0.1 Hz; 1 Hz noise due to motion of the cable;
(B) improved highpass cutoff at 0.65 Hz.

(B) improved highpass cutoff at 0.05 Hz.

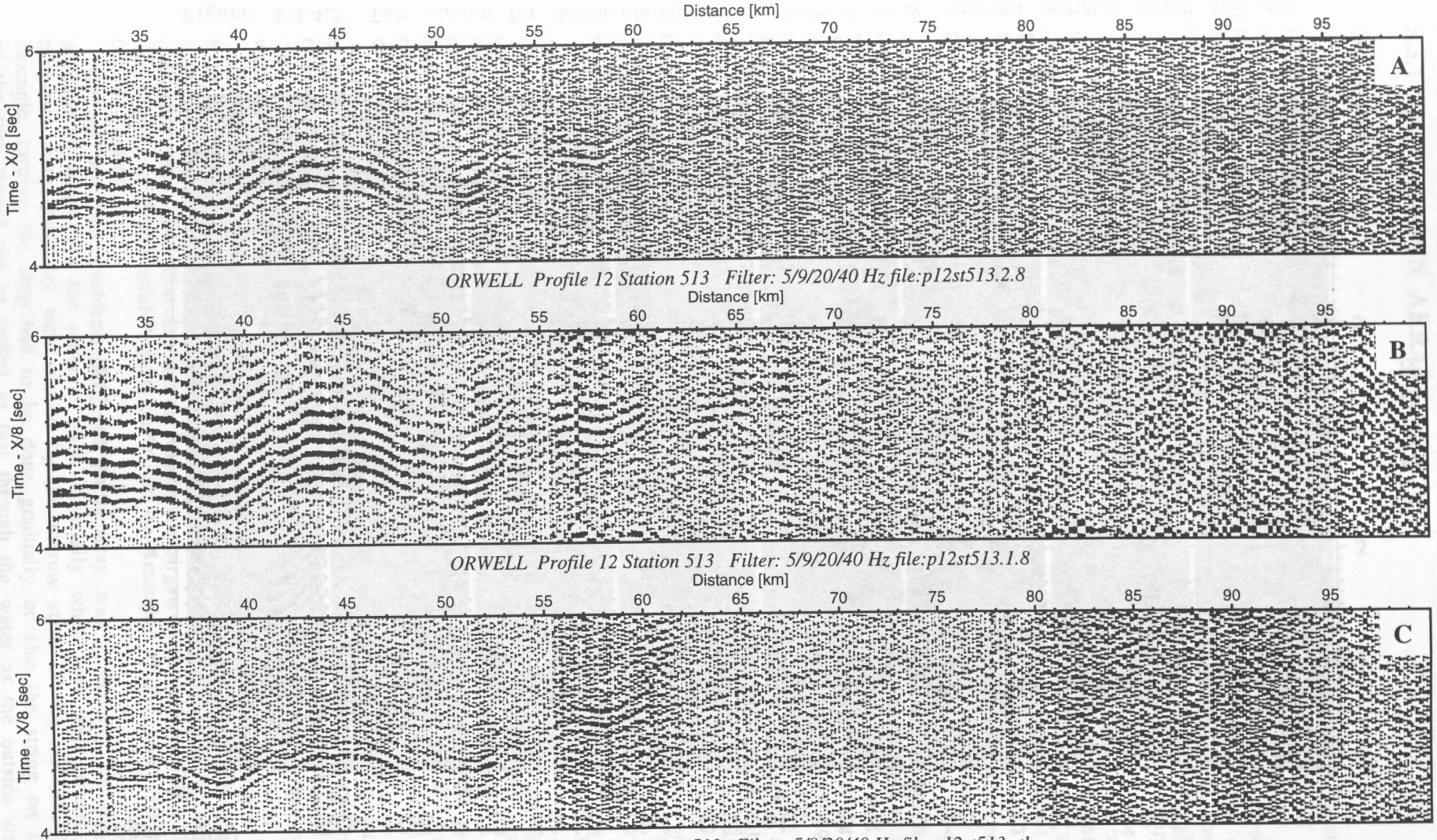

Figure 5.2.4.2: Cutout of the seismogram section from OBH513:
(A) single OAS type hydrophone;
(B) channel 1 of the vertical array; 10 AQ-1 type hydrophones;
(C) stack of channels 1, 3 & 4; spike deconvolution prior to stack.

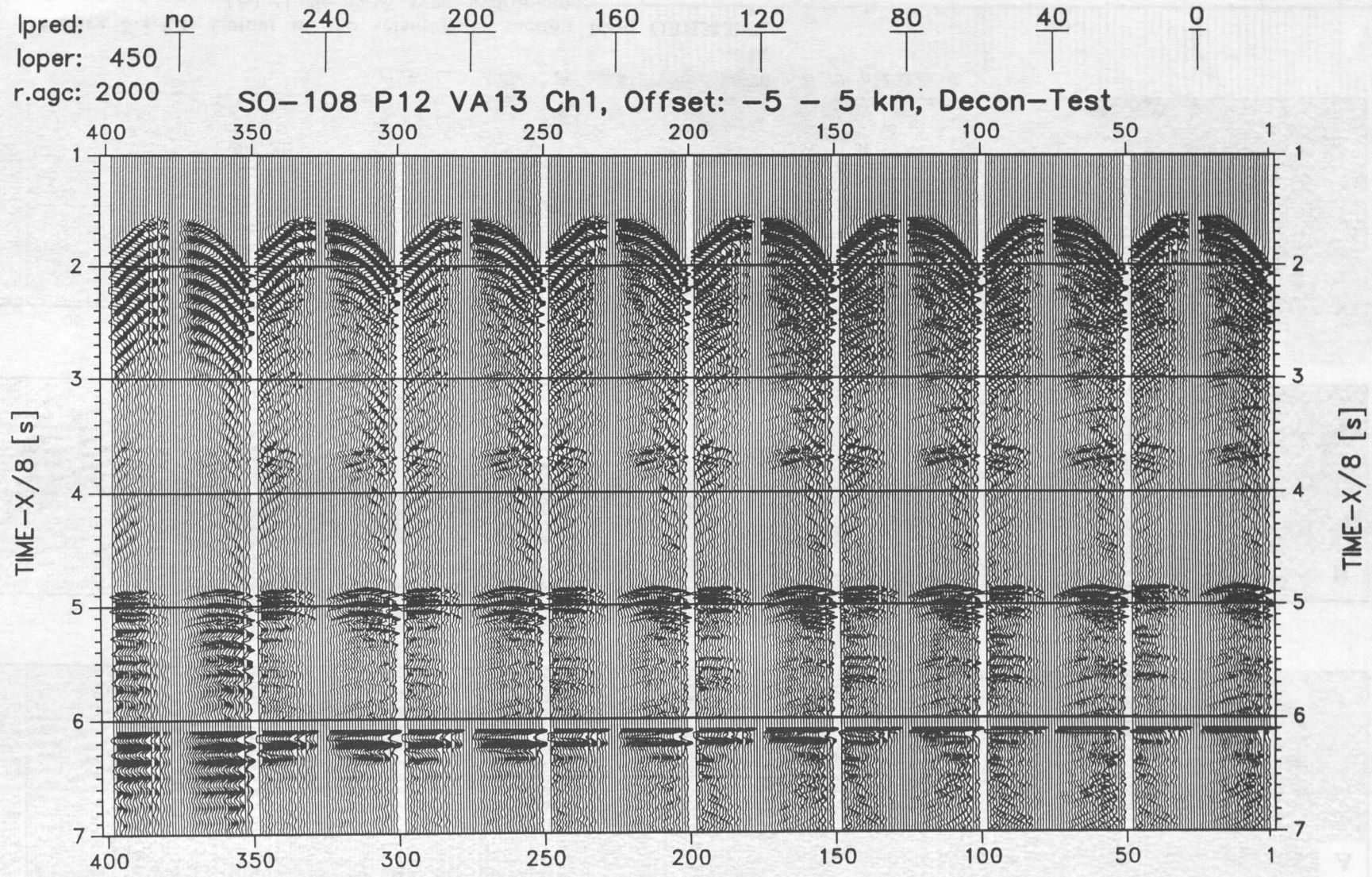

Figure 5.2.4.3: Test section for deconvolution of the vertical array; constant operator length 450 ms; varying prediction lag from 240 to 0 ms; autocorrelation function displayed from 6-7 s; original section displayed at left hand.

5.3 SEISMIC SOURCES
5.3.1 THE AIRGUN ARRAY

(M. Fisher)

We used two different airgun arrays aboard the SONNE during cruise SO108. The larger array was used during the wide-angle shooting and had a volume of 6350 in3 (104 l). The smaller array had a volume of 5352 in3 (88 l) and operated while multichannel seismic data were collected. Figure 5.3.1.1 shows the gun layout in each of these strings. The airgun arrays were arranged linearly, consisted of two strings, each with eight airguns, and the guns were spaced about 8 feet apart. The gun nearest the ship was 40 m back. Foam floats kept the guns at a depth of about 10 m. The main advantage of the linear array proved to be the ease of merging with the deck gear already aboard the SONNE.

Calculations of array characteristics are available only for the 104 l array. Software used in these calculations was supplied by John Diebold at Lamont Doherty Earth Observatory. The vertically directed, sound pressure of the array is 107 bar-m (261 dB re 1 µPa-m), and the peak-to-bubble ratio is about 4 to 1 (Figure 5.3.1.2). However, near-field measurements made from the ship using an uncalibrated hydrophone suggest that this ratio is closer to 2. No calculations were done for the array chosen for the multichannel seismic data acquisition.

During the collection of wide-angle data the airguns were fired at 45 to 90 second intervals, but after experimenting, we settled on a 60 second rate. At this low shot rate it was possible to use one of the SONNE's two compressors, each of which is rated to deliver 780 scfm. For the MCS data, however, shots should occur at 18 to 20 second intervals, which means that the SONNE's compressor had to be supplemented. For this reason, the USGS installed a 285 kW, diesel generator and two compressors on the back deck; each compressor is rated to supply 305 scfm. The combined ship and USGS compressors were rated to supply 1390 scfm, and according to estimates supplied by Price Compressors, Inc., this volume should have been sufficient to support the firing rated required for MCS data collection. However the combined air supply proved insufficient to charge the array in less than about 25 s. Part of the shortfall derives from the ship's continued venting of high-pressure air for about 15 seconds after each shot to ease the load on the compressor. The duration of this venting can be controlled and the ship's engineering department agreed to minimized it during MCS operations.

The air deficit required a choice among three possibilities: 1) lowering the fold of coverage by shooting less often; 2) shortening the length of trackline along which data could be collected by reducing the survey speed; or 3) lowering the airgun power by installing smaller chambers in the strings. We decided that it was not wise to lower the fold of coverage because were some of the airguns to fail, then we would achieve little or no enhancement in signal-to-noise ratio -- The signal to noise ratio in seismic data has a square-root dependence on the fold of coverage, and the sound pressure level of an airgun falls off as the square root of distance.

The strings fabricated by the USGS were patterned after the configuration used by BGR. Welded steel hooks suspend the airguns from rails carried by the ship. The rail are about 2 m above the deck, provide attachment points for floats and tow chains, and constrain the air hoses and trigger lines. The airgun arrays worked well to answer the needs of this survey.

During launch and retrieval, the system proved to be labor intensive, requiring 8 to 12 people, depending on the sea state. Launching would be greatly simplified if a winch, like the one used during retrieval, were available to pull the string overboard. We found that the rail in which the airgun hooks slide ends too close to the ship's stern; the entire operation would be smoother if the rails extended about 0.3 m farther.

One of the main problems with our linear array was a tendency for the hose package to loop over the retrieval wire, especially when seas were abeam. Other problems array problems were caused by the narrow stern of the SONNE. For example, turning the ship had to be done gradually or else the string on the inside of the turn would not be pulled as fast through the water as the outside string; we

speculate that as a consequence the inside guns were able to jerk erratically under the lowered tension. We considered turning off all guns during a turn; this might have reduced the suspected tendency for the impulse of released air to initiate erratic gun motion. A strange asymmetry in damage to the gun strings became evident: The starboard string consistently had more problems with broken hoses and hooks than did the port string.

5.3.2 MARINE MAMMALS VERSUS THE SOUND PRESSURE LEVEL OF AIRGUNS

(M. Fisher)

The size of our airgun array proved to be of concern to biologists who specialized in marine mammals. Deep-crustal research is evolving toward the use of large airgun arrays, and this direction is on a collision course with the increasing demands from biologists and ecologists that the sound level in the ocean be reduced. In particular, the biologists worried that our shots would injure or harass whales. In US law, harassment is defined sensu lato as any action that makes a mammal, particularly a whale, do something it otherwise would not do.

In 1972 the US Congress passed the Marine Mammal Protection Act (MMPA) and then strengthened it in 1994. This act invests the National Marine Fisheries Service (NMFS) with the primary responsibility for curtailing the harassment or killing of marine mammals, including whales, dolphins, porpoises, seals, and otters. Consequently there is immensely increased concern by fisheries regulators about the effects of airguns on marine mammals. Airgun use involves what is called Level B harassment. Level A harassment results in injury or death. Level B harassment is defined as "...any pursuit, torment, or annoyance which has the *potential* (our emphasis) to disturb a marine mammal or mammal stock in the wild by causing disruption of behavioral patterns, including but not limited to migration, breathing, nursing, breeding, or sheltering." The word *potential* in this definition allows virtually unconstrained latitude in how the probable effects of airguns are judged. According to NMFS, for some Level B harassment, such as aerial population surveys, permission can be obtained simply by sending NMFS a certified letter 30 days before the activity. Since late 1995, however, airgun use requires a more stringent permit process that takes 120 days to complete and involves a lengthy period for public comment. The request for a permit for this cruise arrived too late at the US Department of State for NMFS to issue a formal permit, so they wrote a letter containing recommendations (Enclosure 5.3.2.1), which if followed, would greatly reduce the risk of harassing whales.

All large whales are on the list of endangered species, so they are also protected by the Endangered Species Act, which is administered through the Environmental Protection Agency. The Fish and Wildlife Service, another agency of the US government, has unclear jurisdiction in these matters. However to obtain a permit for the SONNE only required contacting NMFS. This permit is in addition to the one required of all foreign vessels by the US Department of State.

During this cruise, gray and humpback whales were migrating from Mexico to Alaska, across the inshore part of the survey area. Gray whales migrate close to shore, with 96% following paths that concentrate within 2 km of the shoreline. We were unlikely to encounter this type of whale. Humpback and other whales, however, migrate farther offshore.

The airgun permit process has produced onerous requirements for some operators. For example, late in 1995 Exxon, Inc. collected seismic lines inside the 3-nm limit off southern California. These lines were astride the whale migration paths. Exxon was required to put an array of sensors on the seafloor to chart, in real time, the location of whales within the survey area. This effort failed to achieve its goals. Overflights were required before, during and after the survey to assess the long- and short-term effect of airguns on whale-migration patterns. Trained whale observers, approved by NMFS, were put aboard the seismic boat and had the authority to shut off the airguns whenever a mammal entered a stipulated protective zone. A prohibition against shooting at night was eventually waived

because Exxon proposed to use night-vision scopes as well as the array of seabottom sensors to detect and avoid whales.

At the beginning of SONNE's negotiations for a permit, NMFS proposed that the Exxon requirements also apply, but NMFS determined that there was insufficient time to issue a permit and instead issued recommendations about how to avoid whales altogether.

Steps taken to mitigate the effect of airguns on whales included lookouts on the bridge of the ship who watched for mammals. Members of the science crew aided the ship's bridge crew to keep vigil. Shooting was stopped once because of the proximity of whales to the airguns. We also ramped the array, i.e. turned on the guns one by one over about one half hour. This ramping seems to have given whales plenty of time to avoid the ship. Typically, we fired the smallest gun for at least 10 minutes before slowly turning on the rest of the array.

Airguns were designed to replace explosives in marine geophysics because 40 years ago, explosives were widely used as the seismic source, and they had a devastating impact on marine life. Airguns produce a sound wave having a slow rise in pressure, and relative to explosives, airguns have low power in the high frequency part of the spectrum. These attributes limit the airgun's potential for damage to sealife. Repeated experiments on fish, fry, and roe have shown that unless an animal is right next to the airgun, there are no ill effects.

The question of how an airgun affects marine mammals is more controversial because of the broad-spectrum sensitivity of their hearing. Experiments have shown that when the sound pressure level from an airgun decays to 164 dB re 1 μPa-m, 90% of whales are unaffected; conversely, at a level of 180 dB re 1 μPa-m, 90% of whales avoid the airgun (Richardson et al., 1995, p. 287).

For the SONNE's array, the level of vertically propagating sound is 107 bar-m or 261 dB re 1 μPa-m. But this sound level will not affect whales unless they are swimming directly under the array. The sound that has greatest effect on whales propagates horizontally. As an approximation, the horizontally propagated sound level of an airgun array is about the same as the level of the array's largest gun. In the case of the 104 l array, the largest airgun had a 580 in3 chamber, and the measured sound level of this gun is 238 dB re 1 μPa-m.

To gauge the effect of airgun sound on whales, a model of sound decay versus distance from the array must be assumed. The literature is full of such models; the two models NMFS and we used are: 1) the decay results from simple spherical spreading, and 2) the decay follows an empirical model developed for an array of airguns. Spherical spreading results in a decay of -20log10(R) in dB re 1 μPa-m, where R is range in meters. The empirical model, -25log10(R) (units as above), describes a faster rate of sound decay than the spherical-spreading model because the airguns are arranged in a spatial pattern that directs sound downward and suppresses horizontal sound.

The NMFS biologists recommended that airguns be turned off when a whale enters a circle within which the sound level exceeds 160 dB re 1 μPa-m. At this level, fewer than 10% of whales should be disturbed. The protective radius calculated using the spherical spreading model is about 8 km (4.3 nm), and that estimated from the empirical model is about 1.3 km (0.71 nm). This radius accords with stipulations developed for earlier projects. For example, during the Exxon survey the array totaled 3959 in3 (65 l) and the protective radius was 0.45 km. For the ACCRETE project aboard the R/V Ewing, a seismic boat operated by the National Science Foundation, the array was 8585 in3 (141 l), and shooting was allowed when whales were within about 2 km of the ship. Both ships had whale biologists onboard, who reported no evident harassment of whales that were within 2-4 km of the arrays. SONNE's array is intermediate in size between the Exxon and Ewing arrays, and appropriately, the protective radius for SONNE that was calculated using the empirical model, is intermediate in size.

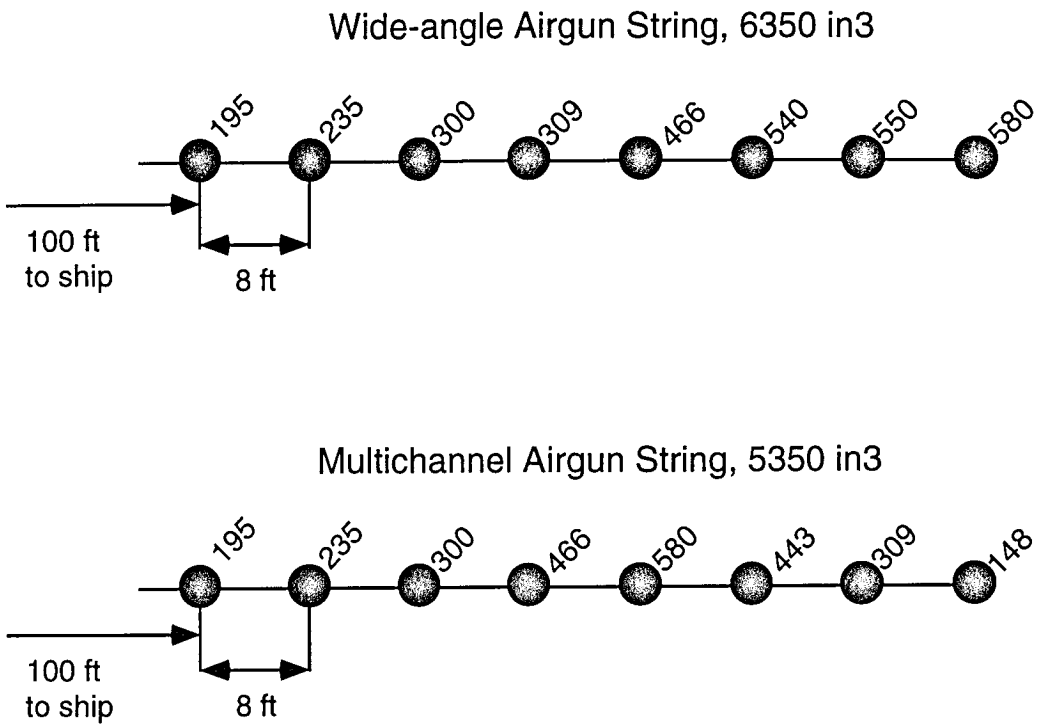

Figure 5.3.1.1: Gun arrangement within the wide-angle and MCS gun strings.

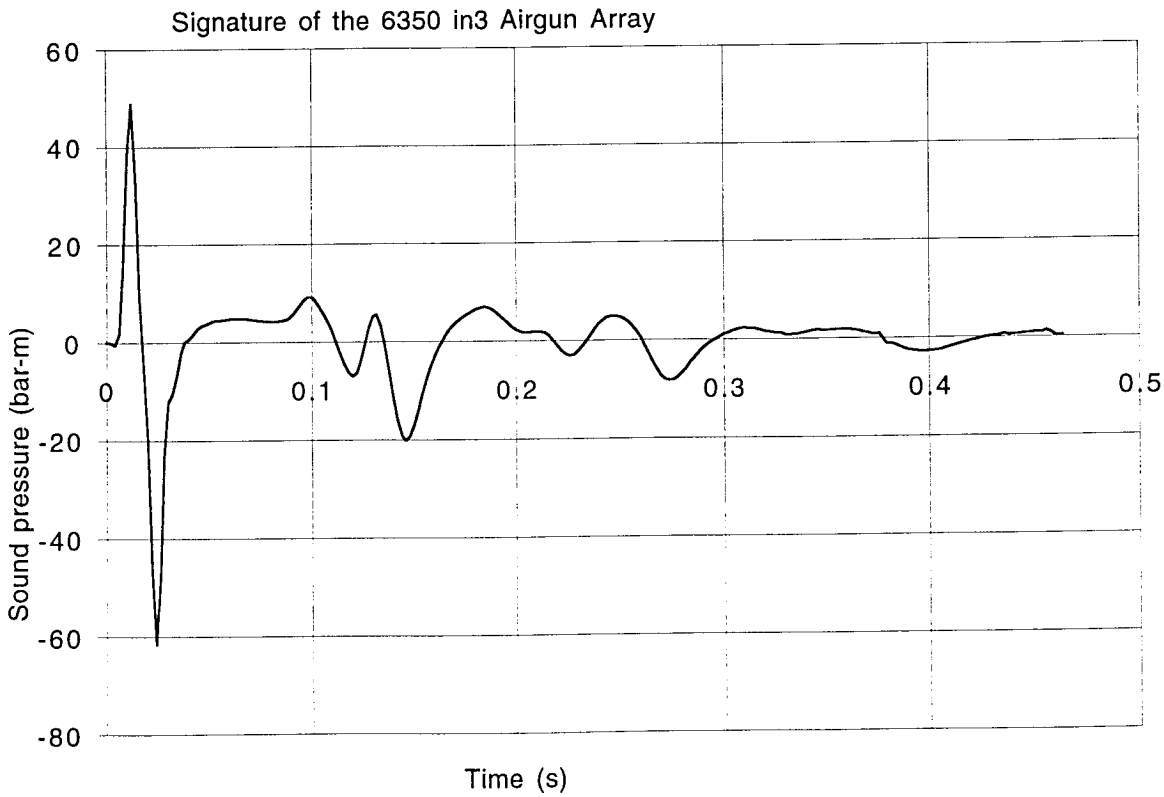

Figure 5.3.1.2: Calculated signature of the wide-angle, 6350 in3 (104 l) airgun array.

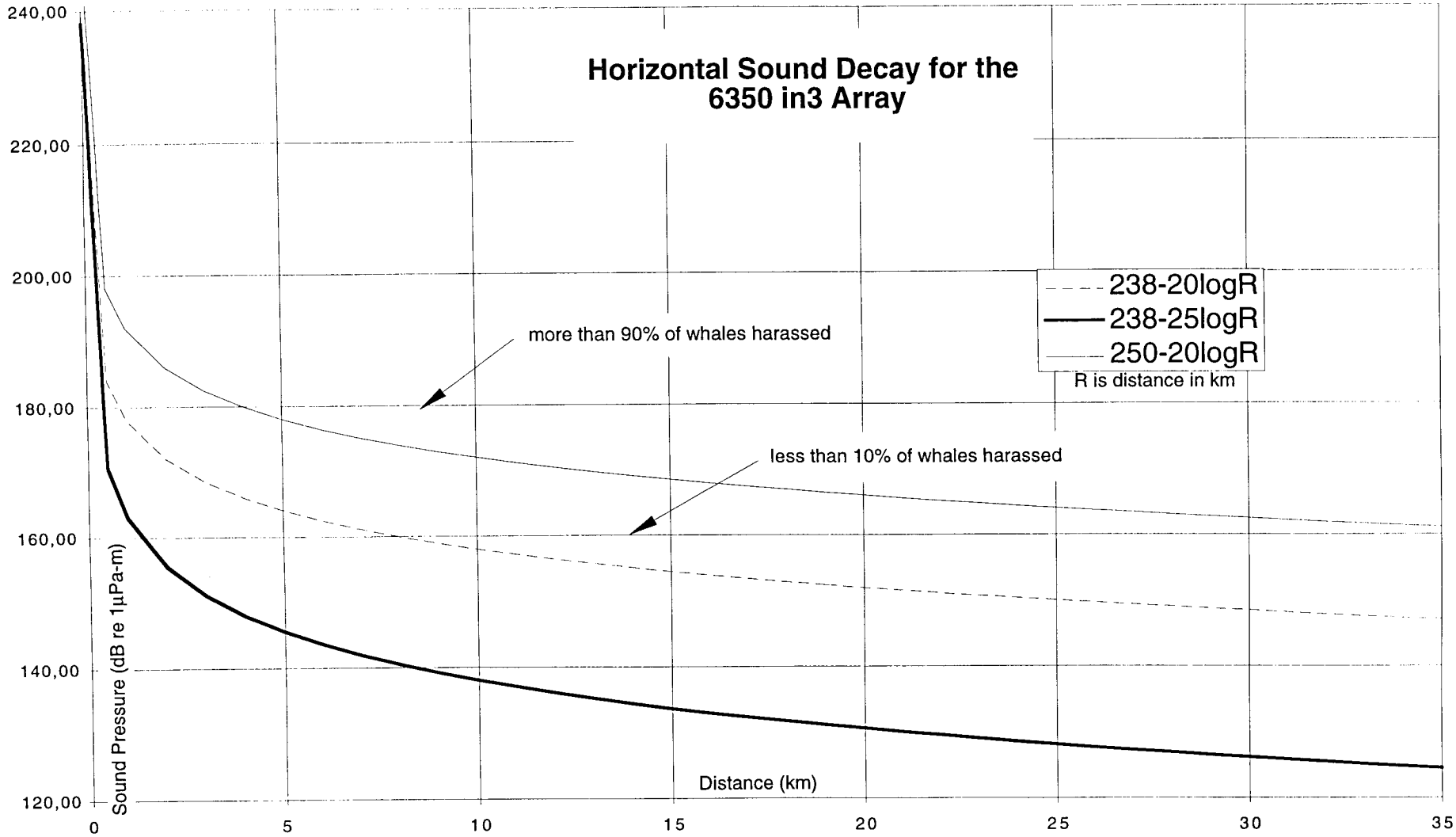

Figure 5.3.2.1: Decay of sound pressure from SONNE's airgun array versus

UNITED STATES DEPARTMENT OF COMMERCE
National Oceanic and Atmospheric Administration
NATIONAL MARINE FISHERIES SERVICE
Silver Spring, Maryland 20910

APR 5 1996

Dr. Michael A. Fisher
U.S. Geological Survey
Marine and Coastal Surveys
345 Middlefield Road, MS 999
Menlo Park, CA 94025

Dear Dr. Fisher:

This is in response to your recent letters informing the National Marine Fisheries Service (NMFS) of your seismic mapping project in the northeast Pacific Ocean off Washington State. In the past, seismic work has been demonstrated to result in the incidental harassment of marine mammals and under the Marine Mammal Protection Act (MMPA), the taking of marine mammals, including harassment, is prohibited unless the activity is exempted by law or permitted under the MMPA.

In that the U.S. Geological Survey (USGS) has not applied for an incidental take authorization under section 101(a)(5) of the MMPA, and, because there is insufficient time for USGS to obtain an authorization under statutory requirements prior to startup of the experiment, we are unable to authorize any takings. As a result, USGS will need to take precautions to avoid taking, including harassing, those marine mammals inhabiting the coastal and offshore waters of the State of Washington.

The purpose of the USGS/GEOMAR research is to conduct a geophysical investigation of the Cascadia continental margin in the Juan de Fuca plate to derive a better understanding of the crustal structure, the earthquake and tsunami generation, the tectonic and thermal history of the subduction zone and its variability through time and space. The research will be conducted from the R/V SONNE, a FRG ship, under the direction of Dr. Ernst R. Flueh, GEOMAR, and Dr. Michael Fisher, USGS, and have a scientific staff of 25. The dates for the expedition are from approximately April 20, 1996 until May 22, 1996, a total of 33 days. Of principal concern to NMFS is the use of the seismic array on the cruise, both during the ocean bottom seismic (OBS) work and the multichannel data seismic (MCS) data collection. During OBS survey work, the seismic array will be used approximately 7-8 days depending upon the number of stations and during the MCS survey work the array will be powered up for approximately 16-17 days.

Enclosure 5.3.2.1: Letter of recommendations from National Marine Fisheries Service outlining ways to avoid harassing whales.

On March 18, 1996, you informed us that the seismic airgun proposed for use on the R/V SONNE has a volume of 6,500 in^3 and a source strength of 100 bar-m. In addition, you estimate that the array will have a sound pressure level (SPL) of 240 dB re 1 μPa @ 1 meter. The largest gun in the array measures 580 in^3 (9.51 liters). However, based upon the pressure measurement you provided (100 bar-meters), NMFS questions the SPL for your array. Based upon the equation from Richardson et al. (1995)

$$L_s \text{ (dB re 1 uPa-m)}_{p\text{-}p} = 20 \log (P_a) + 220,$$

NMFS believes your array has an SPL of 260 dB peak to peak or about 254 dB zero to peak level. This refers to the downward propagation of the source. These levels agree with those found in Richardson et al. (1995) for large seismic arrays.

Of greater importance for assessing impacts on marine mammals however, is the horizontal propagation of sounds, which depends upon array geometry and aspect relative to the long axis of the array (Richardson et al. (1995). SPLs directed ahead of, behind (end-fire), or broadside (beam-fire) to the array may conservatively be estimated to be approximately 10-20 dB less than that projected downward. Also, again depending upon array design, Malme et al. (1984; as quoted in Richardson et al. (1995)) noted the possibility that levels at the bow and stern may not be greater than the largest gun in the array. For your array, the largest gun measures 580 in^3 (9.51 liters) with a pressure level of 8.1 bar-meters or 238 dB peak-to-peak and 232 dB zero-to-peak. Therefore, unless provided with additional information, NMFS will presume that the R/V SONNE's seismic array has a horizontal SPL of between 238-250 dB peak to peak or about 234-244 dB zero to peak level. To be consistent with the precautionary principle, NMFS must calculate the zones of harassment and injury based upon the worst case situation. As a result, NMFS will consider that the R/V SONNE's seismic source has a beam-fire and end-fire SPL of 250 dB.

Seismic airgun arrays emit pulsed energy principally at frequencies in the 20 to 250 Hz range. Based upon calculations using the 20 Log R propagation model, the seismic source used on the R/V SONNE will result in SPLs attenuating to approximately 195 dB at 1,843 ft (562 m), 190 dB at 3,280 ft (1,000 m), 180 db at 10,371 ft (3,162 m) and 160 dB at 17.3 nautical miles (nm) (31.6 km). NMFS believes that smaller marine mammals (including dolphin, porpoise, seal, and sea lion) hearing is poor at frequencies less than 1,000 Hz; thus, it is unlikely that your airgun would significantly affect these animals unless they were very close to the source.

Underwater audiograms indicate that seals, sea lions, and small whales and dolphins are particularly sensitive to sound with frequencies in the 2-12 kHz range (Richardson et al. 1991).

Seals and sea lions have thresholds of roughly 60 to 80 dB (re 1 μPa) in the range of best hearing. Phocid seals have lower thresholds and a wider frequency range of hearing than otariid seals. Pinniped hearing in sub-1 kHz range varies from 85 dB at 1 kHz to 114 dB at 250 Hz for the California sea lion, 70-85 dB at 1 kHz for the harbor seal, and 95 dB at 1 kHz for the northern fur seal (Richardson et al. 1991). No information has been reported concerning the in-water hearing of northern elephant seals (Richardson et al. 1991), although Schusterman (as cited in ARPA 1995) believes they may have mid- to low-frequency hearing ability.

Because no studies to date have focused on pinniped reaction to underwater noise from pulsed, seismic arrays in open water (Richardson et al. 1991), as opposed to in-air exposure to continuous noise, substantive conclusions are unavailable. However, assuming an SPL needed to be 80-100 dB over its threshold in order to cause annoyance and 130 dB for injury (pain), as is the current thought based upon human studies (ARPA, 1995), then it appears unlikely that pinnipeds would be harassed or injured by low frequency sounds from a seismic source unless they were within close proximity of the array (114 dB[1] + 80 dB = 190 dB (harassment); 114 dB[2] + 130 dB = 244 dB (injury)). For permanent injury, marine mammals would need to remain in the high noise field for extended periods of time. Therefore, because the evidence indicates that pinnipeds could be incidentally harassed at an SPL of 190 dB or greater, and because USGS has not been issued an incidental harassment authorization for pinnipeds, NMFS recommends that a safety zone around the source be established at the 190 dB isopleth or 3,280 ft (1,000 m) from the source.

Based upon the best scientific evidence available, NMFS believes that the hearing of dolphins, porpoises and other small whales that inhabit the Pacific coast area is poor at frequencies less than 1,000 Hz, and thus it is unlikely that the airgun noise would significantly affect them, unless they were very close to the source. While odontocetes can hear sounds over a very wide range of frequencies, from as low as 75-125 Hz in bottlenose dolphins and belugas (Johnson, 1967; Awbrey et al. 1988) to 105-150 kHz in several other species (Richardson et al. 1991), underwater audiograms indicate that odontocetes hear best at frequencies above 10 kHz. However, none of the seismic source frequencies will be within the dominant frequencies used by odontocetes for vocalization (Richardson et al. 1991).

In the range of best hearing (10 kHz-90 kHz), odontocetes have thresholds in the range of 40 to 60 dB re 1 μPa. In the

---

[1] Extrapolated from Figure 7.2 in Richardson et al. (1991).

absence of noise, bottlenose dolphins can detect a signal of about 41-42 dB at various frequencies between 10 kHz and 100 kHz (Johnson, 1967, 1968). For frequencies from 100 Hz to roughly 1000 Hz however, hearing thresholds range from 130 dB to 90 dB re 1 μPa, suggesting the potential for an increased tolerance for low frequency sound. Other odontocete species appear to have similar threshold frequencies (see Richardson et al. 1991). Richardson et al. (1991) have concluded, that, based upon studies on humans, SPLs of 80-100 dB over threshold are necessary in order to cause annoyance and 130 dB for injury (pain) in odontocetes. As a result, most odontocetes would probably need to be fairly close to the seismic source, and intentionally remain there, in order to be seriously affected by the seismic array (110 dB[2] + 80 dB (harassment) = 190 dB; 110 dB + 130 dB (injury) = 240 dB). However, NMFS cautions that testing on the similarity between hearing capabilities between humans and marine mammals still needs to be conducted before more than hypothetical conclusions can be drawn. However, similar to pinnipeds, because the evidence indicates that odontocetes (other than the sperm whale) could be incidentally harassed at an SPL of 190 dB or greater, and because USGS has not been issued an incidental harassment authorization for marine mammals, NMFS recommends that USGS establish a safety zone around the source at the 190 dB isopleth or 3,280 ft (1,000 m) from the source.

For the larger whales, such as gray, humpback and sperm whales, that have a greater sensitivity at the low frequencies of the seismic source than smaller whales, NMFS has determined that injury may occur at an SPL of 180 dB or greater and harassment at an SPL of 160 dB (see 60 FR 53753, October 17, 1995). Therefore, because USGS has not been issued an incidental harassment authorization for marine mammals, NMFS recommends that USGS establish a safety zone for these species at the 160 dB isopleth or 17 nautical miles (nm) (31.6 km) from the source. While there are indications, based upon the Heard Island assessment, that injury may occur at the 160 dB SPL (and therefore harassment would occur to some greater distance), because the 164 dB SPL is where Malme et al. (1984) noted 10 percent avoidance behavior for gray whales, and injury by low frequency noise for larger whales appears to be about 20 dB higher than the onset of harassment, 160 dB may not be a realistic level for injury takes. Therefore, until more conclusive evidence becomes available, NMFS considers 160 dB as the SPL at which larger whales may show behavioral response to low frequency noise and for that reason, recommends a safety zone for large whales be established at the 160 dB level.

---

[2] Extrapolated from Figure 7.1 in Richardson et al. (1991).

Of primary importance in conducting your activity is to avoid the serious injury or death of a marine mammal. In order to avoid seriously injuring a marine mammal, your acoustic array should be powered up at a rate no greater than 6 dB per minute between 160 dB and the operating SPL of the array, whenever the array is turned on. For your array, this should take approximately 15-20 minutes. This ramp-up should provide sufficient time for marine mammals that can hear the sounds from the array, and are uncomfortable with those sounds, to either leave the area or move away from the source prior to the onset of any injury to their hearing mechanism.

In addition, because you do not have an authorization to harass marine mammals, efforts must be undertaken during seismic work to determine whether marine mammals are within the vicinity of the ship. This can be accomplished in two ways: (1) visually by biological observers and (2) acoustically by hydrophones. Because the safety zone for small whales, dolphins, seals and sea lions is relatively small (1,000 m), visual monitoring should be sufficient. However, because the safety zone for the larger whales such as the gray and humpback whales is significantly greater, visual monitoring may not be sufficient. Because these large whales vocalize at the low frequencies similar to those used for seismic arrays, acoustic monitoring for these animals can be accomplished with the same equipment used for seismic recording. Information on establishing this acoustic monitoring program is enclosed.

To monitor the safety zones, NMFS recommends a minimum of 2-3 observers be on watch during all daylight hours that the array is operational; one - two observers to view, through 25X Big Eye binoculars, that portion of the 17 nm (31.6 km) monitoring zone that is visible from the bridge of the ship, while another observer will serve as a data recorder and observer of the safety zone. To avoid eye fatigue while observing through the 25X binoculars, observers should rotate their time on watch fairly frequently (two hours recommended). While observations through the Big-Eye binoculars are not necessary when the array is powered down, monitoring of the safety zone should begin one hour prior to ramp-up of the source.

In the event that either a small whale or seal is sighted within 1,000 m of the R/V SONNE or a larger whale is detected, either visually or acoustically, within their 17 nm safety zone, because you are not authorized to incidentally take a marine mammal, you should immediately power down the array to below 160 dB until the marine mammal has left the vicinity of the test. In addition, because the time of your seismic work coincides with the northward migration of gray whales, and because these animals normally remain close to the shoreline, we concur with your

agreement to remain 12 nm offshore. At this distance, we believe that a corridor will be provided that will allow gray whales to continue their migration unimpeded.

If you have any questions concerning this letter, please contact Kenneth Hollingshead, Office of Protected Resources, NMFS at (301) 713-2322.

Sincerely,

for William W. Fox, Jr., Ph.D.
Director
Office of Protected Resources

Enclosure

5.4 SHIPBOARD EQUIPMENT

5.4.1 HYDROSWEEP

(N. Kukowski and T. Schillhorn)

Onboard RV Sonne, the bathymetric contours of the ocean floor can be continuously recorded using the swathmapping system HYDROSWEEP ("HYDROgraphic multi-beam SWEEPing survey echosounder", made by Atlas Elektronik GmbH, Bremen).

The instrument works with a frequency of 15.5 kHz. The input amplifier is situated perpendicular to the longitudinal axis of the ship. With 59 acustic beams and an opening angle of 90°, a swath about twice as wide as the water depth is surveyed. Precision is about 1% if the ship rolls less than 10° and heaves less than about 5°. The central beam has a range of up to 10000 m, the outermost ones can range up to at least 7000 m. There are three ways to deal with acoustic water velocity: 1) it can be calculated during data acquisition by means of an optimising selfcalibration by comparing the forward and downward rays; 2) a constant average velocity can be assumed, or, 3) a depth profile for water velocity can be taken as obtained e.g. from a CDT (Conductivity Depth Temperature) tool. Data (location, time, and water depth) are continously written to magnetic tape and magneto-optical disc and, during acquisition, can also be plotted online as isoline charts.

Postprocessing of HYDROSWEEP data to produce bathymetric maps and couloured 3D perspective views is done onboard with the Hydromap 300 system (Atlas Elektronik GmbH, Bremen). Hydrosweep data can also be edited and processed with the *mbsystem* software developed at the Lamont-Doherty Earth Observatory.

5.4.2 PARASOUND

(N. Kukowski and T. Schillhorn)

By means of the parametric sediment-echosounder PARASOUND (PARAmetric sediment survey echoSOUNDer, Atlas Elektronik GmbH, Bremen), shallow sedimentary layers down to a maximum depth of about 100m can be imaged.

The PARASOUND system, which operates differently from traditional 3.5 kHz echosounders, uses the sound beam that results from the interference of two high-frequency waves of similar frequency (18-23.5 kHz). This process leads to the formation of a low-frequency signal typically of 2 to 5 kHz. The depth of penetration of the parametric 2.5 to 5.5 kHz echo is as great as that of 3.5 kHz systems, but due to the narrower beam width, a clearer and more differentiated image of multi-layer structures is obtained. The beam width of the output sound wave is about 4°, which gives a swath of 7% of the water depth. Therefore, data quality depends to a large amount on the morphology of the ocean bottom, in case of steep slopes, data quality often is quite poor. The same can be valid at high ship's speed (> ca. 8 kn).

Raw analog data are written to a black and white as well as a color printer. With the program PARADIGMA (PARAsound DIGitalisierungs- und Mehrkanal Auswertesystem, V. Spieß, U Bremen), data can also be written digitally to magnetic tape in the SEG-Y format which allows the application of seismic processing techniques.

5.4.3 NAVIGATION

(J. Bialas)

During the cruise SO108 it was decided to shot at constant time intervals rather than on constant waypoint increments. As there was no digital recording of shot times and positions available with the trigger unit, shot lists must be provided

externaly. For this purpose the shot reply of the first airgun was provided as 5 V, 100 ms pulse which was recorded by one of the OBH Methusalem data loggers. Playback of this records was done in the same manner as the OBH recordings (see Chapter 5.2.3). As the analog signal was not covered with noice only a simple algorithm was needed to detect the onset of the rising flank and the duration of that signal to detect the exact shot times. At this time an ASCII file was provided listing all shots with reference to the GPS based synchronization of the OBH recording system. In addition possible misfires or drop outs would have been recognized immediately and need no later trace editing. For positioning purposes the RV SONNE is supplied with two GPS receivers, Transit Navigation and standard naviagtion tools like doppler and gyro. As there is no differential GPS available uncertainties of the satelite positioning need to be corrected by other means. This should be done by the ships navigation computation which provides a so called "Filter" which was recognized as best possible position. These positions and all other values are stored into a ships database. System operators of RV SONNE provided ASCII files with Filter position and water depth based on UTC date and time at intervals of 10 s. According to this navigation files the position for each shot was interpolated with reference to the UTC timing. Following this scheme an UKOOA formated ASCII file with shot position, shot time and water depth could be provided for each line.

Once the OBH and OBS recordings were split into SEG-Y files according to the shot tables the direct water wave could be used to check the navigation precision. Reduced with 1.5 km/s the water wave arrival should line up as one continuous event. Due to changes in the water velocity the arrival might not be horizontal but should not be characterized by short term undulations (Figure 5.4.3.1.A). Statistics of the ships navigations files and the trigger recordings were calculated to check wether these are caused by wrong shot times or positions. Despite a few misfires all shots were released within the designated intervals and could be verfied by the recording of the first gun's reply. Statistics and plots of the navigation data show that there are two major problems (Table 5.4.3.1). Obviously the designated recording interval of 10 s was not achieved during the whole time span. Although the amount of data supplied by the ship's database is equal to the 10 s time interval, the values were often constant for minutes and could not be used for shot positioning (see points 720 to 740 in Figure 5.4.3.1.B). This is perhaps due to the overload of the NavVax, where the memory is not updated as desired. Chart plots of the navigation values (Figure 5.4.3.1.B) show a course which is interrupted by small steps and small peaks. After an arbitrary number of points lining up in a smooth trail there are a few values that cause small scale sidewards steps (see points 740 to 760 in Figure 5.4.3.1.B). Even if the ship is sailing within rough sea these steps must be considered artificial. Consequently the positions of shots calculated with such values will not provide the correct shot receiver distance. Statistics of the shot tables show that despite constant time intervals the distances from shot to shot may vary as much as 30 m which is about 25% to 30% of the desired 90 m spacing.

Several processes were applied to the navigation files in order to minimize these errors. 1-D median filter were tested with a 6, 12 and 24 point sliding window but could not significantly help to improve the data. A promising chance might be given with the help of the unrelated ships gyro and doppler log information. As these values have not been extracted from the database earlier, the database files from the cruise need to be restored from backup tapes by the ship's system operators. This job could not be finished before the end of this cruise because no instructions were available on how to handle this. Therefore any further data processing of the navigation files has to be postponed. Another approach could be achieved using a long term average to proof the quality of each single position. For this purpose a sliding window with an odd number of points was moved through the navigation file. At this time for each point its distance and and the ships velocity was calculated with reference to the previous position. The achieved values were expected to differ not more than 1% from the longterm average. If not this point was dropped and would not be considered for the longterm average. A window of 101 points and an uncertainty of 1% achieved the best results (Figure 5.4.3.2). Short range undulations of the direct water wave were observed with an

wave length of 1 to 2 km. At -47 km and -64 km the arrival steps back by some 100 to 200 ms. This could drastically be improved by application of the longterm quality check. A second indicator for the improvement of the navigation are the variety of events that can be seen all over the section. After the navigation check the phase correlation between the phases became much more continuous and correlate well. This simple algorithm could improve the positioning to nearly meet our demands. Much to everyones surprise no information is available on how the ship's "Filter"-sytem works.

System checks of the ships navigation processor showed that the filter process was not assigned with the highest possible priority on the NavVax. As a first method to improve the situation this process was asigned a high priority. With the higher priority the systems access to the data base seems to be more efficient. Dublicate readings were no longer detected in the navigation files. During discussion with the system operator it turned out that despite several new software releases navigation problems are known since 1991 (see numerous cruise reports by BGR and GEOMAR). Manufacturer Atlas Electronic's reply stated that they are "still working" on this. Further tests of the system manager on board RV SONNE seems to prove that there are some major weight within the filter algorithm that are not consequently checked for reliabilty. One observation is that once the doppler log is ground coupled its readings are apparently choosen at highest reliability without any further consistency check. This might have mislead the system on April 27 when the ship's navigation was off by more than two miles (see Appendix, Systemoperators report). Navigation processing will need some further attention for future seismic operation of the vessel.

H010Description of survey data ORWELL - RV SONNE - SO108
H020Date of survey 22.04.1996
H022Date of this tape 25.04.1996
H030Client GEOMAR
H040Geophisical contractor GEOMAR
H050Positioning contractor RF - RV SONNE
H060Positioning processing cont.GEOMAR
H070Positioning & computer sys. Filter - RV SONNE
H080Coordinate location Source Position
H090Offset to coord. location -80
H100Clock time respect of GMT +1

Profile	Shot	Day & Time	Latitude	Longitude	Depth	Time [S] since last shot	Distance [m]	diff. to ext. time
1	1	113 22:42:59.000	45: 4:40.64N	126:14:27.15W	2751.0	0.000	0.	0.000
1	2	113 22:43:22.000	45: 4:45.23N	126:14:26.47W	2751.0	23.000	143.	0.000
1	3	113 22:43:22.000	45: 4:45.23N	126:14:26.47W	2751.0	0.000	0.	0.000
1	4	113 22:43:22.000	45: 4:45.23N	126:14:26.47W	2751.0	0.000	0.	0.000
1	5	113 22:43:57.000	45: 4:52.21N	126:14:25.53W	2754.0	35.000	217.	0.000
1	8	113 22:44:22.000	45: 4:57.23N	126:14:24.54W	2754.0	20.000	126.	0.000
1	9	113 22:44:22.000	45: 4:57.23N	126:14:24.54W	2754.0	0.000	0.	0.000
1	10	113 22:44:45.000	45: 5: 1.61N	126:14:23.77W	2755.0	23.000	136.	0.000
1	98	113 22:59:28.000	45: 4:55.05N	126:14:48.91W	0.0	10.000	14.	0.000
1	99	113 22:59:29.000	45: 4:55.00N	126:14:48.93W	0.0	1.000	2.	0.000
1	100	113 22:59:48.000	45: 4:54.41N	126:14:49.34W	2751.0	19.000	20.	0.000
1	101	113 22:59:58.000	45: 4:54.13N	126:14:49.48W	2751.0	10.000	9.	0.000
1	102	113 23: 0: 8.000	45: 4:53.87N	126:14:49.54W	2762.0	10.000	8.	0.000
1	124	113 23: 3:48.000	45: 4:48.09N	126:14:58.08W	2751.0	16.000	24.	0.000
1	125	113 23: 3:55.000	45: 4:47.81N	126:14:58.33W	2752.0	7.000	10.	0.000
1	126	113 23: 3:55.000	45: 4:47.81N	126:14:58.33W	2752.0	0.000	0.	0.000
1	127	113 23: 3:55.000	45: 4:47.81N	126:14:58.33W	2752.0	0.000	0.	0.000
1	128	113 23: 3:55.000	45: 4:47.81N	126:14:58.33W	2752.0	0.000	0.	0.000
1	129	113 23: 3:55.000	45: 4:47.81N	126:14:58.33W	2752.0	0.000	0.	0.000
1	168	113 23: 3:55.000	45: 4:47.81N	126:14:58.33W	2752.0	0.000	0.	0.000
1	169	113 23: 3:55.000	45: 4:47.81N	126:14:58.33W	2752.0	0.000	0.	0.000
1	170	113 23:11:25.000	45: 4:30.55N	126:15: 8.95W	2755.0	450.000	582.	0.000
1	171	113 23:11:38.000	45: 4:30.06N	126:15: 9.40W	2751.0	13.000	18.	0.000
1	172	113 23:11:41.000	45: 4:29.93N	126:15: 9.50W	2751.0	3.000	5.	0.000

Table 5.4.3.1: Statistics derived from waypoints of the "Filter" navigation along profile 1.

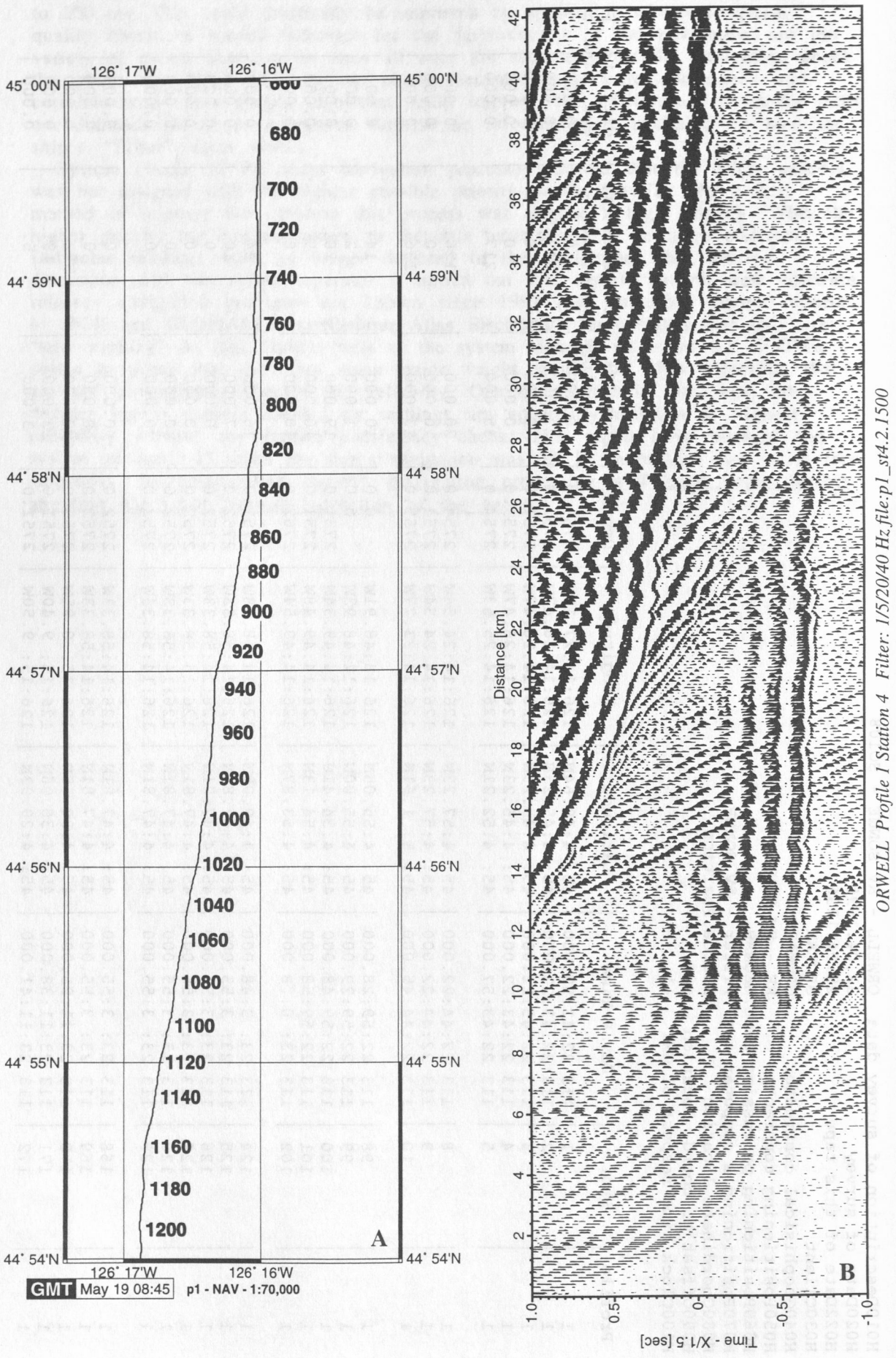

gure 5.4.3.1: Cutout of OBH04 on Line 1. Display of the direct water wave arrival. Reduction velocity 1.5 km/s (A). Cutout of the "Filter" navigation waypoints from Line 1 (B).

Figure 5.4.3.2: Cutout of the direct water wave arrivals at OBH59 on Line 11. Distances calculated according to "Filter" navigation waypoints (A). Cutout of the direct water wave arrivals at OBH59 on Line 11. Distances calculated according to longterm average weighted "Filter" navigation waypoints (B).

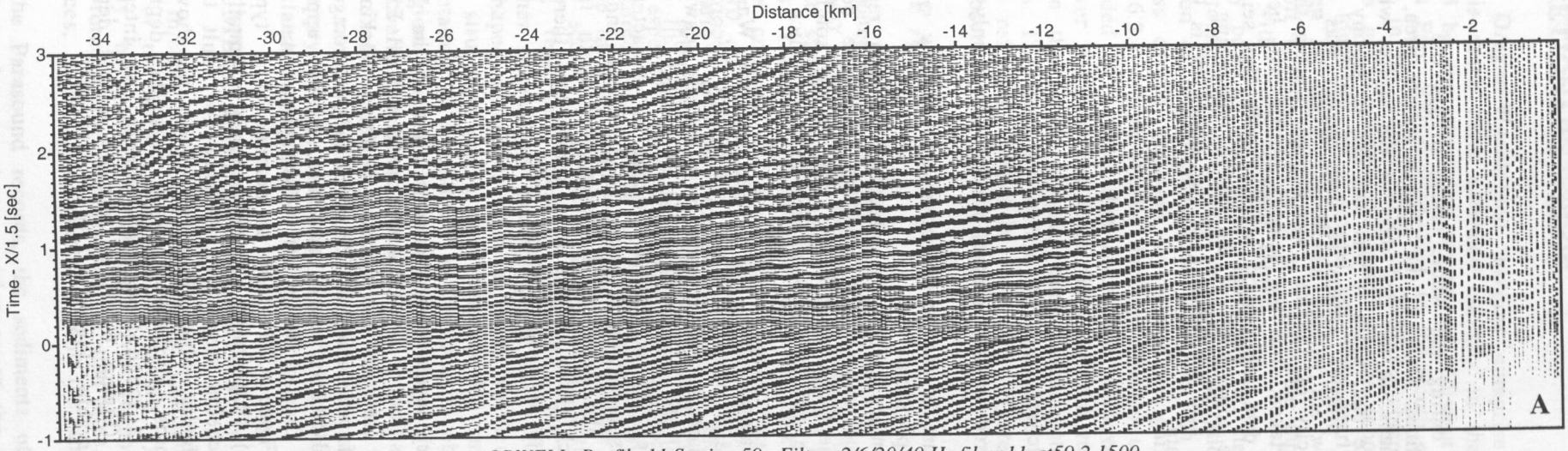

ORWELL Profile 11 Station 59 Filter: 2/6/20/40 Hz file:p11_st59.2.1500

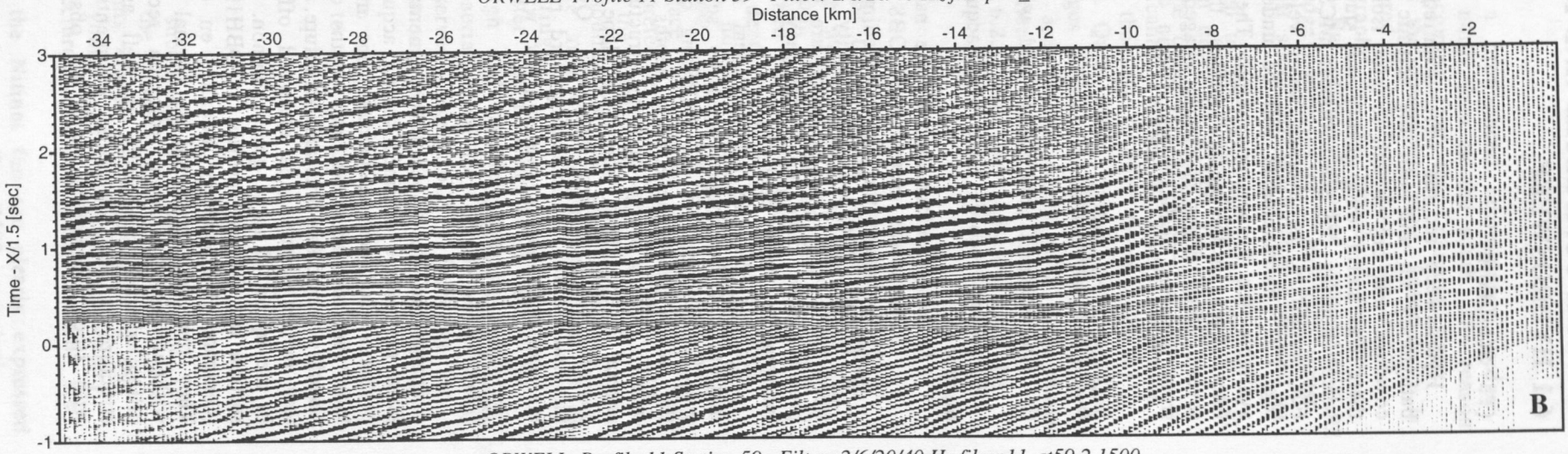

ORWELL Profile 11 Station 59 Filter: 2/6/20/40 Hz file:p11_st59.2.1500

6. WORK COMPLETED AND FIRST RESULTS

6.1 HYDROSWEEP

(T. Schillhorn)

Hydrosweep records were acquired during the whole cruise to get the bathymetry on and near the seismic lines. Only in the Oregon rosette area, coverage was big enough to plot isomaps. In the first days of the cruise, while there was storm, data quality was quite bad, again it was bad due to stormy weather when shooting the southernmost MCS profiles. Otherwise, data quality was good. For simplicity, an average water velocity of $1485ms^{-1}$ was chosen. During the next leg, CTD measurements will be undertaken, thus the velocity profile will be available for further processing. The data are plotted together with the seismic lines. Even in the narrow stripes, the topography of the wedge comprising of several steep ridges is clearly imaged, also the bending of the slopes as is known from previous Seabeam and Gloria data.

6.2 PARASOUND

(N. Kukowski, T. Schillhorn, and watches)

Parasound records have been acquired on all seismic profiles for mainly two purposes:

1) to get information of the nature of the ocean bottom and shallow subsurface around OBH/OBS positions,
2) to image the shallow sedimentary layers and structures in high resolution.

A relation between data quality and underground structure cannot be detected from the records. One exception are the OBSs close to the coast on the southern profiles. Here, quite noisy data may be due to the water rich mud on which the instruments have been set.

Although showing specific local features, both, the Oregon and the Washington margin, can be characterized by several units from the sedimentary record which will be described in the following chapters. The oceanic crust records seaward of the trench shows penetration depths of the Parasound signal of around 40 m mostly, and a fairly uniform structure. The accretionary wedge is characterized by several steep ridges, where the slope is too steep to obtain good signals, and small basinshaped structures inbetween. On the upper shelf, penetration depth is minimal (< 10 m), indicating hard rock (from drilling it is known that there are massive carbonates) overlayn by water rich homogenous mud.

OCEANIC CRUST

Images of the uppermost sedimentary layers of the oceanic crust of the Juan de Fuca plate were obtained during acquisition of the Oregon Rosette and all EW profiles. On average, the sections of the southern and the northern working area look very similar comprising depths of penetration of 35 to 50 m on average and showing no clear internal structure. However, only sometimes, in the uppermost few meters, layering is observed off Oregon, while off Washington, fine layering in the upper 10 m is quite common. Figure 6.2.1 shows an example of a "typical" section off Oregon (profile 7, OBH19). Topography is very smooth regionally (compare Hydrosweep). Locally, en echelon steps give evidence for fault tectonics. They may be interpreted as normal faults, which, however, cannot be shown without doubt without reflexion records. Furtheron, smooth basinlike depressions, pillow shaped topography as well as a rough topography without any internal structure in the penetrated sediments (Figure 6.2.2) or tectonic related depressions with steep, segmented walls are observable (Figure 6.2.3).

ACCRETIONARY WEDGE

The Oregon-Washington margins comprise a pronounced accretionary wedge which is much more extended laterally in the north than in the south. The reason should be the enormous amount of sediment coming from the Columbia river (Astoria Fan, Nitinat Fan). Due to the youth of the downgoing plate, water depth is not big in the trench (2500 to 2900 m) compared to other margins. The trench itself is not dinstinctly expressed in the topography, in the Parasound records it can be identified by a several km wide nearly flat section followed immediatelly by the steep 1st ridge. The frontal part of the wedge comprises of 2 imbricate thrust slices off Oregon, and of 3 to 4 imbricate thrust slices off Washington expressed as ridges with steep seaward flanks.

Many parts of the ridges' flanks are too steep to get good Parasound records, but if the topography is smooth enough, penetration down to around 100 m and resolution of locally more than 10 layers can be obtained (Figure 6.2.4). The thickness of the sediment layers varies significantly. While the layers shown in Figure 6.2.4 are of similar thickness, further to the east, 2 thick layers (~20 m) surrounded by several thin layers are observed. Quite often, slumps are imaged at the lower parts of the steep flanks of the ridges within the accretionary wedge. Between the ridges, slightly curved sediments are visible, partly with wave-shaped surfaces. The fault just before the next ridge often is visible as a quite steeply dipping reflector. Turbiditic sequences (Figure 6.2.5) and fan sediments can be only observed in the Washington area.

SHELF AREA

At water depths of less than about 300 m, the image of the shallow subsurface completely differs from the seaward part of the wedge formed by the ridges with basinlike structures inbetween. This is imaged both, in the E-W as well as in the N-S lines. Therefore, these structures are described here separately.

Quite common are areas where penetration depth is minimal, not exceeding about 10 m. Topography in these areas varies, however: nearly flat regions with very narrow zick-zack topography (A), a narrow scale "zick-zack" surface with dipping reflectors (B), and coarse blocked surface (C) can be distinguished (Figure 6.2.6), especially closest to shore. This is interpreted to be caused by coarse, hard, unstructured rock, which is not penetrated by the Parasound signal with a coverage of fine, water rich mud on top. The southermost part of the Oregon N-S profiles seems to represent a tectonically active area with thrust faults and steeply dipping reflectors, perhaps indicating fracturing.

Further downslope, penetration is much better again. Remarkebly are older wave-shaped reflectors with a large wavelentgh and parallel layering indicating glacial structures which have been eroded subaerially and on top of which young sedimentation of around 20 m thickness is observed (Figure 6.2.7). Typically for this region is also flat topography with penetration around 40 m and well imaged quite coarse layering.

The shelf is cut by several steep canyons, the most expressed of which is the Astoria canyon. Sedimentation is quite similar to the structures observed in the accretionary wedge, slumping (Figure 6.2.8) is quite common, resulting in tilted blocks and rough surface.

COLUMBIA RIVER (NITINAT) FAN

The thickest sediment input in the Cascadia subduction zone occurs in the region of the Astoria Fan, built up mainly by the Colubia river sediments. Recently, however, the Columbia river sediments mostly are transported to the north, forming the Nitinat Fan. In that area, young sediments and sedimentary sequences, differing completely from the structures observed further south, are found.

In the Parasound records, the sediments of the Nitinat fan are clearly expressed as well on the accretionary wedge as on the oceanic crust. The 2500 m isobath

seems to be the seaward border of the fan sediments. Their internal structure (Figure 6.2.9) is very similar in all areas where they are observed. It is a change between layered sequences and sequences of more turbiditic character.

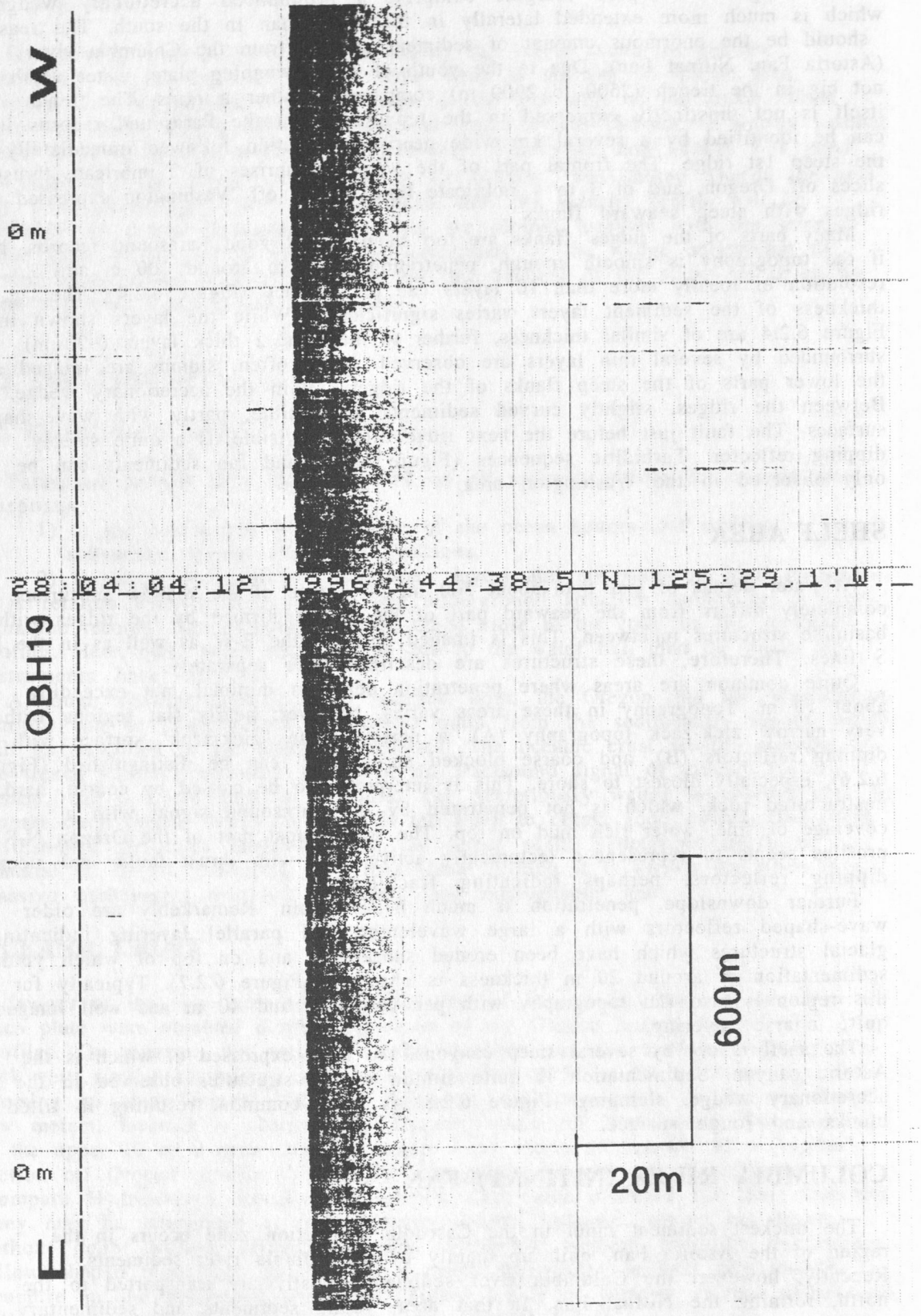

Figure 6.2.1: Typical Parasound section of the Juan de Fuca plate crust in the neighbourhood of OBH 19. Penetration depth ~25-30 m. In the upper 15m, layered structures may be identified.

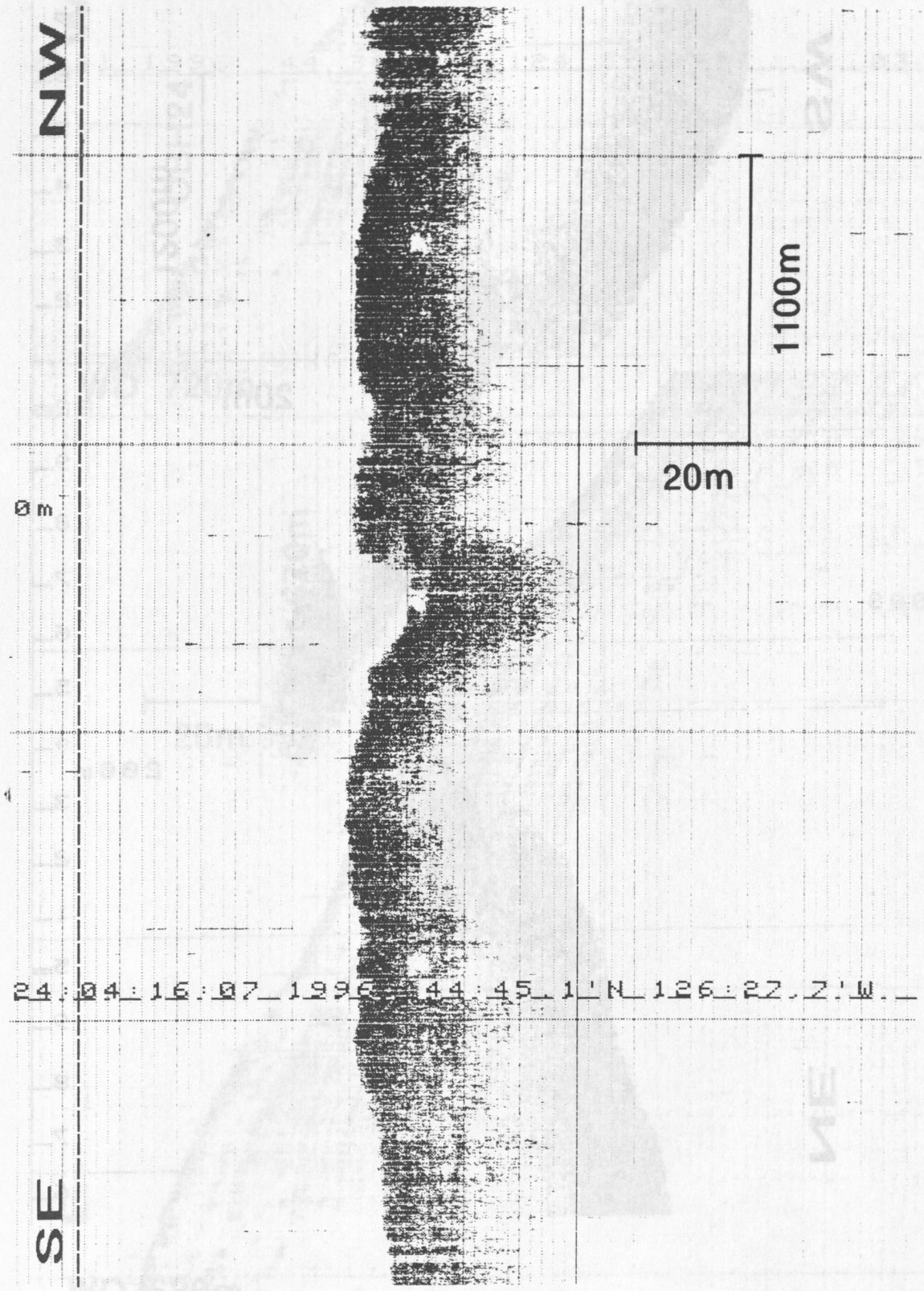

Figure 6.2.2: Parasound section of the Juan de Fuca plate crust between the midpoint of the rosette and OBH 10. Penetration depth ~20 m.

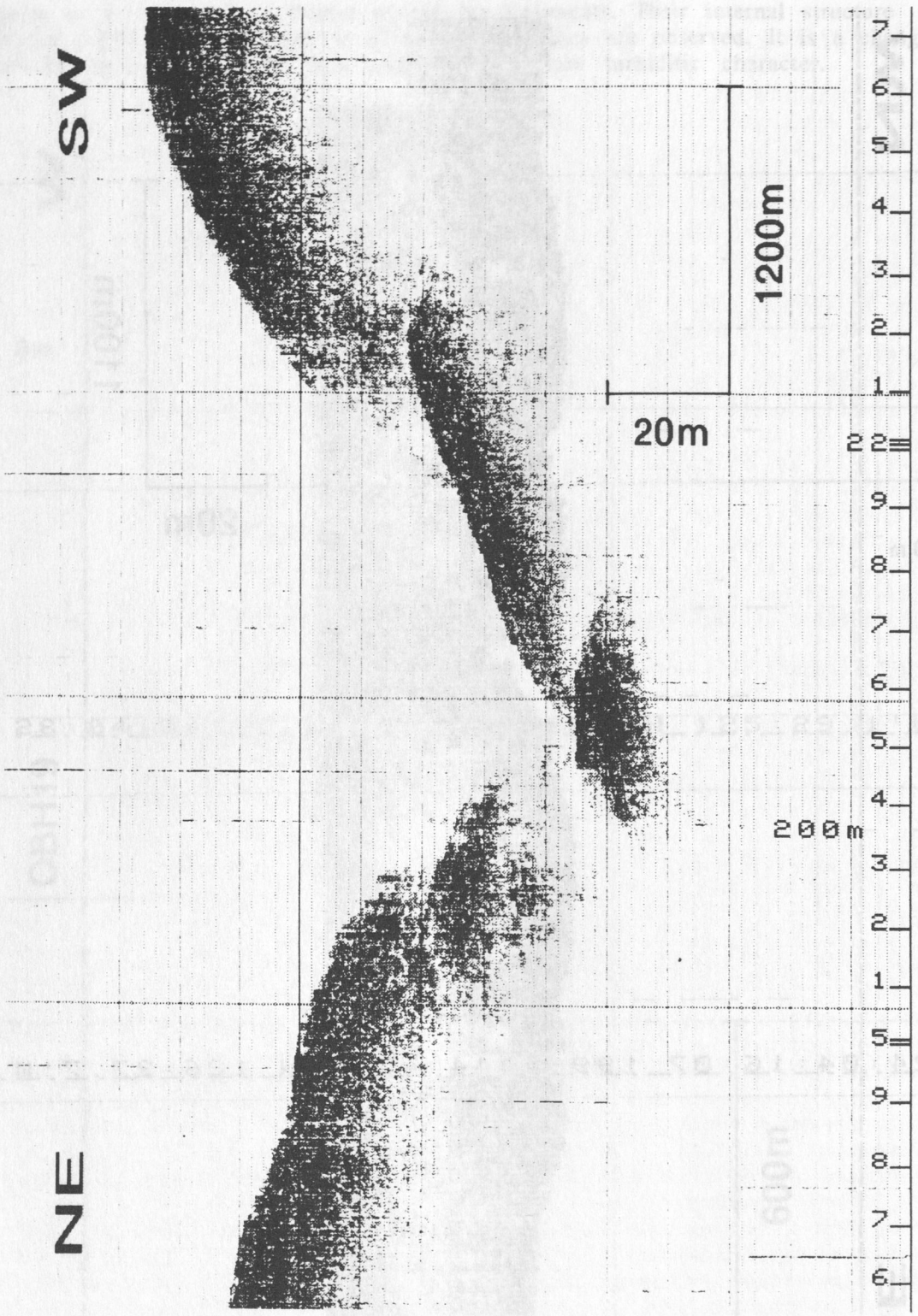

Figure 6.2.3: Parasound section of the Juan de Fuca plate crust east of OBH 40. The structure of the right hand side wall may be caused by slumping.

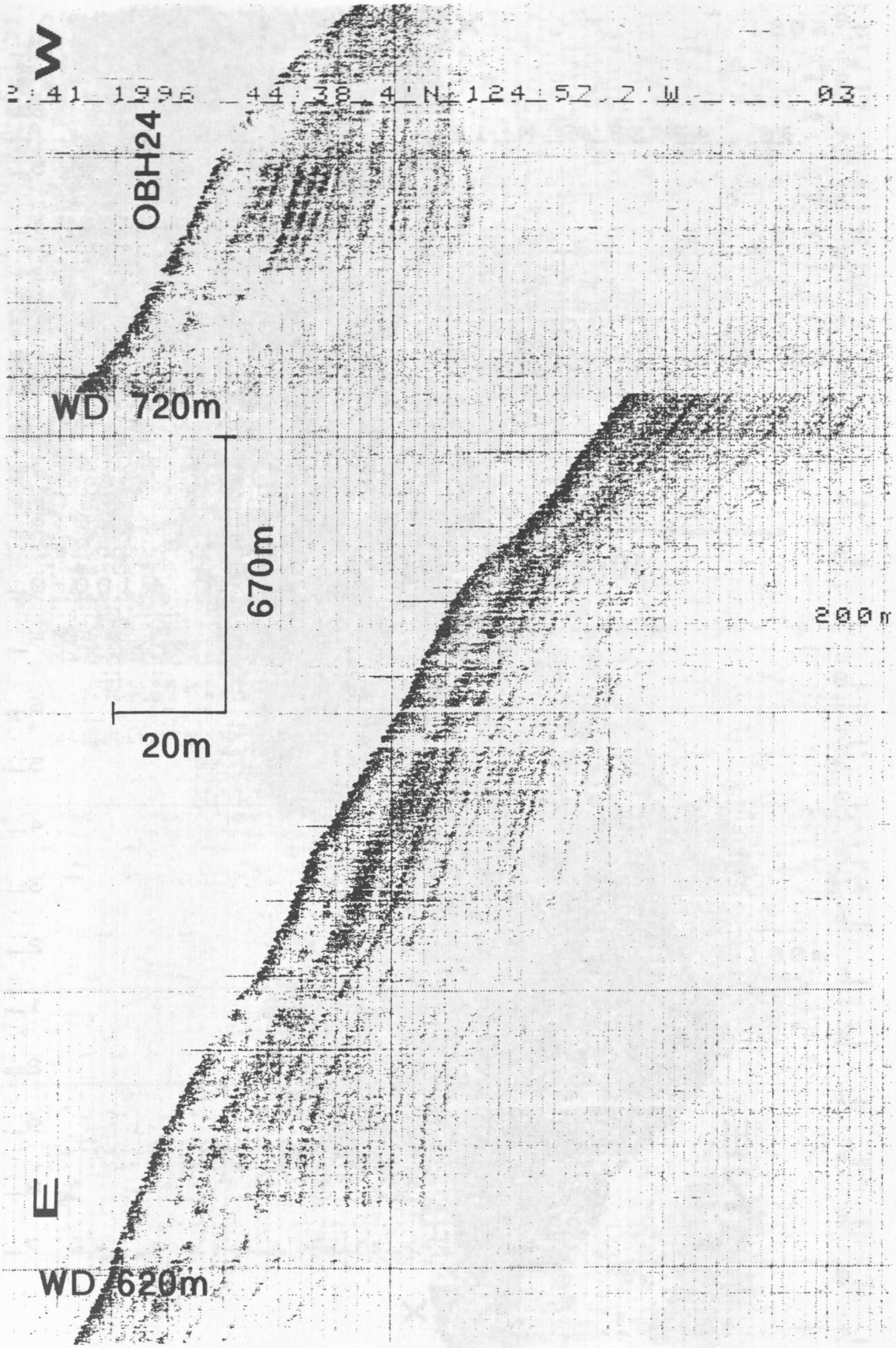

Figure 6.2.4: Sedimentary sequence landward of the second ridge, east of OHB 24, Oregon E-W profile 7. Alltogether, 14 layers can be distinguished.

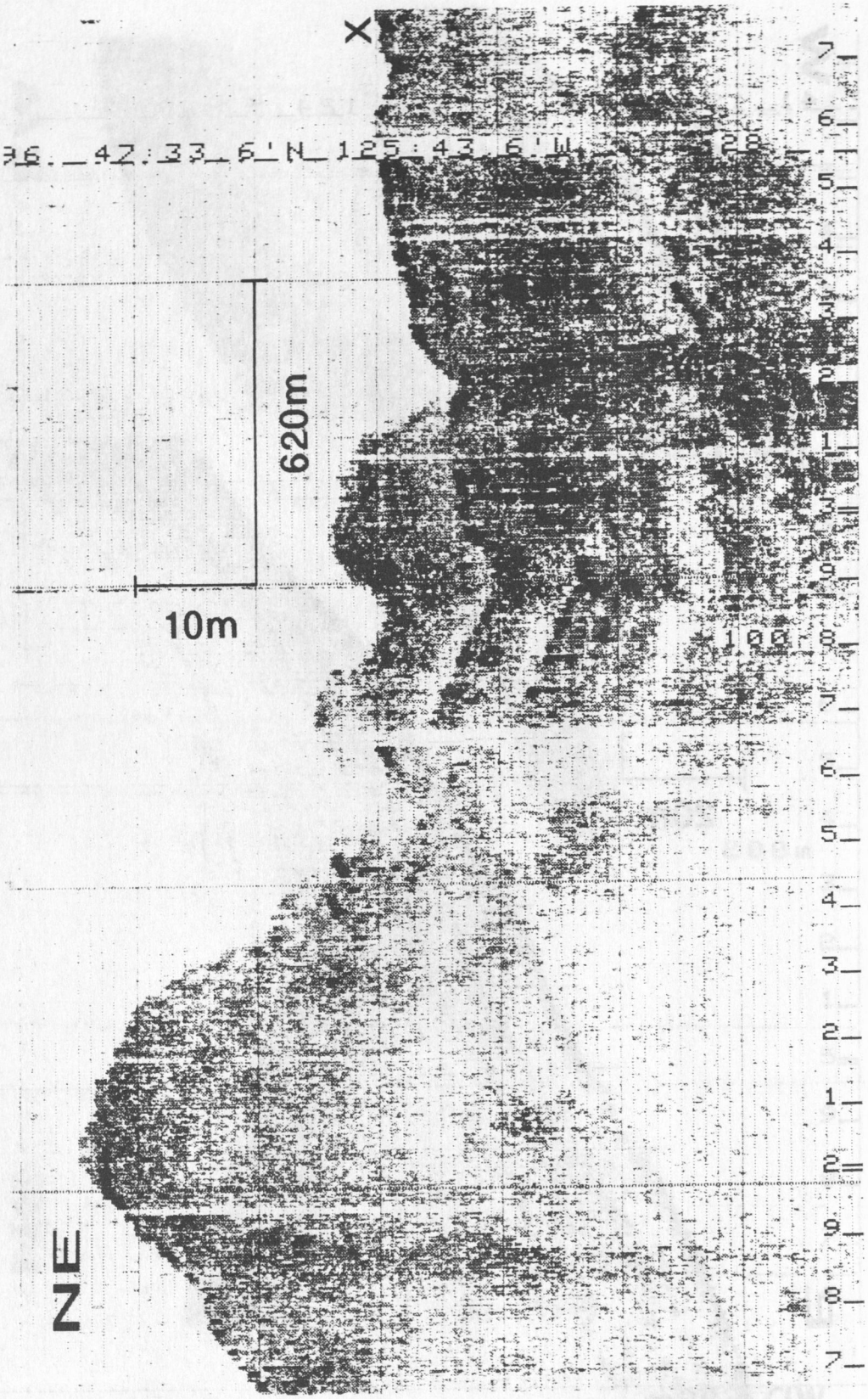

Figure 6.2.5: Slumped turbiditic sequence seaward of the second ridge on the northernmost MCS profile (profile 101) (The cross marks the point of overlap).

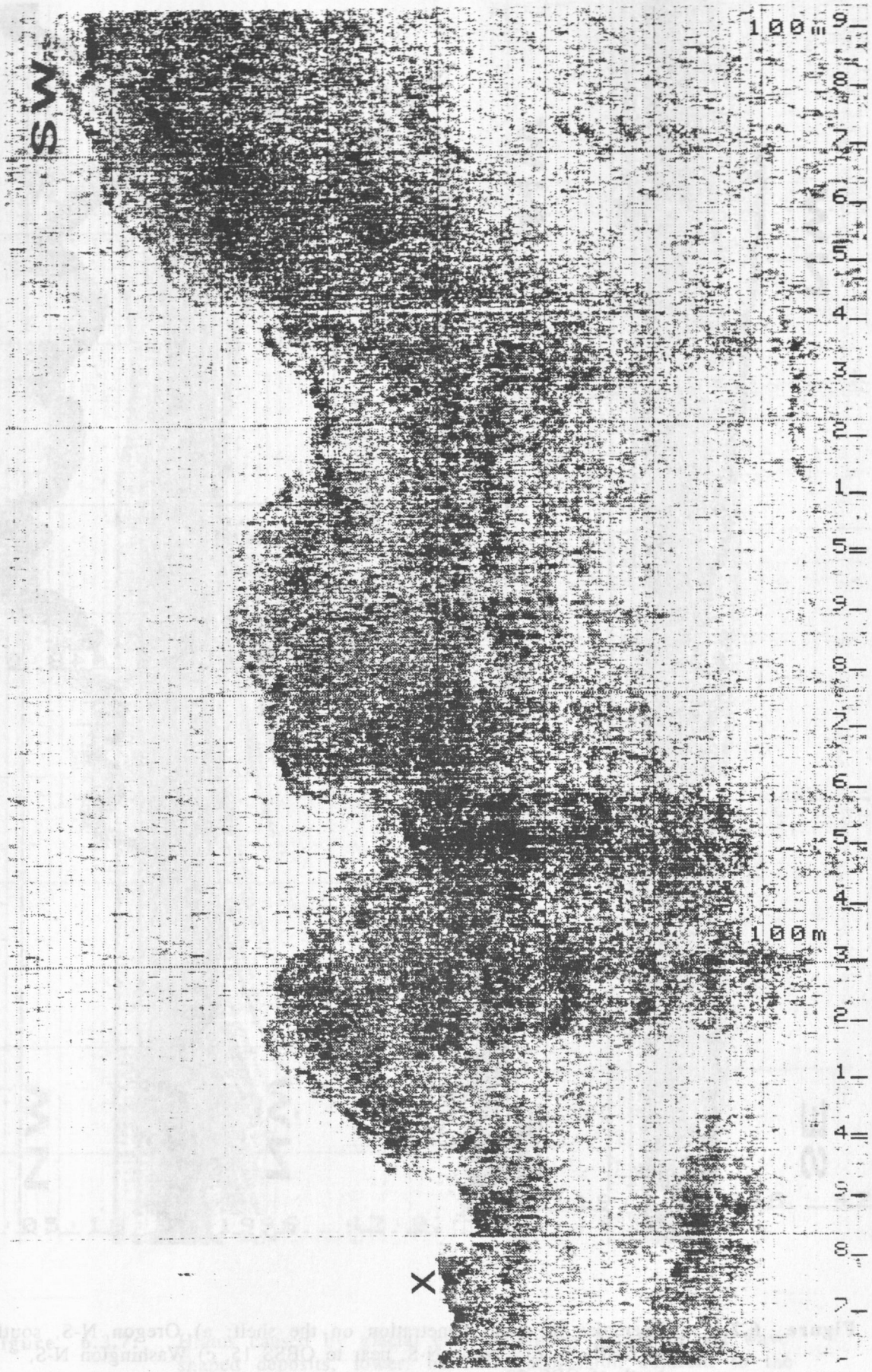
SW
100m
100m
X

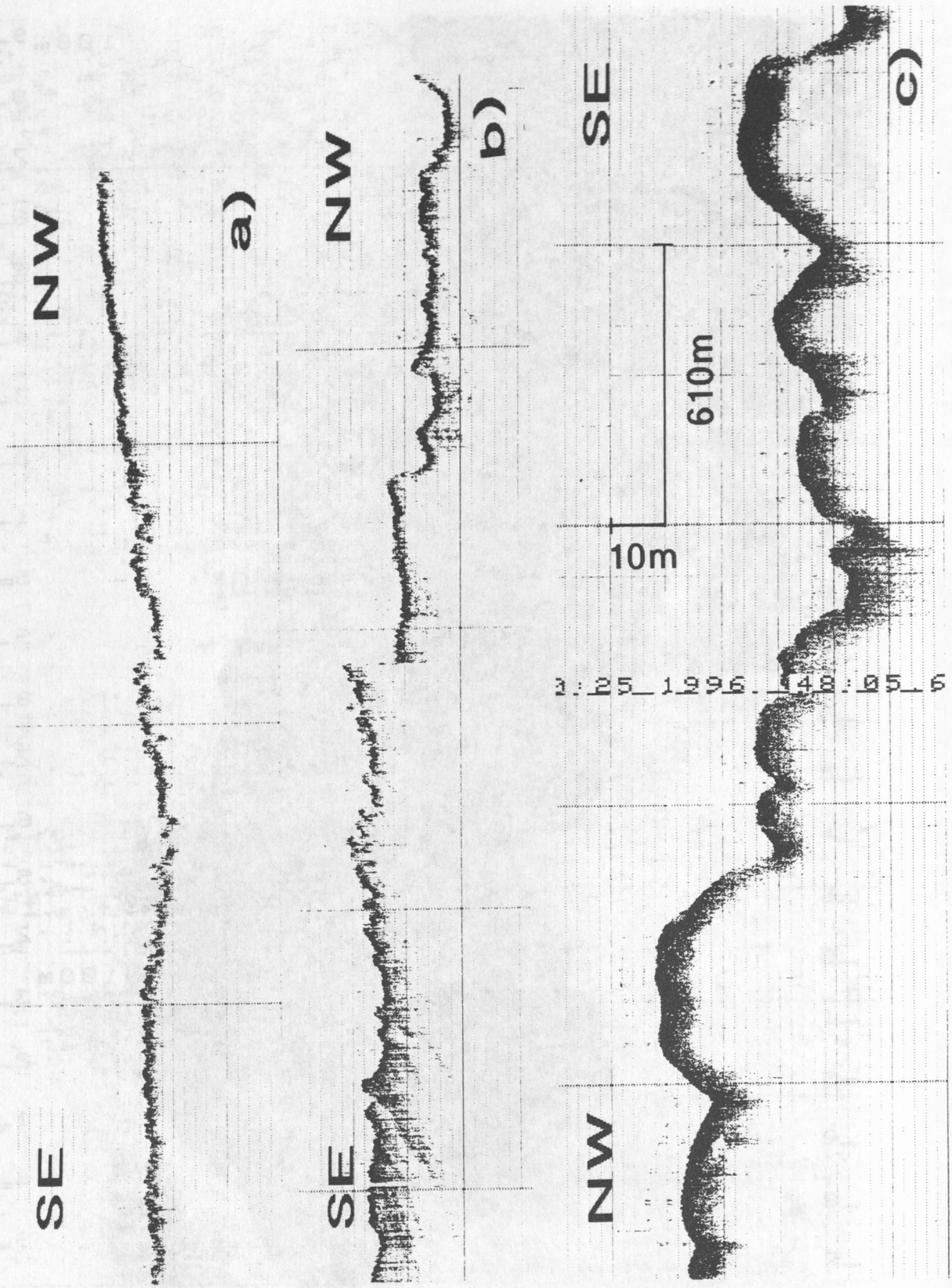

Figure 6.2.6: Examples of small penetration on the shelf: a) Oregon N-S, south of OBH 32, b) Oregon N-S, near to OBSS 15, c) Washington N-S, north of OBS 29,

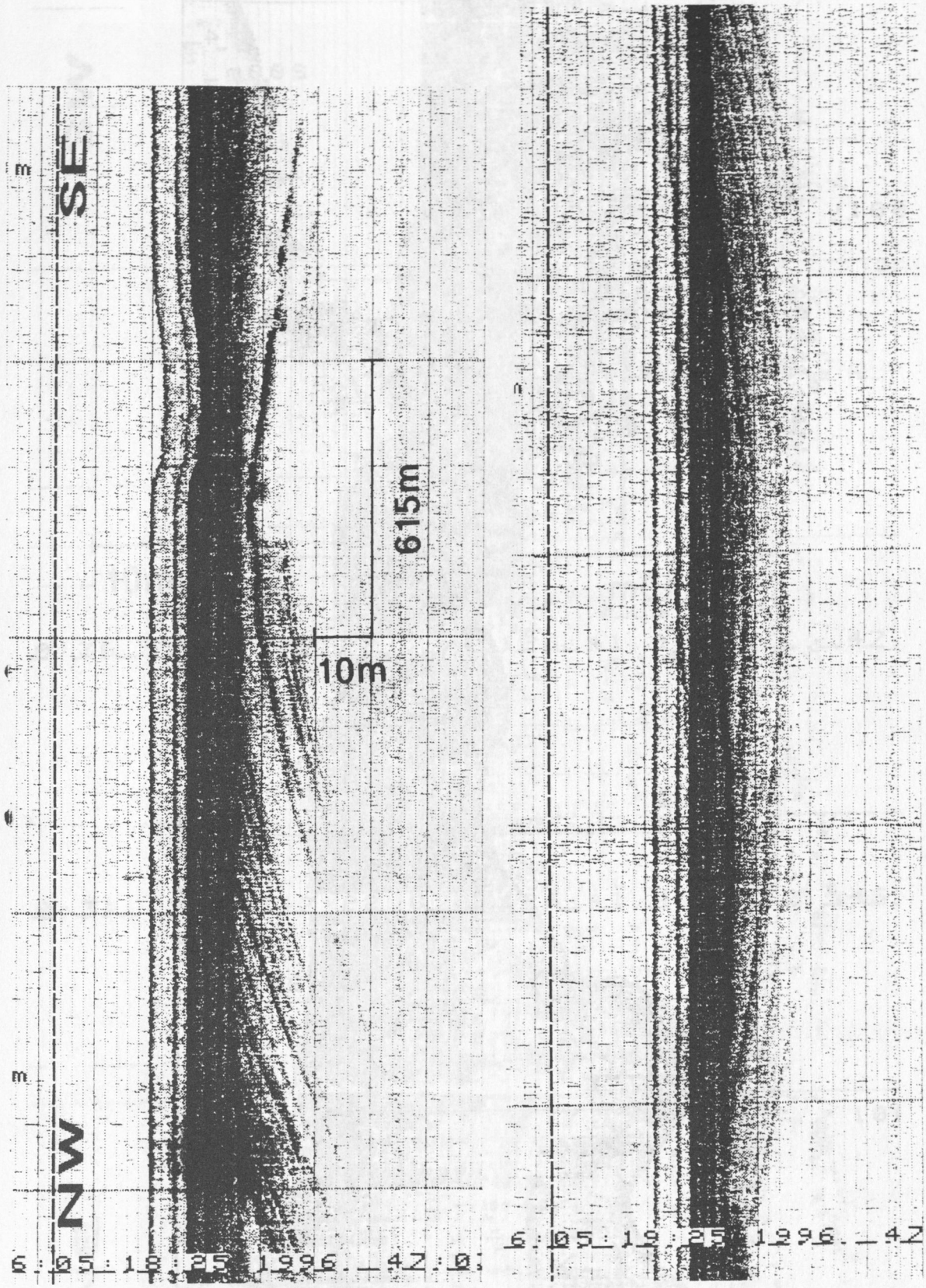

Figure 6.2.7: Hiatus caused by glacial erosion. Upper: buckle of old wave shaped deposits, lower: basinkile depression adjacent to the buckle.

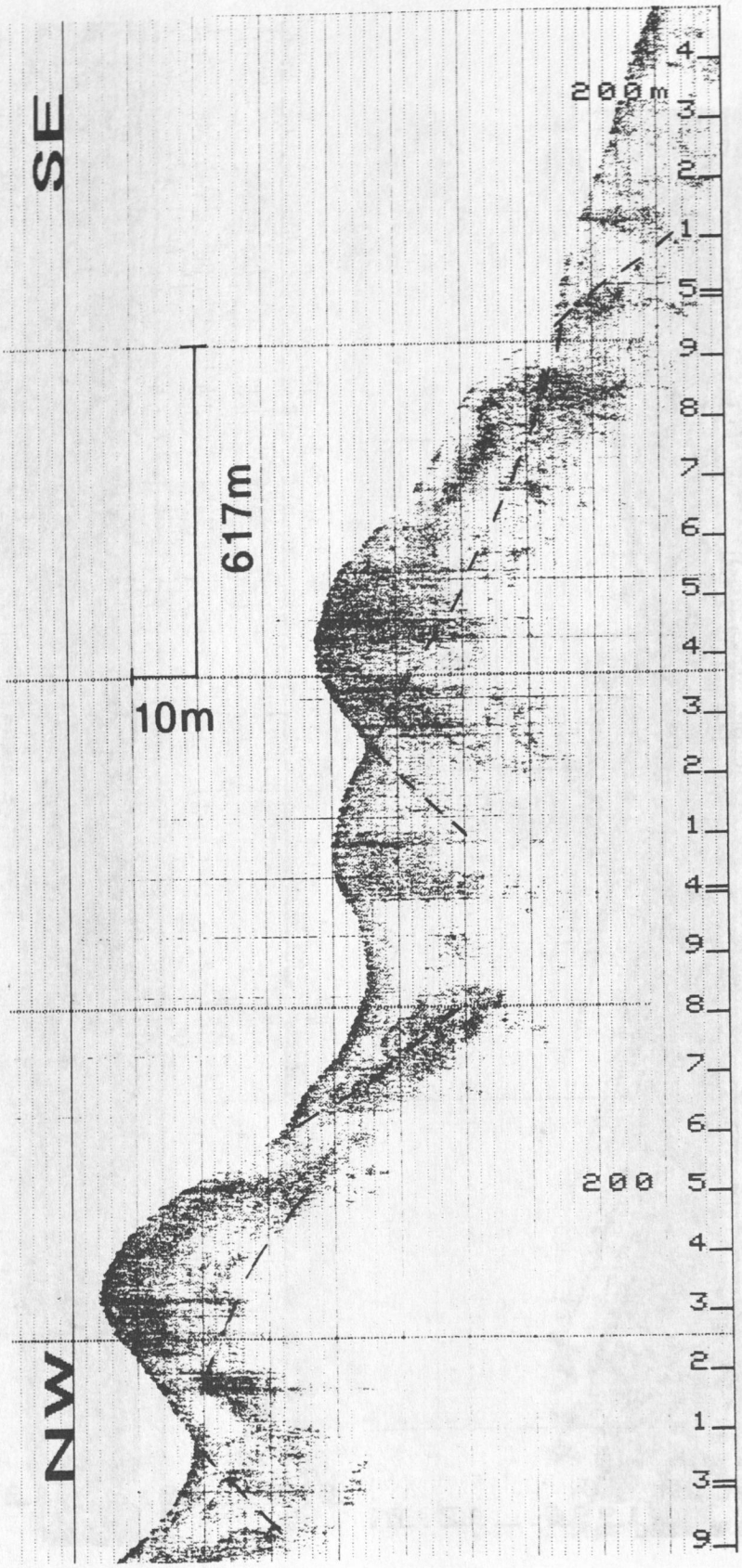

Figure 6.2.8: Slump structures on the shelf near OBS 27, Washington N-S profile.

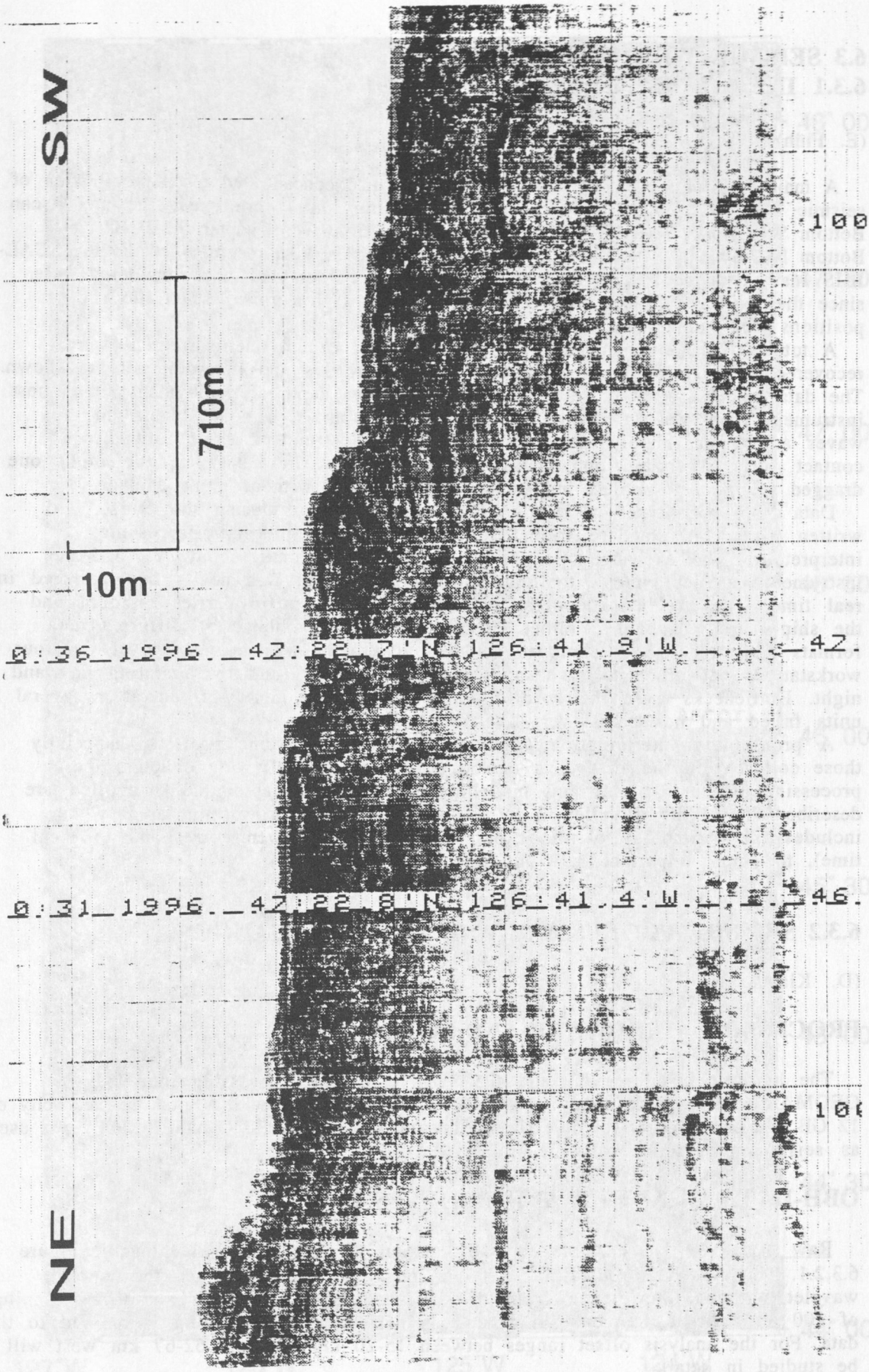

Figure 6.2.9: Fan sediments on the oceanic crust recorded while shooting the MCS Olympic line. Penetration depth up to more than 50m, water depth 2490m. In the upper part of the recorded section, layering and also turbiditic structures can be seen.

6.3 SEISMIC WIDE-ANGLE WORK
6.3.1 INTRODUCTION

(E. Flüh)

A major portion of the SO108 - ORWELL cruise concentrated on the collection of seismic wide-angle data. Three different recording units were used: the are Ocean Bottom Seismometers (OBS) of the USGS, Woods Hole (see Chapter 5.2.2), Ocean Bottom Hydrophones (OBH) of GEOMAR, and REFTEK land recorders of the PASSCAL-IRIS instrument pool. The data from the land recorders are not considered here, since they could only be analyzed after the end of the cruise, when the shot positions and timing are available.

A total of 116 deployments were made, and all except one instrument were recovered. In Figure 6.3.1.1 a summary of the profiles and recording site is shown. The data quality seems closely related to the water depth at deployment sites, most instruments deployed in shallow water suffered from high noise levels due to waves and boats, mainly fishing vessels. Twice instruments came into direct contact with fishermen, one instrument was brought into harbour, the other one dragged for about 4 miles, but both were recovered without great damage.

Data from both types of instruments were played out during the cruise, and written in SEG-Y standard format for data reduction, plotting, processing, interpretation and exchange. Despite the large data volume (about 400 MB per instrument per deployment, totaling 50 GB), this work was nearly accomplished in real time. The excellent cooperation between the scientific parties onboard and the ship´s crew enabled a rather smooth operation. Problems of different data formats and processing techniques could be overcome by making use of the four workstations networked to each other (see Chapter 5.1) and by operating day and night. Bottlenecks were the hard disks, which became nearly filled after several units failed and no spares were available.

A preliminary interpretation could be achieved for some profiles, especially those collected in the first days of the cruise. In the following chapters the processing (Chapter 6.3.2) and modelling techniques (Chapter 6.3.3) applied are described first. This is followed by a description of each working area, which includes the chronology of the experiment (all times given correspond to local time), the most important data and the first results.

6.3.2 SEISMIC PROCESSING AND DATA EXCHANGE

(D. Klaeschen)

PROCESSING HARDWARE AND SOFTWARE

The hardware facilities onboard the SONNE for the processing included 2 GEOMAR SUN® workstations (Sparc 10/40 and Sparc LX) with a total disk capacity of 12 GB and one DAT drive for each workstation. GEOSYS (PRAKLA-SEISMOS) was used as seismic processing software.

OBH-DATA ANALYSIS AND PROCESSING

Raw data: As data example, the OBH station 17 for profile 7 is shown in Figure 6.3.2.1. This was deployed with a 1700 m long anchor line to study the source wavelet without interference from the seafloor reflection. Here an offset binning of 100 m, a broad frequency filter and an offset-dependent scaling is applied to the data. For the analysis offset ranges between 15-20 km east and 62-67 km west will be studied in detail.

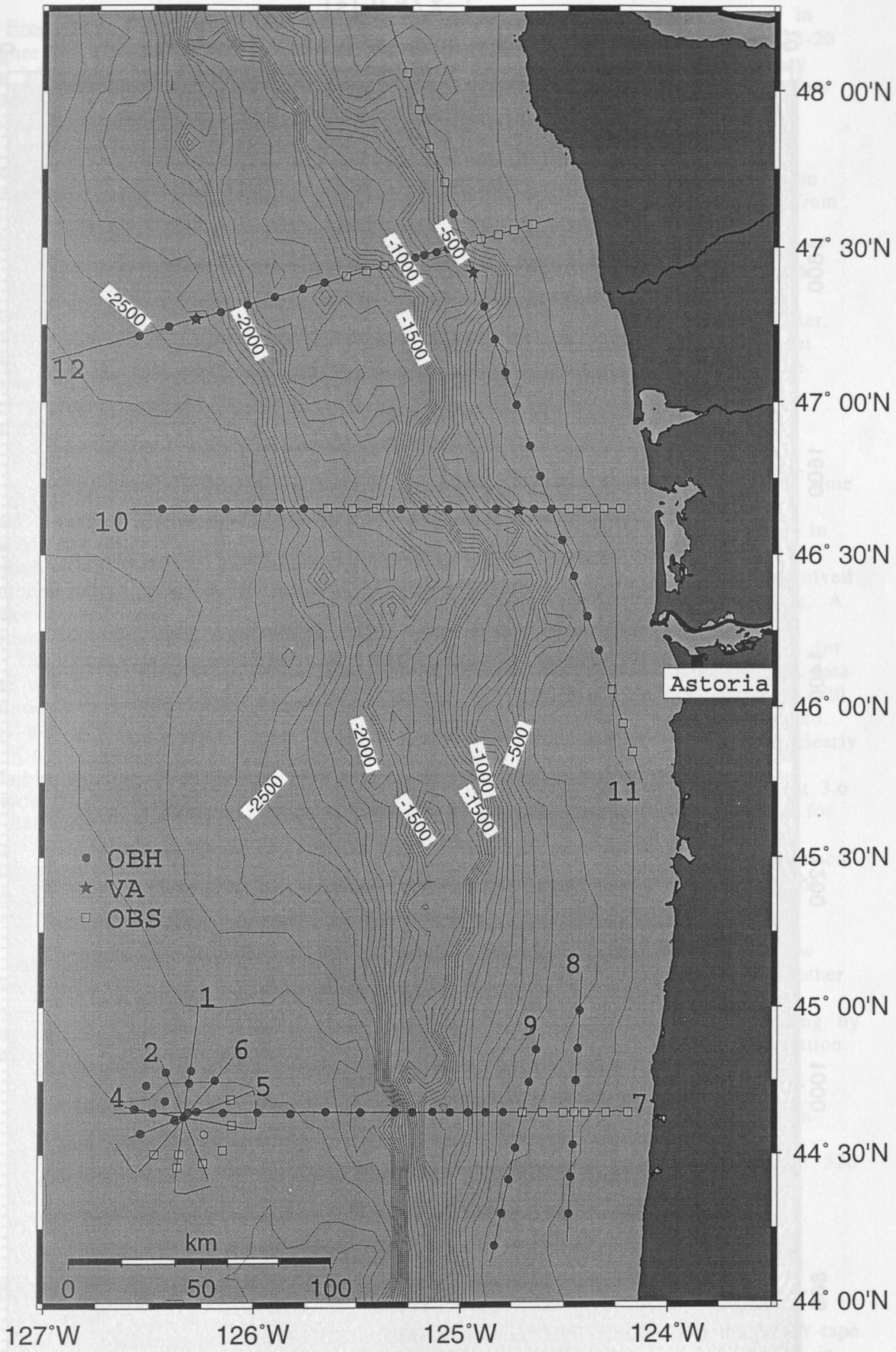

Figure 6.3.1.1: Map showing all wide-angle recording sites and profiles of the ORWELL Project.

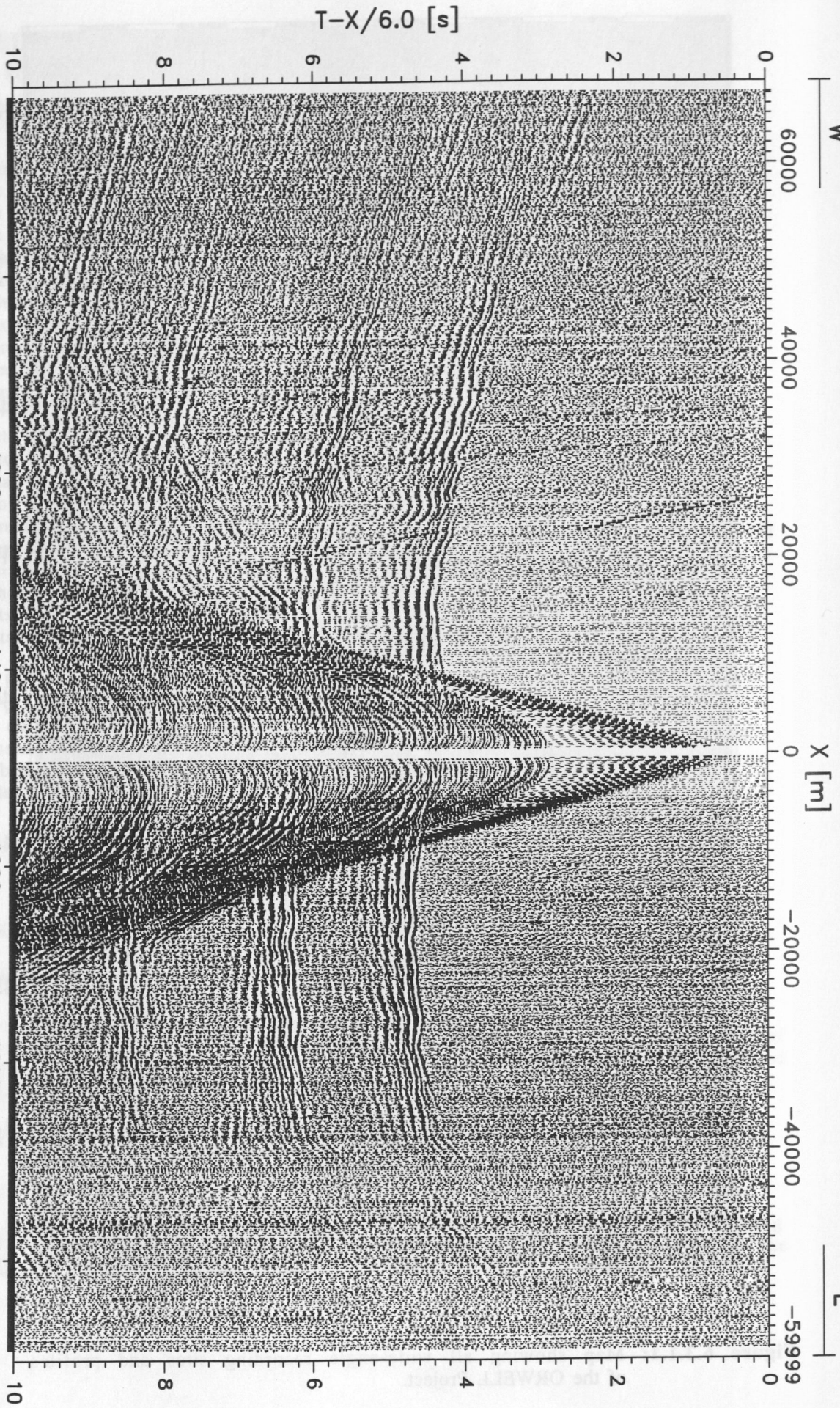

Figure 6.3.2.1: Raw data of OBH17 on profile 7.

Frequency filter test: To determine the frequencies of the seismic energy in Figure 6.3.2.2 and Figure 6.3.2.3 are shown filter panels for the offset range 15-20 km and 62-67 km respectively. The amplitude spectra of the Ormsby frequency filter operators are characterised by linear slopes. The filter is described by four corner frequencies:

Lower stop / pass band boundary and upper pass / stop band boundary. The frequencies on the filter panels correspond to the lower and upper pass frequencies. The main energy for the P_g phase at 3.6 s in the offset range from 15-20 km is between 5-23 Hz and for the P_n phase at 2.5 s in the offset range from 62-67 km between 5-10 Hz.

Deconvolution test: To improve the temporal resolution of the seismic data a deconvolution is applied to compress the basic seismic wavelet. The recorded wavelet has many components, including the source signature, recording filter, and hydrophone response. Ideally, deconvolution should compress the wavelet components and leaving only the earth's reflectivity in the seismic trace. The deconvolution algorithm which was applied is the Wiener deconvolution in sucessive trace segments which is based on the following assumptions:

1. The earth's reflectivity is 'white'.
2. The wavelet shows the minimum-delay phase behavier.

As in wide-angle data the amplitude spectra of the seismic traces vary with time and offset, the deconvolution must be able to follow these time and offset variations. Each trace is therefore devided into 2 s data gates with 1 s overlap, in which time invariant deconvolution operators are computed from the autocorrelation function of the data segment and applied. The overall deconvolved trace results from a weighted merging of the independently deconvolved gates. A removable AGC of 2 s is applied to the traces to keep relative amplitudes.

The deconvolution test panels are shown in Figure 6.3.2.4 and Figure 6.3.2.5 for the offset range 15-20 km and 62-67 km respectively. In the last second of the data window the autorrelation function is appended. A constant operator length of 320 ms and a variation of the predictive length from 0 (spike) to 240 ms is displayed.

On the undeconvolved data in Figure 6.3.2.4 reverberations of 150 ms are clearly visible in the autocorrelation function. The best resolution is obtained for a predictive length of 0 ms. Here a P_mP reflection at 3.75 s below the P_g phase at 3.6 s can now be identified. After deconvolution a Butterworth filter was applied for the final data representation. This filter is showing only a small amount of ringing compared to other filter technics. The Butterworth filter is characterised by a lower and upper cornerfrequency of 3 and 26 Hz. At these frequencies the amplitude are reduced by a factor of 0.5.

Processed data: Comparison of the processed data in Figure 6.3.2.6 to the raw data in Figure 6.3.2.1 shows a clear separation of P_g and P_mP phases. On the other hand, weak events in the raw data may be lost by the deconvolution process especially on the far offset traces. For the picking of events and model building by raytracing both sections must be used to keep all the aviable seismic information.

Processing sequence:

- Input: SEGY-data, 5 ms sample rate with complete geometry information
- Ormsby frequency filter: 4/8-30/40 Hz
- Gated Wiener deconvolution: gate length 2s, overlap 1 s, operater length 320 ms, prediction interval 0 ms (spike)
- Offset binning and stacking: bin width between 100 and 200 m
- Butterworth frequency filter: 3-26 Hz

DATA EXCHANGE

For the exchange between the OBH (GEOMAR) and OBS (USGS) data the SEGY-tape format on DAT was choosen. The complete geometry information is positioned in SEGY-trace header:

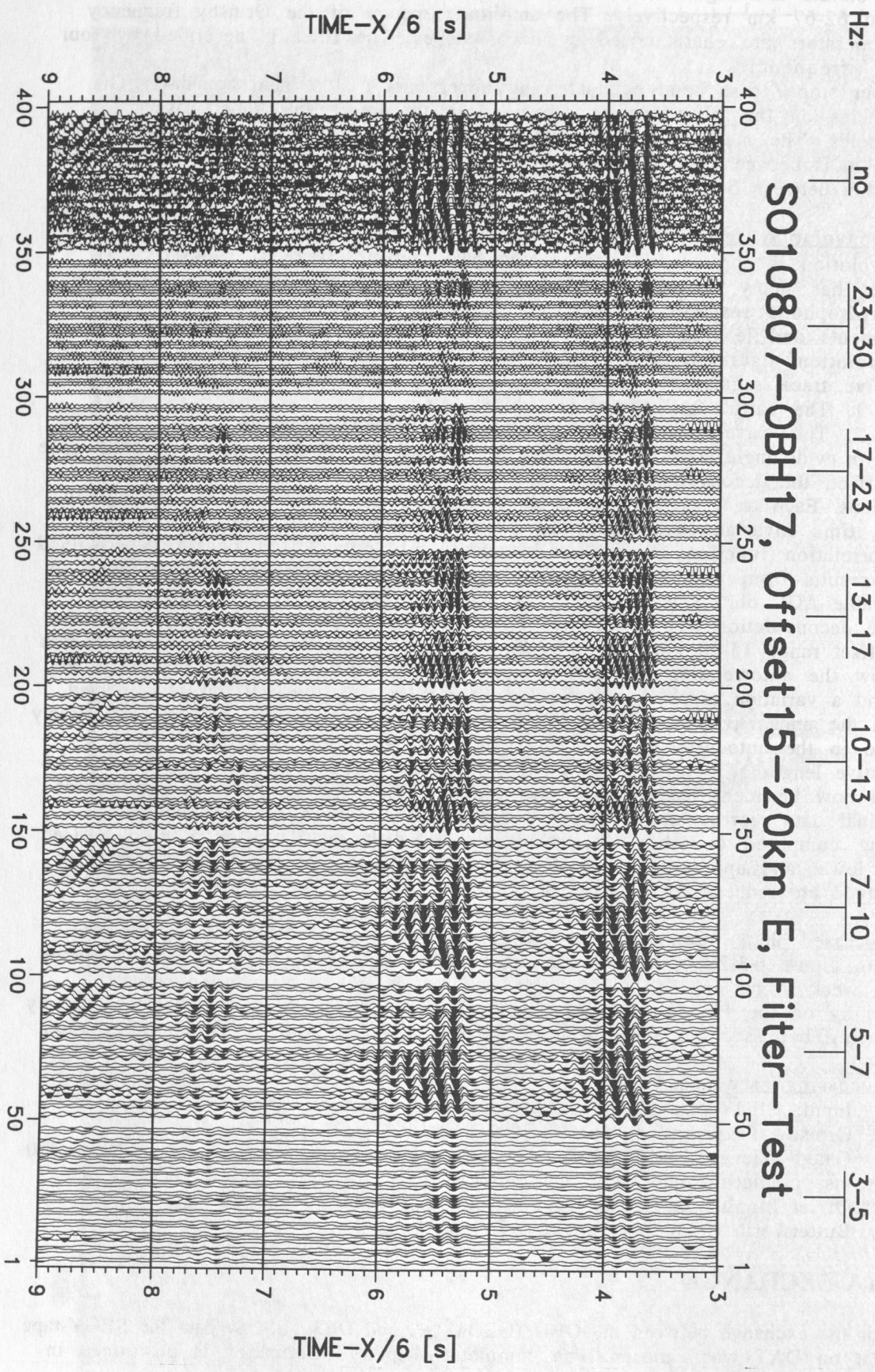

Figure 6.3.2.2: Filter test panels in the offset range 15-20 km East.

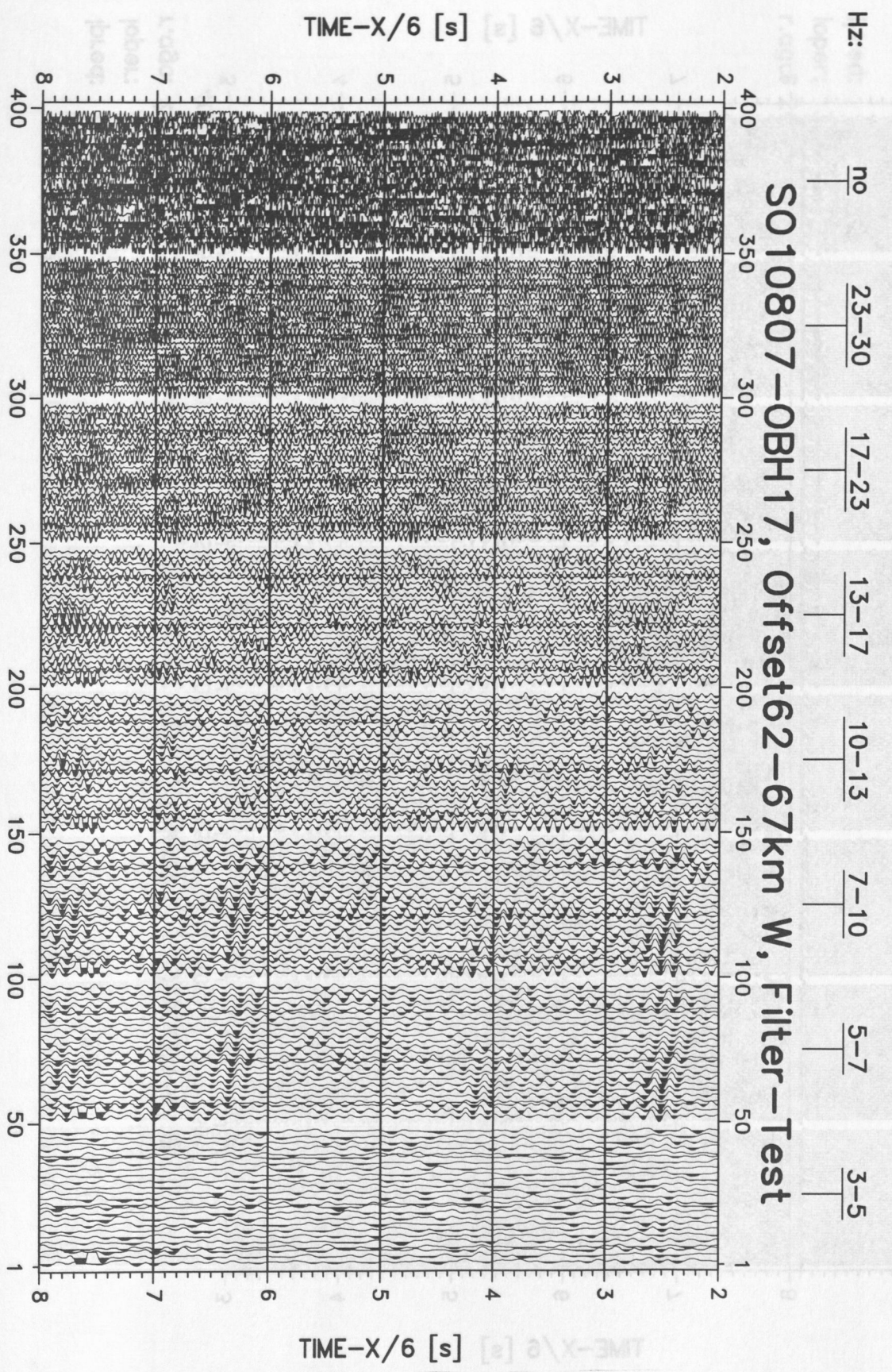

Figure 6.3.2.3: Filter test panels in the offset range 62-67 km West.

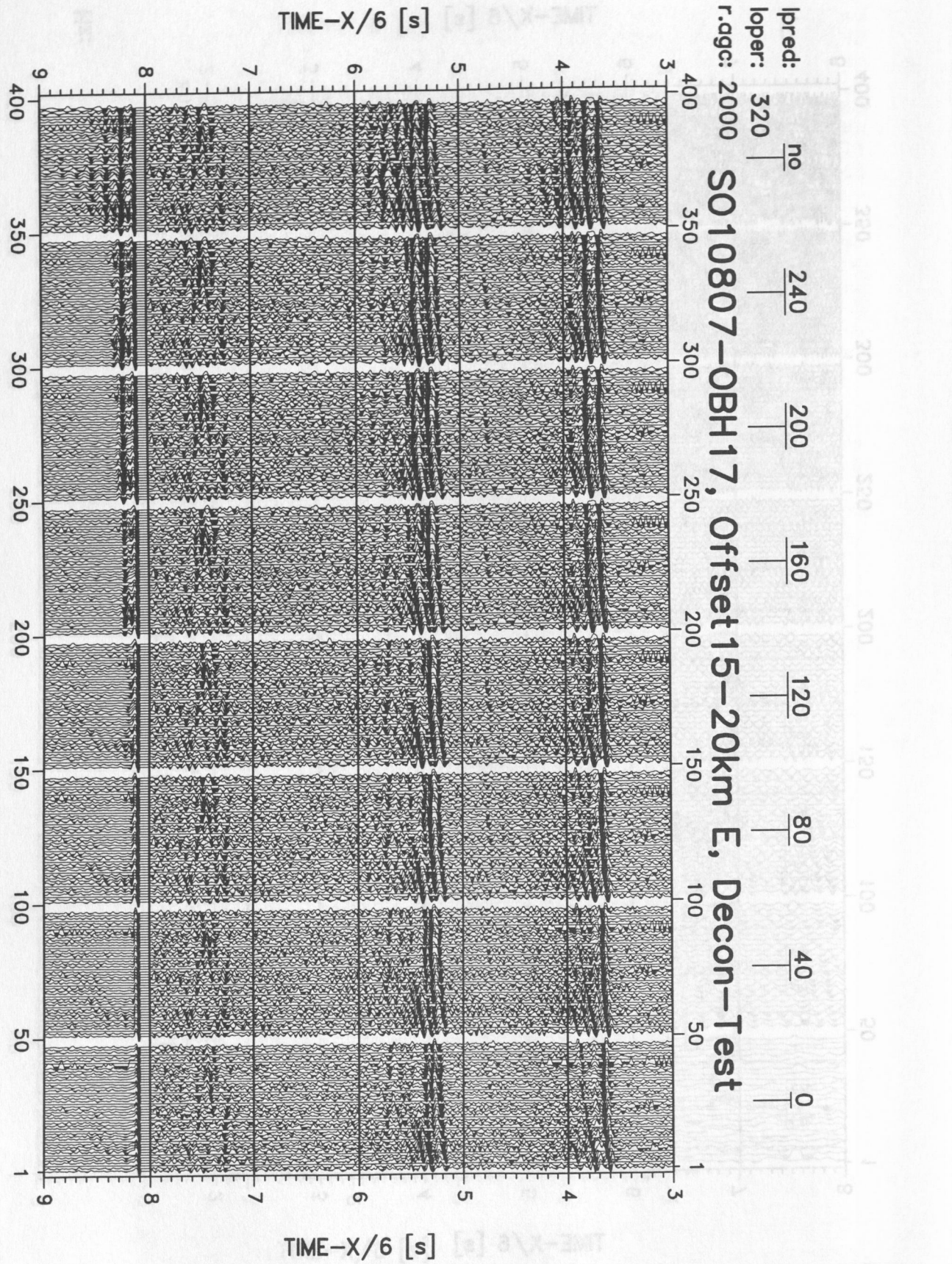

Figure 6.3.2.4: Deconvolution test in the offset range 15-20 km East.

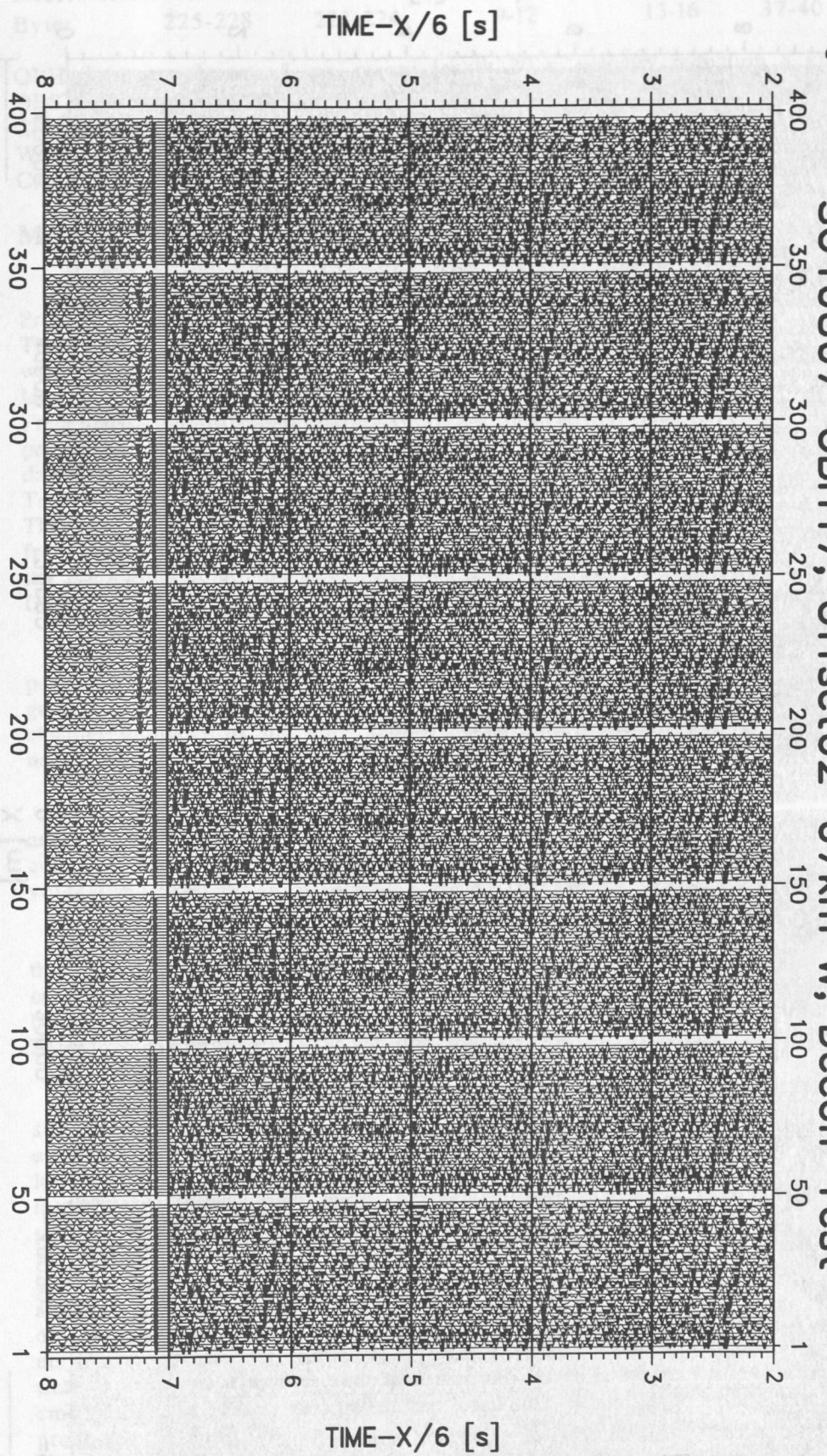

Figure 6.3.2.5: Deconvolution test in the offset range 62-67 km West.

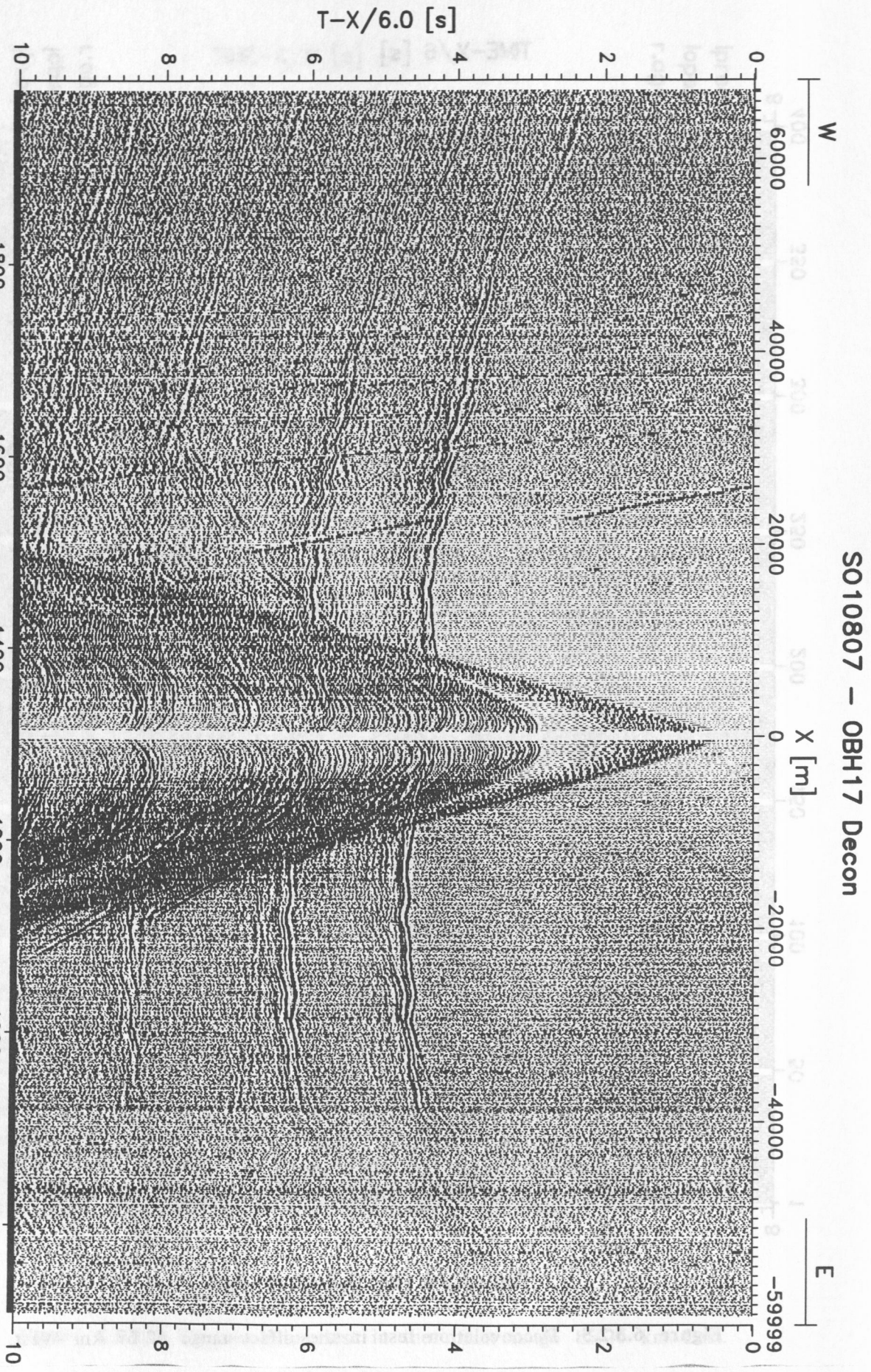

Figure 6.3.2.6: Processed data of OBH17 on profile 7.

Information:	Profile No.	Receiver No.	Channel. No.	Shot No.	Offset
Byte:	225-228	221-224	9-12	13-16	37-40

OBH data: sample rate 5 ms, record length 20 s, velocity reduction 8 km/s.
OBS data: sample rate 10 ms, record length 60 s, no velocity reduction.
Convention for the sign of the offsets depending of the shooting direction: W(-) -> E(+), E(+) -> W(-), N(+) -> S(-), S(-) -> N(+).
Convention for alpha numeric OBS reciever stations: A=1, B=2,.... i.e. C2=32.

MCS-DATA ANALYSIS AND PROCESSING

Raw data: The raw field tapes were demultiplexed by the USGS-group on the ProMax system and copied as SEGY-data to DAT. Each field record contains 48 traces. The original field-file number was checked against aquisition gaps and and written as a shot-record number into the trace header of byte 181-184. The data length was 16 s sampled at 4 ms.
Frequency spectra analysis shows that no significant energy above 60 Hz is present in the raw data, so that resampling to 8 ms was done simultaneously with data copy from DAT to disk.
To define the aquisition geometry a constant shotpoint distance of 50 was assumed. The near trace (channel 48) of the 48 channels with 50 m spacing had a distance from the source of 190 m for profile 101 and 198 m for profile 103 respectively. For the cmp binning a bin width of 25 m was defined resulting in a coverage of 24 fold.

Quality control: To have a representative data sampling of a complete aquisition profile a near-trace section, shot gathers with an increment of 48 shots and cmp gathers with an increment of 49 cmps were plotted (to display even and odd channel numbers in the cmp gathers). The data quality is good with high signal to noise ratio.

Velocity analysis: Based on the near-trace section the positions for the velocity analysis were defined. At 14 positions on profile 101 and 16 positions on profile 103 constant velocity stacks of cmp groups were analysed to define the stacking velocities.

Brute stack: Before stacking the data an outer-trace mute was applied to remove the water wave in the parts of the seismic profiles over shallow water. A trace AGC of 3 s was used for trace equalization. After stacking a time variant Butterworth filter and a time variant scaling was applied before plotting. The brute stack in Figure 6.3.2.7 shows strong multiple energy between 4 s and 5 s.

Mutiple suppression: As multiple energy cover the primary events a multiple supression process based on moveout differences between primary and multiple events was applied to the data. In Figure 6.3.2.8 a raw cmp gather is shown to the left. The multiple energy from the seafloor is seen below 4.3 s. The next panel to the right displays the same cmp gather after normal-moveout correction. The primary events are nearly horizontal whereas the multiple events show down dip. An additional time correction (dlt) leads the primary events to dip upward whereas the multiple energy still dips downward. Based on these differences in the apparent velocity an fk filter can be designed to remove only the downward dipping events. An application of such a filter is shown in the fk panel where most of the multiple energy below 4.3 s is removed. After removing the additional time correction (invdlt) and the normal-moveout correction (invnmo) the filtered cmp gather on the right panal represent the input cmp gather after the cascaded processes of multiple supression. Energy of multiples remains on the near traces where no moveout difference exist between primary and mutiple events. Here an inner-trace mute must be applied before stacking.

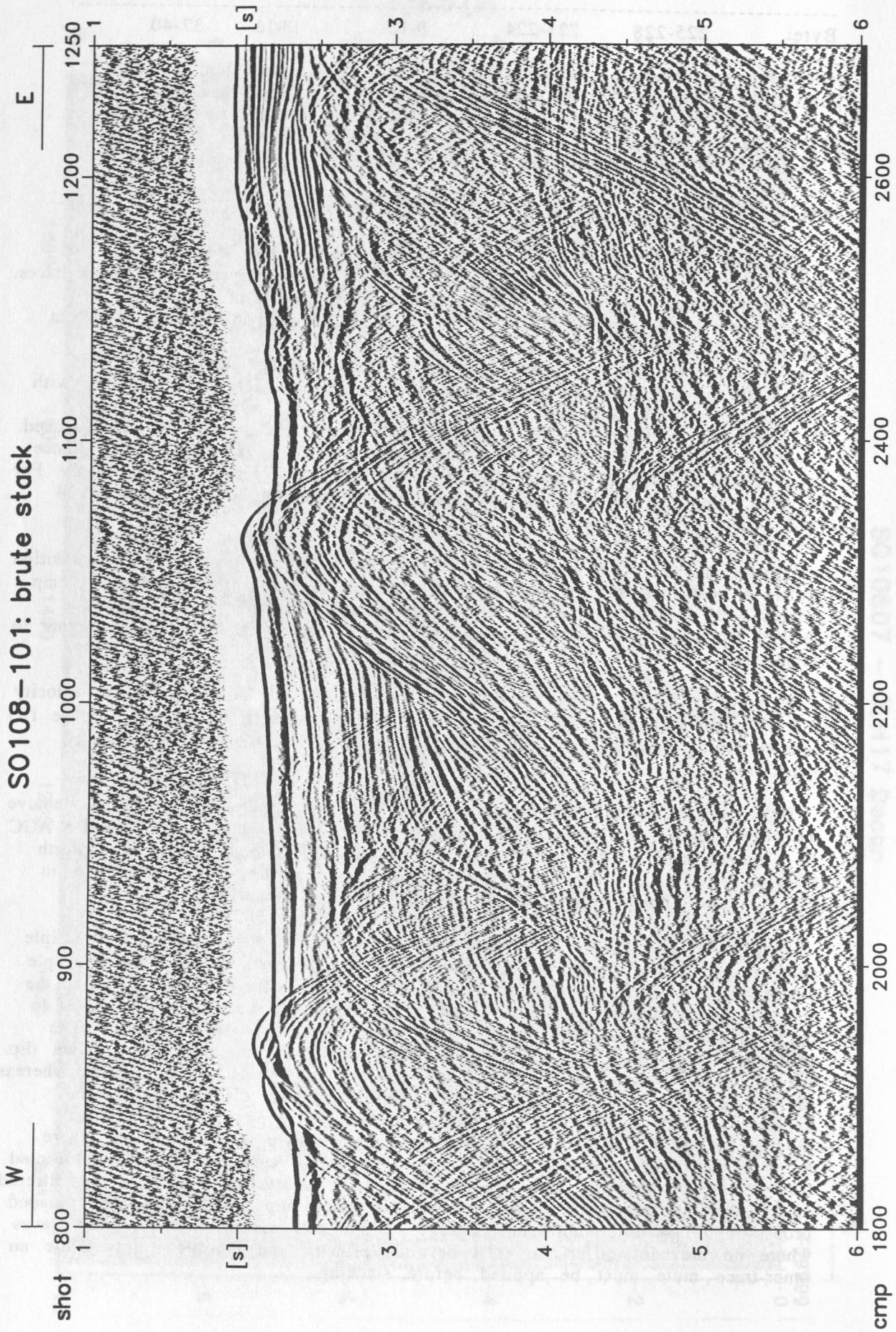

Figure 6.3.2.7: Brute stack of cmp 1800-2700 on profile 101.

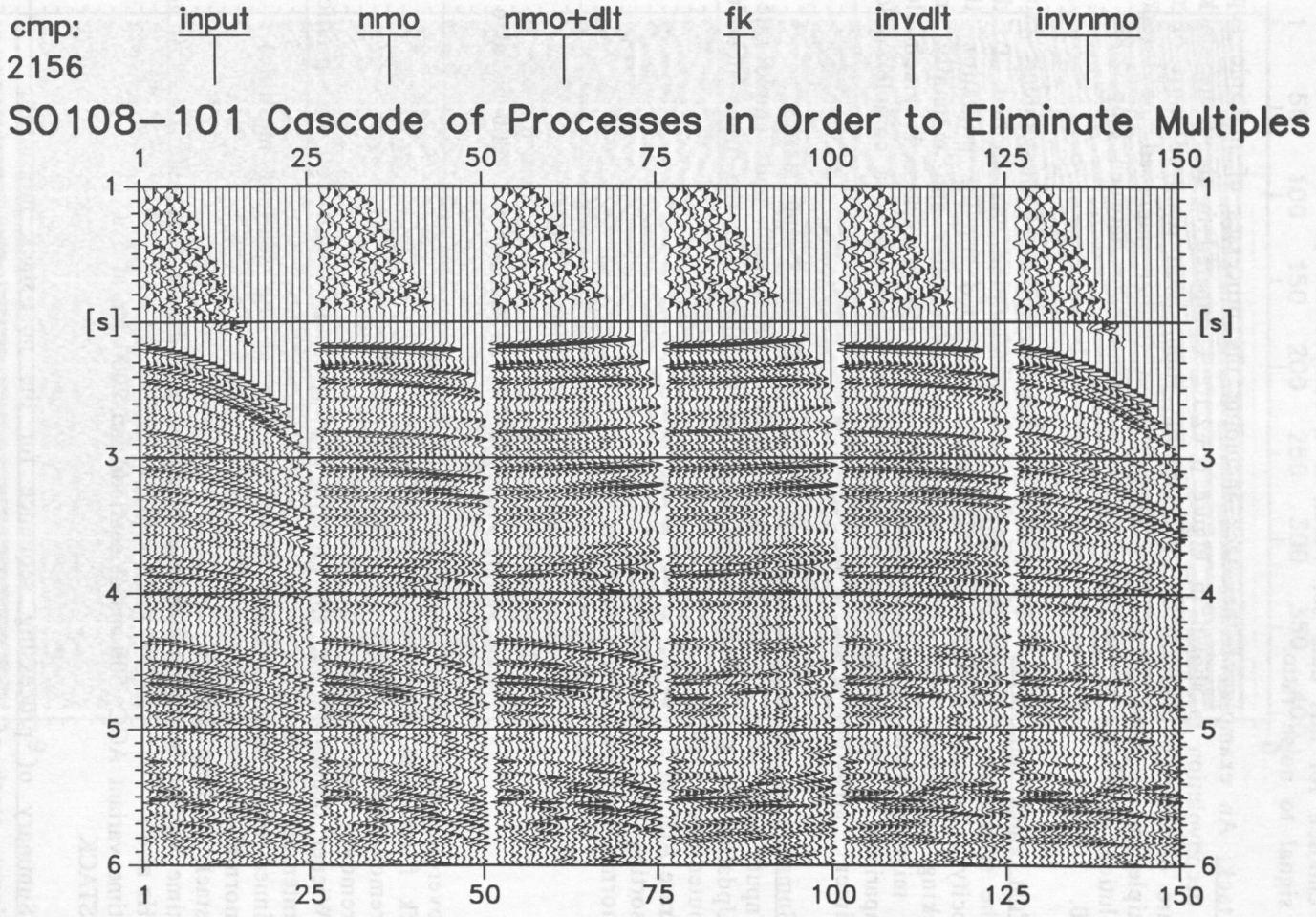

Figure 6.3.2.8: Suppression of multiple energy.

Deconvolution: To improve the temporal resolution of the seismic data a deconvolution is applied. For each trace a 2 s data gate below the seafloor was used to compute the deconvolution operators from the autocorrelation function of the data gate. In Figure 6.3.2.9 the deconvolution test panels are shown. In the last second of the data window the autocorrelation function is appended. A constant operator length of 160 ms and a variation of the predictive length from 0 ms (spike) to 240 ms is displayed.
Reverberation of 110 ms are clearly visable in the autocorrelation function on the undeconvolved data to the right on Figure 6.3.2.9. A predictive length of 160 ms was choosen for this data set which is a compromise between temporal resolution and signal to noise ratio.

Stack: An example of the stack including the processes of multiple suppression and deconvolution is shown in Figure 6.3.2.10. Compared to the brute stack in Figure 6.3.2.7 the processes of the multiple suppression removed most of the multiple energy below 4 s. The deconvoution further improved the temporal resolution especially of the upper most sediment layer between cmp 2000 and cmp 2200.

Post stack migration: As stacked data do not represent the geologic cross section if the subsurface structure is complex, a time migration was applied. To define the velocity information (macro model) which is needed for the migration, the stacking velocities were converted to interval velocities and manually smoothed. The migrated time section in Figure 6.3.2.11 of the subsurface is much clearer in comparison to the stacked data in Figure 6.3.2.10 and shows a complex folded sediment structure.

Summary of processing sequence of the brute stack and stack:

- Input: SEGY-data of shot-gathers with 48 channels each and sample rate of 8 ms
- Updating of the aquisition geometry information into the trace headers
- outer trace mute
- trace AGC of 3 s
- sorting into cmp gathers
- normal-moveout correction (nmo)
- stack of cmp gathers
- variant Butterworth frequency filter:
- 5-45 Hz at 4 s, 5-23 Hz at 6 s, and 5-25 Hz at 8 s
- time variant AGC: 500 ms at seafloor and 2000 ms at 6 s
- BRUTE STACK
- over-correction with delta time function (dlt)
- fk filter with time variant application
- remove over correction of delta time function (invdlt)
- remove nmo correction (invnmo)
- Wiener deconvolution: gate length 2 s, operator length 160 ms, prediction interval 160 ms
- inner trace mute (channel 44-48, starting at the seafloor multiple)
- normal-moveout correction (nmo)
- stack of cmp gathers
- time variant Butterworth frequency filter: 5-45 Hz at 4 s, 5-23 Hz at 6 s, and 5-25 Hz at 8 s
- time variant AGC: 500 ms at seafloor and 2000 ms at 6 s
- STACK

Summary of processing sequence for the post-stack migration:

- Input: stack of cmp gathers
- spatial and time variant application of fk filter (profile 103) to supress side swipes on the shelf area
- spatial and time variant weighting for the deeper section to supress long period mutiples
- finite-difference migration in space time domain (63 degree operator)
- spatial and time variant application of fk filter (profile 101) to supress migration noise

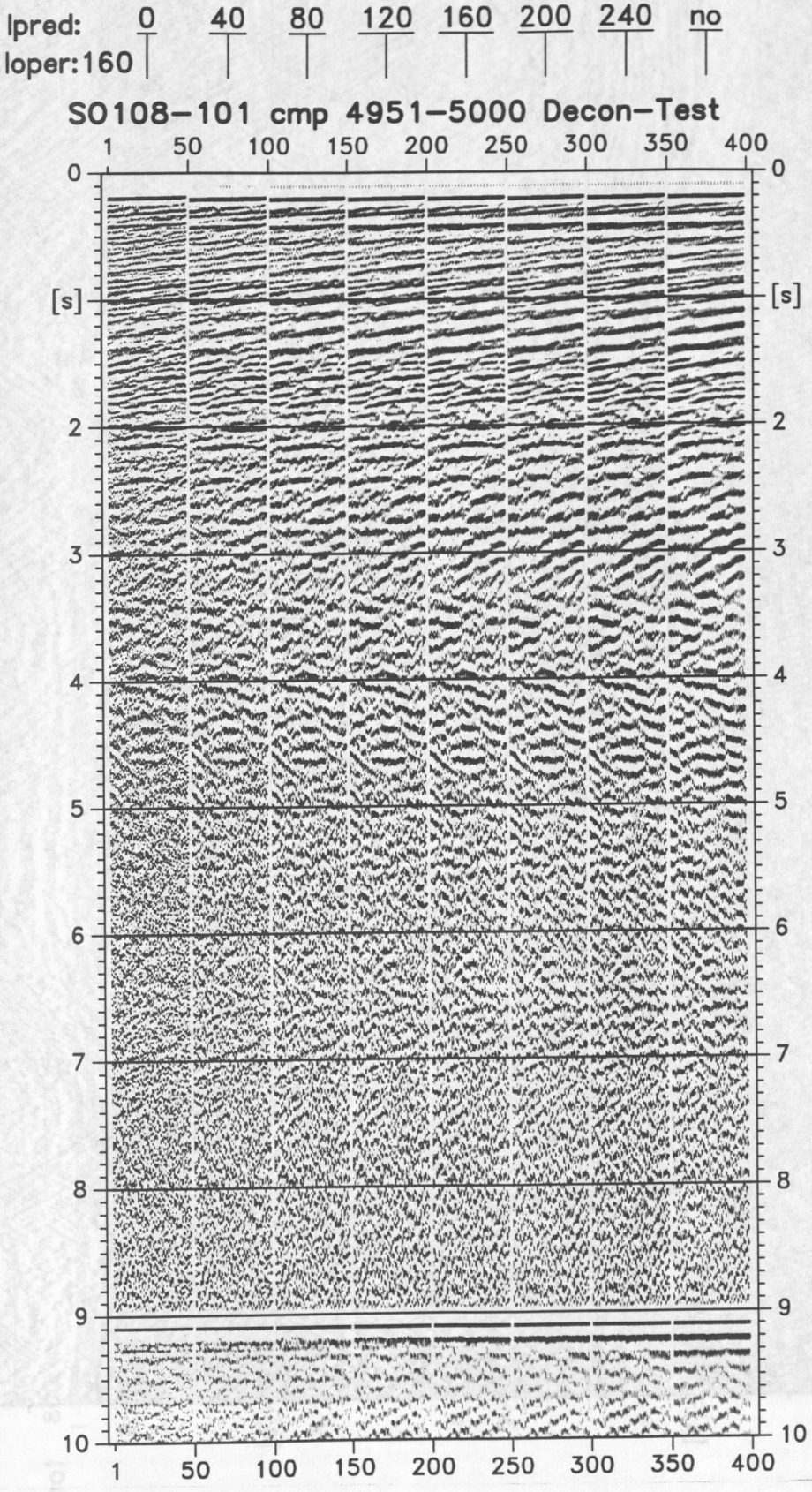

Figure 6.3.2.9: Deconvolution test panels on profile 101.

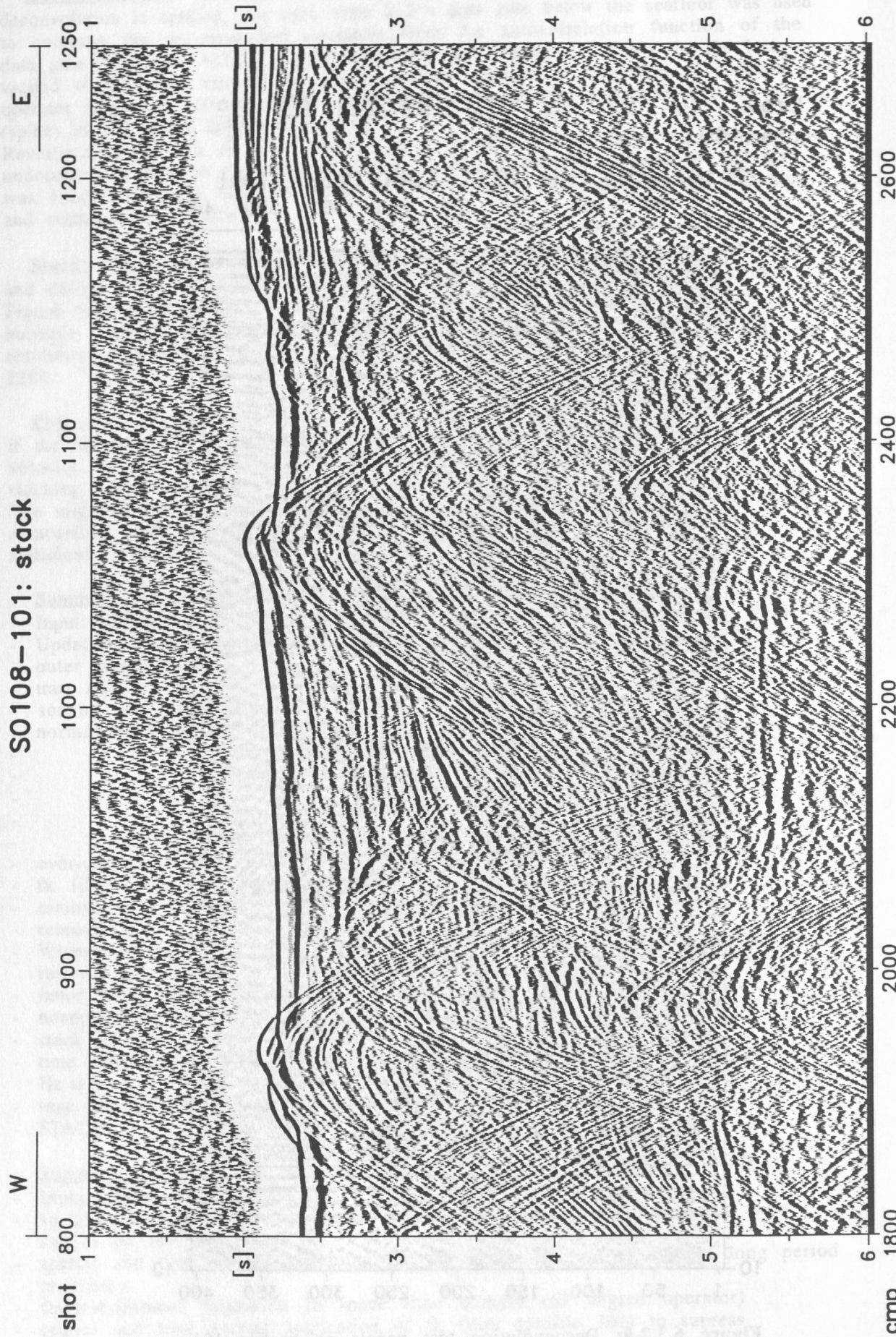

Figure 6.3.2.10: Stack of cmp 1800-2700 on profile 101.

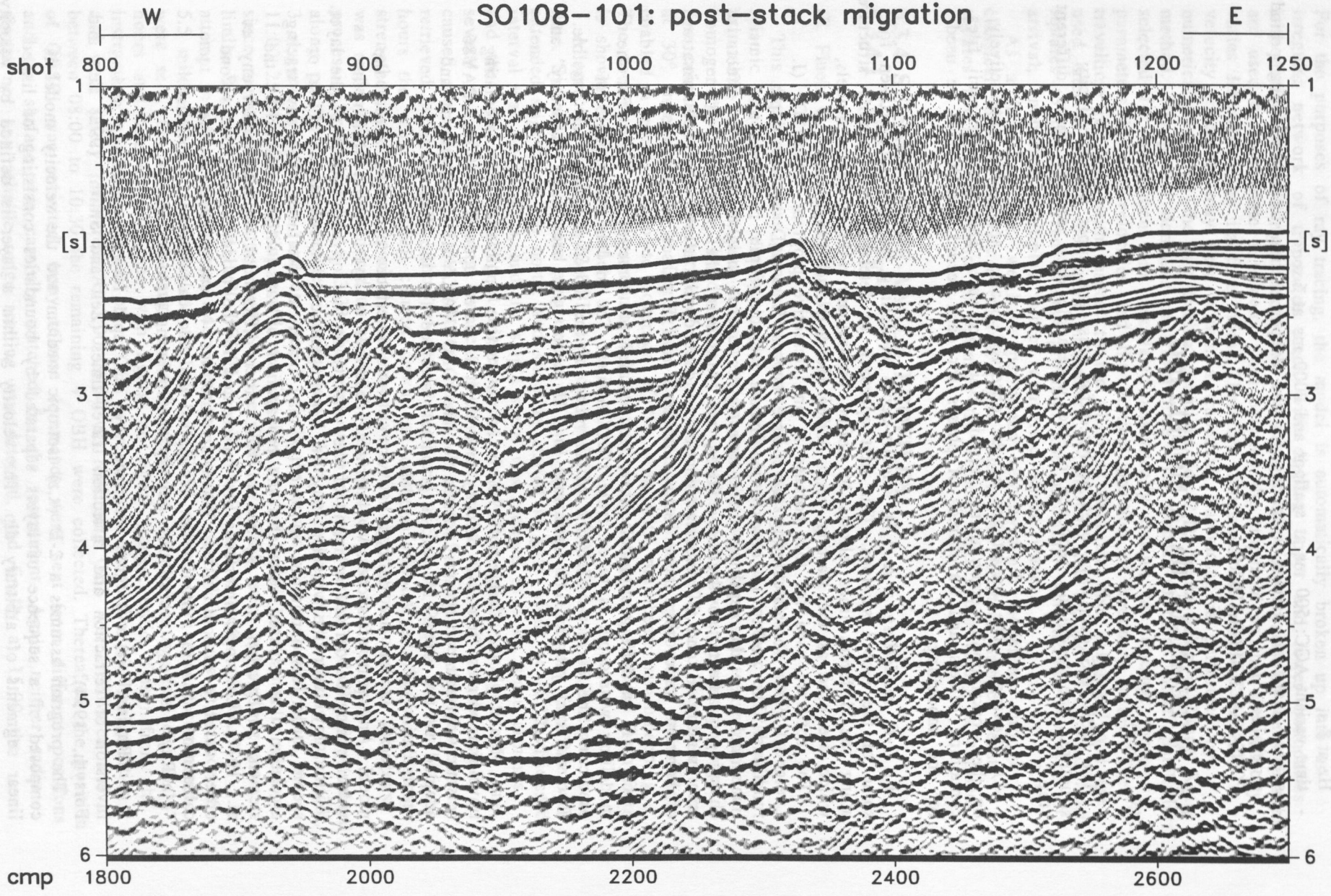

Figure 6.3.2.11: Post-stack migration of cmp 1800-2700 on profile 101.

- time variant Butterworth frequency filter: 5-45 Hz at 4 s, 5-23 Hz at 6 s, and 5-25 Hz at 8 s
- time variant AGC: 500 ms at seafloor and 2000 ms at 6 s
- spatial and time variant weighting for the deeper section to supress long period mutiples
- POST-STACK MIGRATION

6.3.3 WIDE-ANGLE DATA MODELLING

(N. Vidal)

The OBH/OBS data have been analyzed for crust and upper mantle velocity structure. The modelling sequence of the wide-angle data involves three different steps:

A) Picking : The traveltimes of the observed phases are picked interactively on the workstation's screen using Seismic Unix Software. This provides ascii files, containing offsets and traveltimes of phases for each record, which will be used for the modelling.

B) 1-D modelling : A 1-D velocity-depth modelling has been undertaken for some of the record sections. This first approach to determine the velocity structure along the different lines allows to define preliminary velocity-depth models, which are used as the starting point during the 2-D modelling.

The software used for this porpuse is an interactive program "MacR1D" (J. Luetgert, 1992) for calculating travel-time curves from 1-D velocity-depth functions. The ability to quickly manipulate velocity-depth functions and inmediately see the resulting travel-times gives useful insights into the effects of changing gradients, low-velocity zones, etc. Moreover, the possibility of manipulating P and S velocity functions independently allows the determination of Poisson's ratio from those sections where P and S phases are observed.

C) 2-D modelling : Models have been created for some of the lines. For the modelling waterdepth is taken from UKOOA-files. The models are capable of predicting the correct offset/time of as many of the observed phases as possible. Two different programs to trace rays in 2-D media have been used: "MacRay" and "Rayinvr".

-- "MacRay" (J. Luetgert, 1992) is an interactive application for calculating travel-time curves from 2-D velocity models. It is based upon RAY84 and RAY86 seismic raytracing programs written for the DEC VAX/VMS environment and adapted to the Apple Macintosh graphical interface for the display and manipulation of the velocity models.

Velocity models are defined by two or more interfaces extending across the model. Any pair of successive interfaces describes a layer, within which the velocity may be defined in terms of the velocity at the top and bottom of the layer. Within any layer the velocity may be inhomogeneous but continuous. First or second order discontinuities in velocity may occur at interfaces. The ray tracing algorithm that is used calculates the propagation of rays within a layer by the stepwise integration of a system of first order differential equations (Cerveny et al., 1977). Lithologic interfaces are represented in the model as first or second order velocity discontinuities. When an interface is encountered in the calculation of a ray, Snell's law is applied and the calculation is continued. "MacRay" is very usefull for quickly manipulating velocity models.

-- "Rayinvr" is a program to trace rays for rapid forward modelling and inversion of refraction and reflection travel times (Zelt and Smith, 1992; Zelt and Forsyth, 1994).

The program assumes a 2-D (x,z) isotropic medium and the velocity model is composed of a sequence of layers separated by boundaries consisting of linked linear segments of arbitrary dip. The velocity within a layer is defined by velocity

values specified at arbitrary x-coordinates along the top an bottom of the layer. For the purposes of ray tracing, the model is automatically broken up into an irregular network of trapezoids, each with dipping upper and lower boundaries and vertical left and right sides. The velocities at the four corners of the trapezoid are used to interpolate a velocity field between the trapezoid so that the velocity varies linearly along its four sides. Therefore, horizontal as well as vertical velocity gradients may exist within a trapezoid. Raytracing is performed by numerically solving the ray tracing equations for 2-D media using a Runge Kutta method. The partial derivates of travel time with respect to those model parameters selected for adjustment are calculated analytically during ray tracing; these parameters include velocities and the vertical position of boundary nodes. The traveltime residuals with respect to the observed data are also calculated and are used later to update the model parameters by applying the method of damped least-squares to the linearized inverse problem. The algorithm can include any type of arrival, including multiples and/or converted shear waves.

As a first approach, we have performed velocity-depth modelling through classical forward analysis of arrival times. Finally, an iterative damped least-squares inversion procedure to optimize the velocity and depth values is applied.

6.3.4 SEISMIC WIDE-ANGLE PROFILES
6.3.4.1 THE ROSETTE

(E. Flueh, C. Kopp, U. ten Brink, and J. Fest)

This experiment was planned to consist of 6 crossing profiles to study the seismic structure and velocity of the oceanic crust and its intrinsic lateral and azimuthal variations. It was choosen in an aera that was supposed to be rather homogeneous and flat. The direction of the profiles was choosen such, that one line coincides with the strike of the magnetic lineations (10°), and the others are at 30° increments to it. During the operation, continuous hydrosweep recording enabled a nearly complete coverage of the area with multibeam swathmapping. The location of the instruments and seismic profiles together with the bathymetry is shown in Figure 6.3.4.1.1.

Altogether 8 OBS and 12 OBH were deployed from 23:00 21.04. to 13:00 22.04. local time. Since the OBS were programmed to start recording at 18:00, the first line was extended slightly to the north, and shooting started in gale winds at 16:12. The shot interval was set to 45 s, and the ship's speed was reduced to 4 kn, since airhoses and the wire were tangling at higher speed. Soon after the beginning of the line, several guns failed. During the next hours wind speed increased and the swell caused more damage to the airhoses. Finally, in force 9 winds the arrays were retrieved at 11:00 23.04., short of the intended end of line 2. During the next 26 hours the wind and swell calmed down and repair of the airgun array, including strengthening the hose package and modifying the rigging of some of the guns was made. OBH12 was picked up at 10:20 24.04. to check the data and study processing parameters. At 13:30 the guns were deployed again and shooting started along profile 4 in moderately rough seas. With increasing winds during the night, 3 airguns dropped out, and at force 8 winds the arrays were retrieved again at 11:00 25.04. after finishing profile 6. The last planned profile could not be made, since recording and battery supply of the OBH and OBS were approaching their limits. Between 14:00 and 19:30 OBH02, 11, 10, 09, 07 and 06 were retrieved. An attempt to release OBS01 was made after the recovery of OBH06 from a distance of 5.5 miles, but not confirmed. At the site of OBS01 several more release commands were sent, but no reliable range could be read and despite waiting for several hours and searching the sea with lights, no signal (range, radio, flash) from the instrument was detected. All other OBS were released from the previous position and were safely recovered. At 7:00 26.04. all remaining OBS were recovered and between 08:00 to 10:30 the remaining 4 OBH were collected. Thereafter, the position of OBS01 was revisited, many release commands were sent from different positions and the surface was carefully watched for the instrument. Again neither radio signal nor any reliable range reading was detected, and finally at 15:00 the instrument was sadly given up.

Due to downtime and some unknown reasons, about half of the OBH did not record all profiles, and one instrument refused to record any data at all. Detailed information about the positions and instrument codes are given in the appendix. In Figure 6.3.4.1.2 the desired (top) and the actual coverage (bottom) obtained are shown, including data from the Oregon dip line (profile 7), which was shot later. Due to downtime and instrument failure, the 3-D inversion of the experiment will not be obtained as desired.

Following the routines described in Chapter 6.3.2, all data were processed. Some record sections are shown in Figures 6.3.4.1.3 to 6.3.4.1.16. The record sections obtained using the hydrophon channel of the OBS are similar to those obtained from the OBH. The vertical and horizontal components of the OBS provide additional information on the nature of the individual phases. In Figure 6.3.4.1.17 all for channels from OBS05 recording profile 1 are shown for comparison.

The amplitude of the P-wave first arrivals is strong on the vertical geophone and the hydrophone and is weak or missing on the horizontal geophones. The hydrophone channel shows strong water multiples whereas the geophones channels, in particular the horizontals have strong pegleg multiples and weak water multiples. (The pegleg multiples are arrivals which bounce within the sedimentary layer either under the source or under the receiver). The converted P-to-S- wave arrivals are similar to the first arrivals. They are clear on the vertical geophone and the hydrophone but are missing on the horizontals. Their pegleg on the other hand has a strong amplitude on the horizontals. The P-to-S converted waves are not expected to be stronger on the horizontal channels than on the vertical channel or the hydrophone, because they also emerge as P-waves. The peglegs may be better detected by the horizontal channels than by the vertical geophone or hydrophone either because their angle of emergence is low, or because the peglegs are vibrations of the sediment layers, which cause the OBS to rock and tilt. The hydrophone, on the other hand, always shows a water multiple that is stronger than the first arrival due to constructive interference of the downgoing wavefield and the seafloor reflection travelling upwards.

The peglegs are probably amplified by the constructive interference between bounces under the source and bounces under the receiver, which occurs when the sediment thickness and velocity are uniform across an area. Another cause for amplification is resonance. If the seismic waves have frequencies similar to the characteristic frequency of the layer, the layer may resonate. Note that while the frequency of the first arrivals is fairly broad, the peglegs have a narrow frequency band of about 6-8 Hz (Figure 6.3.4.1.17). The sediment characteristic frequency is defined by its thickness and velocity, $f = 4v/l$ where v is the velocity and l is the layer thickness. Because $TWTT = 2l/v$, the resonant frequency $f = 8/TWTT$. The sediment TWTT around OBS05 in the Rosette experiment was 1.0-1.3 s, hence, f = 6-8 Hz.

Records from other environments also show differences among the four components (e.g., Figure 6.4.3.5.4). Where peglegs are not generated (e.g., high velocity sediments), the horizontal records show good quality first arrivals. In shallow waters they sometimes even record the first arrivals with a better signal-to-noise ratio than the vertical geophone and the hydrophone (e.g. Figure 6.3.4.5.11; Figure 6.3.4.4.19). The differences may not be due to the response of the different component to the signal, but rather due to their sensitivity to the ambient noise (waves, engine noise, etc.). The reason for the differences, we believe, is that the OBS can be considered as being embedded in two layers, the geophones being embedded in the sediment layer and the hydrophone in the water layer. If our assessment is correct, the different channels will produce different quality data in different environments. In deep water with soft sediments and high impedance contrast at the basement, water multiples do not contaminate the data of interest whereas peglegs do. In these environments the hydrophone may be advantageous. In shallow water and in hard bottom where water multiples are frequent and of high amplitude, the geophones may be advantageous. Horizontal geophones may also be less sensitive than the hydrophone to noise in the water column from nearby fishing vessels on the shelf.

On all sections, clear refractions from the oceanic crust and sometimes the upper mantle are seen, but the critical distance for PMP is highly variable from 19

Due to downtime and some unknown reasons, about half of the OBH did not record all profiles, and one instrument refused to record any data at all. Detailed information about the positions and instrument codes are given in the appendix. In Figure 6.3.4.1.2 the desired (top) and the actual coverage (bottom) obtained are shown, including data from the Oregon dip line (profile 7), which was shot later. Due to downtime and instrument failure, the 3-D inversion of the experiment will not be obtained as desired.

Following the routines described in Chapter 6.3.2, all data were processed. Some record sections are shown in Figures 6.3.4.1.3 to 6.3.4.1.16. The record sections obtained using the hydrophon channel of the OBS are similar to those obtained from the OBH. The vertical and horizontal components of the OBS provide additional information on the nature of the individual phases. In Figure 6.3.4.1.17 all for channels from OBS05 recording profile 1 are shown for comparison.

The amplitude of the P-wave first arrivals is strong on the vertical geophone and the hydrophone and is weak or missing on the horizontal geophones. The hydrophone channel shows strong water multiples whereas the geophones channels, in particular the horizontals have strong pegleg multiples and weak water multiples. (The pegleg multiples are arrivals which bounce within the sedimentary layer either under the source or under the receiver). The converted P-to-S- wave arrivals are similar to the first arrivals. They are clear on the vertical geophone and the hydrophone but are missing on the horizontals. Their pegleg on the other hand has a strong amplitude on the horizontals. The P-to-S converted waves are not expected to be stronger on the horizontal channels than on the vertical channel or the hydrophone, because they also emerge as P-waves. The peglegs may be better detected by the horizontal channels than by the vertical geophone or hydrophone either because their angle of emergence is low, or because the peglegs are vibrations of the sediment layers, which cause the OBS to rock and tilt. The hydrophone, on the other hand, always shows a water multiple that is stronger than the first arrival due to constructive interference of the downgoing wavefield and the seafloor reflection travelling upwards.

The peglegs are probably amplified by the constructive interference between bounces under the source and bounces under the receiver, which occurs when the sediment thickness and velocity are uniform across an area. Another cause for amplification is resonance. If the seismic waves have frequencies similar to the characteristic frequency of the layer, the layer may resonate. Note that while the frequency of the first arrivals is fairly broad, the peglegs have a narrow frequency band of about 6-8 Hz (Figure 6.3.4.1.17). The sediment characteristic frequency is defined by its thickness and velocity, $f = 4v/l$ where v is the velocity and l is the layer thickness. Because $TWT = 2l/v$, the resonant frequency $f = 8/TWT$. The sediment TWT around OBS05 in the Rosette experiment was 1.0-1.3 s, hence, f = 6-8 Hz.

Records from other environments also show differences among the four components (e.g., Figure 6.4.3.5.4). Where peglegs are not generated (e.g., high velocity sediments), the horizontal records show good quality first arrivals. In shallow waters they sometimes even record the first arrivals with a better signal-to-noise ratio than the vertical geophone and the hydrophone (e.g. Figure 6.3.4.5.11; Figure 6.3.4.4.19). The differences may not be due to the response of the different component to the signal, but rather due to their sensitivity to the ambient noise (waves, engine noise, etc.). The reason for the differences, we believe, is that the OBS can be considered as being embedded in two layers, the geophones being embedded in the sediment layer and the hydrophone in the water layer. If our assessment is correct, the different channels will produce different quality data in different environments. In deep water with soft sediments and high impedance contrast at the basement, water multiples do not contaminate the data of interest whereas peglegs do. In these environments the hydrophone may be advantageous. In shallow water and in hard bottom where water multiples are frequent and of high amplitude, the geophones may be advantageous. Horizontal geophones may also be less sensitive than the hydrophone to noise in the water column from nearby fishing vessels on the shelf.

On all sections, clear refractions from the oceanic crust and sometimes the upper mantle are seen, but the critical distance for PMP is highly variable from 19

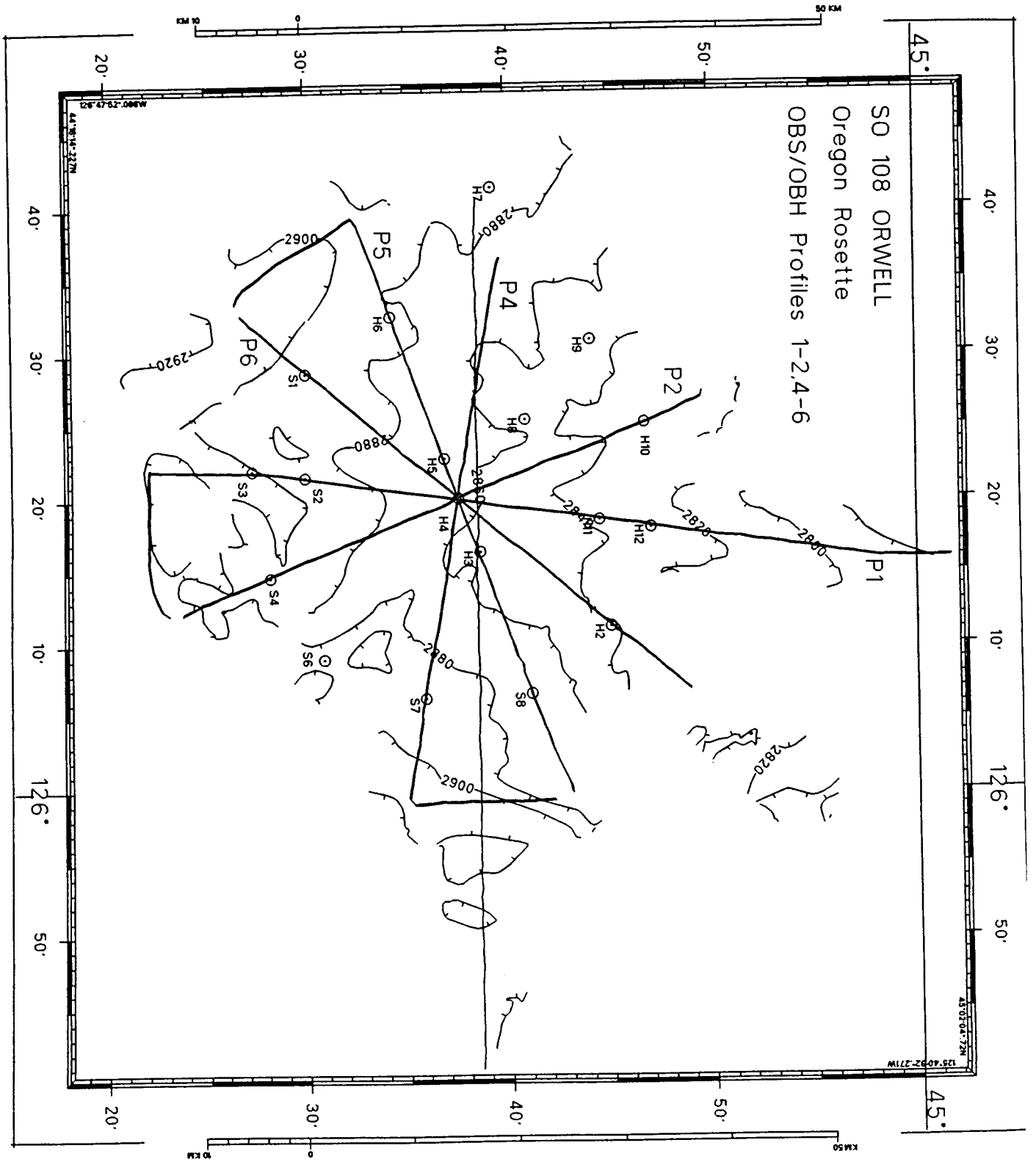

Figure 6.3.4.1.1: Location map of the Rosette area. Contour intervall 20 m. S* and H** mark OBS/OBH stations.

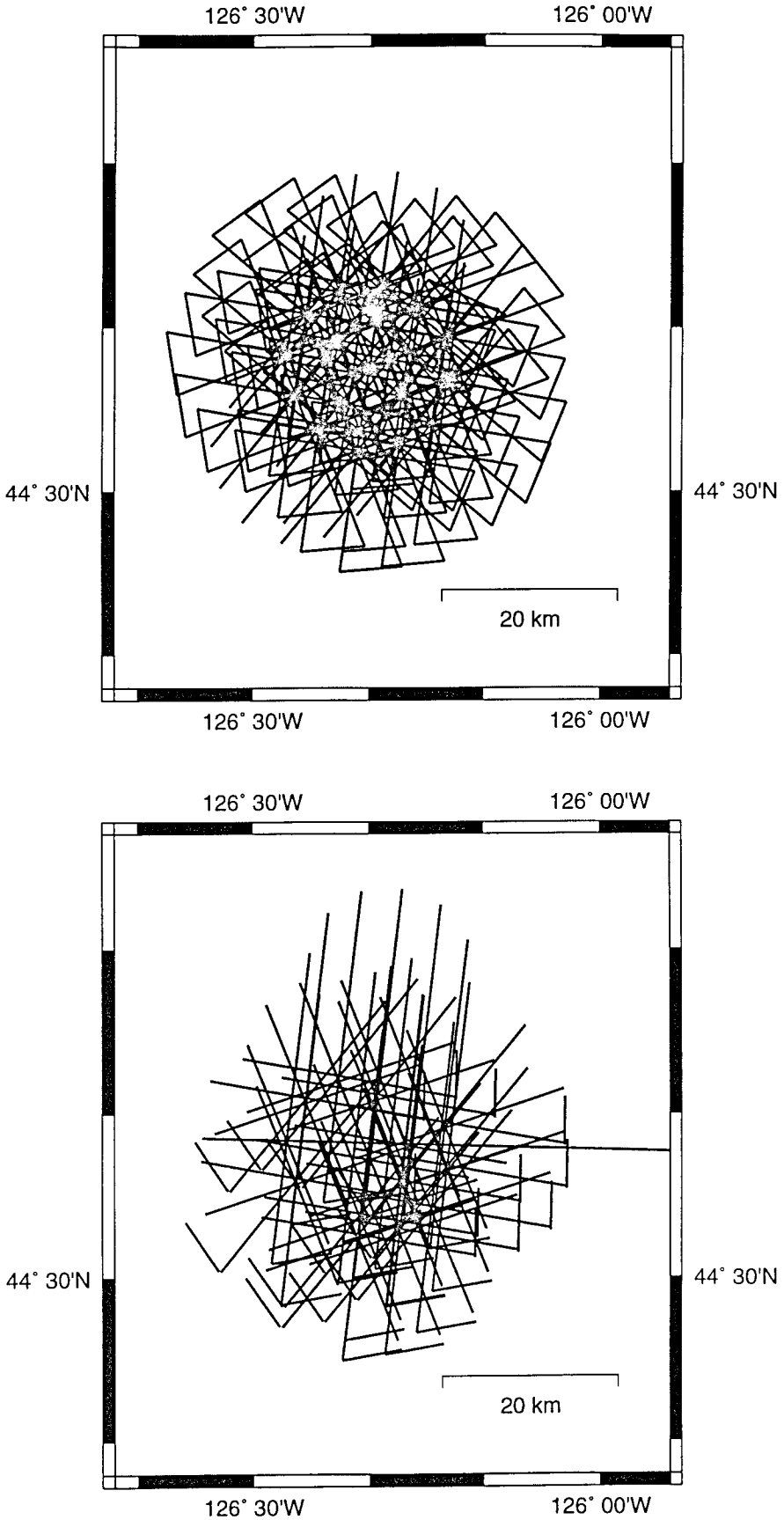

Figure 6.3.4.1.2: Midpoint coverage for the Rosette area. Top: desired coverage, bottom: achieved coverage including data from profile 7 (chapter 6.3.4.2) .

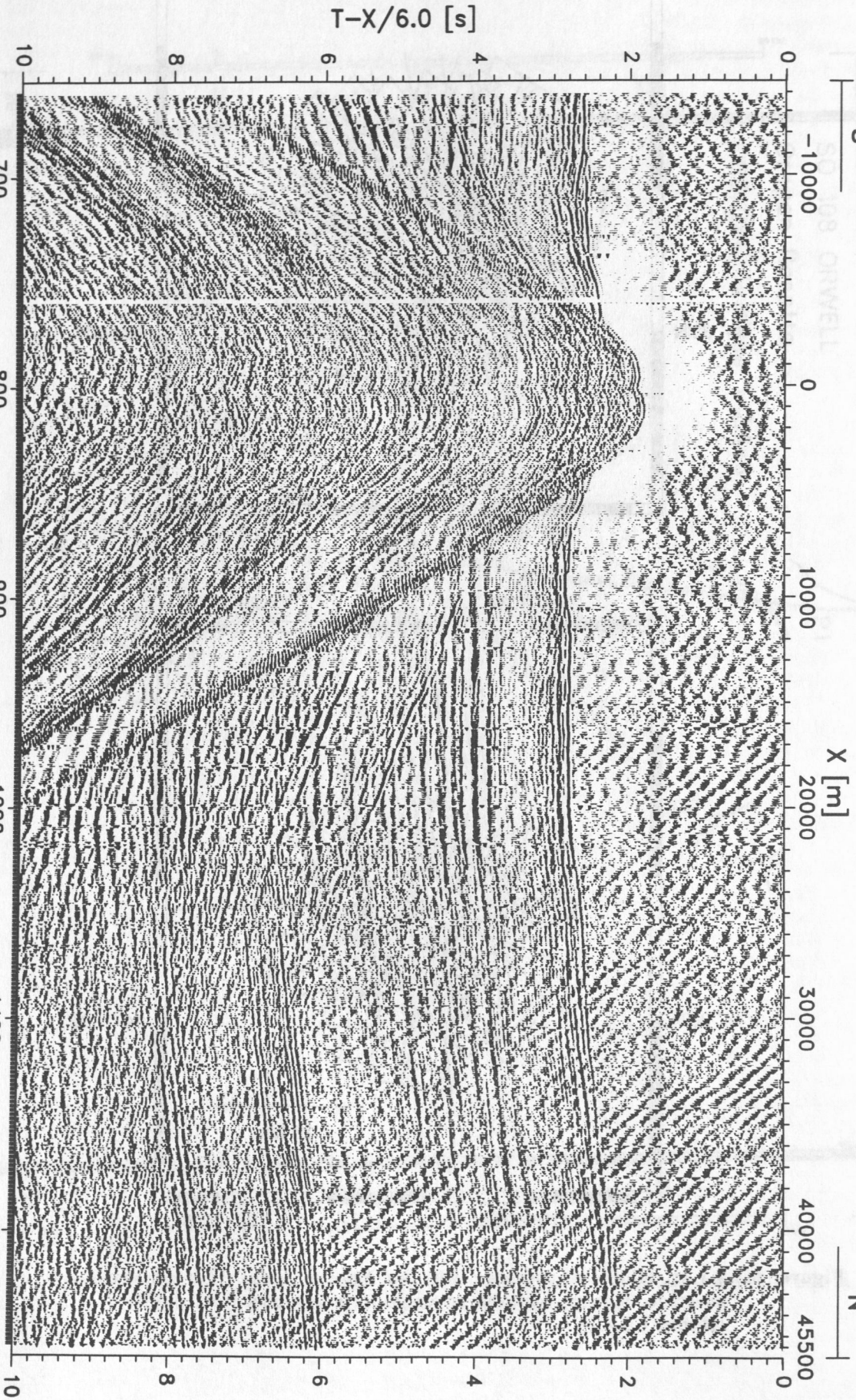

Figure 6.3.4.1.3: Record section of OBS02 for profile 1, vertical component.

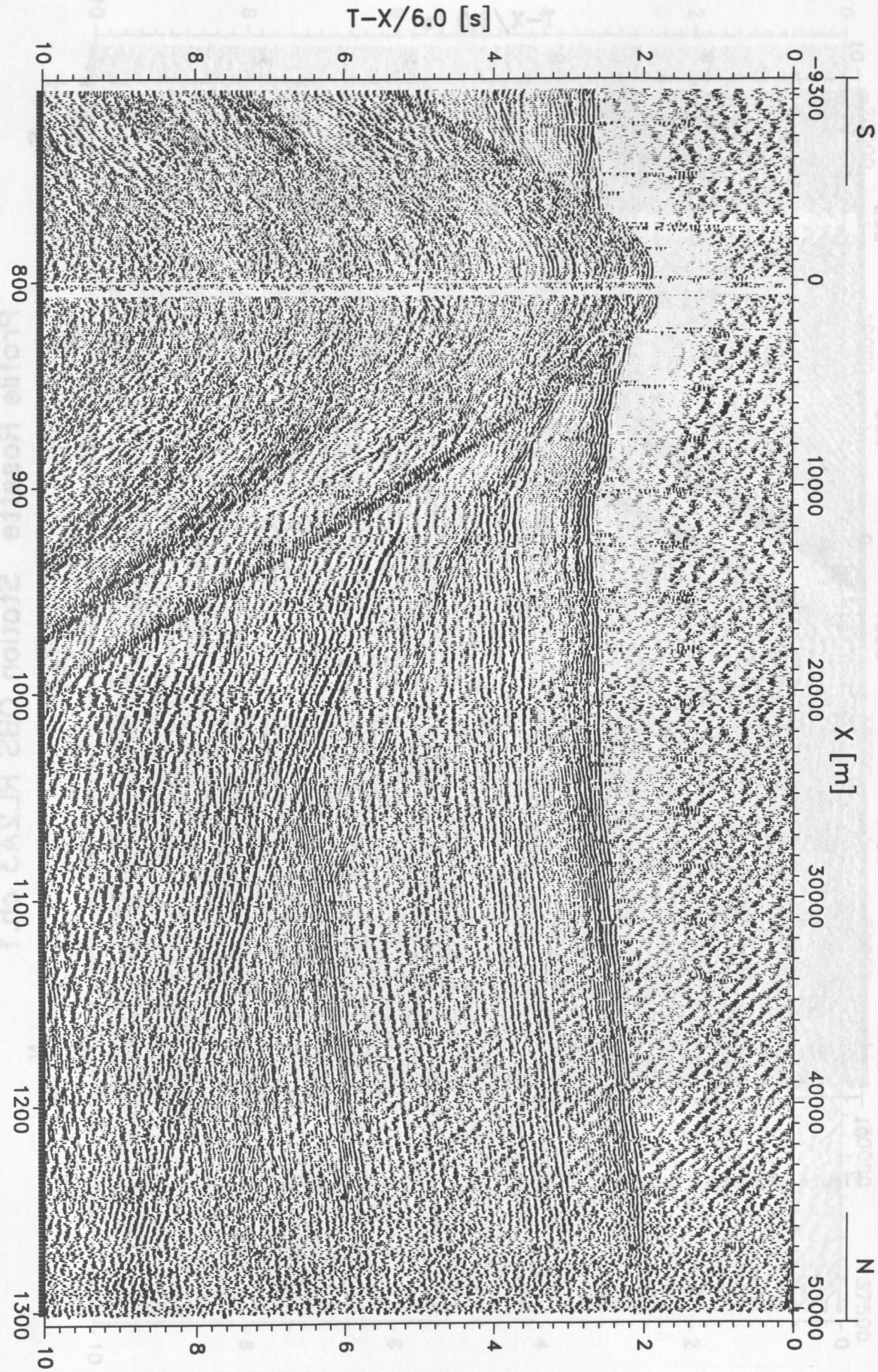

Figure 6.3.4.1.4: Record section of OBS03 for profile 1, vertical component.

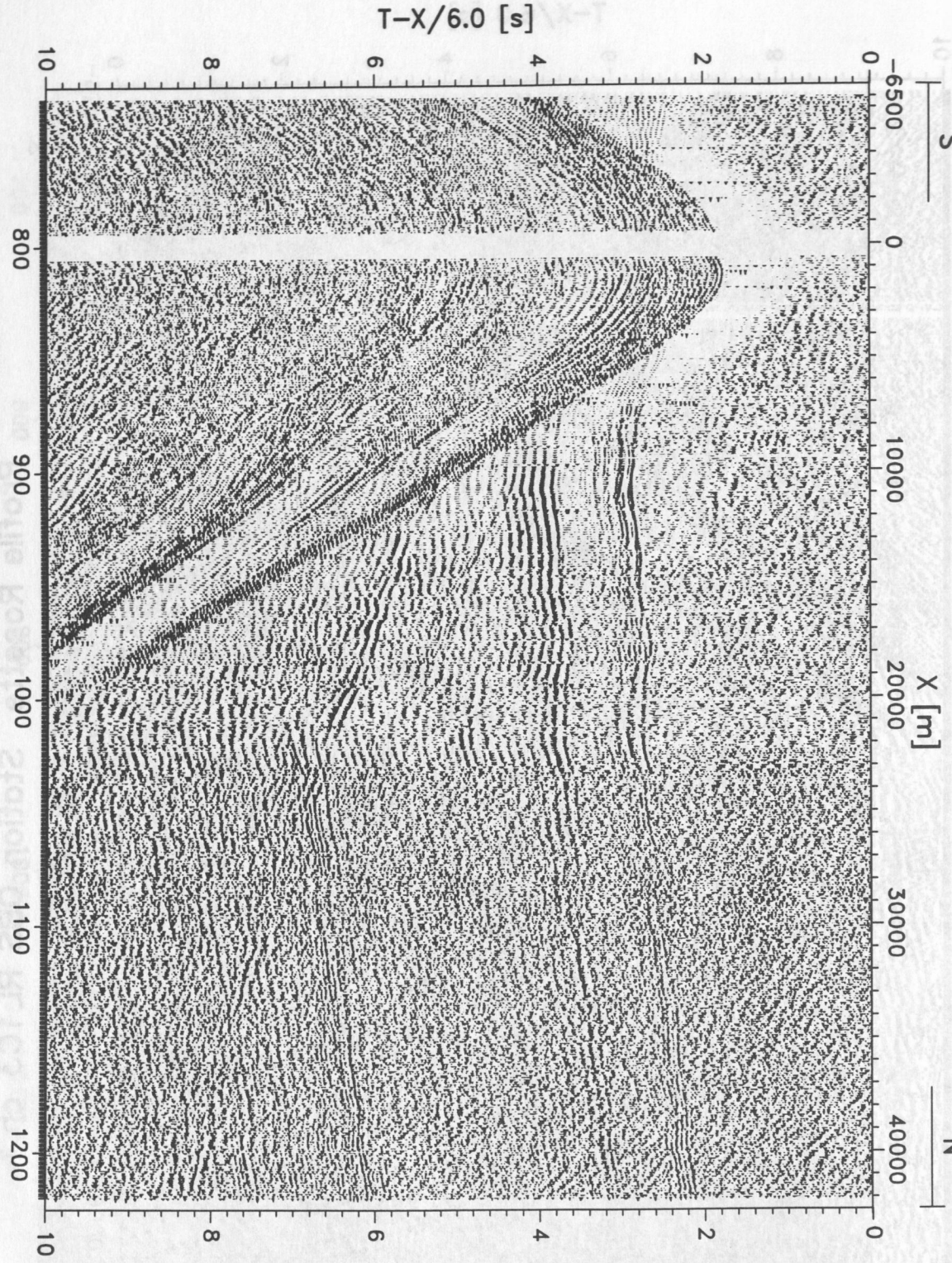

Figure 6.3.4.1.5: Record section of OBS04 for profile 2, vertical component.

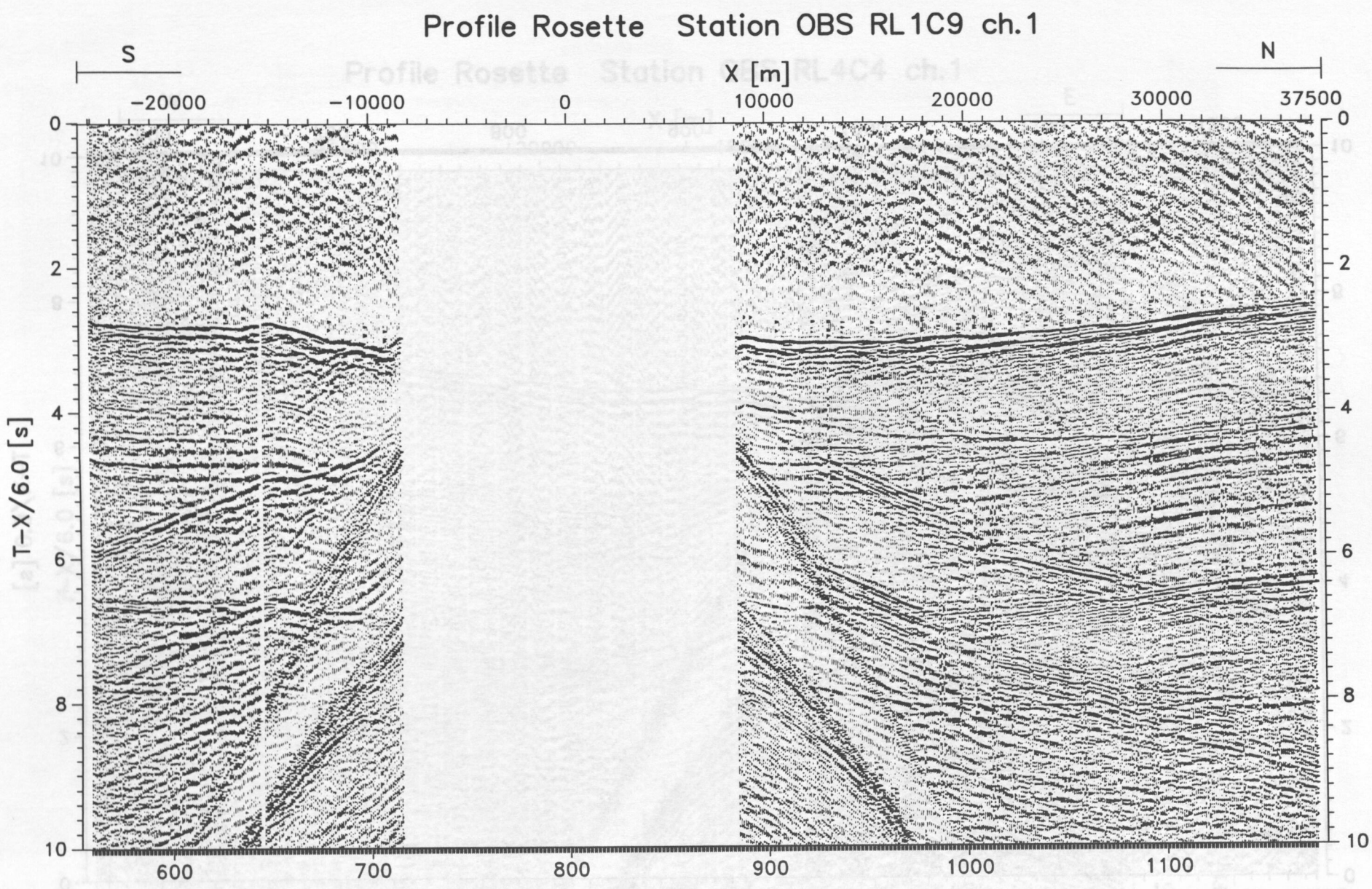

99

Fig. 4.3.11c: Record section of OBS05 for profile 1, vertical component.

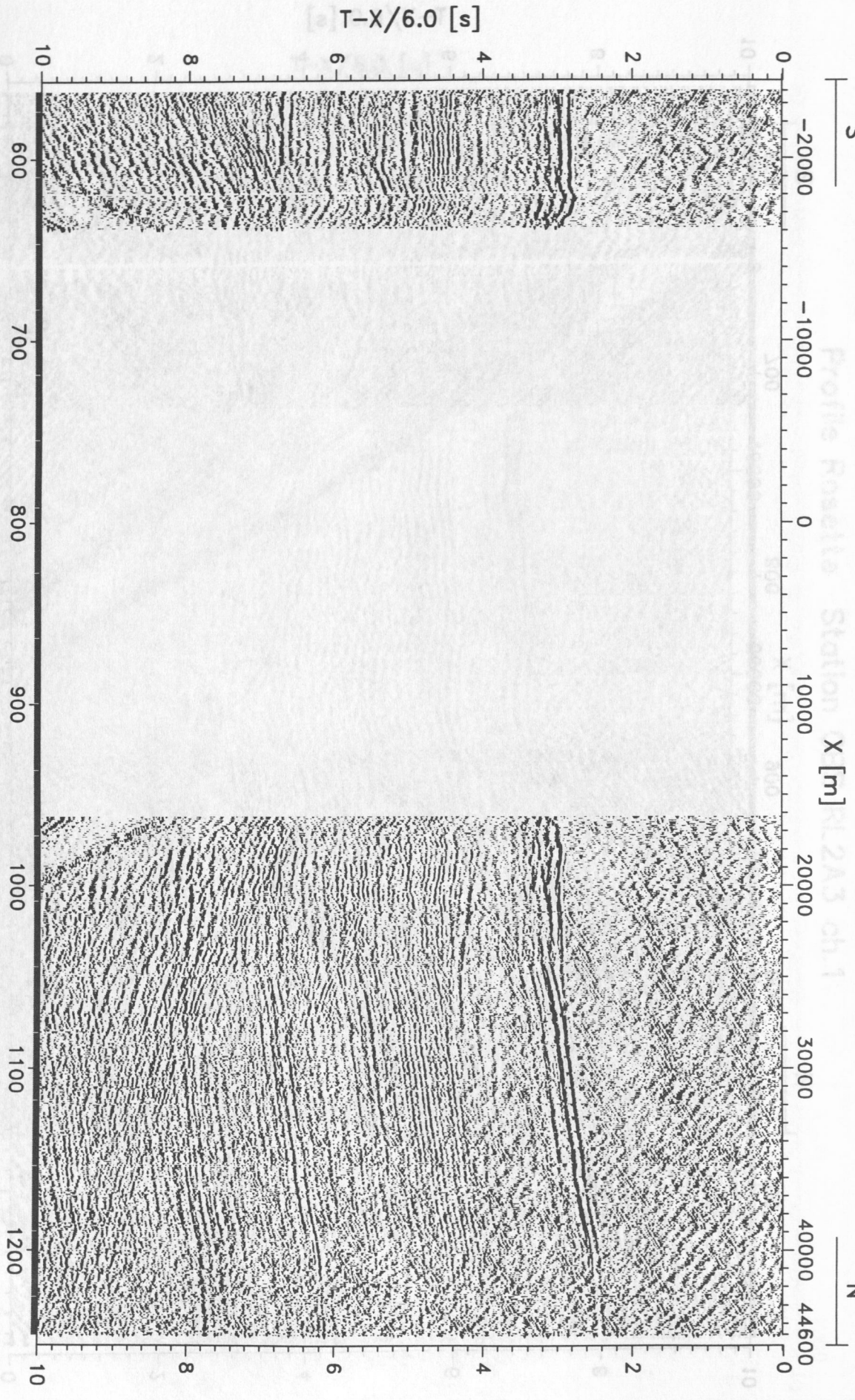

Figure 6.3.4.1.7: Record section of OBS06 for profile 1, vertical component.

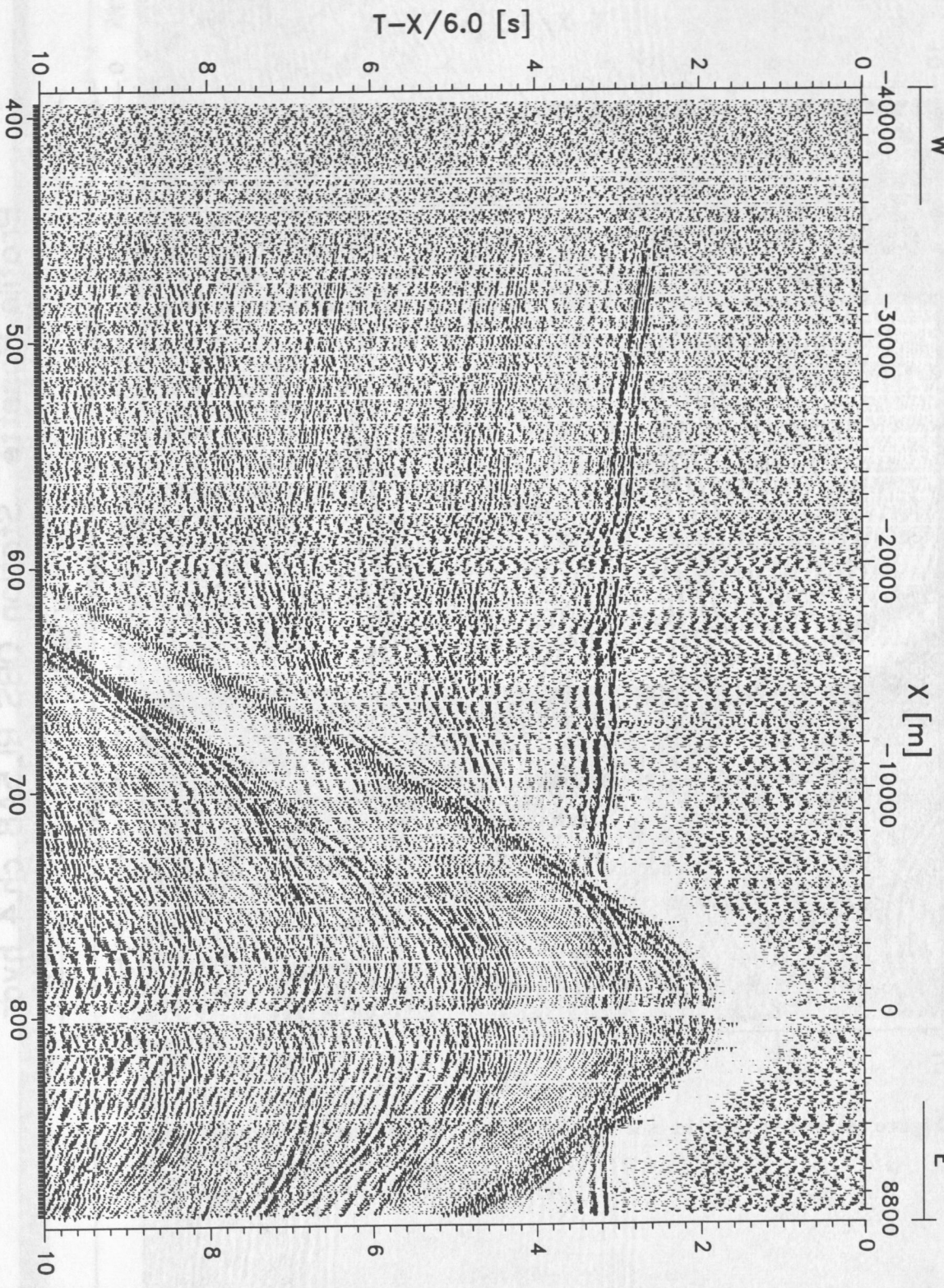

Figure 6.3.4.1.8: Record section of OBS07 for profile 4, vertical component.

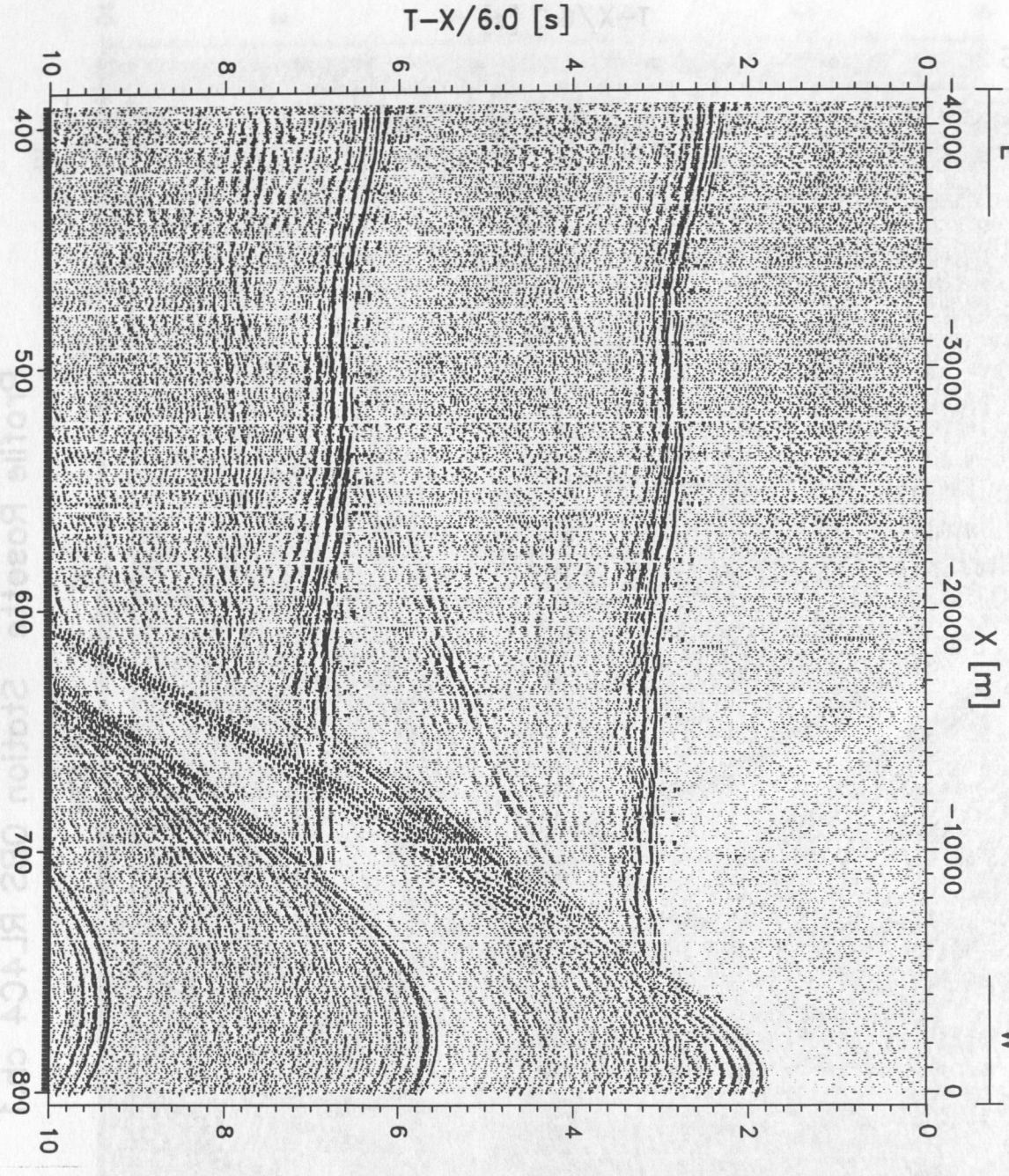

Figure 6.3.4.1.9: Record section of OBS08 for profile 5, hydrophone.

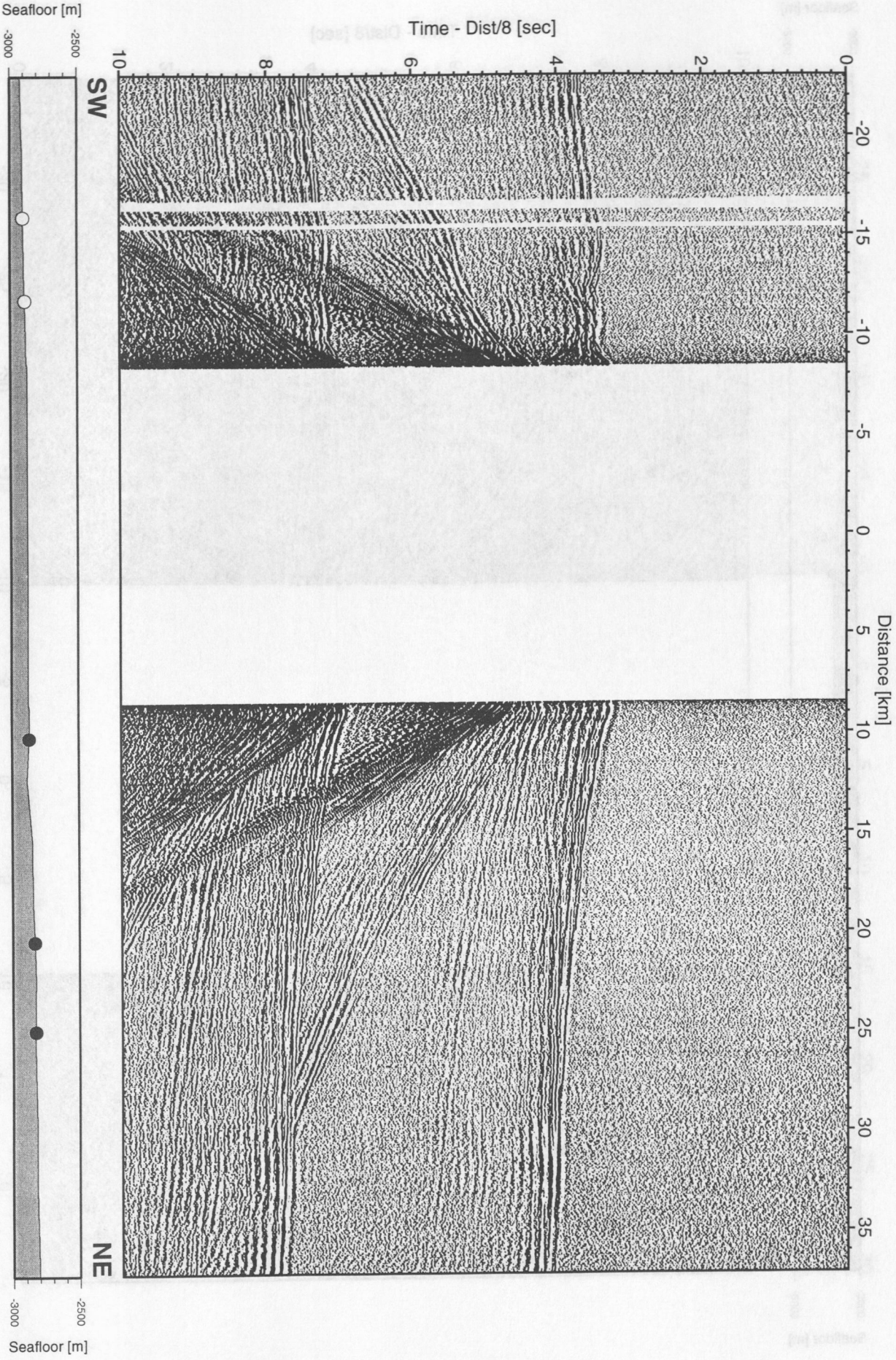

Figure 6.3.4.1.10: Record section from OBH 1, Profile 1.

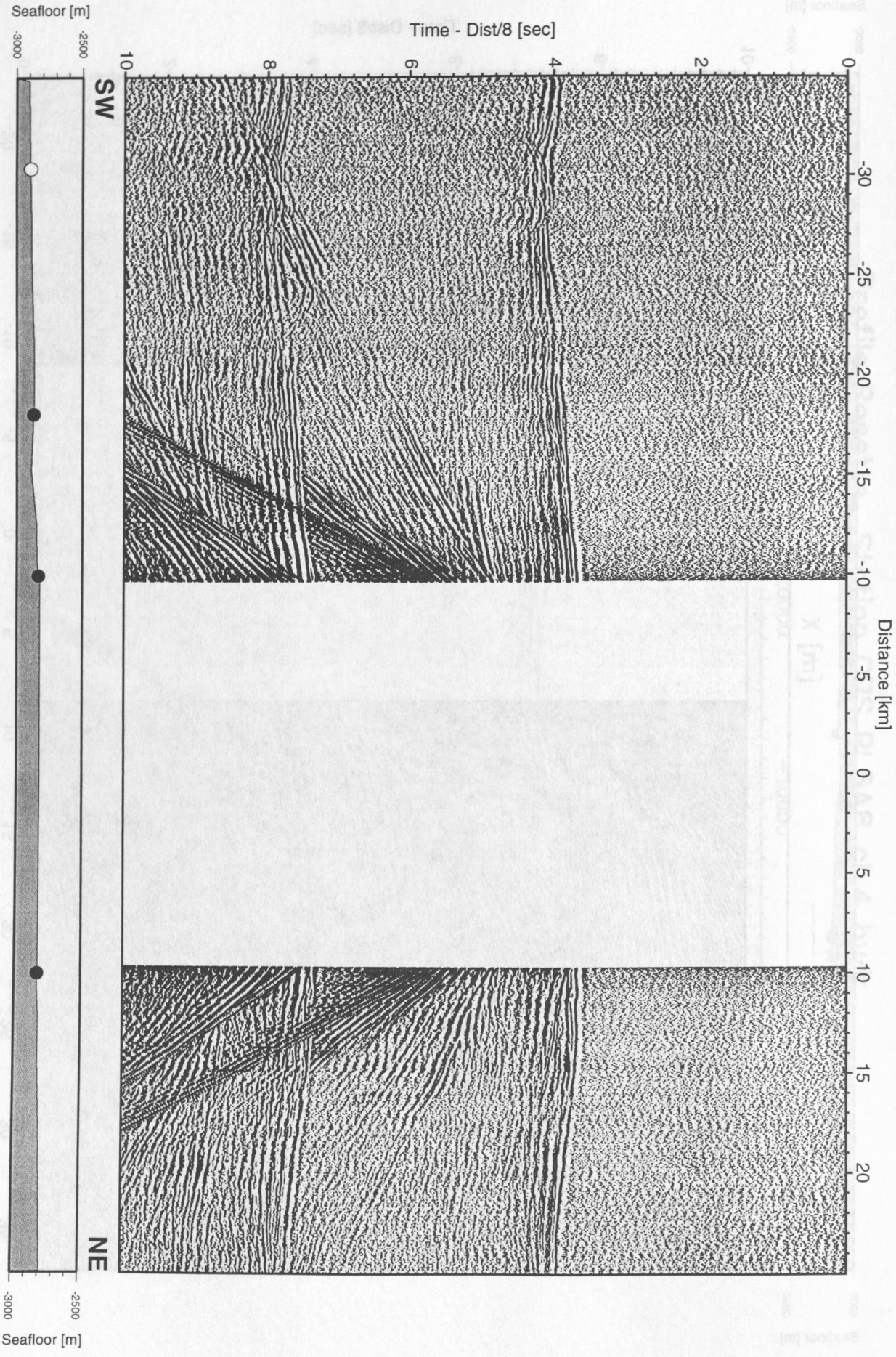

Figure 6.3.4.1.11: Record section from OBH 2, Profile 1.

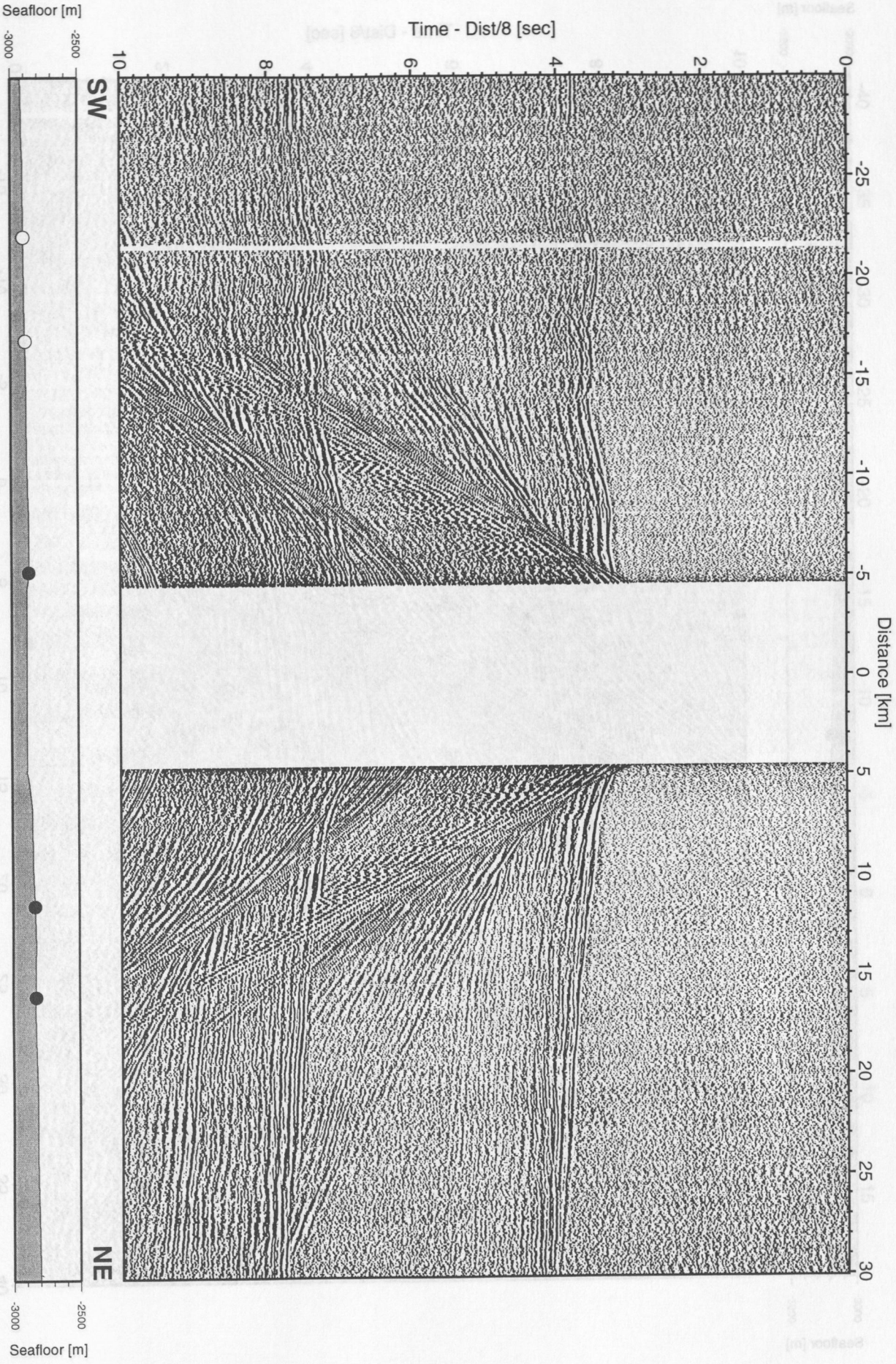

Figure 6.3.4.1.12: Record section from OBH 3, Profile 1.

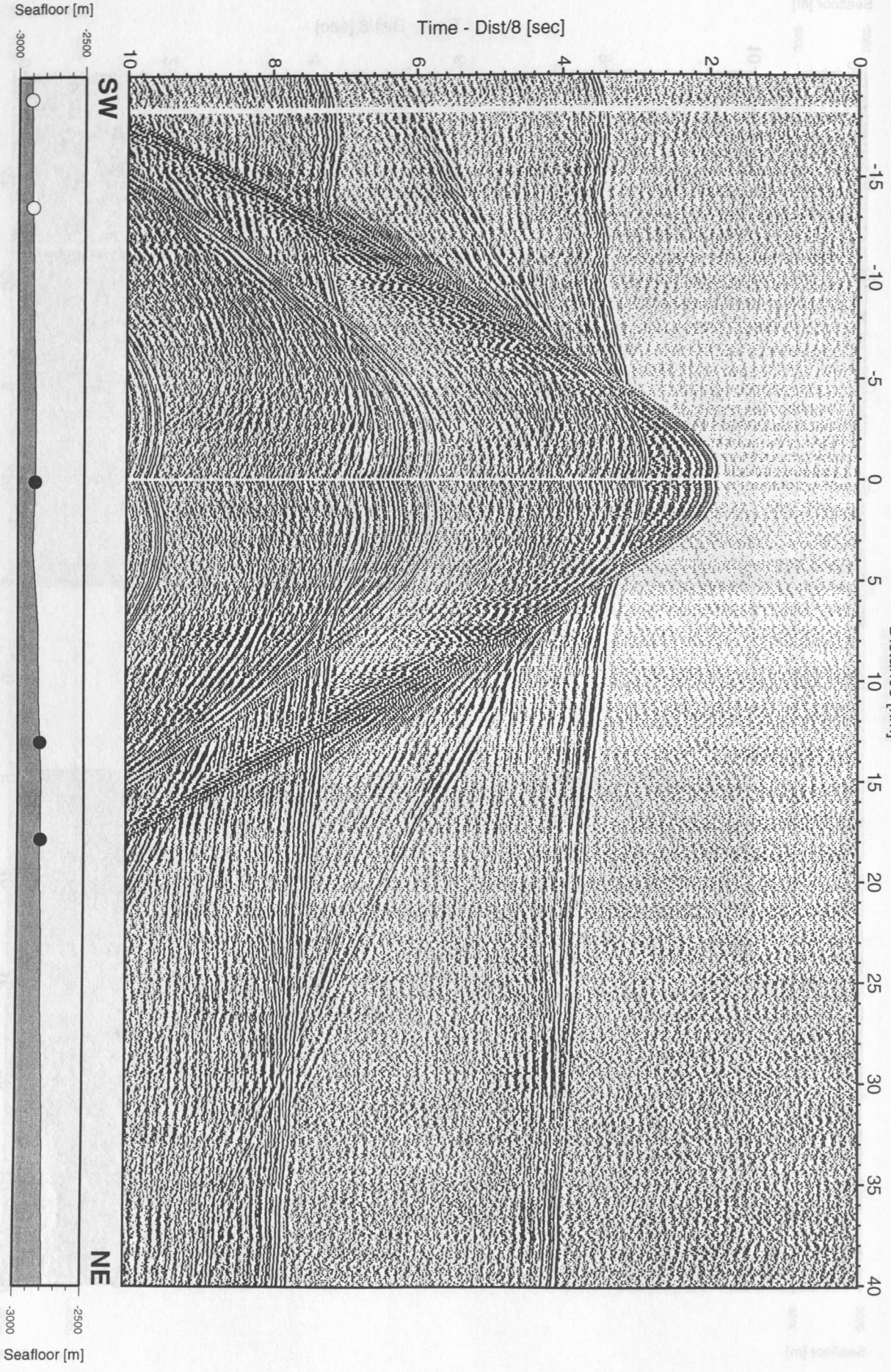

Figure 6.3.4.1.13: Record section from OBH 4, Profile 1.

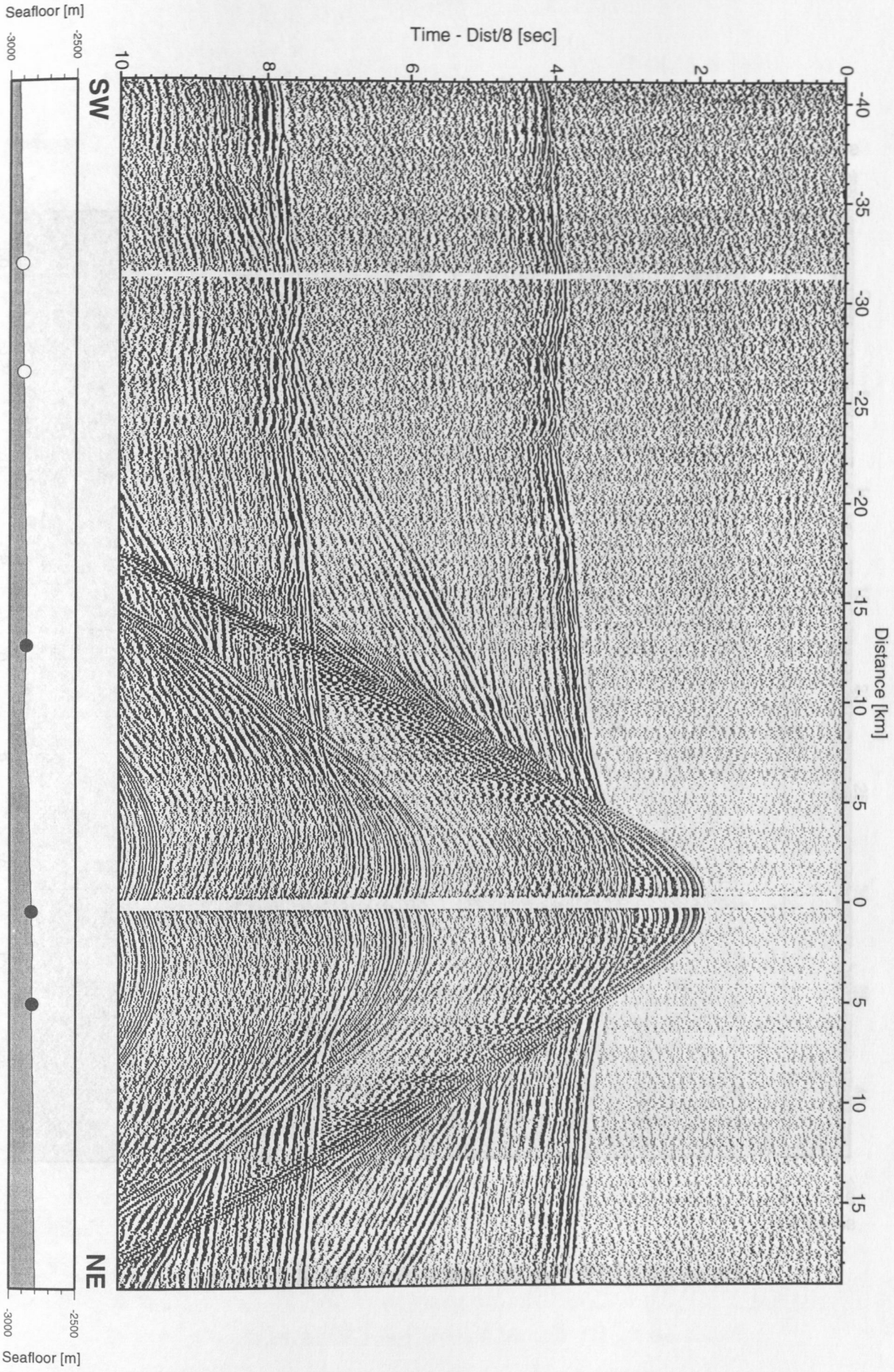

Figure 6.3.4.1.14: Record section from OBH 11, Profile 1.

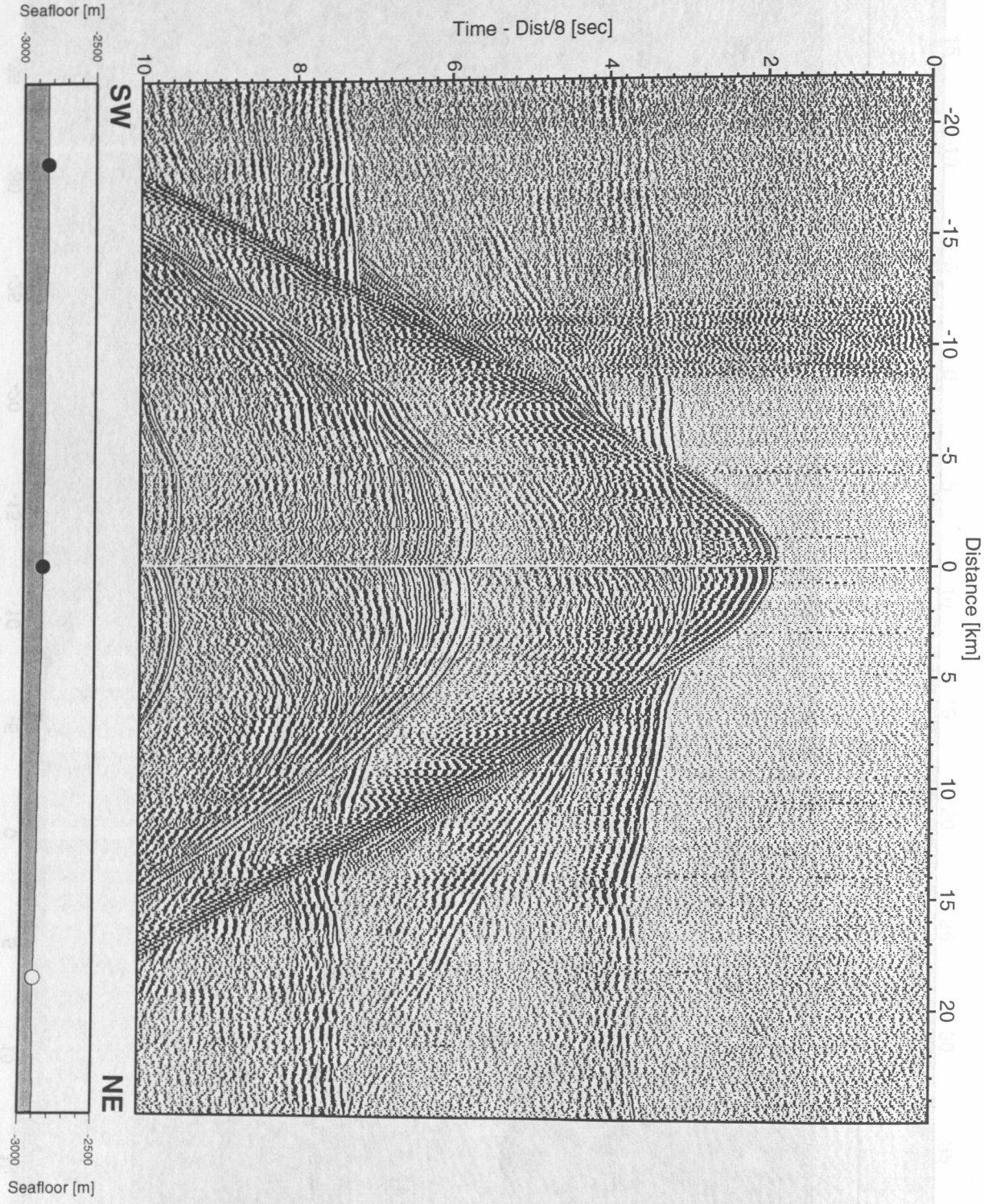

Figure 6.3.4.1.15: Record section from OBH 4, Profile 2.

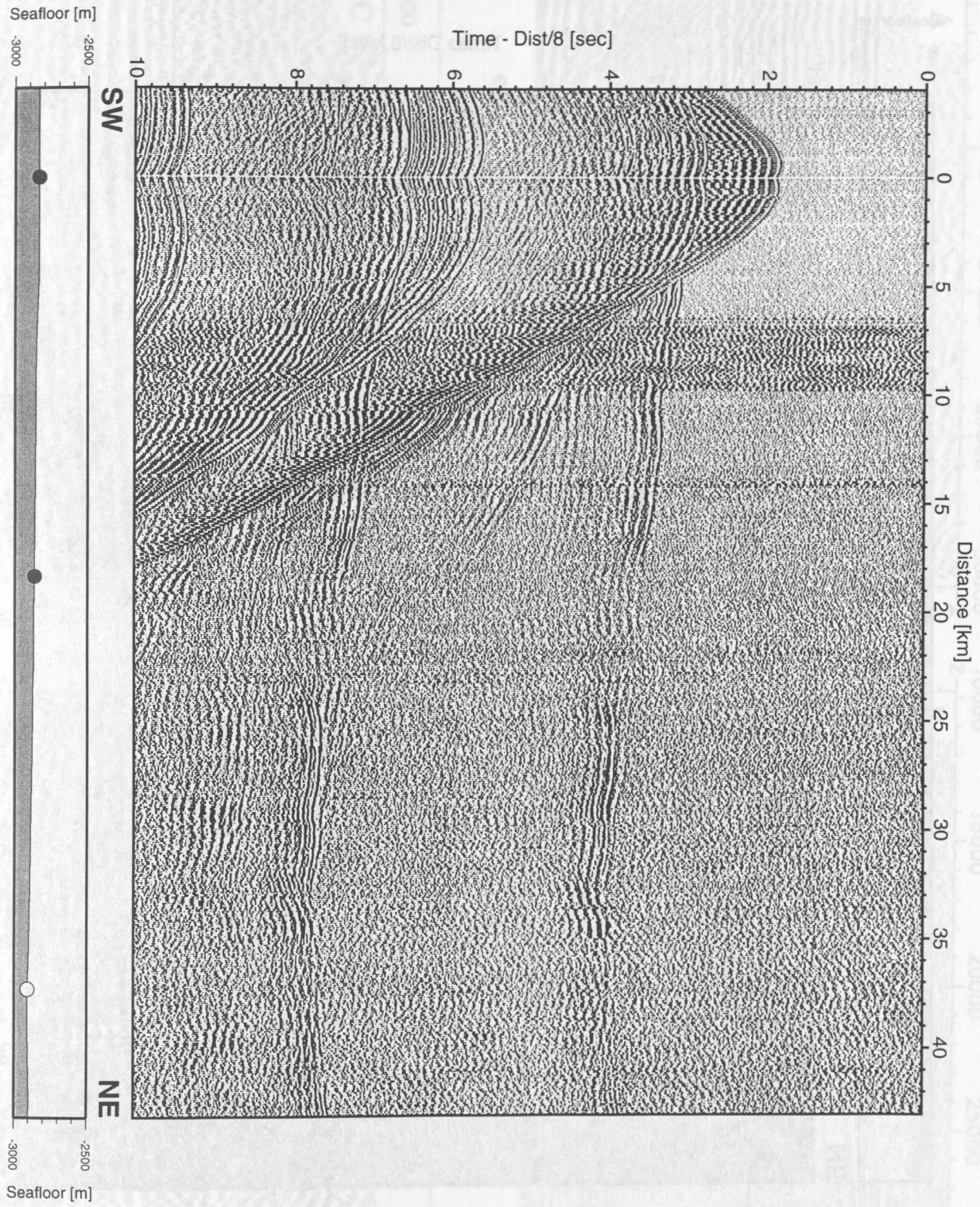

Figure 6.3.4.1.16: Record section from OBH 10, Profile 2.

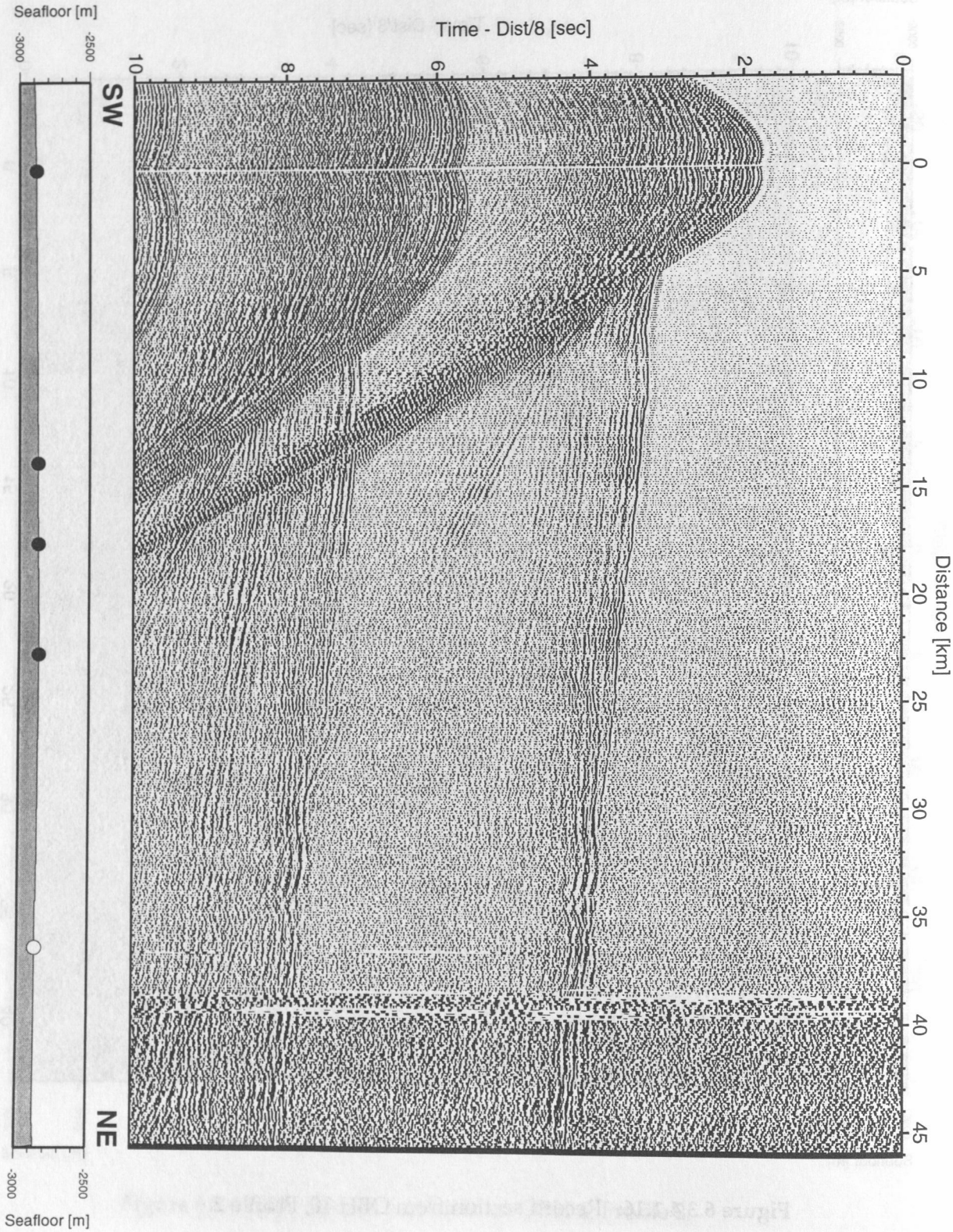

Figure 6.3.4.1.17: Record section from OBH 6, Profile 5.

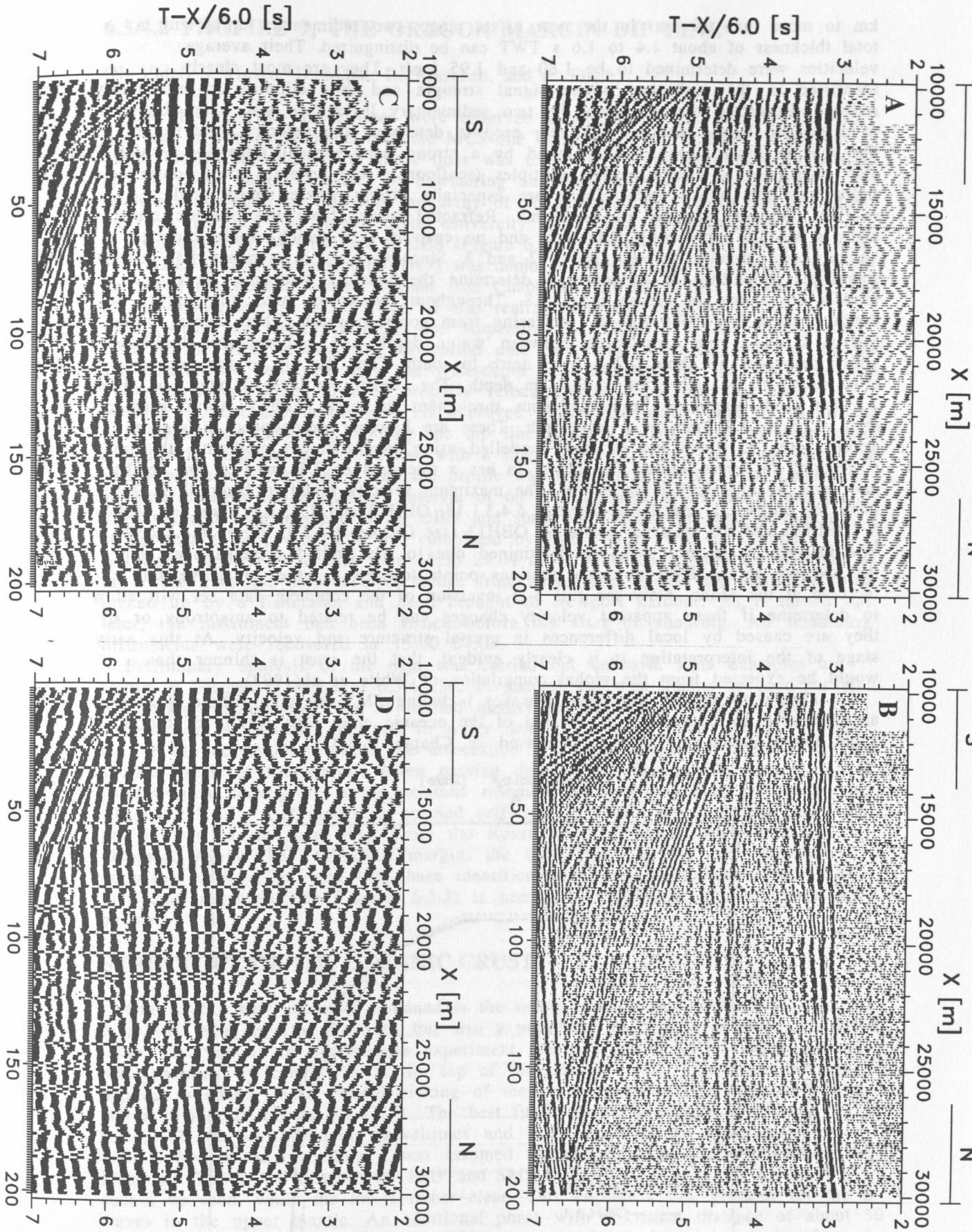

Figure 6.3.4.1.18: Record section for all 4 channels of OBS05 for profile 1. top: Hydrophone (A) and vertical (B), bottom: 2 horizontals (C and D). Butterworth bandpass filter: 4-7-25-42 Hz.

km to more than 30 km. In the near offset range, two sedimentary units with a total thickness of about 1.4 to 1.6 s TWT can be distinguised. Their average velocities were determined to be 1.80 and 1.95 km/s. They are most clearly identified in the multiples, where signal strength and thus clipping is sufficiently reduced. Refracted arrivals from the two sedimentary layers are also seen, but due to dispersion they cannot be uniquely used to determine the velocity. The top of the oceanic crust (layer 2) is marked by a strong near vertical reflection, which also gives rise to strong pegleg multiples (seafloor to top oceanic crust), observed throughout the survey area. These are especially strong where source and receiver peglegs coincide in traveltime. Refracted waves from the oceanic crust show a steadily decreasing curvature, and no cusp is seen which would indicate a velocity discontinuity between layers 2 and 3. Since the region is rather flat, a 1-D traveltime modelling is adequate to determine the velocity structure. Several models are shown in Figure 6.4.3.1.18. Throughout the survey area, the water depth changes by about 100 m, increasing from north to south. There seems to be nearly a one-to-one correlation between water depth and sedimentary thickness, which decreases by about 0.2 s from north to south. Thus the top of the oceanic crust seems to be rather flat at 3.5 km depth. The velocity in layer 2, which is about 1.5 km thick, seems to be homogenous throughout the area, with a strong gradient from 4.75 to 6.2 km/s at 5 km depth. There are however pronounced differences within layer 3, which can be best modelled using two different gradients, that may correspond to layers 3a and 3b. Layer 3a has a thickness of 2.5 km (7.5 km depth), and layer 3b of 1.7 (9.2 km depth). The maximum velocity found in layer 3b is 7.2 km/s for profiles 1 and 2 (see Figures 6.4.3.1.18, OBH10 and 11), 6.9 km/s for profile 5 (OBH06) and 6.6 km/s for profile 7, OBH13 (see Chapter 6.4.3.2, Figure 6.4.3.2.32). The Pn-velocity in not uniquely determined due to the limited offset ranges, but the absence of the PMP on some sections points towards a rather small velocity increase at the Moho. Only the full 3-D inversion of the complete data set will allow to determine if these apparent velocity changes can be related to anisotropy or if they are caused by local differences in crustal structure and velocity. At this early stage of the interpretation it is clearly evident, that the crust is thinner than would be expected from the global compilation of White et al.(1992).

On almost all section also clear S-waves including SMS are seen. These S-waves are generated by conversion at the top of the oceanic crust. The results of the S-wave interpretation are further discussed in Chapter 6.4.3.2.

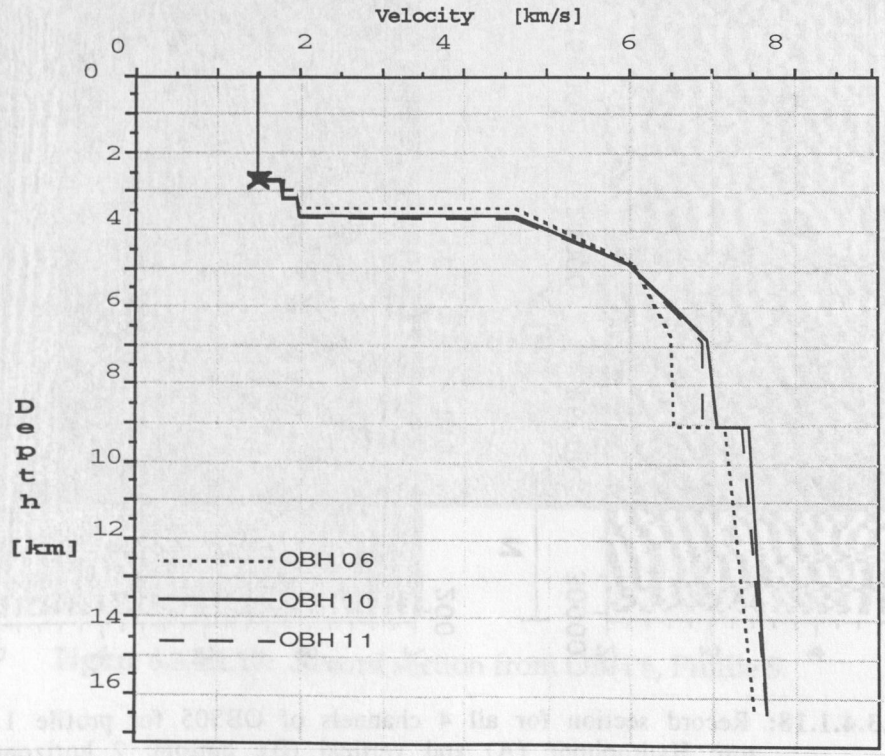

Figure 6.3.4.1.19: 1-D velocity functions for several receivers (OBH06 on profile 5, OBH10 on profile 2, and OBH11 on profile 1).

6.3.4.2 PROFILE 7, THE OREGON MARGIN DIP LINE

(N. Vidal, S. Husen, D. Mann, D. Kläschen, and E. Flueh)

One dip and two strike lines were observed along the Oregon margin. The dip line was chosen to coincide with the MCS-line Oregon 5, shot in 1989 (McKay et al., 1992; 1996). The purpose of these lines was to determine the detailed velocity field and to allow better estimates of dewatering and fluid expulsion. Along the landward extension of this line, an array of 36 seismometers spread out over 100 km was operated by Oregon State Univercity (A. Trehu) simultaneously.

Deployment of 14 OBH and 6 OBS (Figure 6.3.4.2.1) started in the Rosette area at 15:30 26.04. One instrument (OBH17) was deployed with a 1500 m long anchor cord to record the farfield source wavelet (see Chapters 5.3.1 and 6.3.2). Toward the end of the deployment at 06:00 27.04. it was realized that the ships navigation filterprocess was malfunctioning (see Appendix and Chapter 5.4.3). During the reset of the filter process, the navigation data bank was destroyed, and for the last six instruments deployed only the waterdepth was known from the observers logs. These positions were however properly relocated during recovery of the instruments, because these were all deployed in shallow water, and no significant drift could have occurred. Shoting the dip line (profile 7) from east to west started in perfectly calm sea at 7:30 27.04. with a ships speed of 4 kn. The trigger rate was varied between 60 and 90 s, and the profile was finished at 09:00 28.04. Later analysis showed that a shooting interval of 60 s is superior to the 90 s interval. Retrieval and redeployment of all OBH and some OBS along the two north-south strike lines (Figure 6.3.4.2.2) was completed by 16:00 29.04. The strike lines (profiles 8 and 9) were shot from 18:30 29.04 to 00:00 01.05. During the shooting of the strike lines the ship received notice from shore, that one of the OBH had been picked up by a fisherman and been brought to Newport harbour. As it turned out later, the instrument had been fished before the start of shooting. All remaining instruments were recovered at 15:00 01.05.

Preliminary analysis of the data was carried out onboard. Data examples are shown in Figures 6.3.4.2.3 to 6.3.4.2.30. In general, the data quality is good for all deep water deployments, but of limited quality for the strike lines and the easternmost instruments deployed in water depths shallower than 500 m. On the toe of the accretionary prism the attenuation is rather strong, as indicated by the sudden break of the arrivals when passing this region. The profile started in the Rosette area, where the record sections resemble the previous ones in detail (see Chapter 6.3.4.1). 1-D modelling seemed sufficient to obtain good results. Since the profile was longer than those from the Rosette, even deeper penetration was obtained. Along the continental margin, the travel time of the first arrivals undulates with offset, and the phase identification is no straightforward. A 2-D raytracing approach (see Chapter 6.3.3) is needed to model the data as described below.

STRUCTURE OF THE OCEANIC CRUST

One of the best examples obtained is the record section from OBH13 (Figure 6.3.4.2.3). Not only the P-waves, but also a prominent S-wave is observed, similar to other observations in the Rosette experiment (see Chapter 6.3.4.1). These S-waves are generated by conversion at the top of the oceanic crust. Deconvolution was applied to enable more careful picking of the seismic phases (see Chapter 6.3.2) and is shown in Figure 6.3.4.2.31. The best fitting model is shown in Figure 6.3.4.2.32, the corresponding traveltimes and Poissons ratio are seen in Figure 6.3.4.2.33. For the modelling it was assumed that the interfaces for both waves are identical. The critical distance for PMP and SMS is at 19 to 20 km. An Sn phase cannot be seen, while the Pn is rather clear. This implies a low gradient for the S-waves in the upper mantle. An additional phase with a critical distance of about 50 km is seen for both P and S waves. This phase can be explained by an interface at 16.5 km depth, where a positive velocity jump is required to match the critical distances. The crustal thickness is slightly less than 6 km, and no velocity discontinuity is seen, as already described in Chapter 6.3.4.1. Changes of the velocity gradient at 5 and 7.5 km depth can be used to indicate the separation into

layer 2, 3a and 3b. The S-wave velocity shows no change in gradient between layers 3a and 3b. The P-wave velocities are generally low (not exceeding 6.7 km/s in the crust), and especially the upper mantle velocity of 7.7 km/s for the P-waves is surprisingly low. Poissons Ratio is only well constrained in the crust, where it decreases from 0.28 to 0.25. Since no Sn phase is observed, the upper mantle S-wave velocity is only constrained by the critical distance for SMS, and therefore Poissons ratio is poorly constrained in the upper mantle. When taking the reverse observations into account (OBH16 and 18, Figures 6.3.4.2.6 and 6.3.4.2.8), it is evident that the crust is not as homogeneous as thought before. The 1-D models for these records are also shown in Figure 6.3.4.2.32. They show higher crustal velocities and a thickness about 2 km in excess of the model derived from OBH13. Also the sedimentary thickness increases landwards. This shows that there is already a considerable dip of the oceanic plate about 100 km seaward of the trench.

PROFILE 7

A preliminary 2-D model for profile 7 has been developed using 11 OBH and 4 OBS records avalaible along the line. Modelling has been done using the method described in Chapter 6.3.3. The starting model for the profile was constructed considering the known bathymetry recorded during data acquisition and the velocity profiles derived from the 1-D modelling.

Profile 7 is coincident with the reflection line OR5, collected by MacKay et al. (1992). A post stack time migration together with the positions of all recording instruments is shown in Figure 6.3.4.2.34. The observed sedimentary thickness has been also considered for the starting model.

Different seismic phases have been identified and included in the modelling: the water wave, the reflected and refracted waves within the sediments, the refracted waves within the oceanic crust, the reflected waves from the oceanic Moho and the refracted waves from the oceanic upper mantle.

The velocity model of the crust beneath profile 7 is shown in Figure 6.3.4.2.35 and comparison of observed and calculated traveltimes for each OBH/OBS used in the preliminary modelling is displayed in Figure 6.3.4.2.36 together with the ray diagram connecting source-receiver pairs.

The oceanic crust is well imaged along the first 110 km. It is characterized by 3 different main units: a) the sedimentary layers with velocities around 2 km/s for the Neogene sediments and ranging from 2.3 to 4 km/s for older sediment; b) upper oceanic crust (layer 2) with velocities between 5.0 to 6.3 km/s and c) lower oceanic crust (layer 3) of the Juan de Fuca plate with values of 6.5-6.9 km/s. Velocities in the uppermost mantle range between 7.9-8.0 km/s.

The deformation front is observed in the sediments at km 110 (in the model) to the east. This area is considered to correspond to a zone of highly deformed sediments (Trehu et al., 1994). This is clearly imaged from OBH20 to OBS14, which show prominent undulations in the observed phases. These undulations should be attributed to the deformed sedimentary cover. The velocity model in this area has been constructed considering several sedimentary layers (Figure 6.3.4.2.35) which try to fit the average velocities observed in the seismic sections. Nevertheless, this smoothed representation should be replaced by a complex structure consisting of blocks of high/low velocity material. Velocities of 5.0 km/s have been obtained from 5 to 9 km depth. There, a high velocity interface (6.5 km/s) marks the transition from upper/lower crust. There is no evidence in the data for a lateral change in velocities which could determine the position of the Fulmar fault and characterize the Siletz terrane. According to previous interpretations in the area (Trehu et al., 1994) this fault should be located around km 190 in our model, between OBS11 and OBS12. The low coverage of the eastern most OBS yields to a lack of resolution in this zone, because it is located close to the eastern end of the line. In this respect, the integration of the land data will be crucial to constrain the crustal structure and the Siletz terrane transition.

The subducted oceanic crust can be clearly imaged along the model by the reflected and refracted waves coming from the top and the bottom of the slab. Velocities range from 6.5 to 7.0 km/s along the whole area and upper mantle velocities are 7.9-8.0 km/s. The data does not show, offshore, a pronounced arch in the subducted plate as proposed by previous interpretations (Crosson and Owens,

1987). It rather images a gently deepening and locates the base of the crust at about 21 km depth below the coast line. This is constrained by OBS9 which shows PmP arrivals at short offsets and at 8 seconds (Figures 6.3.4.2.13 and 6.3.4.2.36). This result is in agreement with the previous interpretations by Trehu et al. (1994) who gave a range between 20 and 28 km for the Moho depths at the shoreline.

PROFILE 8

1-D modelling of Profile 8 illustrates the complexity of placing the plate boundary and the base of the crust in the area, and adds new costrains in this respect. Reverse coverage from OBH34 (Figure 6.3.4.2.26) and OBH38 (Figure 6.3.4.2.30) show below the sedimentary cover and upper crustal phases, a high velocity arrivals at about 7 s reduced traveltime at critical distance of 60 km. Figure 6.3.4.2.37 shows two different possible models for the OBH34/38 dataset. Model "a" considers an intracrustal discontinuity at about 15 km depth, the top of the subducting slab around 20 km and the base of the oceanic crust at 26 km. If we look at the arrival times for this tree interfaces half a second difference between them is observed. The slope shows that this phase should rather correspond to the lower crust or to the Moho but there are no arguments to point in favor one of them. A Moho located at slightly shallower depth will provide the same arrival times as the ones obtained from the lower crust. A weak energetic area between 45 to 60 km offsets in the record sections masks the critical distance which may help to constrain the model. Model "b" shows and average upper-lower crustal velocity profile and places the base of the oceanic crust at about 21 km depth, in accordance with modelling along profile 7.

The fan recordings along profile 9 and profile 8 introduce new constrains in the placement of the base of the crust. The fan-record section (from OBH34) shows the same 7 seconds high velocity arrivals but with larger offsets to about 95 km and displays the critical distance at about 50 km. A Pn phase with a velocity greater than 8 km/s at distances larger than 70 km clearly favorous model "b" with vaues of 21 km depth for the moho in this zone, instead of deeper depths. This has been also constrained by the 2-D modelling of profile 7 which shows a gently deepening of the subducting slab to the east and places the Moho around 21 km at the shoreline.

PROFILE 9

1-D modelling of profile 9 has been done using OBH28 to OBH32 and OBS09. At the location of OBS09 there is the intersection with the EW profile 7.

The modelling results (Figure 6.3.4.2.38) show relatively thick sedimentary layers up to 4.5 km depth. In the northern part we can distinguish three of them with velocities of 1.8, 2.1 and 3.5 km/s. As a probable result of lateral inhomogenities we only find the 1.8 (to 1.9) and 3.5 km/s layer in the southern part.

Phases associated with the upper oceanic crust show velocities around 4.5 km/s and extend homogeneously from 4 to 9 km depth, thickening under the locations of OBS09 to OBH29.

A more or less 2 km thick transition zone of velocities ranging between 6 and 6.8 km/s is found in all sections. Remarkable is the deepening of this zone from about 9-11 km at the north and southend to 11-14 km depth in the central part of the line.

Below this we obtain velocities of 7.0 km/s, which indicate the top of the lower oceanic subducting crust.

2-D modelling of profile 7 (Figure 6.3.4.2.35) is in agreement with these 1-D results. The differences concern only small deviations of velocity and depth estimates.

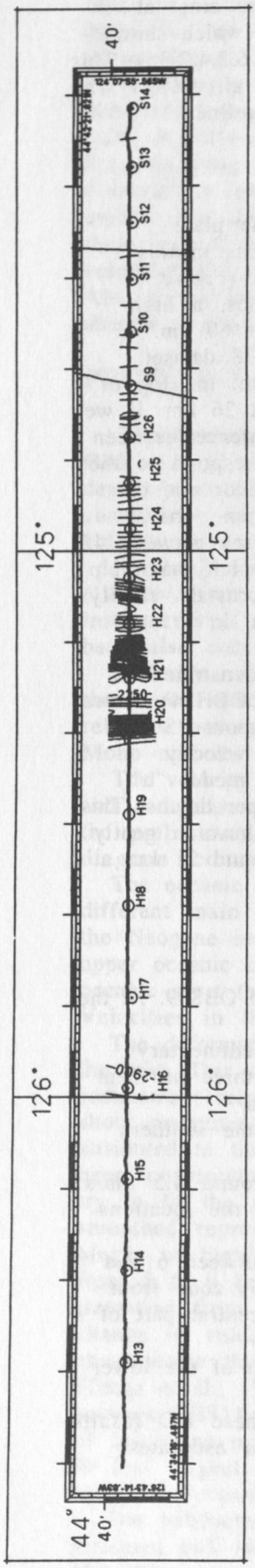

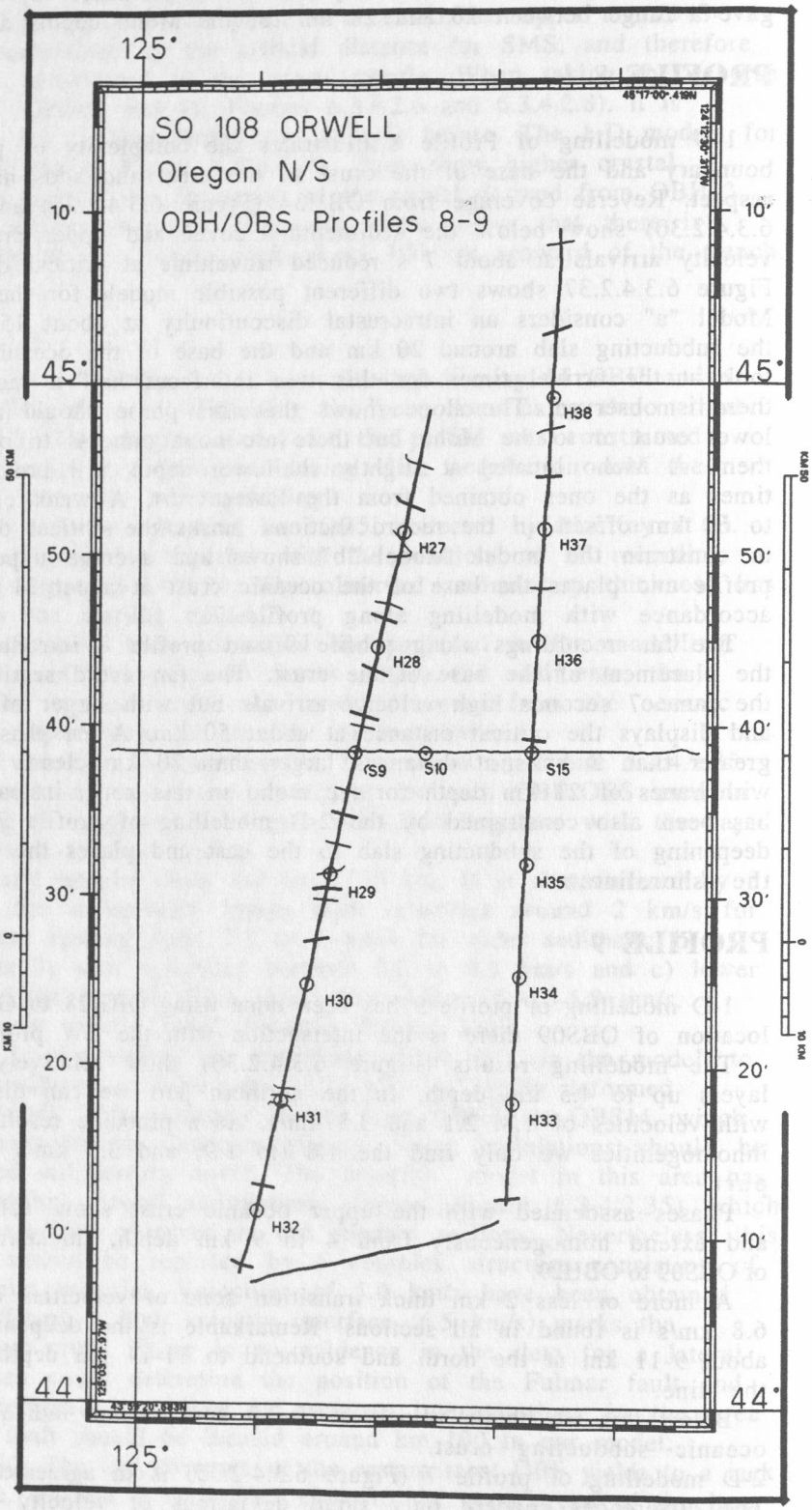

Figure 6.3.4.2.1: Location map of profile 7. Contour intervall 100 m. S* and H** mark OBS/OBH stations.

Figure 6.3.4.2.2: Location map of profile 8 and 9. Contour intervall 5(S* and H** mark OBS/OBH stations.

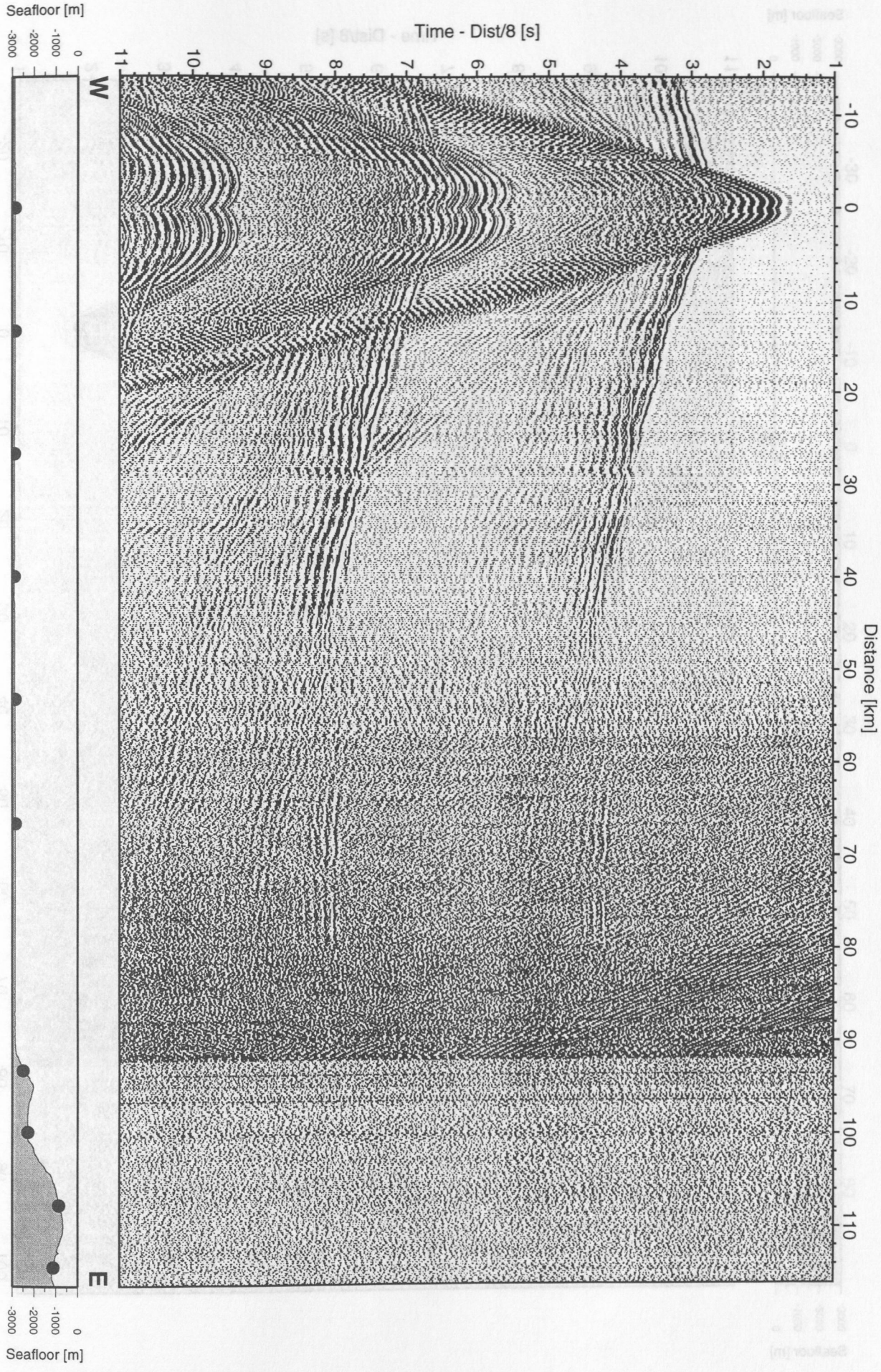

Figure 6.3.4.2.3: Record section from OBH 13, Profile 7.

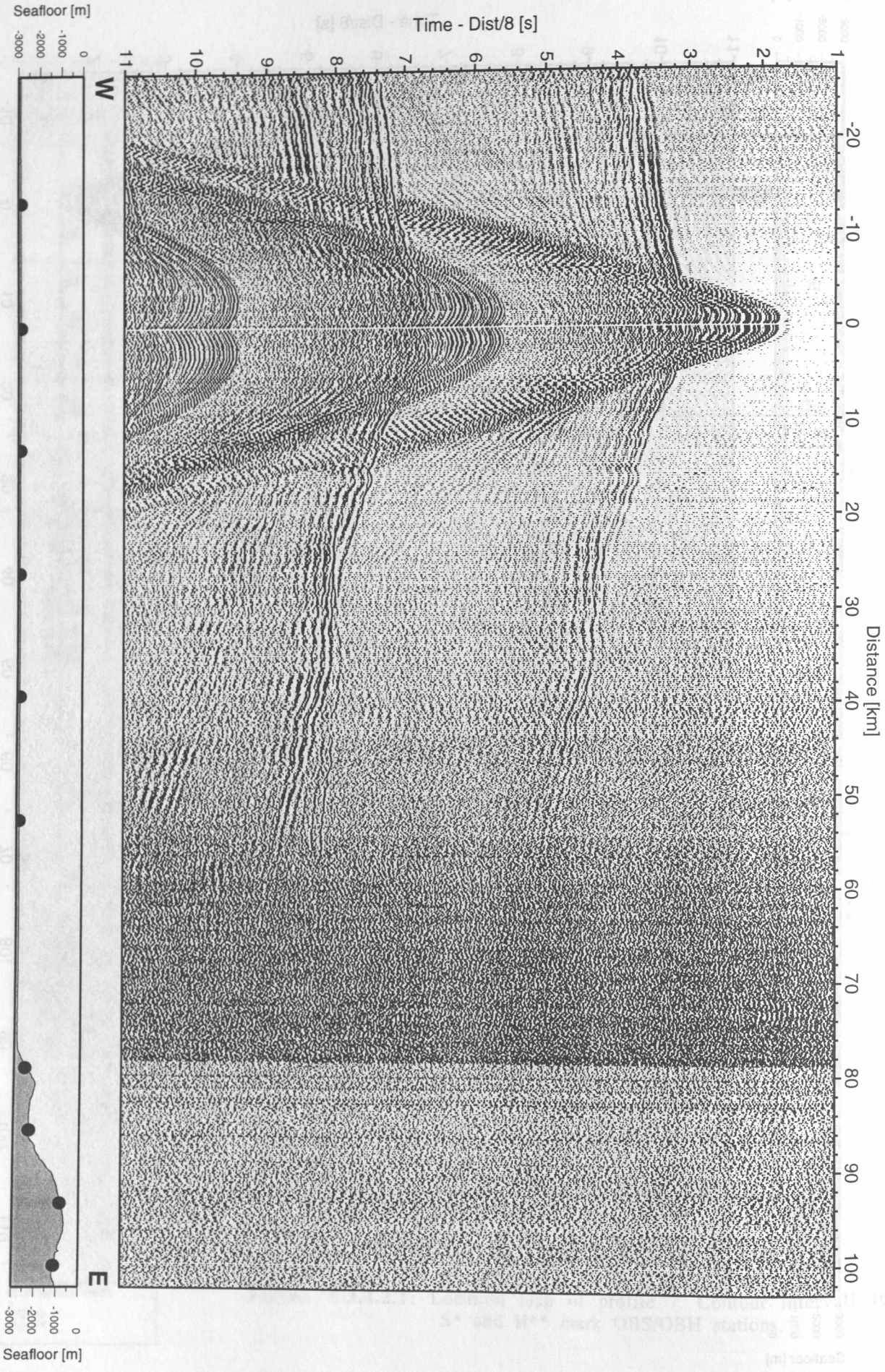

Figure 6.3.4.2.4: Record section from OBH 14, Profile 7.

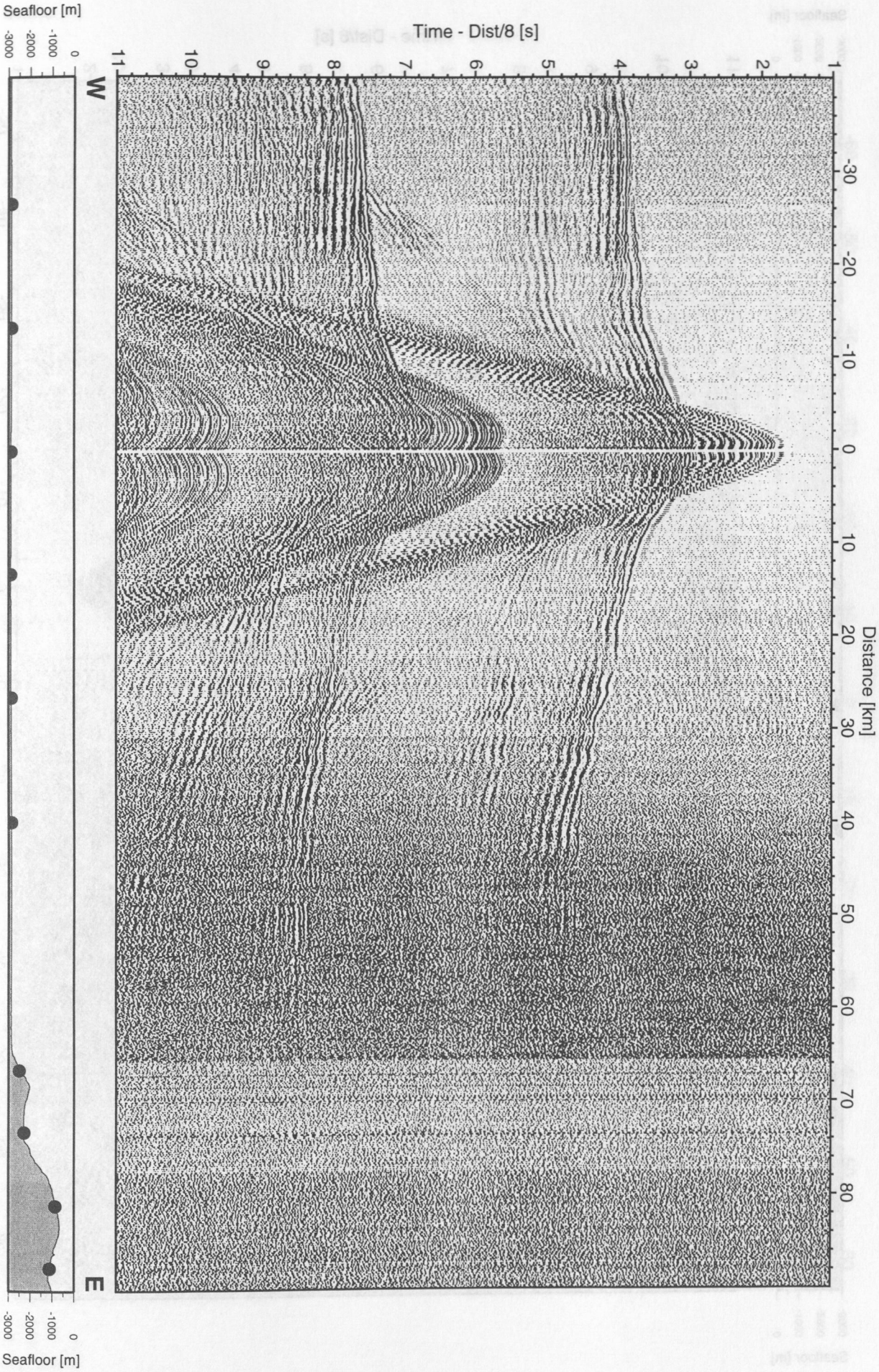

Figure 6.3.4.2.5: Record section from OBH 15, Profile 7.

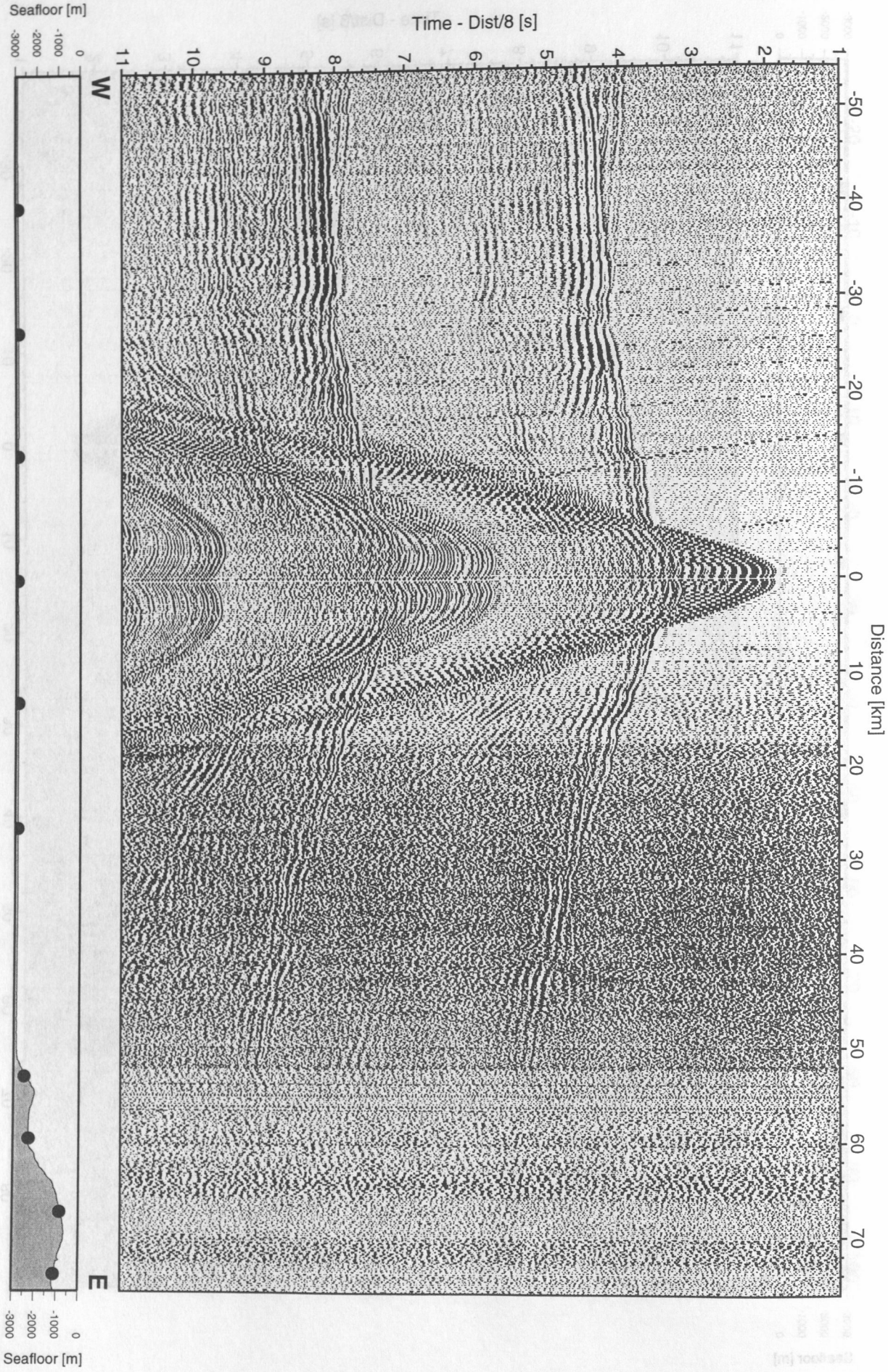

Figure 6.3.4.2.6: Record section from OBH 16, Profile 7.

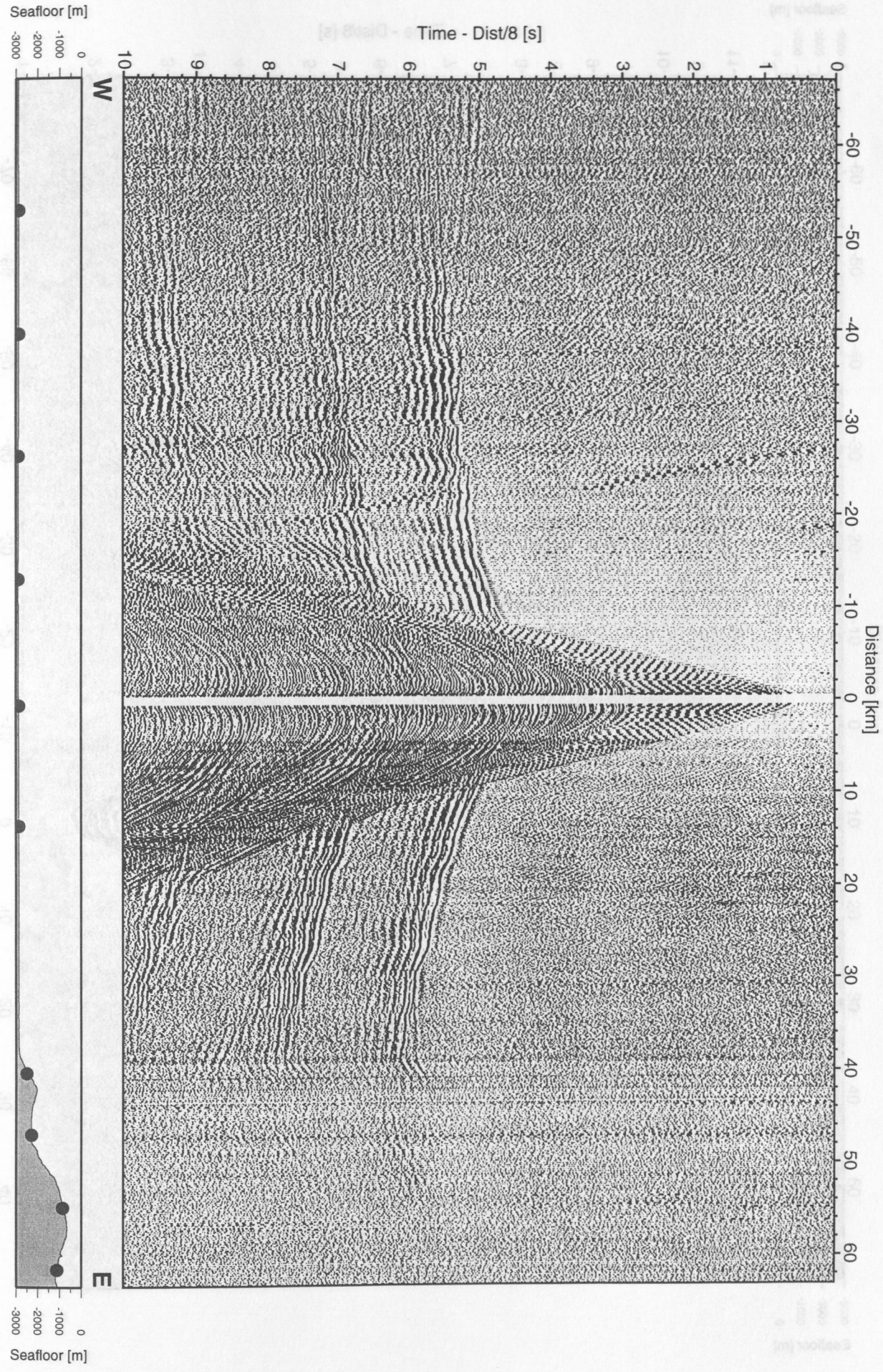

Figure 6.3.4.2.7: Record section from OBH 17, Profile 7.

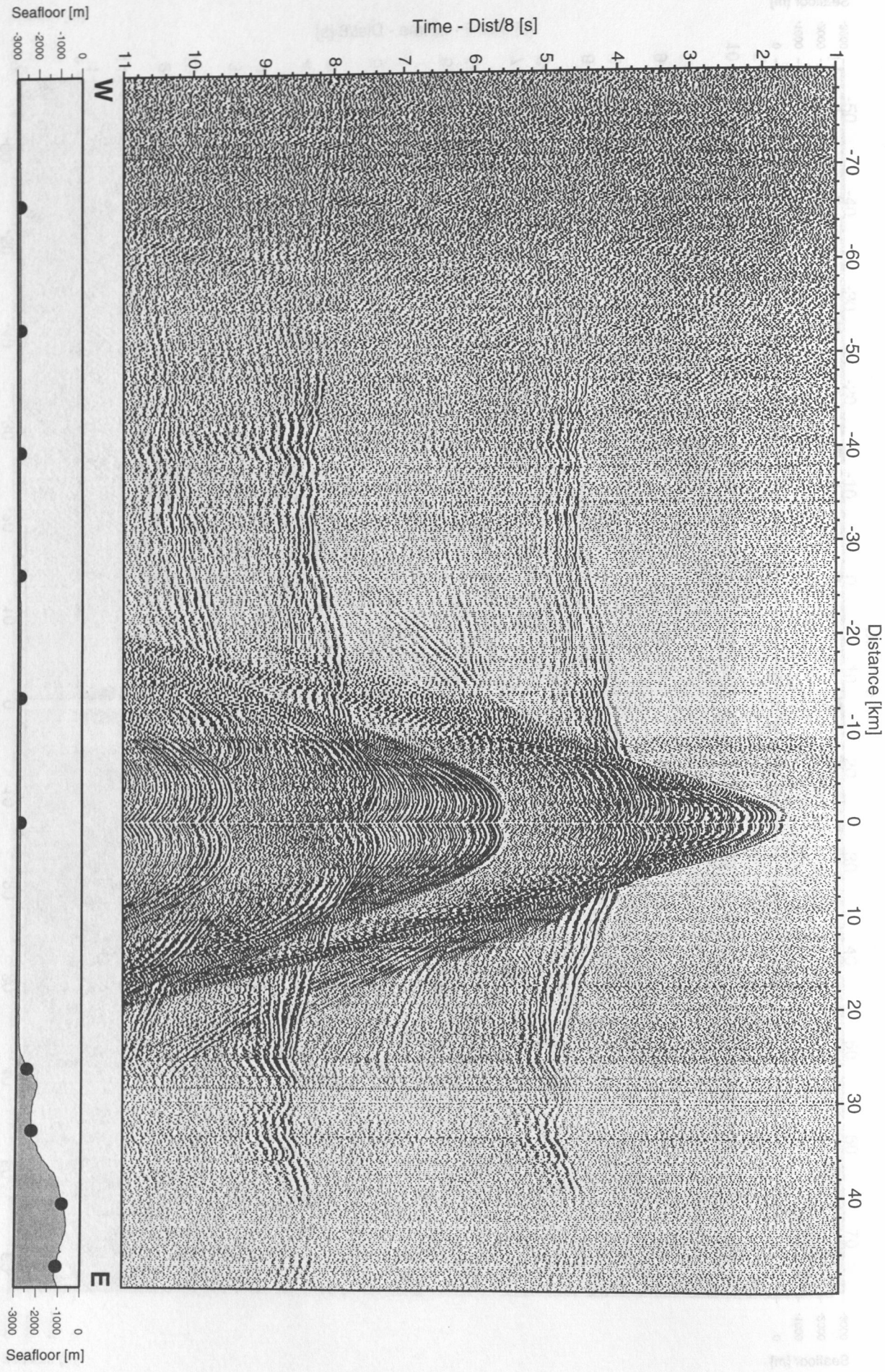

Figure 6.3.4.2.8: Record section from OBH 18, Profile 7.

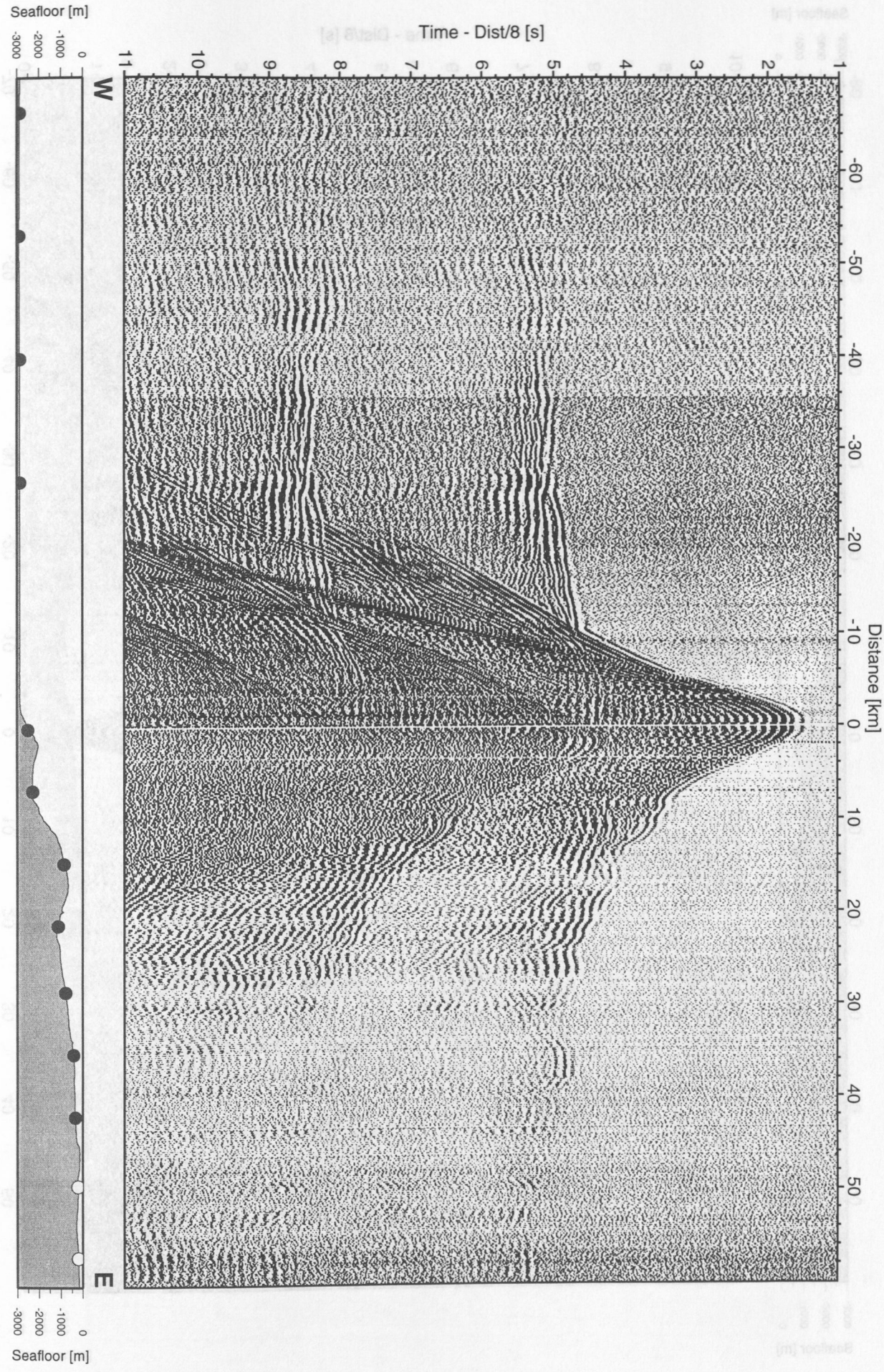

Figure 6.3.4.2.9: Record section from OBH 20, Profile 7.

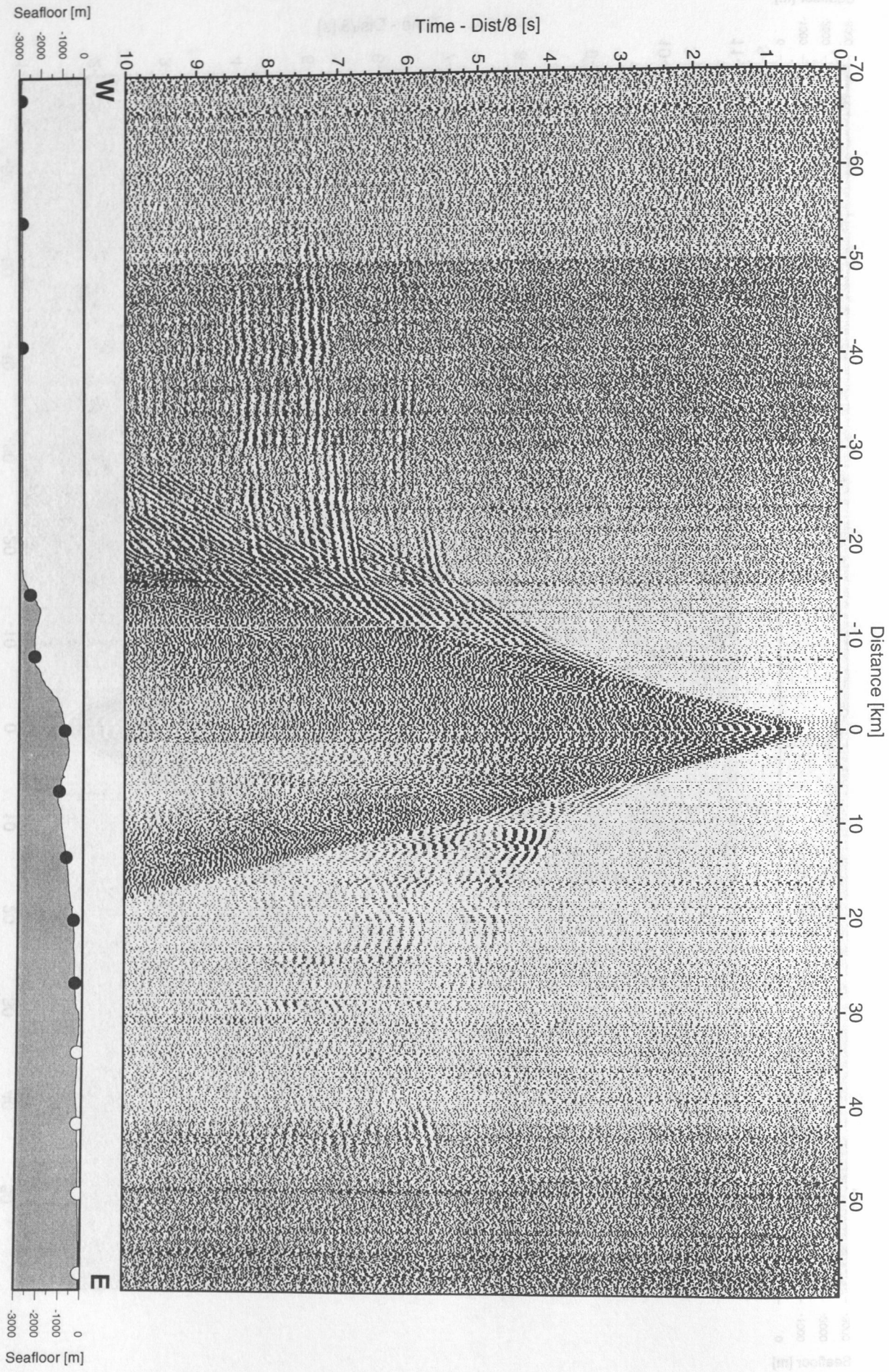

Figure 6.3.4.2.10: Record section from OBH 22, Profile 7.

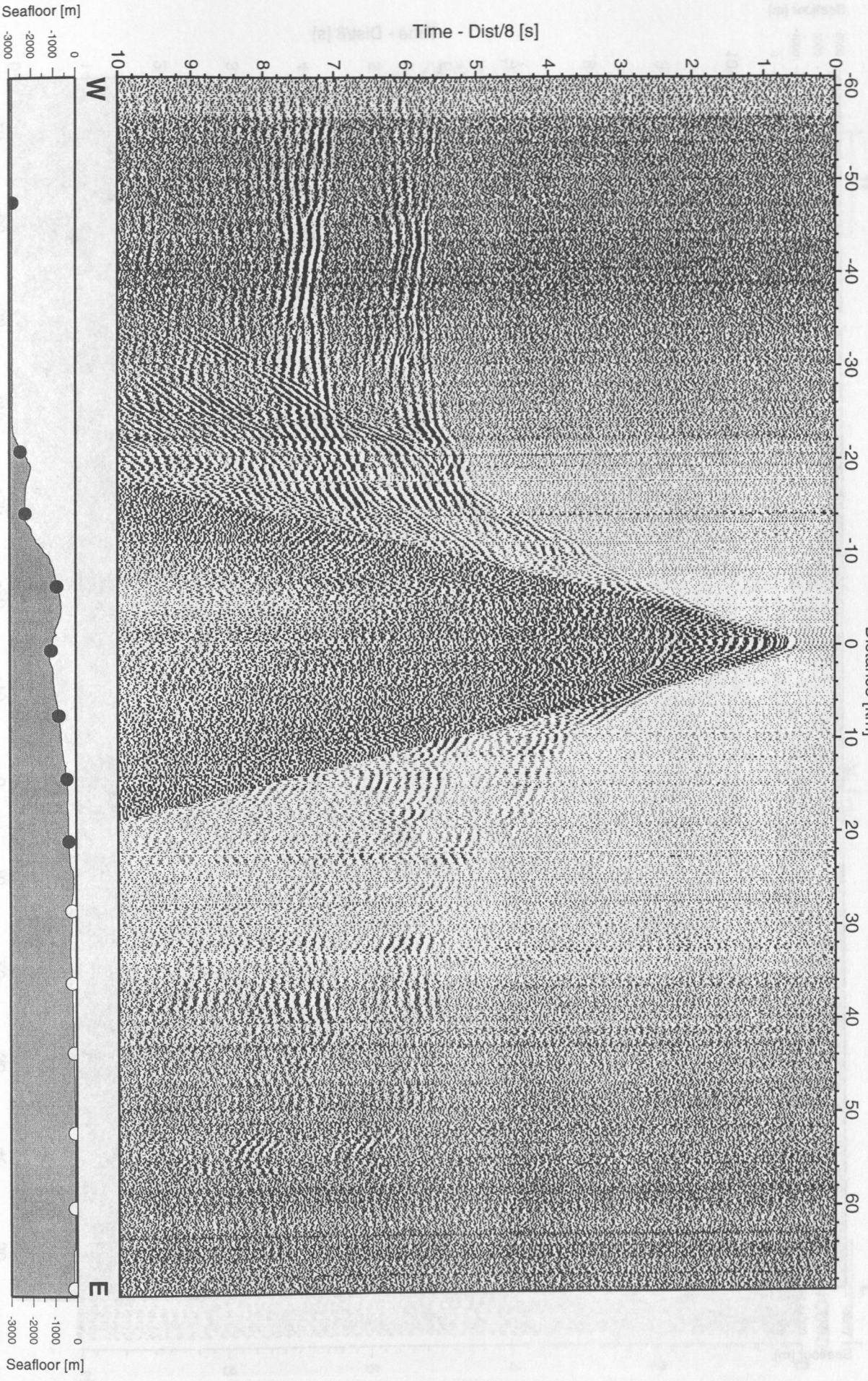

Figure 6.3.4.2.11: Record section from OBH 23, Profile 7.

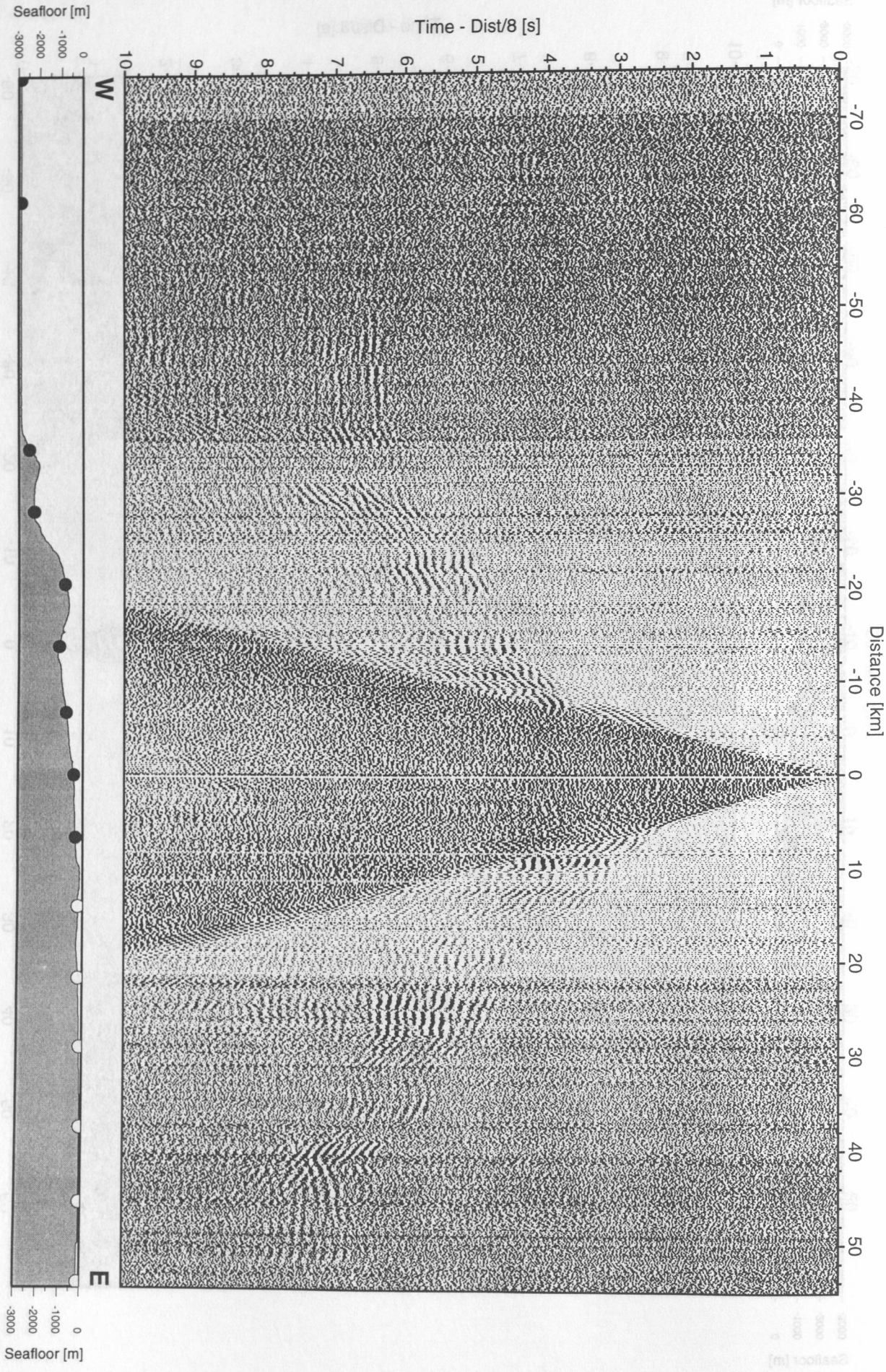

Figure 6.3.4.2.12: Record section from OBH 25, Profile 7.

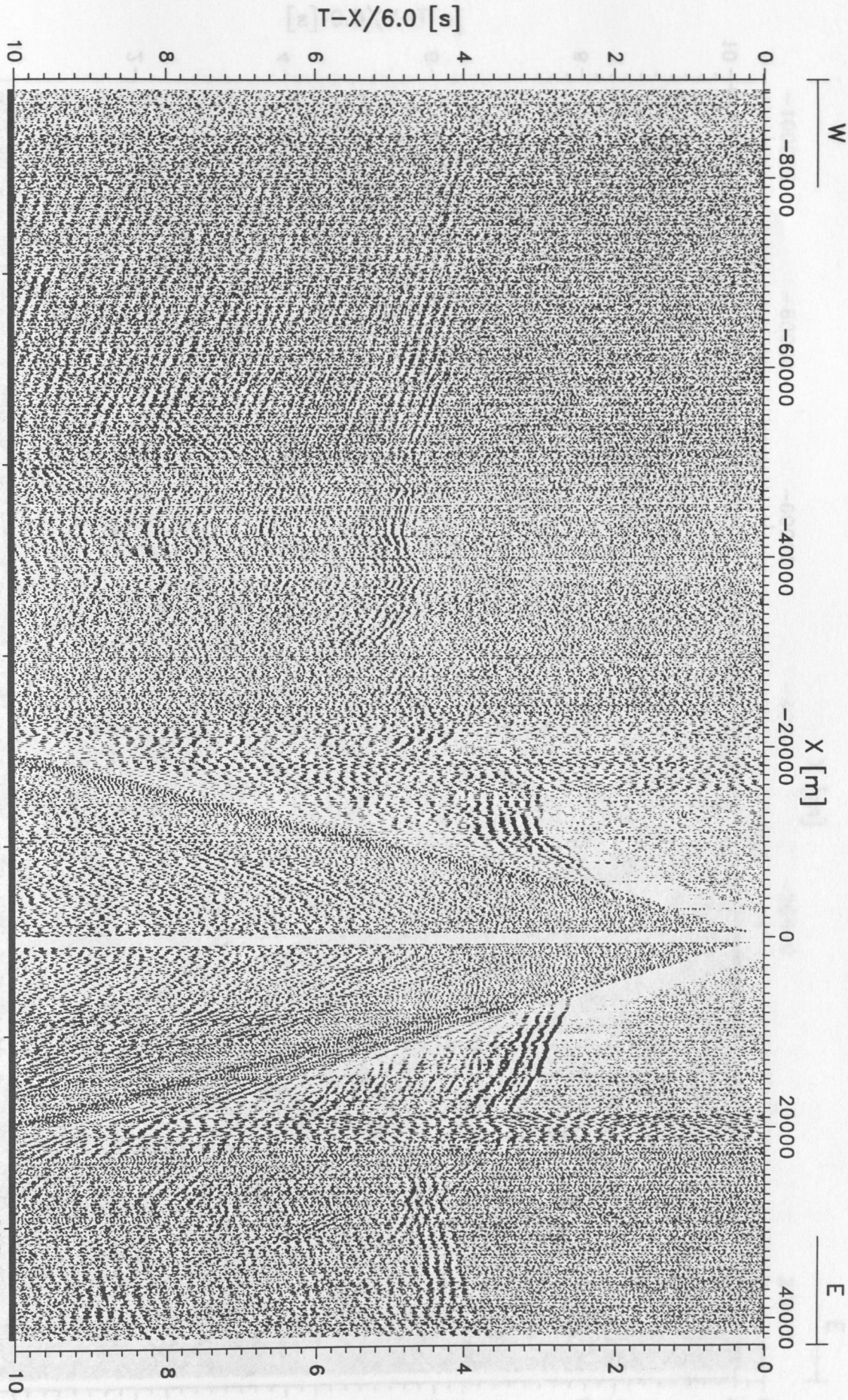

Figure 6.3.4.2.13: Record section for OBS09, vertical component.

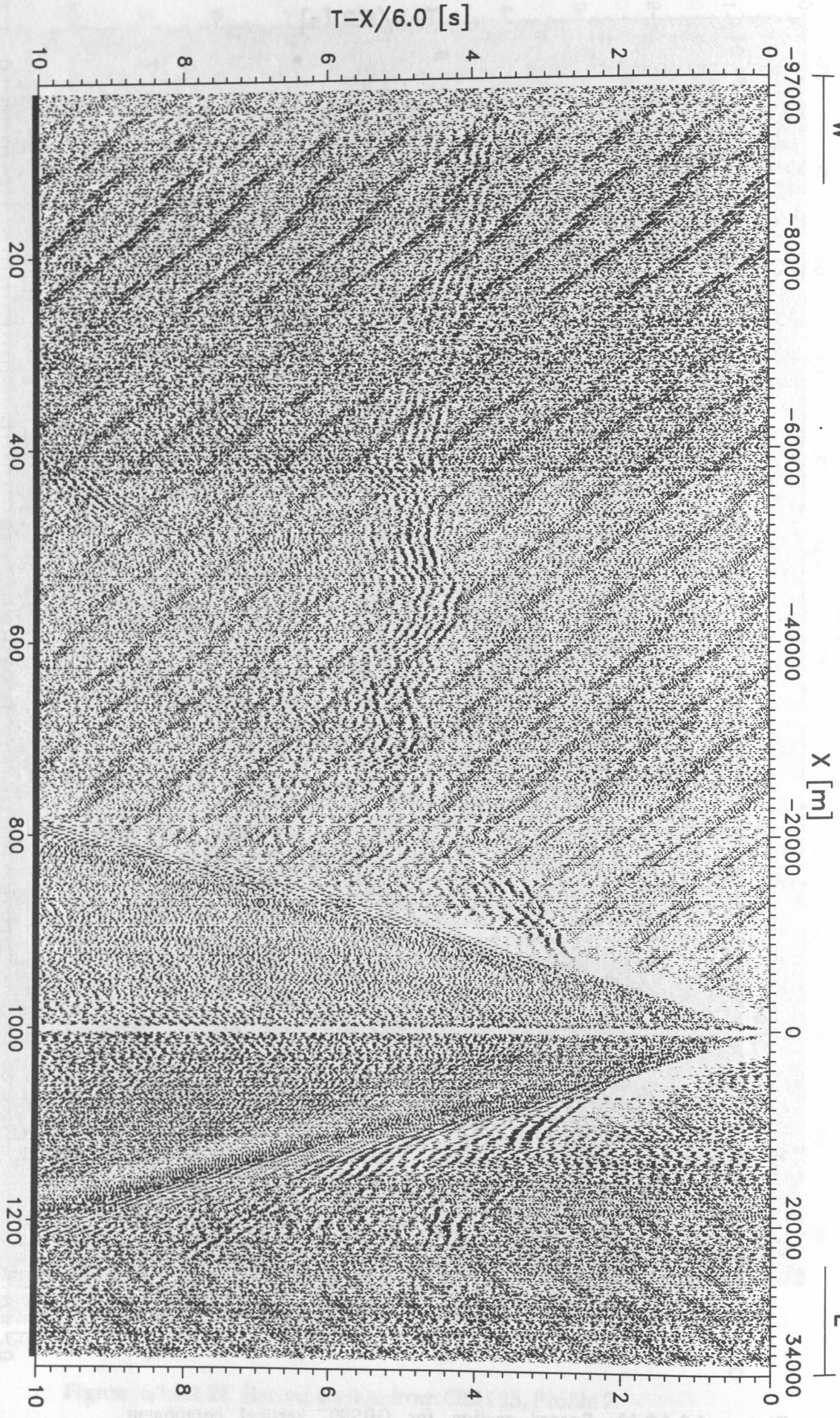

Figure 6.3.4.2.14: Record section for OBS10, vertical component.

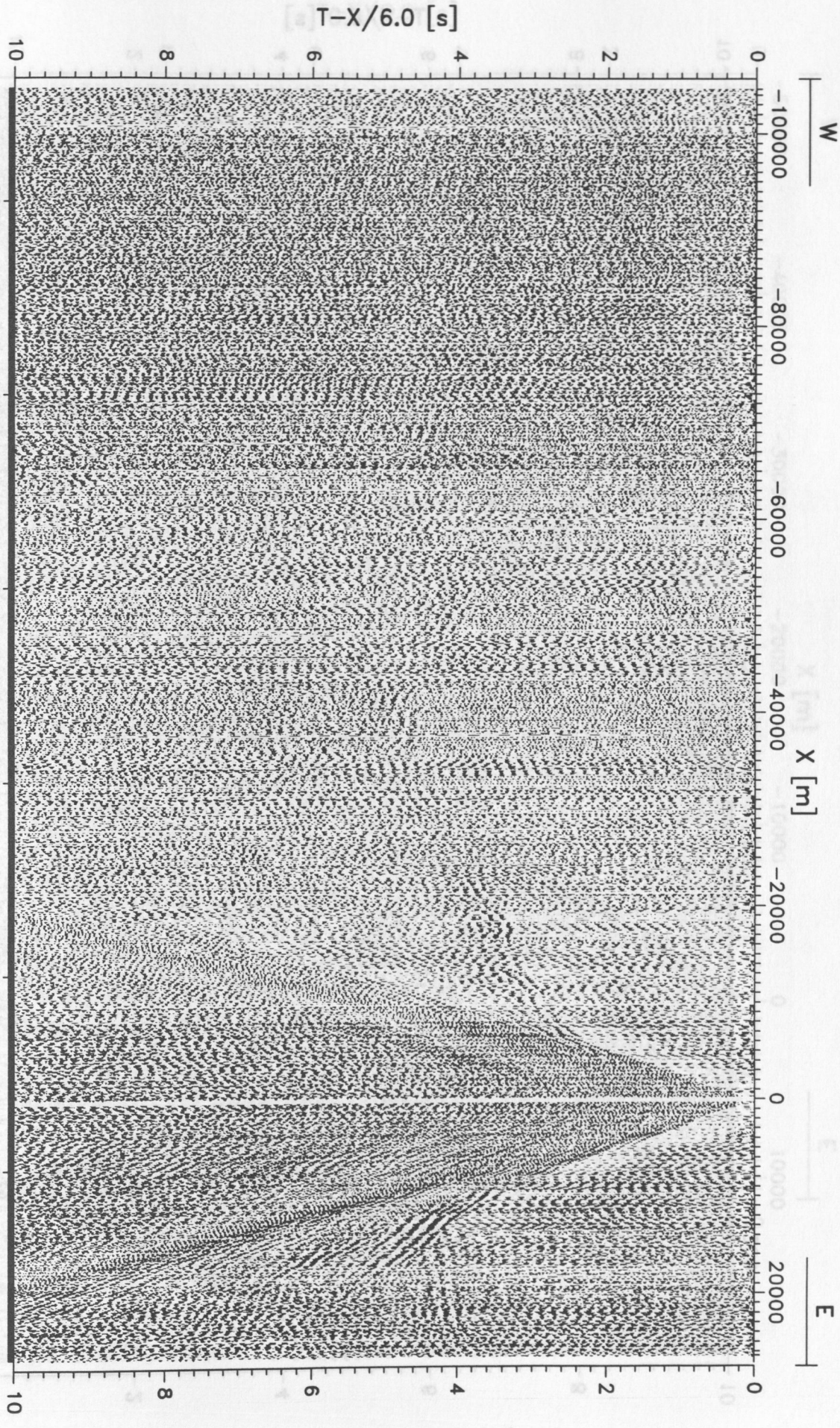

Figure 6.3.4.2.15: Record section for OBS11, vertical component.

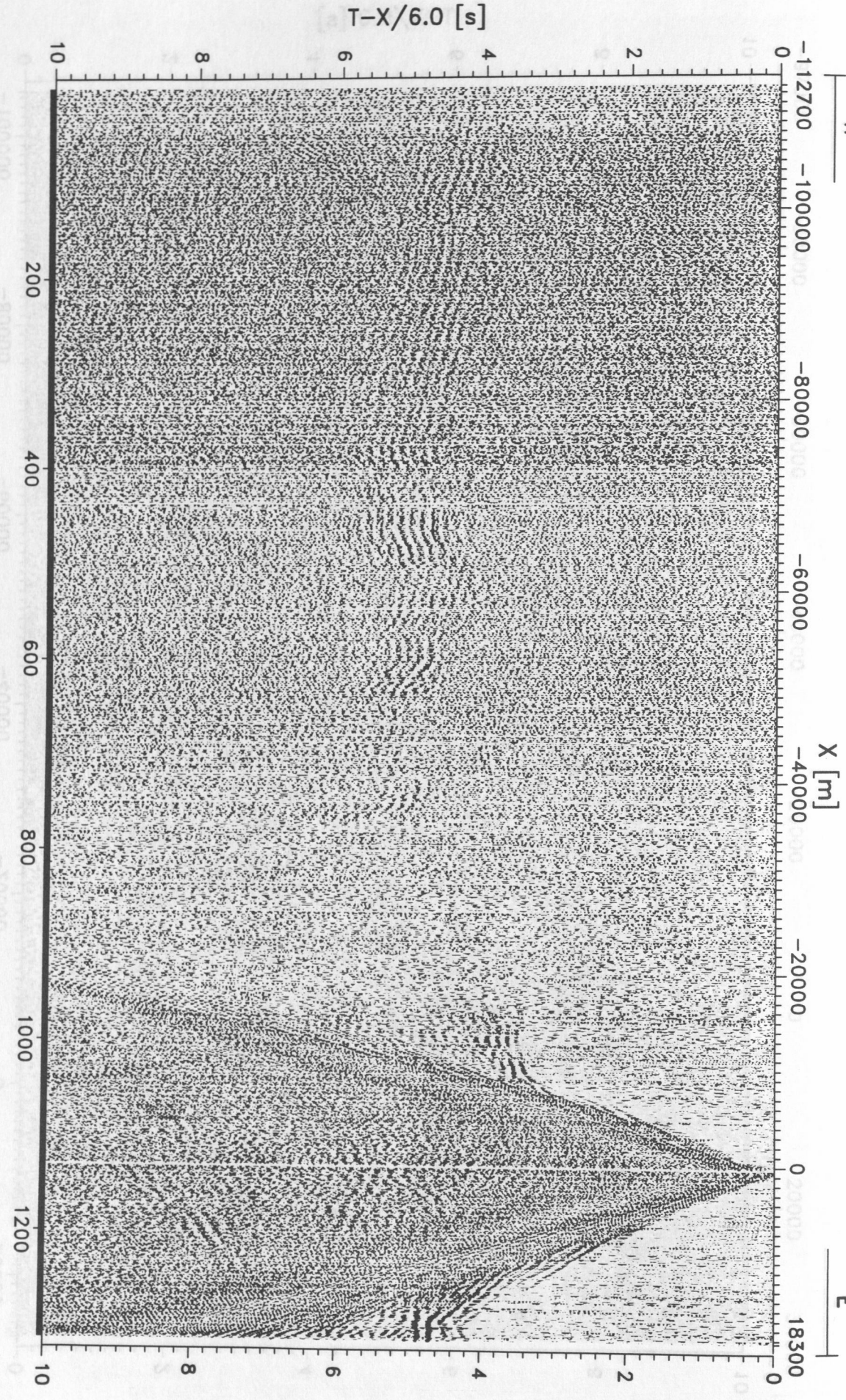

Figure 6.3.4.2.16: Record section for OBS12, hydrophone.

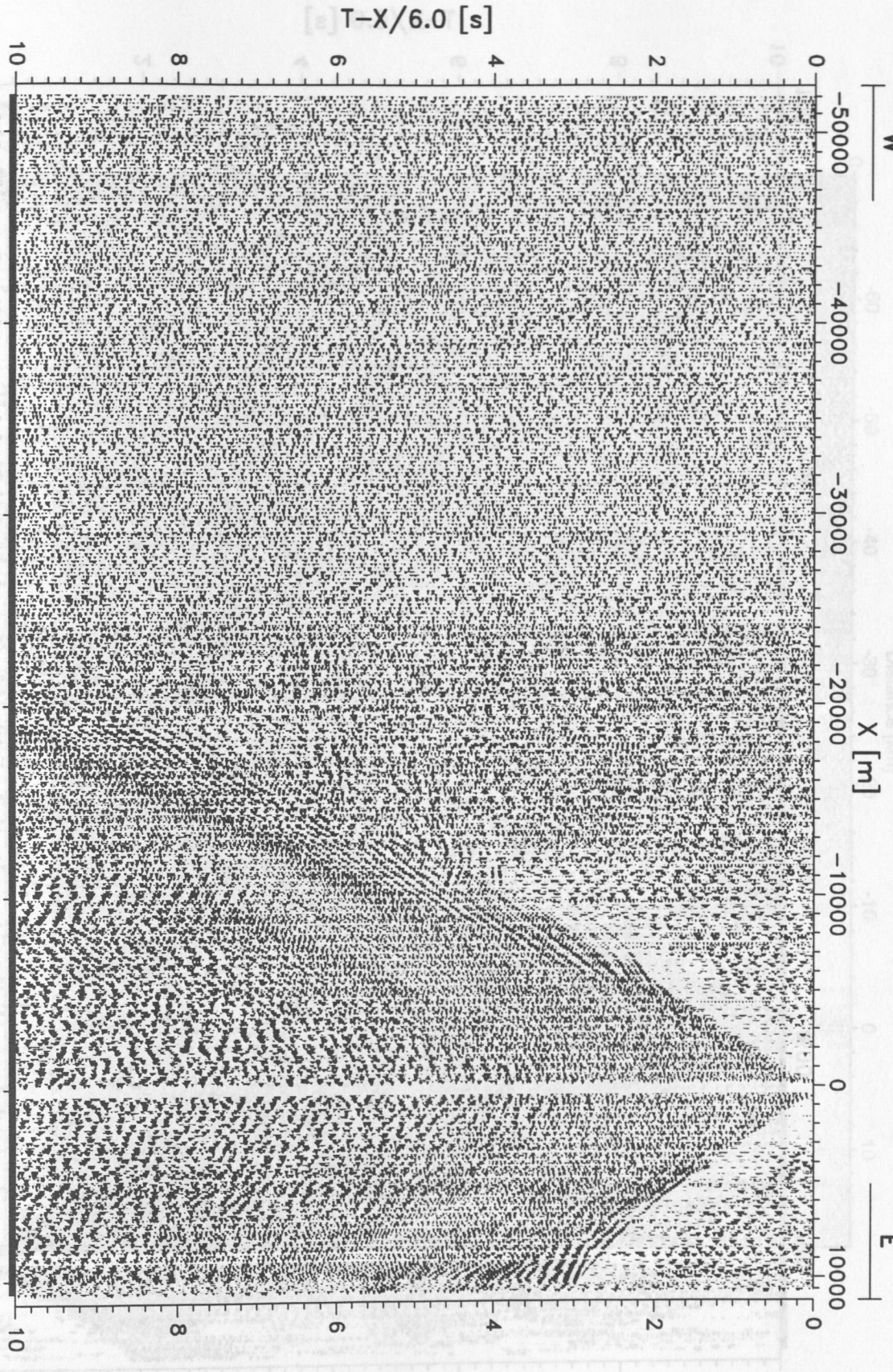

Figure 6.3.4.2.17: Record section for OBS13, vertical component.

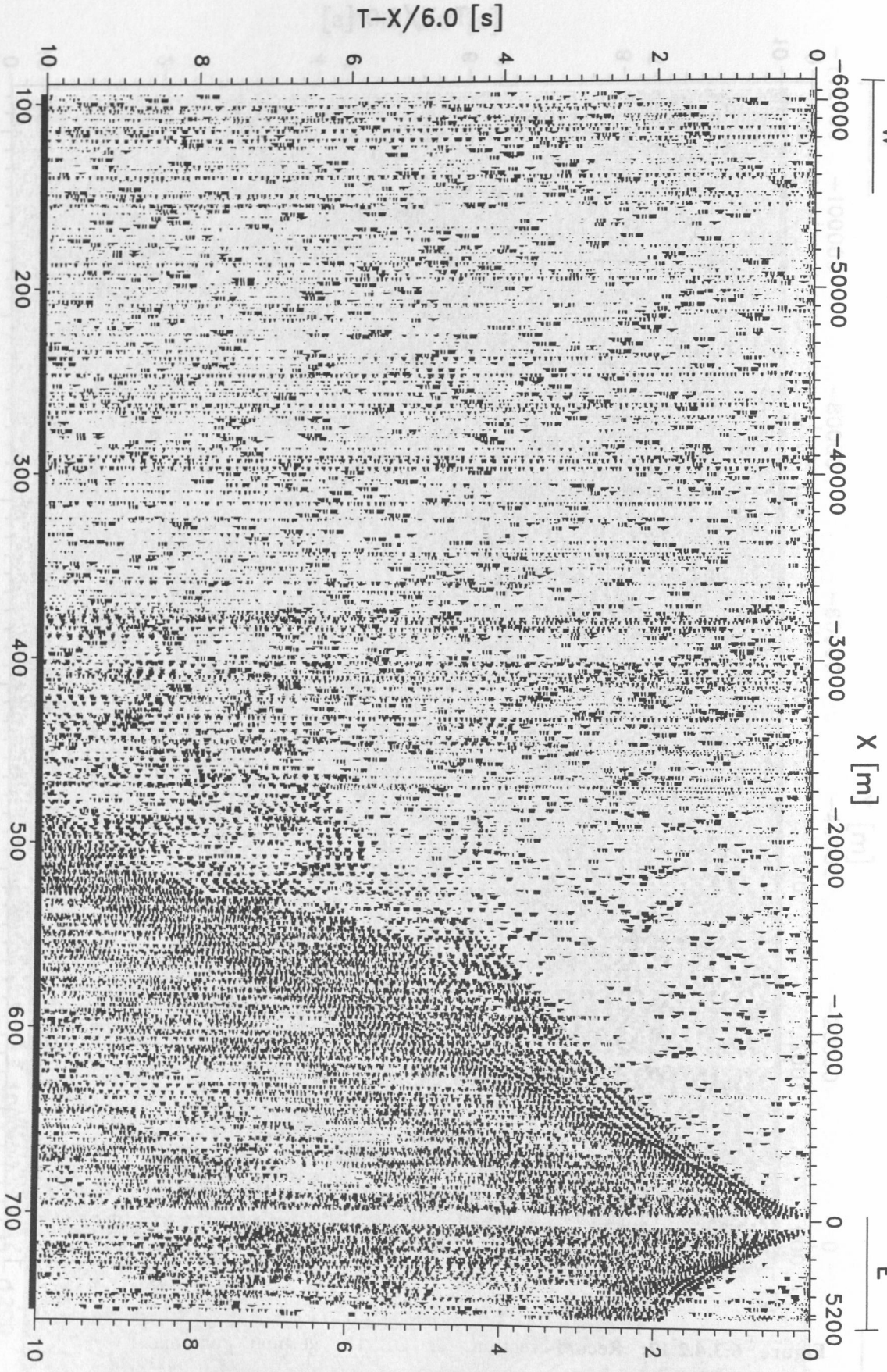

Figure 6.3.4.2.18: Record section for OBS14, hydrophone.

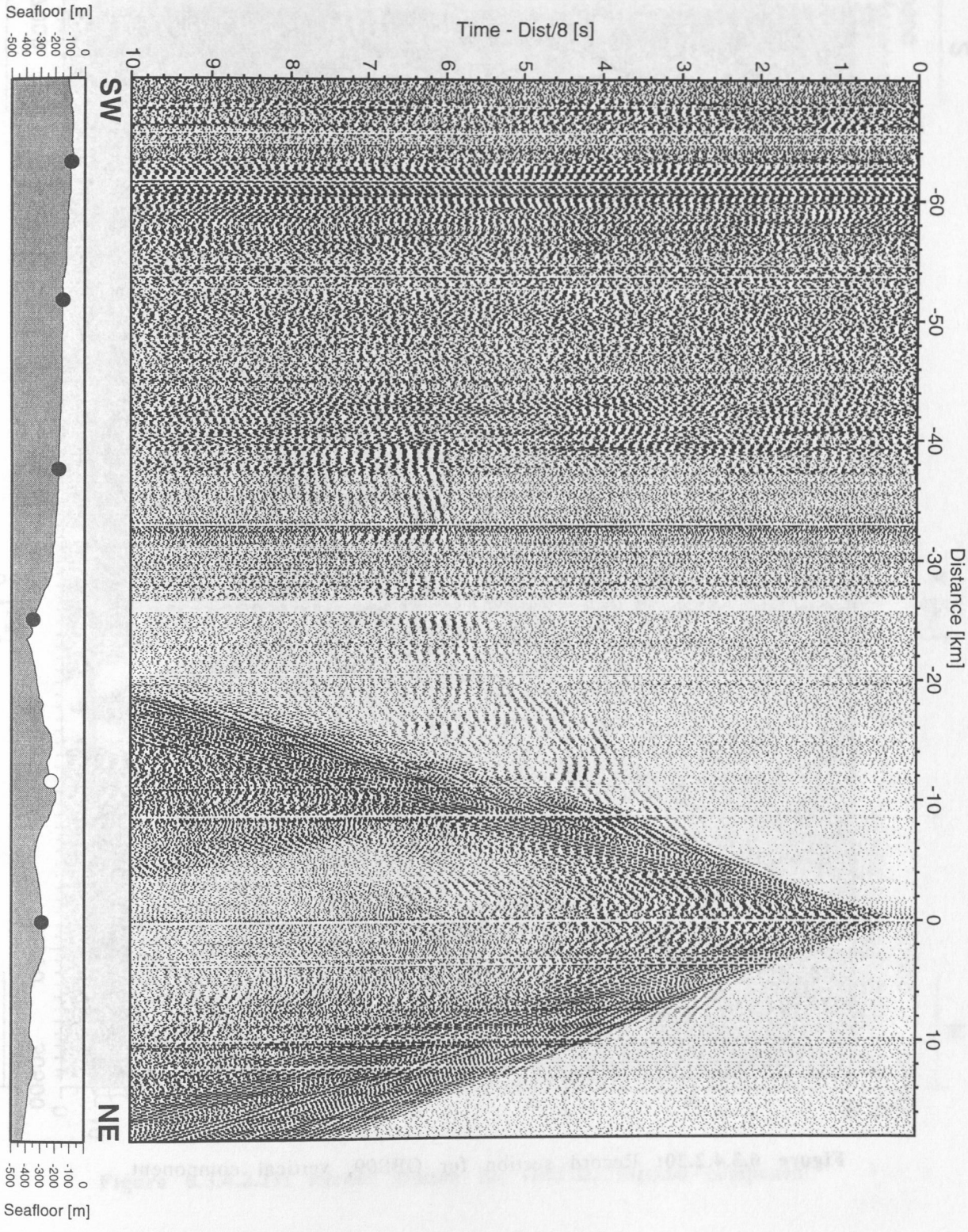

Figure 6.3.4.2.19: Record section from OBH 28, Profile 9.

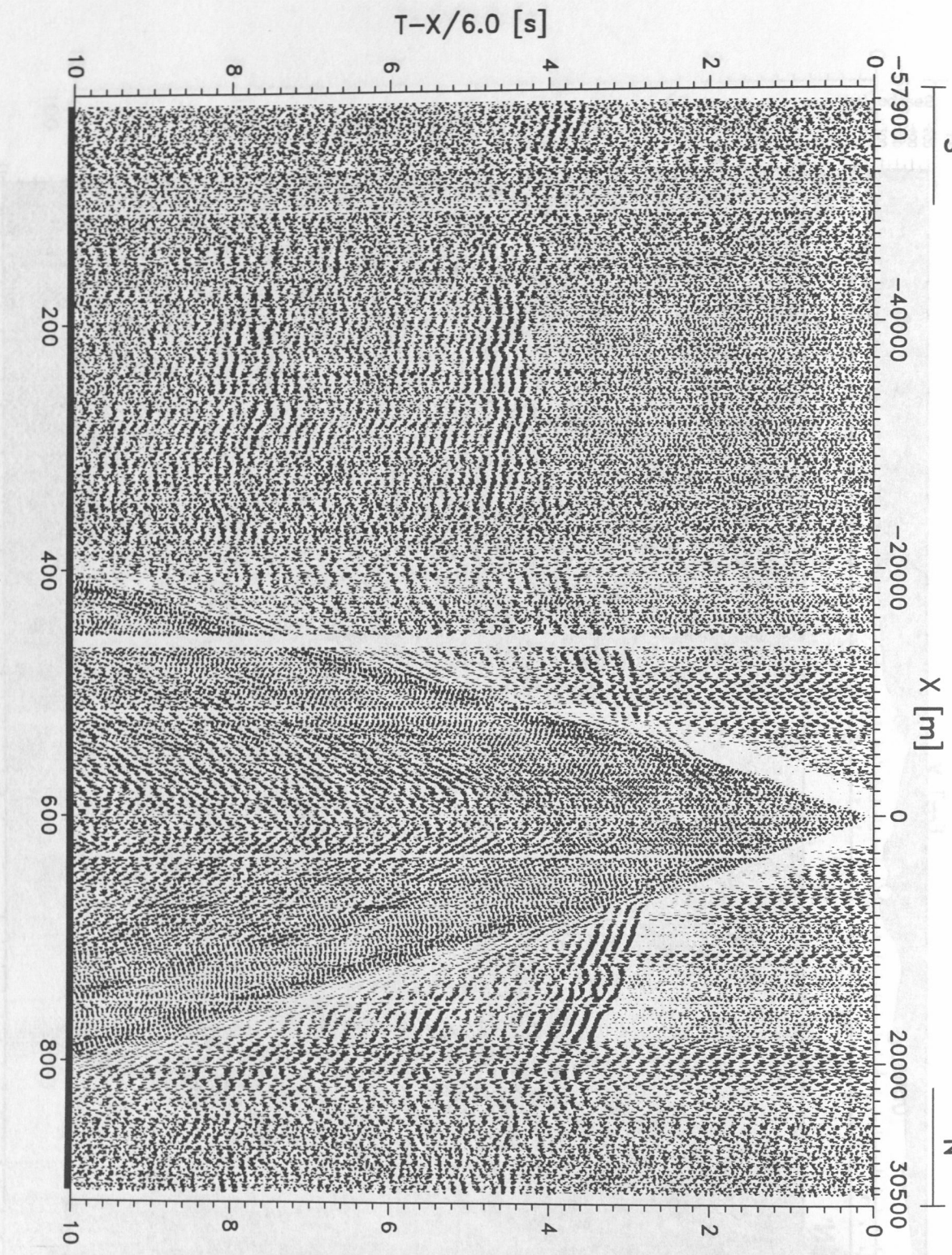

Figure 6.3.4.2.20: Record section for OBS09, vertical component.

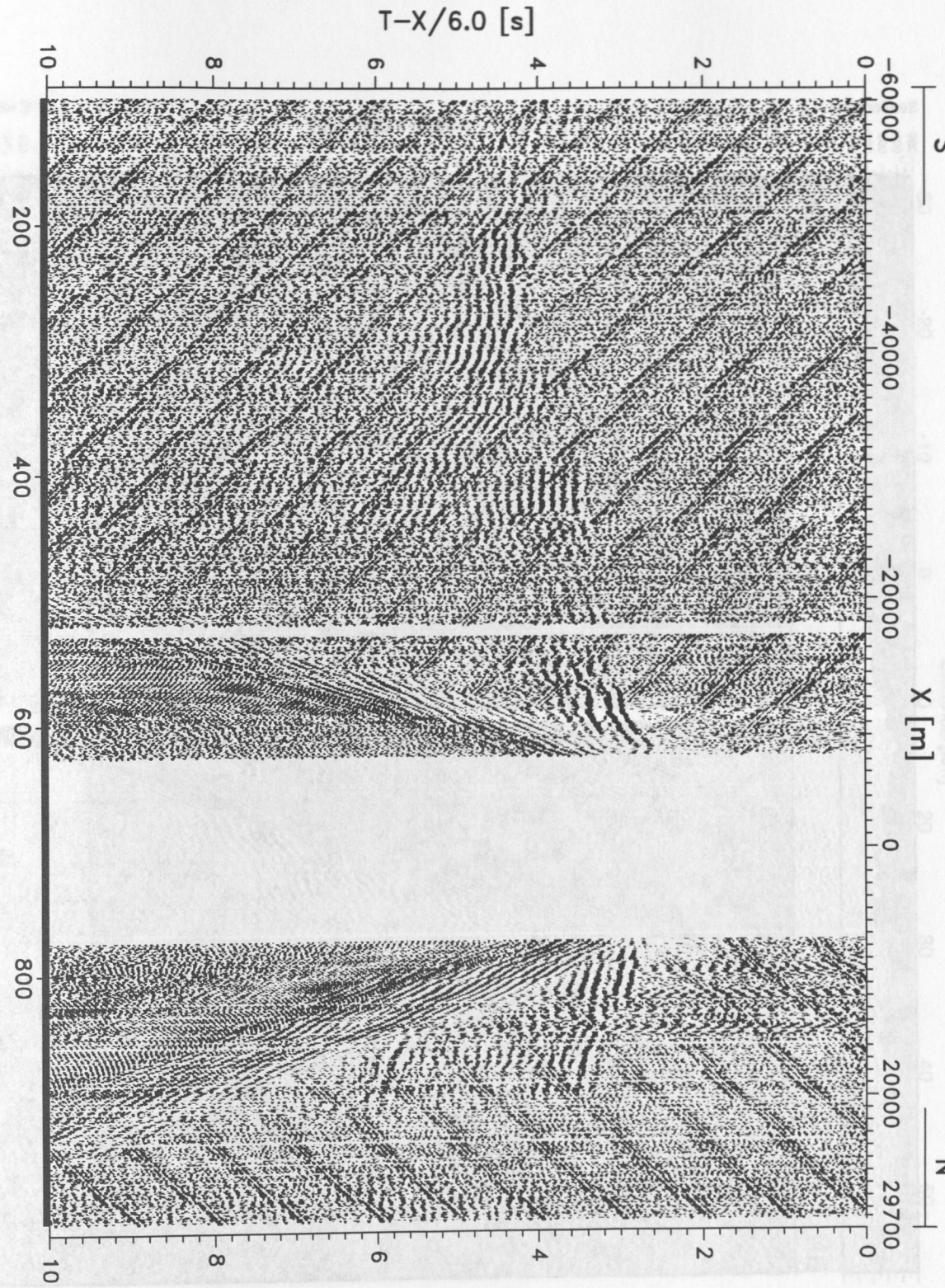

Figure 6.3.4.2.21: Record section for OBS10, vertical component.

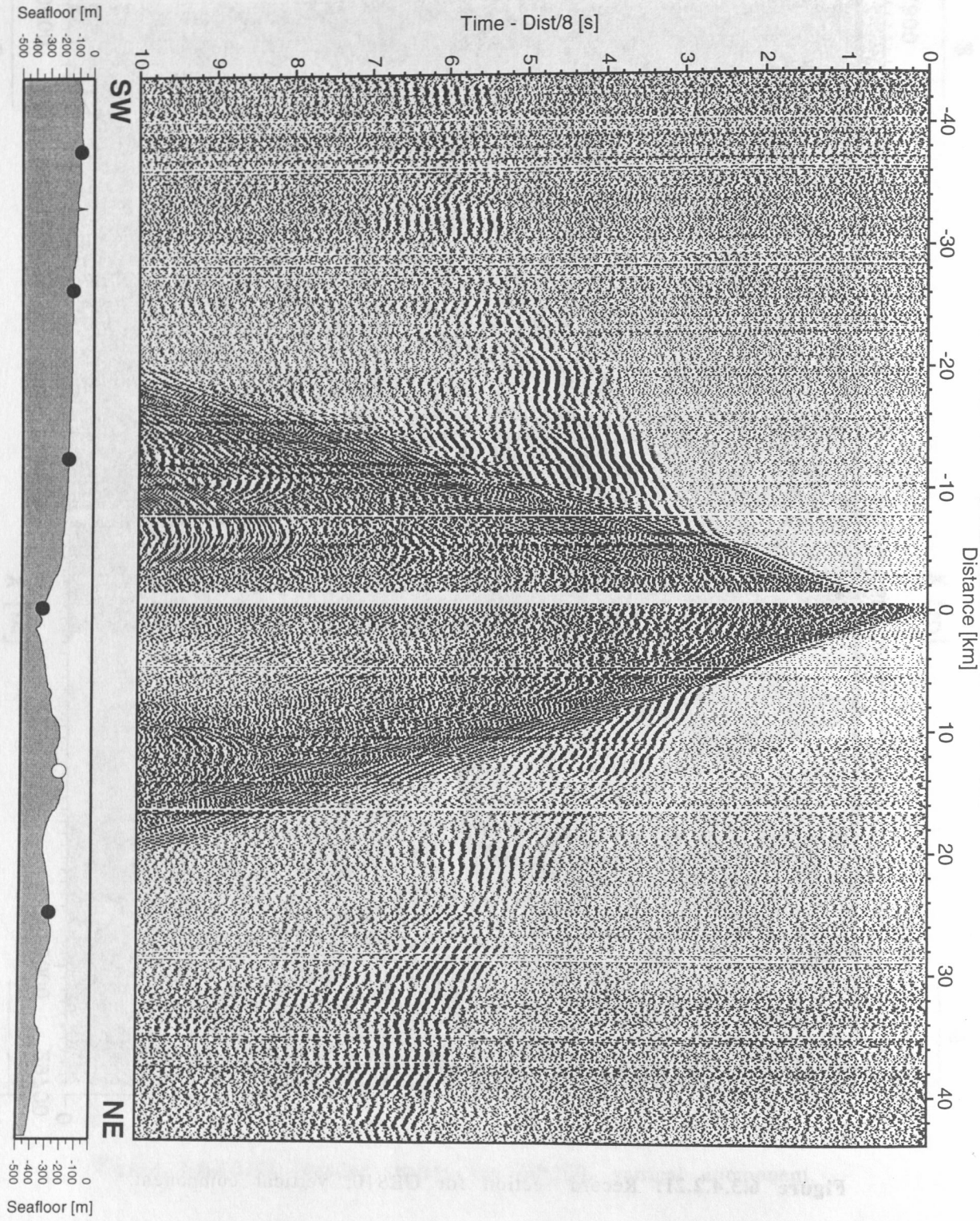

Figure 6.3.4.2.22: Record section from OBH 29, Profile 9.

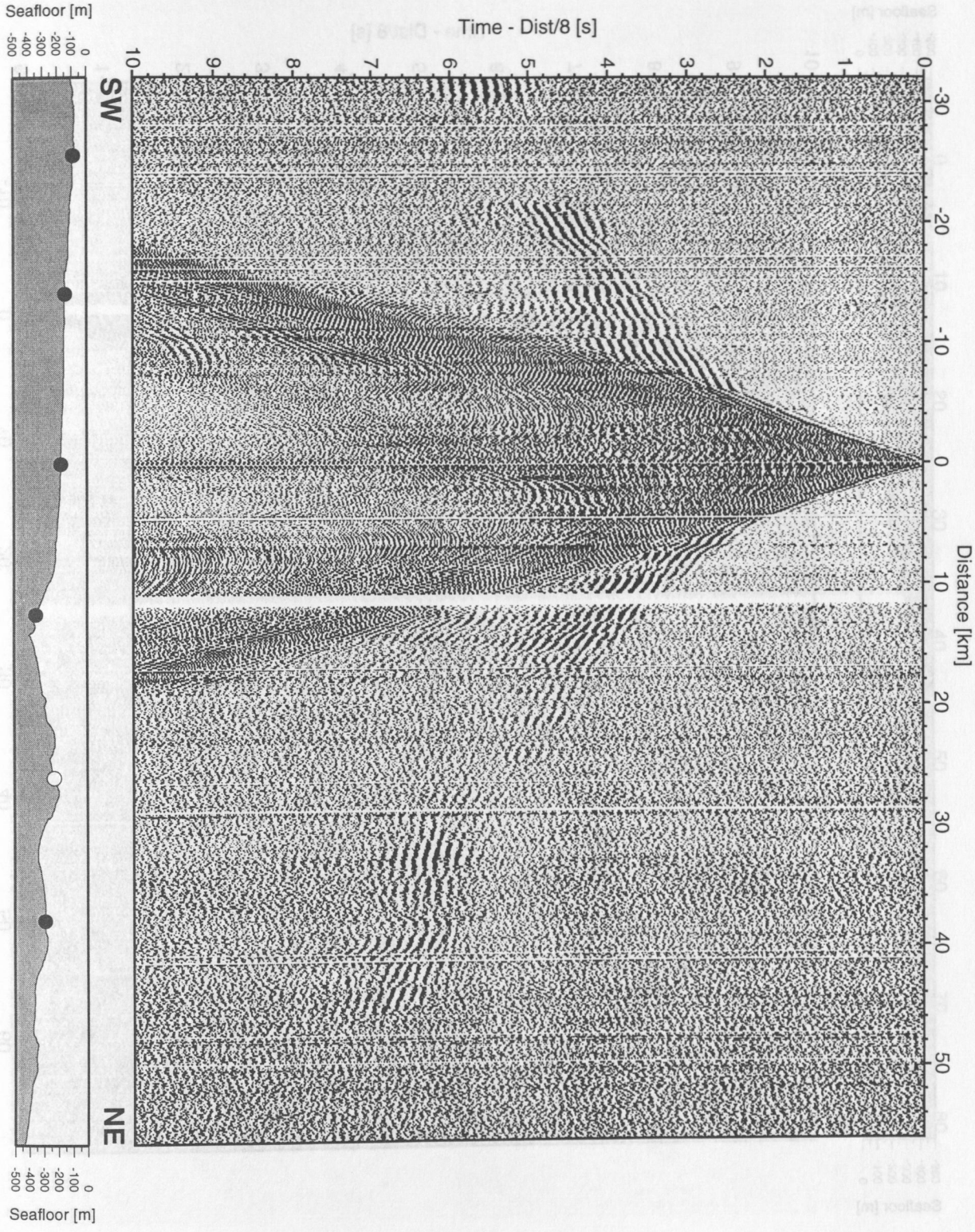

Figure 6.3.4.2.23: Record section from OBH 30, Profile 9.

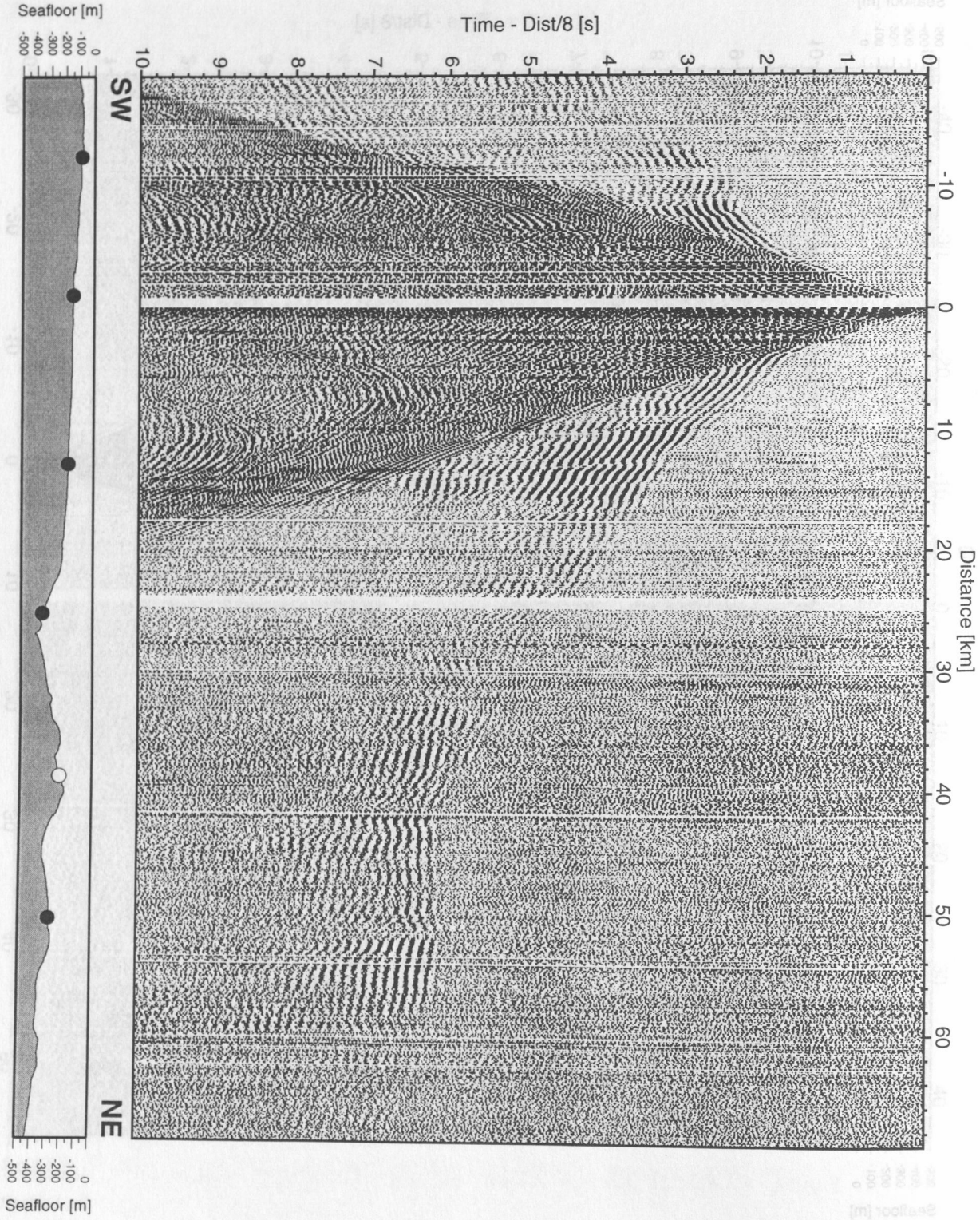

Figure 6.3.4.2.24: Record section from OBH 31, Profile 9.

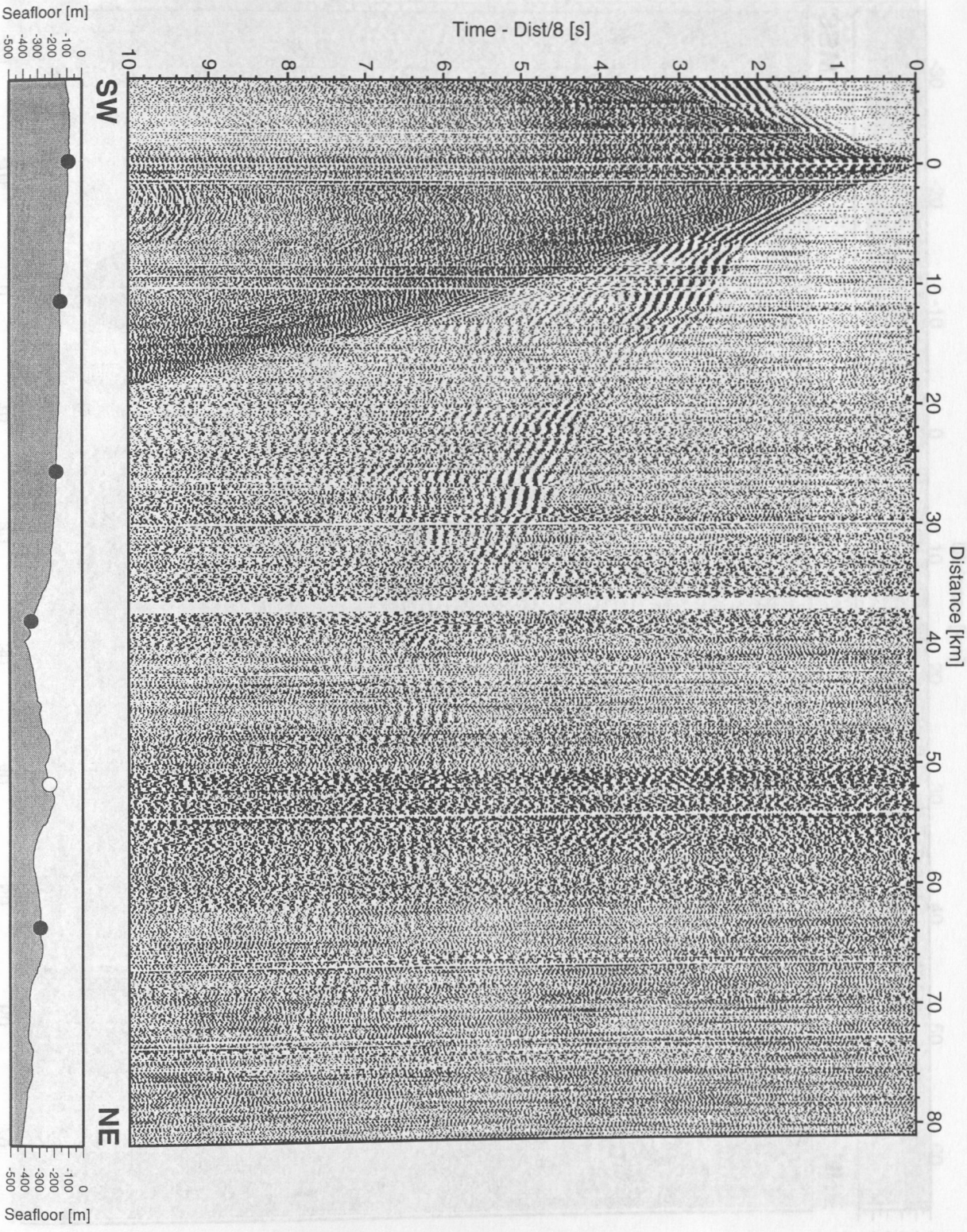

Figure 6.3.4.2.25: Record section from OBH 32, Profile 9.

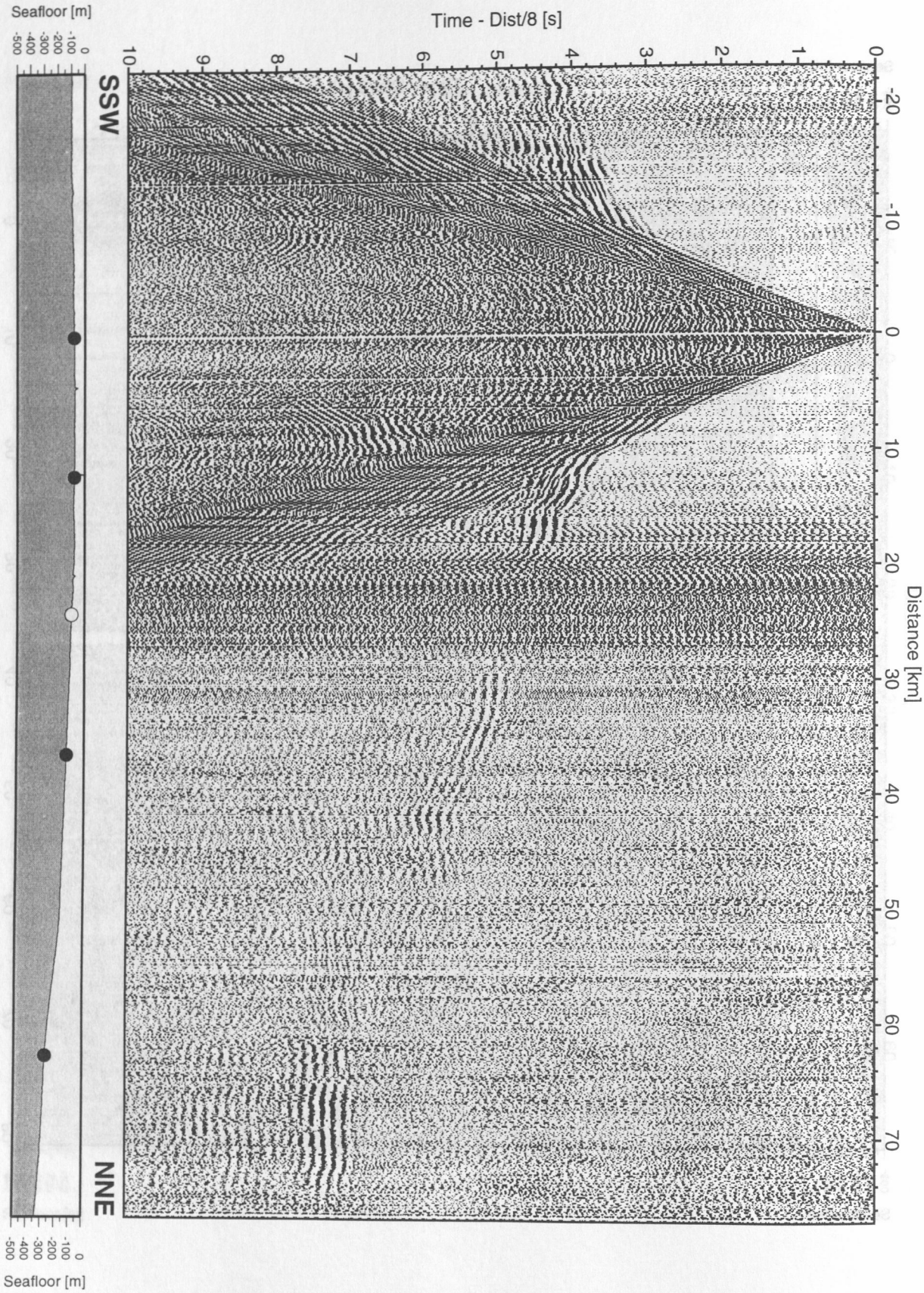

Figure 6.3.4.2.26: Record section from OBH 34, Profile 8.

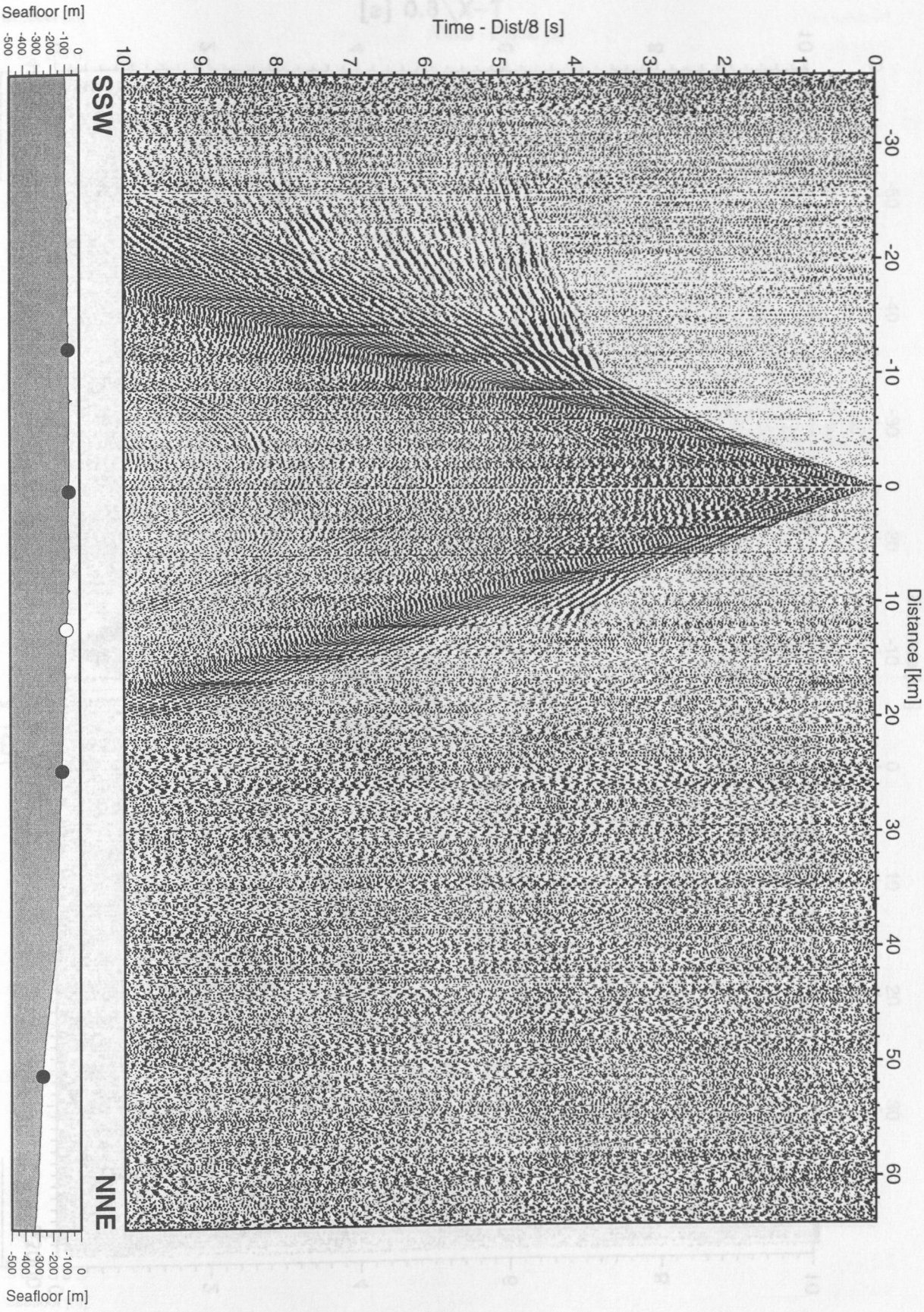

Figure 6.3.4.2.27: Record section from OBH 35, Profile 8.

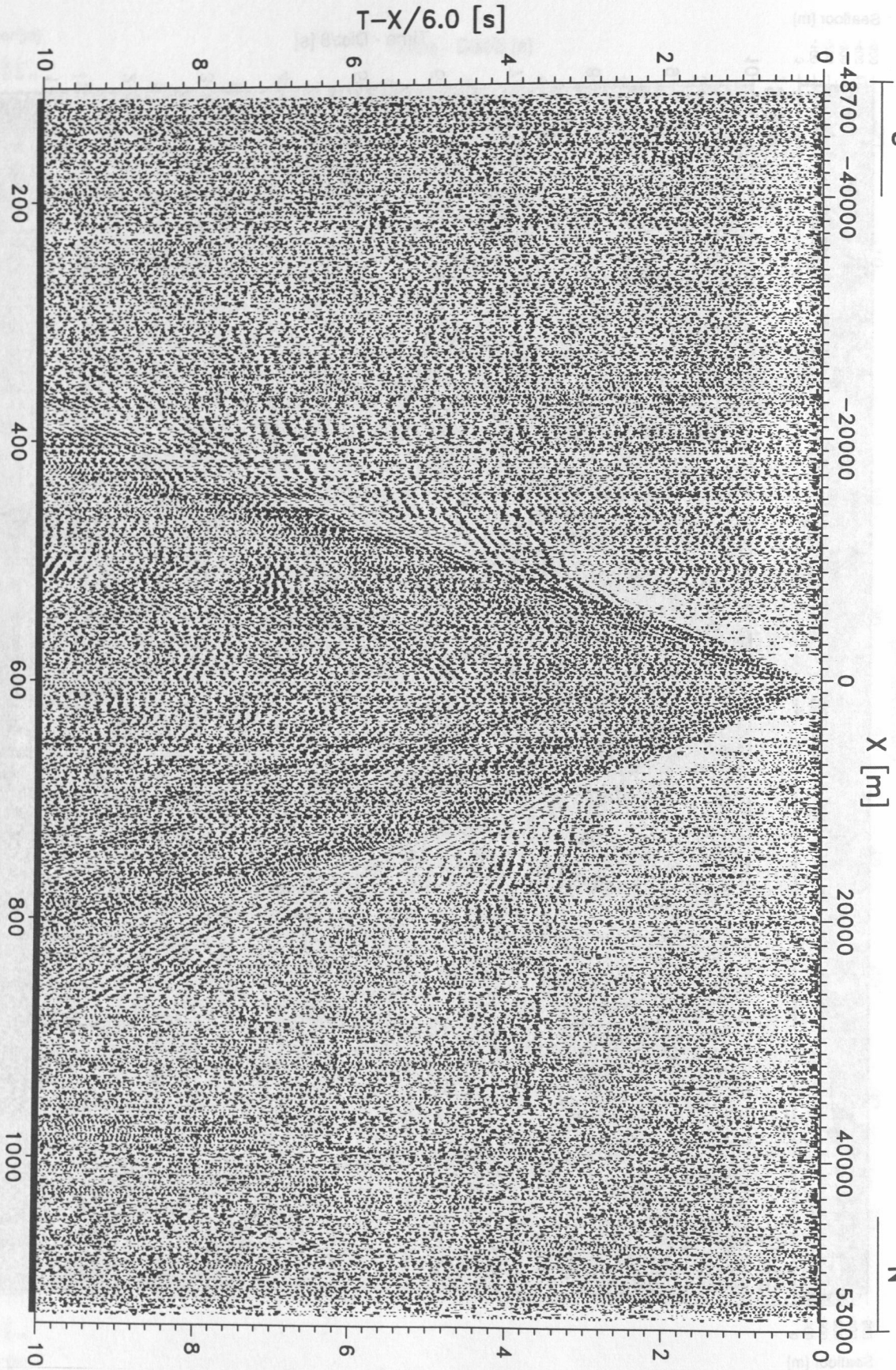

Figure 6.3.4.2.28: Record section for OBS15, hydrophone.

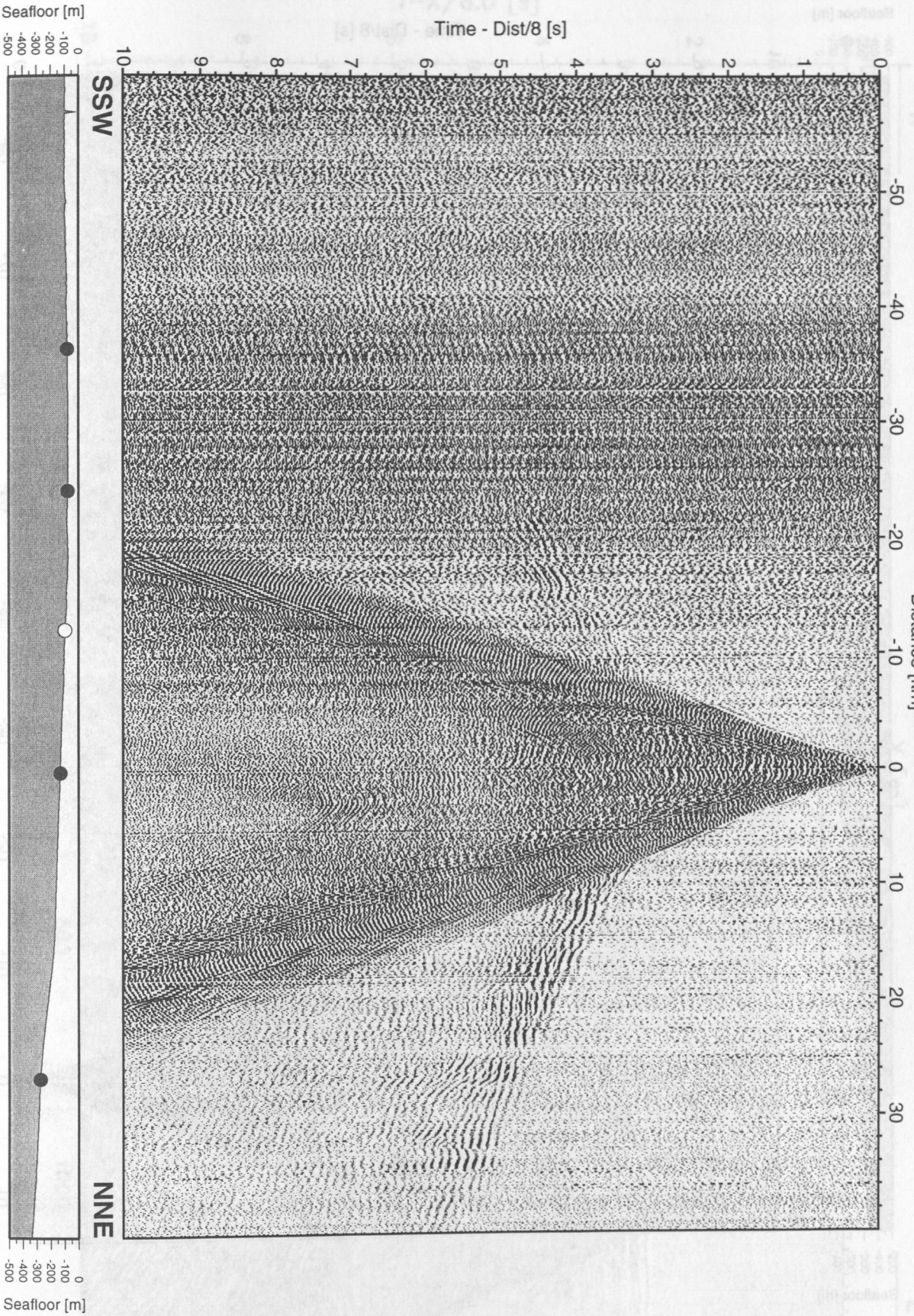

Figure 6.3.4.2.29: Record section from OBH 36, Profile 8.

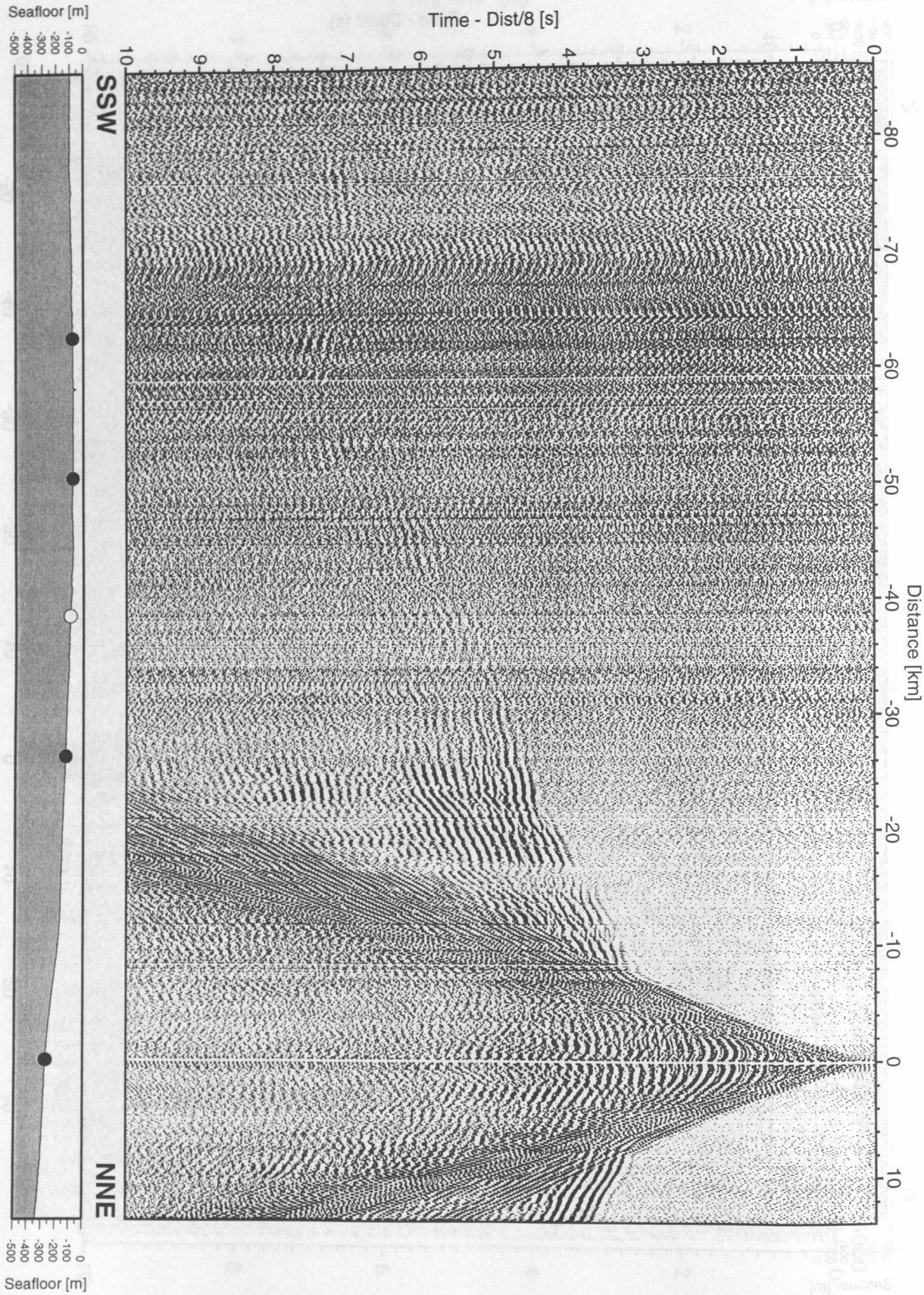

Figure 6.3.4.2.30: Record section from OBH 38, Profile 8.

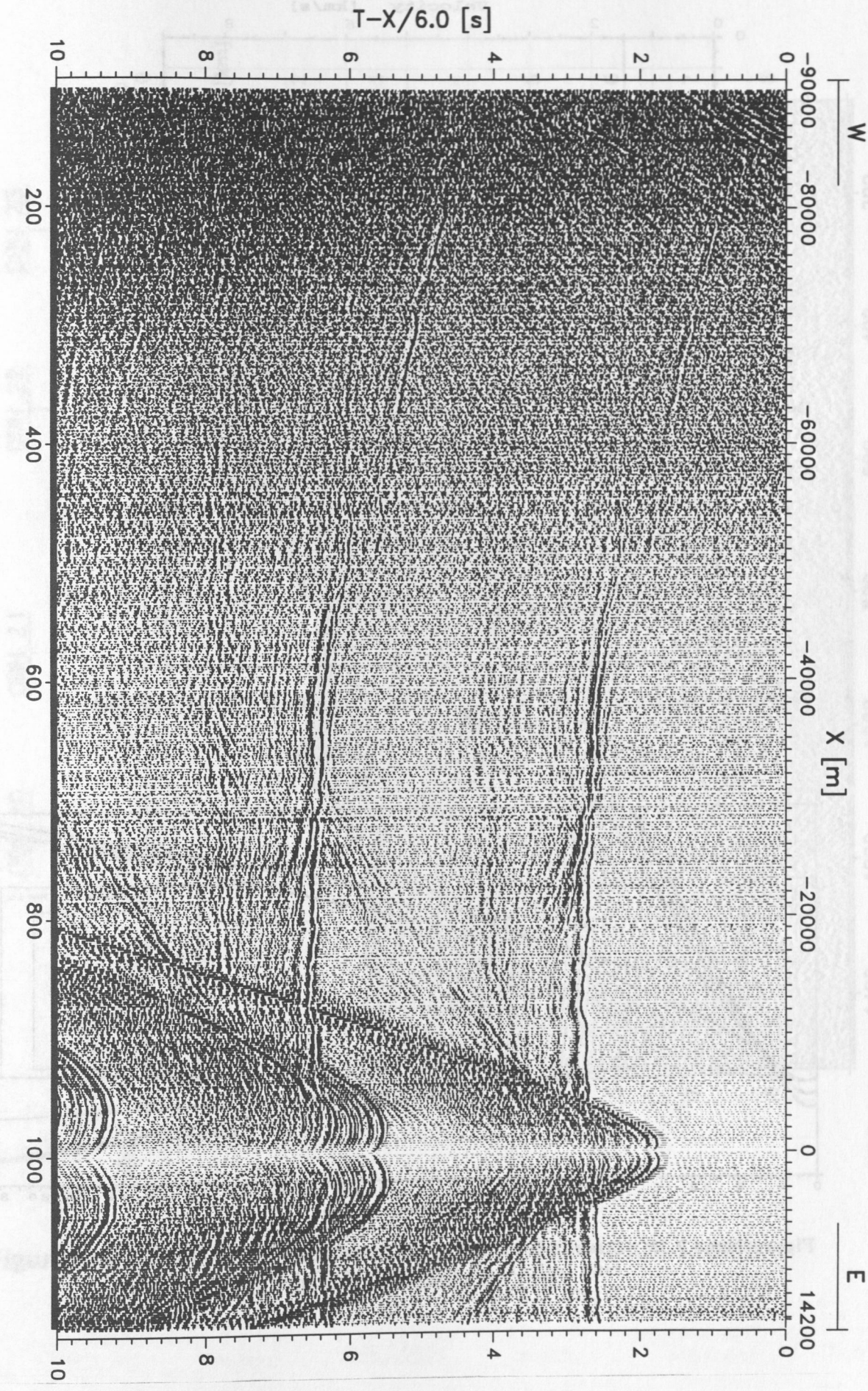

Figure 6.3.4.2.31: Record section for OBH13 after deconvolution (compare to Figure 6.3.4.2.3).

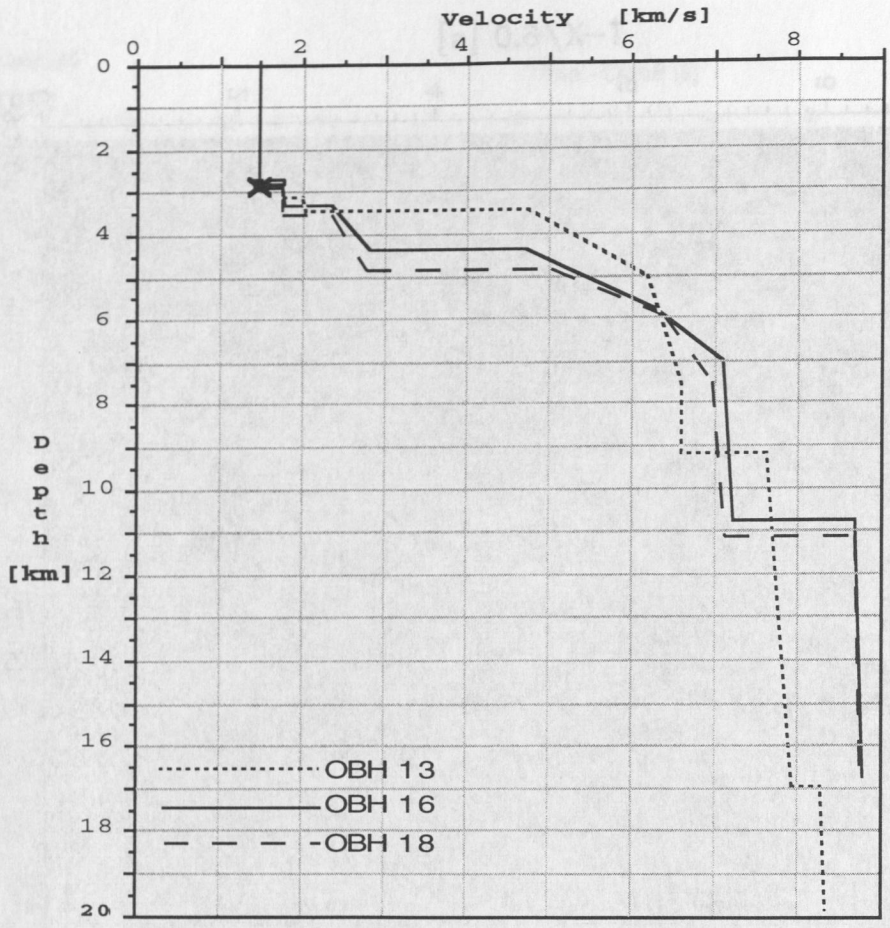

Figure 6.3.4.2.32: Best fitting 1-D velocity depth from OBH13-East and OBH16 and 18-West.

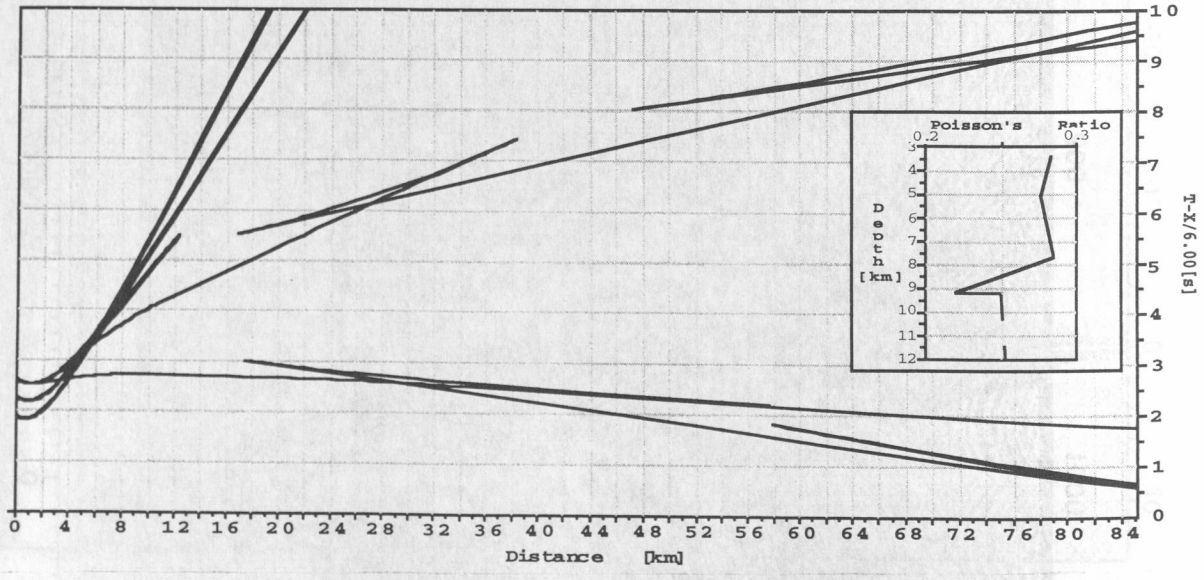

Figure 6.3.4.2.33: Traveltimes for P- and S-waves for OBH13 and Poisson's ratio calculated from the velocity depth function of Figure 6.3.4.2.32.

Figure 6.3.4.2.34: Poststack depth migration of Line 89OR-5. OBH-locations are indicated on top.

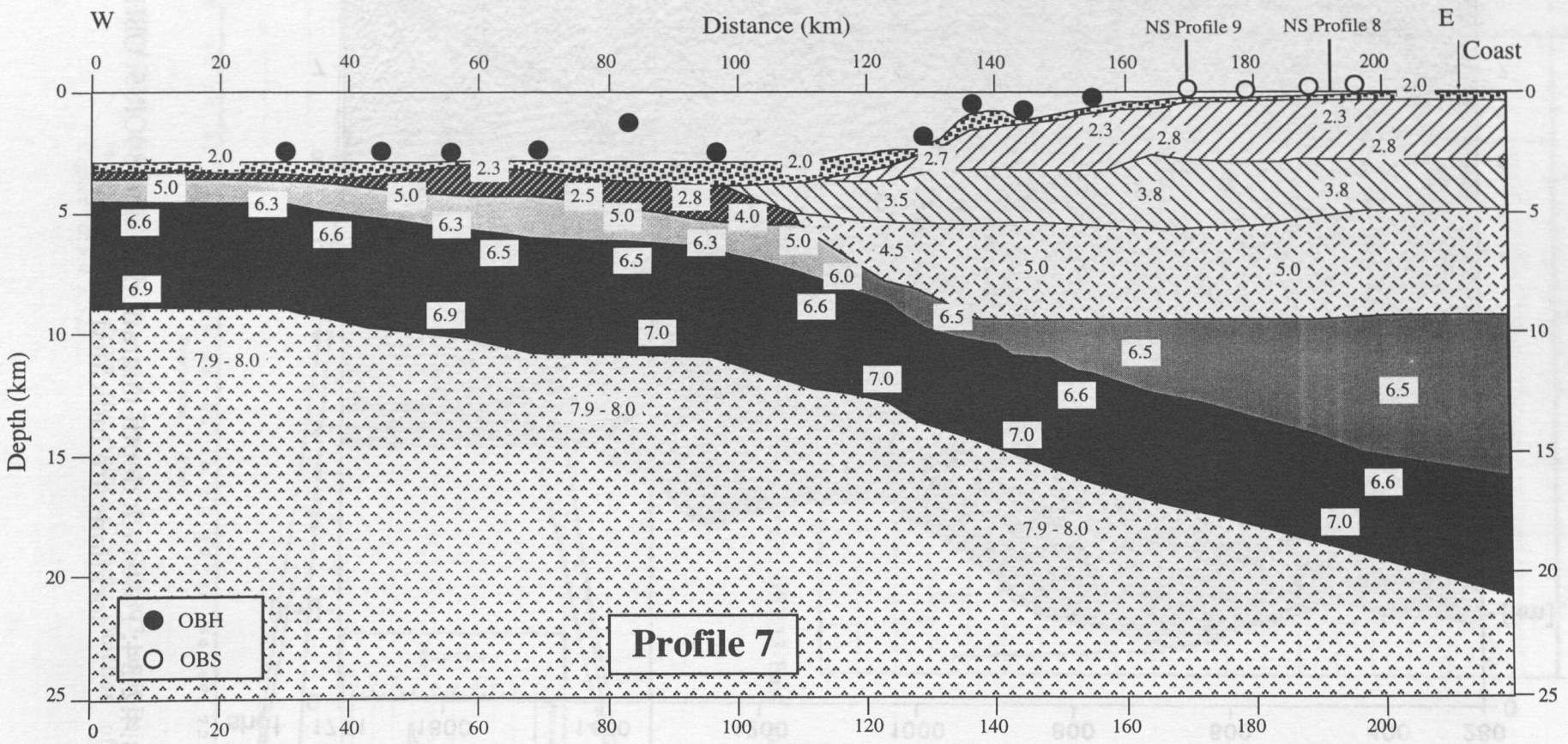

Figure 6.3.4.2.35: Preliminary results of the modelling along profile 7. Numbers are velocities in km/s

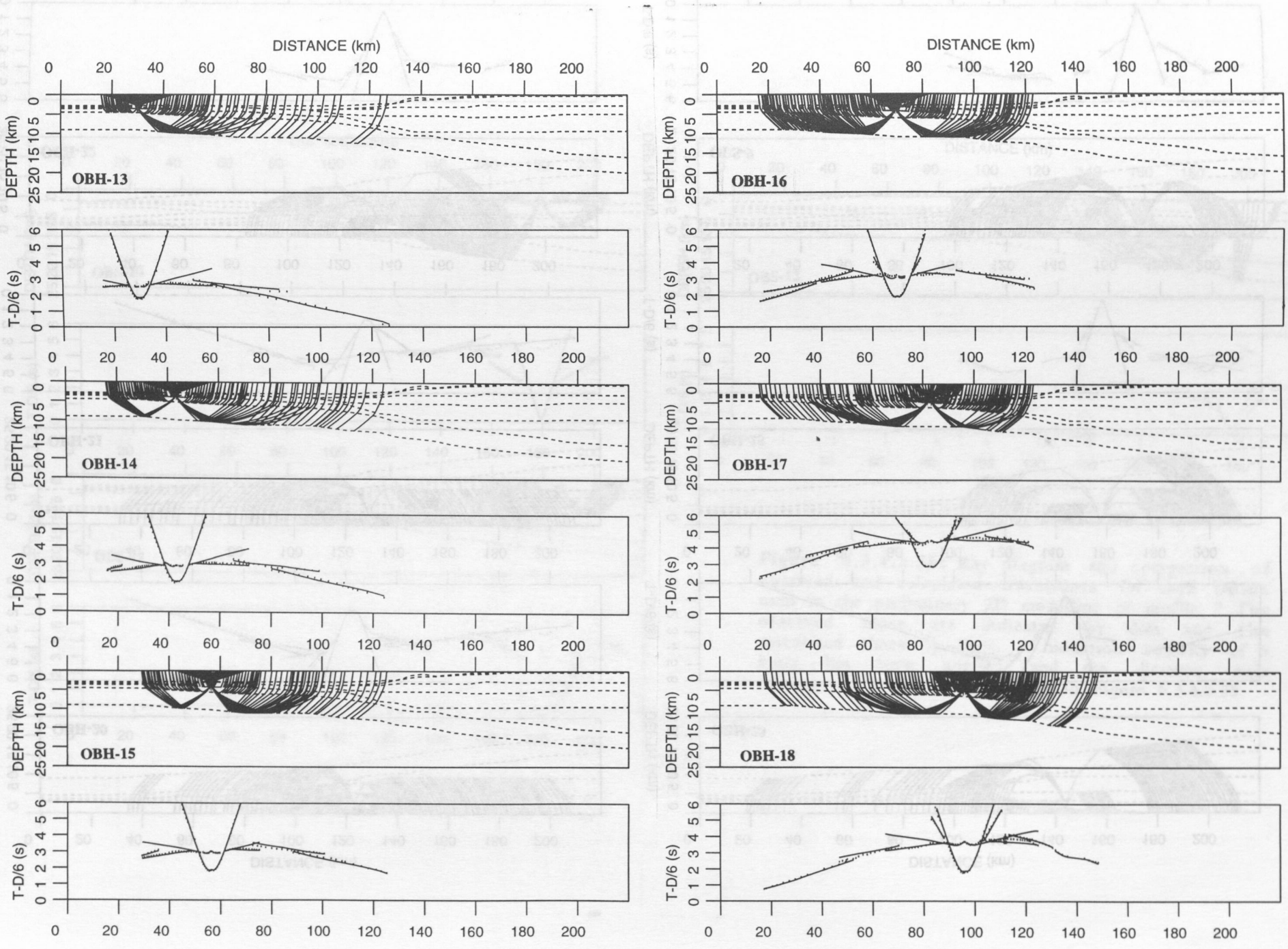
DISTANCE (km)
0 20 40 60 80 100 120 140 160 180 200
DEPTH (km)
0 5 10 15 20 25
OBH-13
T-D/6 (s)
0 1 2 3 4 5 6
OBH-14
OBH-15
OBH-16
OBH-17
OBH-18

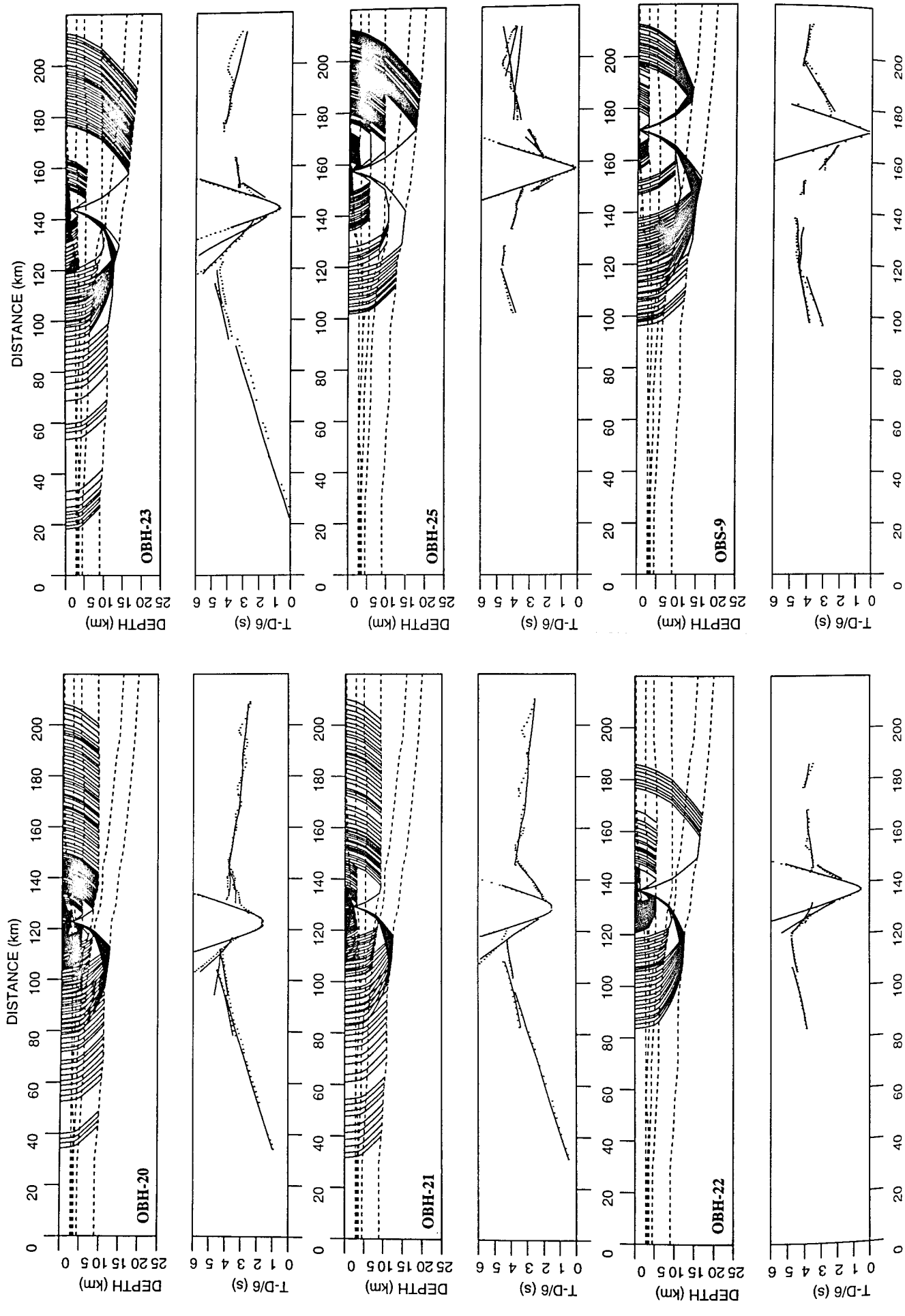
DISTANCE (km)
OBH-20
OBH-21
OBH-22
OBH-23
OBH-25
OBS-9
DEPTH (km)
T-D/6 (s)

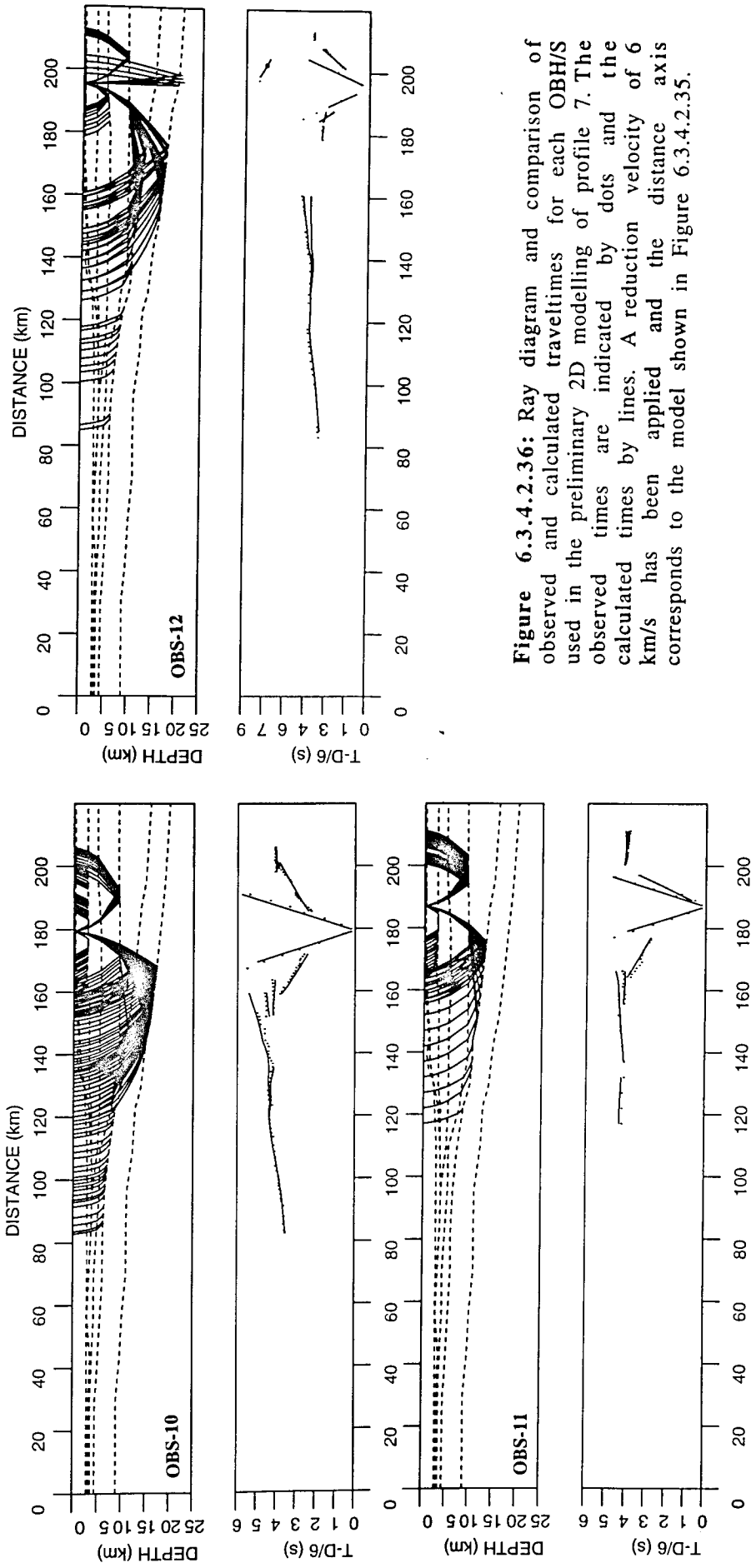

Figure 6.3.4.2.36: Ray diagram and comparison of observed and calculated traveltimes for each OBH/S used in the preliminary 2D modelling of profile 7. The observed times are indicated by dots and the calculated times by lines. A reduction velocity of 6 km/s has been applied and the distance axis corresponds to the model shown in Figure 6.3.4.2.35.

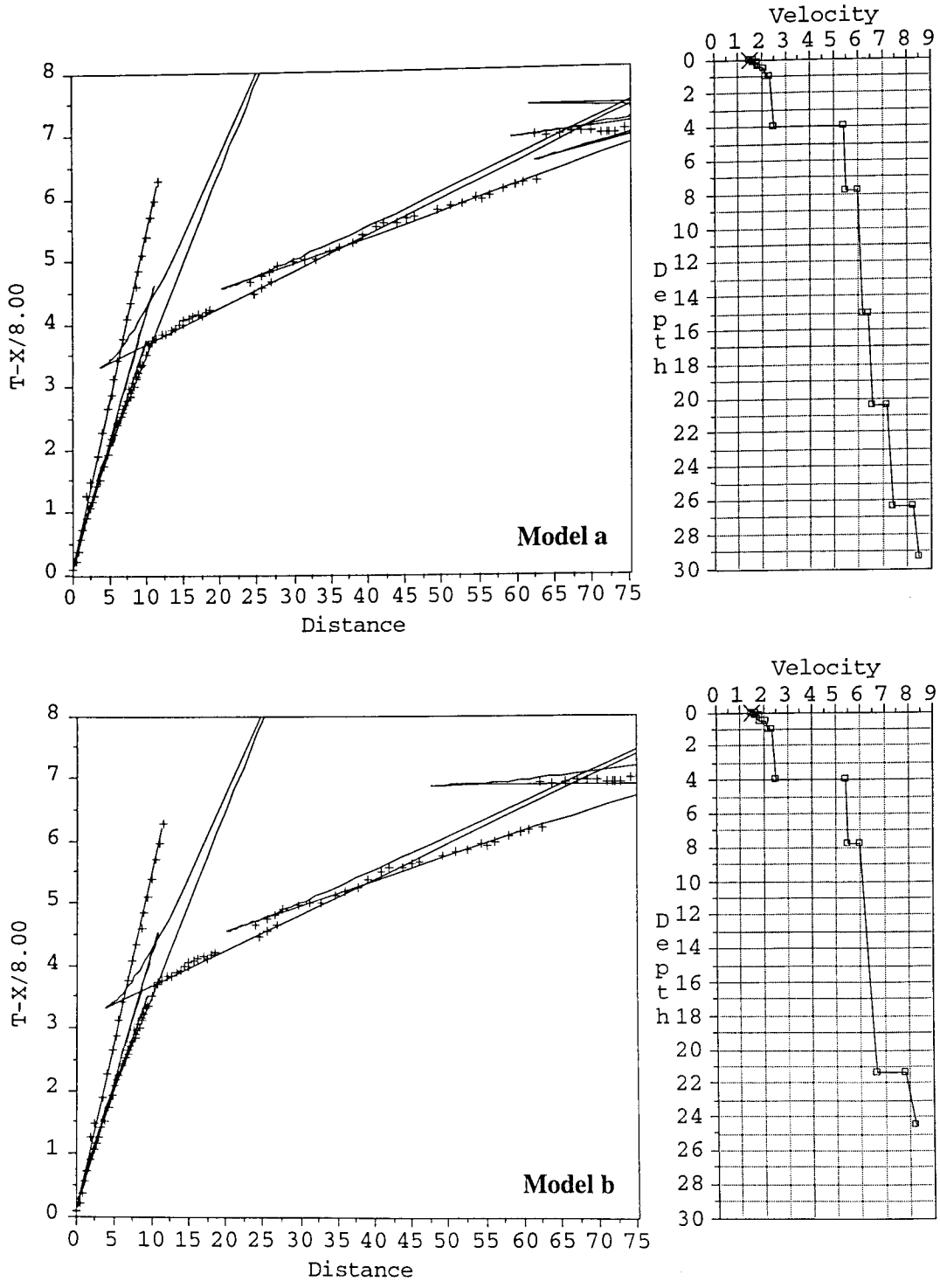

Figure 6.3.4.2.37: 1-D modelling for OBH34 (Profile 8).

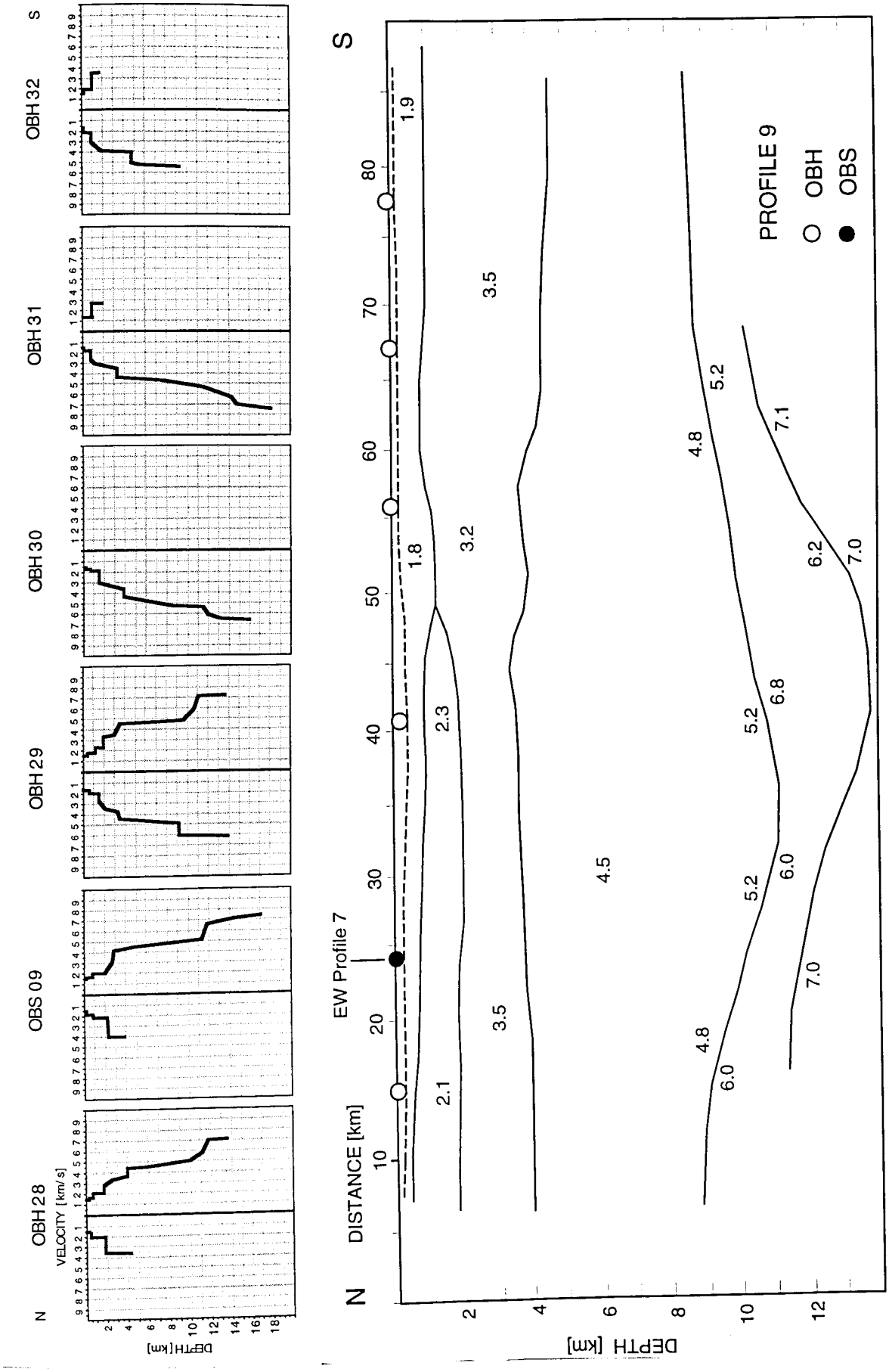

Figure 6.3.4.2.38; Profile 9 - Results of 1-D modelling.

6.3.4.3 THE SW-WASHINGTON TRANSECT, PROFILE 10

(E. Flueh, S. Husen, and K. Henneberg)

Twentyone instruments were deployed across the SW-Washington margin. These were deployed from 04:00 to 15:00 02.05. The offshore instruments were augmented by a 60 receiver array deployed onshore. For the first time during this cruise, the vertical array was deployed (see Chapter 5.2.4). Shooting started around 16:00 with a ship's speed of 3.5 kn and a trigger interval of 60 s.

The ITT ministreamer was also deployed for parts of the line to monitor the source signal and near-vertical seismic reflection data. During the shooting, when all instruments were listening, the magnitude 5.2 Duvall earthquake occured near Seattle and was recorded by most instruments (see Chapter 6.5). The profile was terminated at 21:00 03.05., and the retrieval of the instruments was interrupted on 04.05. to meet a supply vessel off Astoria, which also returned the OBH picked up by a fisherman from the deployment for profile 8 (see Chapter 6.3.4.2). Thereafter, to save transit time, several instruments were redeployed along the north-south transect (profile 11) before the remaining instruments were picked up by 03:00 05.05. The location map of the profile and the deployment positions are given in Figure 6.3.4.3.1. Some of the record sections are shown in Figures 6.3.4.3.2 to 6.3.4.3.20. Especially the OBS deployed in shallow water show very little seismic energy, apparently the noise level was too high.

Record sections from the instruments on the Juan de Fuca Plate, OBH39 to OBH42, show two sedimentary units and the basement as clear near-vertical reflections. Refracted waves sample the oceanic crust and upper mantle, the PMP critical distance is around 30 km. The sedimentary units thicken towards the trench by about 0.5 s TWT. Along the slope, strong undulations of the first arrivals are evident, which are only partly caused by topography. All instruments on the slope were able to record the PMP, and sometimes even a weak Pn phase is seen. Those instruments placed on the shelf show a pronounced traveltime delay of a about 6 s TWT for the PMP, indicating the presence of deep sedimentary basins.

MCS data were collected along this profile, but they could not be processed in time for this report. We attempted to model the wide-angle data without constraints from MCS data. As for all other profiles, we only intended to model the main features, many details will be filled in later. Based on 2-D raytracing, a velocity model was obtained and is shown in Figure 6.3.4.3.21. The oceanic plate is well imaged and dips 3 to 4° east, and reaches a depth of 13 km near the coast. A velocity anomaly was introduced between kilometer 100 and 140 of the model to explain some early PMP arrivals, where the travel time anomaly could not be accommodated in the overlying plate. Two sedimentary units are observed across the profile, the first one has velocities of about 2.0 km/s and has a nearly constant thickness of 1 km. The second unit has an average velocity of about 3.0 to 3.5 km/s, and shows strong lateral variations. In places, this unit reaches depth of 8 km. Across the margin, this unit is underlain by two more units, showing velocities between 4.5 and 5.2 km/s. These may still be sedimentary rocks, but certainly of a much older age and higher metamorphic grade. The model will certainly be refined and updated, once the MCS data are processed.

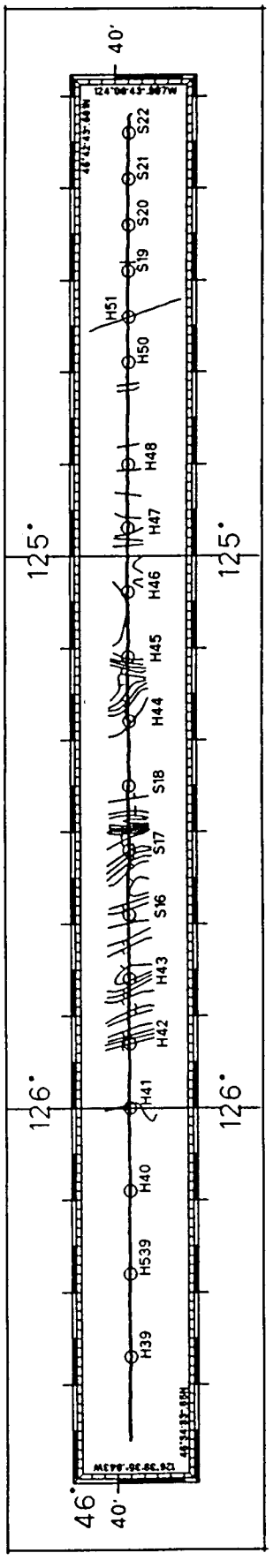

Figure 6.3.4.3.1: Location map of profile 10. Contour intervall 100 m. S* and H** mark OBS/OBH stations.

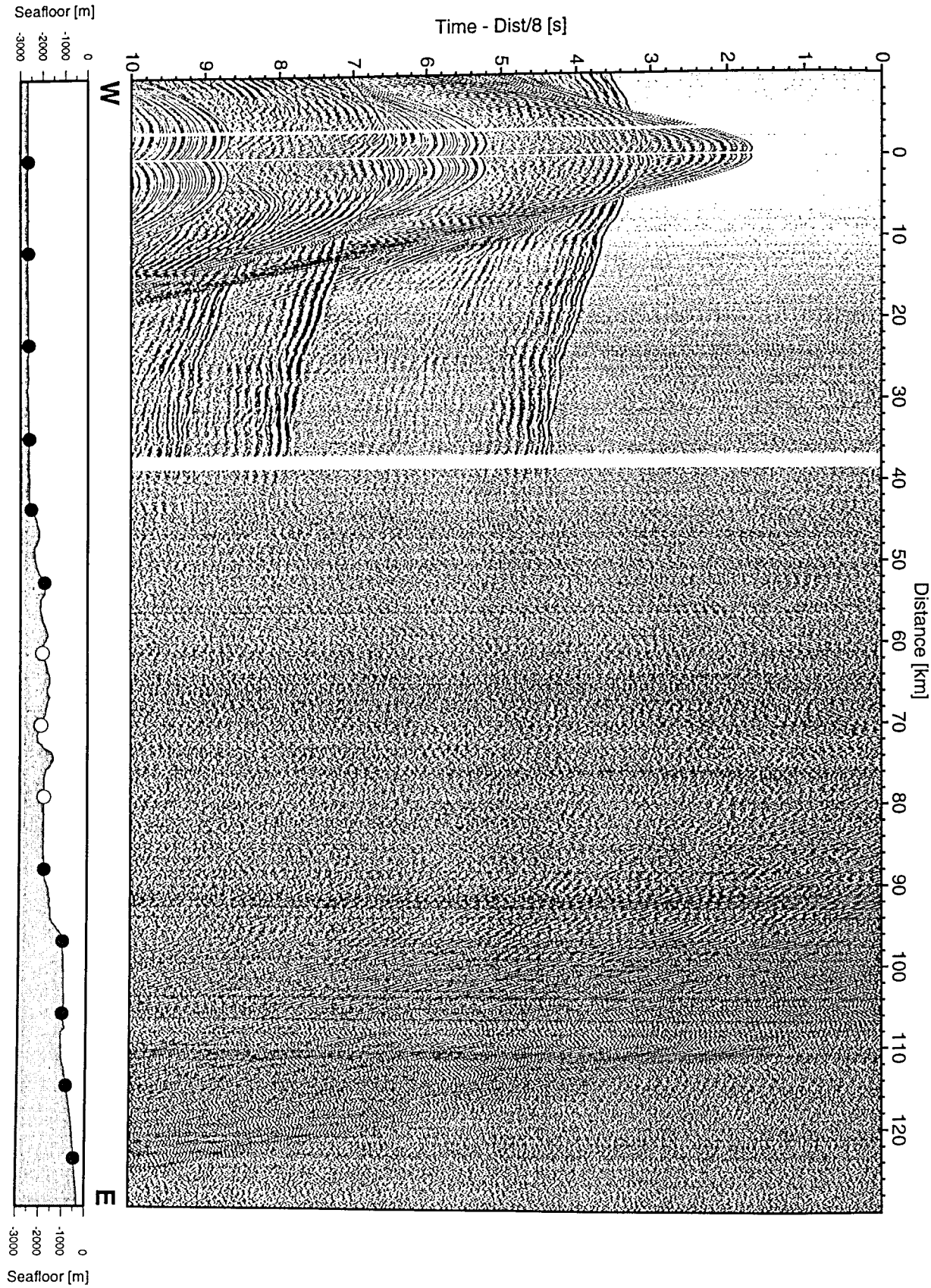

Figure 6.3.4.3.2: Record section from OBH 39, Profile 10.

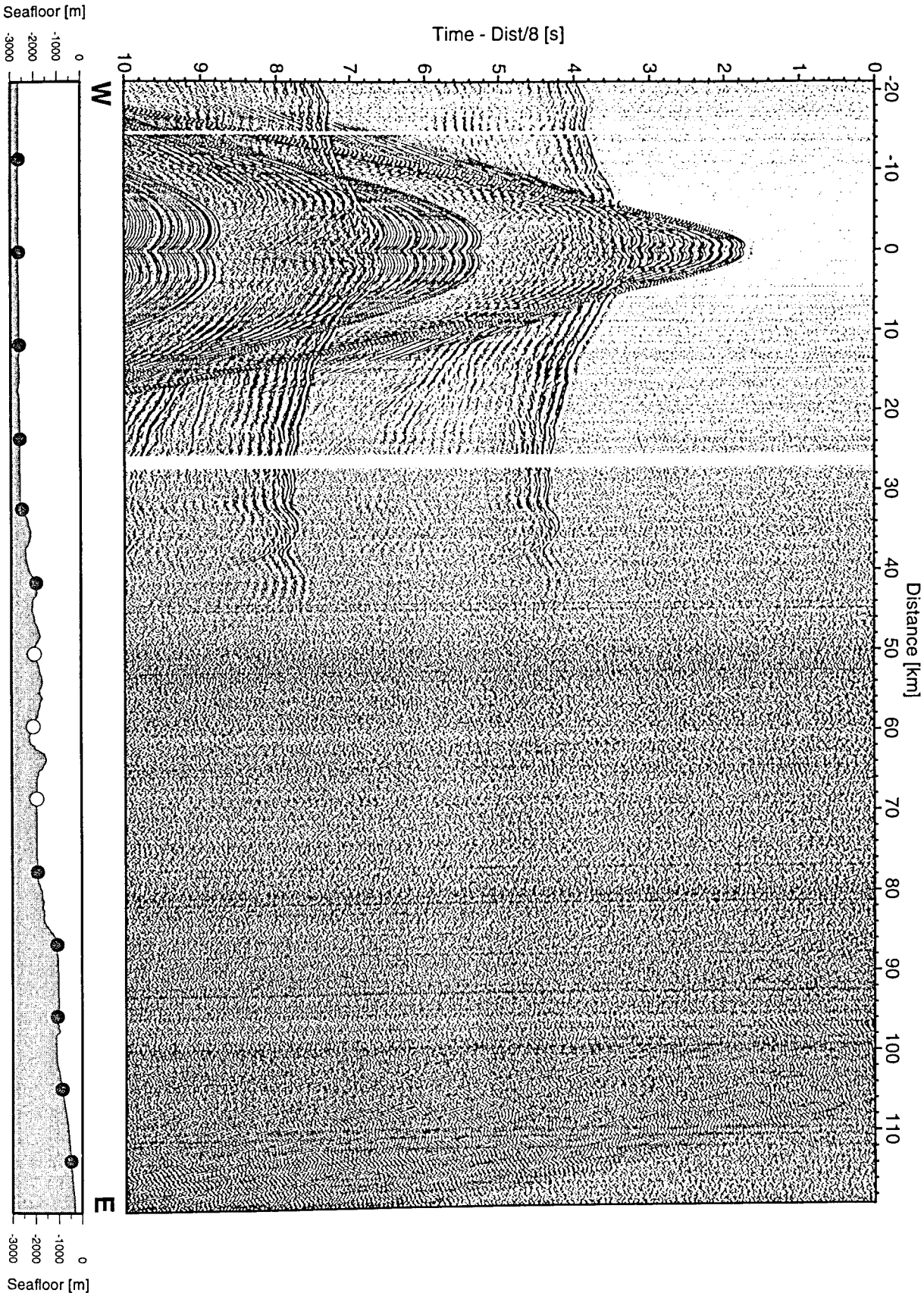

Figure 6.3.4.3.3: Record section from OBH 539, Profile 10.

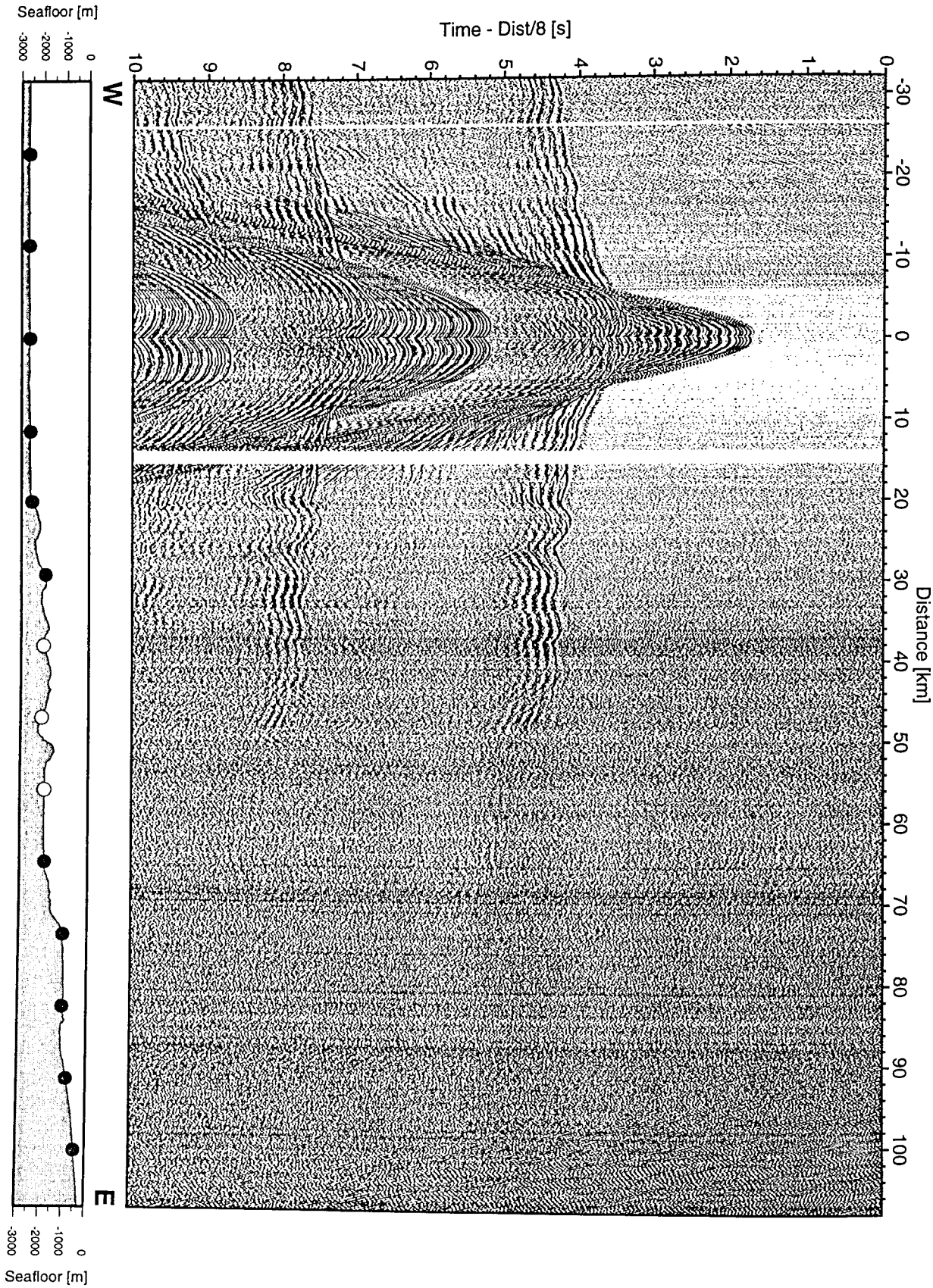

Figure 6.3.4.3.4: Record section from OBH 40, Profile 10.

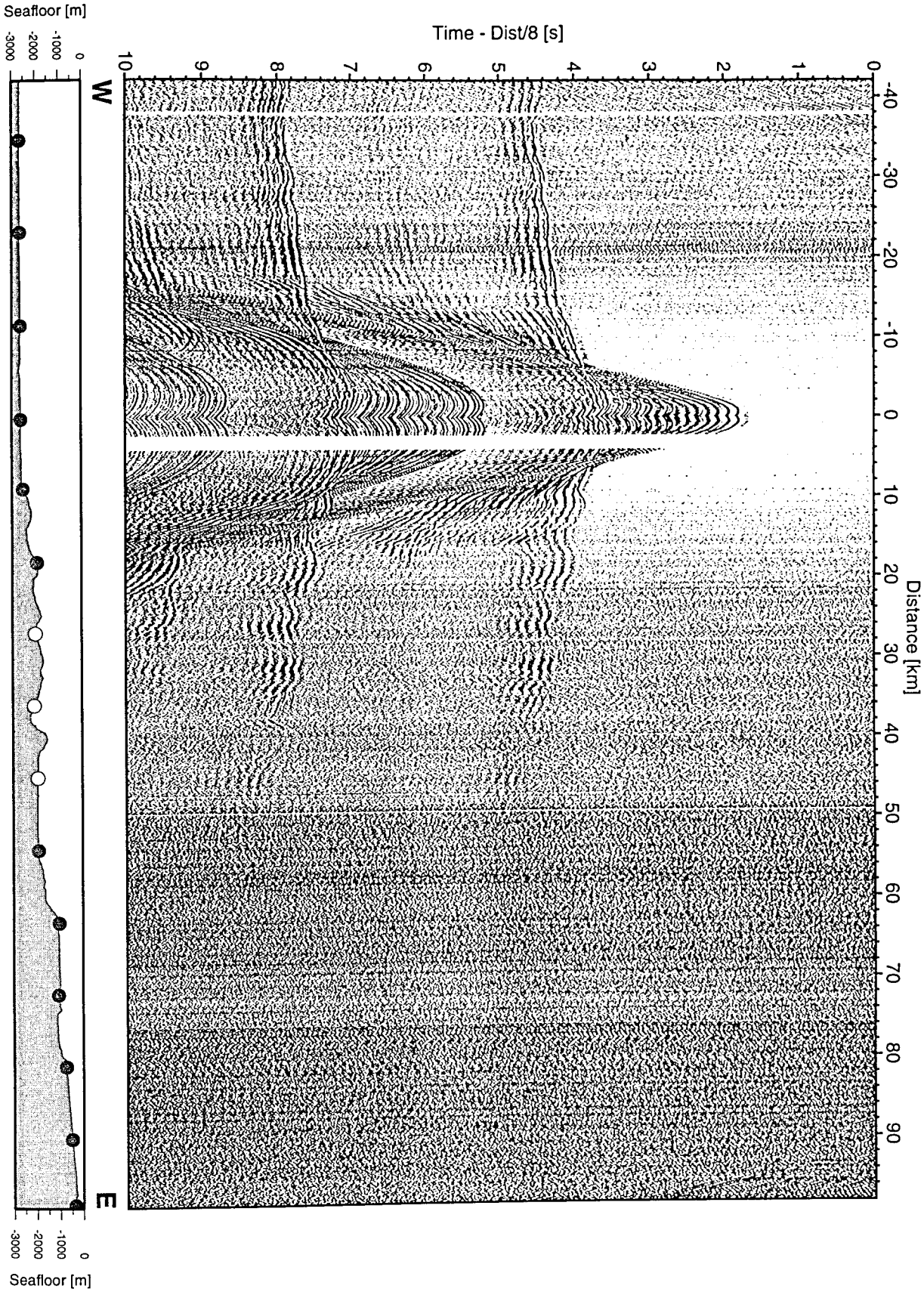

Figure 6.3.4.3.5: Record section from OBH 41, Profile 10.

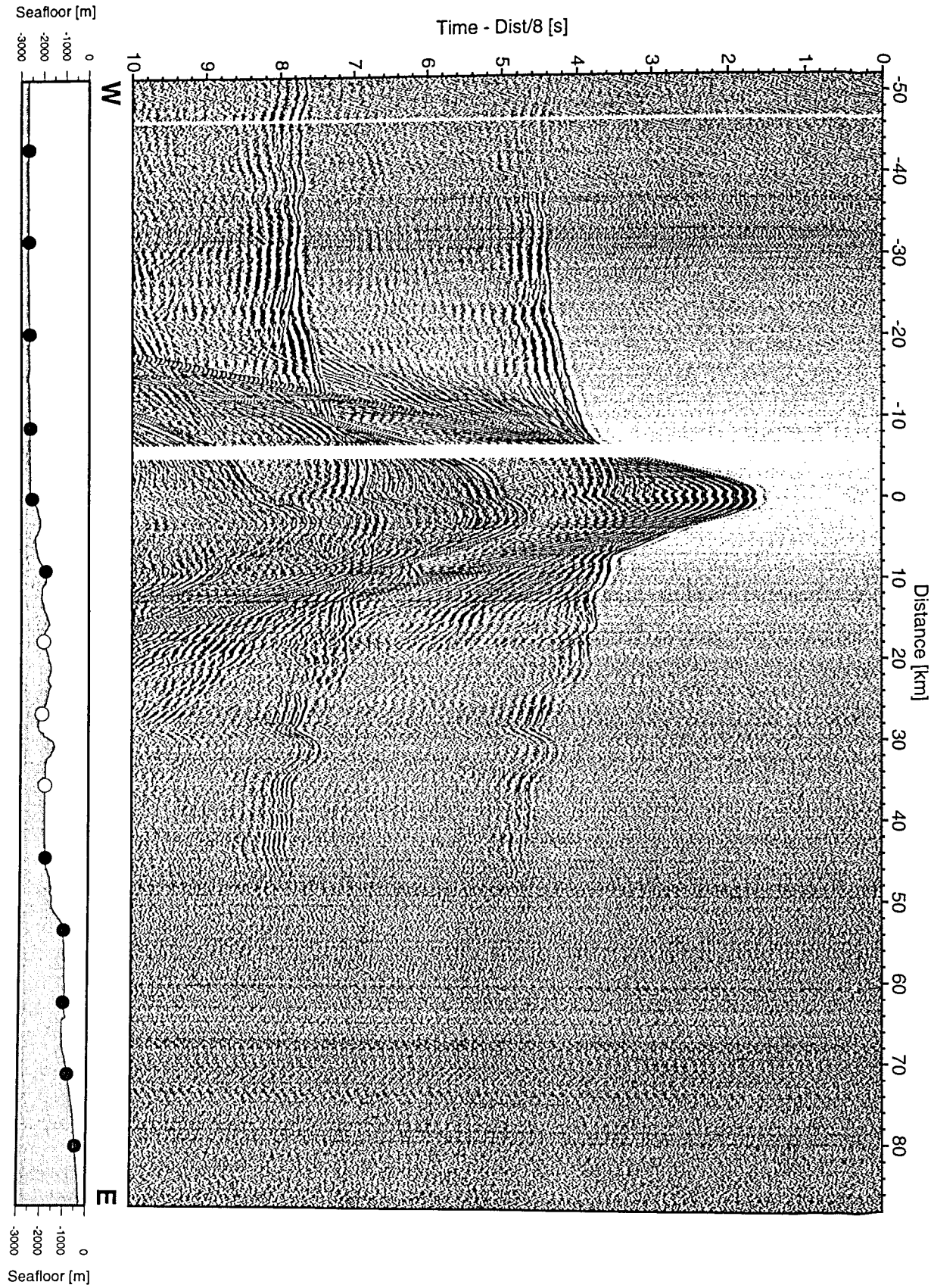

Figure 6.3.4.3.6: Record section from OBH 42, Profile 10.

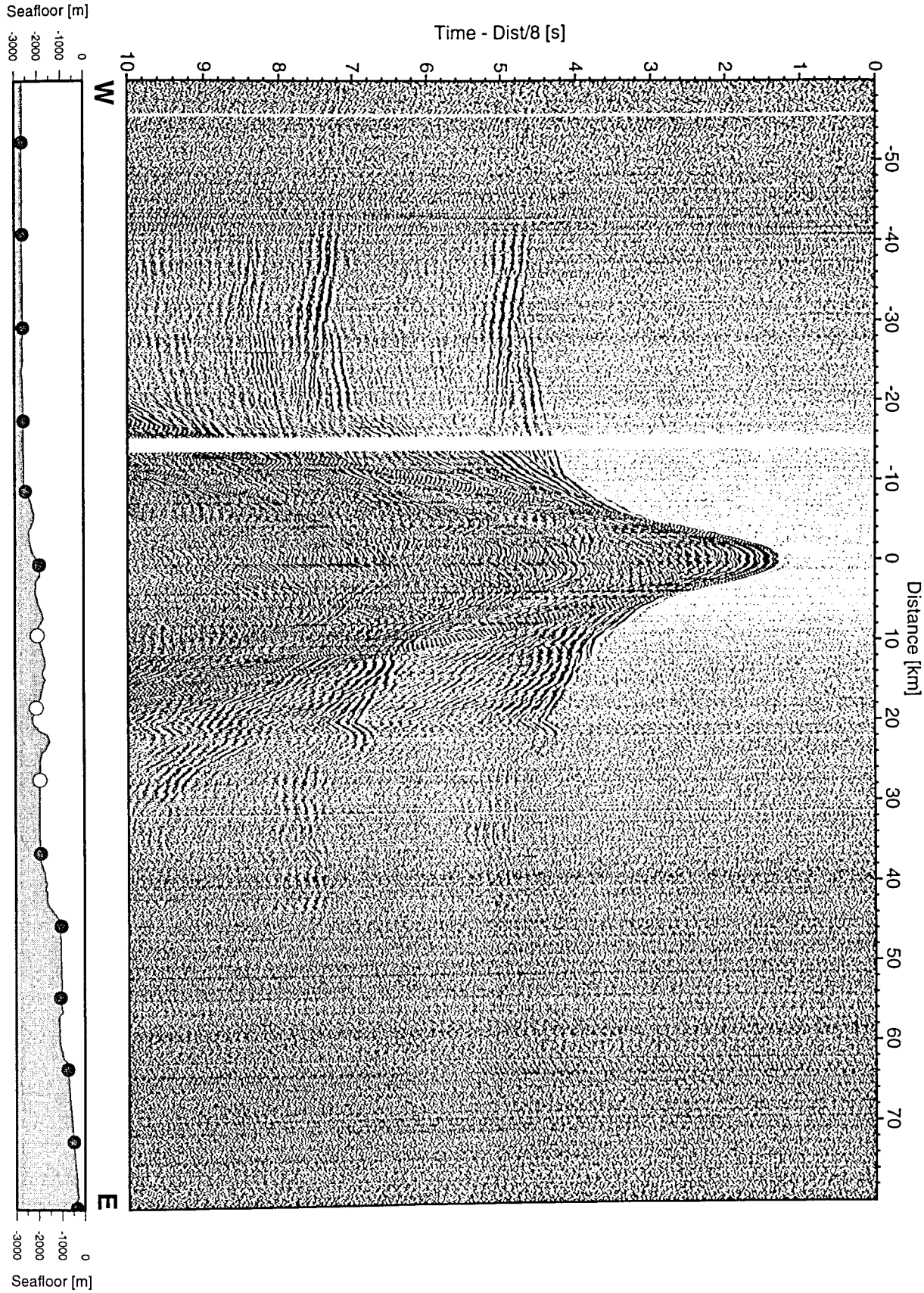

Figure 6.3.4.3.7: Record section from OBH 43, Profile 10.

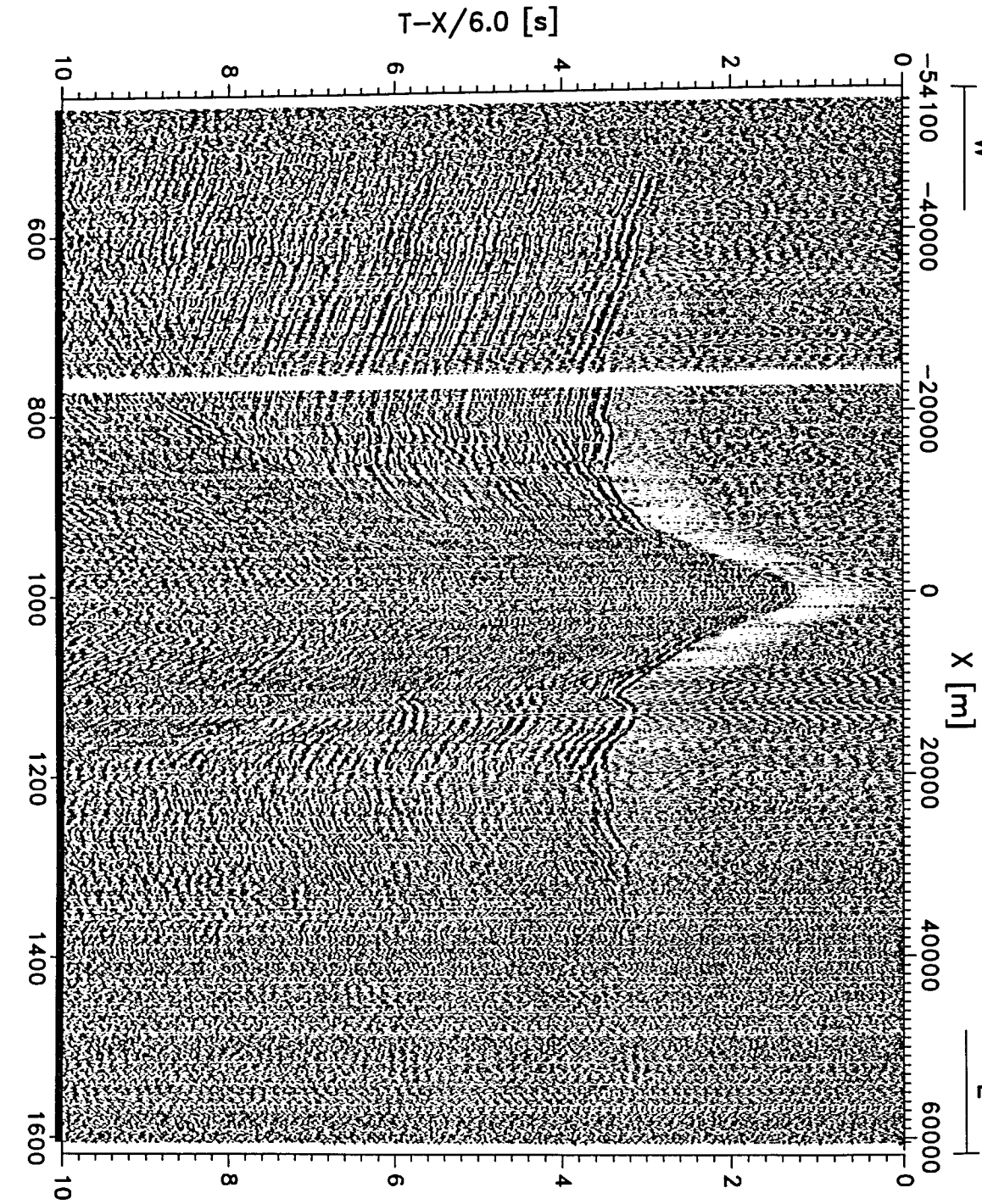

Figure 6.3.4.3.8: Record section for OBS16, vertical component.

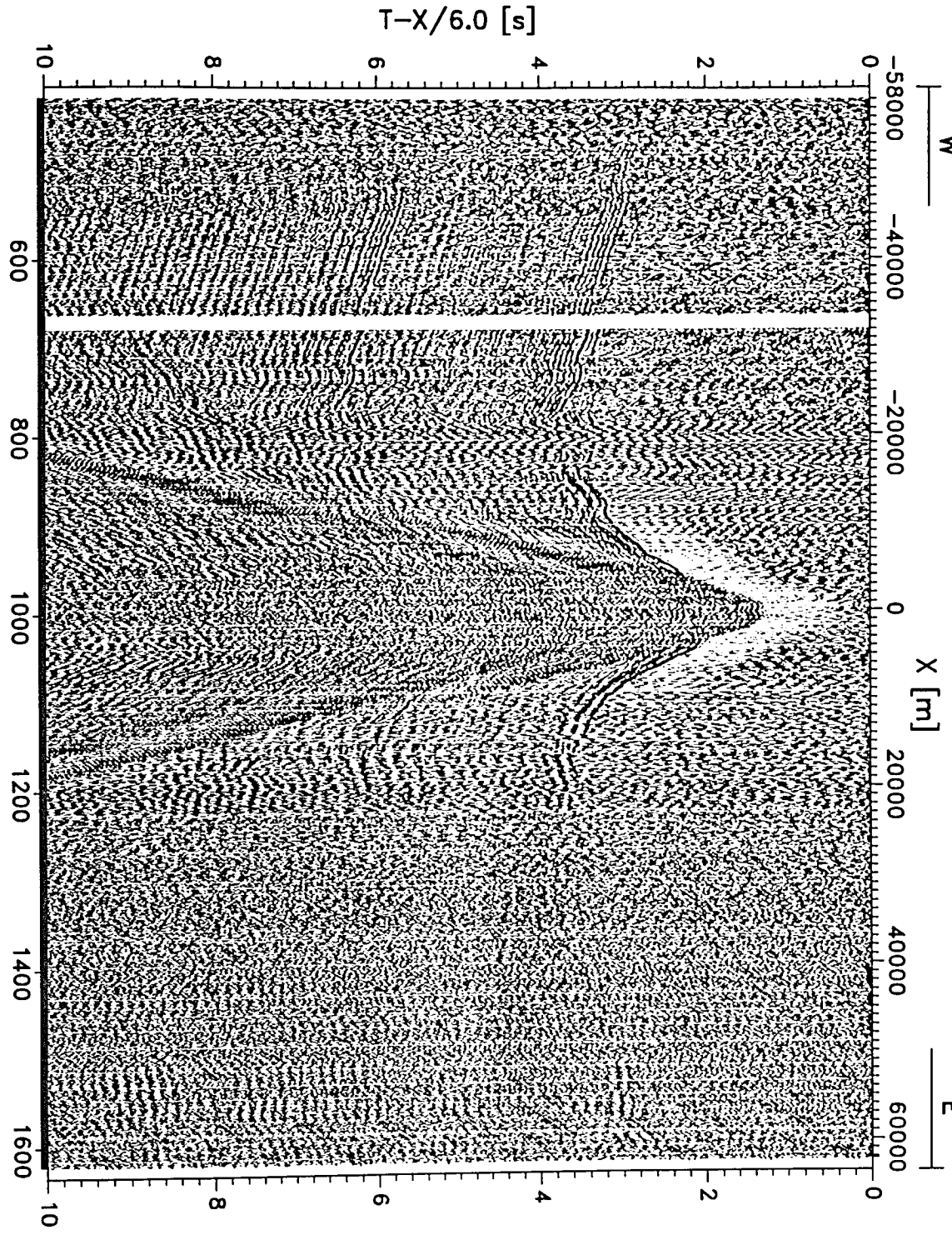

Figure 6.3.4.3.9: Record section for OBS17, vertical component.

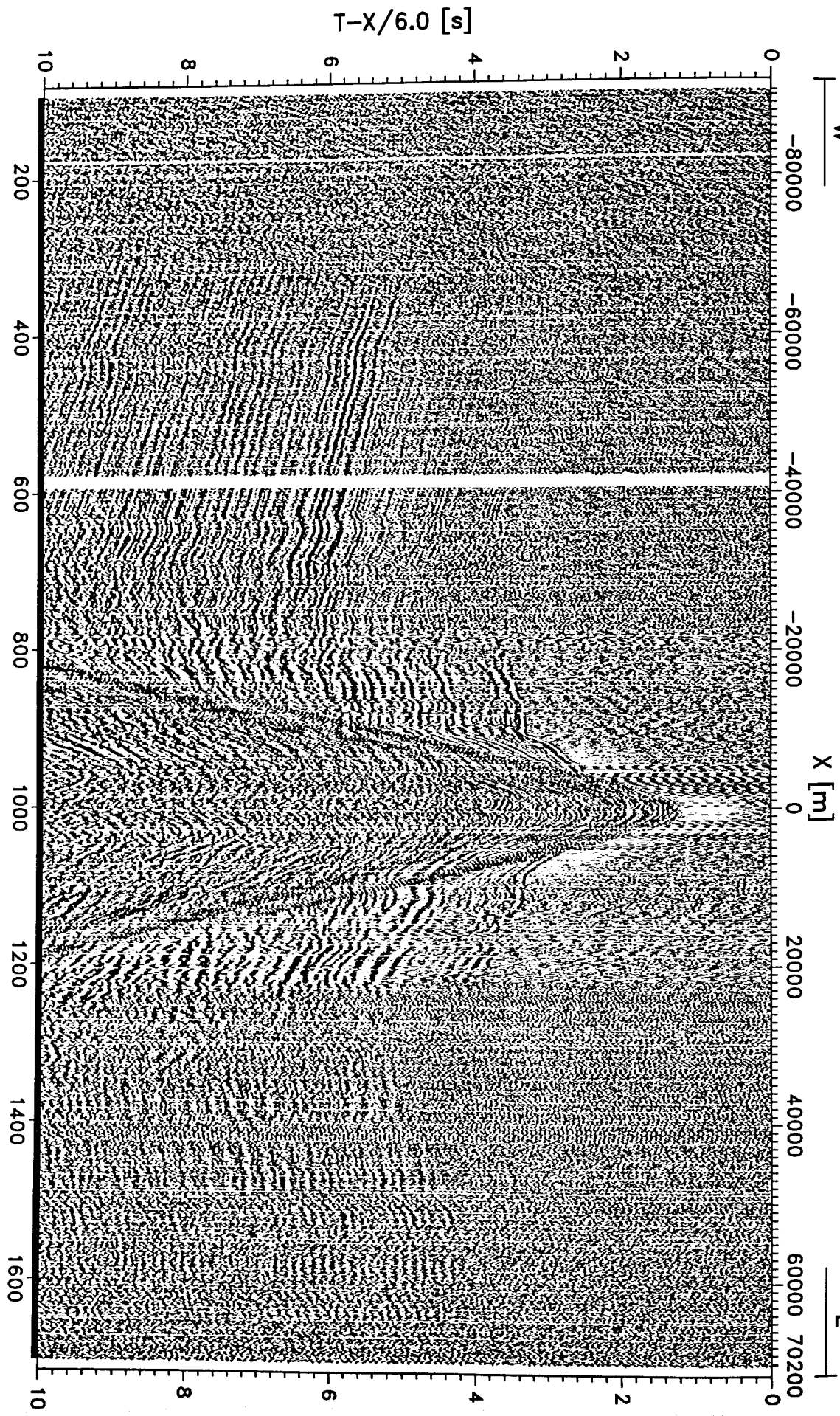

Figure 6.3.4.3.10: Record section for OBS18, vertical component.

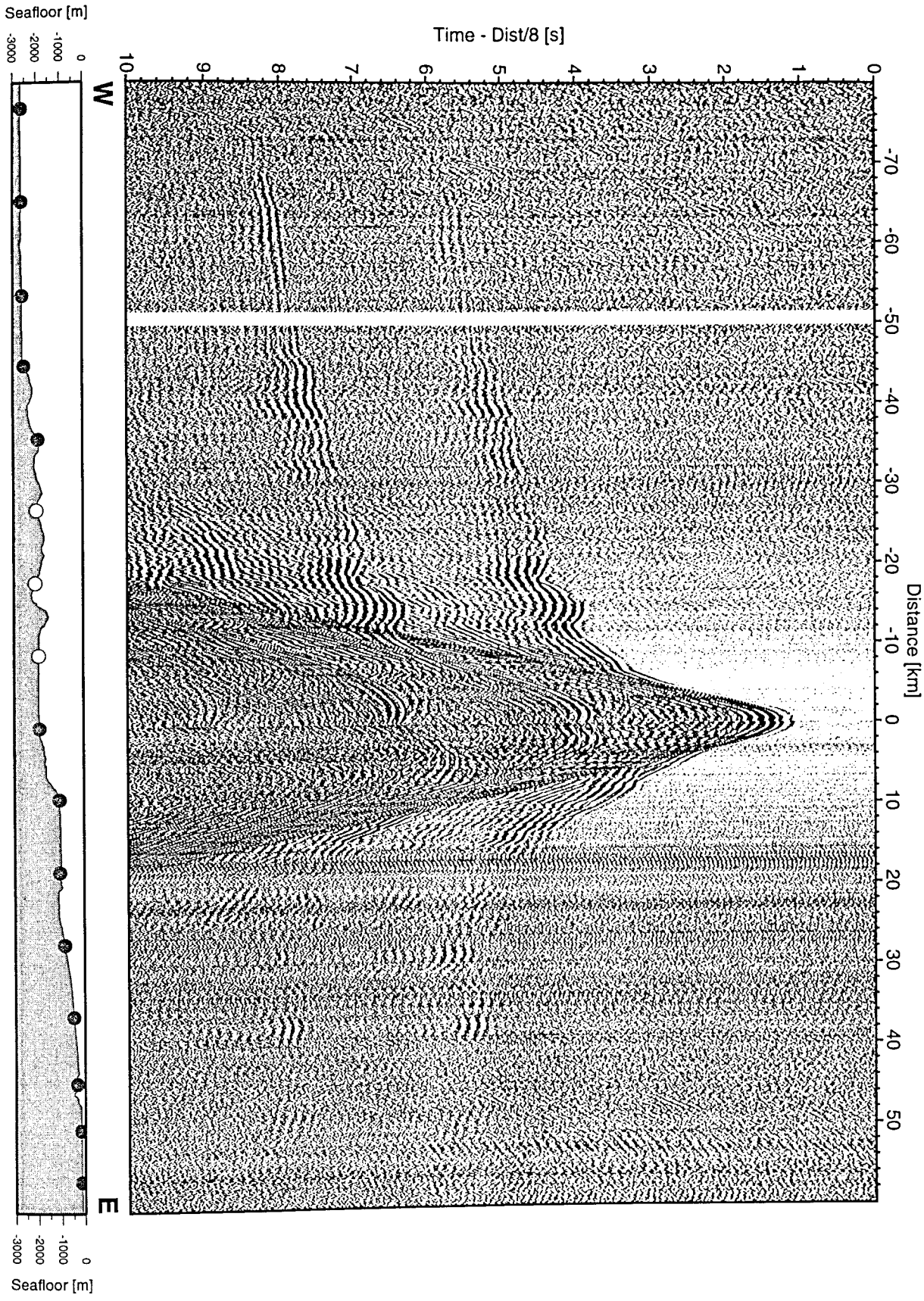

Figure 6.3.4.3.11: Record section from OBH 44, Profile 10.

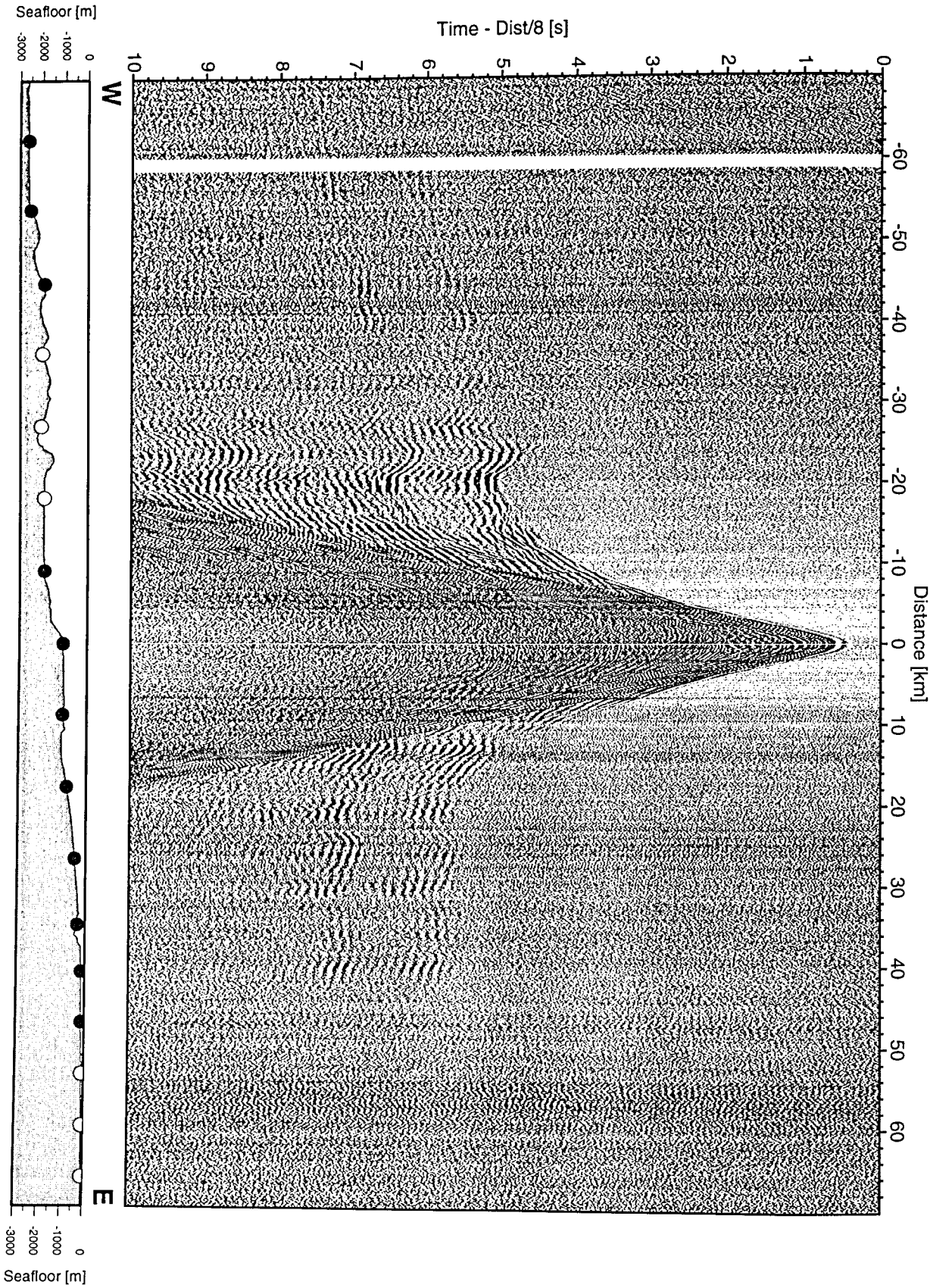

Figure 6.3.4.3.12: Record section from OBH 45, Profile 10.

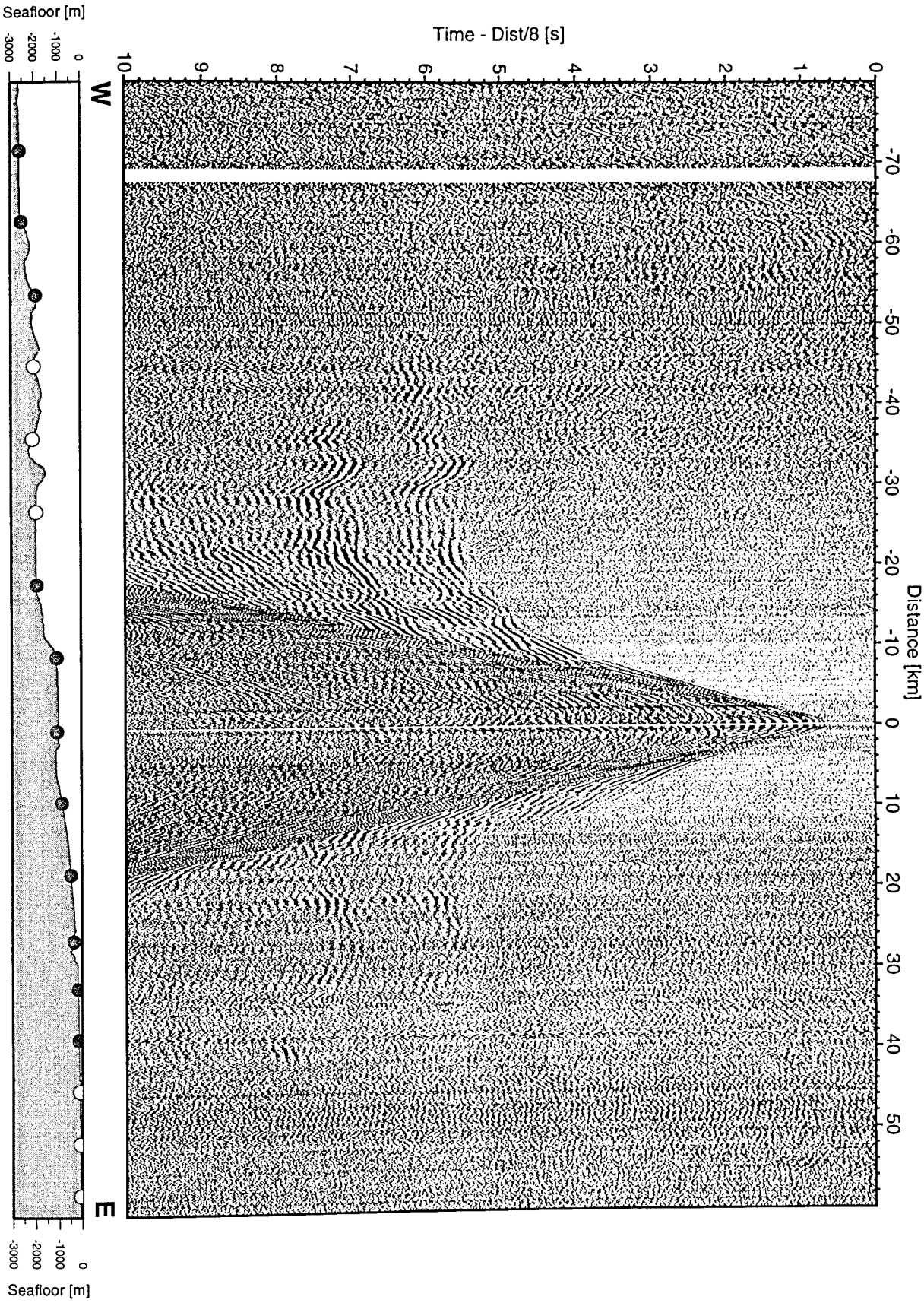

Figure 6.3.4.3.13: Record section from OBH 46, Profile 10.

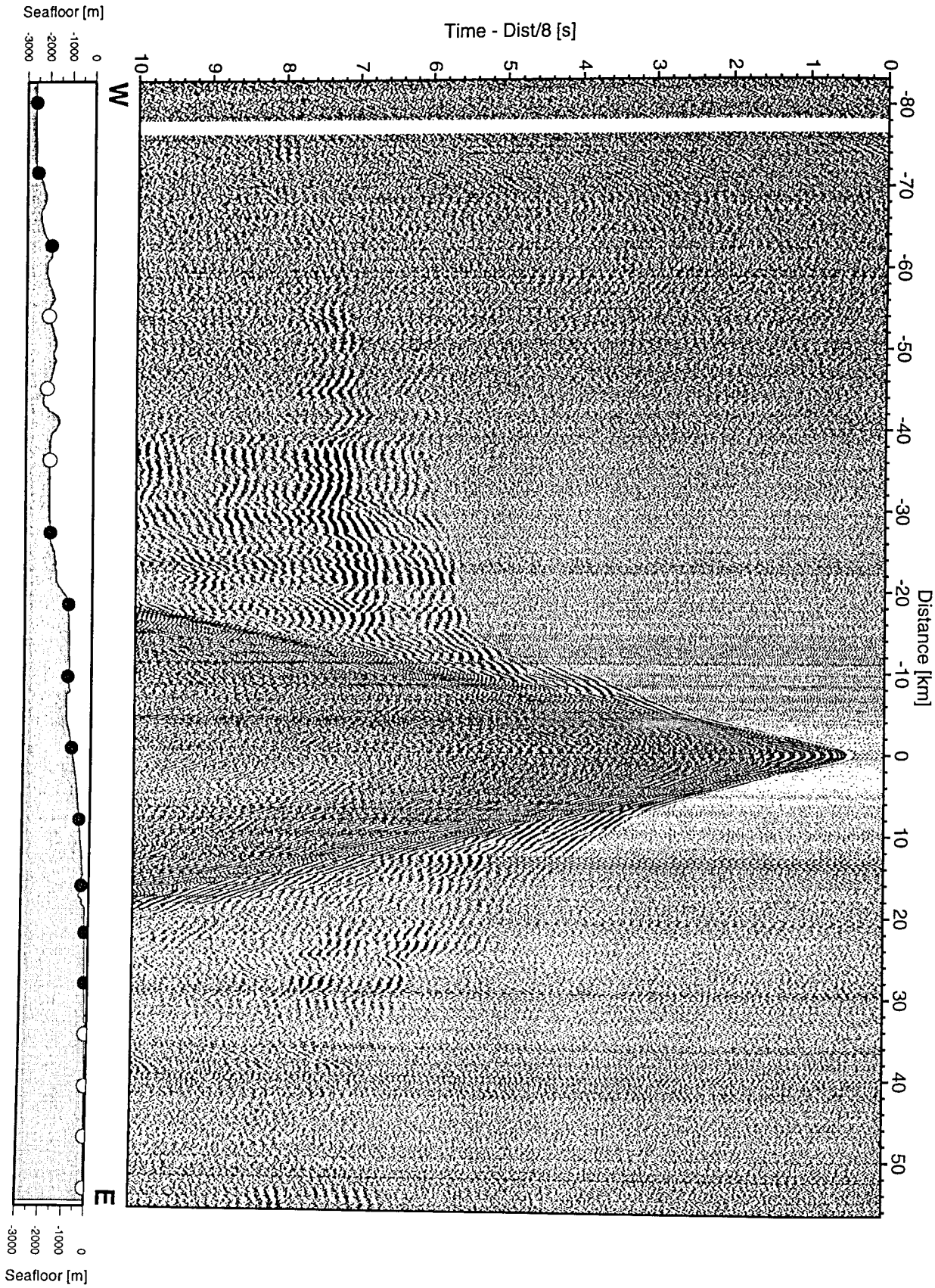

Figure 6.3.4.3.14: Record section from OBH 47, Profile 10.

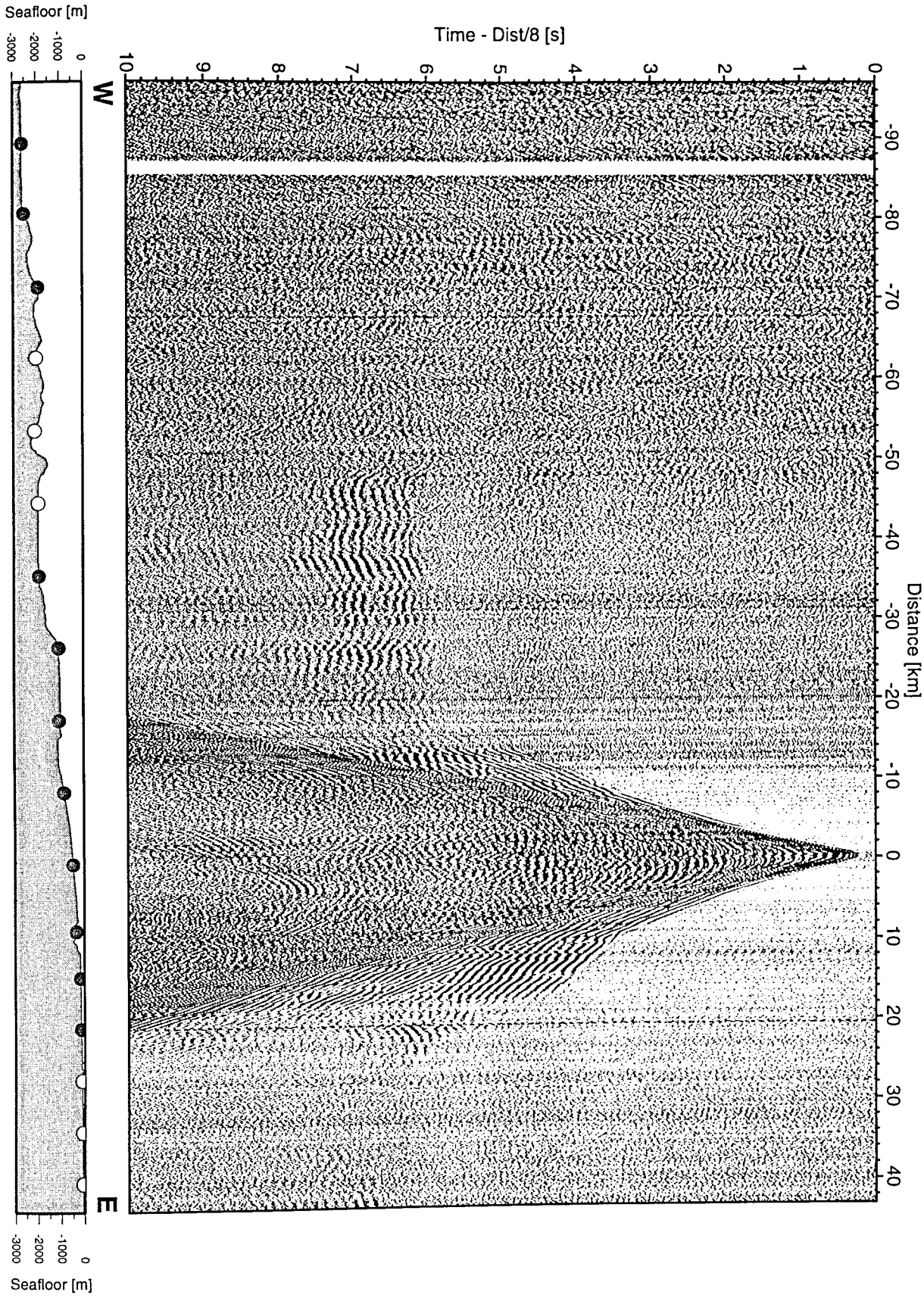

Figure 6.3.4.3.15: Record section from OBH 48, Profile 10.

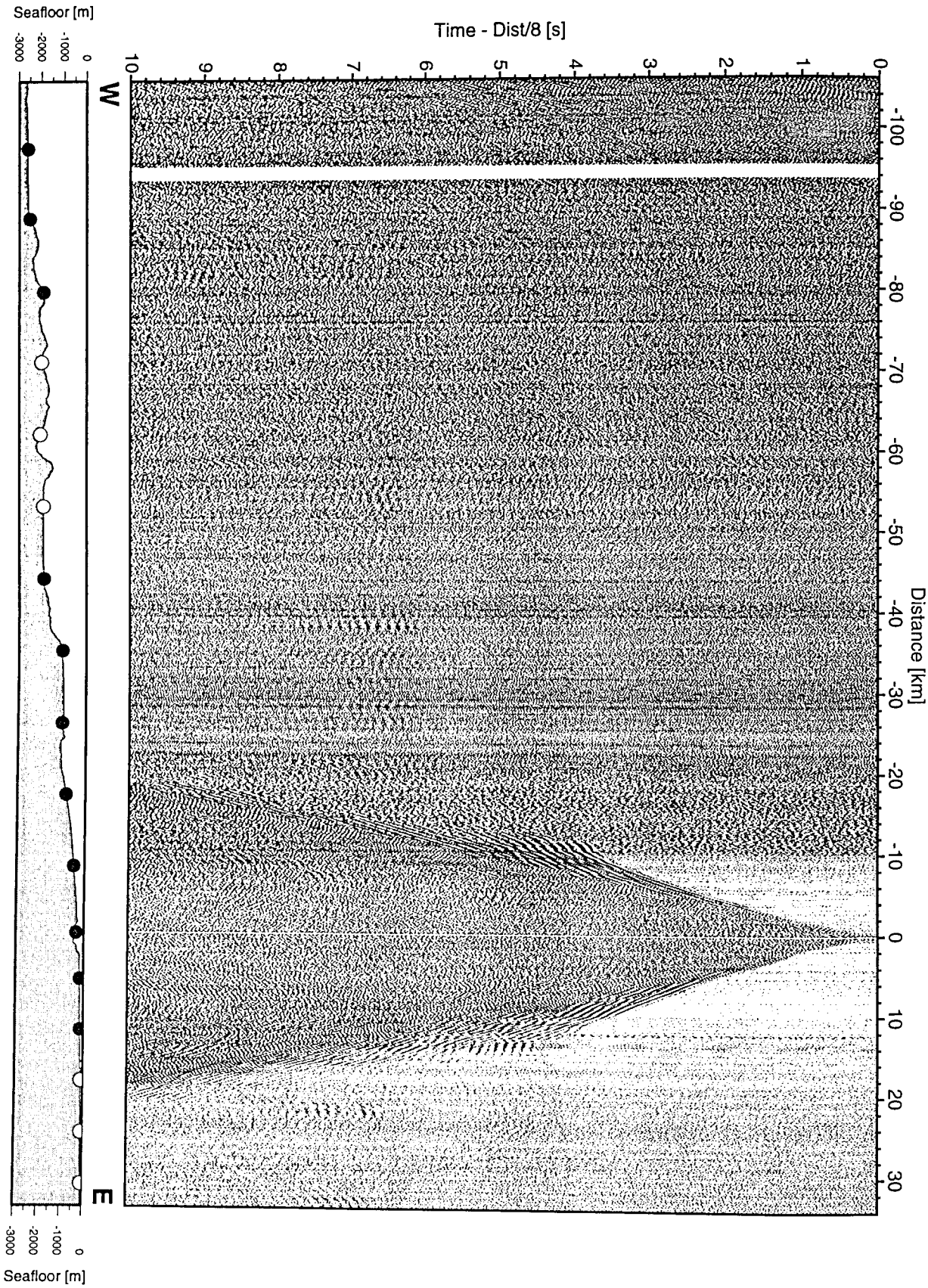

Figure 6.3.4.3.16: Record section from OBH 49, Profile 10.

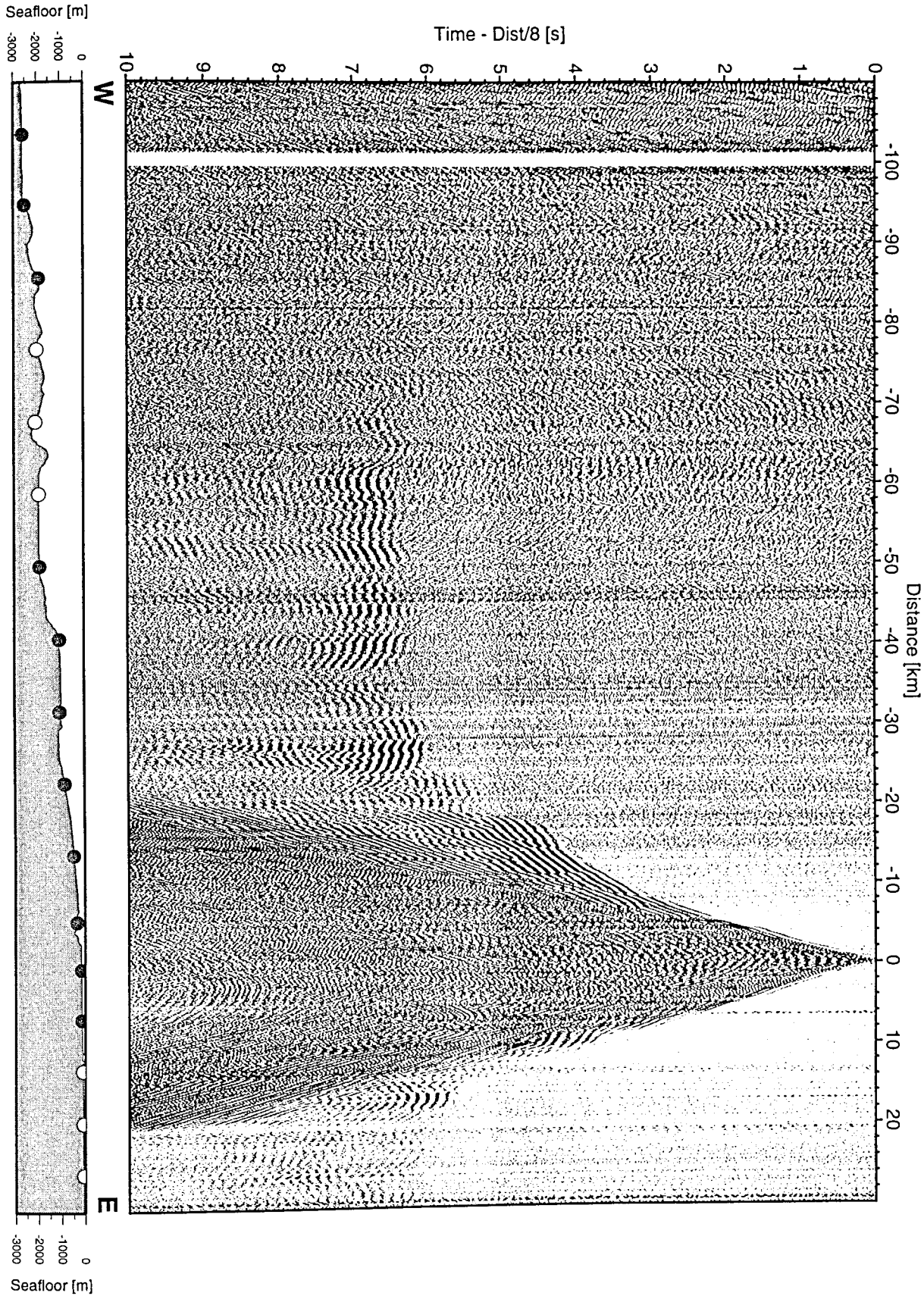

Figure 6.3.4.3.17: Record section from OBH 50, Profile 10.

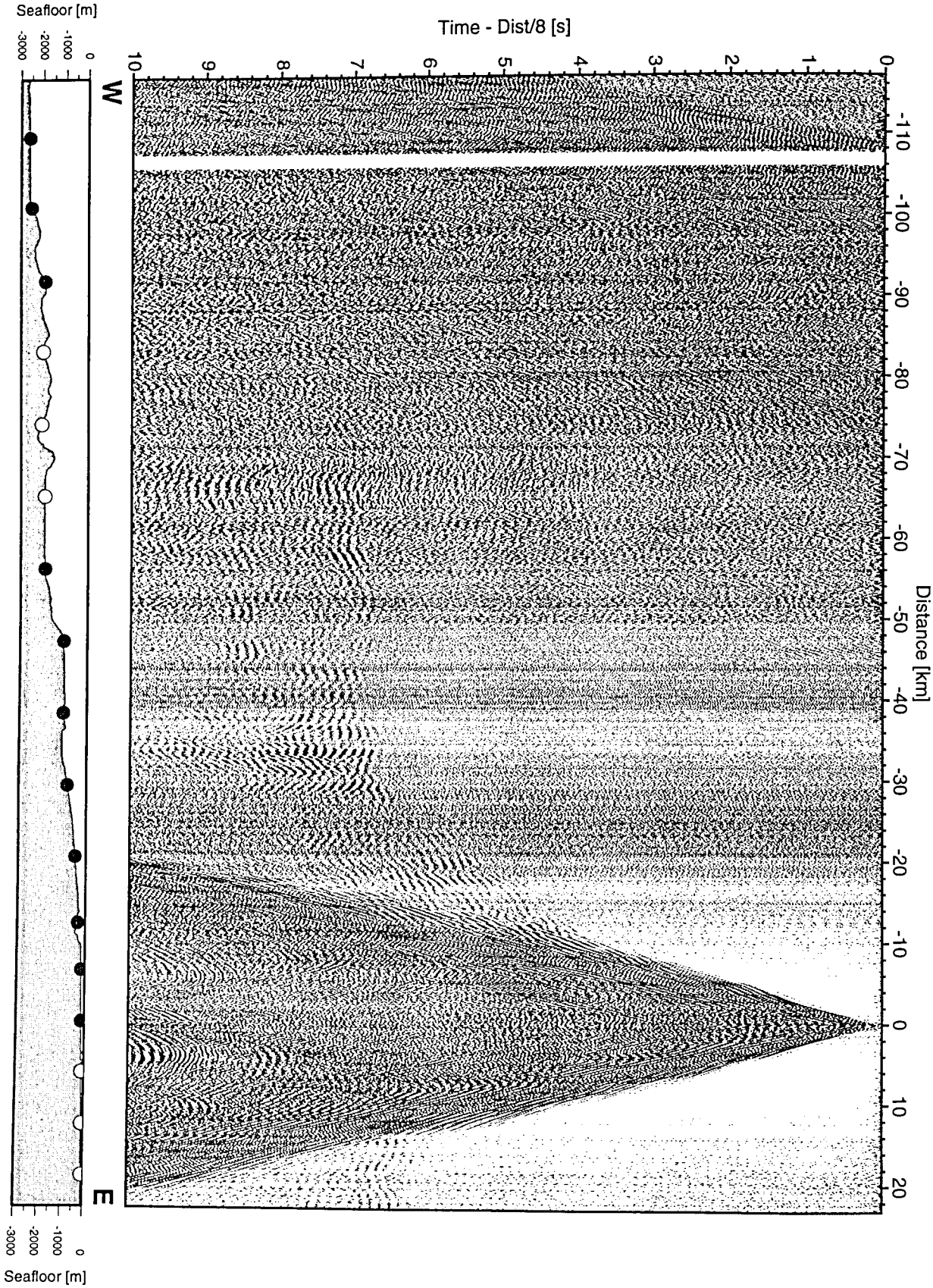

Figure 6.3.4.3.18: Record section from OBH 51, Profile 10.

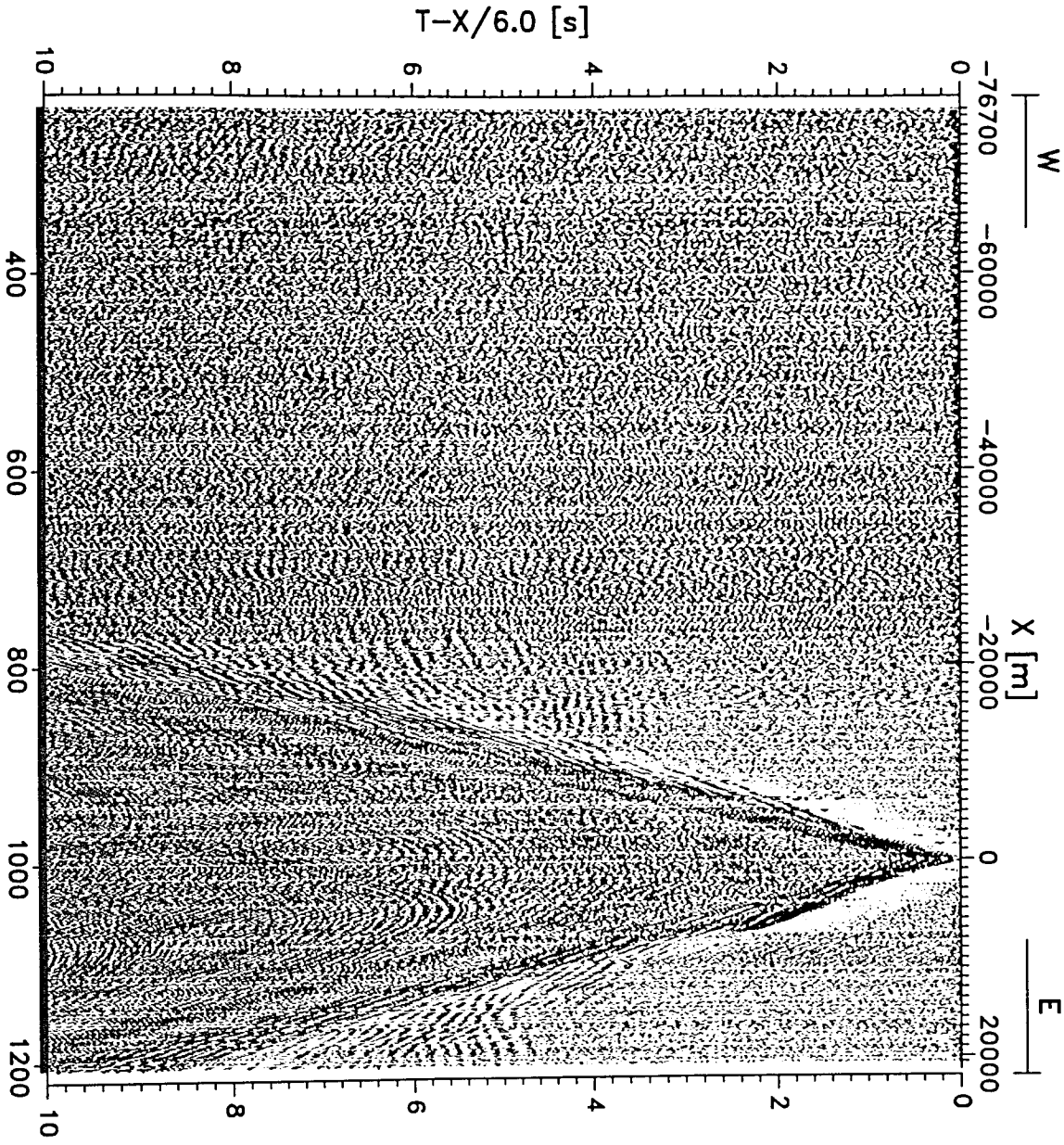

Figure 6.3.4.3.19: Record section for OBS19, hydrophone.

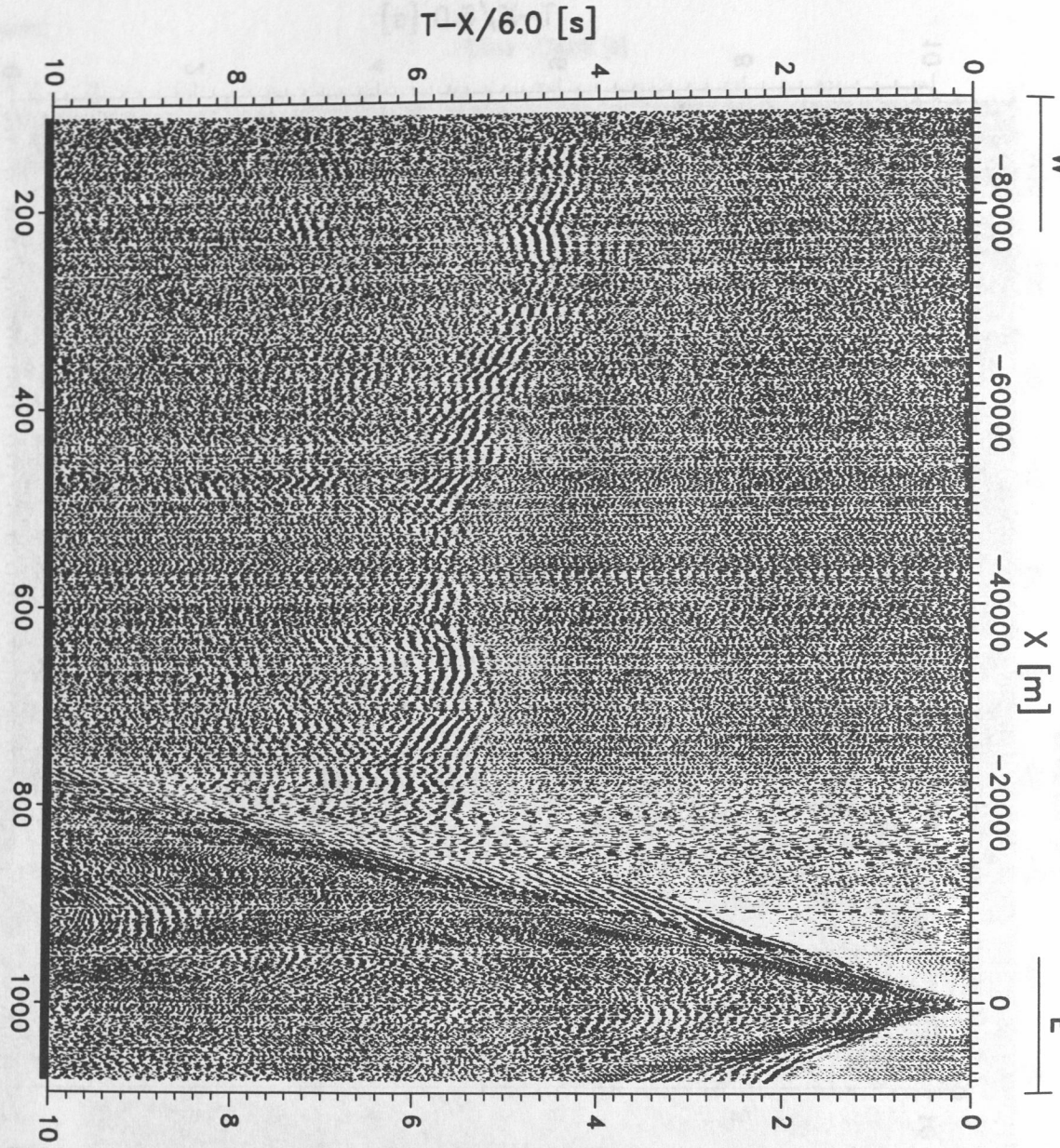

Figure 6.3.4.3.20: Record section for OBS21, hydrophone.

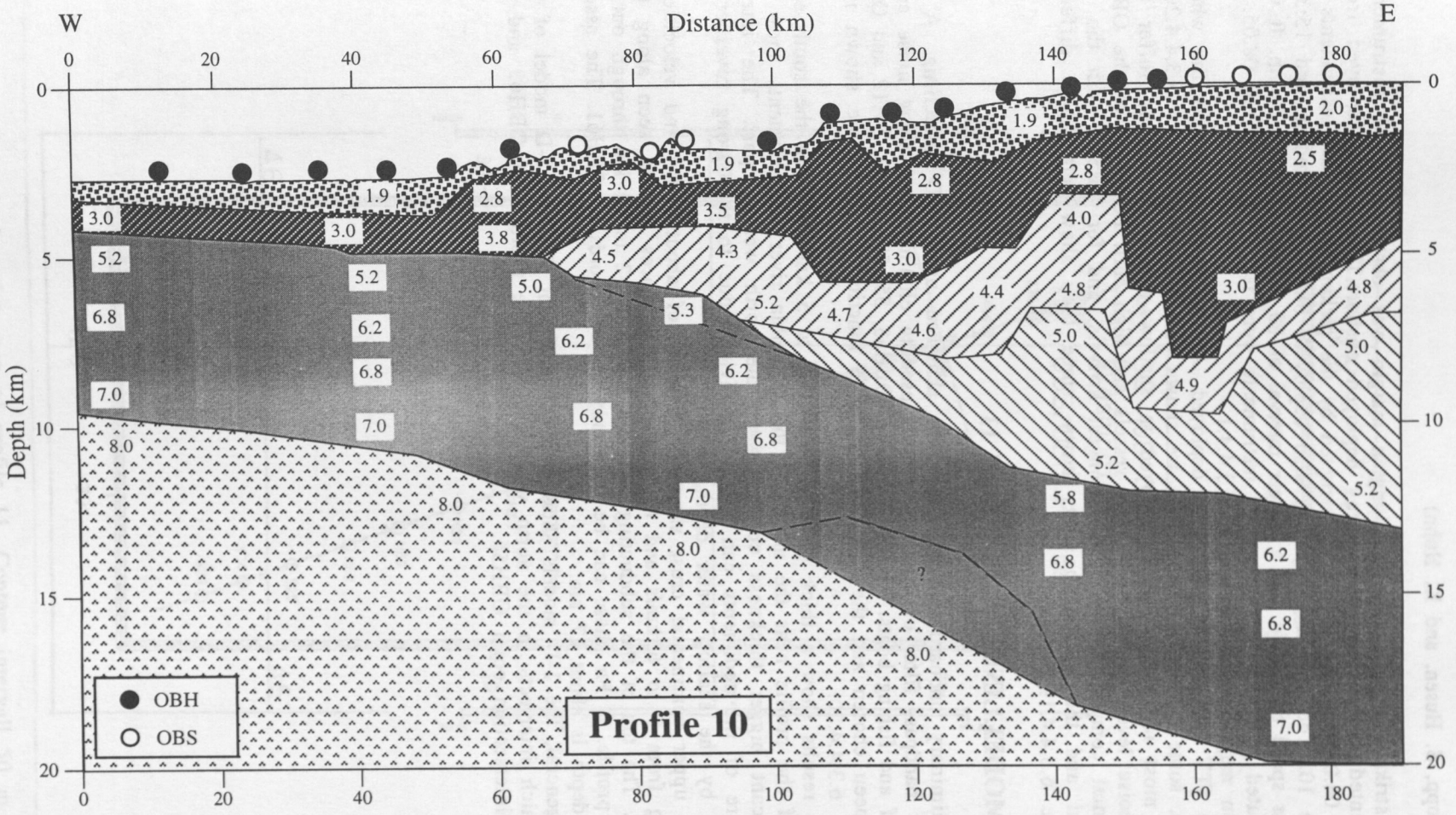

Figure 6.3.4.3.21: Preliminary results of the modelling along profile 10. Numbers are velocities in km/s.

6.3.4.4 THE WASHINGTON N-S TRANSECT, PROFILE 11

(C. Kopp, S. Husen, and K. Huhn)

A strike line along the Washington margin was observed by 21 instruments, augmented by a 60 receiver array deployed onshore.These were deployed from 15:30 04.05. to 12:30 05.05., interrupted by the pickup of the last instruments from profile 10. The vertical array was also deployed. Shooting started around 15:30 with a ships speed of 3.5 kn and a trigger interval of 60 s from North to South. It was terminated at 10:00 07.05., and all instruments were recovered by 07:00 08.05. A location map is shown in Figure 6.3.4.4.1.

The ITT ministreamer was also deployed. All instruments recorded the whole profile, some of the record sections are shown in Figures 6.3.4.4.2 to 6.3.4.4.20. Since most instruments were deployed in shallow water, the records suffer from high noise levels caused by fishing vessels and high surf. For some of the OBS the horizontal component shows the strongest arrivals, and for OBS29 both the vertical and the hydrophone are shown, since they show remarkable differences (Figure 6.3.4.4.19).

1-D MODELLING OF PROFILE 11

Preliminary onboard interpretation was achieved using 1-D modelling. A more narrow bandpass filter of 9 to 20 Hz was used to eliminate the strong noise caused by surf and fishing boats. Finally 7 stations (OBH53, 55, 58, 61, 62, VA12 and QBH64) have been chosen and the 1-D velocity depth functions of these are shown in Figure 6.3.4.4.20.

The results show a thick sediment layers up to 5 km depth. In the south eastern part of the profile near the mouth of the Columbia river the sediments show a significant bigger thickness comparing to the north western part. The internal structure of the sediments can hardly be divided due to the strong reverberations caused by the shallow water depth.

The upper continental crust shows a thickness of about 5 km and velocities ranging from 5 to 6 km/s and no significant differences can be seen along the profile. The top of the subducting slab can traced in 12 to 14 km through out the whole profile. A Pn phase can be seen only in the records of OBH61. The associated Moho depth is about 17 km.

In general, the 1-D models show a good agreement with the 2-D model of profile 12, which intersects in the north western part at the position of OBH63 and profile 10 at intersection point OBH56.

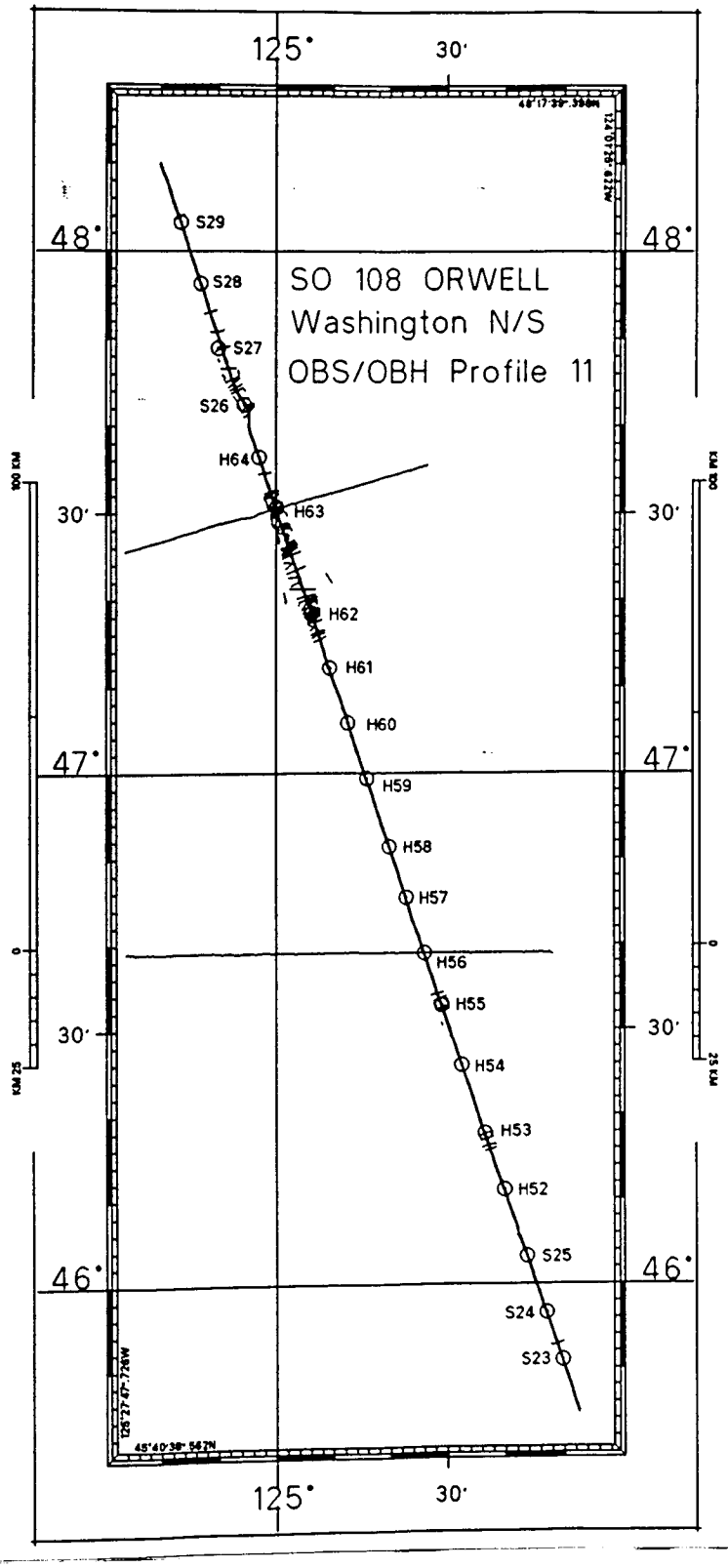

Figure 6.3.4.4.1: Location map of profile 11. Contour intervall 50 m. S* and H** mark OBS/OBH stations.

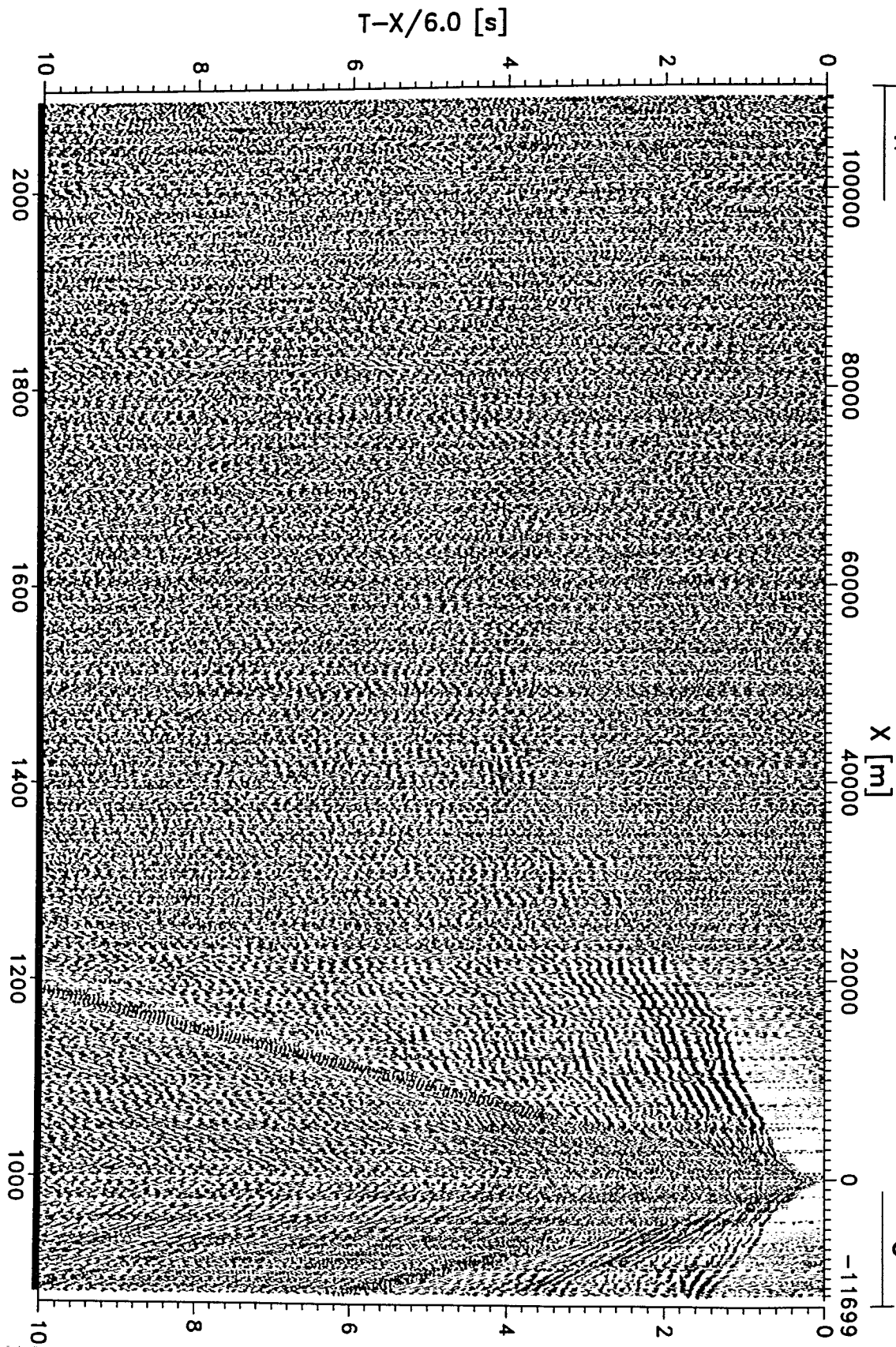

Figure 6.3.4.4.2: Record section for OBS23, vertical component.

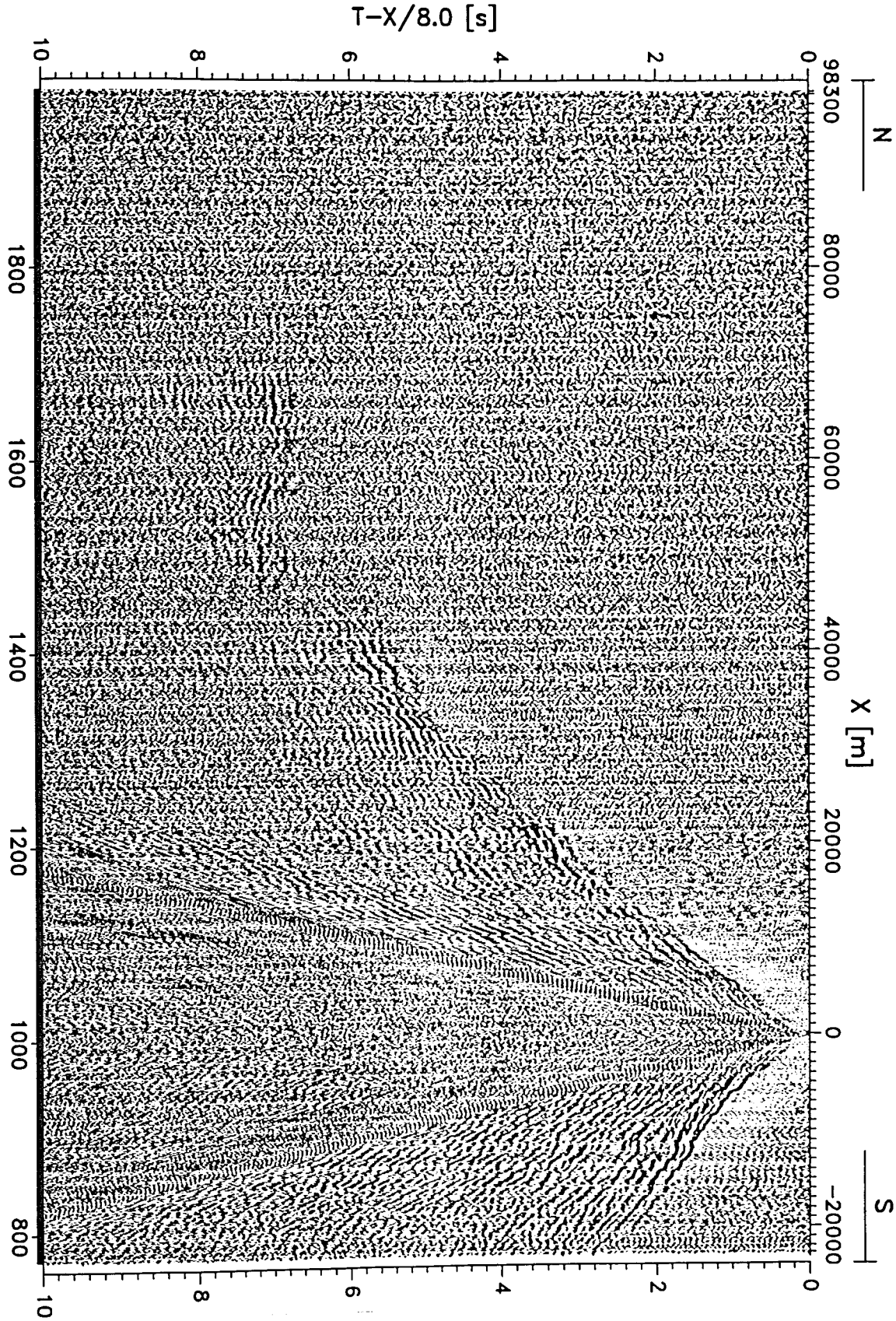

Figure 6.3.4.4.3: Record section for OBS24, hydrophone.

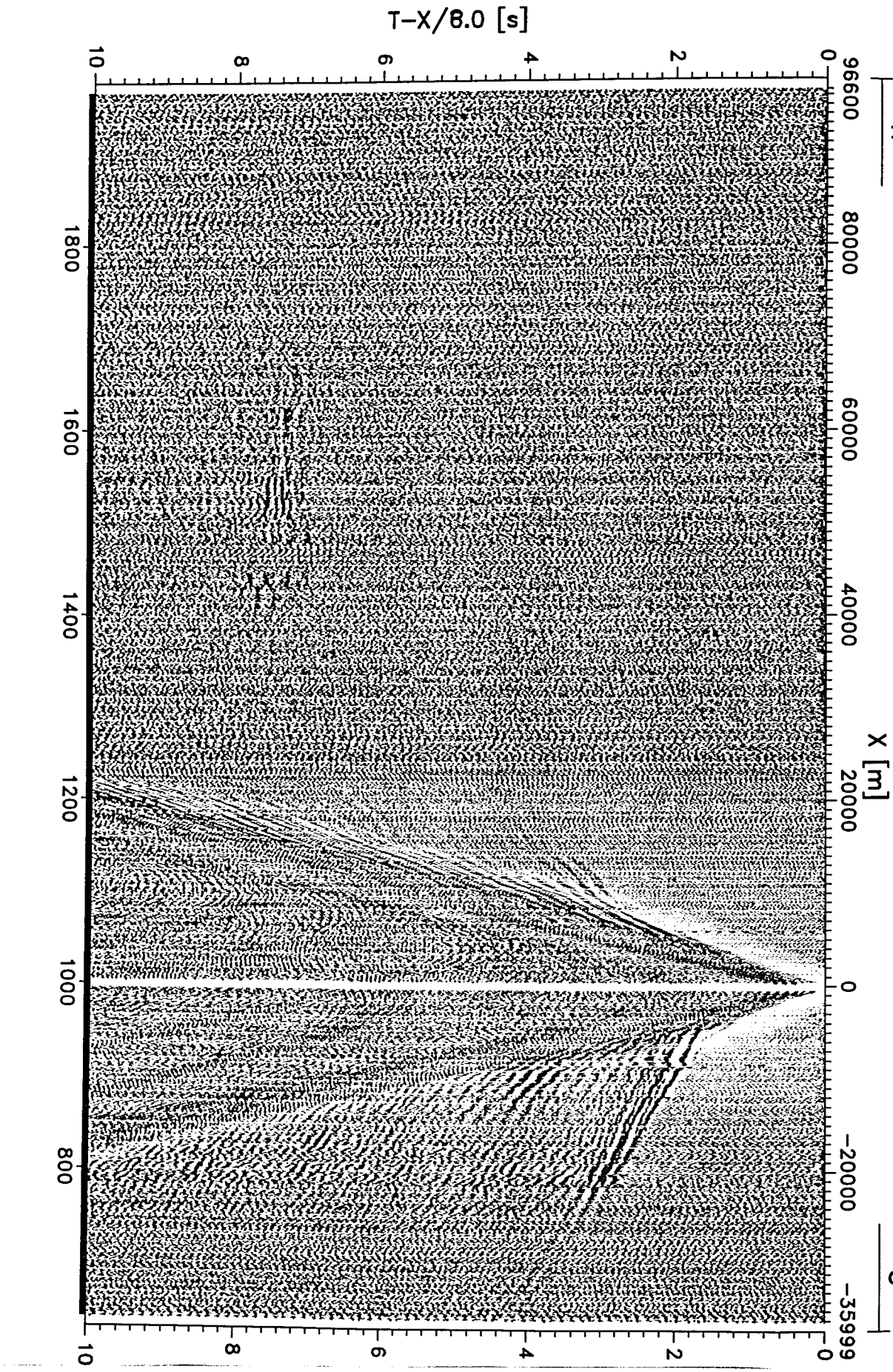

Figure 6.3.4.4.4: Record section for OBS25, horizontal component.

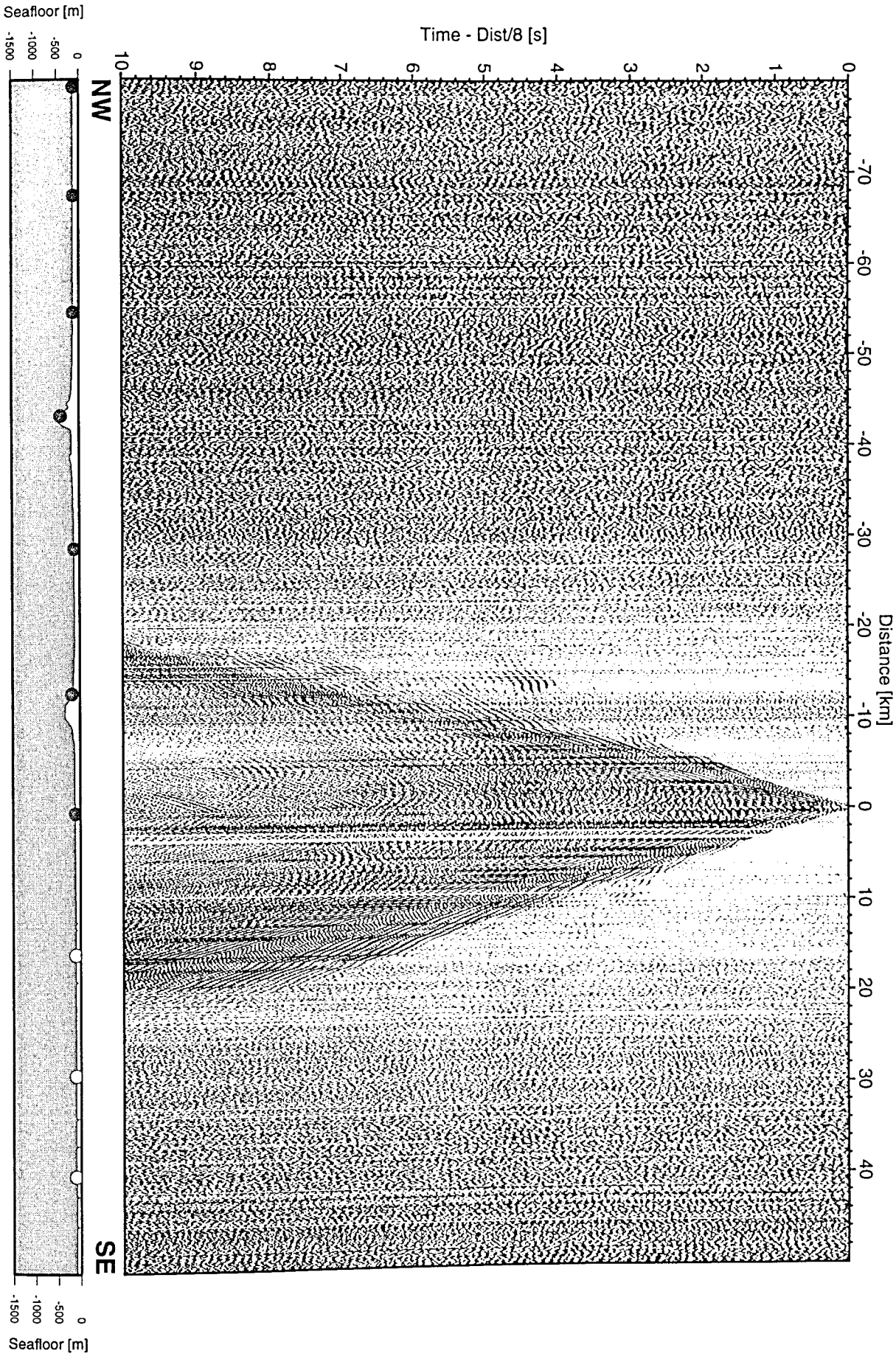

Figure 6.3.4.4.5: Record section from OBH 52, Profile 11.

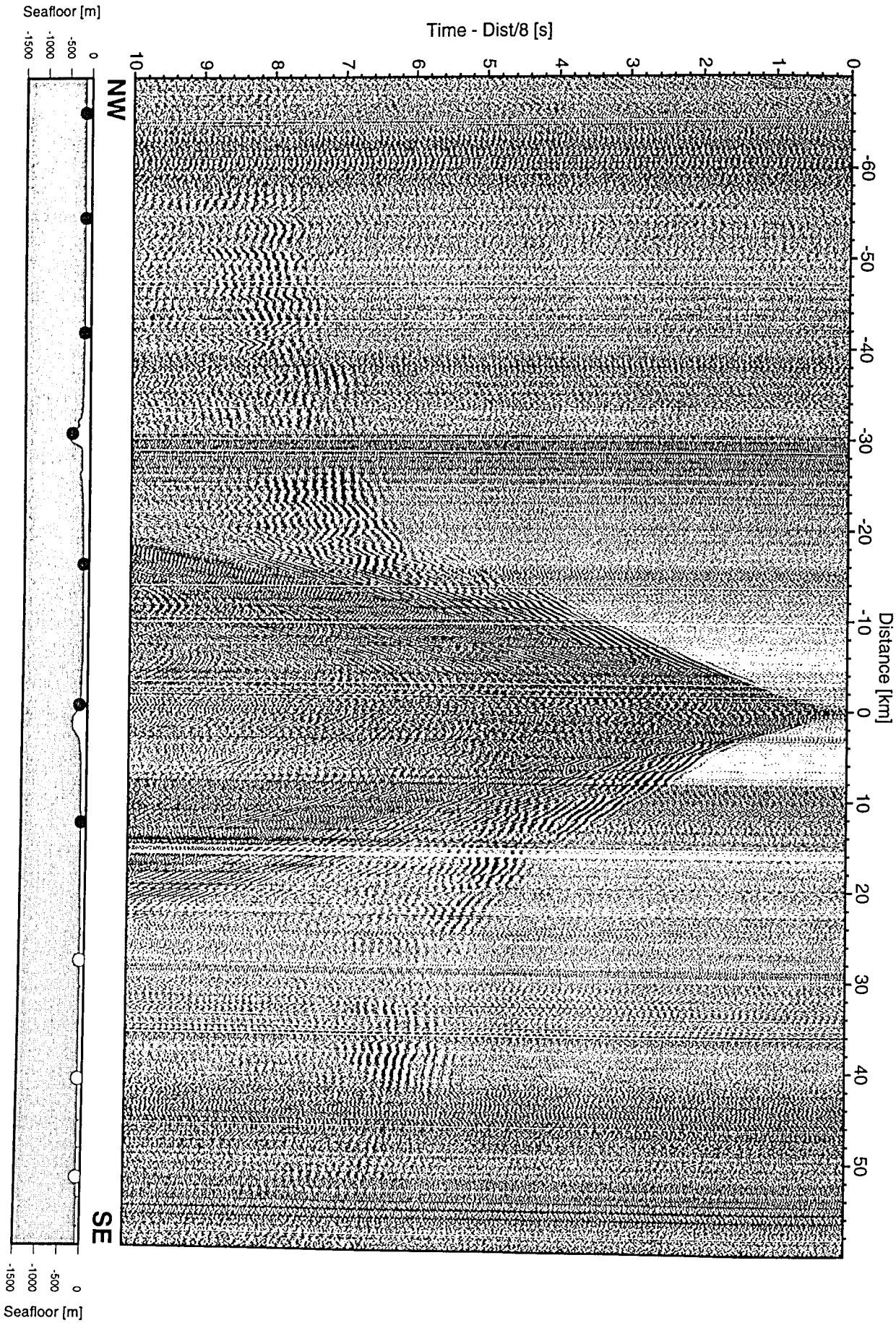

Figure 6.3.4.4.6: Record section from OBH 53, Profile 11.

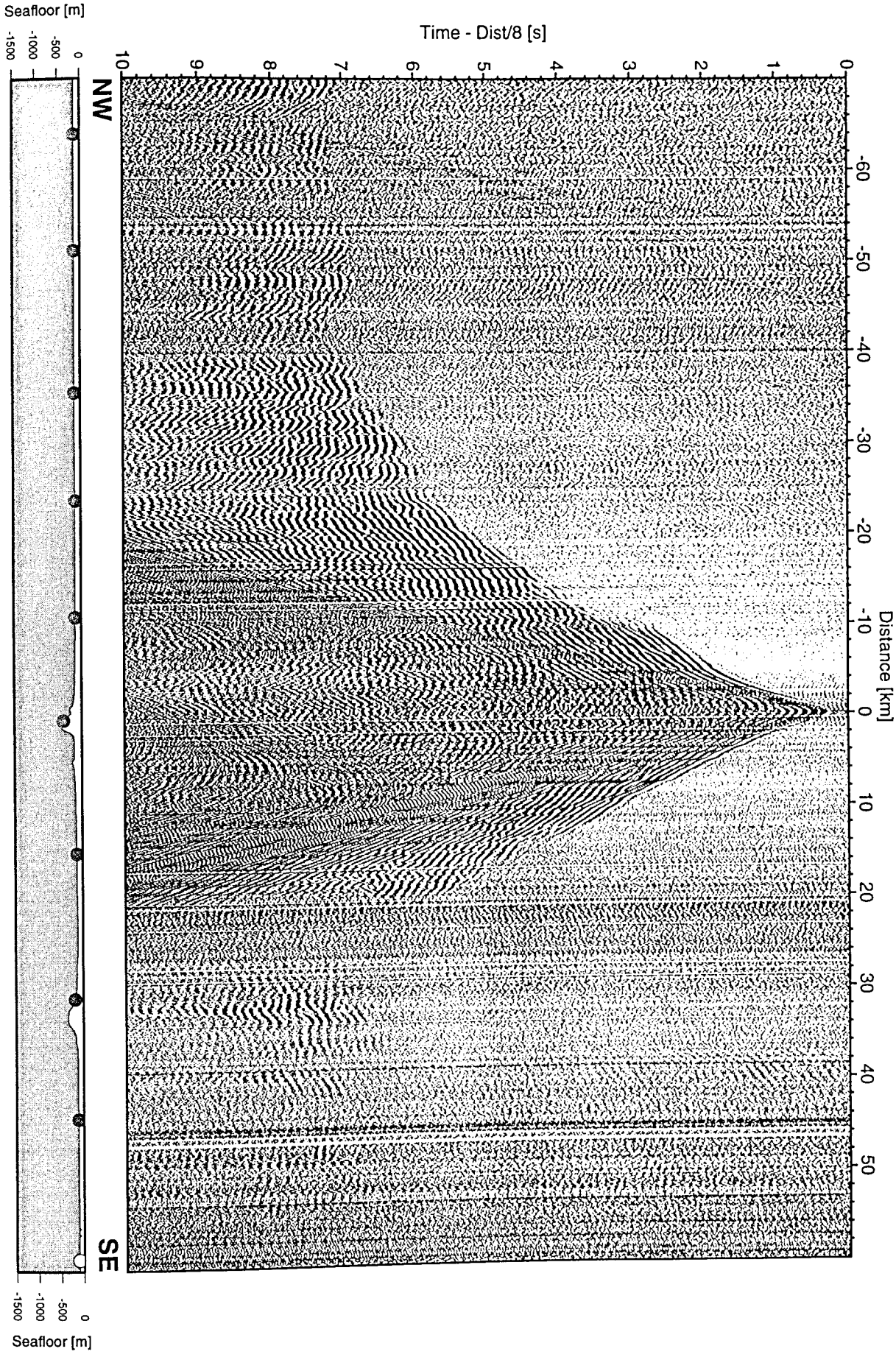

Figure 6.3.4.4.7: Record section from OBH 55, Profile 11.

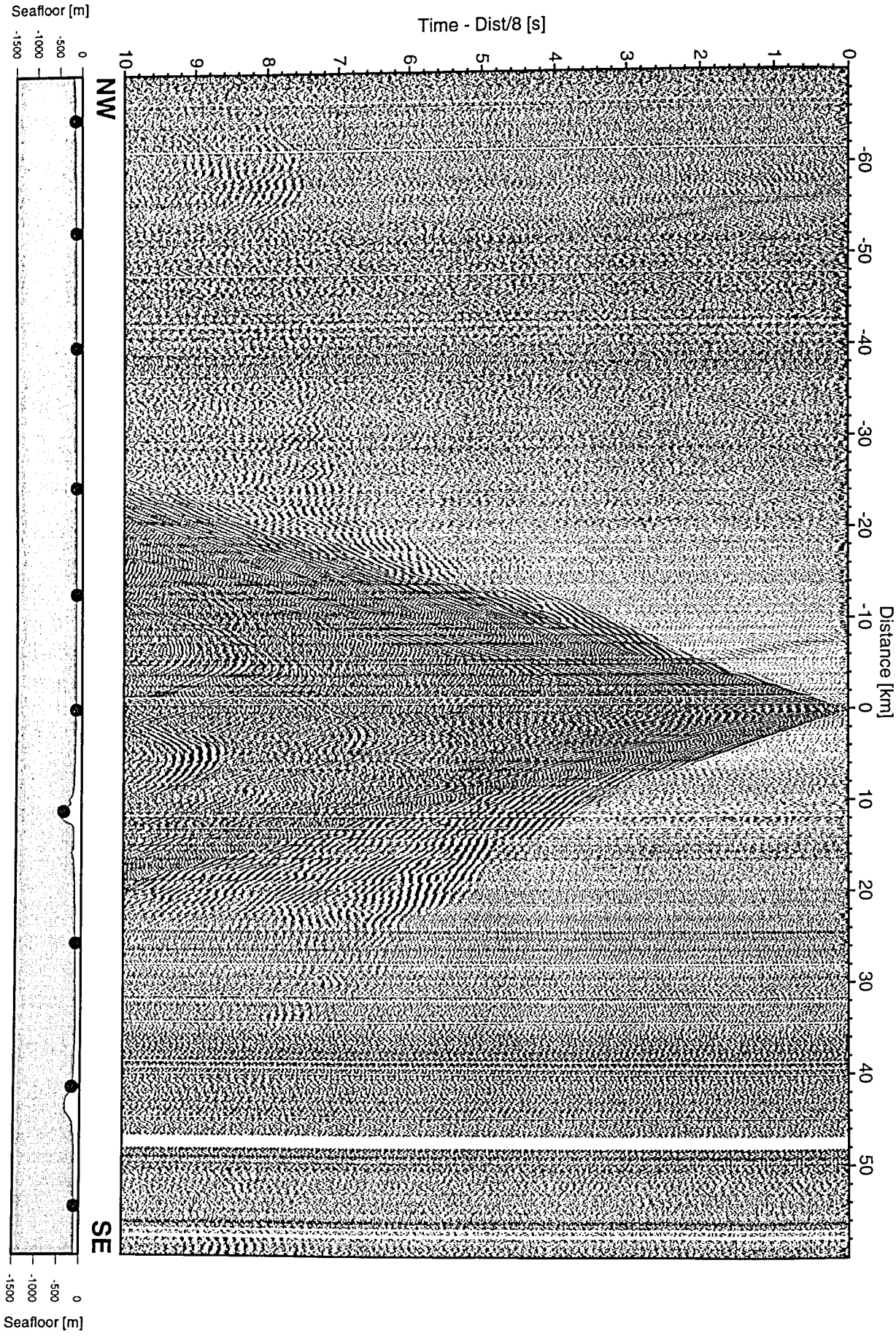

Figure 6.3.4.4.8: Record section from OBH 56, Profile 11.

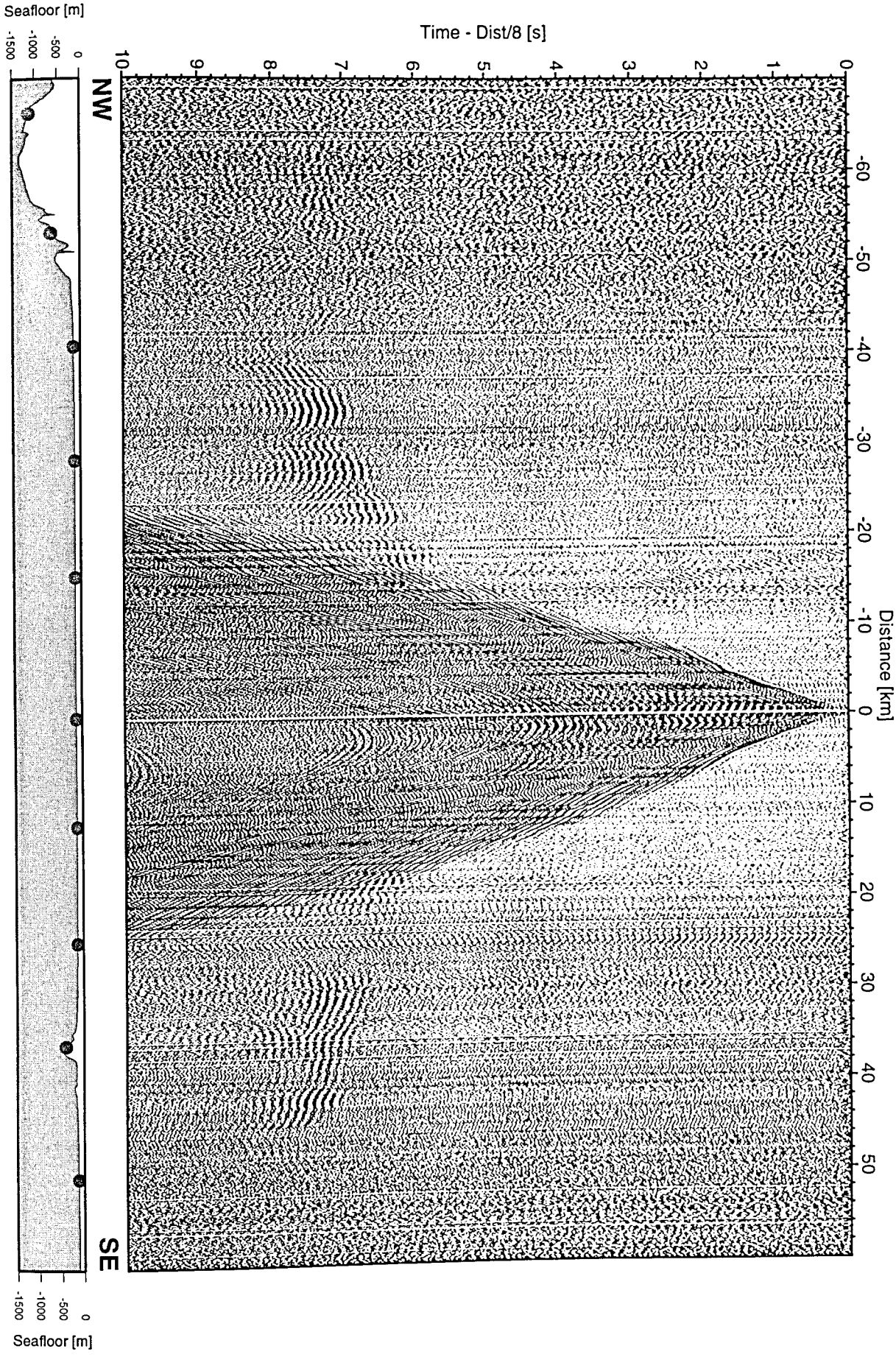

Figure 6.3.4.4.9: Record section from OBH 58, Profile 11.

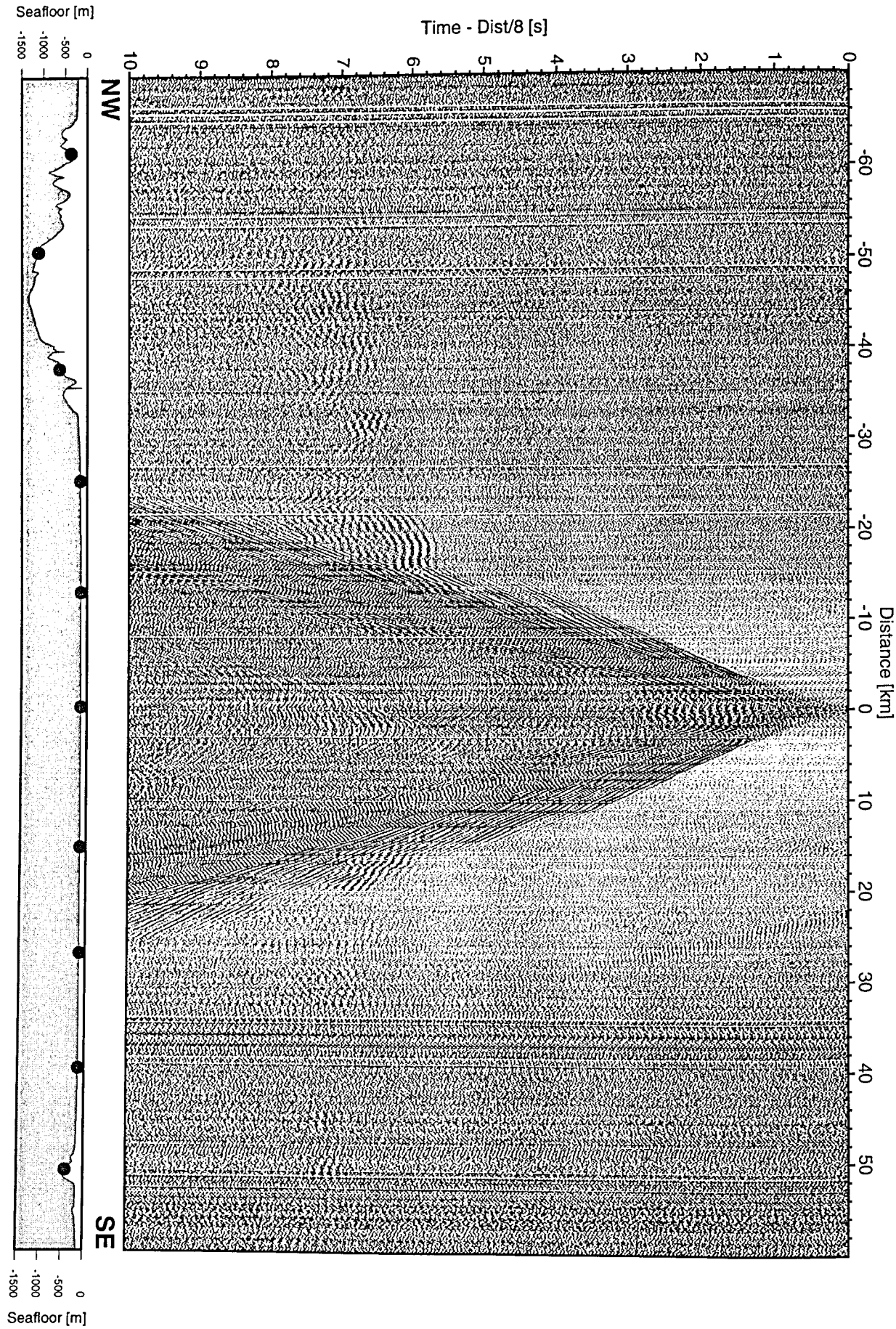

Figure 6.3.4.4.10: Record section from OBH 59, Profile 11.

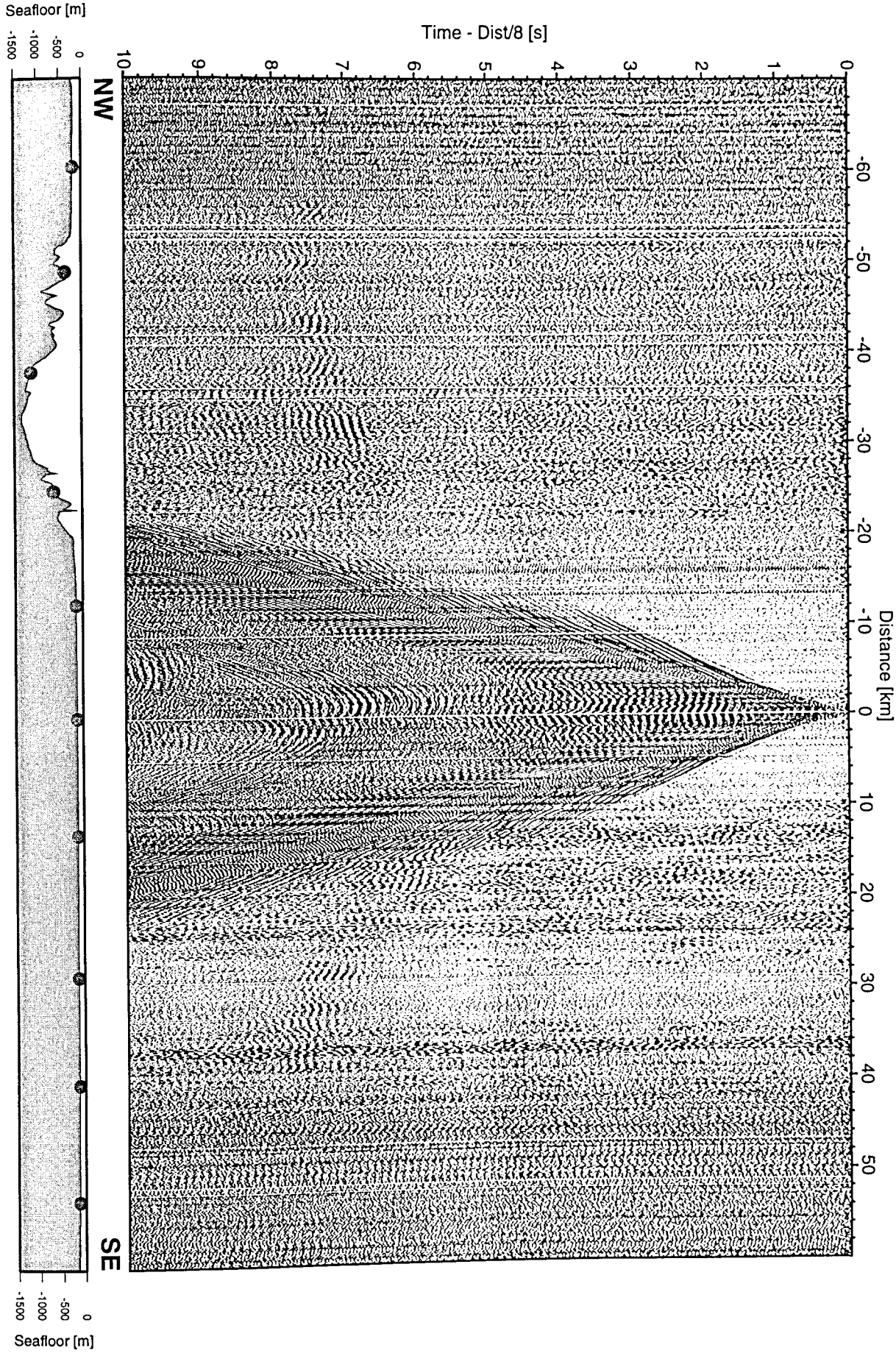

Figure 6.3.4.4.11: Record section from OBH 60, Profile 11.

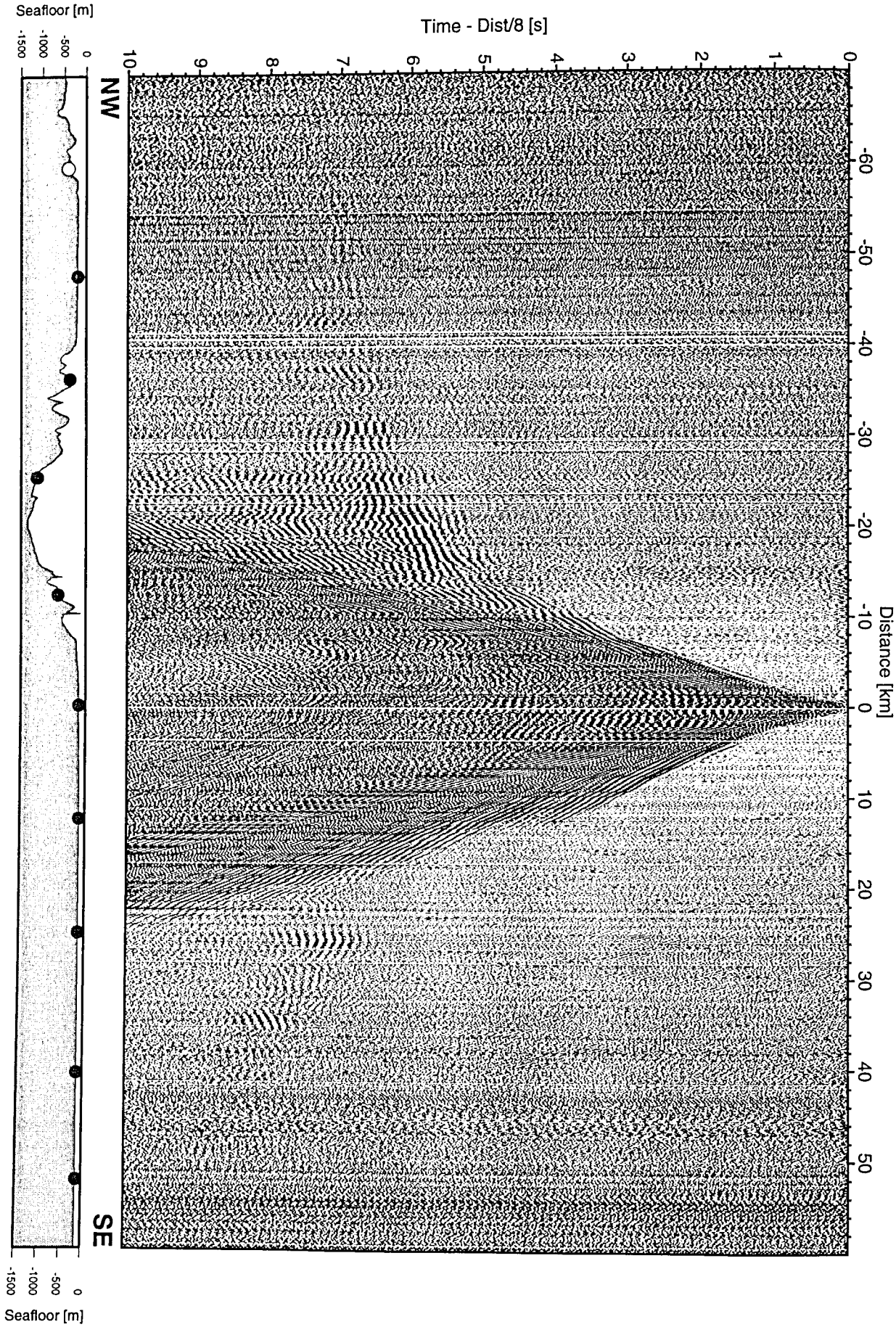

Figure 6.3.4.4.12: Record section from OBH 61, Profile 11.

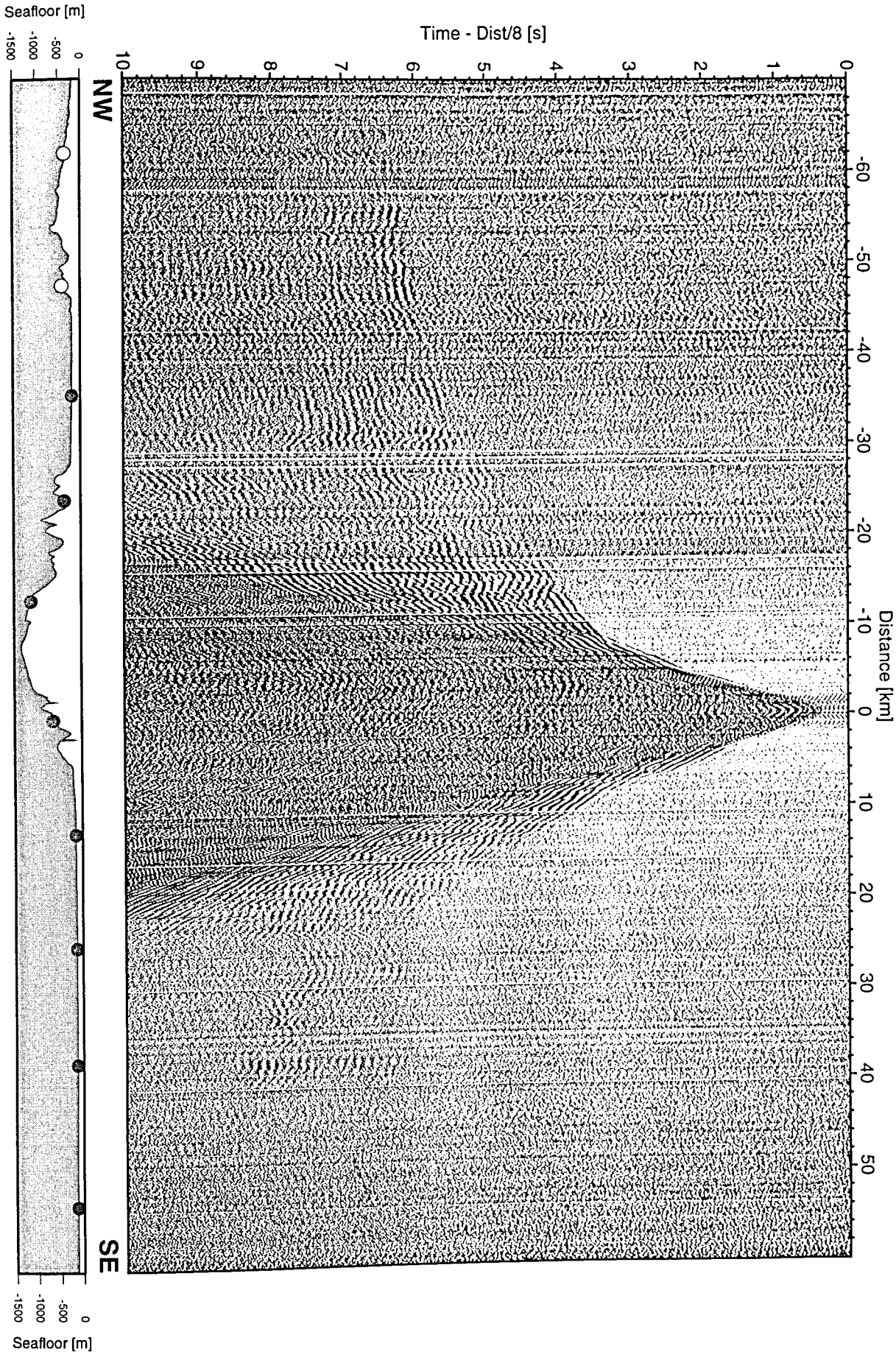

Figure 6.3.4.4.13: Record section from OBH 62, Profile 11.

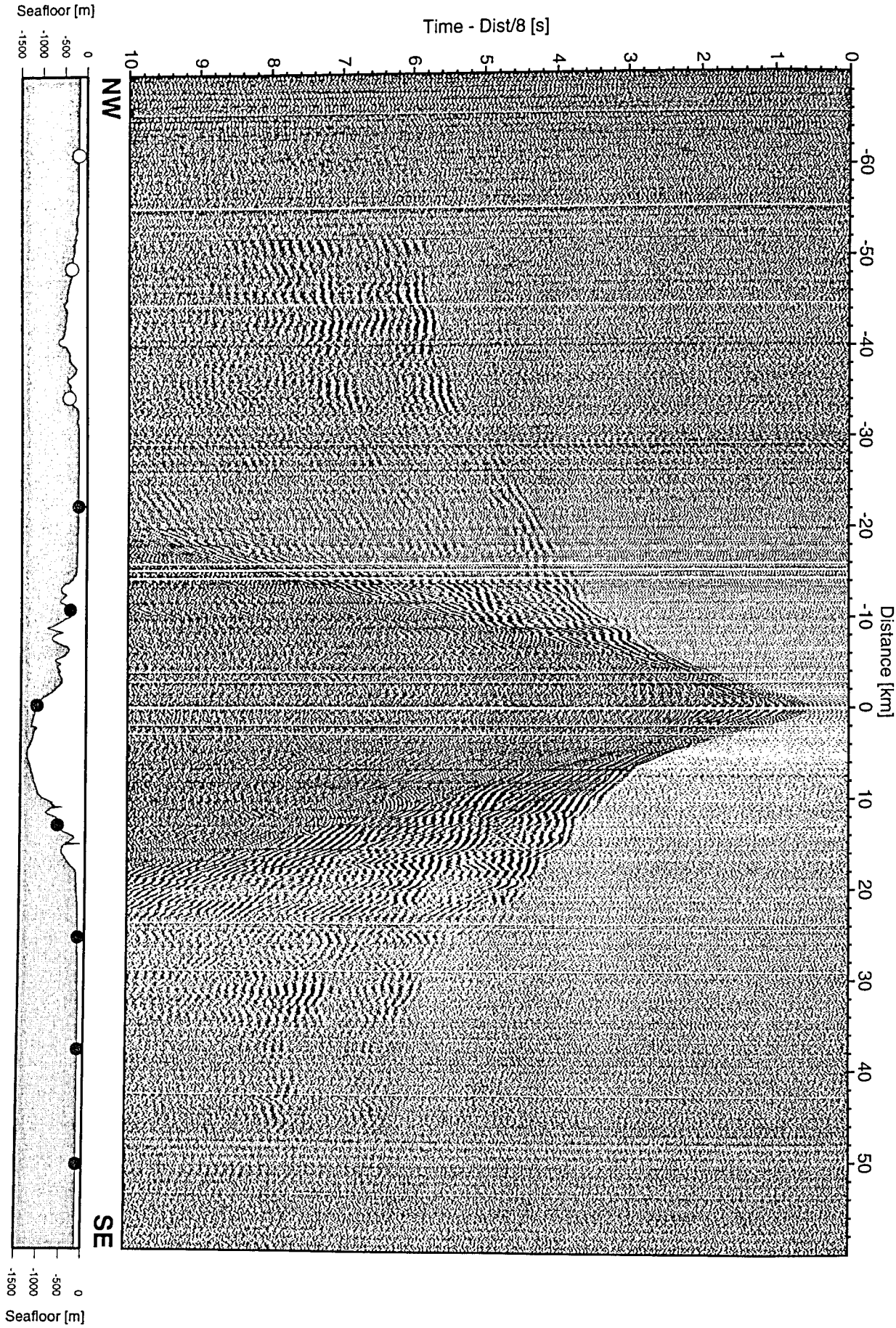

Figure 6.3.4.4.14: Record section from OBH 562, Profile 11.

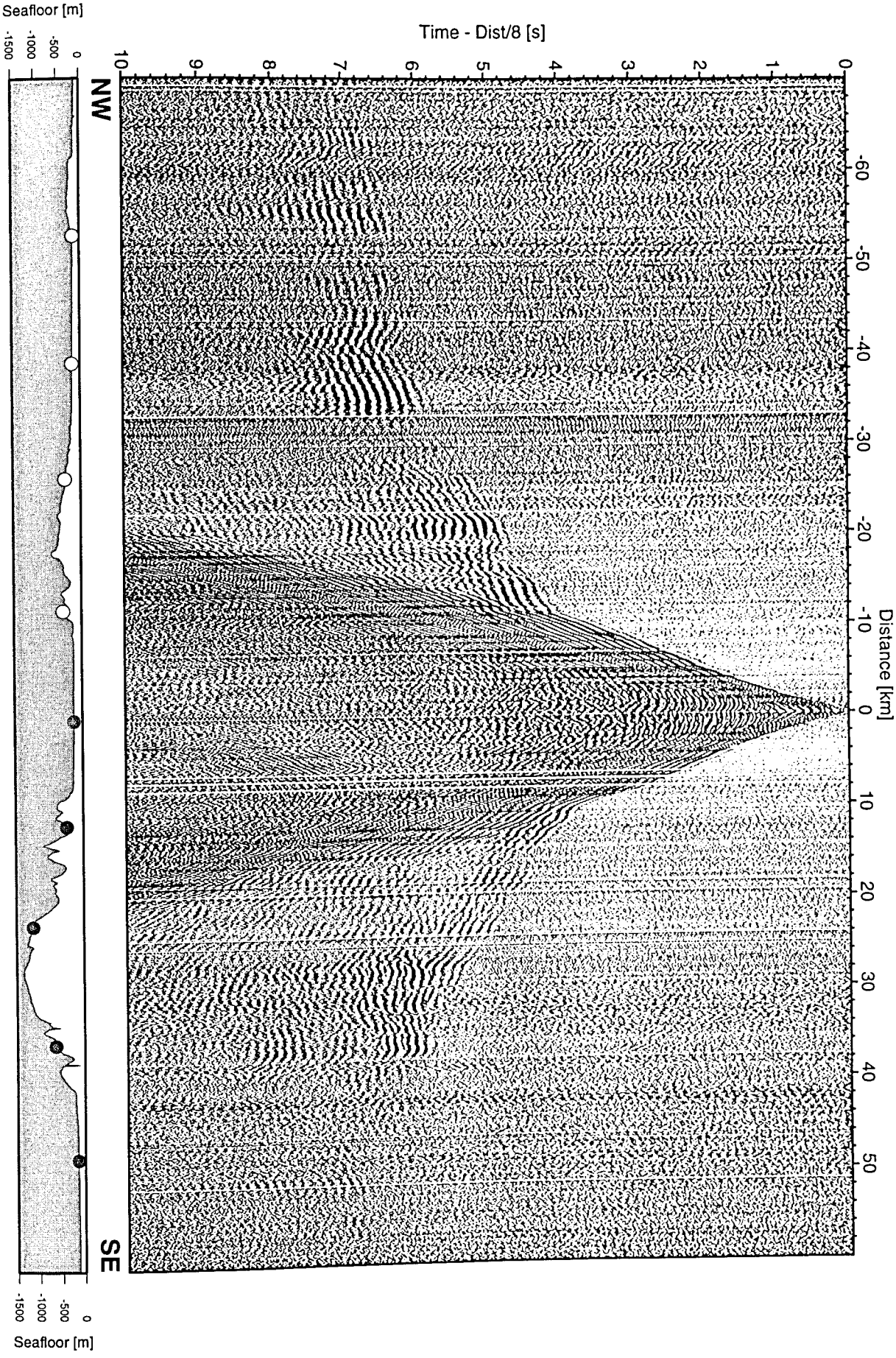

Figure 6.3.4.4.15: Record section from OBH 64, Profile 11.

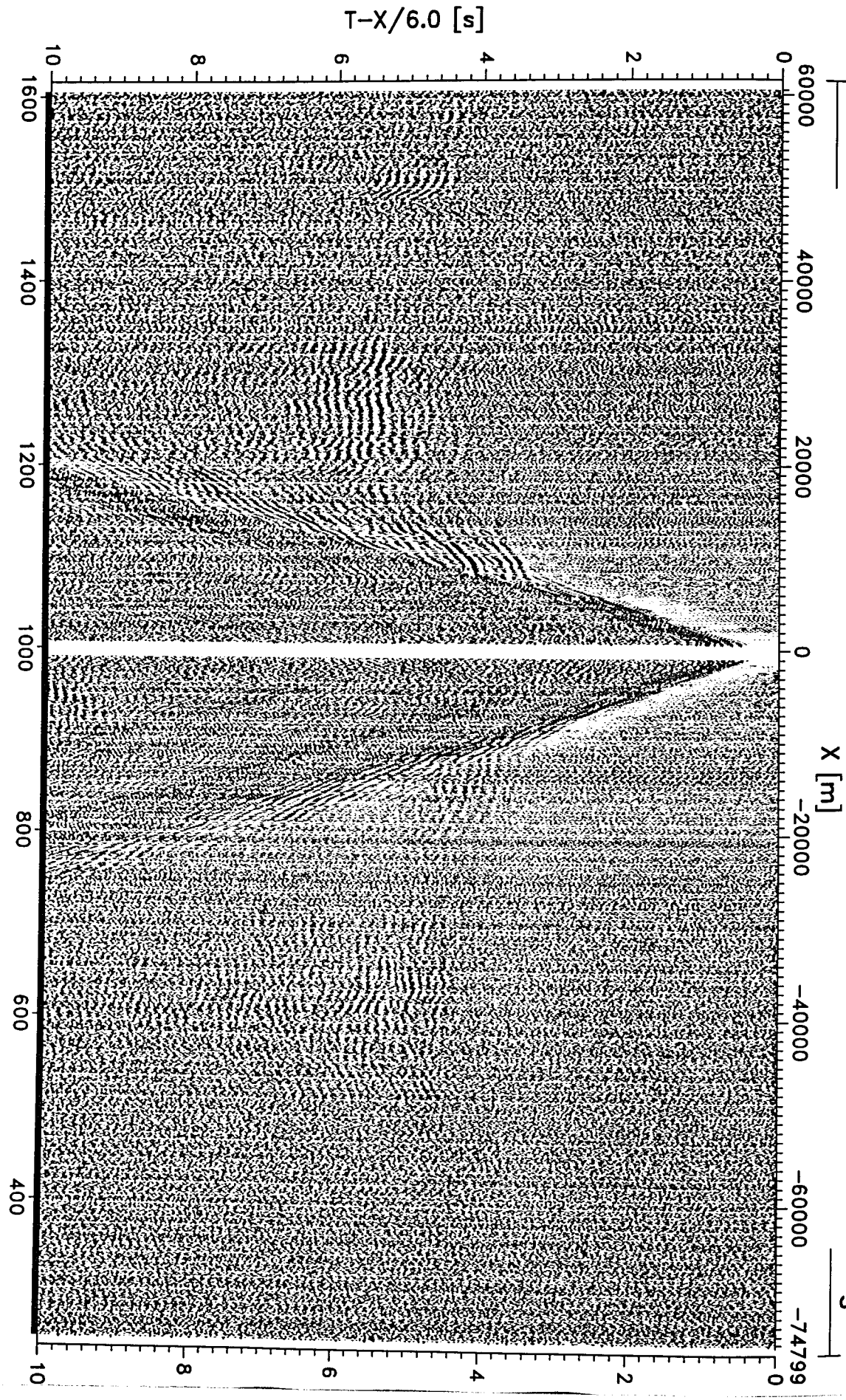

Figure 6.3.4.4.16: Record section for OBS26, hydrophone.

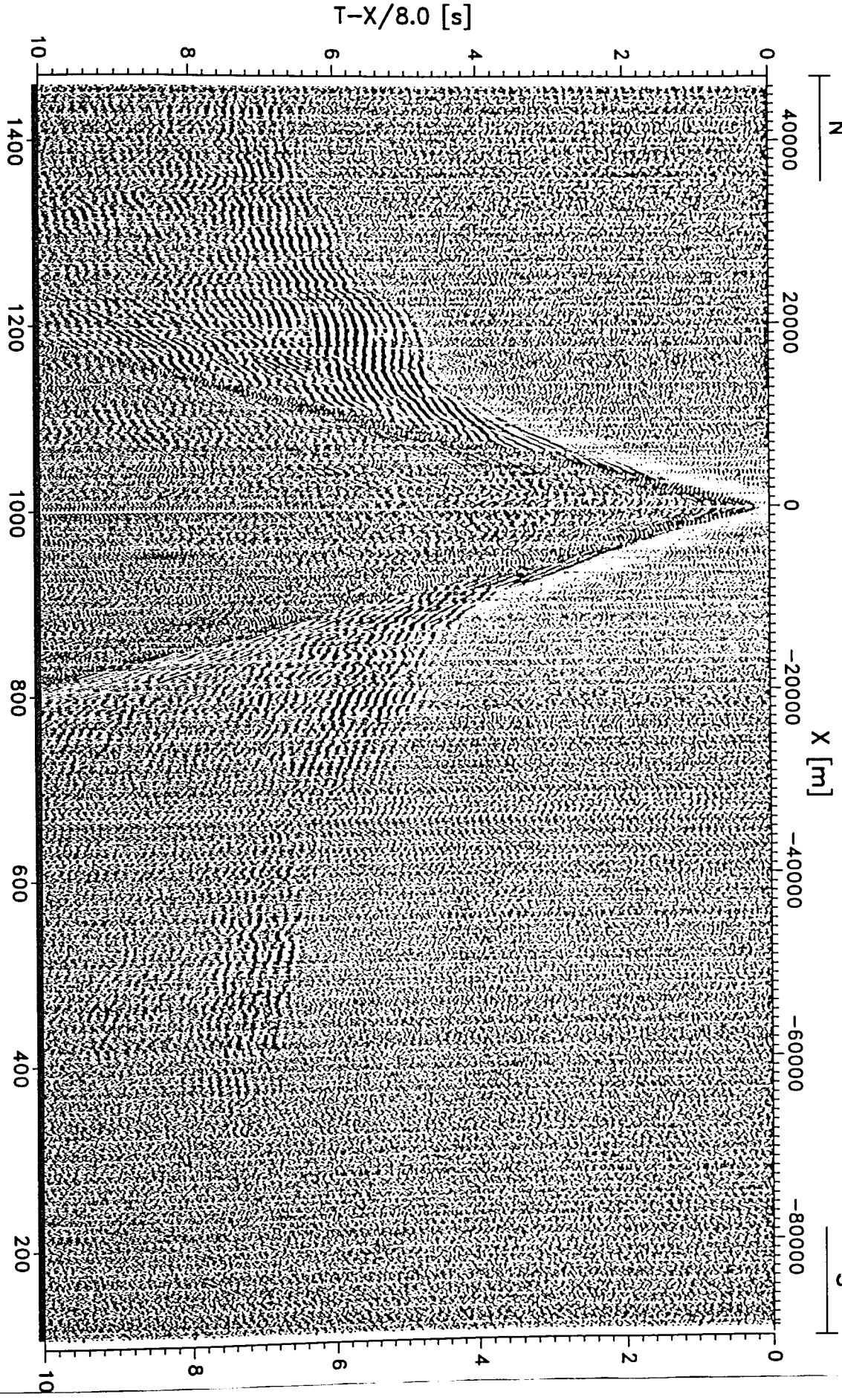

Figure 6.3.4.4.17: Record section for OBS27, hydrophone.

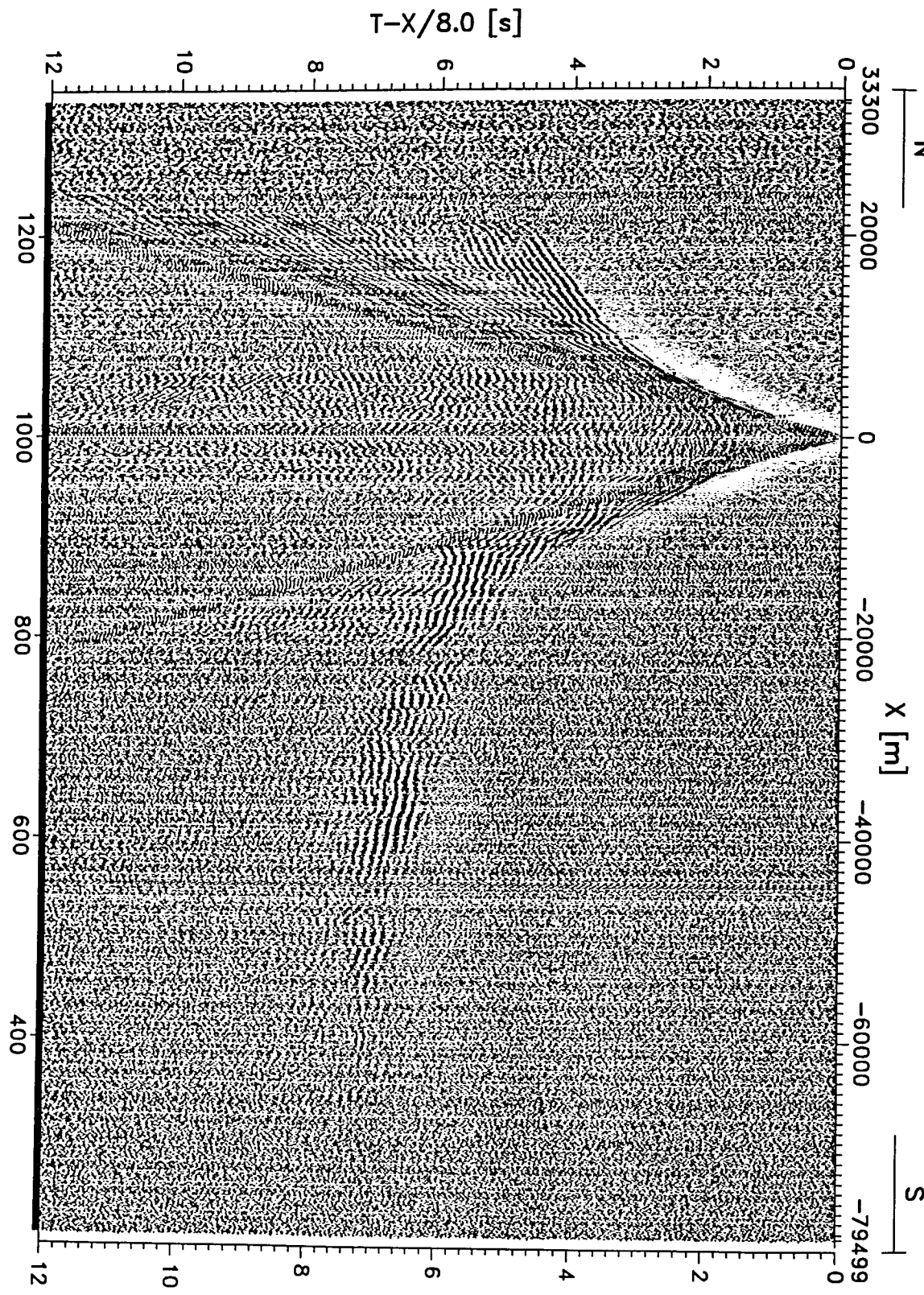

Figure 6.3.4.4.18: Record section for OBS28, horizontal component.

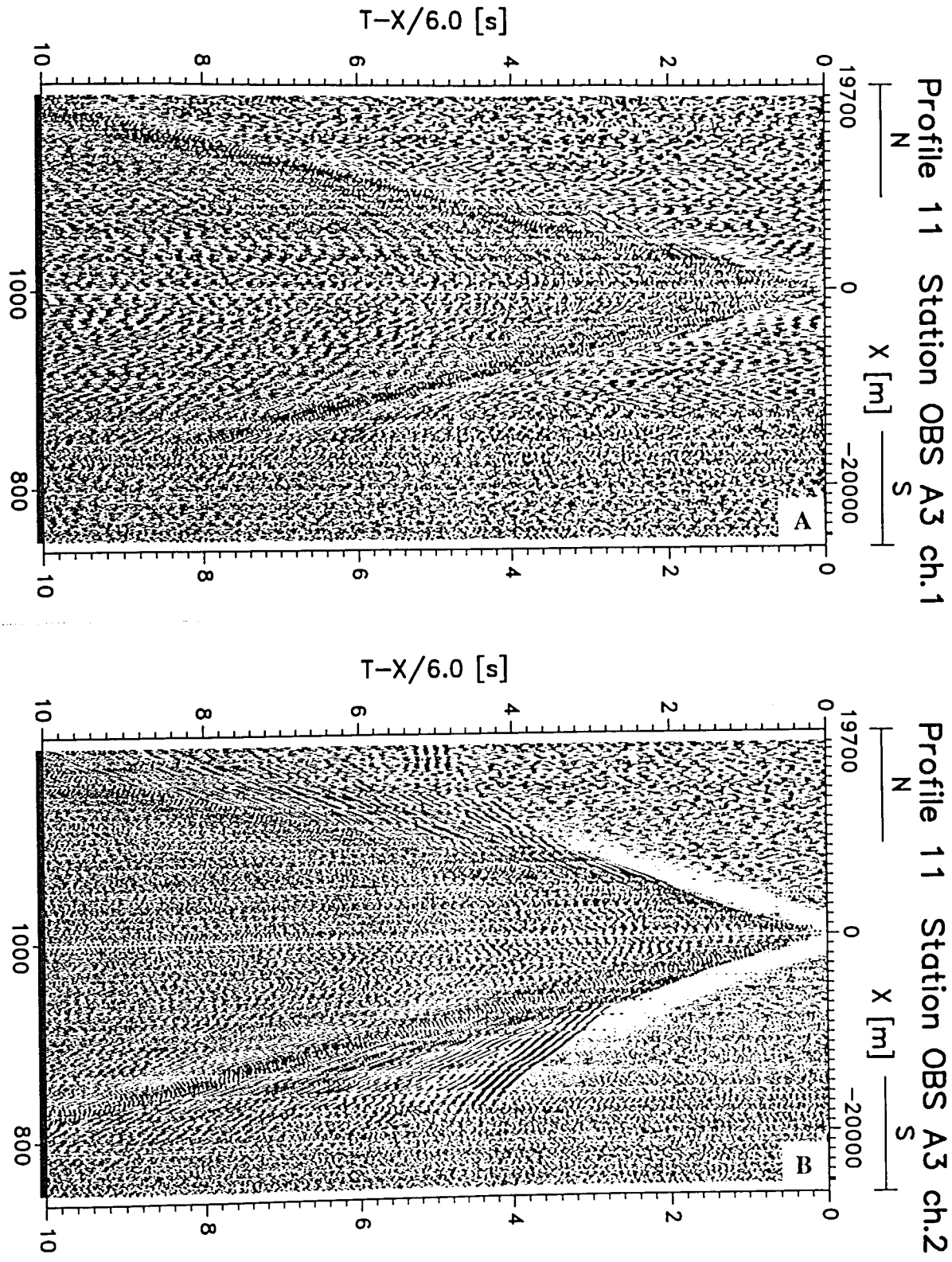

Figure 6.3.4.4.19: Record section for OBS29, vertical (A) and horizontal component (B).

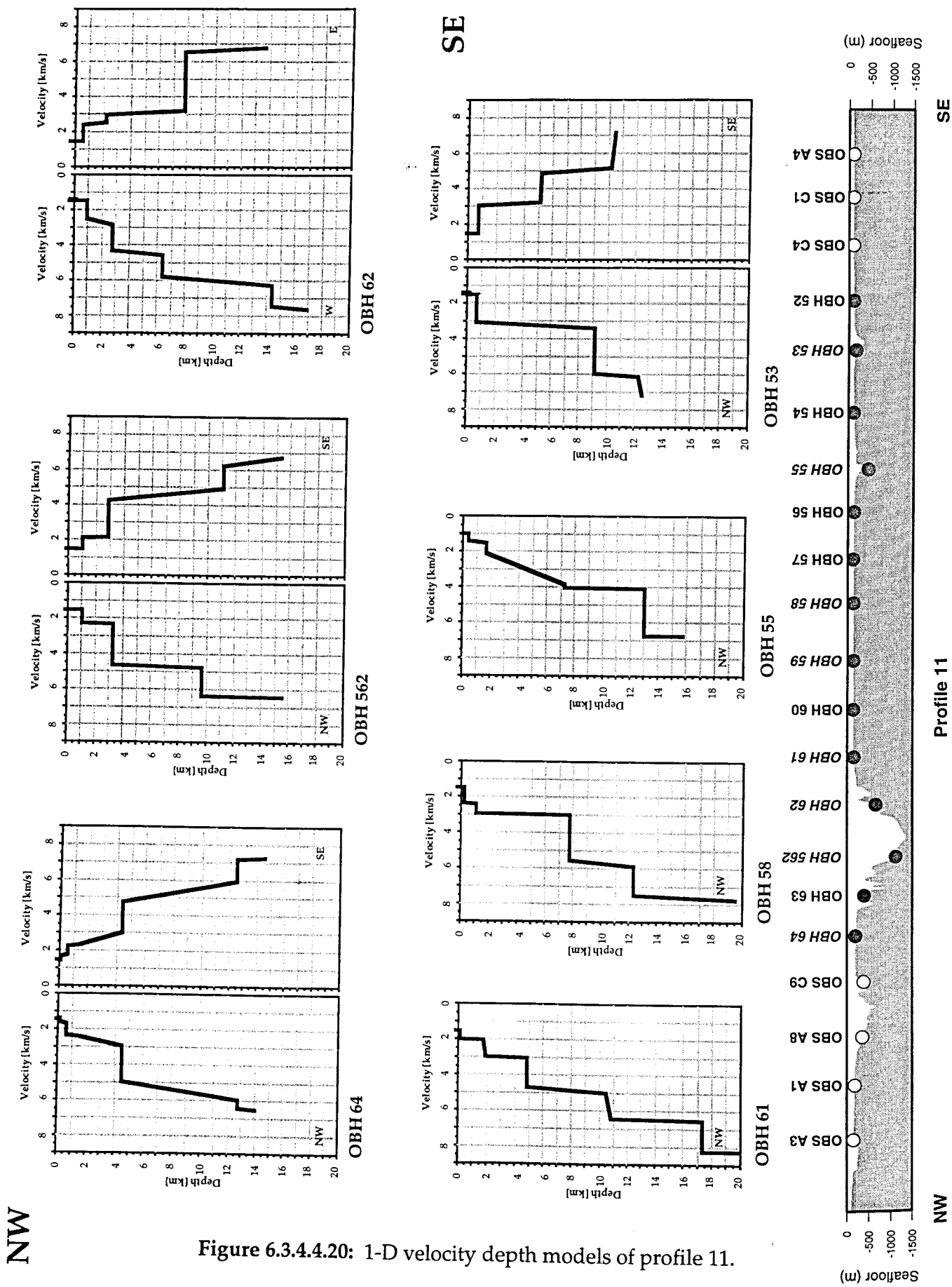

Figure 6.3.4.4.20: 1-D velocity depth models of profile 11.

6.3.4.5 THE OLYMPIC TRANSECT, PROFILE 12

(C. Kopp and E. Flueh)

A dip line across the accretionary wedge off Northern Washington was obtained using 21 instruments that were augmented by a 60-receiver array deployed onshore. The offshore insttruments were deployed from 10:00 to 21:00 on 08.05. The vertical array was also deployed, and OBH77 was lowered on a 1600 m long anchor rope, so it stayed at nearly 1000 m below sea level. This was done to monitor the source signal without interference from the seafloor reflection. Shooting started around 00:00 on 09.05. with a ships speed of 3.5 kn and a trigger interval of 60 s from East to West in totally calm seas. It was terminated at 06:30 09.05., and all instruments were recovered by 23:00. A location map is shown in Figure 6.3.4.5.1. During recovery, OBH65 did not respond to the release command, but it ascended to the surface several minites after the release command had been sent. A weak radio signal was received, and the OBH was located about 4 miles from its point of deployment. Several scratches and a broken flag indicated it had been dragged by a fishing vessel, and the data analysis proved that this had happened before the profile was shot. The data are still useful, although not recorded in line. It was to our extreme good fortune, that the instrument released upon command; had it been dragged a little further, it would have probably been out of range.

The ITT ministreamer was also deployed during this profile. All instruments except OBS33 recorded the whole profile, some of the record sections are shown in Figures 6.3.4.5.2 to 6.3.4.5.21. The easternmost OBS were deployed in shallow water, but since there was very little fishing activity and perfect weather conditions, these recordings are among the best shallow water recordings obtained during the cruise.

For some of the shallow water OBS the horizontal component shows the strongest arrivals, and for OBS32 both the vertical and the hydrophone are shown, since they show remarkable differences (Figure 6.3.4.5.4, see also discussion in Chapter 6.3.4.5.1). On the shelf, the first three instruments show a pronounced assymetry of the first arrivals, suggesting a steeply seaward dipping interface. Along the mid- and lower slope, all records sections show a pronounced undulation in the first

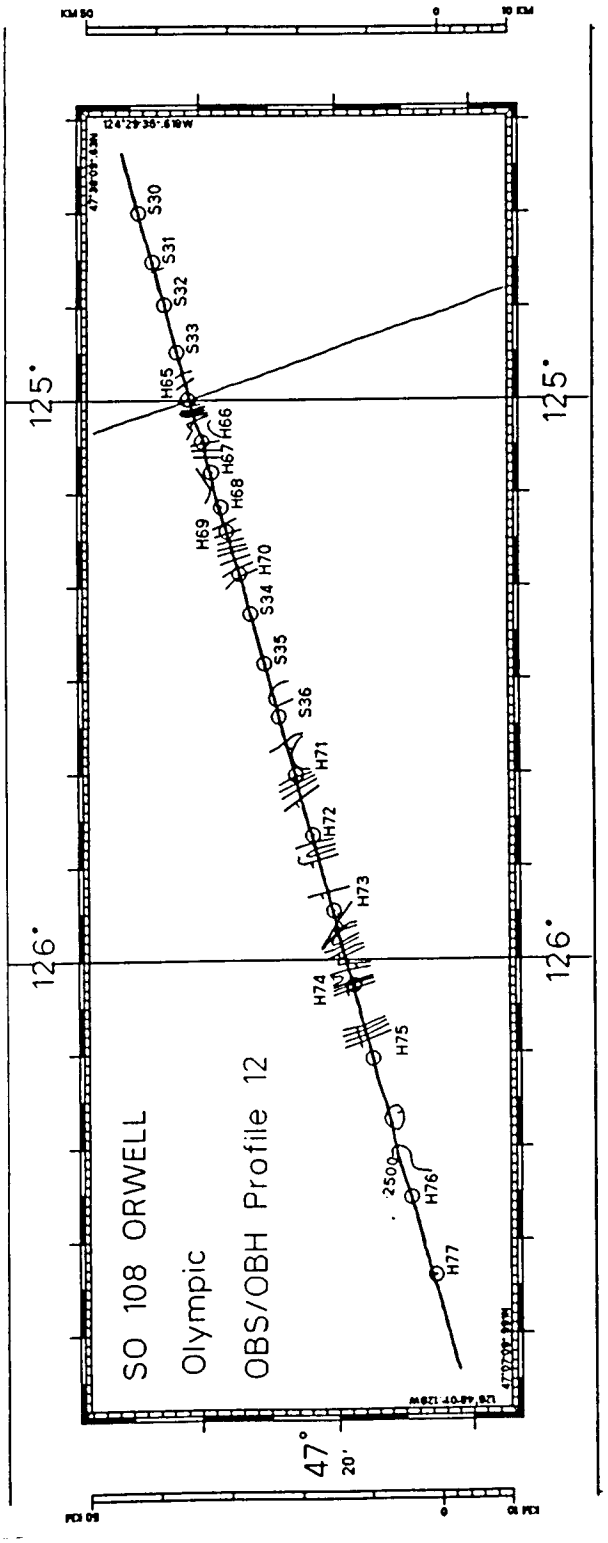

Figure 6.3.4.5.1: Location map of profile 12. Contour intervall 100 m. S* and H** mark OBS/OBH stations.

arrivals, which only in part can be explained by topography. Besides crustal phases the PMP is always clear, and a weak Pn is also evident on most sections. Crossover distance for Pn is between 40 and 50 km. On records from the lower slope and the oceanic crust the basement is seen as a prominent near-vertical reflection.

Along this profile, MCS data (profile 103) were also collected and processed onboard (see Chapter 6.4). The MCS records were used for the preliminary interpetation of the wide-angle data. The MCS section clearly images the plate boundary down to 7 s TWT at the eastern end of the line and also gives some indication of the internal sedimentary structure. Using 2-D raytracing, a velocity model for profile 12 was developed, and is shown in Figure 6.3.4.5.22. We did not attempt to model the velocity structure of the sediment in detail, but evidently a low velocity layer about 1 km thick is found along the profile. On the shelf this layer locally thickens to 3 km. A steeply dipping interface (10° in profile projection) explains the observed assymetry of the first arrivals at the easternmost stations. A second sediment layer with velocities around 3 km/s thickens towards the trench and can also be followed across the profile. Near the trench the velocities within this layer increase to 3.5 km/s, indicating pore fluid loss which may occur along the prominent fault zone observed on the MCS data (see Chapter 6.4). The oceanic crust is clearly imaged by both data sets. The MCS data define the TWT to its top, and the wide angle data in addition map the Moho well. The plate dips at 2 to 3° and reaches depth of 13 km near the coast, the Moho is at 19 km. This is considerably shallower than along profile 7 (see Chapter 6.3.4.2, Figure 6.3.4.2.35). On the shelf two other units are seen with velocities of about 4.4 and 5.5 km/s. The western part of the 4.4 km/s layer most likely consists of dewatered sediments, while the remaining parts are older rock units of unknown age and history. A joint inversion of both the MCS and wide-angle data will provide a more detailed picture during the post cruise interpretation.

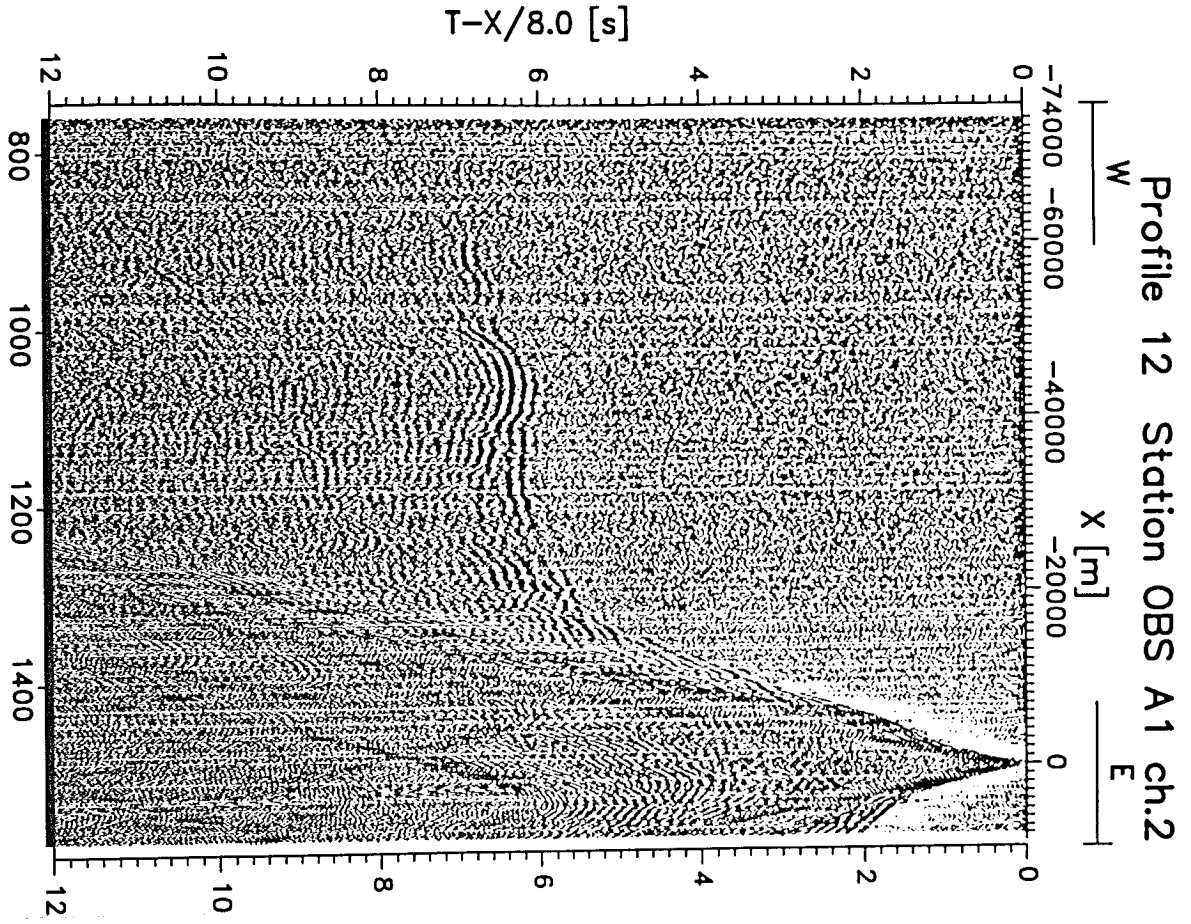

Figure 6.3.4.5.2: Record section for OBS30, horizontal component.

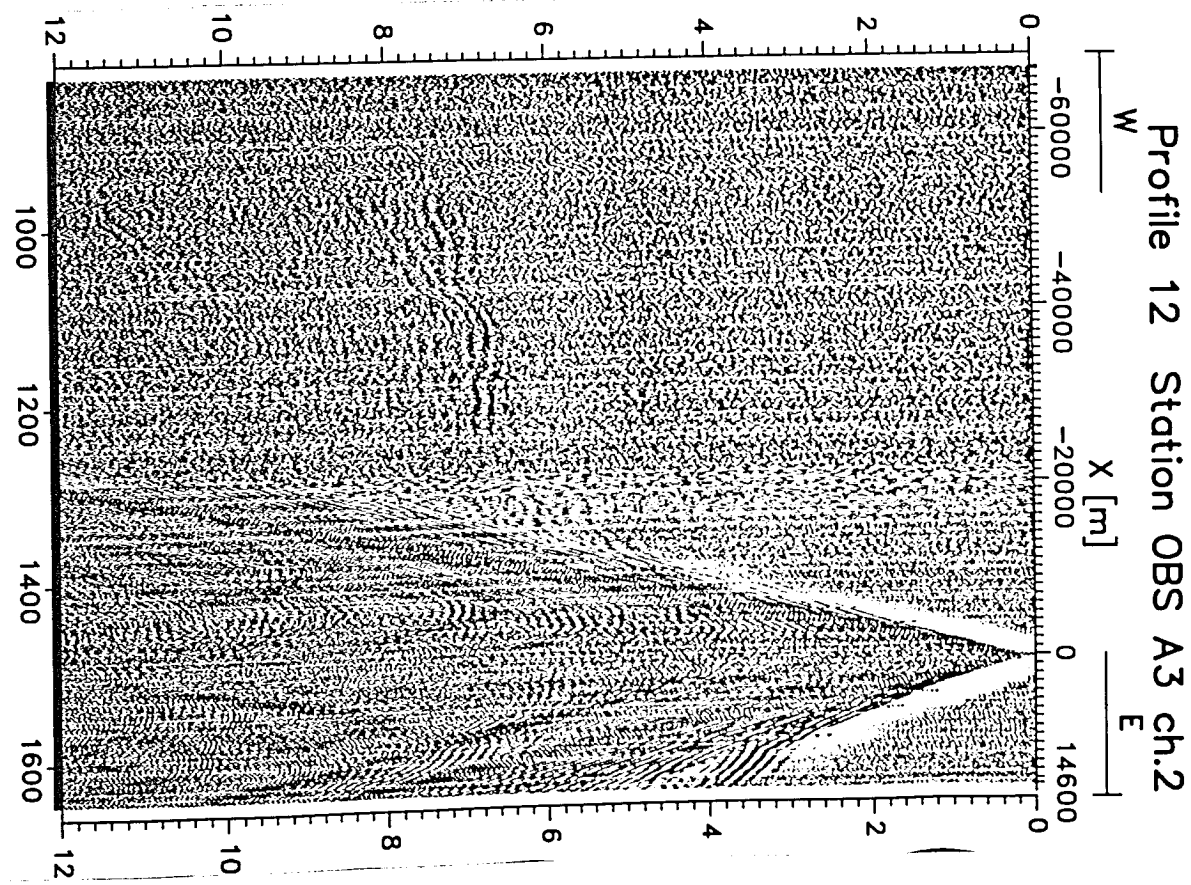

Figure 6.3.4.5.3: Record section for OBS31, horizontal component.

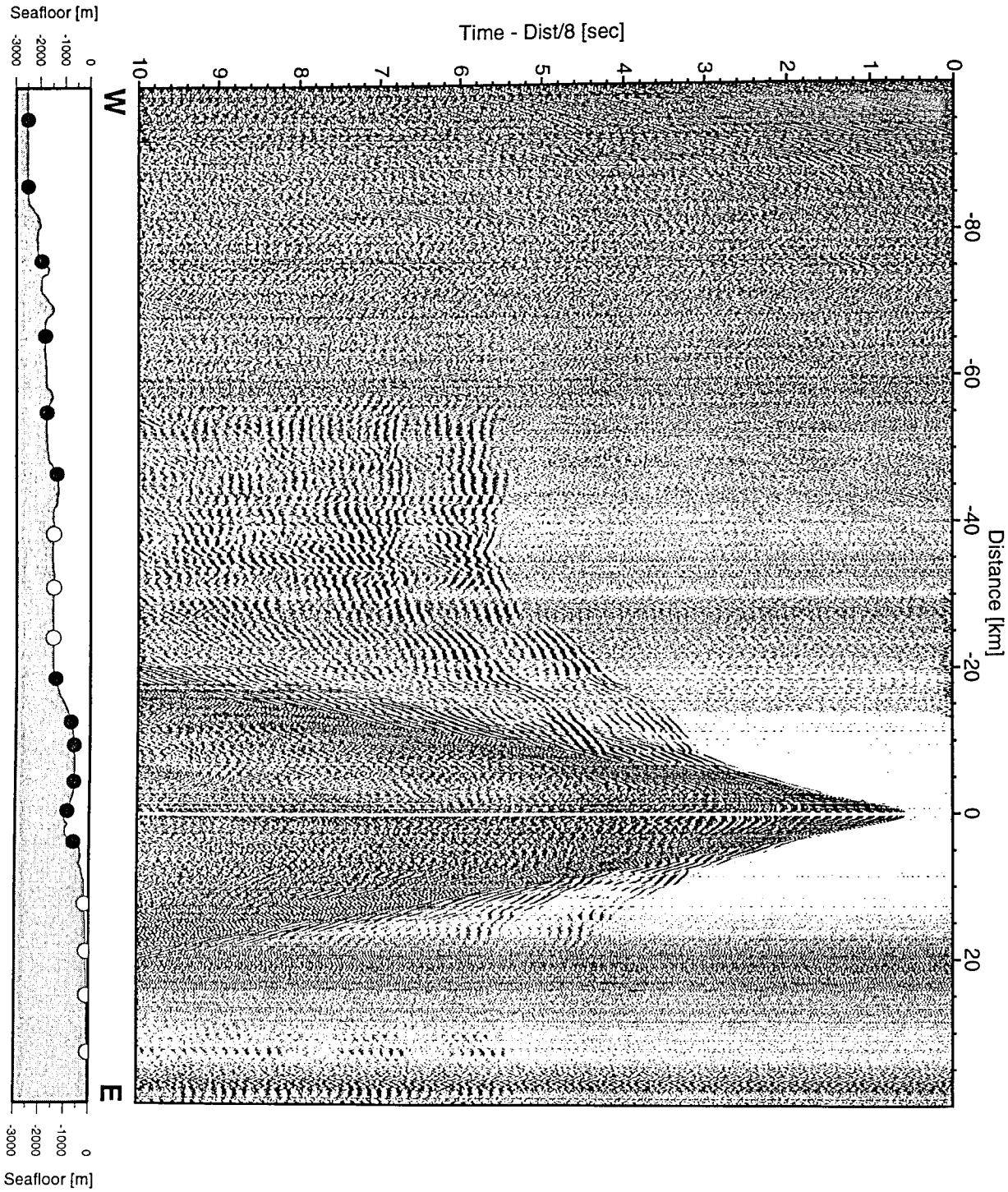

Figure 6.3.4.5.6: Record section from OBH 66, Profile 12.

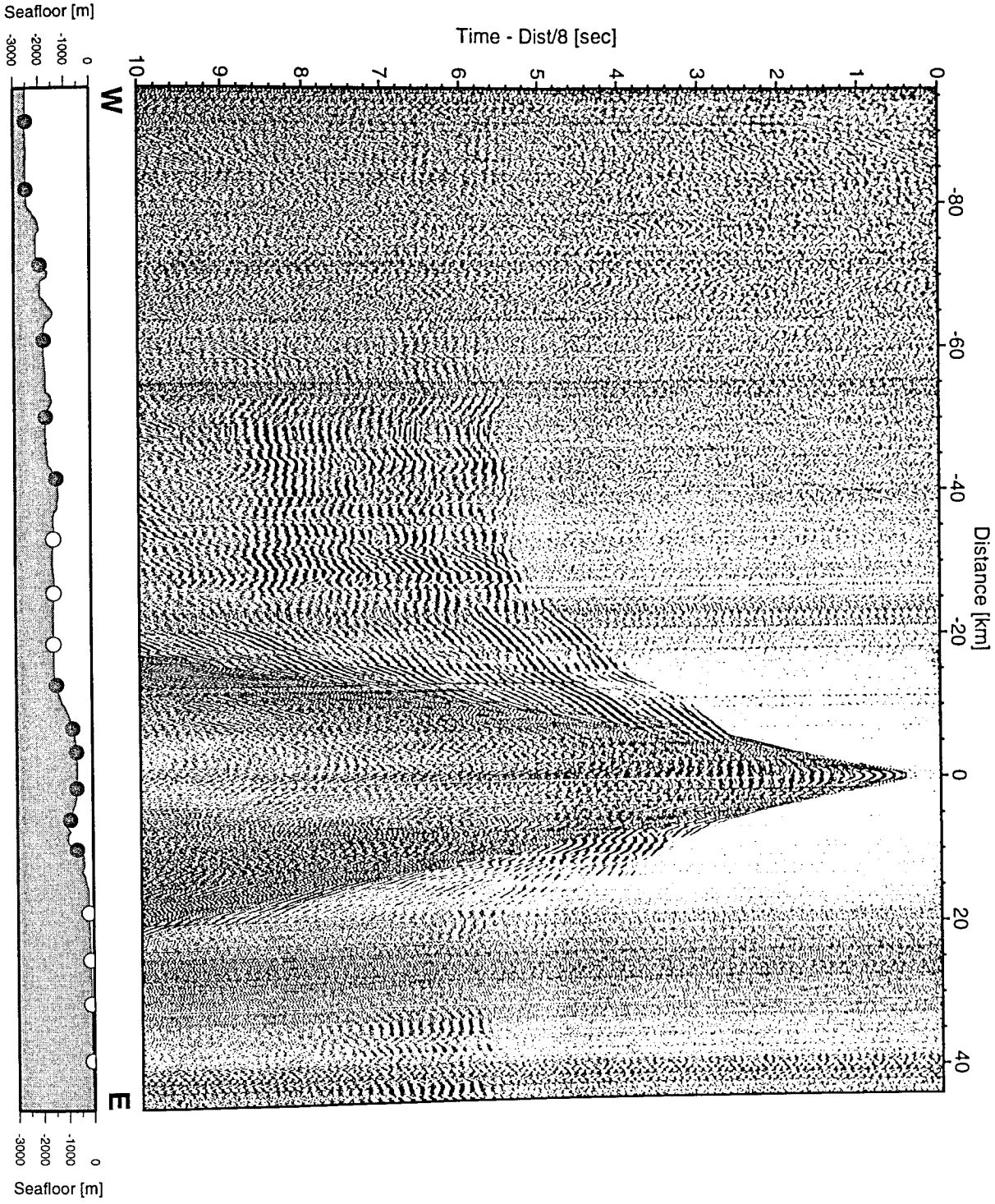

Figure 6.3.4.5.7: Record section from OBH 67, Profile 12.

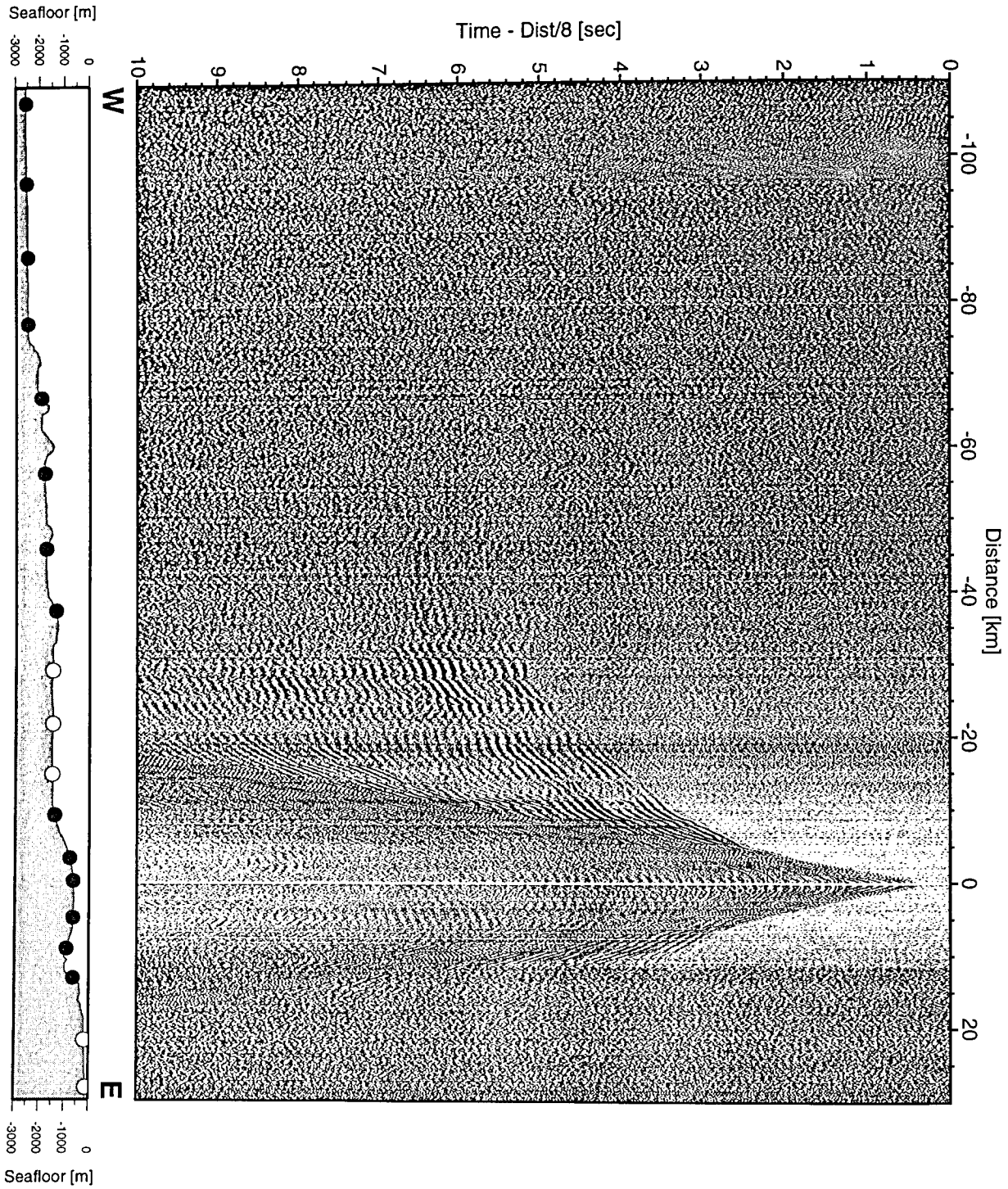

Figure 6.3.4.5.8: Record section from OBH 68, Profile 12.

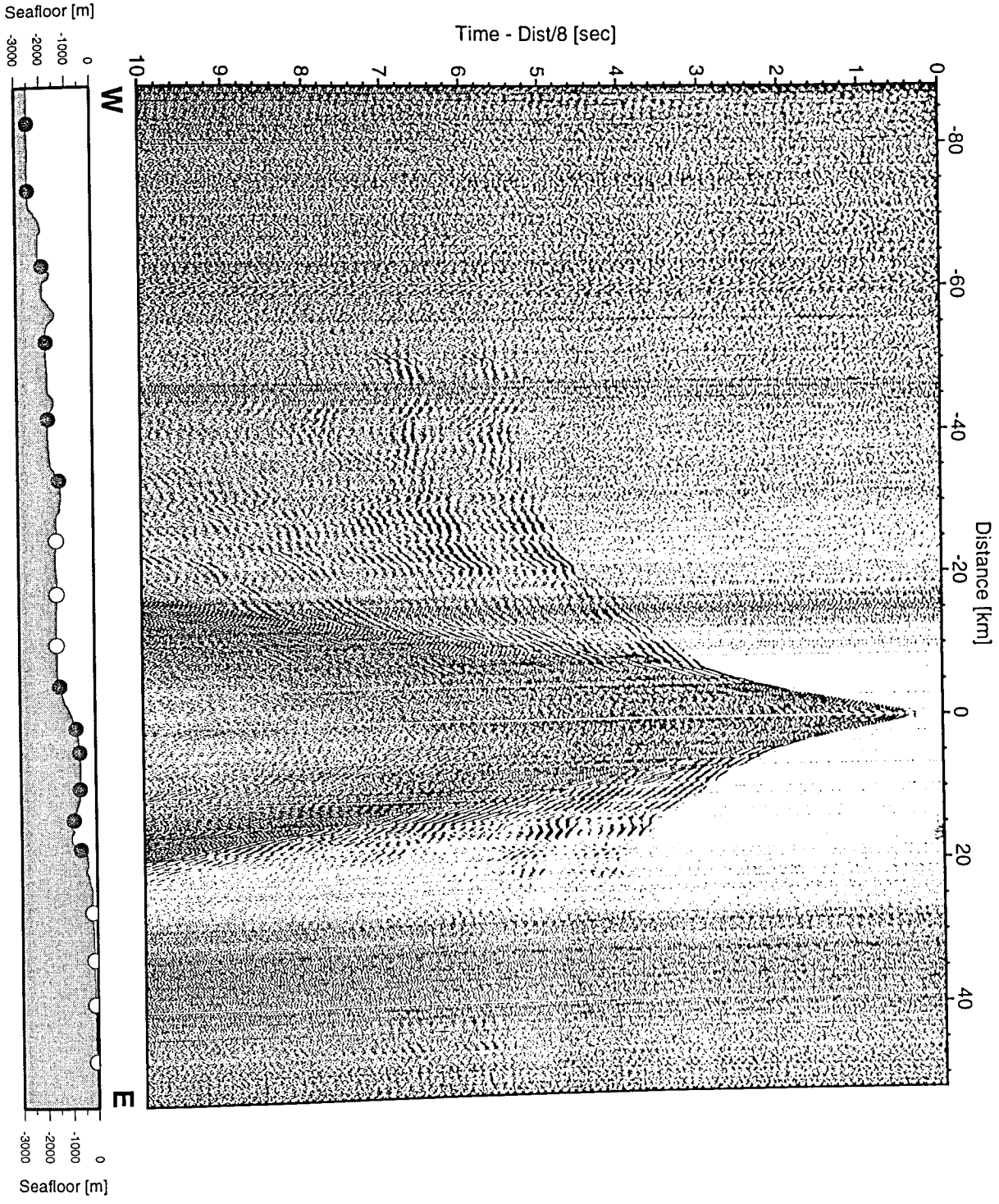

Figure 6.3.4.5.9: Record section from OBH 69, Profile 12.

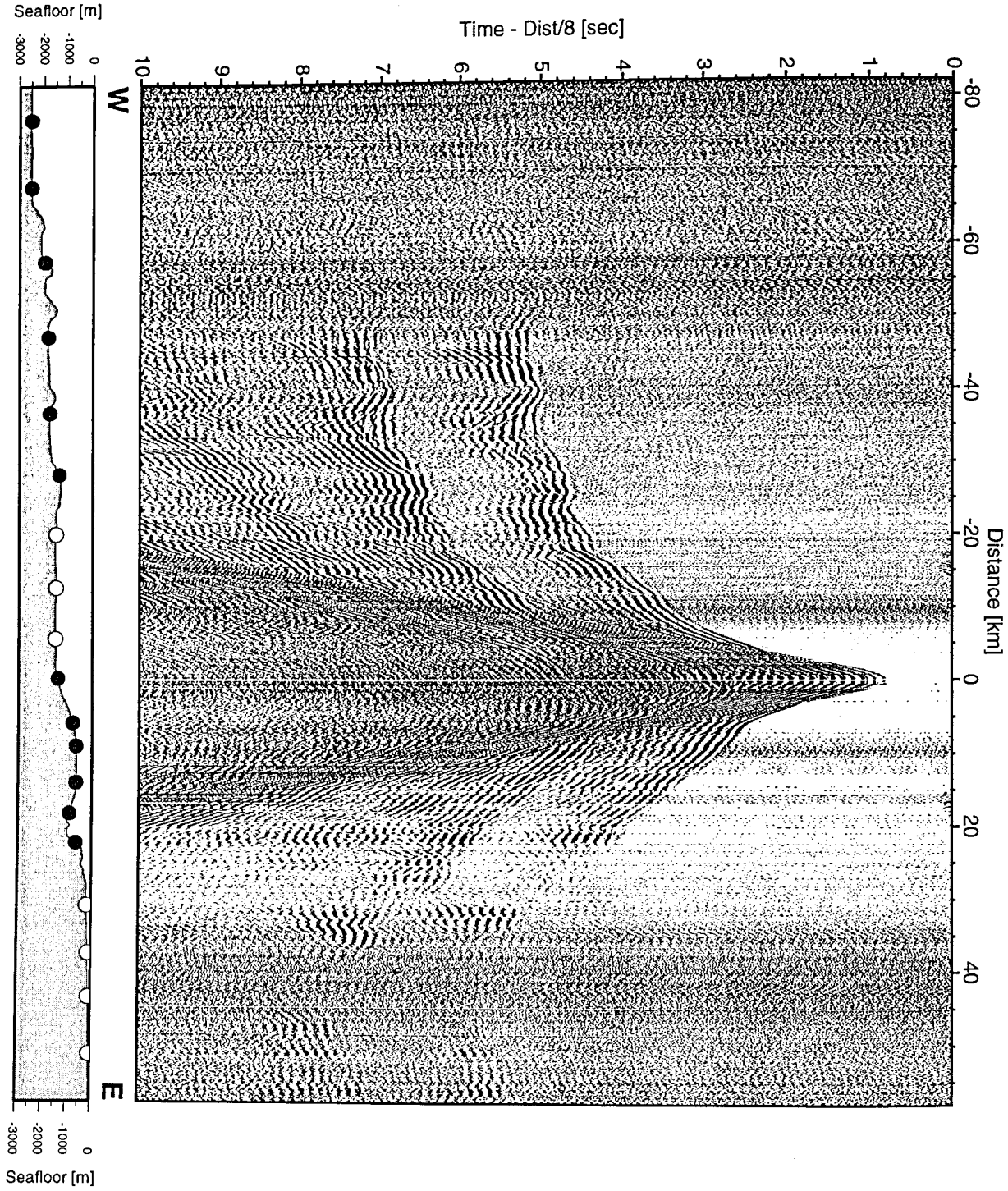

Figure 6.3.4.5.10: Record section from OBH 70, Profile 12.

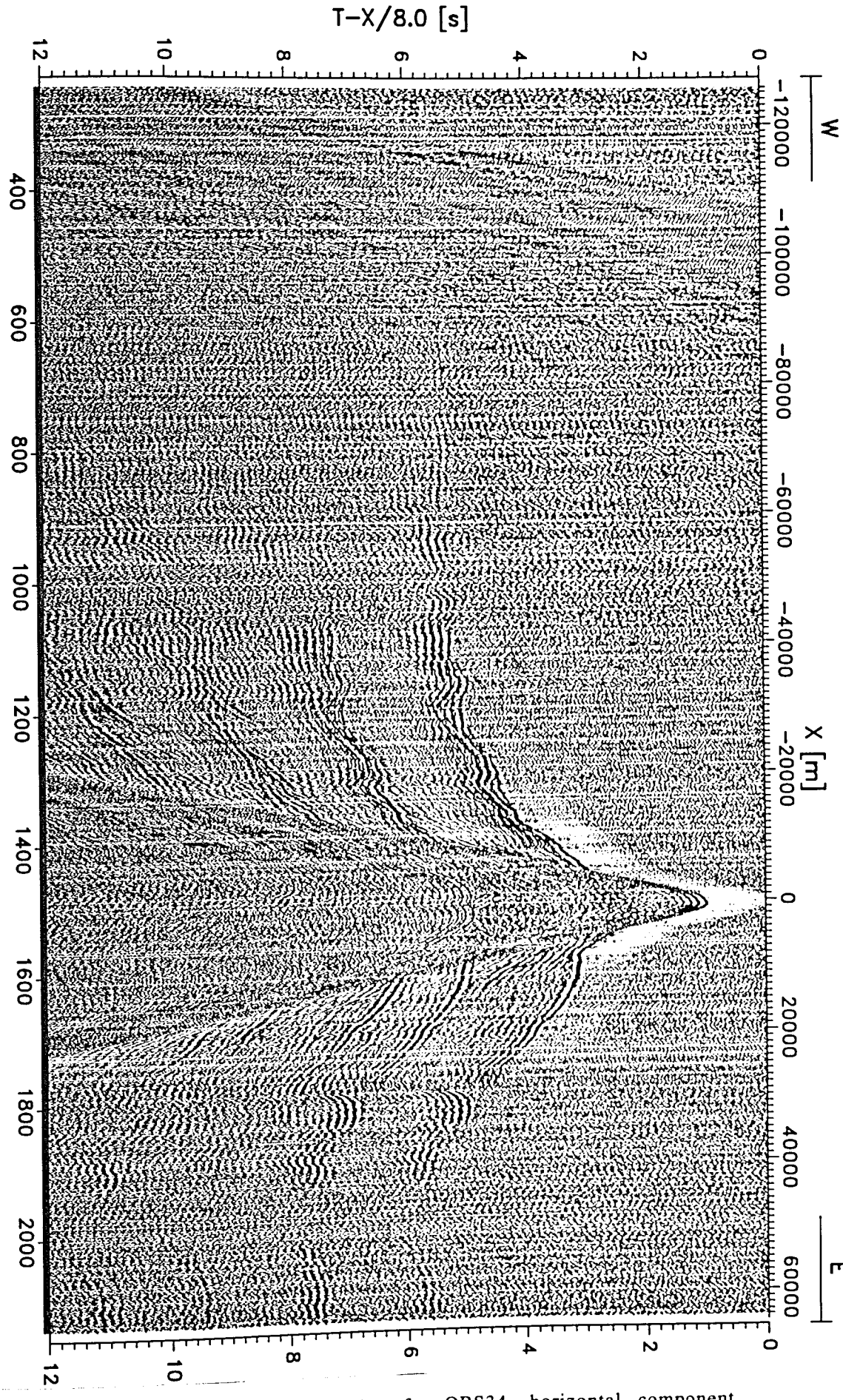

Figure 6.3.4.5.11: Record section for OBS34, horizontal component.

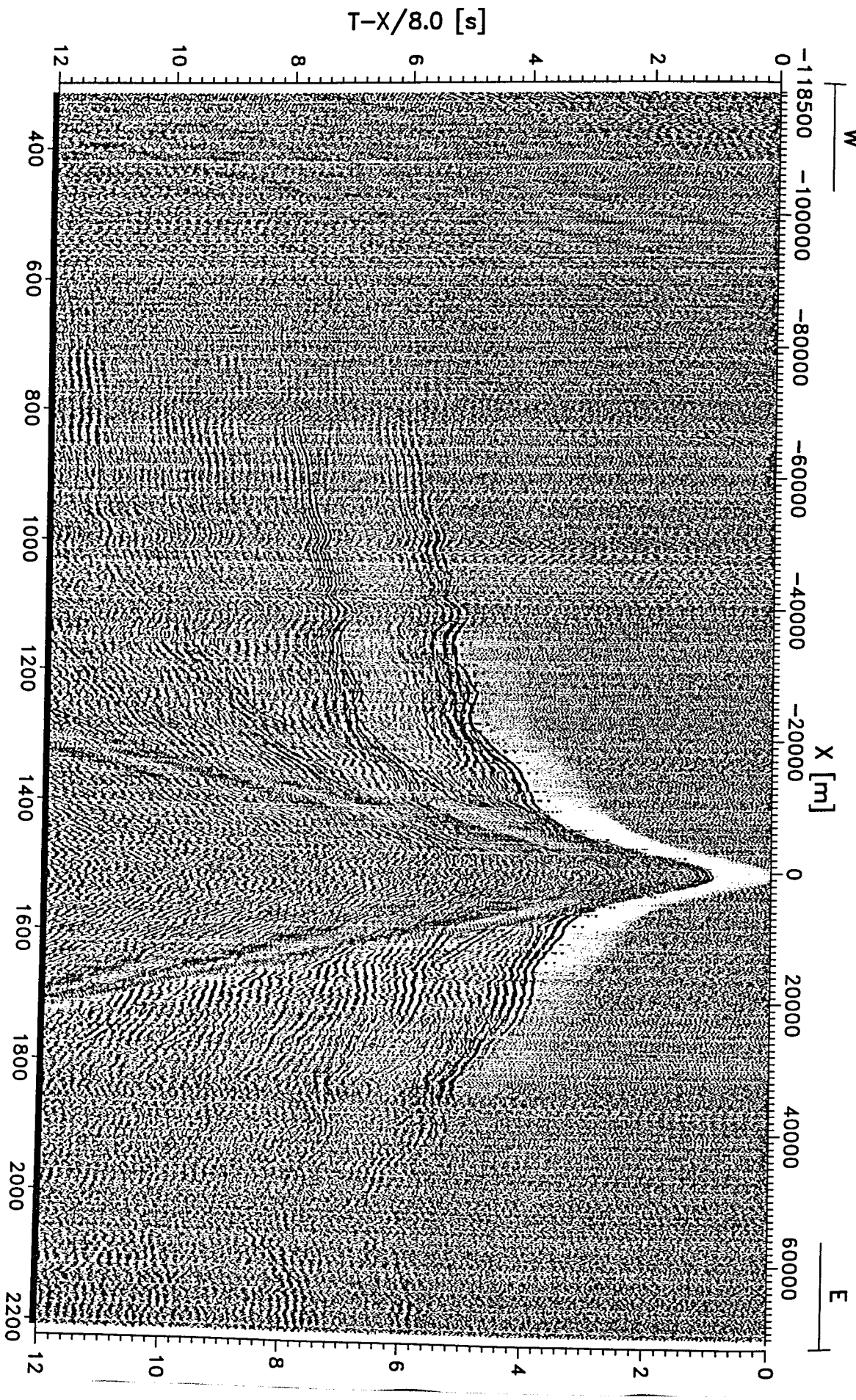

Figure 6.3.4.5.12: Record section for OBS35, vertical component.

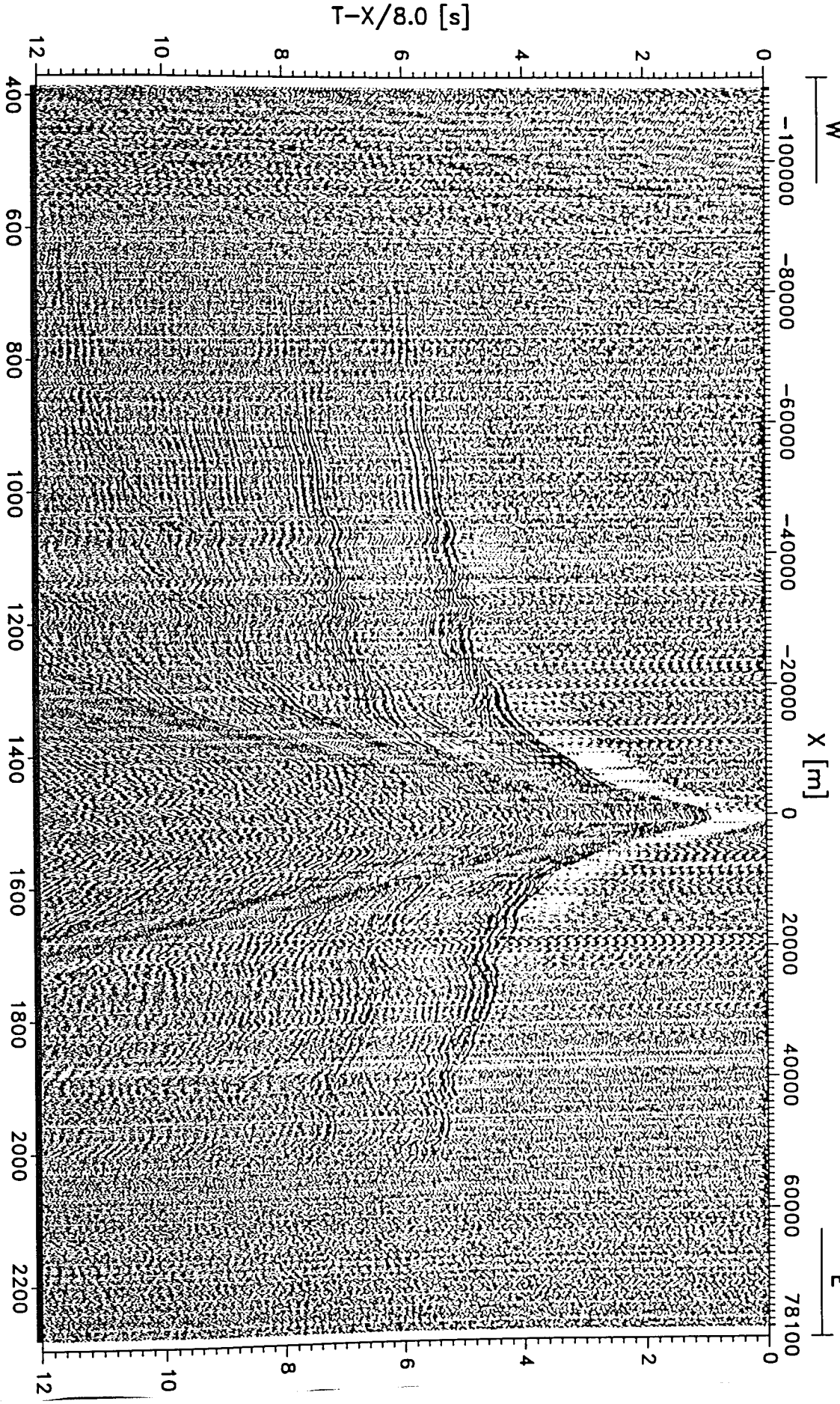

Figure 6.3.4.5.13: Record section for OBS36, vertical component.

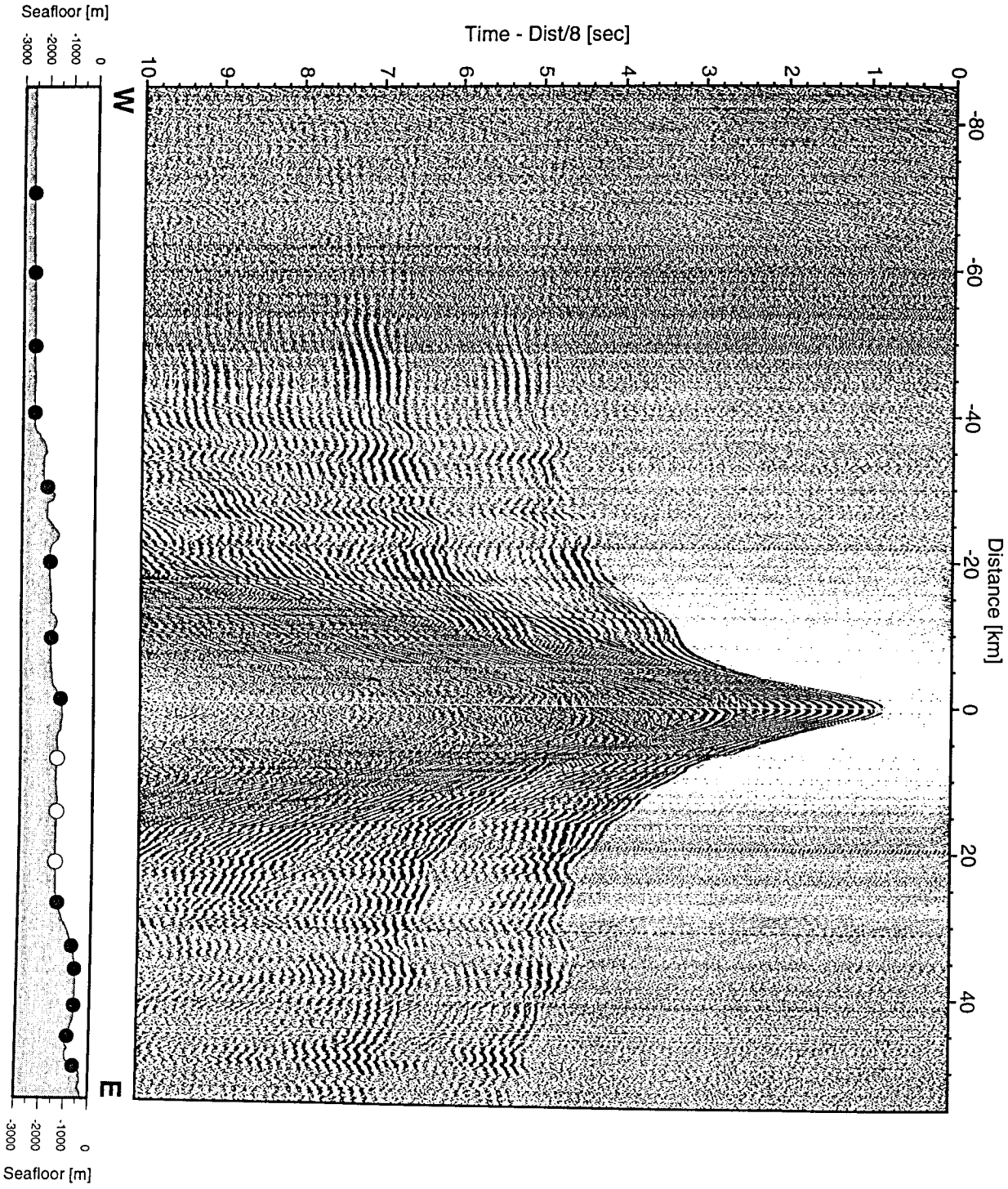

Figure 6.3.4.5.14: Record section from OBH 71, Profile 12.

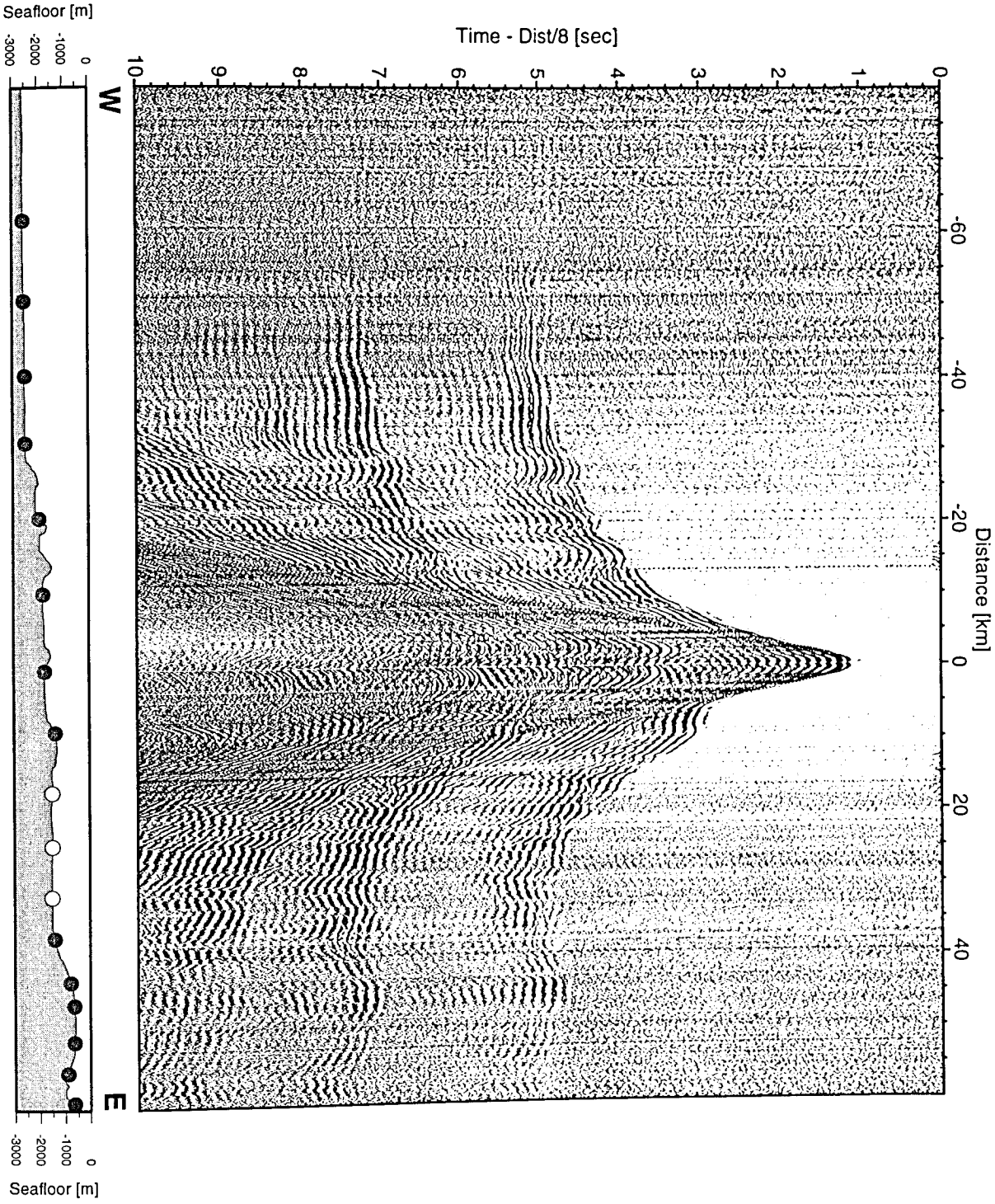

Figure 6.3.4.5.15: Record section from OBH 72, Profile 12.

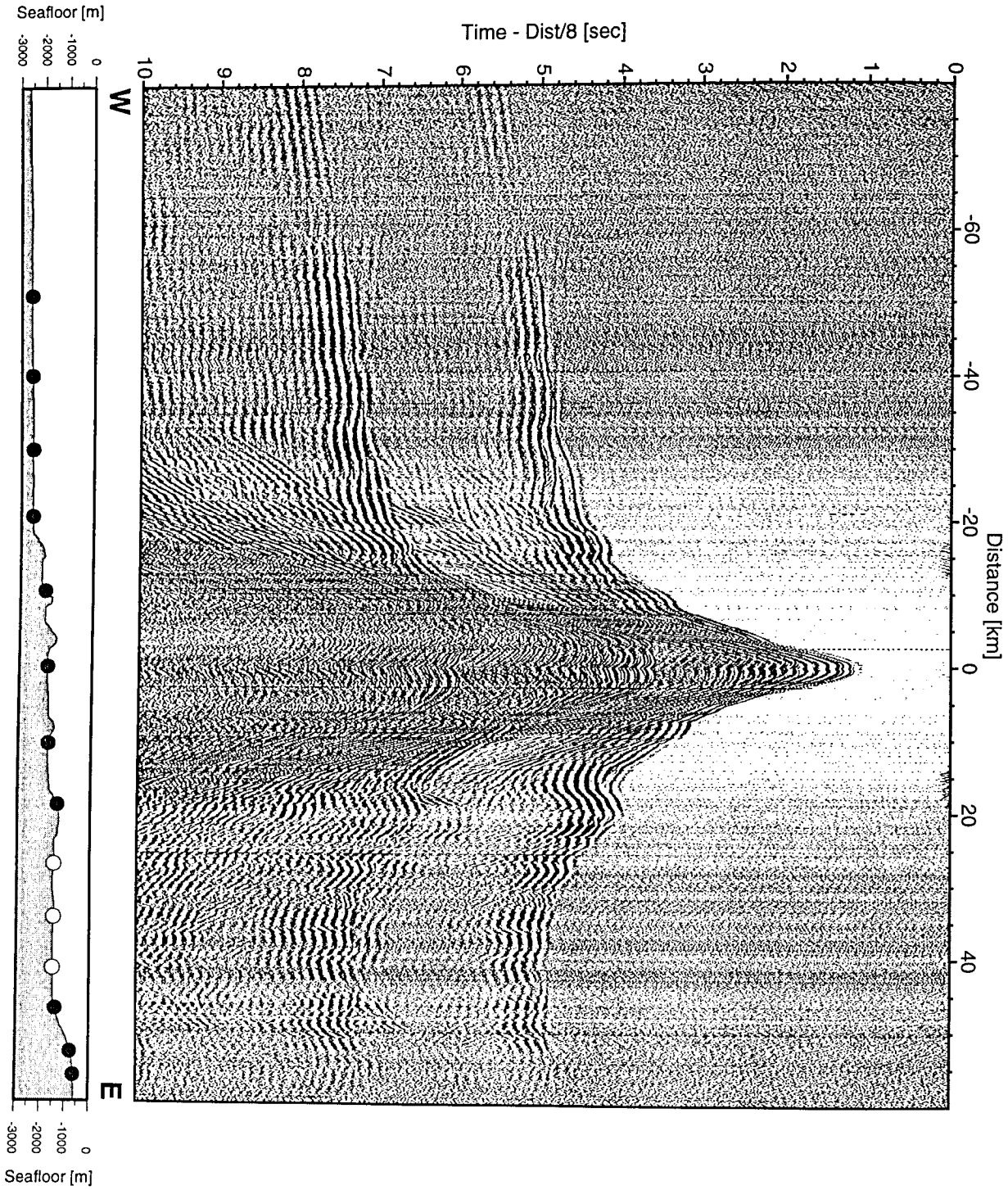

Figure 6.3.4.5.16: Record section from OBH 73, Profile 12.

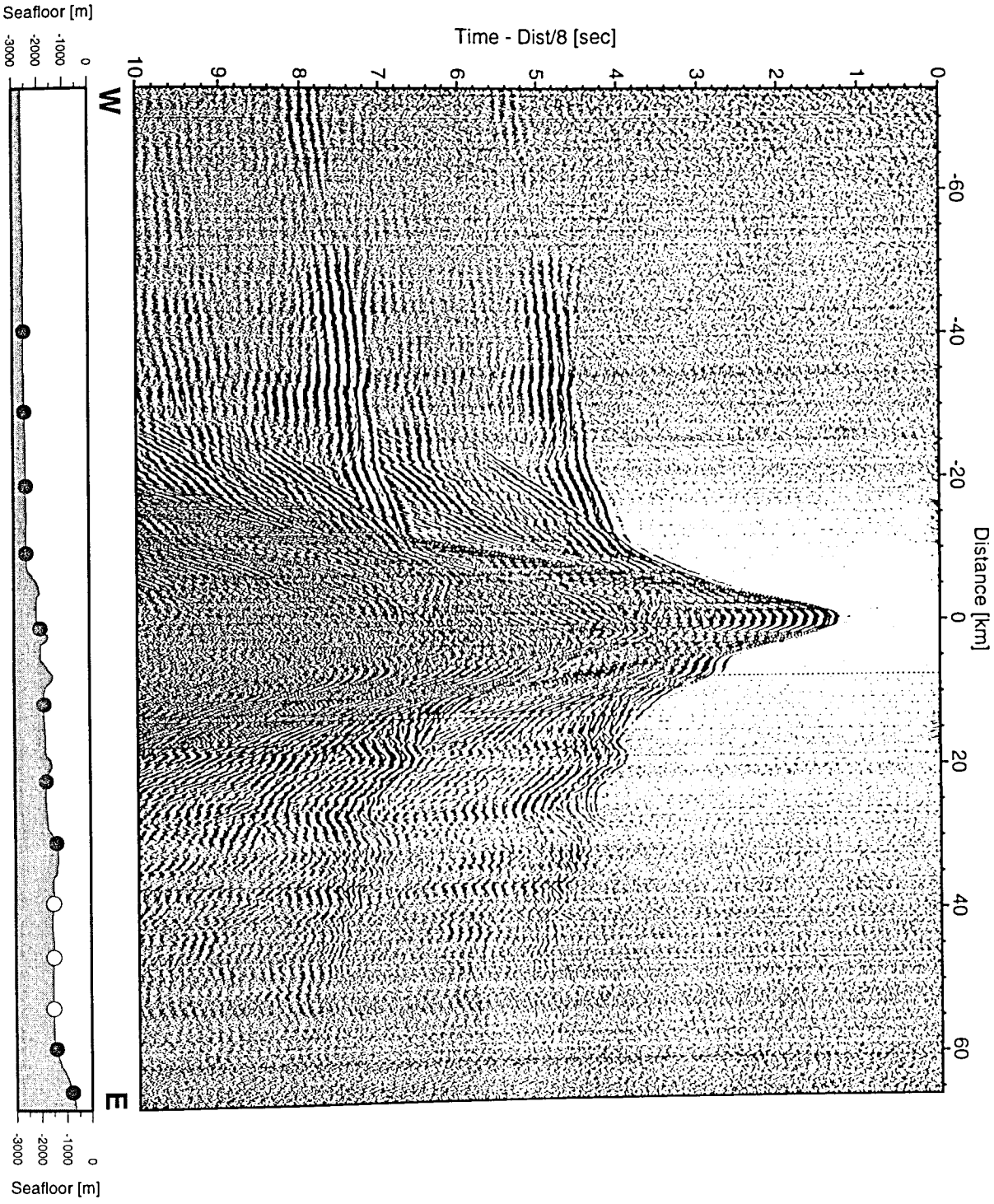

Figure 6.3.4.5.17: Record section from OBH 74, Profile 12.

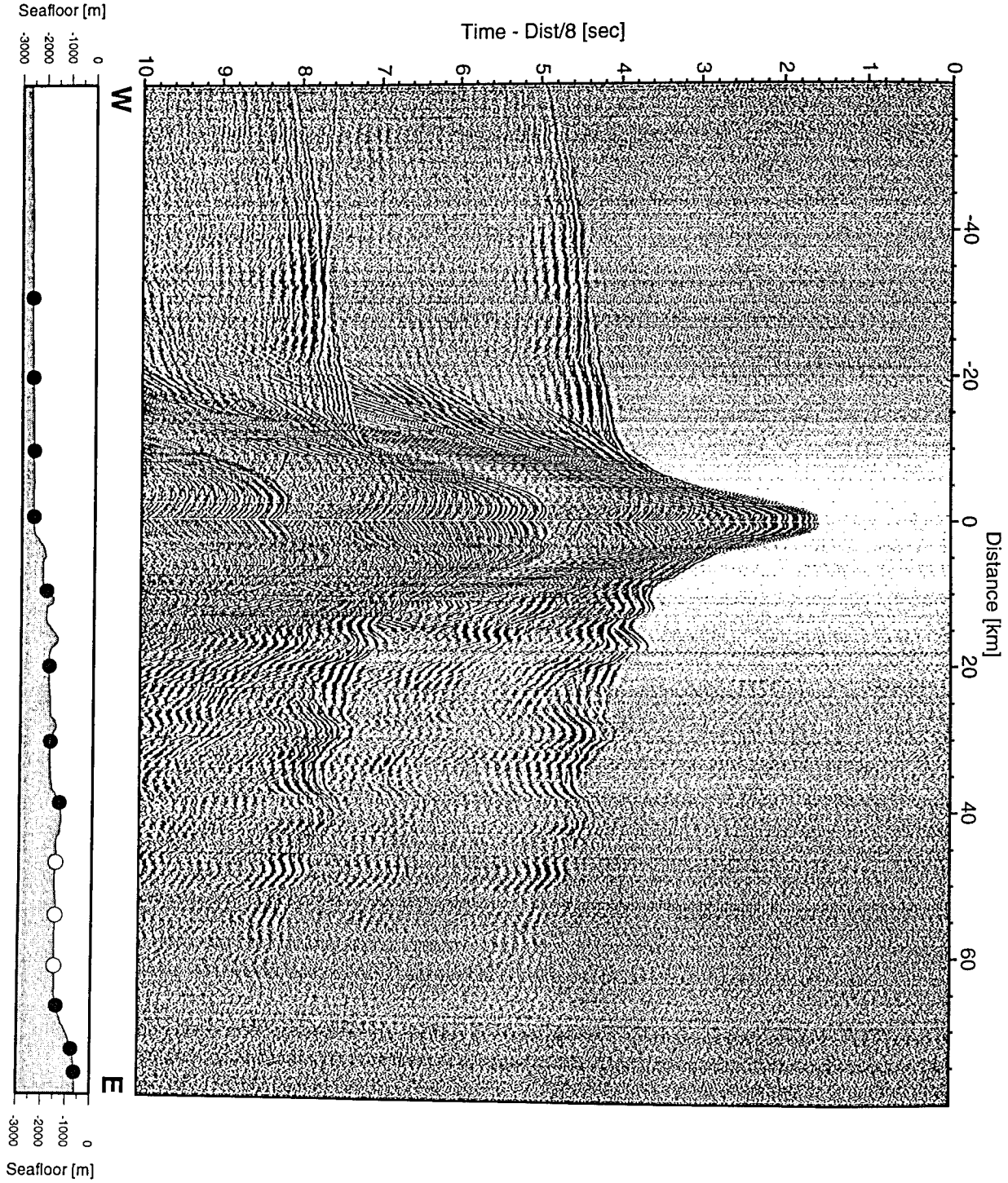

Figure 6.3.4.5.18: Record section from OBH 75, Profile 12.

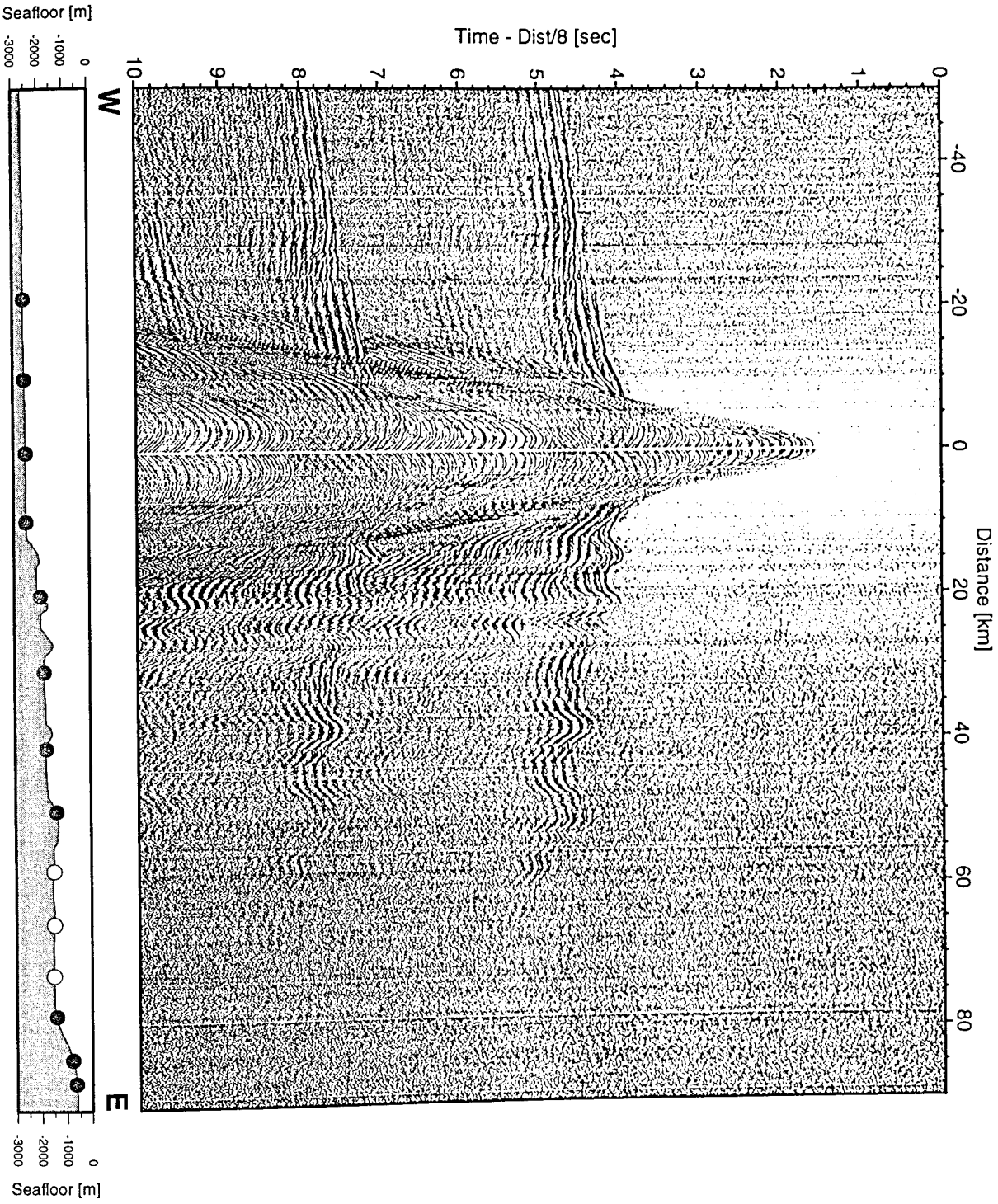

Figure 6.3.4.5.19: Record section from VA13, single hydrophone, Profile 12.

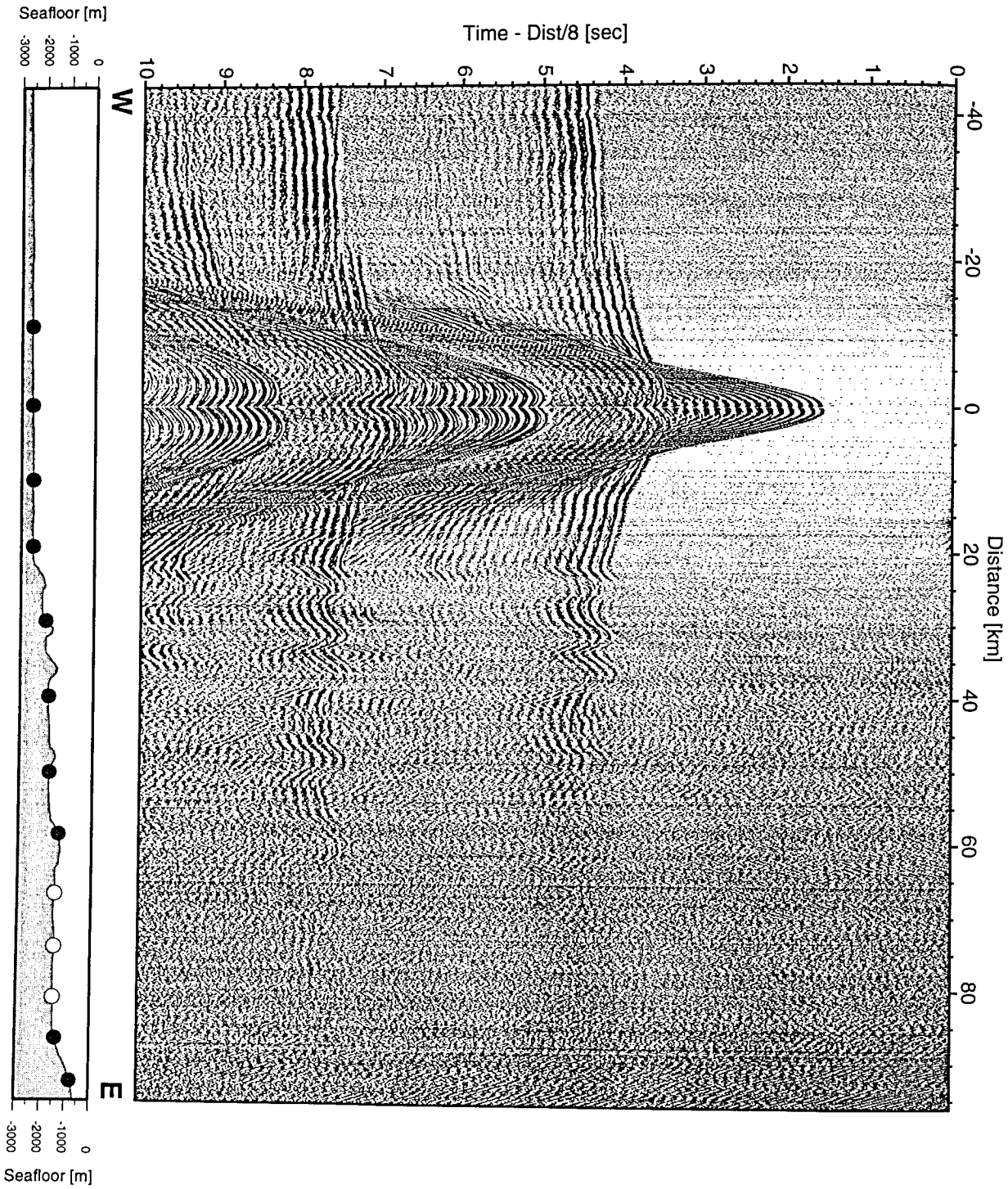

Figure 6.3.4.5.20: Record section from OBH 76, Profile 12.

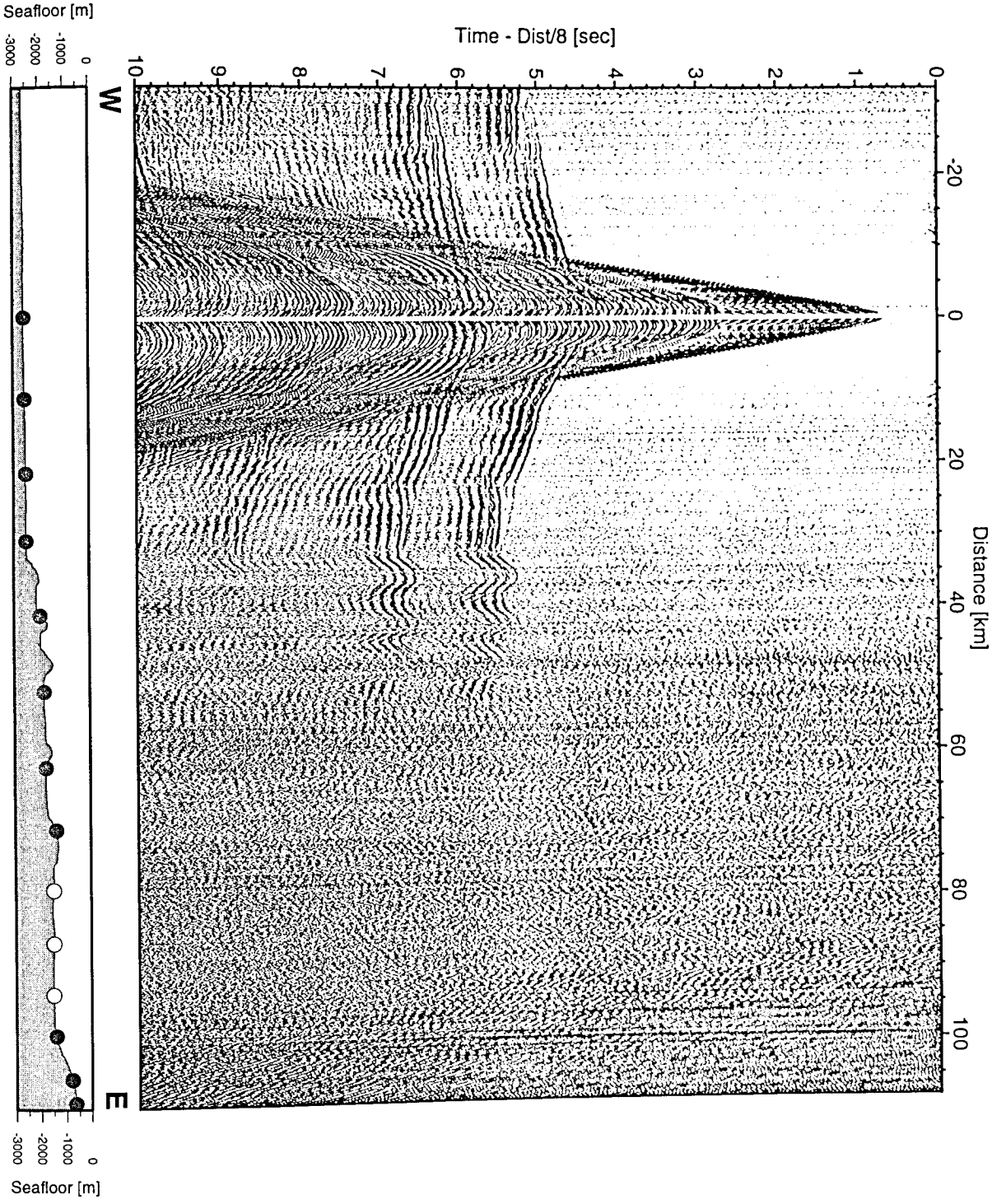

Figure 6.3.4.5.21: Record section from OBH 77, Profile 12.

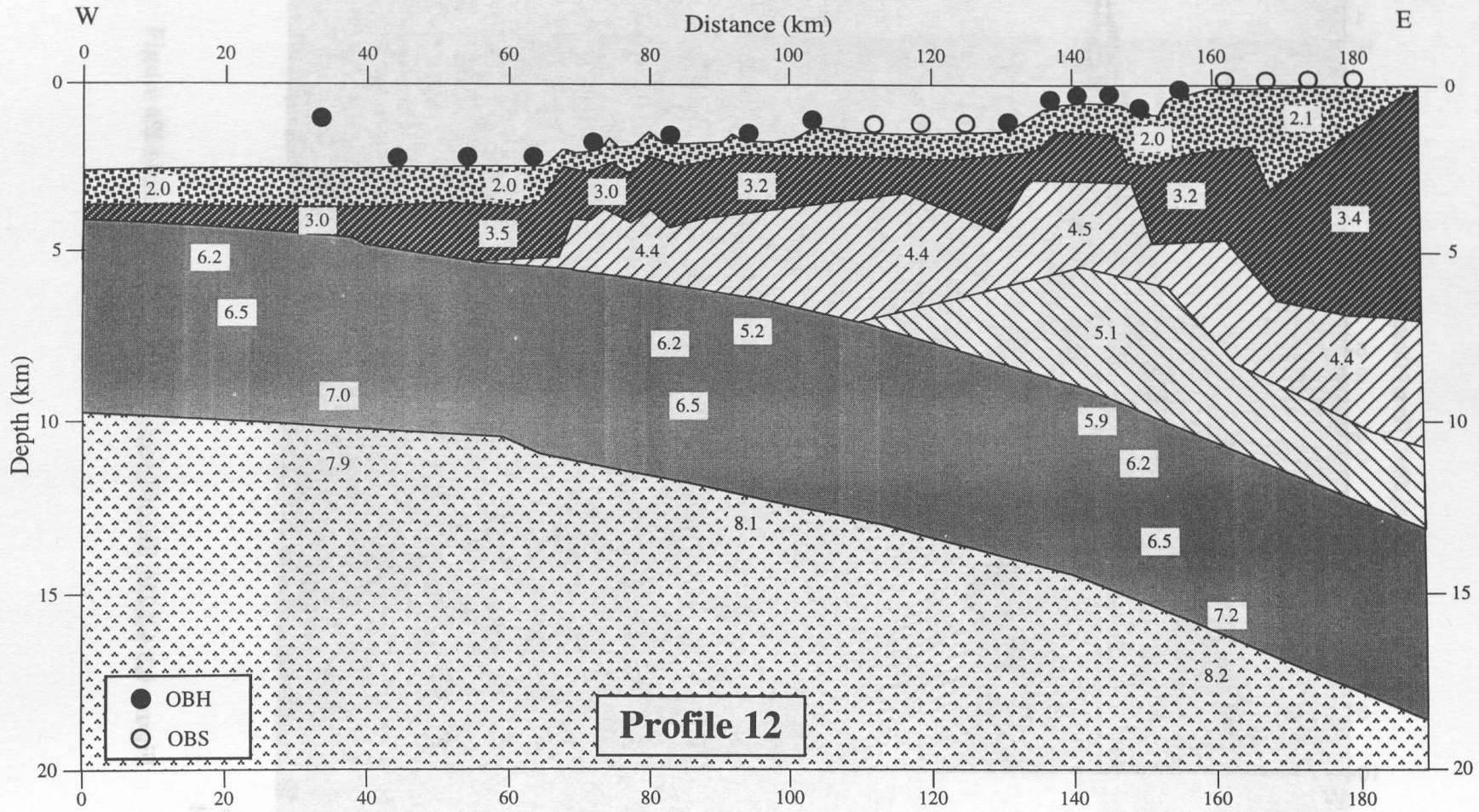

Figure 6.3.4.5.22: Preliminary results of the modelling along profile 12. Numbers are velocities in km/s

6.3.4.6 INITIAL INTERPRETATION OF THE WASHINGTON WIDE-ANGLE PROFILES 10, 11, AND 12 AND COMPARISON WITH THE OREGON PROFILE 7

(U. ten Brink, E. Flueh, and N. Vidal)

The Washington margin can be divided physiographically into 5 zones (Figure 6.3.4.6.1): A flat shelf (< 200 m), the first terrace, the second terrace, the thrust-faulted ridges, and the trench. We compare wide-angle seismic records from profiles 10 and 12 and the preliminary results of our modelling, which are located at a similar distance from the trench axis. In addition, we discuss the wide angle records from the N-S profile 11, which provide the third dimension of the sedimentary and crustal structure on the shelf.

SEDIMENT THICKNESS ON THE SHELF

South of the mouth of the Columbia River low velocity (1.6-3.5 km/s) sedimentary rocks are no more than 0.4 s TWT thick (Figures 6.3.4.4.2, 6.3.4.4.3). Sediment thickness increases dramatically a few km south of OBS C4 around lat. 46° 01' as can be seen by the termination of the first arrival at 20 km offset north of OBS A4 (Figure 6.3.4.4.2) and by the vastly different apparent velocity of the first arrivals north and south of OBS C4 (Figure 6.3.4.4.3). Sediment thickness to the north of OBH53, located in the Astoria canyon, is more than 5 s (Figure 6.3.4.4.6). Hence, sediment thickness increases toward the North by almost 5 s within a 25 km wide zone between OBS C4 and the Astoria canyon. This area coincides with the NE-SW magnetic anomaly interpreted to mark the northern termination of the offshore Siletz River basalts (R. Wells, Pers. comm., 1996).

Sediment thickness increases to ~6 s on OBH55 (Figure 6.3.4.4.7) at lat. 46° 33' opposite Willapa Bay. These sediments maintain their thickness north to lat. 47° 22' opposite Cape Elizabeth, where their thickness decreases abruptly to ~4 s (Figures 6.3.4.4.13, 6.3.4.4.17). This area is the offshore extension of a WNW-ESE-trending strike-slip fault which separates the Eocene-Oligocene melange along the coast of the Olympic peninsula from the younger Cenozoic sedimentary rocks to the south (Snavely, 1987).

Records from seven adjacent instruments on the outer shelf and the first terrace along profile 10 (Figures 6.3.4.3.12 to 6.3.4.3.19) are characterized by an arrival with unusually high apparent velocity that is located along the easternmost 8-15 km of the profile. This arrival may be due to an inclined surface dipping away from the coast that begins about 10-15 km offshore. If this arrival indeed originates from an inclined surface, then it may mark the western boundary of the Siletz block in this area as suggested by Snavely (1987).

The seaward extent of the thick sedimentary section can be defined with the aid of profiles 10 and 12 and MCS profile 101 (Double profiles on Figure 6.3.4.6.1). On profile 10 west of Willapa Bay the thick sedimentary unit extends seaward of the shelf edge. Sediment thickness on OBH48 is 5 s and by the edge of the first terrace, which lies 37 km seaward of the shelf edge (Figure 6.3.4.3.12, water depth of 1020 m) the thickness is ~3 s. Sediment thickness west of the edge of the terrace decreases considerably and is 1.5-2 s across the deeper part of the margin (e.g., Figure 6.3.4.3.11).

In contrast, the thick sedimentary section on profile 12 north of Cape Elizabeth thins rapidly beyond the shelf edge and is only 2-2.5 s thick beneath the first terrace (Figure 6.3.4.5.6).

On MCS profile 101, the 3.5-4 s thick sedimentary section thins beyond the shelf edge and is less than 1.5 s thick at the first terrace.

Initial forward ray-tracing model of the wide-angle reflection data along profile 10 (Figure 6.3.4.6.2) shows that the shelf sedimentary basin is up to 8 km deep and is centered under the outer shelf. The sediment velocity is low (2-3 km/s). The basin ends seaward under the edge of the first terrace where the thickness changes from 5 km to 2.5 km. The basin thins landward due to an inclined bottom surface.

Along profile 12, the basin is slightly more shallow (maximum of 7 km) and its main part has a higher velocity (3.0-3.5 km/s) than on profile 10. The basin terminates seaward in the outer shelf, but there is no evidence for thinning landward. The three OBS closest to shore (Figures 6.3.4.5.2 to 6.3.4.5.4) are characterized by a higher sediment velocity on their eastward side than on their northward due to an inclined boundary. The model shows the uppermost sediments with velocity of 1.9-2.3 km/s to taper out toward the shore. According to Snavely (1987), the Eocene-Oligocene melange, which is exposed along the coast of the Olympic peninsula, underthrusts Pliocene sediments in the offshore drill hole P-0141. The inclined boundary between the lower and higher velocity sediments along the eastern edge of profile 12 may be this thrust fault.

In summary, the wide-angle seismic data provide evidence for a deep, narrow, and elongate sedimentary basin under the Washington shelf, which is fault-bounded to the south and possibly to the east. The greatest sediment thickness under the shelf is located between the mouth of Columbia river and Cape Elizabeth, offshore the coastal region of low topography (Figure 6.3.4.6.1). This is also the region to which most of the fine-grained sediments from the Columbia River are being transported.

CRUSTAL THICKNESS OF THE MARGIN

Crustal thickness under the thrust-faulted ridges appears to be similar to or only slightly larger than the adjacent oceanic crust, because the upper mantle refracted wave, Pn, crosses the crustal diving waves and the Moho reflection to become a first arrival at ~30 km offset (e.g., Figures 6.3.4.3.8 and 6.3.4.5.16). The crust does not appear to thicken much under the slope terraces on profile 10, as evidenced by the cross-over offset of 30 km east of OBS L10C4 and OBH44 (Figures 6.3.4.3.10, 6.3.4.3.11), located on the second terrace. Pn in instruments at the same relative location on profile 12, however, appear as a first arrival at an offset of 50 km (OBH71, L12A4). Pn on records from instruments located between the first terrace and the shelf in both profiles 10 and 12, does not appear as a first arrival until at least 50 km offset (Figures 6.3.4.4.12 and 6.3.4.4.14 for profile 10 and Figures 6.3.4.5.10 and 6.3.4.5.11 for profile 12). On the N-S strike profile (profile 11) on the shelf, Pn cross-over is at offsets of at least 55 km (Figure 6.3.4.4.13, 6.3.4.4.18). Thus, it appears that crustal thickness under the outer shelf is generally similar in both profiles, but is different between profile 10 and 12 under the second terrace of the continental slope. On MCS profiles 101 and 103, the top of the oceanic crust deepens by 0.75-1 s between the thrust-faulted ridges and the second terrace (Figure 6.4.3, SP1100-1300).

The ray-tracing models confirm these observations: On profile 12 the subducted plate starts dipping down from the trench axis, but on profile 10 it starts dipping 20 km landward from the trench edge. The total crustal thickness to the base of the subducting plate under the shelf is 18-20 km. The dip of the subduction zone is 3.4° for profile 12 and 5° on profile 10. Analysis of arrival times with offset for the Duvall earthquake suggested a dip of 5.6 ° under the shelf edge and the first terrace along profile 10 (Section 6.5).

COMPARISON WITH THE OREGON PROFILE

There are two major differences between the continental margins of Washington and Oregon. The first is the width of the margin. The distance from the trench to the coast is 100 km along profile 7 (Figure 6.3.4.6.2) in Oregon and 140-160 km along profiles 10 and 12 in Washington. The dip of the subducting plate under the margin is highest in Oregon (5.2°), slightly less in SW Washington (5°) and is the smallest along the Olympic profile (3.4°). However, these offshore dips may not be indicative of the overall dip of the subducting plate, as shown by Trehu et al. (1994).

The other major difference is in the average velocity of the sedimentary and crustal rocks overlying the subducting plate. Offshore Washington, the rock velocity never exceeds 5.3 km/s even at depths as large as 10-12 km. Offshore

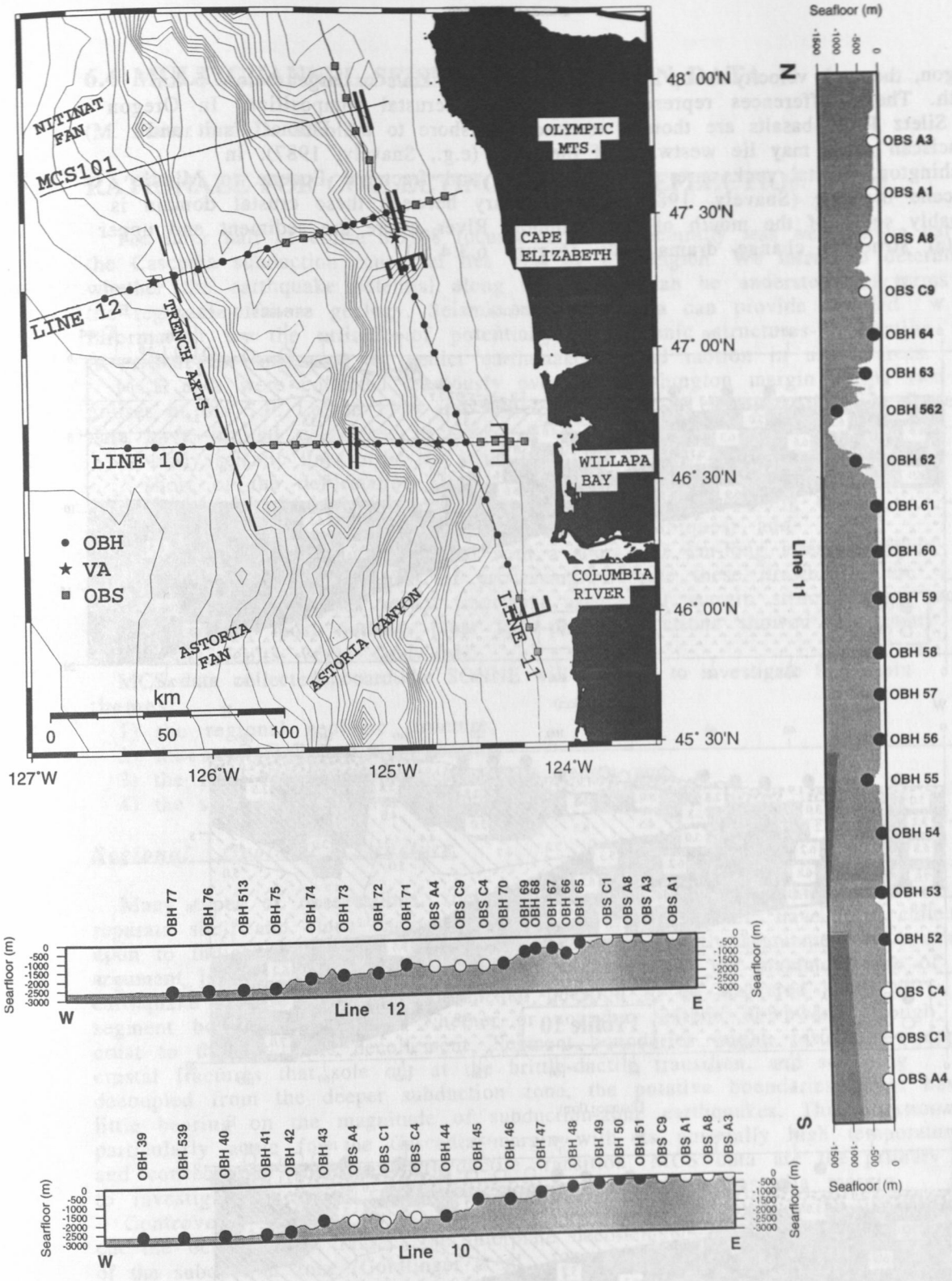

Figure 6.3.4.6.1: Location map and bathymetric profiles of refraction profiles 10, 11 and 12. Pour pronged profile - suggested locations of faults which offset the sediments (see text). Double profile - seaward edge of the sedimentary basin. A deep elongate sedimentary basin probably underlies the shelf between the four-pronged symbols and the double-profile symbols. It is wider in the south near profile 10 and narrower to the north on profiles 12 and MCS101.

Oregon, the rock velocity is up to 6.5 km/s and is 5 km/s or larger below 5 km depth. These differences represent differences in crustal composition. In Oregon the Siletz River basalts are thought to extend offshore to the Fulmar Fault and Franciscan rocks may lie westward of the fault (e.g., Snavely, 1987). In Washington, crustal rocks are probably broken and fractured Eocene to Middle Miocene melange (Snavely, 1987). The boundary between these crustal domain is probably south of the mouth of the Columbia River where the sediment and upper crustal structure change dramatically (Figure 6.3.4.6.1).

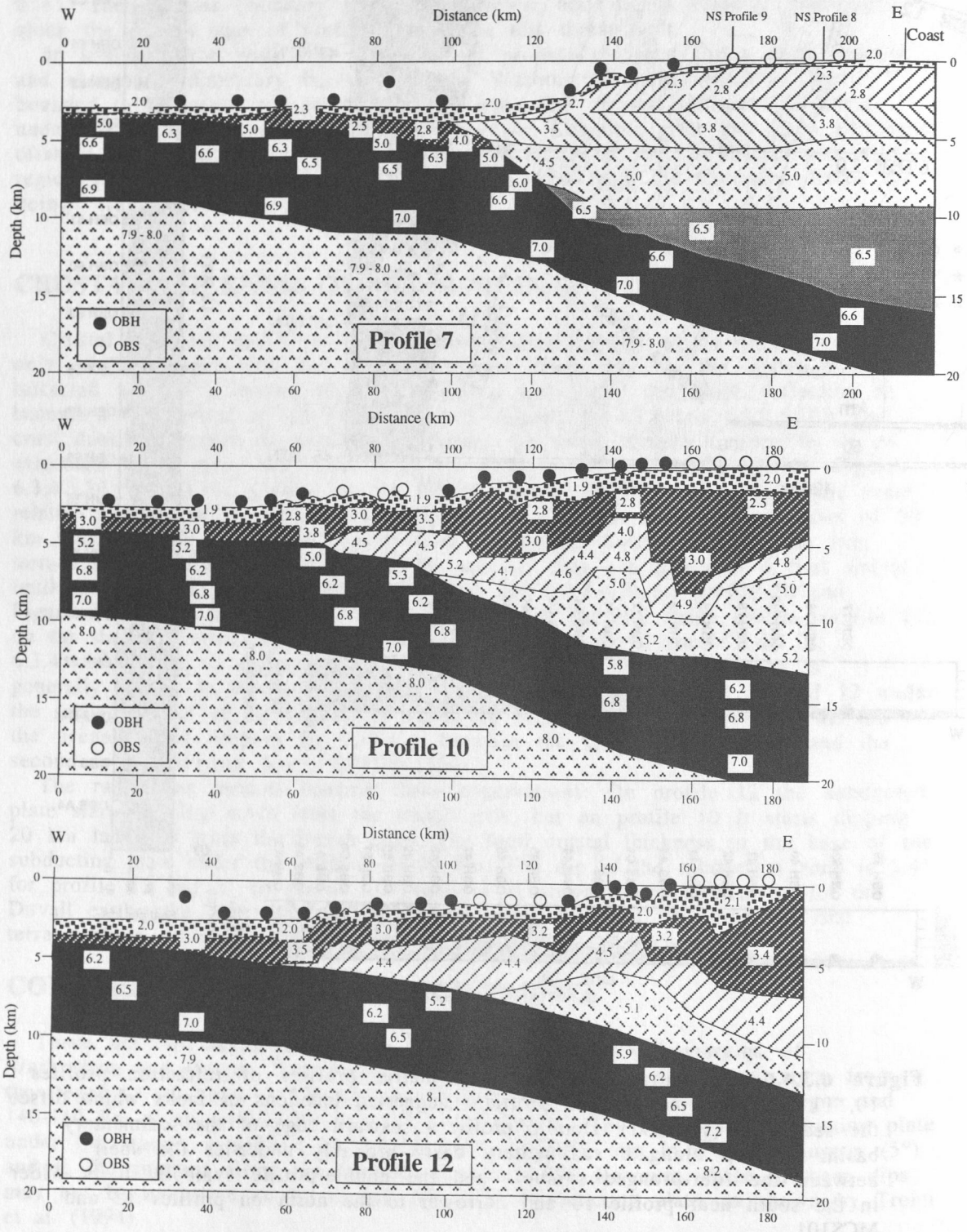

Figure 6.3.4.6.2: Crustel cross-sections for profile 7, 10 and 12 from preliminary analysis of wide-angle data.

6.4 MULTICHANNEL SEISMIC REFLECTION DATA

(M. Fisher and D. Scholl)

RATIONALE FOR COLLECTING SEISMIC REFLECTION DATA

The later half of cruise SO108 focused on the structurally less well known part of the Cascadia subduction zone that lies west of Washington. We intend to determine whether the earthquake potential along the margin can be understood in terms of the regional offshore geology. Seismic reflection data can provide detailed information on the attitude of potentially seismogenic structures-information that is critical for engineers to predict earthquake ground motion in urban areas.

MCS data were collected previously over the Washington margin during two cruises of the S.P. Lee in 1976 and 1980. For studies of earthquake hazards, these data have limited usefulness because:

1) many seismic lines cross the shelf and slope but typically stop 10 to 30 km short of the deformation front;
2) nearly all lines cross regional structure obliquely, reducing the effectiveness of advanced, data-processing techniques; and
3) one entire cruise was obtained with a short, 1.2 km-long streamer, again reducing the effectiveness of processing. Despite these drawbacks, the earlier seismic lines reveal important aspects of margin structure and rock sequences; most notably, clear fault-plane reflections showed that many thrust faults verge landward.

MCS data collected aboard the SONNE will be used to investigate four main themes:

1) the regional geologic structure;
2) the stratigraphy of slope basins;
3) the fluid regime of the accretionary wedge; and
4) the sediment budget of the subduction zone.

Regional Geologic Structure

Many types of observations, such as transverse faults, basement highs that separate shelf and slope basins, and potential-field anomalies, have been called upon to indicate where the Cascadia margin is structurally segmented. A common argument is offered that the implied segmentation limits the maximum size of earthquake rupture zones. A fundamental question to be answered about all segment boundaries concerns whether or not they extend downward through the crust to the interplate decollement. Segment boundaries might, instead, be upper-crustal fractures that sole out at the brittle-ductile transition, and so being decoupled from the deeper subduction zone, the putative boundaries might have little bearing on the magnitude of subduction-zone earthquakes. This question is particularly acute for the Cascadia margin with its unusually high temperature and consequently shallow, brittle/ductile transition. MCS data are the primary tool to investigate questions concerning segmentation of the Cascadia margin.

Controversy also surrounds the interpretation that vertical, strike-slip faults cut the ocean crust, transect the interplate decollement, and offset the upper plate of the subduction zone (Goldfinger et al., 1992). Such faults are suggested to segment the margin into numerous small blocks, placing an upper limit on the magnitude of earthquakes. The mechanics of how such faults form and maintain themselves are a puzzle.

MCS data can be used to investigate along-strike changes in the regional style of crustal deformation. For example, off southern Oregon thrust faults in the accretionary wedge verge mainly seaward, whereas off northern Oregon and Washington, large-displacement thrust faults verge landward (MacKay, 1992). One proposed explanation for this vergence change is that in the north, the interplate decollement is particularly weak. By studying the mechanics of the wedge as well as wedge structure and fluid regime, we should be able to determine the main mechanical attributes of the decollement. Other variations in regional structure might stem from the sequence of sedimentary deposits entering the subduction zone. The large Astoria and Nitnat submarine fans are being swept into the

subduction zone along the Cascadia margin, so locally the entering sedimentary section might be richer in course channel material than where distal fan sediment predominates. We planed several lines to investigate the style of deformation associated with subduction of the fan bodies.

Slope-basin stratigraphy

Locally, slope basins lie between zones of relatively greater deformation, and strata within these basins record the history of structural development. Using MCS data we want to decipher this record to investigate the recurrence interval of major earthquakes or episodes of deformation.

Fluid regime

Understanding the fluid regime along the interplate decollement is central to analyzing earthquake hazards. Fluids within plate-boundary faults are thought to be contained within separate hydrologic compartments, and earthquakes are thought to nucleate within compartments where fluid pressure is relatively low (Byerlee, 1992). Fluid pressures can be investigated using MCS data because overpressured zones typically are more negatively reflective than are normally pressured ones (e.g. Barbados: Bangs and Westbrook, 1991; Oregon: Moore et al., 1995; Nankai Trough: Karig et al., 1995). In addition a LITHOPROBE MCS survey west of Vancouver Island revealed a possible overpressured zone at about 20 km depth (Calvert and Clowes, 1990, Cassidy and Ellis, 1991).

Sediment Budget

Whether oceanic sediment is subducted or accreted has problematic implications for earthquake nucleation. On the one hand subducted sediment could be ready-made fault gouge, rich in clay minerals and fluids, that facilitates fault slip; on the other hand, global statistical analyses indicate that thick trench sediment is associated with large-magnitude earthquakes, suggesting that thick sediment somehow impedes slip. In either case MCS data will be used to investigate the sediment flux through the subduction zone to determine what proportion has been subducted and what this portends for seismogenesis.

INTERPRETATION OF MCS DATA COLLECTED ABOARD SONNE

A total of 13 MCS lines was collected during the cruise. Their location are shown in Figure 6.4.1. MCS lines 101 and 103 were demultiplexed and processed onboard. See Chapters 5.2.1, 5.3.1 and 6.3.2 for details on, respectively, data collection and processing. The two processed seismic sections provide excellent images of the subsurface, suggesting that many of the goals outlined above can be achieved.

MCS Line 101

This line is shown here as both stacked (Figures 6.4.2, 6.4.3, and 6.4.4) and post-stack migrated versions (Figures 6.4.5, 6.4.6, and 6.4.7), but the following discussion is based solely on the migrated section. MCS line 101 crosses the Nitnat fan about 20 km south of where the fan's main channel debouches onto the Juan de Fuca oceanic plate. One reason for collecting data along this line is to investigate the structural style of an accretionary wedge where the deforming fan sediment is thick.

MCS line 101 reveals that sediment on the ocean plate is about 2 km thick (Figure 6.4.5). The high-amplitude reflection from the top of the igneous crust clearly delimits the base of this sedimentary pile. At the toe of the accretionary wedge, the main channel of the Nitnat fan departs from its sinuous but generally westward course across the margin by hooking sharply southward to follow the western border of the wedge toe. This channel appears in MCS line 101 as the wide, shallow depression in the seafloor centered below shotpoint (SP) 400. The broad, gentle rise in the seafloor that extends westward from the side of the channel is the channel's levee.

Frontal deformation of the accretionary wedge is a ramp anticline above a landward verging thrust fault. The west boundary of this anticline is a kink fold with a steeply inclined fold axis (below SP 480). The thrust fault that forms the eastern and lower limit of this fold extends downward to the level of the igneous oceanic crust. This geometry indicates that all of the incoming sediment on the oceanic crust is being frontally accreted. Reflections from the fault plane are clearly evident at 4.5 s below SP 550. This fault flattens upward to form a local flat, and then it steepens near the seabottom to form another ramp. This ramp-flat-ramp geometry causes the small seafloor fold below SP 580 to develop. The plane of this thrust fault locally returns strong reflections, perhaps indicating overpressured fluids.

A landward succession of about six main thrust faults form anticlinal ridges, most of which deform rocks at the seafloor. However, the landwardmost anticlinal ridge, below SP 1050, is buried except for its sharply curved apex, which structurally controls the location of the channel centered below SP 1100. This channel is the main one feeding the Nitnat fan.

A major structural boundary within the accretionary wedge is the thrust fault at 3.5 s below SP 1100 (Figure 6.4.6). Well bedded rocks in the hangingwall of this thrust yield the same, coherent seismic image as the accreted oceanic rocks in the folds to the west. Rocks in the footwall, however, return a less coherent image. Even in the migrated section, reflections from the footwall rocks are strongly curved and irregular. We propose that these rocks are from an older episode of accretion, that they are indurated, and that they form a backstop to the recently accreted rocks to the west. The west face of the backstop dips seaward and merges downward with the oceanic plate near SP 950.

In accretionary wedges elsewhere, seaward dip of the backstop promotes landward verging thrust faults. Hence backstop dip as well as the possibility of a weak decollement must be considered in trying to explain the landward vergence of thrust faults off Washington.

Rocks near the seafloor, east of SP 1100, overlie the proposed backstop and are essentially undeformed. An interesting idea is that rocks forming the backstop are competent, so this part of the accretionary wedge resisted deformation during the recent accretion. The smooth seafloor over this backstop forms a wide, midslope terrace. If other seismic lines show this same relationship between terrace and backstop, it may be possible to map the extent of the backstop by circumscribing the terrace.

The terrace off Washington contrasts strongly with the steep, narrow slope west of Oregon. Most of this smoothness results from sediment deposition that buried old structures. Abundant sediment would have followed the channel, below SP 1100, that leads to the Nitnat fan.

The broad seafloor rise centered below SP 1600 is cored by an apparent, near-vertical offset (below SP 1600) in the top of the older, backstop rocks, so this rise has a structural origin. Low frequency reflections at 2.5 s under the east flank of this rise dip gently east.

Reflections from the igneous oceanic crust are clearly evident below the folds within the toe of the accretionary wedge. These reflections, however, become more difficult to discern below the proposed backstop. Nonetheless a series of discontinuous events can be followed eastward from the young folds to about 6.5 s below the shelf break at the east end of this seismic line. This traveltime is equivalent to a depth of 12 km to 15 km.

Reflections from rocks at shallow depth below and east of the shelf edge are flat lying or dip gently seaward. Deep reflections (below about 2 s) are faint, even so they define a consistent eastward dip. Hence the overlying rocks disconformably overlie the deeper rocks.

MCS Line 103: The Olympic Transect

This transect is one of the seismic lines along which both MCS and wide-angle data were collected, so detailed analysis of the geology will be possible. Eventually, this transect will become part of a cross section through Seattle to enhance our understanding of earthquake hazards in this metropolitan region.

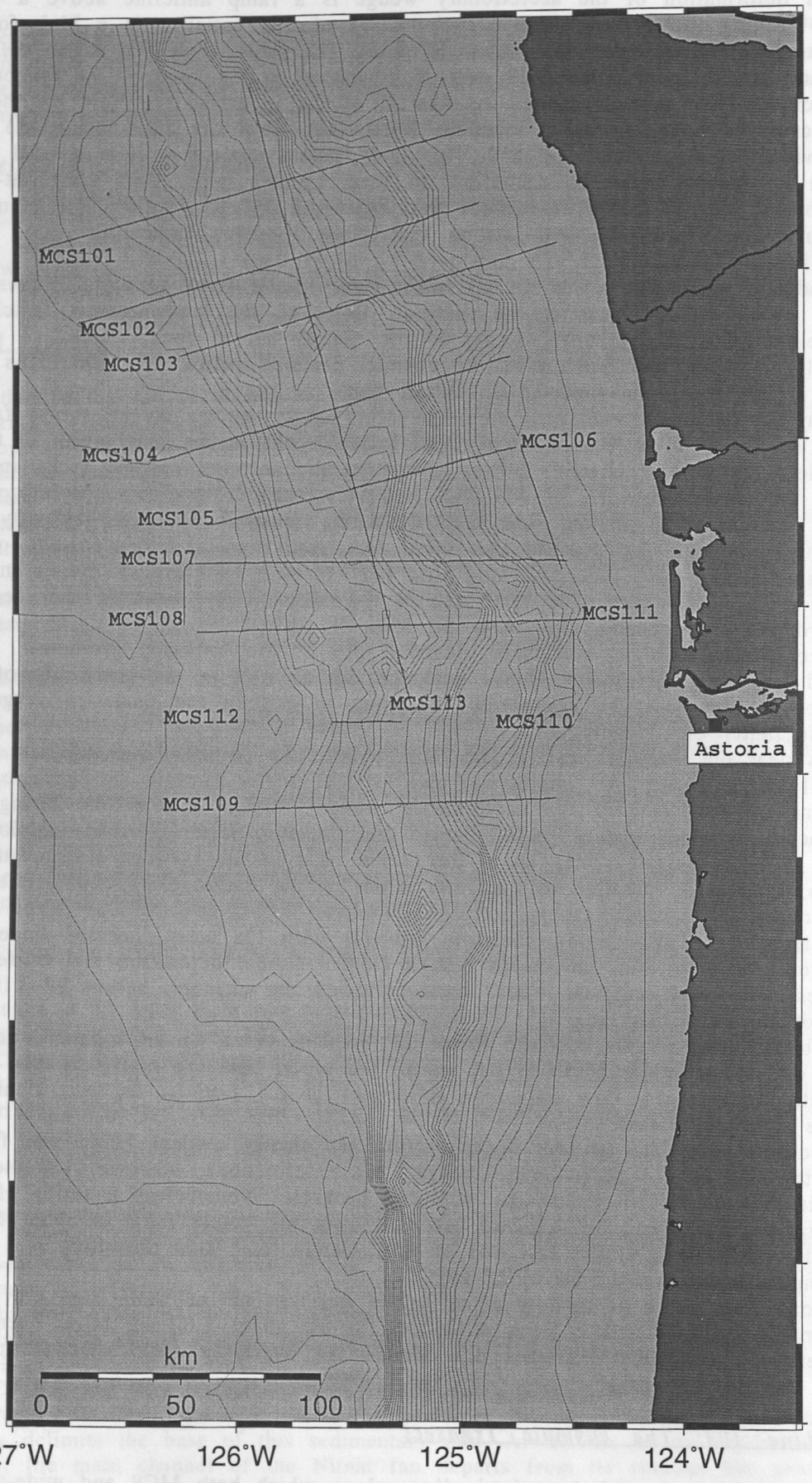

Figure 6.4.1: Location map of the MCS-lines collected during SO108.

Line 103 is shown in both stacked (Figures 6.4.8, 6.4.9, 6.4.10, and 6.4.11) and migrated versions (Figures 6.4.12, 6.4.13, 6.4.14, and 6.4.15). In the migrated version of line 103, a distributary channel from the Nitnat fan is evident just west of the toe of the accretionary wedge. This channel is about 7.5 km wide, and it's west side is evident below SP 850 (Figure 6.4.11).

A landward-vergent thrust fault has developed below this channel and defines the next block of sediment that will be accreted to the edge of the continent. As faulting continues, thick and potentially coarse-grained channel deposits will be incorporated into the wedge. These deposits could have a marked effect on the fluid dynamics of the wedge. Clearly, the wide accretionary wedge off Washington is at least locally, still growing seaward to maintain its critical taper.

Strong reflections from the igneous oceanic crust can be readily traced beneath both the sediment on the Juan de Fuca plate and the deformed rocks in the outer part of the accretionary wedge, up to SP 1800, where reflections from the top of the slab occur at 5 s. Landward of this shot point a series of laterally discontinuous events, like the one below SP 2500 at 5.5 s, define the downgoing plate eastward to the end of the line, where reflections from the slab occur at about 7 s. Thus with a good degree of confidence, the downgoing plate can be traced for 120 km beneath the continental edge. This circumstance will help guide modeling of wide angle data.

As noted above in describing line 101, fault plane reflections are clearly evident beneath each of the thrust-faulted ridges of the lower accretionary wedge. Six anticlinal ridges are evident, but the one in the fourth position, below SP 1400, is not well developed. As on section 101, we recognize two episodes of accretion under what is now the lower slope: the contact between rocks of these episodes is the landwardmost thrust fault that produces an anticlinal ridge at the seafloor. We propose that on section 103, this fault occurs below SP 1750 at 3 s. It stacks rocks on the west that have a coherent seismic image over rocks on the east that produce laterally discontinuous or sharply curved reflections. An exception to this generalization is the anticlinally deformed stack of coherent beds below SP 1900. Certainly east of SP 1900, accreted rocks below 2.5 s are poorly reflective.

We propose that the rocks in the footwall of the fault below SP 1750 form the backstop; they are older and more competent than are rocks in the hangingwall. The footwall rocks taper downward to end at the igneous crust below SP 1550 at 5 s. The seaward dip of this backstop could be part of the reason why thrust faults west of the backstop developed landward vergence.

The broad seafloor bulge centered below SP 2500 appears to be both a structural and sedimentary construct. The structural influence is evident in the small folds and possible thrust faults that deform rocks between SP 2500 and SP 2600 at 2 s. The sedimentary aspect is evident in the shallow beds that are not deformed by the folds or faults but instead unconformably overlie them. Furthermore, beds in the canyon below SP 2700 are truncated at the seafloor, indicating active erosion along the east side of the bulge. Part of the bulge could be overbank deposits or a sedimentary basin that is now being eroded by channelized currents. Bathymetric charts indicate that the canyon is a tributary to a large submarine canyon that ends abruptly eastward at the shelf break.

Rocks under the shelf are more complexly deformed that are shelf rocks evident on line 101. On line 103 at least one large anticline is evident, which could be cored by a diapir of melange, as in onshore rocks.

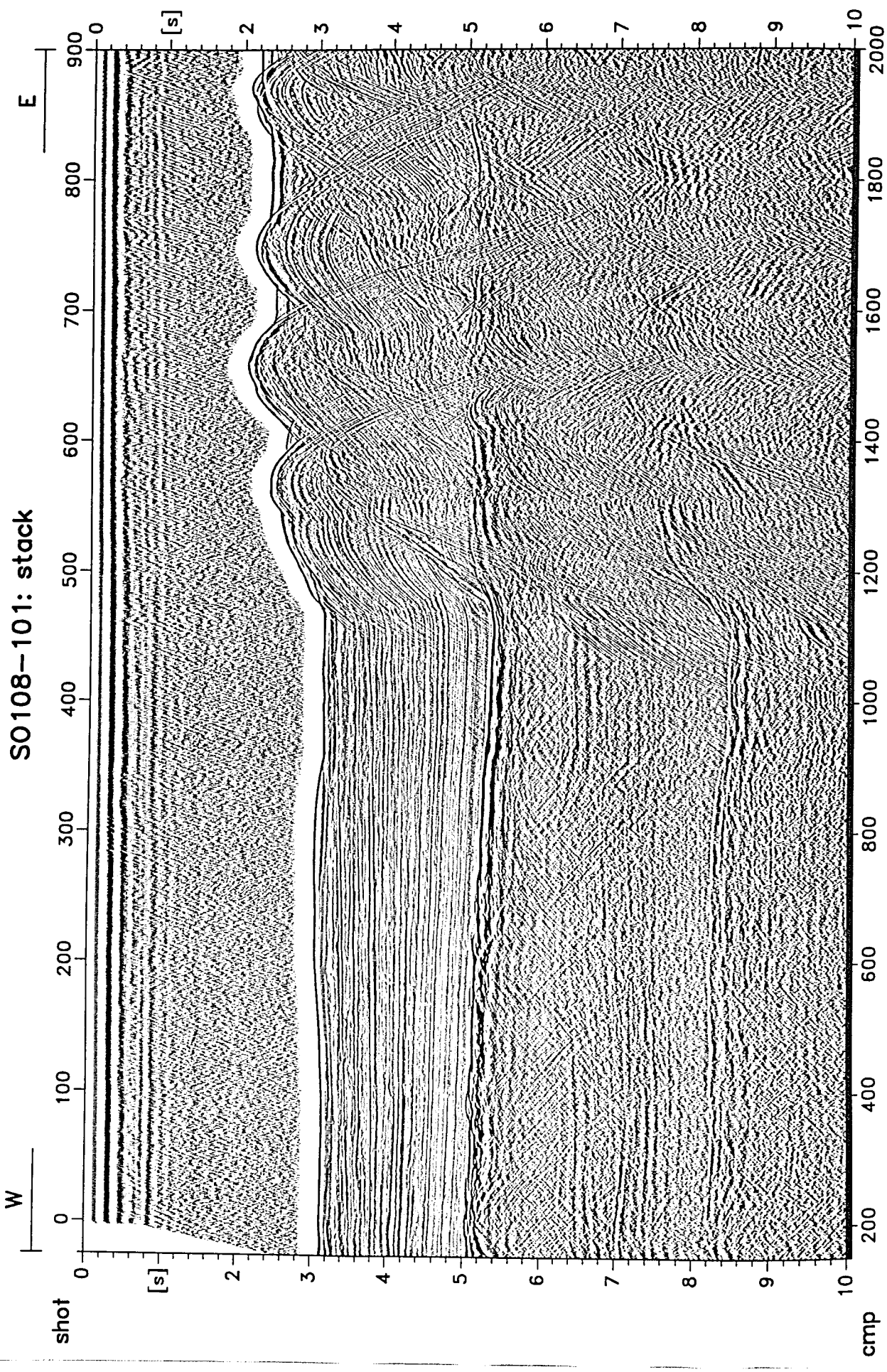

Figure 6.4.2: Line 101, stack, shots 0-900.

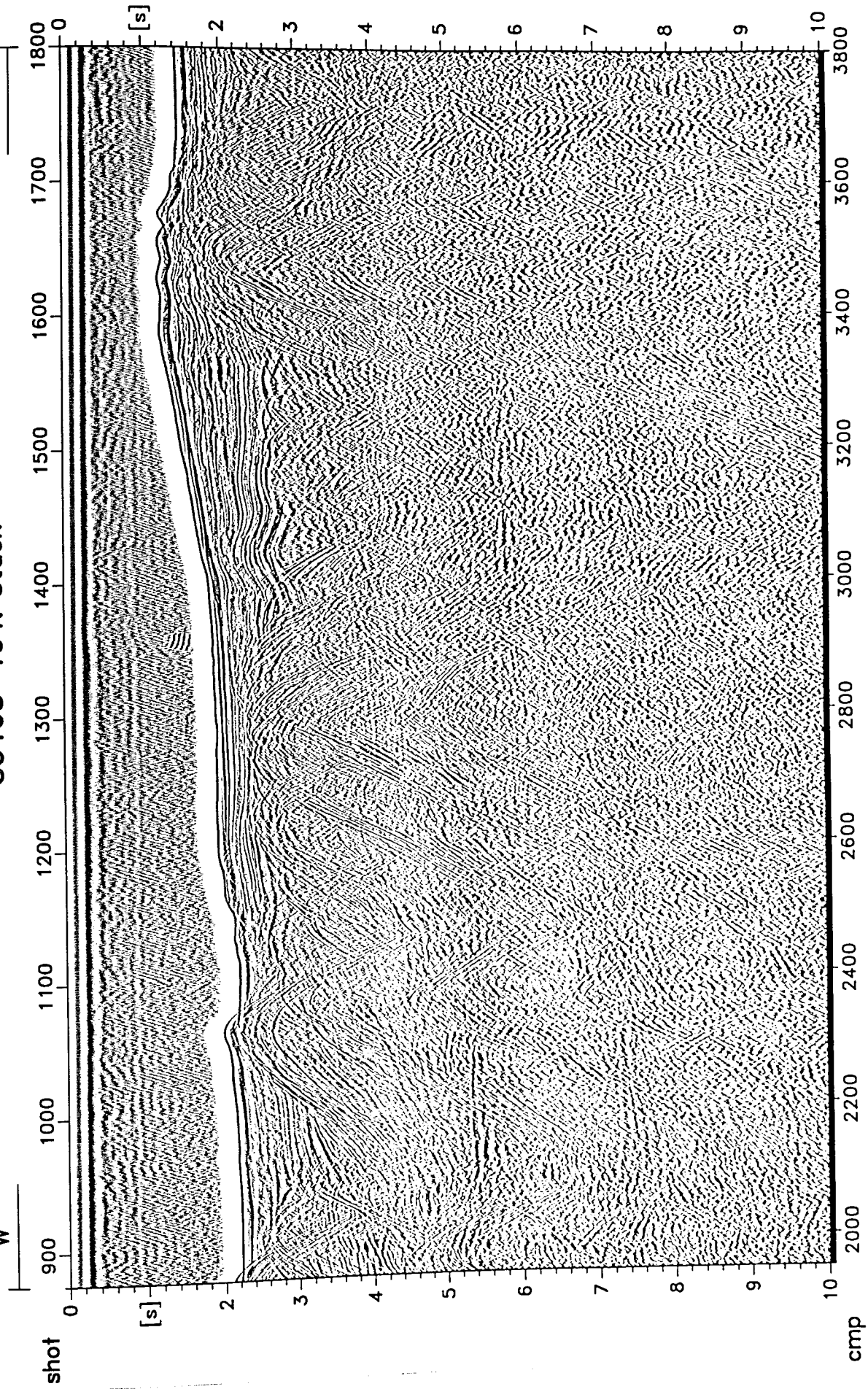

Figure 6.4.3: Line 101, stack, shots 850-1800.

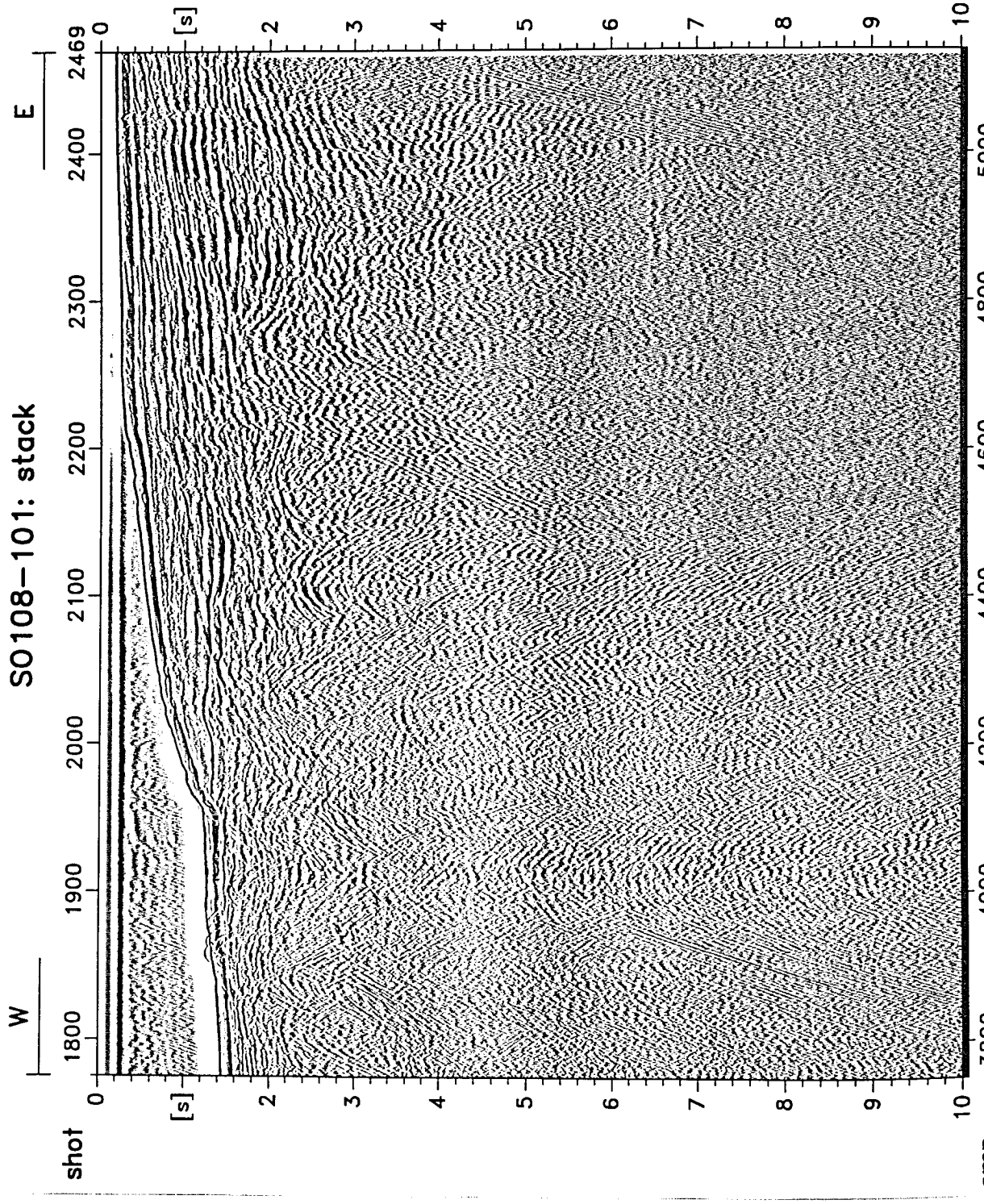

Figure 6.4.4: Line 101, stack, shots 1750-2469.

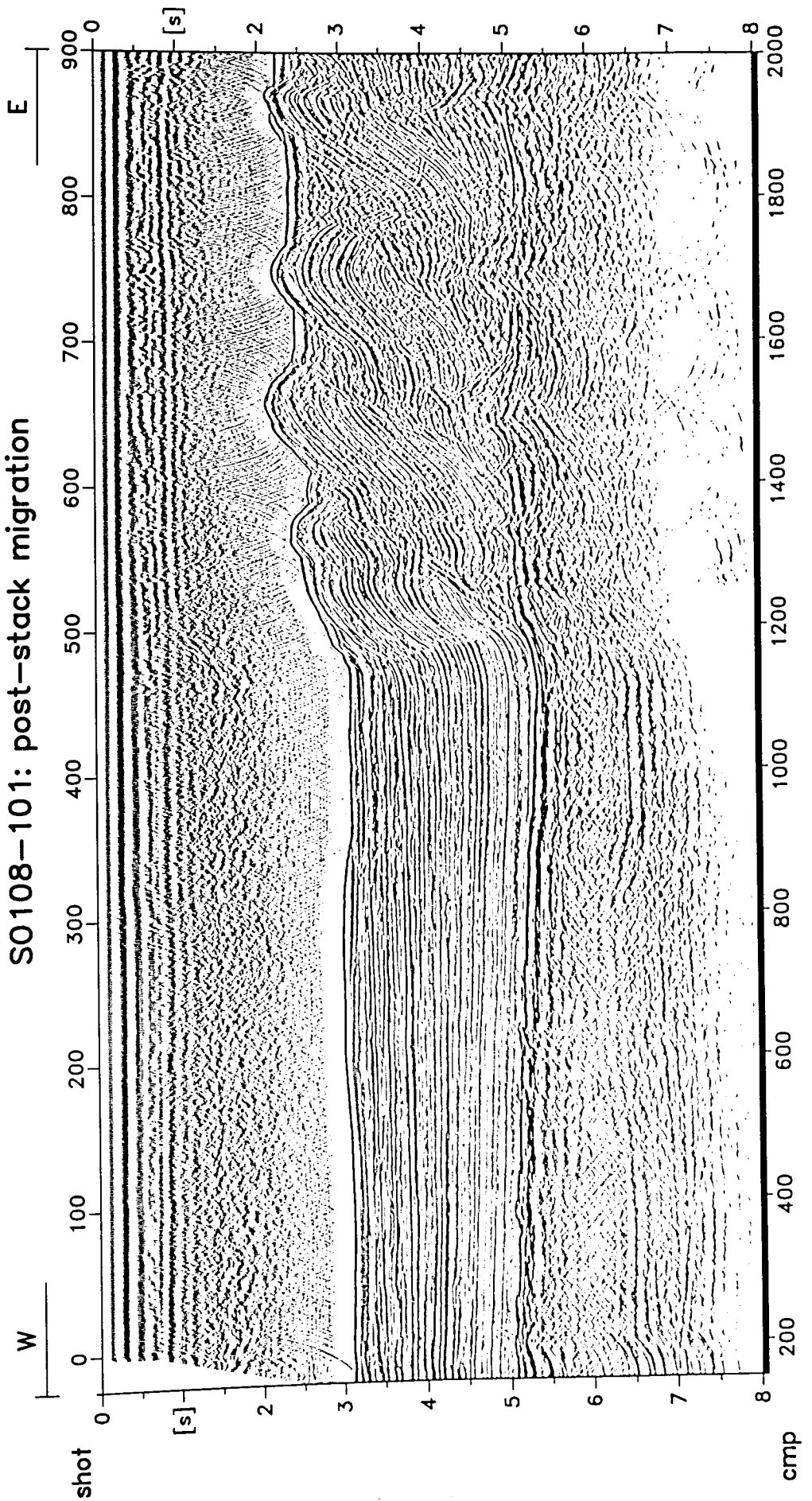

Figure 6.4.5: Line 101, migration, shots 0-900.

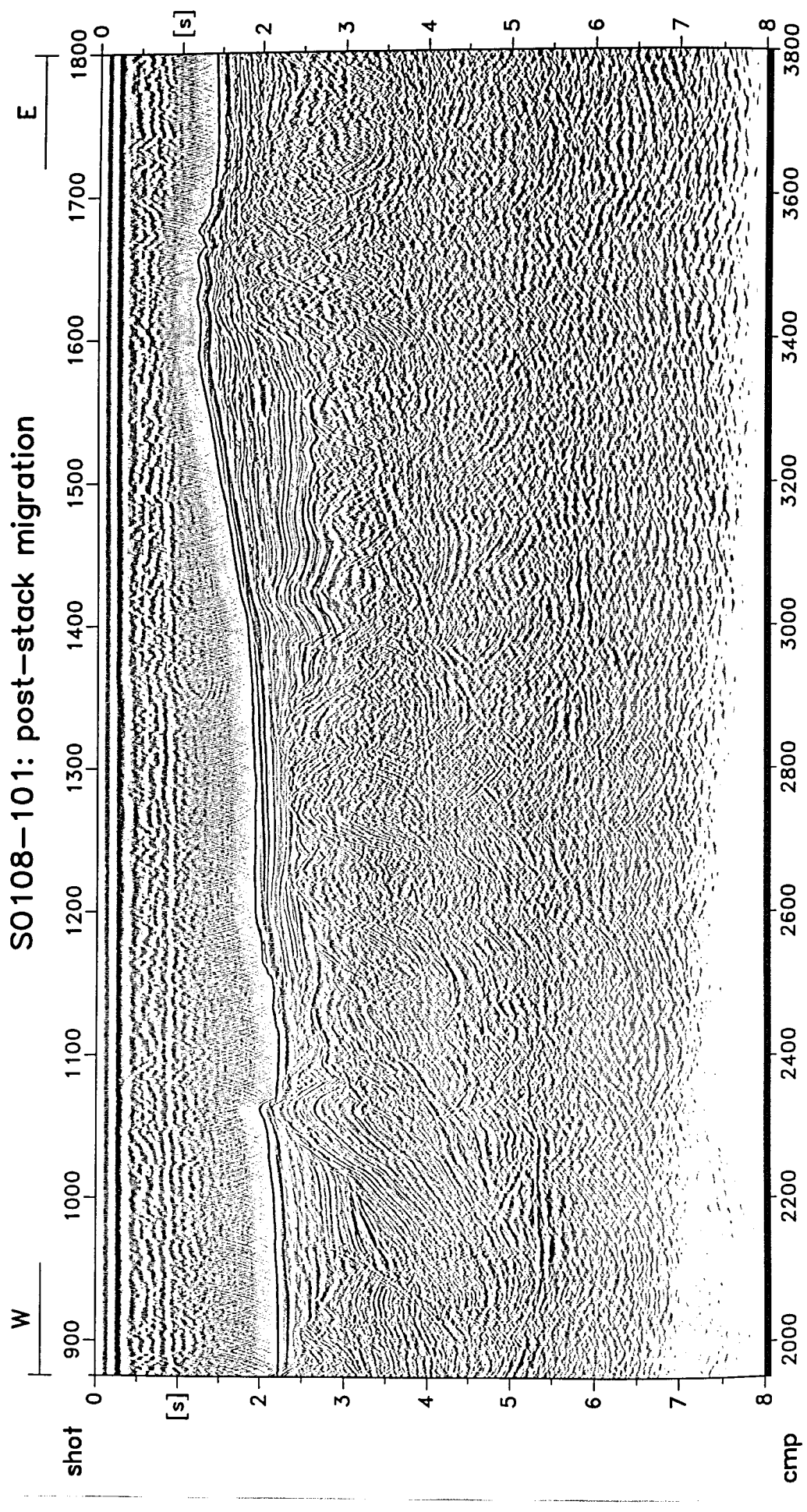

Figure 6.4.6: Line 101, migration, shots 850-1800.

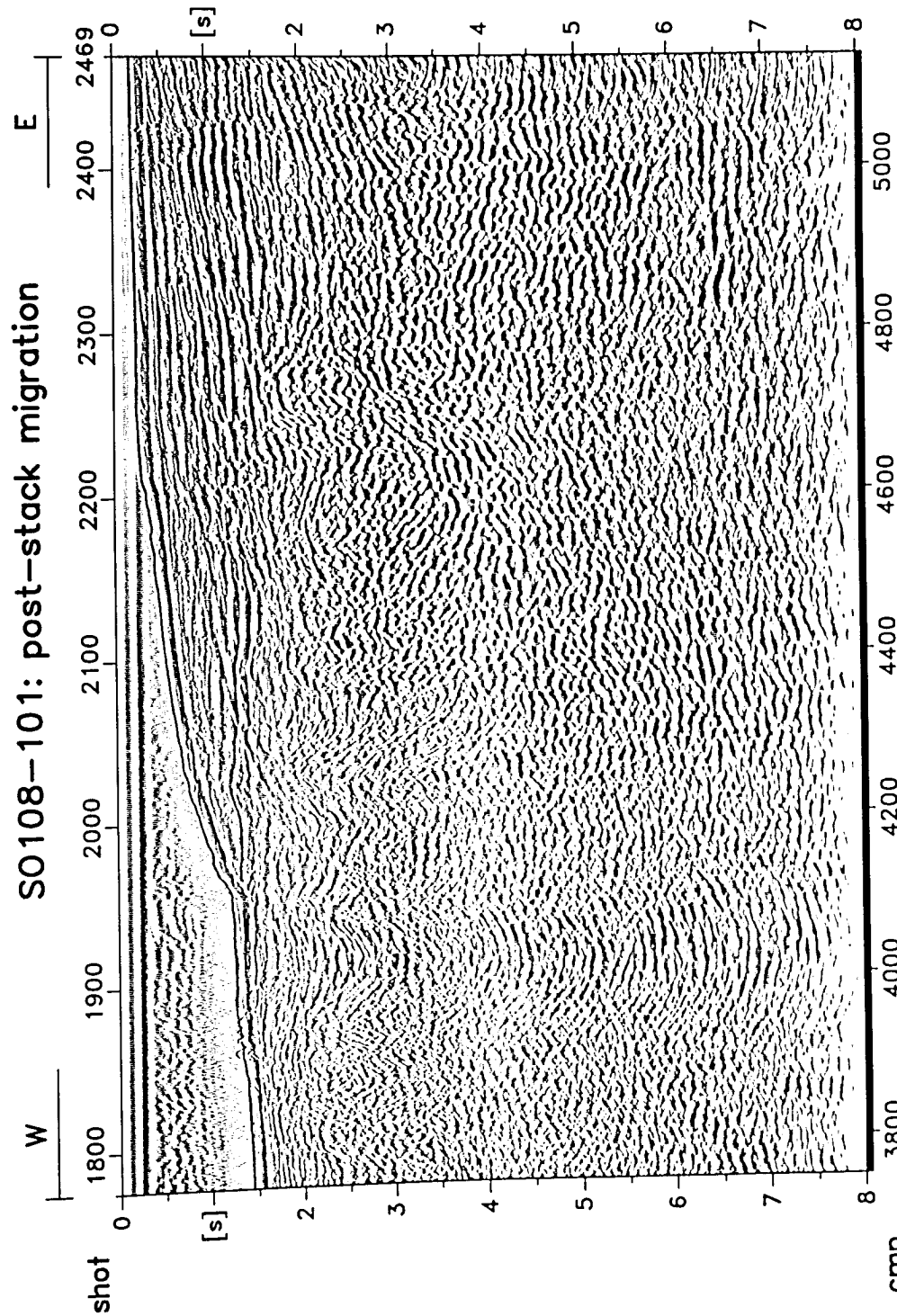

Figure 6.4.7: Line 101, migration, shots 1750-2469.

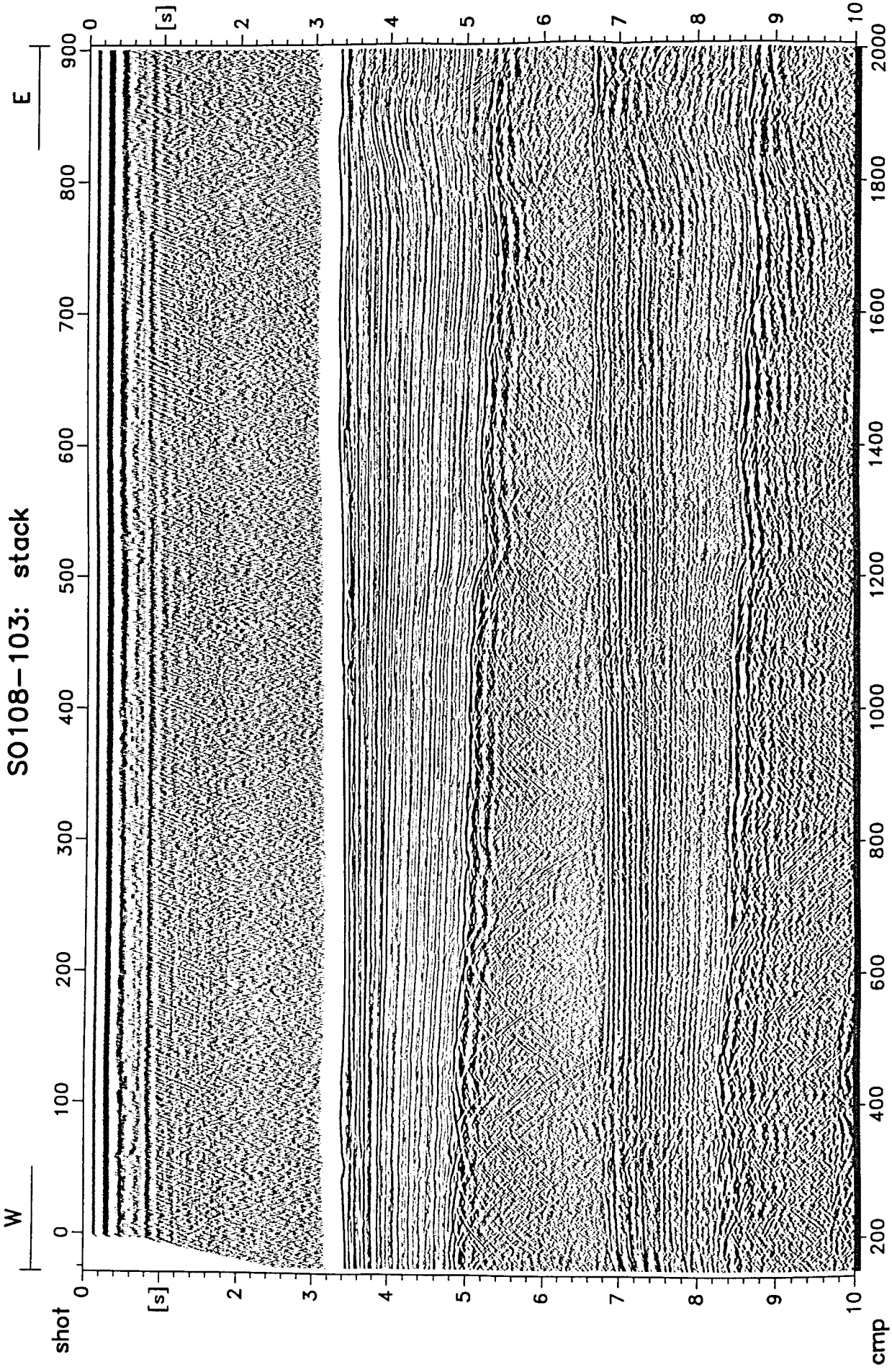

Figure 6.4.8: Line 103, stack, shots 0-900.

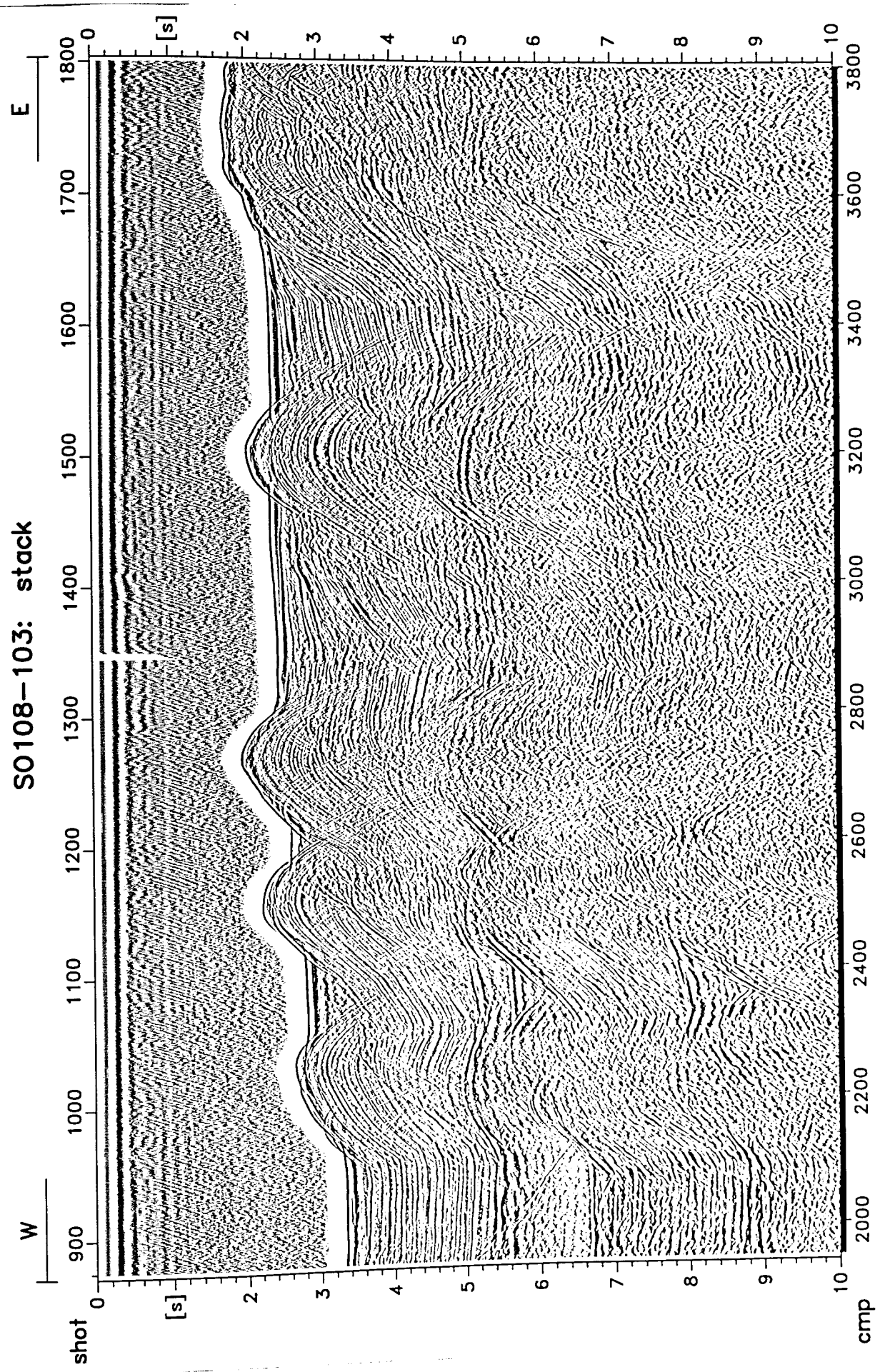

Figure 6.4.9: Line 103, stack, shots 850-1800.

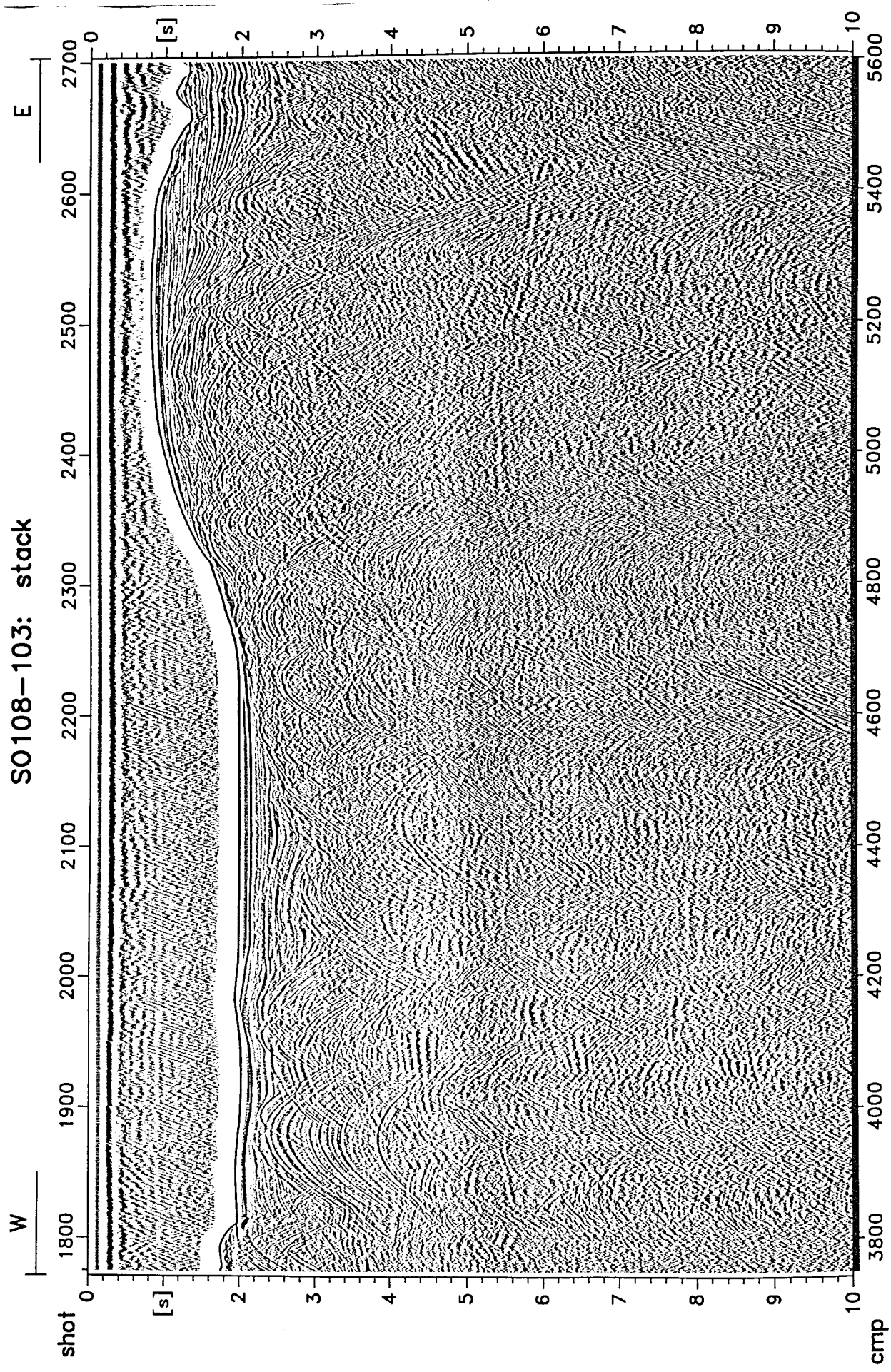

Figure 6.4.10: Line 103, stack, shots 1750-2700.

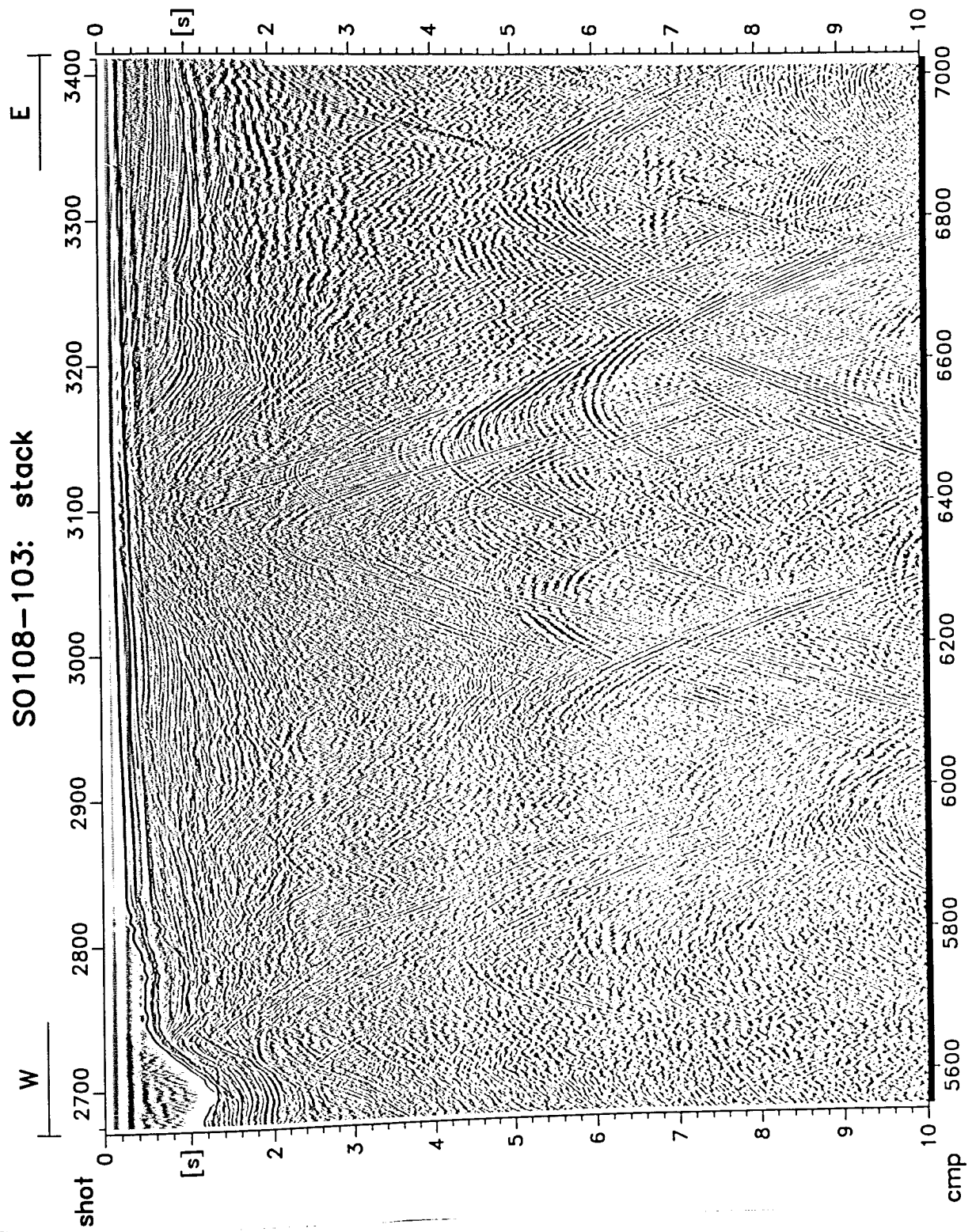

Figure 6.4.11: Line 103, stack, shots 2650-3420.

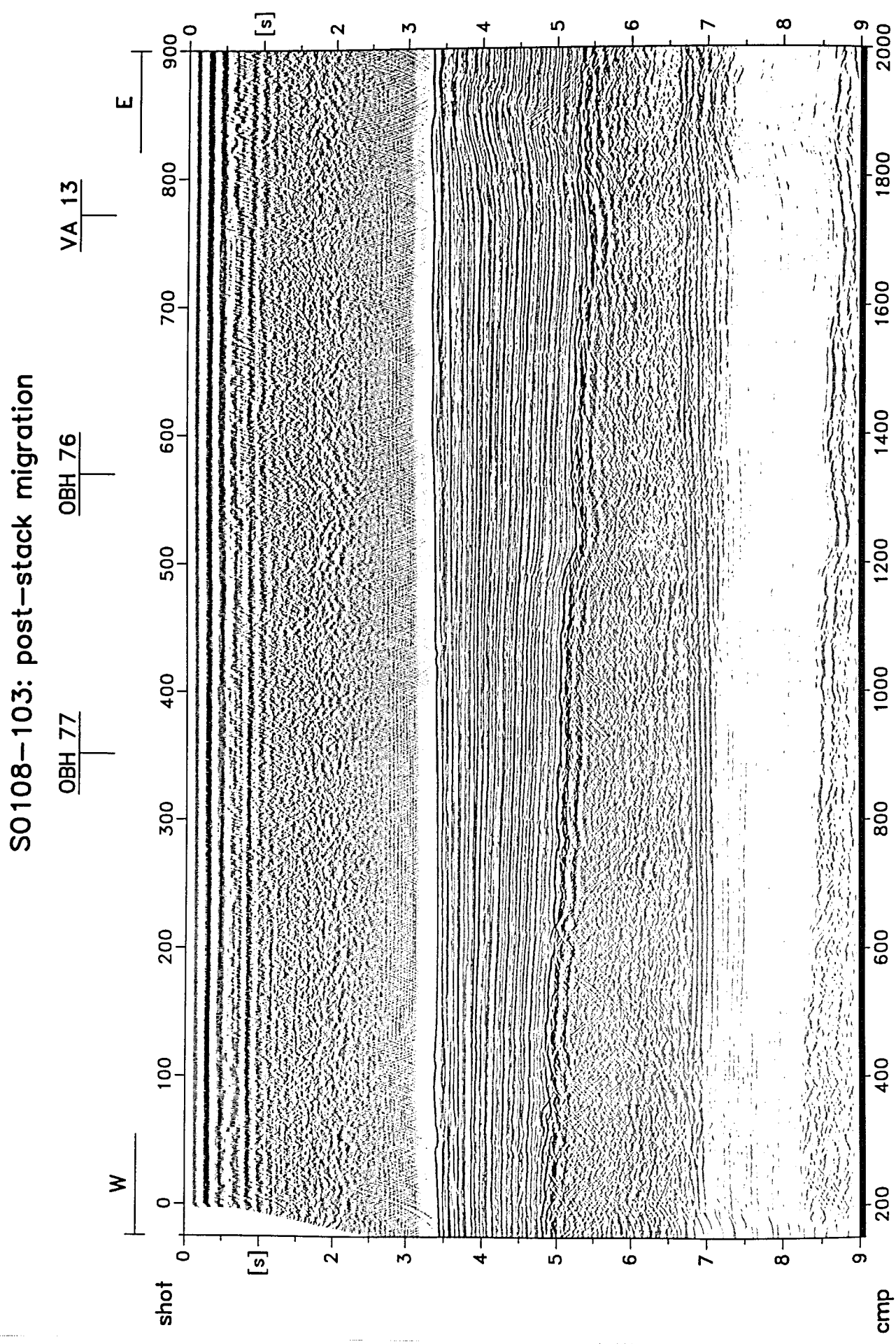

Figure 6.4.12: Line 103, migration, shots 0-900.

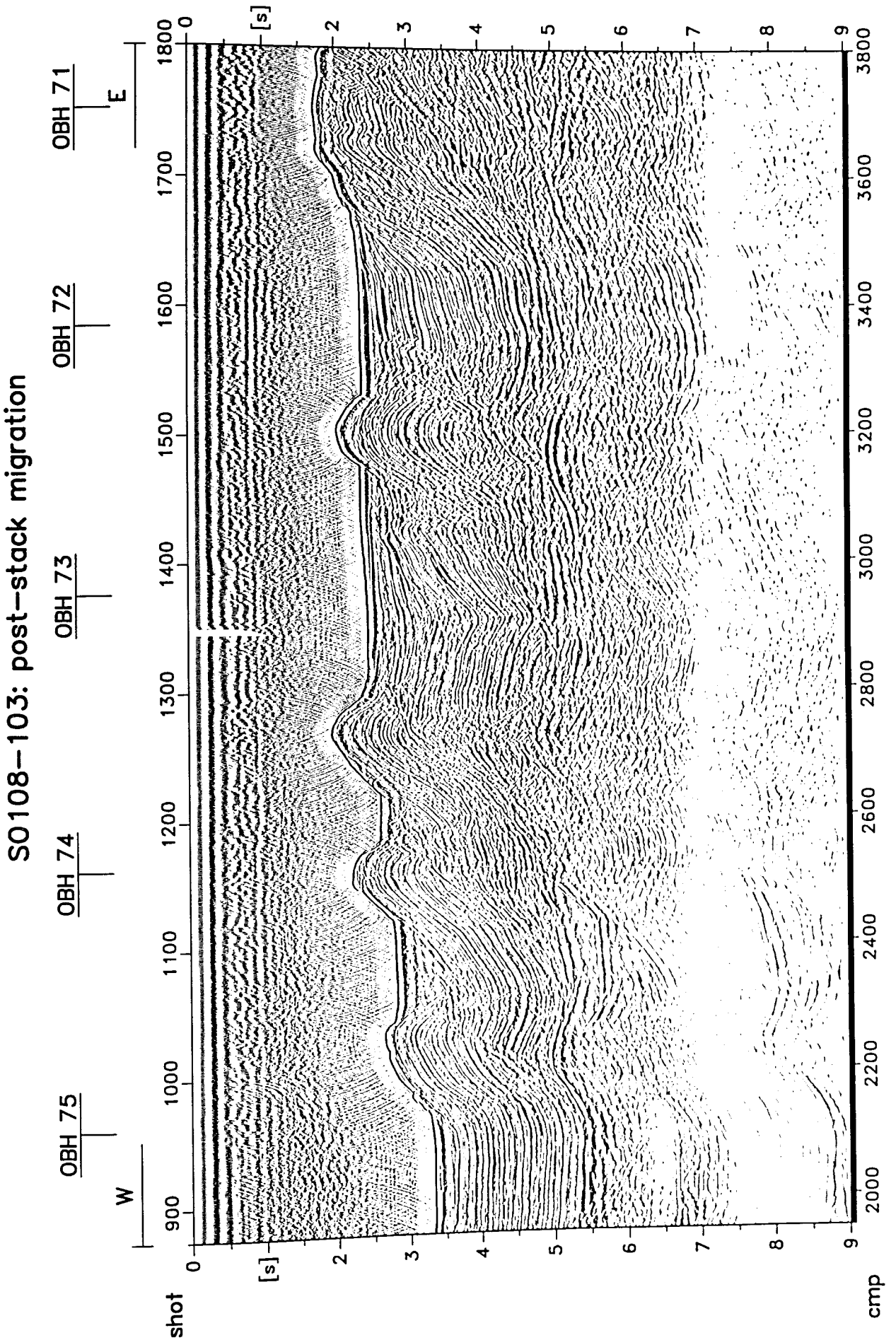

Figure 6.4.13: Line 103, migration, shots 850-1800.

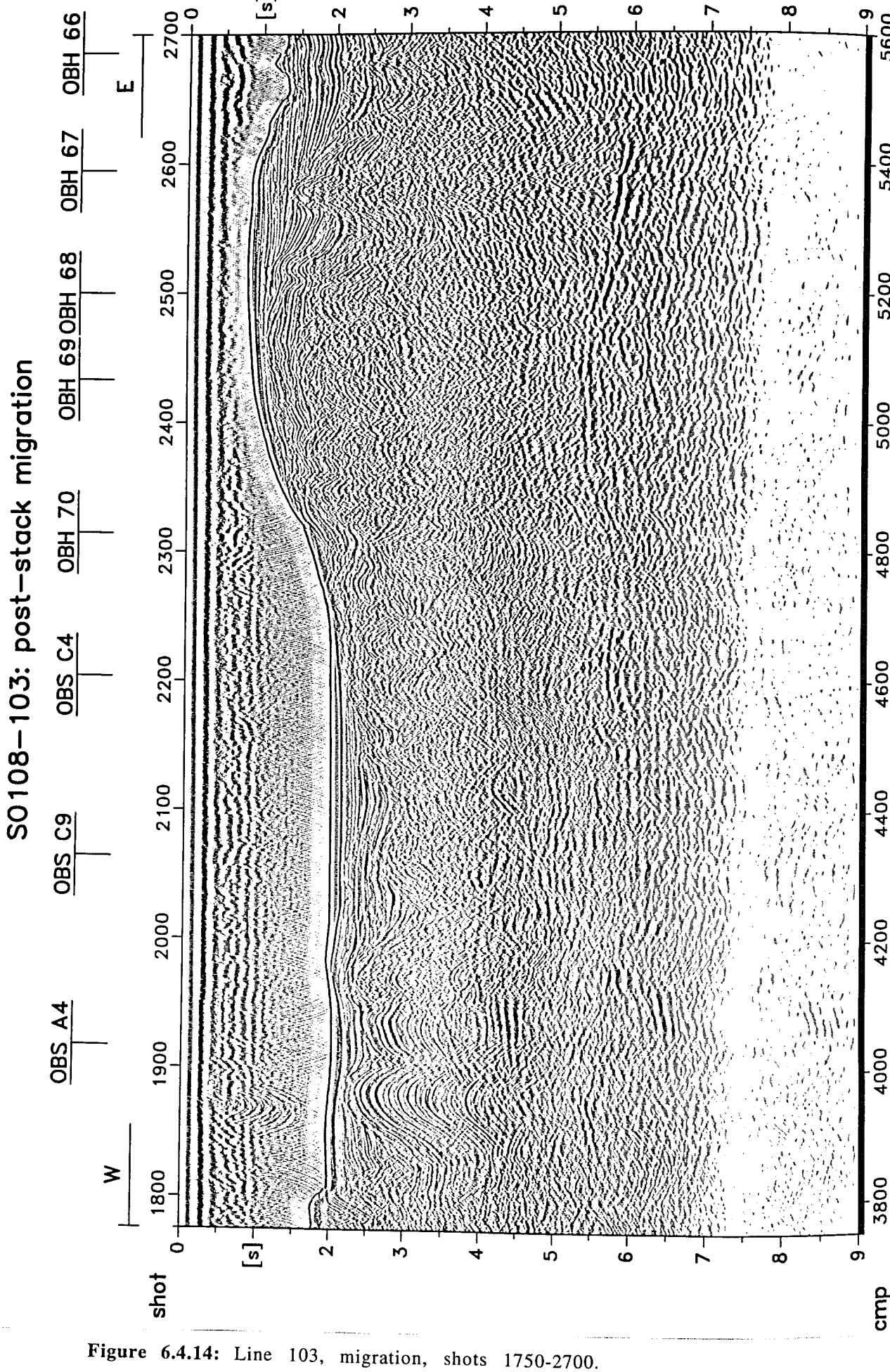

Figure 6.4.14: Line 103, migration, shots 1750-2700.

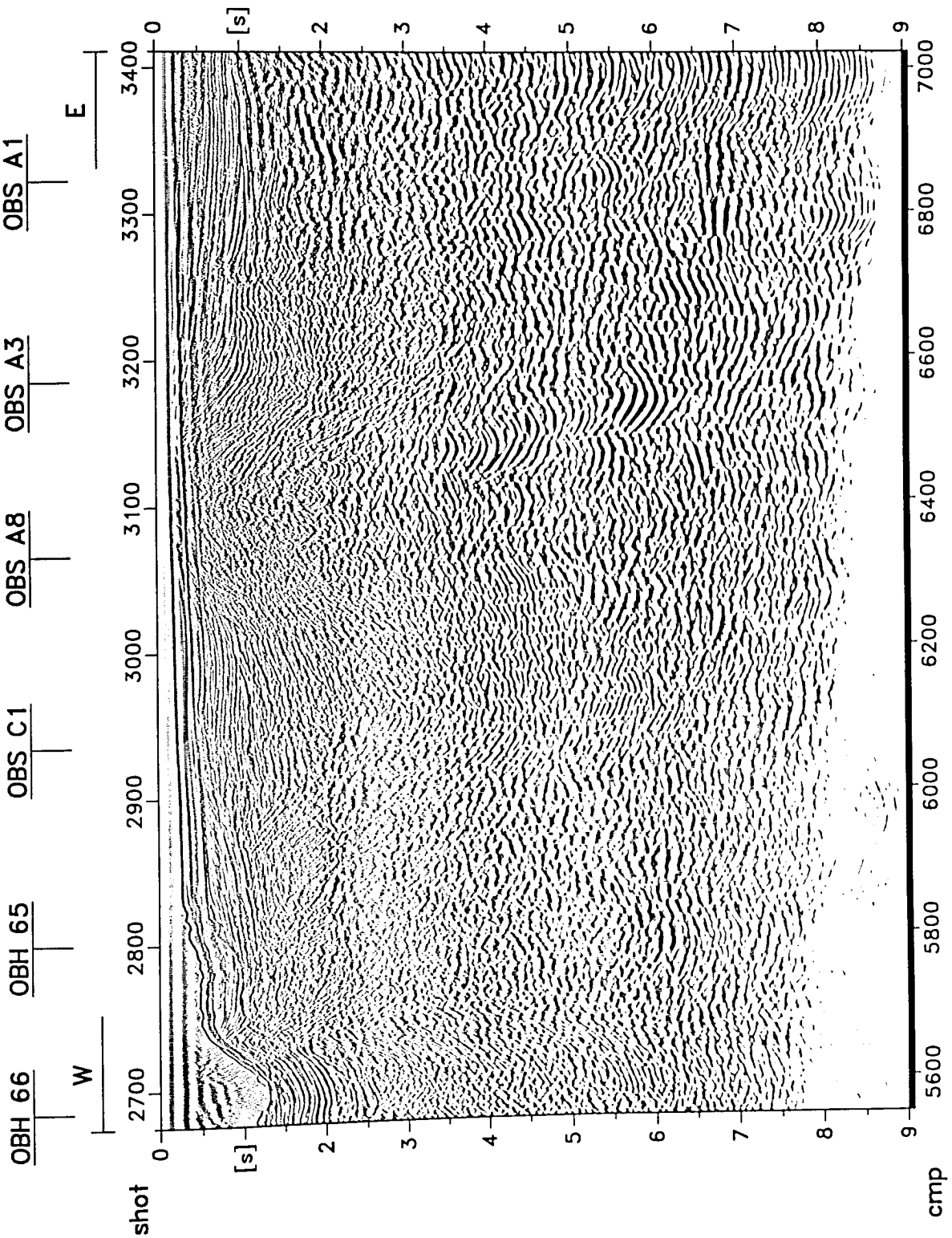

Figure 6.4.15: Line 103, migration, shots 2650-3420.

6.5 THE DUVALL EARTHQUAKE

(U. ten Brink, J. Bialas, and R. Busby)

The Duvall Earthquake is the largest earthquake to occur near Seattle in the last 15 years. Because one of the principal goals of this experiment is to aid in the assessment of earthquake hazard in the Pacific Northwest, the recording of this earthquake is of particular interest to us. The earthquake and many of its aftershocks occurred while the OBS and OBH were deployed along Line 10 (SW Washington line; Figure 6.5.1). The earthquake also gives us an unprecedented opportunity to evaluate the suitablity of the OBS and OBH for earthquake aftershock monitoring. In particular the comparison of the sensitivity of OBS and OBH is of interest to the GEOMAR group as their systems were already used for seismological recordings off Chile (SO103) and Nicaragua (SO107).

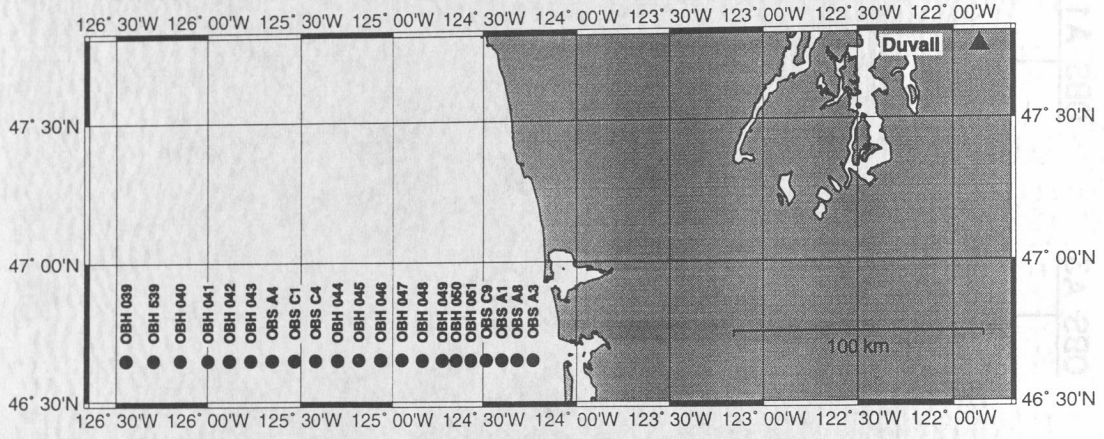

Figure 6.5.1: Location map of the OBS and OBH positions during the Duvall earthquake.

The parameters of the earthquakes are given below. They were determined independently by the University of Washington, University of California at Berkeley and Oregon State University, and ranges represent the variance between the three determinations.

DATE/TIME: 96/05/03 04:04:23 (UTC); 96/05/02 21:04:23 PM PDT (Local)
DEPTH: 6-8 km
MAGNITUDE: 5.3 - local magnitude; 5.4 - body-wave magnitude; Mw - 5.1-5.21
Reported felt in western Washington and from southern British Columbia to northern Oregon and east to Wenatchee.
LOCATION: 47.76 N, 121.85 W (U. Washington)
47.754 N, 121.881 W (OSU)
10.2 km ENE of Duvall, 13.3 km SE of Monroe
FOCAL MECHANISM: thrust with fault plane striking almost N-S
strike = 350 -360; 177 - 182
rake = 83 - 89; 91 - 100
dip = 50 - 53; 37 - 40

Duvall Mainshock and largest aftershocks:

Evt #	date	time UTC	latitude	longitude	depth	Mag	(local)
1	96/05/03	04:04:22	47.75N	121.86W	4.1	5.3 B	8.5 km ENE of Duvall
2	96/05/03	04:13:36	47.75N	121.85W	3.8	3.0 B	9.1 km E of Duvall
3	96/05/03	04:21:23	47.75N	121.86W	5.3	3.0 B	9.2 km ENE of Duvall
4	96/05/03	16:02:30	47.76N	121.86W	4.4	3.1 B	9.1 km ENE of Duvall
5	96/05/03	23:14:50	47.75N	121.88W	0.0	3.4 B	7.8 km ENE of Duvall

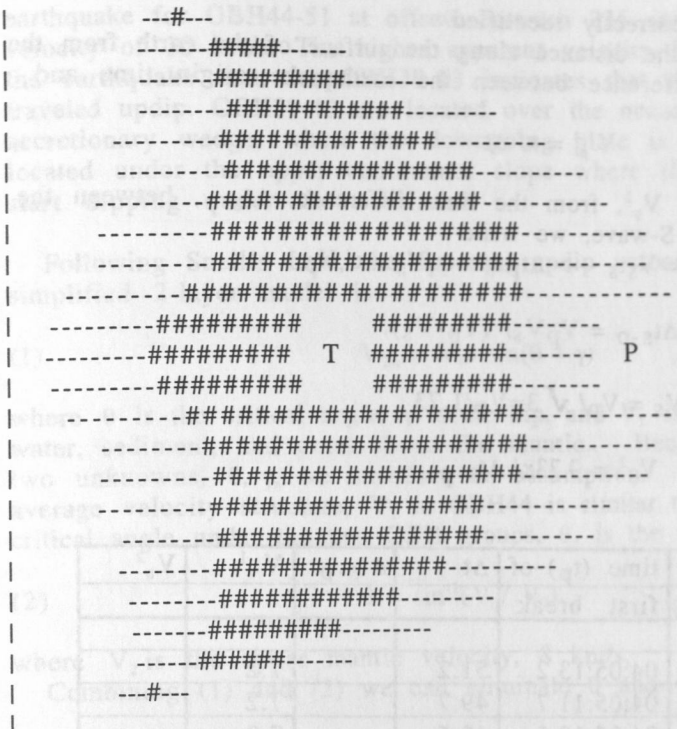

Lower Hemisphere Equal Area Projection

RECORDINGS OF THE EARTHQUAKE

The main shock was recorded on all the OBS and OBH for varying durations between 1-2.5 minutes. Figure 6.5.2.A shows 60 seconds of data recorded by the vertical (1), horizontals (2,3), and the hydrophone (4) of OBS C4 starting 37 seconds after the onset of the earthquake. Note the different responses of the 4 channels. None of the channels exhibit the earthquake wave train, typically recorded on land instruments. The onset of P wave is not sharp and the amplitude increases with time (Figure 6.5.3.B). The onset of S-wave is sharp on channels 3 and 4, but not on channels 1 and 2 (Figure 6.5.3.C). The earthquake record on the adjacent OBS, C1, ~6 km farther away is different than on C4 (Figure 6.5.2.B). For example, channel 1 on OBS C1 shows the onset of S-wave (Figure 6.5.2.B), but on C4 it does not (Figure 6.5.2.A). On C1, the trace amplitude is high from the onset of P-wave arrival (Figure 6.5.3.A) whereas on C4 the amplitude increases within the first several seconds (Figure 6.5.3.B). At present, it is not clear whether the differences between the channels and between the instruments, and the difference from typical land records are due to instrument response, or other causes. Figure 6.5.4 shows the main shock recordings of the hydrophones from the 14 OBH instruments. The display starts at 124:04:04:20, two seconds earlier than the occurance of the quake and continuous for three minutes. The higher amplitudes of OBH49 are due to an eight times higher amplification than on the other stations. Generally the OBH system records the signals with two different amplifications which were not available at station 49 as there was a vertical array attached. As described for the OBS a weak onset of the event is observed at all stations. Figure 6.5.5 displays an enlargement of the stations indicating that the type of onset is not depending on distance. Water wave arrivals of the regular airgun shots can be seen on the records of stations 45 to 51 (Figure 6.5.4).
To verify that the instruments indeed recorded the first P-wave break and not the later surface waves, we calculated the average velocity along the surface of the earth, V_p^1, between the earthquake and the OBS/OBH. (The average velocity along the ray path will be higher than V_p^1. If the average velocity is high (> 5 km/s), then the arrivals are not surface waves. We also calculated the velocity, V_p^2, from the time difference between the first break and the onset of the S-waves. If this velocity roughly matches the average velocity between the earthquake and the

OBS, then our picks have been correctly identified.

The average velocity, V_p^1, is the distance along the surface of the earth from the earthquake, x, divided by the difference between the earthquake origin time and the onset of the first break, Δt,

$$V_p^1 = x/\Delta t$$

To derive the average velocity, V_p^2, from the time difference, Δt_{S-p}, between the onset of P-wave and the onset of S-wave, we write

$$x = V_p t_p = V_s t_s \text{ ---> } \Delta t_{p-s} = x/V_s - x/V_p$$

Rearrange

$$x/\Delta t_{S-p} = V_p V_s/(V_p - V_s).$$

Assume

$$V_S = V_p/\sqrt{3} = V_p/1.73$$

Hence,

$$V_p^2 = 0.73x/\Delta t_{S-p}$$

OBS#	Channel	Distance (x)	time (t_p) of	Δt	Δt_{S-p}	V_p^1	V_p^2
OBH#	Rec. Type	from e.q. (km)	first break				
39	4	368.60	04:05:13.2	51.2		7.2	
539	4	357.93	04:05:11.7	49.7		7.2	
40	4	347.27	04:05:10.5	48.5		7.2	
41	4	336.62	04:05:09.0	47.0		7.2	
42	4	328.42	04:05:07.5	45.5		7.2	
43	4	320.22	04:05:06.4	44.4		7.2	
C1	1	302.23	04:05:05.3	42.3	30	7.14	7.34
	2-4		04:05:05.3	42.3		7.14	
C4	1	294.57	04:05:04.7	41.7		7.06	
	2-3		04:05:03.6	40.6	33.5	7.26	6.42
	4		04:05:06.8	43.8	30.5	6.73	7.03
44	4	287.85	04:05:02.7	40.7		7.1	
45	4	279.85	04:05:02.4	40.4		6.9	
46	4	271.86	04:05:01.7	39.7		6.8	
47	4	264.02	04:05:01.5	39.5		6.7	
48	4	256.38	04:05:00.7	38.7		6.6	
49	4	249.22	04:05:00.3	38.3		6.5	
50	4	244.16	04:05:00.0	38.0		6.4	
51	4	238.75	04:04:59.0	37.0		6.5	
A1	1-2	226.92	04:04:58.1	35.1		6.46	
	3		04:04:57.5	34.5		6.58	

TABLE 6.5.1: Average p-wave velocities for event 1 (main shock).

We find that the velocities up to 290 km are reasonable average crustal velocities. Furthermore, they increase with distance. We are, therefore, confident of our identification of the onset of earthquake energy as being indeed the onset of P wave, despite the unusual character of the wave train. At larger distances between 290 and 370 km the average velocity is kept constant at 7.2 km/s. The well distinguished velocity pattern indicates that different wave pathes are observed.

Dip of the downgoing slab

A true distance display of the 14 OBH recordings of the main shock (Figure 6.5.5) was used to analyse the average velocity within the line. The onset of the earthquake for OBH39-43 at offsets larger than 320 km line up at an apparent velocity of 8 km/s identifying them as mantle refracted phase. The onset of the

earthquake for OBH44-51 at offsets between 235 and 290 km line up at an apparent velocity of 10 km/s. The higher apparent velocity for OBH44-51 which are closer to the earthquake than for OBH39-43 indicates that the arrivals reaching these OBH traveled updip. OBH39-43 are located over the oceanic crust and at the tow of the accretionary wedge, where the downgoing plate is almost horizontal. OBH44-51 are located under the upper continental slope where the downgoing slab is expected to start dipping under the continent.

Following Snell's Law, the apparent updip velocity of the mantle, V_{2u}, in a simplified 2-layer model is

(1) $$V_{2u} = V_1 / \sin(\theta - \gamma)$$

where θ is the critical angle, γ is the dip, and V_1 is the average velocity of the water, sediment, and crust above the mantle.. Because this is one equation with two unknowns, θ, γ, we introduce an assumption. The assumption is that the average velocity structure, V_1 at OBH44 is similar to that of OBH43, hence the critical angle under the two OBH groups, θ, is the same. Again from Snell's Law,

(2) $$\theta = \sin^{-1}(V_1 / V_2)$$

where V_2 is the upper mantle velocity, 8 km/s.

Combining (1) and (2) we can eliminate θ and write

$$\gamma = \sin^{-1}(V_1 / V_2) - \sin^{-1}(V_1 / V_{2u})$$

with V_2 = 8 km/s, V_{2u} = 10 km/s, and V_1 = 3.2 km/s, the slab dip, γ = 4.9°.

This dip is, however, the apparent dip of the slab because the Duvall earthquake lay at an angle of 29° off the axis of OBH/OBS Line 10. The true dip along the line equals the apparent dip divided by cos(29°). Hence, the true dip under OBH44-51 is 5.6°, which translates to deepening of the slab by 5.4 km in this portion of the line.

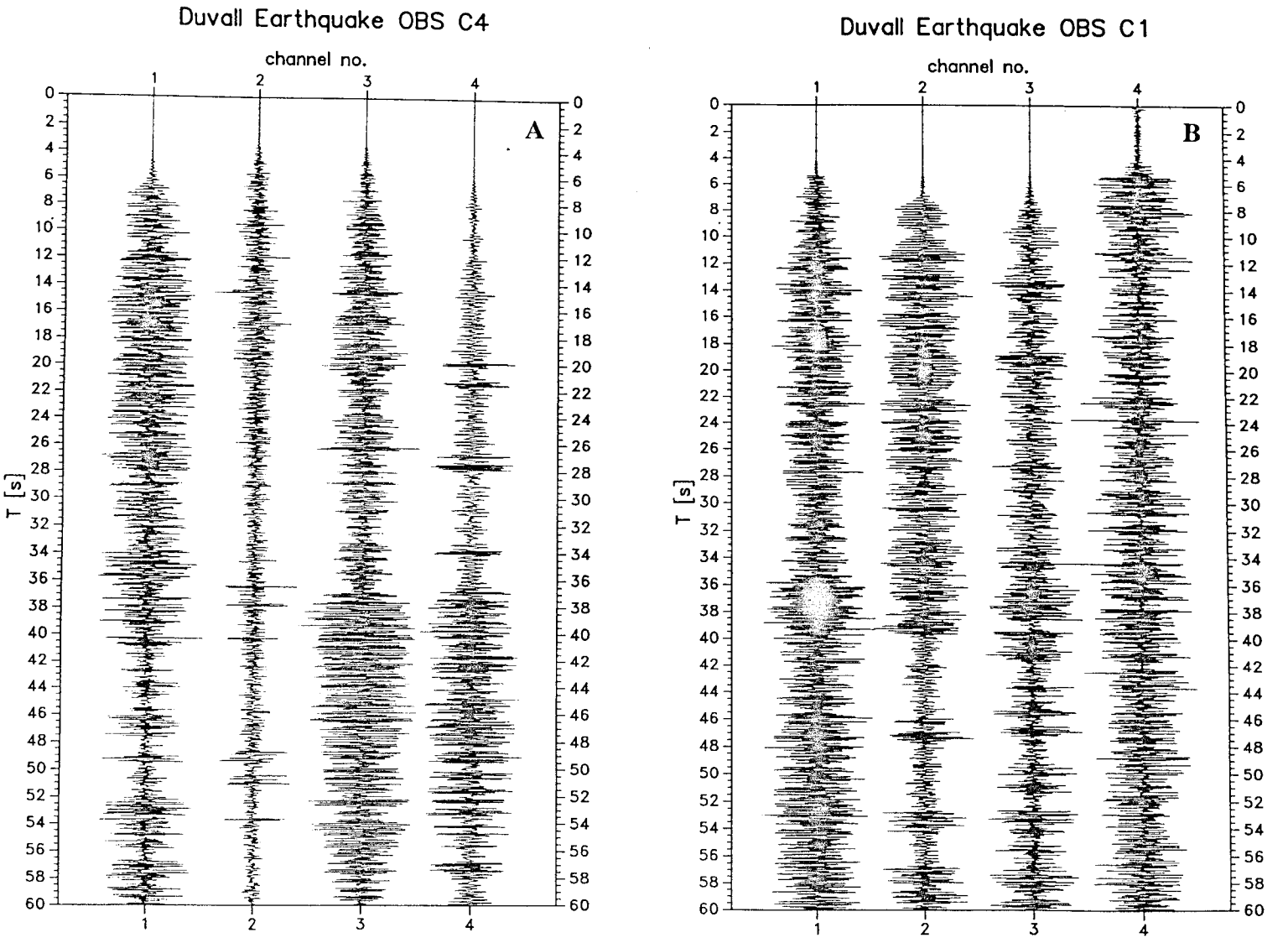

Figure 6.5.2: 60 second record of the 4 OBS channels (1 - vertical geophone; 2 and 3 - horizontal geophones; 4 - hydrophone) starting at 04:05:00, or 37 seconds after the earthquake occurred. (A) OBS C4, (B) OBS C1. The geophone pack is mounted inside the sphere and the hydrophone is mounted on the outside. The sphere is tightly held by a spring against a flat wide anchor which sits on the bottom.

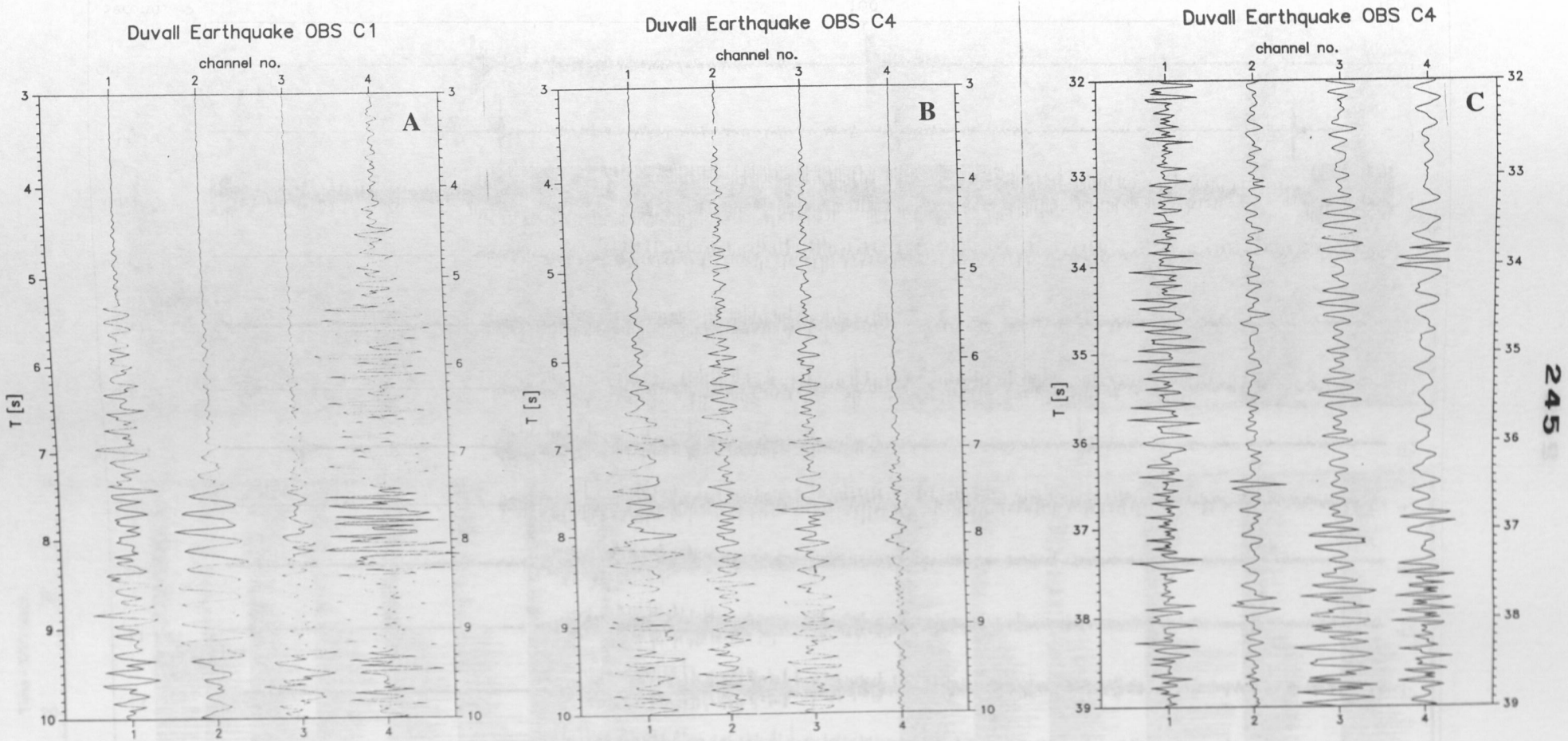

Figure 6.5.3: Enlargements of sections of Figure 6.5.2 showing (A) the onset of the P waves and details of the wavelet for OBS C1, (B) the onset of the P waves and details of the wavelet for OBS C4 and (C) the onset of the S waves and details of the wavelet.

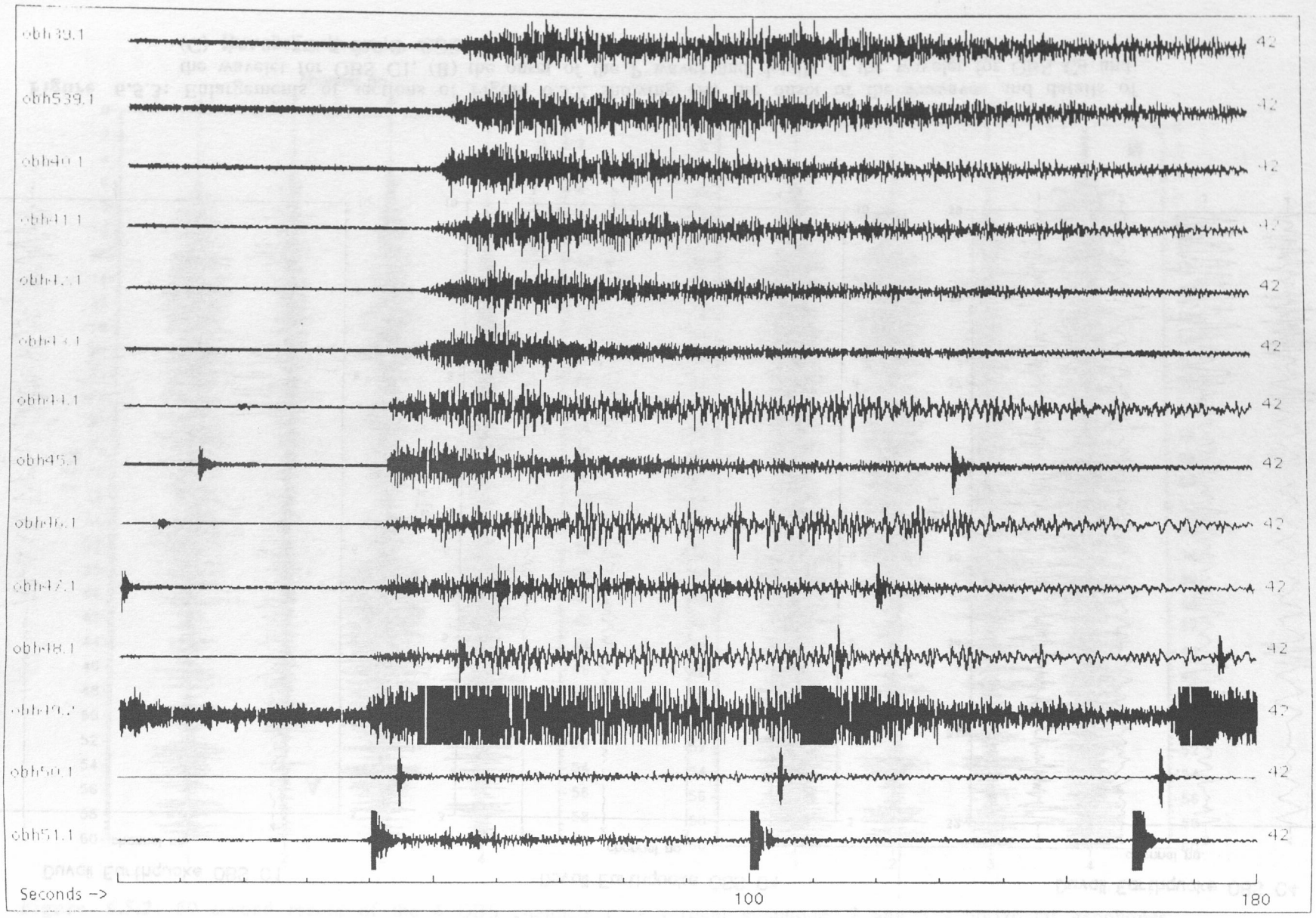

Figure 6.5.4: minute record of all 14 OBH starting at 124:04:04:20; Stations are ordered by distance (largest on top, equaly spaced).

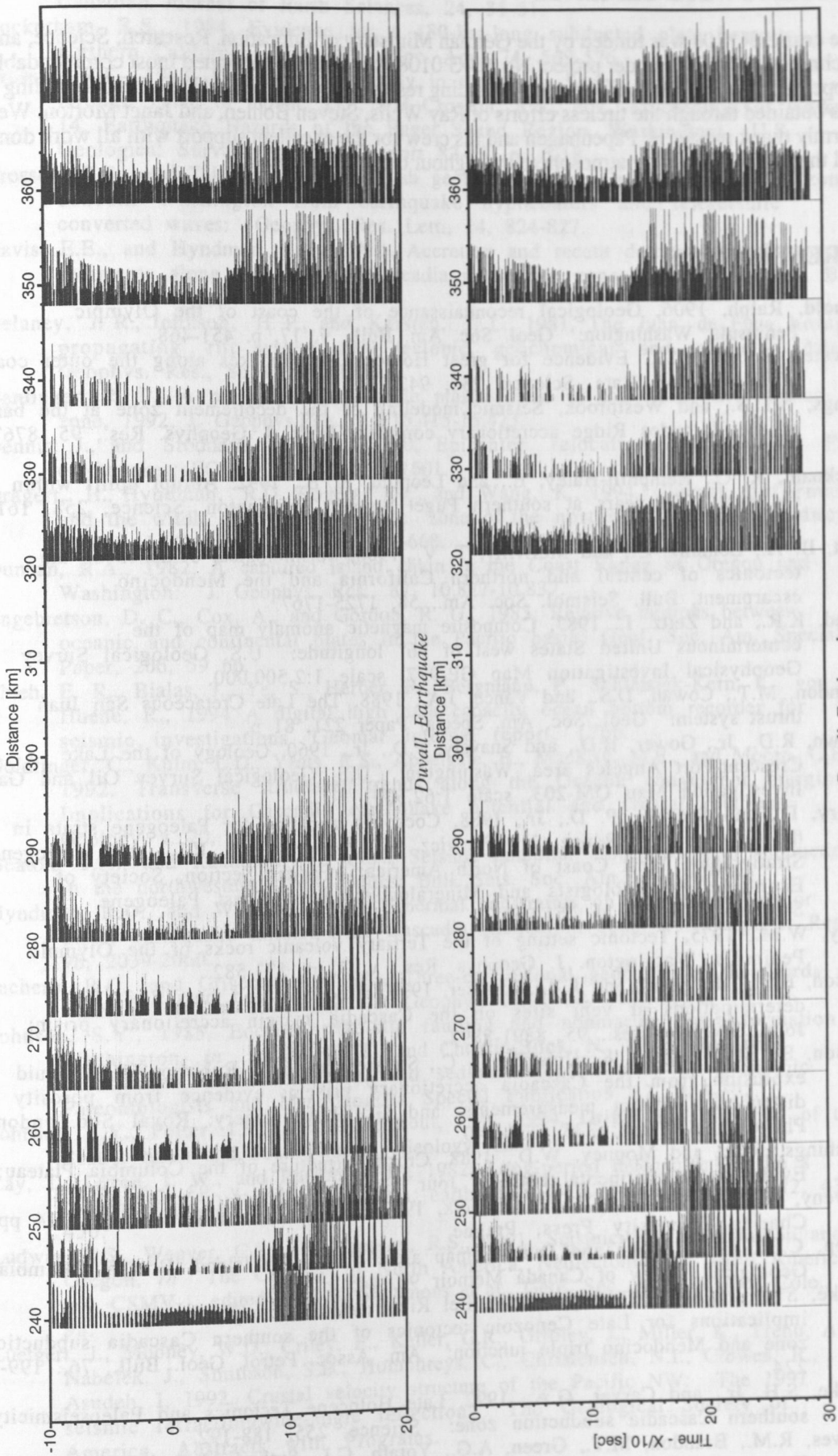

Figure 6.5.5: True distance display of all 14 OBH recordings of the Duvall Earthquake plotted at reduced travel time of 8 km/s and 10 km/s.

7. ACKNOWLEDGEMENTS

The cruise SO 108 was funded by the German Ministery of Education, Research, Science, and Technologie (BMBF) under project No. 03 G 0108 A within the continued most commendable support for marine sciences with an oustanding research vessel like SONNE. USGS funding was obtained through the tireless efforts of Ray Wells, Steven Bohlen, and Janet Morton. We warmly thank master H. Papenhagen and his crew for the excellent support with all work done and the splendid working atmosphere throughout the whole cruise.

8. REFERENCES

Arnold, Ralph, 1906, Geological reconnaissance of the coast of the Olympic Peninsula, Washington: Geol. Soc. Am. Bull., v. 17, p. 451-468.

Atwater, B. F. ,1987,. Evidence for great Holocene earthquakes along the outer coast of Washington State. Science, 236, 942-944.

Bangs, N.L.B., and Westbrook, Seismic modeling of the decollement zone at the base of the Barbados Ridge accretionary complex. 1990, J. Geophys. Res., 95, 8767-8782.

Bucknam, R. C., Hemphill-Haley, E., and Leopold, E. B., 1992. Abrupt uplift within the past 1700 years at southern Puget Sound, Washington. Science, 258, 1611-1614.

Bolt, B. A., Lomnitz, C., and McEvilly, T. V., 1968, Seismological evidence on the tectonics of central and northern California and the Mendocino escarpment, Bull. Seismol. Soc. Am., 58, 1725-1767.

Bond, K.R., and Zeitz, I., 1987, Composite magnetic anomaly map of the conterminous United States west of 96° longitude: U.S. Geological Survey Geophysical Investigation Map GP-977, scale 1:2,500,000.

Brandon, M.T., Cowan, D.S., and Vance, J.A., 1988, The Late Cretaceous San Juan thrust system: Geol. Soc. Am. Special Paper 221, 81 p.

Brown, R.D., Jr., Gower, H.D., and Snavely, P.D., Jr., 1960, Geology of the Lake Crescent-Port Angeles area, Washington: U.S. Geological Survey Oil and Gas Investigation Map QM-203, scale 1:62,500.

Bukry, D., and Snavely, P. D., Jr., 1988, Coccolith zonation for Paleogene strata in the Oregon Coast Range, *in* Filewicz, M.V., and Squires, R.L., eds., Paleogene Stratigraphy, West Coast of North America: Pacific Section, Society of Economic Paleontologists and Mineralogists, West Coast Paleogene Symposium, v. 58, p. 251-263.

Cady, W.M., 1975, Tectonic setting of the Tertiary volcanic rocks of the Olympic Peninsula, Washington. J. Geophys. Res., v. 3, p. 573-582.

Carson, B., E., E. Suess, and J. C., Strasser, 1990, Fluid flow and mass flux determinations at vent sites on the Cascadia margin accretionary prism: Jour. Geophys. Res., 95, 8891-8897.

Carson, B., M.L. Holmes, K. Umstattd, J. C., Strasser, and H.P. Robinson, 1991, Fluid explusion from the Cascadia accretionary prisem: evidence from porosity distrubution, direct measurements, and GLORIA imagery: Royal Soc.London Philosphical Trans, 335, 331-340.

Catchings, R.D., and Mooney, W.D., 1988, Crustal structure of the Columbia Plateau; Evidence for continental rifting: Jour. Geophys. Res., v. 93, p. 459-474.

Cerveny, V., I.A. Molotkov, and I. Psencik, 1977. Ray Method in Seismology, 214 pp., Charles University Press, Prague.

Clapp, C.H., 1917, Sooke and Duncan map area, Vancouver Island, British Columbia: Geological Survey of Canada Memoir 96, 445 p.

Clarke, S.H. Jr., 1992, Geology of the Eel River basin and adjacent region: implications for Late Cenozoic tectonics of the southern Cascadia subduction zone and Mendocino triple junction: Am. Assoc. Petrol. Geol. Bull., 76,. 199-224.

Clarke, S.H. Jr., and Carver, G.A., 1992, Late Holocene Tectonics and Paleoseismicity, southern Cascadia subduction zone: Science, 255, 188-192.

Clowes, R.M., Brandon, M.T., Green, A.G., Yorath, C.J., Sutherland Brown, A., Kanasewich, E.R., and Spencer, C., 1987, LITHOPROBE - Southern Vancouver

Island: Cenozoic subduction complex imaged by deep seismic reflections: Canadian Journal of Earth Sciences, 24, 31-51.

Cockerham, R.S., 1984, Evidence for a 180-km-long subducted plate beneath northern California: Bull. Seis. Soc. Am., 74, 569-576.

Crosson, R.S., 1983, Review of seismicity in the Puget Sound region from 1970, through 1978, *in* Yount, J.C., and Crosson, R.S., eds., Proceedings of workshop 14, Earthquake Hazards of the Puget Sound Region, Washington: U.S. Geological Survey Open-File Report 83-19, p. 6-18.

Crosson, R.S., and T.J. Owens, 1987, Slab geometry of the Cascadia subduction zone beneath Washington from earthquake hypocenters and teleseismic converted waves: Geophys. Res. Lett., 14, 824-827.

Davis, E.E., and Hyndman, R.D., 1989, Accretion and recent deformation of sediments along the northern Cascadia subduction zone: Geol. Soc. Am. Bull., 101, 1465-1480.

Delaney, J. R., Johnson, H. P., and Karsten, J. L., 1981, The Juan de Fuca hotspot-propagating rift system: new tectonic, geochemical and magnetic data: J. Geophys. Res., 86,.11747-11750.

Denlinger, R. P., A model for large-scale plastic yield of the Gorda deformation zone, 1992, J. Geophys.Res., 9., 15,415-15,423.

Dennis J., and Stoddard, Paul R., 1990, Epicenter relocations of Explorer Plate earthquakes: EOS, v. 71, p. 1600-1601.

Dragert, H., Hyndman, R.D., Rogers, G.C., and Wang, K., 1994, Current deformation and the witdh of the seismogenic zone of the northern Cascadia subduction thrust: J. Geophys. Res., 99, 653-668.

Duncan, R.A., 1982, A captured island chain in the Coast Range of Oregon and Washington: J. Geophys. Res., 87, 10,827-10,837.

Engebretson, D. C., Cox, A., and Gordon, R. G., 1985, Relative motions between oceanic and continental plates in the Pacific basin: Geol. Soc. Am. Special Paper, 206, 59 pp.

Flueh, E. R., Bialas, J., Ye, S., Herber, R., Bergmann, P., Schleisiek-Kern, K., von Huene, R., 1994 A digital high data caoacity ocean bottom recorder for seismic investigations. Geomar internal report, 17pp.

Goldfinger, C., Kulm, L.D., Yeats, R.S., Appelgate, B., MacKay, M.E., and Moore, G.F., 1992. Transverse structural trends along the Oregon convergent margin: Implications for Cascadia earthquake potential and crustal rotations: Geology, v. 20, p. 141-144.

Heaton, T.H., and Kanamori, H., 1984, Seismic potential associated with subduction in the northwestern United States: Bull. Seis. Soc. Am., 74, 933-941.

Hyndman, R.D., and Wang, K., 1993, Thermal constraints on the zone of major thrust earthquake failure: the Cascadia subduction zone: J. Geophys. Res., 98, 2039-2060.

Jachens, R.C., and Griscom, A., 1983, Three-dimensional geometry of the Gorda plate beneath northern California: J. Geophys. Res., 88, 9375-9392.

Johnson, S.Y., 1985, Eocene strike-slip faulting and nonmarine basin formation in Washington, *in* Biddle, K. T., and Christie-Blick, N., eds., Strike-slip deformation, basin formation, and sedimentation: Society of Economic Paleontologists and Mineralogists Special Publication 37, 283-302.

Johnson, S.Y., Potter, J.M., and Armentrout, J.M., 1994, Origin and evolution of the Seattle basin and Seattle fault: Geology, 22.

Lay, T., Given, J. W., and Kanamori, H., 1982, Long-period mechanism of the 8 November 1980 Eureka, California, earthquake: Bull. Seis. Soc. Am., 72, 439-456.

Ludwin, R.S., Weaver, C.S., and Crosson, R.S., 1991, Seismicity of Washington and Oregon, *in* The Geology of North America, Neotectonics of North America, vol. CSMV-1, edited by D.B. Slemmons et al., Geol. Soc. Am., Boulder, Colo., 77-98.

Luetgert, J., Mooney, W.D., Criley, E., Keller, G.R., Gridley, J., Miller, K., Trehu, A. Nabelek, J., Smithson, S.B., Humphreys, C., Christensen, N.I., Clowes, R., Asudeh, I, 1992, Crustal velocity structure of the Pacific NW: The 1991 seismic refraction/wide-angle reflection: The Geological Society of America, Abstracts with Programs.

Luetgert, J., 1992. One-Dimensional Seismic Travel Time Modelling, USGS Open File Report, 17pp.

Luetgert, J., 1992. Interactive Two-Dimensional Seismic Raytracing for the Macintosh, USGS Open File Report, 43pp.

MacKay, M.E., Moore, G.F., Cochrane, G.R., Moore, J.C., and Kulm, L.D.l, 1992. Landward vergence and oblique structural trends in the Oregon margin accretionary prism: Implications and effect on fluid flow. Earth Planet. Sci. Lett., v.109, p. 477-491.

MacKay, M.E., Moore, G.F., Klaeschen, D., and von Huene, R., 1995. The case against porosity change: Seismic velocity decrease at the toe of the Oregon accretionary prism. Geology, 23, 827-830.

Masson, D. G., D. A. Cacchione, and D. E. Drake, 1988, Tectonic evolution of Gorda Ridge inferred from sidescan sonar images, Marine Geophysical Researches, 10, 191-204.

Meyers, R. A., D.G. Smith, H.M., Jol. and C.D. Peterson, 1996, Evidence for eight great earthquake-subsidence events detected with ground-penetrating radar, Willapa barrier, Washington: Geology, 24, 99-102.

Muller, J.E., 1977, Evolution of the Pacific margin, Vancouver Island, and adjacent regions: Canadian Journal of Earth Sciences, 14, 2062-2085.

Niem, A.R., Snavely, P.D., Jr., and Niem, W.A., 1990, Onshore-offshore geologic cross section from the Mist Gas field, northern Oregon Coast Range, to the northwest Oregon continental shelf and slope: Oregon Department of Geology and Mineral Industries Continental Margin Transect OGI-17, 46 pp., 1 plate.

Pelayo, A.M., and D.A. Wiens, 1992,Tsunami earthquakes: slow thrust-faulting events in the accretionary wedge: J. Geophys. Res., 97, 15,321-15,337.

Rau, W.W., 1975, Geologic map of the Destruction Island and Taholah quadrangles, Washington: Washington Division of Geology and Earth Resources, Geologic Map GM-13, scale 1:62,500.

Satake, K, K. Shimazaki, Y. Tsuji, and K. Ueda, 1996, Time and size of a giant earthquake in Cascadia inferred from Japanese tsunami records of January, 1700: Nature, 379, 246-249

Savage, J.C., 1983. A dislocation model of strain accumulation and release at a subduction zone, J. Geophys. Res., 88, p. 4984-4996.

Savage, J.C., Lisowski, M., and Prescott, W.H., 1991, Strain accumulation in western Washington: J. Geophys. Res., v. 96, p. 14,493-14,507

Silver, E. A., Late Cenozoic underthrusting of the continental margin off northernmost California, 1969, Science, 166, 1265-1266.

Silver, E. A., pleistocene tectonic accretion of the continental slope off Washington. 1972, Mar. Geol. 13, 239-249.

Simpson, R.W., and Cox, A., 1977, Paleomagnetic evidence for tectonic rotations of the Oregon Coast Range: Geology, 5, 585-589.

Sinton, J. M., and Detrick, R. S., 1992, Mid-ocean ridge magma chambers: J. Geophys. Res., 97,197-216.

Snavely, P.D., Jr., MacLeod, N. S. and Wagner, H.C., 1968, Tholeiitic and alkalic basalts of the Eocene Siletz River Volcanics, Oregon Coast Range: American Journal of Science, v. 266, p. 454-481.

Snavely, P.D., Jr., and MacLeod, N.S., 1974, Yachats Basalt—An upper Eocene differentiated volcanic sequence in the Oregon Coast Range: U.S. Geological Survey Journal of Research, 2, 395-403.

Snavely, P.D., Jr., Pearl, J.E., and Lander, D.L., 1977, Interim report on petroleum resources potential and geologic hazards in the outer continental shelf--Oregon and Washington Tertiary province: U.S. Geological Survey Open-File Report 77-282, 64 p.

Snavely, P.D., Jr., Wagner, H.C, and Lander, D.L., 1980, Geological cross section of the central Oregon continental margin: Geol. Soc. Am., Map and Chart Ser., MC-28J.

Snavely, P.D., Jr., and Wagner, H.C., 1981, Geologic cross section across the continental margin off Cape Flattery, Washington and Vancouver Island, Brithish Columbia: U.S. Geological Survey Open-File Report 81-978.

Snavely, P.D., Jr., and Wagner, H.C., 1982, Geologic cross section across the continental margin of southwestern Washington: U.S. Geological Survey Open-File Report 82-459, 10 p

Snavely, P.D., Jr., Wagner, H.C., and Lander, D.L., 1980b, Geological cross section of the central Oregon continental margin: Geological Society of America Map and Chart Series MC-28J, scale 1:250,000.

Snavely, P.D., Jr., Wagner, H.C., and Rau, W.W., 1982, Sections showing biostratigraphy and correlation of Tertiary rocks penetrated in wells drilled on the southern Oregon continental margin: U.S. Geological Survey Miscellaneous Field Studies Map MF-1482, 1 sheet.

Snavely, P.D., Jr., and Wells, R.E., 1984, Tertiary volcanic and intrusive rocks on the Oregon and Washington continental shelf: U.S. Geological Survey Open-File Report 84-282, 17 pp

Snavely, P.D., Jr., and McClellan, P.H., 1987, Preliminary geologic interpretation of USGS *S.P. Lee* seismic-reflection profile WO 76-7 on the continental shelf and upper slope, northwestern Oregon: U.S. Geological Survey Open-File Report 87-612, 12 p.

Snavely, P.D., Jr., von Huene, Roland, and Miller, J., 1987, The central Oregon margin Lines WO76-4, ***in*** von Huene, R. (ed.), Seismic images of convergent margin tectonic structure: American Association of Petroleum Geologists Studies in Geology No. 26, 24-27.

Snavely, P.D., Jr., 1987, Tertiary geologic framework, neotectonics, and petroleum potential of the Oregon-Washington continental margin, ***in*** Scholl, D.S., Grantz, A., and Vedder, J.G., eds., Geology and resource potential of the continental margin of western North American and adjacent ocean basins; Beaufort Sea top Baja California: Circum-Pacific Council for Energy and Mineral Resources Earth Science Series, 6, 305-335.

Snavely, P.D., Jr., Niem, A.R., and MacLeod, N.S., 1989, Geology of the coastal area between Cape Flattery and Cape Alava, northwest Washington: U.S. Geological Survey Open-File Report 89-141.

Snavely, P.D. Jr., and Kvenvolden, K.A., 1989, Chapter A, Geology and hydrocarbon potential, Preliminary evaluation of the petroleum potential of the Tertiary accretionary terrane, west side of the Olympic Peninsula, Washington: U.S. Geological Survey Bulletin 1892 A-C, 1-17.

Snavely, P.D., Jr., MacLeod, N.S., Niem, A.R., and Minasian, D.L., 1993, Geologic map of Cape Flattery area, Northwestern Olympic Peninsula, Washington: U.S. Geological Survey Miscellaneous Investigations Map; 1:48,000.

Stoddard, P. R., 1991, A comparison of brittle deformation models for the Gorda plate: Tectonophysics,187, 205-214.

Tabor, R.W., and Cady, W.M., 1978, The structure of the Olympic Mountains, Washington—analysis of a subduction zone: U.S. Geological Survey Professional Paper 1033, 38 pp.

Trehu, A.M., Asudeh, I., Brocher, T.M., Luetgert, J.H., Mooney, W.D., Nabelek, J.L. and Y. Nakamura, 1994. Crustal Architecture of the Cascadia Forearc. Science, 266.

U.S. National Research Council, 1993, Solid-earth sciences and society, by the National Research Council, Academy of Sciences Press

Velasco, A. A., Ammon, C. J., and Lay, T., 1993, Recent large earthquakes near Cape Mendocino and in the Gorda Plate: Broadband source time-functions, fault orientations and rupture complexities: J. geophy. Res.

Wannamaker, P.E., Booker, J.R., Jones, A.G., Chave, A.D., Filloux, J.H., Waff, H.S., and Law, L.K., 1989, Resistivity cross section through the Juan de Fuca Subduction system and its tectonic implications, J. Geophys. Res., 94, 14,127-14,444.

Weaver, C.S., and Baker, G. E., 1988, Geometry of the Juan de Fuca plate beneath Washington and northern Oregon from seismicity: Bull. Seis. Soc. Am., 78, 264-275.

Wells, R.E., Engebretson, D.C., Snavely, P.D., Jr., and Coe, R.S., 1984, Cenozoic plate motions and the volcano-tectonic evolution of western Oregon and Washington: Tectonics, 3, 275-294.

Wells, R.E., and P.L.,Heller, 1988, The relative contribution of accretion, shear, and extension to Cenozoic tectonic rotation in the Pacific Northwest: Geol. Soc. Am. Bull., 100, 325-338.

Wells, R. E., Mechanisms of Cenozoic tectonic rotation, Pacific Northwest convergent margin, U.S.A., 1989, *in* Paleomagnetic rotations and continental deformation, NATO ASI Series, edited by C. Kissel and C. Laj, Kluwer Academic Publishers, Dordrecht, 1-16.

Wells, R. E., Paleomagnetic rotations and the Cenozoic tectonics of the Cascade arc, Washington, Oregon, and California, 1990, J. Geophys. Res., 95, 19409-19417.

White, R.S., D. MCKenzie, and R.K. O'Nions, Oceanic crustal thickness from seismic measurements and rare earth element inversions, J. Geophys. Res., 97, 19,683-19,715, 1992

Wilson, D.S., 1989, Deformation of the so-called Gorda Plate: J. Geophys. Res., 94, 3065-3075.

Zandt, G., and Furlong, K.P., 1982, Evolution and thickness of the lithosphere beneath coastal California: Geology, 10, 376-381.

Zelt, C.A. and R.B. Smith, 1992. Seismic traveltime inversion for 2-D crustal velocity structure. Geophys. J. Int., 108, p 16-34.

Zelt, C.A. and D.A. Forsyth, 1994. Modelling wide-angle seismic data for crustal structure: southeastern Grenville province, J. Geophys. Res., 99, p 11687-11704.

9 APENDICES

9.1 REPORT OF THE LAND RECORDING

9.2 DETAILS OF OBH/OBS DEPLOYMENTS

9.3 REPORT ABOUT NAVIGATION ERROR

9.4 CAPTAINS REPORT

9.5 PRESS CLIPPINGS

Onshore Recording of Airgun Sources

Tom Parsons (U.S. Geological Survey; MS 999 345 Middlefield Rd.; Menlo Park, CA 94025; (415)354-3102; FAX (415) 354-3191; tparsons@octopus.wr.usgs.gov)

Anne Trehu (College of Oceanic and Atmospheric Science; Oregon State Un.; Corvallis, OR 97331; (541)737-2655; FAX (541) 737-2064; trehu@oce.orst.edu)

Airgun sources detonated by the Sonne were recorded by 5 east-west trending on-land seismometer deployments (Figure A1). Two of these deployments were installed and maintained in the state of Oregon by Oregon State University (OSU) (Anne Trehu), and three deployments were installed and maintained in the State of Washington by the U.S. Geological Survey (USGS) (Tom Parsons). In all, 93 Reftek seismographs were installed, each of which recorded continuous data from a single 4.5 Hz L28 geophone at a rate of 125 samples/s. The objective of these deployments is to record traveltime and amplitude information about primary and secondary seismic arrivals in order to derive the velocity structure of the North American plate and underlying Juan de Fuca plate beneath the coastal region. Of particular interest is the shape and nature of the boundary between the thick, mafic Siletz terrane and accretionary complex rocks to the west of it; this boundary varies significantly from Oregon, where it occurs offshore, and the Olympic Peninsula in Washington, where it occurs more than 100 km east of the coast in places.

The southernmost east-west profile was located in central Oregon and was located approx. 20 km south of a similar profile recorded in 1989 [Trehu et al., 1994]. This profile included 29 stations located about 3 km apart and recorded airgun sources from the offshore-Oregon east-west and north-south OBS profiles. Seven additional sites were located north and south of the primary profile for comparison with the 1989 data and to provide additional 3-dimensional control on structure. The second Oregon profile was located in northern Oregon near the latitude of the city of Portland; this profile comprised 10 instruments located at 8 km intervals.

The southernmost Washington profile was coincident with the western half of an onshore refraction line that was recorded in September of 1995 by the USGS, OSU, and the University of Texas, El Paso (UTEP) (Kate Miller); this profile extended from Willapa Bay to the town of Centralia (46°30') and had 14 stations at 5 km intervals. The second Washington profile extended from Greys Harbor towards the city of Olympia (47°) and had 15 stations at 5 km intervals. The northernmost Washington profile extended from the town of Klaloch on the coast along the southern boundary of Olympic National Park towards the city of Seattle (47°35'), and had 18 stations at 5 km intervals.

A M5.3 earthquake occurred at 21:04 22.67 PST on May 2, 1996, and was located at 47°45'62"N and 121°52'53"W (near the town of Duval, Washington, east of Seattle). This earthquake was recorded by all stations on the southern Washington profile and by 4 stations on the northern Washington profile (the only stations that were in operation when the earthquake occurred). At least 50 aftershocks were recorded in the following days by all three Washington profiles. Traveltimes from these aftershocks will be used to supplement velocity models generated from offshore airgun sources.

Because shot navigation and timing information are not yet available, only single trace data have been inspected. Clear arrivals are observed from airguns on both the Oregon and Washington deployments. A thorough evaluation of data quality, however, awaits formatting of the data into reduced record sections.

Trehu, A.M., I. Asudeh, T.M. Brocher, J. Luetgert, W.D. Mooney, J.L. Nabelek, Y. Nakamura, Crustal architecture of the Cascadia forearc, Science,v. 265, pp. 237-243, 1994.

Figure A1. Map of western Oregon and Washington showing the location of the seismographs deployed to record airgun shots during this project (black squares). The locations of major cities and of onshore seismic refraction profiles obtained in 1991 and 1995 (dots - seismographs; stars - shots) are also shown.

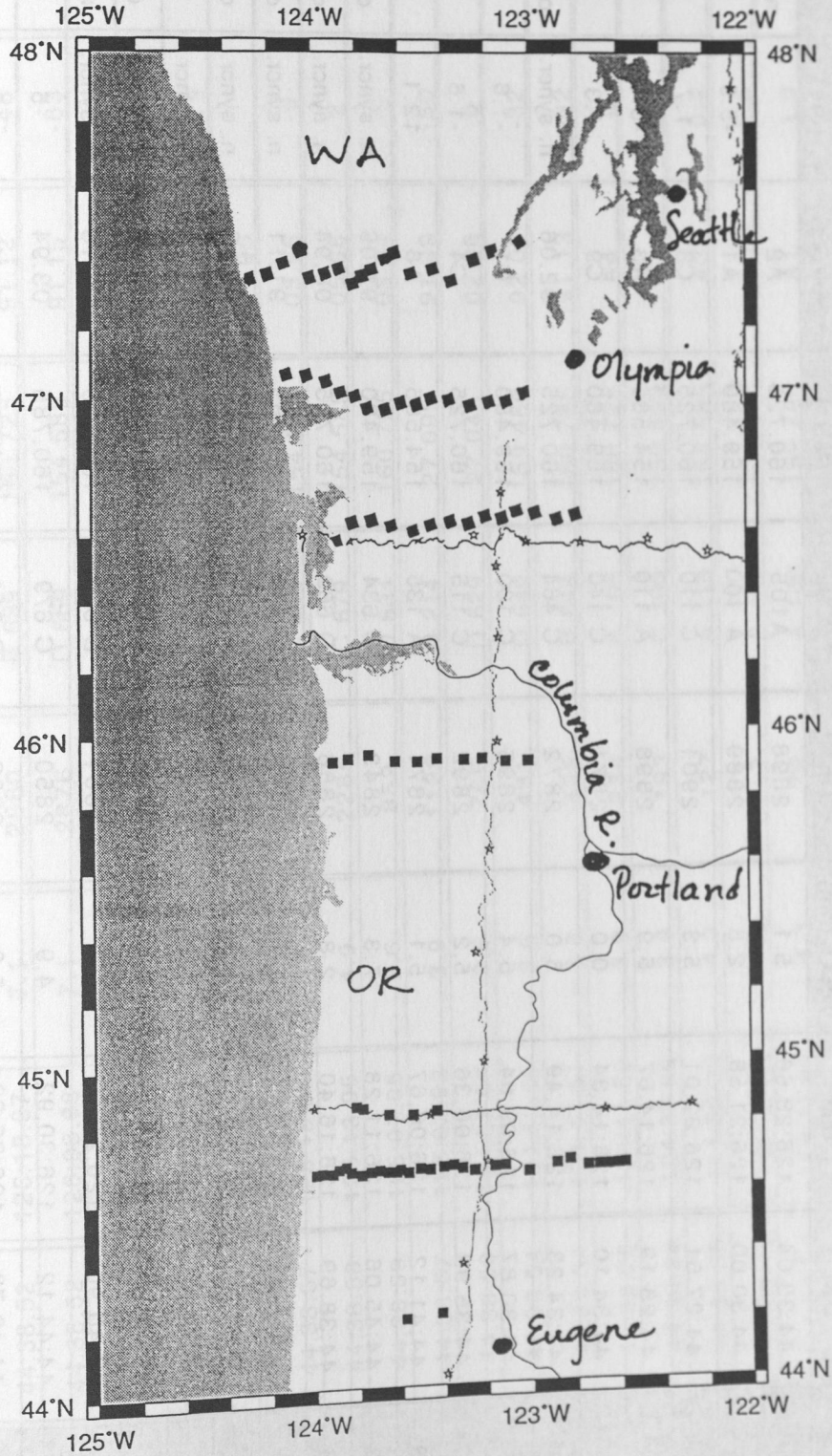

SO108 - ROSETTE, PROFILES 1, 2, 4, 5 and 6

INSTRUMENT	LAT (N)	LON (W)	DIST. TO	DEPTH	RELEASER-	FREQUENCY	RECORDER	SKEW	REMARKS
	D:M	D:M	NEXT (nm)	(m)	CODE	(MHz)	NUMBER	(ms)	
OBS 01	44:30.04	126:28.66	5.1	2898	A105	160.725	A2		not recovered
OBS 02	44:30.00	126:21.58	2.5	2889	A 100	159.480	A1	-5.9	
OBS 03	44:27.51	126:22.01	5.3	2901	C 110	160.725	C3	1.7	
OBS 04	44:28.19	126:14.67	5.9	2898	A 110	154.585	A3	-0.1	
OBS 05	44:34.10	126:14.34	0.0	2871	C 140	159.480	C9	4.3	
OBH 01	44:34.23	126:14.49	5.0	2872	C 464	160.725	92.06	n. syncr.	only profile 1
OBS 06	44:30.87	126:09.04	5.4	2895	C 100	159.480	C1	-1.6	
OBS 07	44:35.92	126:06.36	5.2	2892	C 115	160.725	C4	-1.6	
OBS 08	44:41.12	126:06.67	5.1	2871	A 135	154.585	A8	12.1	
OBH 02	44:45.06	126:11.28	7.3	2843	D 634	159.480	91.09	n. syncr.	only prof. 1, 2
OBH 03	44:38.69	126:16.40	2.8	2886	D 669	160.725	08.94	n. syncr.	only prof. 1, 2, 4
OBH 04	44:37.66	126:20.07	2.1	2887	C 444	154.585	91.11	n. syncr.	only prof. 1, 2
OBH 05	44:36.96	126:22.79	7.4	2895	A 324	159.480	91.12	n. syncr.	only prof. 1, 2, 4
OBH 06	44:34.32	126:32.53	5.1	2881	C 454	159.480	91.15	n. syncr.	
OBH 07	44:39.34	126:34.13	6.4	2865	D 644	154.585	02.95	n. syncr.	only prof. 1, 2
OBH 08	44:40.90	126:25.46	5.1	2851	B 639	160.725	91.13	n. syncr.	no data rec.
OBH 09	44:44.12	126:30.92	4.9	2850	C 679	160.785	03.94	-6	
OBH 10	44:46.78	126:25.23	5.3	2832	B 214	154.585	01.95	-6	
OBH 11	44:44.53	126:18.57	2.6	2838	C 459	160.785	05.96	3	
OBH 12	44:47.05	126:18.04		2831	D 629	160.725	91.14	-92	only prof. 1, 2
Trigger							06.96	-2	

SO108 - OREGON E-W, PROFILE 7

INSTRUMENT	LAT (N)	LON (W)	DIST. TO	DEPTH	RELEASER-	FREQUENCY	RECORDER	SKEW	REMARKS
	D:M	D:M	NEXT (nm)	(m)	CODE	(MHz)	NUMBER	(ms)	
OBH 13	44:38.52	126:28.98	7.1	2859	A 324	159.480	91.14	-89	
OBH 14	44:38.52	126:18.97	7.1	2860	B 639	160.725	91.12	-48	
OBH 15	44:38.52	126:08.98	7.1	2876	D 669	154.585	91.15	-63	
OBH 16	44:38.54	125:59.01	7.1	2908	C 444	160.785	91.11	-18	
OBH 17	44:38.28	125:49.09	7.1	2871	C 454	160.725	02.95	-14	at 1300 mbsl
OBH 18	44:38.59	125:39.00	7.1	2863	C 464	160.785	08.94	-13	
OBH 19	44:38.57	125:28.96	7.1	2858	D 644	154.585	01.95		no data rec.
OBH 20	44:38.57	125:18.95	3.6	2909	C 459	154.585	03.96	-9	
OBH 21	44:38.56	125:13.95	4.9	2285	C 679	154.585	05.96	2	
OBH 22	44:38.59	125:07.95	3.6	859	D 634	160.725	03.94	-5	
OBH 23	44:38.57	125:02.92	3.9	1139	B 214	27.095	91.09	-50	
OBH 24	44:38.50	124:57.57	3.6	769	D 629	27.045	02.96	0	very noisy
OBH 25	44:38.54	124:52.55	3.6	431	D 649	159.480	92.06	-32	
OBH 26	44:38.54	124:47.51	3.6	335	B 644	160.785	91.13	-32	very noisy
OBS 09	44:38.28	124:41.80	3.9	234	A 105	160.725	A4	0	
OBS 10	44:38.34	124:35.99	3.9	193	C 100	159.480	C1	-0.6	
OBS 11	44:38.35	124:30.20	4.3	127	A 110	154.585	A3	0.4	
OBS 12	44:38.44	124:23.96	4.0	75	A 135	154.585	A8	2.5	
OBS 13	44:38.34	124:17.91	4.3	79	A 100	159.480	A1	1.9	
OBS 14	44:38.30	124:11.41		59	C 140	159.480	C9	-2.6	
TRIGGER							06.96	-5	

SO108 - OREGON N-S, PROFILES 8 and 9

INSTRUMENT	LAT (N)	LON (W)	DIST. TO	DEPTH	RELEASER-	FREQUENCY	RECORDER	SKEW	REMARKS
	D:M	D:M	NEXT (nm)	(m)	CODE	(MHz)	NUMBER	(ms)	
OBH 27	44:51.35	124:37.87	6.9	352	B 644	154.585	91.09	-50	
OBH 28	44:44.63	124:39.99	6.6	291	D 649	160.785	05.96	0	
OBS 09	44:38.45	124:41.89	3.5	234	A 105	160.725	A4	0	
OBS 10	44:38.42	124:35.97	9.2	193	C 100	159.48	C1	-0.6	
OBH 29	44:31.32	124:43.89	6.6	349	B 214	159.48	02.96	-2	
OBH 30	44:24.83	124:45.81	7.1	181	D 629	160.725	92.06	-34	
OBH 31	44:17.93	124:47.94	6.6	152	C 679	160.785	03.94	0	
OBH 32	44:11.44	124:49.92	16	89	D 634	159.48	03.96	-12	
OBH 33	44:17.87	124:28.52	7.5	99	D 644	160.725	01.95	-3	
OBH 34	44:25.33	124:27.99	6.6	81	C 459	154.585	08.94	-14	
OBH 35	44:31.92	124:27.41	6.6	77	C 454	160.725	02.95	-12	
OBS 15	44:38.49	124:27.01	6.5	100	C 115	160.725	C4	-0.8	
OBH 36	44:45.02	124:26.54	6.5	130	C 464	160.785	91.11	-12	
OBH 37	44:51.52	124:26.02	7.6	165	D 669	154.585	91.15	recovered	by fisherman
OBH 38	44:59.17	124:25.38		271	A 324	154.585	91.14	-90	
TRIGGER							04.96	-3	

SO108 SOUTH-WEST - WASHINGTON E-W, PROFILE 10

INSTRUMENT	LAT (N)	LON (W)	DIST. TO	DEPTH	RELEASER-	FREQUENCY	RECORDER	SKEW	REMARKS
	D:M	D:M	NEXT (nm)	(m)	CODE	(MHz)	NUMBER	(ms)	
OBH 39	46:38.99	126:26.99	6.2	2650	A 324	160.725	91.14	-90	
OBH539(VA01)	46:39.01	126:18.02	6.2	2649	C 464	160.725	08.94	-13	Cass. VA 01
OBH 40	46:38.98	126:08.99	6.2	2629	C 454	160.785	02.95	-13	
OBH 41	46:38.99	125:59.97	4.8	2602	C 459	154.585	01.95	n. syncr.	
OBH 42	46:39.01	125:53.01	4.8	2498	D 644	159.480	03.96	-8	
OBH 43	46:39.01	125:45.99	4.8	1934	B 639	160.725	91.12	n. syncr.	
OBS 16	46:38.99	125:38.93	4.8	1989	A 115	160.725	A 4	0.4	
OBS 17	46:38.99	125:31.59	4.8	2129	C 100	159.480	C 1	0.3	
OBS 18	46:38.99	125:24.94	4.8	1913	C 115	160.225	C 4	-0.9	
OBH 44	46:38.97	125:17.94	4.8	1900	D 634	159.480	03.94	0	
OBH 45	46:39.04	125:10.98	4.8	1020	D 629	160.785	01.96	1	
OBH 46	46:39.02	125:03.92	4.8	1059	C 679	160.725	91.09	-55	
OBH 47	46:39.04	124:56.94	4.8	736	B 214	154.585	02.91	-2	
OBH 48	46:39.01	124:50.06	4.1	474	D 649	160.725	91.11	-18	
OBH 49 (VA11)	46:38.93	124:43.50	3.4	335	D 738	159.480	15.93	-42	Vertikalarray
OBH 50	46:38.98	124:38.94	3.4	157	C 444	154.585	05.96	1	Cass. "OBH49"
OBH 51	46:39.00	124:33.99	3.4	135	B 644	160.725	92.06	-51	
OBS 19	46:38.98	124:29.00	3.4	108	C 140	159.480	C 9	-0.4	
OBS 20	46:38.99	124:24.00	3.4	84	A 100	159.480	A 1	-0.3	
OBS 21	46:38.98	124:18.99	3.4	68	A 135	154.585	A 8	6	
OBS 22	46:38.99	124:14.03		48	A 110	154.585	A 3	0.6	
TRIGGER							06.96	-4	

SO108 - WASHINGTON N-S, PROFILE 11

INSTRUMENT	LAT (N)	LON (W)	DIST. TO	DEPTH	RELEASER-	FREQUENCY	RECORDER	SKEW	REMARKS
	D:M	D:M	NEXT (nm)	(m)	CODE	(MHz)	NUMBER	(ms)	
OBS 23	45:50.97	124:10.29	5,9	99	A 105	160.785	A4	-2.6	
OBS 24	45:56.59	124:13.04	7,2	105	C 100	159480	C1	0.3	
OBS 25	46:03.28	124:16.383	8,2	105	C 115	160.725	C4	-0.5	
OBH 52	46:11.13	124:20.20	7,1	112	D 649	159.480	91.15	-86	
OBH 53	46:17.82	124:23.51	8,5	172	D 669	160.785	91.11	172	
OBH 54	46:25.85	124:27.52	7,5	124	C 679	154.585	91.09	-70	
OBH 55	46:32.89	124:30.96	6,4	456	B 214	160.785	96.02	-7	
OBH 56	46:38.99	124:34.02	6,9	137	B 644	160.725	91.12	-57	
OBH 57	46:45.49	124:37.25	6,3	123	C 444	154.585	96.03	-11	
OBH 58	46:51.40	124:40.25	8,4	128	D 634	159.480	95.02	-18	
OBH 59	46:59.37	124:44.18	6,9	130	D 629	154.585	91.14	-128	
OBH 60	47:05.83	124:47.49	6,7	130	C 459	160.725	94.08	-17	
OBH 61	47:12.19	124:50.65	6,7	150	B 639	154.585	92.06	-54	
OBH 62	47:18.52	124:53.77	6,9	655	C 454	160.785	94.03	0	
VA 12	47:25.20	124:57.08	6,1	1105	D 738	160.725	93.15	-61	
OBH 63	47:30.75	124:59.94	6,1	387	C 464	159.480	95.01	-3	
OBH 64	47:36.52	125:02.94	6,0	187	A 324	160.725	96.04	-7	
OBS 26	47:42.50	125:05.47	7,2	376	C 140	159.480	C9	-0.3	
OBS 27	47:48.94	125:09.97	7,8	353	A 135	154.585	A8	13.9	
OBS 28	47:56.34	125:13.05	7,3	176	A 100	159.480	A1	-0.6	
OBS 29	48:03.30	125:16.57	7,1	150	A 110	154.585	A3	0.6	
TRIGGER							06.96	-6	

SO108 - OLYMPIC E-W, PROFILE 12

INSTRUMENT	LAT (N)	LON (W)	DIST. TO	DEPTH	RELEASER-	FREQUENCY	RECORDER	SKEW	REMARKS
	D:M	D:M	NEXT (nm)	(m)	CODE	(MHz)	NUMBER	(ms)	
OBS 30	47:34.34	124:39.95	3.7	67	A 100	159.480	A 1	-0.5	
OBS 31	47:33.34	124:45.19	3.2	93	A 110	154.585	A 3	-0.3	
OBS 32	47:32.46	124:49.75	3.5	121	A 135	154.585	A 8	-2.8	
OBS 33	47:31.58	124:54.82	3.6	171	C 100	159.480	C 1	N/A	no data
OBH 65	47:30.60	124:59.97	3.2	356	C 454	159.480	04.96	-5	
OBH 66	47:29.75	125:04.47	2.3	915	C 459	160.725	03.94	1	dragged 4 miles by fisherman
OBH 67	47:29.07	125:07.76	2.6	633	A 324	154.585	92.06	-37	
OBH 68	47:28.38	125:11.51	1.9	632	C 464	160.785	01.95	-1	
OBH 69	47:27.98	125:14.12	3.2	778	B 639	160.725	91.14	-100	
OBH 70	47:27.07	125:18.67	3.8	1402	D 629	159.480	91.12	-51	
OBS 34	47:26.26	125:22.90	2.8	1492	C 115	160.725	C 4	0.4	
OBS 35	47:25.27	125:28.29	3.9	1484	C 140	159.480	C 9	-0.5	
OBS 36	47:24.25	125:33.94	4.4	1478	A 115	160.785	A 4	-2.9	
OBH 71	47:23.01	125:40.19	4.6	1365	D 634	160.725	08.94	-12	
OBH 72	47:21.78	125:46.67	5.8	1766	C 444	154.585	03.96	-9	
OBH 73	47:20.26	125:54.77	5.6	1827	B 214	160.785	02.95	n. syncr.	
OBH 74	47:18.74	126:02.74	5.5	1987	B 644	159.480	91.09	-57	
OBH 75	47:17.37	126:10.57	4.8	2494	D 669	160.725	91.11	-18	
VA 13	47:16.07	126:17.61	5.7	2506	D 738	160.785	15.93	-52	
OBH 76	47:14.53	126:25.41	5.8	2539	C 679	154.585	91.15	-68	
OBH 77	47:12.78	126:33.74		2558	D 649	159.480	06.96	-6	at 1000 mbsl
TRIGGER							01.96	4	

Betr.: Fehlerhafte Positionsausgabe des Navigationsfilters

Am 27.04.1996 um 12:50 Uhr UTC (05:50 Uhr Ortszeit) wurde vom wachhabenden nautischen Offizier durch Radarortung festgestellt, dass das Schiff rund 2,6 Minuten in der Laengenposition vom angezeigten Filterwert entfernt war. (Radarort = Istposition: 124 Grad 10,624 Minuten West; Filterwert des Systems: 124 Grad 08,0 Minuten West; Breite einheitlich bei 44 Grad 38,55 Minuten Nord.)

Zum Vergleich wurde der ungefilterte GPS-Wert herangezogen. Der Abstand von GPS zu Filterposition stimmte mit dem der Radarpeilung bis auf wenige hundertstel Laengenminuten ueberein.

Nach dem unverzueglichen Ruecksetzen des Navigationsfilters durch den Systemmanager "sprang" das Schiff, in der auf dem Brueckenmonitor angezeigten Filterposition, um die erwaehnten rund 2 Seemeilen, auf die mittels Radar und GPS errechnete Position.

Um die Filterpositionen des 27. mit den reinen GPS-Daten des gleichen Zeitraumes vergleichen zu koennen wurde am 28. um 02:40 (UTC), also nach dem Backup der 24h-Datenbank auf Tape, versucht die GPS-Daten aus den Nav-Datenbank auszulesen. Dabei wurde festgestellt, dass die Datenbank des 27. nur einen Bruchteil der normalen Groesse besass. Auf der Datenbank waren lediglich rund 40 Minuten der Zeit UNMITTELBAR NACH dem Reset des Navigationsinterfaces, sowie ungefaehr zwei Stunden von 20 bis 22 Uhr des Tages, protokolliert. Es muss davon ausgegangen werden, dass der Reset des Navigationsinterfaces unverstaendlicherweise auch einen Reset der Datenbank verursachte. Da die GPS-Daten leider auch nicht in die Wiss-Datenbank eingelesen werden, konnte das Entstehen des Fehlers nicht nachvollzogen werden.

Nach Bericht der Nautik besteht dieMoeglichkeit eines Zusammenhanges mit einem Ausfall des Doppler-Logs zu Beginn der fraglichen Stoerungszeit. Gegen 01 Uhr Ortszeit wurde beim Aussetzen eines OBH bemerkt, dass das DOLOG noch 5,7 Knoten Fahrt anzeigte waehrend das Schiff schon ohne Fahrt an der gewaehlten Aussetzposition lag. Darauf wurde vom diensthabenden Nautiker auf das EM-Log gewechselt, welches korrekte Werte anzeigte. Nach dem Aussetzvorgang (ca. 7-10 min) reagierte das Display des DOLOG wieder normal und es wurde auf DOLOG zurueckgeschaltet.

Waehrend des Vorfalls waren die Eingaengssensoren Position, Fahrt ueber Grund und Fahrt durchs Wasser auf "Filter" geschaltet.

Durch die Auftauchpositionen der waehrend des fraglichen Zeitraumes (nach Filterpositionen) ausgesetzten OBHs war es moeglich einen groben Ueberblick ueber die Entstehung des Positionsfehlers zu erhalten. Demnach hat sich der Fehler nach Einschalten des EM-Logs progressiv bis zum Reset des Filters erhoeht. Es folgen die Soll- und Istpositionen der OBHs, wobei nur die Laengenwerte beider Positionen getrennt angegeben werden, da sich alle Positionen annaehernd auf einer Breite von 44 Grad 38,5 Minuten Nord befinden:

Geraet	fehlerhafter Filterwert	Tatsaechlicher Wert	Breitenwert
OBH 26:	124 Grad 47,507 Min W	124 Grad 47,2 Min W	44 Grad 38,5 Min N
OBS 9	124 Grad 42,500 Min W	124 Grad 41,8 Min W	44 Grad 38,5 Min N
OBS 10	124 Grad 37,000 Min W	124 Grad 35,9 Min W	44 Grad 38,5 Min N
OBS 11	124 Grad 31,500 Min W	124 Grad 30,2 Min W	44 Grad 38,5 Min N
OBS 12	124 Grad 25,500 Min W	124 Grad 24,1 Min W	44 Grad 38,5 Min N
OBS 13	124 Grad 19,947 Min W	124 Grad 17,9 Min W	44 Grad 38,5 Min N
OBS 14	124 Grad 14,000 Min W	124 Grad 11,42 Min W	44 Grad 38,5 Min N

Des Weiteren konnte ein erneutes Versagen des Positionsfilters protokolliert werden:

Waehrend des Aufnehmens der OBHs (und OBSse) am 10.05. um 02 Uhr Ortszeit wurde durch den diensthabenden Nautiker beim Beschleunigen nach der Aufnahme eines OBHs festgestellt, dass das DOLOG "nachging". Das Dolog gab noch eine Fahrt von 2,05 Knoten im "Bottom-Track", und eine Fahrt von 7.03 Knoten im "Water-Track" an, waehrend das EM-Log schon 9 Knoten anzeigte. Letzteres konnte durch Beobachtungen des Nautikers als realer Wert bestaetigt werden. Die Anzeige des Dolog hat sich nach wenigen Minuten der Realitaet angepasst. Auch zu diesem Zeitpunkt waren die schon oben angesprochenen Systemeingaenge, wie praktisch staendig, auf "Filter" eingestellt

In der folgenden Zeit konnte durch die Nautik und einen hinzugerufenen Systemmanager beobachtet werden, dass die Filterposition mit progressivem Verhalten von der GPS-Position Abwich. Das Schiff befand sich zur Zeit des Vorfalls auf einem Nord-Sued-Kurs. Als Beispiel folgende Positionsangaben:

Zeit	Fehlerhafter Filterwert	Tatsaechlicher Wert (nach GPS)
02:08	44:50,68N; 124:37,80W	44:50,19N; 124:38,03W
02:20	44:47,7N; 124:38,63W	44:48,32N; 124:38,83W

Um 02:30 wurde der Filter von dem BAP aus zurueckgesetzt. Der Sprung betrug laut Positionsalarm beim Zuruecksetzen des Filters 1231 m. Die Positionswerte der fraglichen Zeit sind sowohl als reine GPS-Daten als auch als Filterwerte verfuegbar.

In einer Besprechung der Systemmanager und der Nautiker am folgenden Tag wurde als Resumee festgestellt, dass der Filterwert nicht zuverlaessig und gefahrlos zur Navigation verwendet werden kann. Die groesste Gefahr entsteht dadurch, dass sich der Filterwert OHNE ALARM und vermutlich mit zunehmender Geschwindigkeit von der realen (oder GPS-) Position entfernt. Dies ist fuer die Forschung (Nutzer), die zumeist auf exakte Positionierung angewiesen ist,unzumutbar und, besonders im kuestennahen Bereich auch eine Gefaehrdung von Schiff und Besatzung.

Wenn ein solches Auseinanderklaffen der tatsaechlichen- und der Filterpositionen in zukuenftigen Filterversionen nicht ausgeschlossen werden kann, sollte als Minimalanforderung ein Positionsalarm ausgeloest werden, wenn sich der Filterwert ueber einen bestimmten Grenzwert von den GPS-Werten entfernt (ein Entfernungsbereich, der mit dem des Positionssprungalarms gekoppelt ist, erscheint hier angebracht).

R. F. Reedereigemeinschaft
Forschungsschiffahrt GmbH

F.S. "S O N N E"
Kapt. H.Papenhagen

STATIONSPROTOKOLL "FS S O N N E" Reise SO - 108

Gebrauchte Abkürzungen für die eingesetzten Geräte und Anzahl der Einsätze mit Winde:

Releaser	Releaser-Test OBH's	2 mal	Geo-Winde 6
CTD/ROS	Kranzwasserschöpfer mit CTD-Sonde	1 mal	W 5
OBH	Ocean Bottom Hydrophon (12 Stck)	77 mal	
OBS	Ocean Bottom Seismograph (8 Stck)	36 mal	
OBH	mit Vertikalhydrofonen (1 Stk)	3 mal	

Eingesetzte Winden: Reise: **SO 108**

Winde	Bestückt mit	RF-Nummer	Einsatzzeit	gesamt Einsatzzeit	gefahrene. SL	max. SL	Zustand
W1	NSW-Kabel 18,2 mm	813004	0,0 h	141,6 h	-- m	-- m	2
W2	LWL-Kabel 18,2 mm	865017	0,0 h	165,6 h	30.688 m	3.961 m	2
W4	Bedea-Kab. 11,0 mm	815300	0,0 h	0,0 h	-- m	-- m	1
W5	NSW-Kabel 11,0 mm	814117	1,0 h	46,4 h	6.970 m	2.899 m	2
W6	Drako-Dra. 18,2 mm	813005	4,8 h	654,0 h	171.200 m	2.900 m	3

Profilmeilen: Reflexionsseismik 1233 km
Refraktionsseismik 1385 km

Geräteverluste:

1 OBS

Abkürzungen im Stationsprotokoll :

z.W.	Zu Wasser
a.D.	An Deck
Boko	Bodenkontakt
Bosi	Bodensicht
SL	Ausgesteckte Seillänge
WT	Wassertiefe (alle Angaben nach Hydrosweep)
(W x)	eingesetzte Winde
HS./PS.	Hydrosweep/Parasound
Releaser	Releaser für OBH's
OBH	Ocean Bottom Hydrphon
OBS	Ocean Bottom Seismograph
RF	Reflexionsseismik
RS	Refraktionsseismik

Stationsarbeiten alle Zeiten UTC - 7 Stunden

20.04.1996 Teststation 1 W 06

0835	Beginn Testation 1	40 50,0 N 125 05,0 W
0843	Releaser z.W.	
0944	SLmax = 2750 m WT = 2900 m	
0945 - 1008	Test von 12 Releasern	
1008	Beginn Hieven	
1123	Release a.D. , Ende Station	

1315 - 1410	bringen Stb. airgun-array aus		
1440	Schießbwginn		
1530 - 1544	bringen Bb. airgun-array aus		
1635	Schießende		
1645 - 1658	holen Bb.-array ein		
1700 - 1720	holen Stb.-array ein		
20.04.1996	**Teststation 2 W 06**		
1720	Beginn Station	41 23,6 N	125 17,4 W
1725	Releaser z.W.		
1823	SLmax = 2900 m WT = 3131 m		
1824 - 1840	Test 12 Releaser		
1840	Beginn Hieven		
1943	Releaser a.D., Ende Station		
21.04.1996			
Wetter : max. SSW 7 ; 6 ; bedeckt, Regen			
0800		43 46,5 N	126 11,7 W
0815	Beginn Auslegen streamer		
	Entfernung Bleibeschwerung		
2055	Ende Ausbringung, Beginn Hieven		
2153	Streamer a.D.	44 16,6 N	126 31,7 W
2320	OBS 01 z.W. WT = 2898 m	44 30,30 N	126 28,65 W
22.04.1996			
max. SSW 8 ; 7 ; bedeckt, Regen			
0006	OBS 02 z.W. WT = 2892 m	44 29,98 N	126 21,58 W
0040	OBS 03 z.W. WT = 2903 m	44 27,49 N	126 22,40 W
0124	OBS 04 z.W. WT = 2900 m	44 28,18 N	126 14,69 W
0221	OBS 05 z.W. WT = 2872 m	44 34,10 N	126 14,33 W
0231	OBH 01 z.W. WT = 2872 m	44 34,23 N	126 14,49 W
0317	OBS 06 z.W. WT = 2896 m	44 30,85 N	126 09,03 W
0406	OBS 07 z.W. WT = 2890 m	44 35,90 N	126 06,40 W
0451	OBS 08 z.W. WT = 2871 m	44 41,14 N	126 06,63 W
0532	OBH 02 z.W. WT = 2843 m	44 45,03 N	126 11,30 W
0638	OBH 03 z.W. WT = 2826 m	44 38,63 N	126 16,40 W
0712	OBH 04 z.W. WT = 2888 m	44 37,65 N	126 20,05 W
0736	OBH 05 z.W. WT = 2894 m	44 36,95 N	126 22,80 W
0843	OBH 06 z.W. WT = 2882 m	44 34,33 N	126 32,52 W
0920	OBH 07 z.W. WT = 2872 m	44 39,35 N	126 34,12 W
1006	OBH 08 z.W. WT = 2851 m	44 40,90 N	126 25,47 W
1045	OBH 09 z.W. WT = 2850 m	44 44,10 N	126 30,92 W
1127	OBH 10 z.W. WT = 2831 m	44 46,77 N	126 25,24 W
1217	OBH 11 z.W. WT = 2829 m	44 44,50 N	126 18,62 W
1313	OBH 12 z.W. WT = 2833 m	44 47,07 N	126 18,06 W
1500 - 1523	bringen Stb.-airgun-array aus		
1525 - 1547	bringen Bb.-airgun-array aus		
1612	Beginn Profil 01 RF/HS	45 01,6 N	12616,0 W
2118	2 airguns defekt	44 30,6 N	126 21,5 W
2400			
23.04.1996			
max. SzW 9 ; 8 ; bedeckt, Regen , südliche Dünung 5 m			
0200	Ende Profil 01	44 22,7 N	126 23,0 W
0408	Beginn Profil 02 RF/HS/PS	44 23,4 N	126 12,1 W
1054	brechen Profil 02 ab wegen Schlechtwetter	44 49,2 N	126 26,7 W
	insgesamt 5 airguns ausgefallen		

1111 - 1125	holen Bb.-airgun-array ein		
1136 - 1207	holen Stb.-airgun-array ein		
24.04.1996			
max. WSW 7 ; 6 ; bedeckt, Regen, w`liche Dünung 5 m			
0800 - 1005	Anfahrt OBH 12		
0932	lösen OBH aus		
1017	OBH 12 a.D.	44 47,2 N	126 18,0 W
1200 - 1310	setzen Bb.-airgun-array aus		
1313	Beginn Profil 03 RF/HS/PS	44 39,0 N	126 31,9 W
1814	Ende Profil 03	44 35,0 N	125 59,6 W
1832 - 2000	setzen Stb.-airgun-array aus		
2031	Beginn Profil 04 RF/HS/PS	44 43,0 N	126 00,1 W
25.04.1996			
max. W 8 ; 7 ; bedeckt, regen , WSW`liche Dünung, 5 m			
0254	Ende Profil 04	44 32,6 N	126 39,1 W
0424	Beginn Profil 05 RF/HS/PS	44 26,3 N	126 33,1 W
1052	Ende Profil 05	44 49,8 N	126 06,0 W
1055 - 1135	holen Stb.-airgun-array ein		
1142 - 1155	holen Bb.-airgun-array ein		
1354	lösen OBH 02 aus		
1437	OBH 02 a.D.	44 45,2 N	126 11,3 W
1457	lösen OBH 11 aus		
1536	OBH 11 a.D.	44 44,7 N	126 18,6 W
1550	lösen OBH 10 aus		
1637	OBH 10 a.D.	44 46,9 N	126 25,2 W
1657	OBH 09 ausgelöst		
1737	OBH 09 a.D.	44 44,2 N	126 30,8 W
1802	OBH 07 ausgelöst		
1837	OBH 07 a.D.	44 39,4 N	126 34,2 W
1900	OBH 06 ausgelöst		
1935	OBH a.D.	44 34,3 N	126 32,6 W
2025 - 2240	versuchen OBS zu releasen, kein Erfolg		
2315	OBS 02 ausgelöst		
2332	OBS 02 a.D.	44 30,2 N	126 21,6 W
2337	OBS 03 ausgelöst		
26.04.1996			
max. W 4 ; 3 ; wolkig , W`liche Dünung 5 - 3 m			
0042	OBS 03 a.D.	44 27,6 N	126 22,1 W
0045	OBS 04 ausgelöst		
0147	OBS 04 a.D.	44 28,4 N	126 14,8 W
0151	OBS 05 ausgelöst		
0254	OBS 05 a.D.	44 34,3 N	126 14,4 W
0259	OBH 01 ausgelöst		
0405	OBH 01 a.D.	44 34,4 N	126 14,5 W
0414	OBS 06 ausgelöst		
0508	OBS 06 a.D.	44 31,2 N	126 09,0 W
0515	OBS 07 ausgelöst		
0614	OBS 07 a.D.	44 36,0 N	126 06,3 W
0618	OBS 08 ausgelöst		
0710	OBS 08 a.D.	44 41,3 N	126 06,8 W
0742	OBH 03 ausgelöst		
0818	OBH 03 a.D.	44 38,7 N	126 16,5 W
0820	OBH 04 ausgelöst		
0902	OBH 04 a.D.	44 37,7 N	126 20,1 W
0905	OBH 05 ausgelöst		
0939	OBH 05 a.D.	44 37,0 N	126 22,8 W

0944	OBH 08 ausgelöst					
1019	OBH 08 a.D.				44 40,9 N	126 25,4 W
1130	versuchen OBS 01 zu releasen, kein Erfolg					
1135 - 1420	fahren Suchkurse für OBH 01 und machen 3 Horchversuche					
1420	brechen Suche nach OBS 01 ab					
1530	OBH 13	geslipt	WT = 2859 m		44 38,50 N	126 28,96 W
1615	OBH 14	geslipt	WT = 2856 m		44 38,50 N	126 18,87 W
1659	OBH 15	geslipt	WT = 2877 m		44 38,50 N	126 08,98 W
1748	OBH 16	geslipt	WT = 2911 m		44 38,50 N	125 59,01 W
1832 - 1902	OBH 17	mit 1500 m Ankerleine ausgesetzt				
1902	OBH 17	geslipt	WT = 2871 m		44 38,27 N	125 49,10 W
2010	OBH 18	geslipt	WT = 2863 m		44 36,60 N	125 39,00 W
2106	OBH 19	geslipt	WT = 2858 m		44 38,60 N	125 29,00 W
2158	OBH 20	geslipt	WT = 2516 m		44 38,60 N	125 19,00 W
2230	OBH 21	geslippt	WT = 2283 m		44 38,50 N	125 14,00 W
2306	OBH 22	geslipt	WT = 858 m		44 38,51 N	125 08,91 W
2340	OBH 23	geslipt	WT = 1140 m		44 38,50 N	125 03,09 W

27.04.1996

NW 4 ; 3 ; wolkig , W`liche Dünung 3 m

0019	OBH 24	geslipt	WT = 769 m		44 38,50 N	124 57,55 W
0055	OBH 25	geslipt	WT = 429 m		44 38,50 N	124 52,55 W
0133	OBH 26	geslipt	WT = 334 m		44 38,50 N	124 27,50 W
0207	OB1 09	geslipt	WT = 234 m		44 38,54 N	124 42,48 W
0247	OBS 10	geslipt	WT = 191 m		44 38,55 N	124 37,02 W
0325	OBS 11	geslipt	WT = 127 m		44 38,54 N	124 31,51 W
0402	OBS 12	geslipt	WT = 77 m		44 38,55 N	124 25,51 W
0436	OBS 13	geslipt	WT = 76 m		44 38,57 N	127 19,95 W
0525	OBS 14	geslipt	WT = 54 m		44 38,54 N	124 14,00 W
0600	stellen fest das INS-Navigation ca. 2 sml Längsfehler hat					
0632 - 0642	setzen Stb.-airgun-array aus					
0645 - 0657	setzen Bb.-airgun-array aus					
0702	Beginn schießen					
0725	alle airguns in Betrieb					
0740	Beginn Profil 06		RF/HS/PS		44 38,4 N	124 11,0 W
2400					44 38,5 N	125 45,8 W

28.04.1996

NE 4 ; 3 ; wolkig, z.T. sonnig , WNW`liche Dünung 3 m ;

0852	Ende Profil 06				44 38,6 N	126 40,0 W
0855 - 0908	holen Stb.-airgun-array ein					
0916 - 0925	holen Bb.-airgun-array ein					
1002	OBH 13	ausgelöst			44 38,6 N	126 29,0 W
1045	OBH 13	a.D.				
1112	OBH 14	ausgelöst			44 38,6 N	126 19,0 W
1146	OBH 14	a.D.				
1214	OBH 15	ausgelöst			44 38,5 N	126 09,0 W
1255	OBH 15	a.D.				
1257	OBH 16	ausgelöst			44 38,4 N	125 59,0 W
1342	OBH 16	a.D.				
1345	OBH 17	ausgelöst			44 38,3 N	125 49,0 W
1431	OBH 17	a.D.				
1433	OBH 18	ausgelöst			44 38,4 N	125 39,1 W
1534	OBH 18	a.D.				
1537	OBH 19	ausgelöst			44 38,5 N	125 29,1 W
1634	OBH 19	a.D.				
1652	OBH 20	ausgelöst			44 38,2 N	125 19,2 W
1734	OBH 20	a.D.				
1737	OBH 21	ausgelöst				

1813	OBH 21 a.D.				44 38,4 N	125 14,1 W
1815	OBH 22 ausgelöst					
1849	OBH 22 a.D.				44 38,3 N	125 08,2 W
1900	OBH 23 ausgelöst					
1925	OBH 23 a.D.				44 38,5 N	125 03,9 W
1940	OBH 24 ausgelöst					
2000	OBH 24 a.D.				44 38,4 N	124 57,8 W
2015	OBH 25 ausgelöst					
2032	OBH 25 a.D.				44 38,5 N	124 52,5 W
2050	OBH 26 ausgelöst					
2110	OBH 26 a.D.				44 38,4 N	124 47,2 W
2140 - 2155	ranging OBS 09				44 38,4 N	124 41,8 W
2222 - 2233	ranging OBS 10				44 38,4 N	124 35,9 W
2315	OBS 11 ausgelöst					
2322	OBS a.D.				44 38,4 N	124 30,2 W
2349	OBS 15 geslipt				44 38,5 N	124 27,0 W

29.04.1996

NNE 5/6 ; 4/5 ; wolkig ; wenig Dünung

0031	OBS 12 ausgelöst					
0057	OBS 12 a.D.				44 38,4 N	124 04,5 W
0144	OBS 13 ausgelöst					
0201	OBS 13 a.D.				44 38,4 N	124 17,9 W
0235	OBS 14 ausgelöst					
0321	OBS 14 a.D.				44 37,9 N	124 11,5 W
0532	OBH 27 geslipt	WT =	351 m		44 51,35 N	124 37,86 W
0617	OBH 28 geslipt	WT =	290 m		44 44,62 N	124 39,98 W
0739	OBH 29 geslipt	WT =	348 m		44 31,32 N	124 43,89 W
0829	OBH 30 geslipt	WT =	181 m		44 24,83 m	124 45,81 W
0909	OBH 31 geslipt	WT =	152 m		44 17,93 m	124 47,94 W
0952	OBH 32 geslipt	WT =	87 m		44 11,44 N	124 49,91 W
1125	OBH 33 geslipt	WT =	99 m		44 17,86 N	124 28,52 W
1217	OBH 34 geslipt	WT =	80 m		44 25,33 N	124 27,99 W
1302	OBH 35 geslipt	WT =			44 31,93 N	124 27,43 W
1420	OBH 36 geslipt	WT =	130 m		44 45,02 N	124 26,53 W
1504	OBH 37 geslipt	WT =	164 m		44 51,52 N	124 26,02 W
1553	OBH 38 geslipt	WT =	271 m		44 59,20 N	124 25,40 W
1600 - 1615	DP-Test					
1732 - 1755	bringen Stb.-airgun-array aus					
1800 - 1808	bringen Bb.-airgun-array aus					
1810	1. Schuß	WT =	354 m		45 08,6 N	124 24,8 W
1830	alle airguns in Betrieb					
1840	Beginn Profil 07	RF/HS/PS			45 06,3 N	124 24,8 W
2400					44 44,7 N	124 25,9 W

30.04.1996

max, NNE 6 ; 5 ; wolkig ; NW`liche Dünung 3 m

0725	Ende Profil 07	44 12,0 N	124 29,0 W
0740	Beginn Profil 08	44 10,9 N	124 29,7 W
1121	Profilwechsel 08/09	44 07,8 N	124 51,3 W
1330 - 1400	Test Vertikalarray		
1653 - 1702	Unterbechung Schießen wegen Wale	44 30,4 N	124 45,2 W
2345	Ende Profil 09	44 58,9 N	124 35,5 W
2350	Beginn einholen STBb.-airgun-array		

01.05.1995

NE 4 ; 3 ; wolkig ; leiche NW`liche Dünung

0006	STb.-array a.D.
0009 - 0030	Einholen Bb.-airgun-array

0119	OBH 27 ausgelöst		
0123 - 0150	suchen OBH 27, Sender und Lampe defekt		
0157	OBH 27 a.D.	44 41,5 N	124 37,7 W
0235	OBH 28 ausgelöst		
0255	OBH 28 a.D.	44 44,6 N	124 40,0 W
0335	OBS 09 ausgelöst		
0352	OBS 09 a.D.	44 38,3 N	124 41,8 W
0423	OBS 10 ausgelöst		
0445	OBS 10 a.D.	44 38,3 N	124 35,9 W
0538	OBH 29 ausgelöst		
0555	OBH 29 a.D.	44 31,3 N	124 43,8 W
0633	OBH 30 ausgelöst		
0644	OBH 30 a.D.	44 24,8 N	124 45,6 W
0728	OBH 31 ausgelöst		
0734	OBH 31 a.D.	44 17,8 N	124 47,9 W
0810	OBH 32 ausgelöst		
0823	OBH 32 a.D.	44 11,5 N	124 50,0 W
0947	OBH 33 ausgelöst		
0955	OBH 33 a.D.	44 17,8 N	124 28,5 W
1041	OBH 34 ausgelöst		
1050	OBH 34 a.D.	44 25,3 N	124 27,9 W
1128	OBH 35 ausgelöst		
1139	OBH 35 a.D.	44 31,8 N	124 27,4 W
1230	OBS 15 ausgelöst		
1244	OBS 15 a.D.	44 38,3 N	124 27,1 W
1320	OBH 36 ausgelöst		
1331	OBH 36 a.D.	44 44,9 N	124 26,6 W
1410	OBH 37 nicht auf Position	44 51,5 N	124 26,0 W
	von einem Fischer geborgen und an Land verbracht		
1446	OBH 38 ausgelöst		
1458	OBH 38 a.D.	44 59,2 N	124 25,4 W

02.05.1996

max. W 5 ; 4 ;	wolkig, einige Schauer			
0232	OBH 39 z.W.	WT = 2650 m	46 38,99 N	126 27,01 W
0317	OBH 40 z.W.	WT = 2646 m	46 39,02 N	126 18,01 W
0356	OBH 41 z.W.	WT = 2628 m	46 38,99 N	126 09,00 W
0435	OBH 42 z.W.	WT = 2598 m	46 38,99 N	125 59,98 W
0505	OBH 43 z.W.	WT = 2504 m	46 39,00 N	125 53,01 W
0537	OBH 44 z.W.	WT = 1936 m	46 39,00 N	125 45,98 W
0613	OBS 16 z.W.	WT = 1984 m	46 39,00 N	125 38,94 W
0651	OBS 17 z.W.	WT = 2126 m	46 39,00 N	125 31,60 W
0730	OBS 18 z.W.	WT = 1915 m	46 39,01 N	125 24,96 W
0813	OBH 45 z.W.	WT = 1899 m	46 38,98 N	125 17,94 W
0848	OBH 46 z.W.	WT = 1023 m	46 39,03 N	125 11,00 W
0921	OBH 47 z.W.	WT = 1069 m	46 39,02 N	125 03,94 W
0954	OBH 48 z.W.	WT = 732 m	46 39,04 N	124 56,96 W
1026	OBH 49 z.W.	WT = 474 m	46 39,01 N	124 50,06 W
1118 - 1120	Schwimmtest Vertikal-OBH-array			
1135 - 1200	Aussetzen OBH VA-01	WT = 326 m	46 38,95 N	124 43,48 W
1232	OBH 50 z.W.	WT = 156 m	46 38,98 N	124 38,95 W
1305	OBH 51 z.W.	WT = 135 m	46 38,99 N	124 33,99 W
1331	OBH 52 z.W.	WT = 108 m	46 38,98 N	124 29,00 W
1401	OBS 20 z.W.	WT = 84 m	46 38,99 N	124 24,00 W
1426	OBS 21 z.W.	WT = 68 m	46 38,98 N	124 19,00 W
1454	OBS 22 z.W.	WT = 48 m	46 39,00 N	124 14,03 W
1528			46 33,9 N	124 11,9 W
1535 - 1548	bringen Stb-airgun-array aus			
1550 - 1601	bringen Bb-airgun-array aus			

1606	1. Schuß	46 35,8 N	124 11,6 W
1655	Beginn Profil 10 RF/HS/PS	46 39,0 N	124 12,3 W
2400		46 39,0 N	124 49,0 W

03.05.1996

NW 4/5 ; wolkig, ab nachmittags aufkommende NW`liche Dünung , 3 m

1327 - 1340	bringen kurzen streamer aus	46 39,0 N	125 56,8 W
1945 - 1951	holen streamer ein	46 39,0 N	126 29,3 W
2105	Ende Profil 10	46 39,0 N	126 36,0 W
2110 - 2124	holen Stb.-airgun-array ein		
2128 - 2137	holen Bb.-airgun-array ein		
2205	OBH 39 ausgelöst		
2308	OBH 39 a.D.	46 38,7 N	126 26,7 W
2328	OBH 40 ausgelöst		

04.05.1996

N`lich 2 ; 1 ; wolkig, leichte NW`liche Dünung

0005	OBH 40 a.D.	46 39,1 N	126 17,9 W
0025	OBH 41 ausgelöst		
0101	OBH 41 a.D.	46 38,9 N	126 09,0 W
0116	OBH 42 ausgelöst		
0155	OBH 42 a.D.	46 39,0 N	125 59,9 W
0200	OBH 43 ausgelöst		
0236	OBH 43 a.D.	46 39,0 N	125 52,9 W
0245	OBH 44 ausgelöst		
0312	OBH 44 a.D.	46 39,0 N	125 45,9 W
0331	OBS 16 ausgelöst		
0405	OBS 16 a.D.	46 38,9 N	125 38,8 W
0432	OBS 17 ausgelöst		
0500	OBS 17 nochmal ausgelöst		
0542	OBS 17 a.D.	46 38,9 N	125 31,4 W
0600	OBS 18 ausgelöst		
0640	OBS 18 a.D.	46 38,9 N	125 24,7 W
0658	OBH 45 ausgelöst		
0728	OBH 45 a.D.	46 38,9 N	125 17,4 W
0744	OBH 46 ausgelöst		
0806	OBH 46 a.D.	46 39,0 N	125 10,8 W
0828	OBH 47 ausgelöst		
0845	OBH 47 a.D.	46 38,9 N	125 03,8 W
0905	OBH 48 ausgelöst		
0920	OBH 48 a.D.	46 39,1 N	124 56,9 W
0940	OBH 49 ausgelöst		
0955	OBH 49 a.D.	46 39,0 N	124 50,0 W
1016	VA 11 ausgelöst		
1028	Kopfboje a.D.		
1043	VA 11 a.D.	46 39,0 N	124 43,5 W
1300 - 1312	übernehmen Ersatzteile für SO 108 vom Kutter Triumph H	46 18,0 N	124 18,7 W
1534	OBS 23 z.W. WT = 99 m	45 50,97 N	124 10,28 W
1617	OBS 24 z.W. WT = 105 m	45 56,95 N	124 13,04 W
1704	OBS 25 z.W. WT = 104 m	46 03,29 N	124 16,70 W
1800	OBH 52 z.W. WT = 112 m	46 11,14 N	124 20,20 W
1852	OBH 53 z.W. WT = 173 m	46 17,82 m	124 23,51 W
1949	OBH 54 z.W. WT = 124 m	46 25,87 N	124 27,51 W
2040	OBH 55 z.W. WT = 456 m	46 32,90 N	124 30,96 W
2155	OBS 22 ausgelöst		
2205	OBS 22 a.D.	46 38,96 N	124 14,06 W
2237	OBS 21 ausgelöst		
2249	OBS 21 a.D.	46 38,92 N	124 19,08 W

2321	OBS 20	ausgelöst			
2333	OBS 20	a.D.		46 38,96 N	124 24,07 W

05.05.1996

max. N`lich 5 , 4 ; bedeckt ;

0005	OBS 19	ausgelöst			
0020	OBS 19	a.D.		46 38,85 N	124 29,00 W
0045	OBH 51	ausgelöst			
0059	OBH 51	a.D.		46 38,90 N	124 34,01 W
0109	OBH 56	z.W.	WT = 136 m	46 39,00 N	124 34,02 W
0147	OBH 50	a.D.		46 38,80 N	124 38,90 W
0253	OBH 57	z.W.	WT = 123 m	46 45,49 N	124 37,26 W
0315	OBH 58	z.W.	WT = 128 m	46 51,41 N	124 40,25 W
0407	OBH 59	z.W.	WT = 130 m	46 59,35 N	124 44,18 W
0455 - 0501	OBH 60	im Wasser			
0518	OBH 60	z.W.	WT = 131 m	47 05,83 N	124 47,47 W
0600	OBH 61	z.W.	WT = 150 m	47 12,21 N	124 50,65 W
0647	OBH 62	z.W.	WT = 662 m	47 18,51 N	124 53,78 W
0735 - 0740	Aussetzen VA 11		WT = 1105 m	47 25,20 N	124 56,95 W
0828	OBH 63	z.W.	WT = 385 m	47 30,76 N	124 59,95 W
0907	OBH 64	z.W.	WT = 187 m	47 36,57 N	125 02,96 W
0959	OBS 26	z.W.	WT = 373 m	47 42,50 N	125 05,97 W
1050	OBS 27	z.W.	WT = 352 m	47 49,94 N	125 09,78 W
1138	OBS 28	z.W.	WT = 177 m	47 56,37 N	125 13,04 W
1232	OBS 29	z.W.	WT = 146 m	48 03,29 N	125 16,57 W
1358 - 1405	bringen ministreamer aus			48 17,6 N	125 24,0 W
1406 - 1416	bringen Stb.-airgun-array aus				
1417 - 1441	bringen Bb.-airgun-array aus				
1444	1. Schuß			48 15,2 N	125 22,6 W
1612	Beginn Profil 11	RF/HS/PS		48 09,97 N	125 20,09 W
2400				47 43,4 N	125 06,0 W

06.05.1996

max. NW 4 ; 3 ; wolkig ;

1200				47 01,7 N	124 45,4 W
2400					

07.05.1996

max. WNW 6 ; 5 ; wolkig und Schauer ;

0352 - 0355	Ausfall GPS				
1000	Ende Profil 11		WT = 86 m	45 44,87 N	124 07,40 W
1005 - 1011	nehmen streamer auf				
1012 - 1020	nehmen Stb.-airgun-array a.D.				
1023 - 1033	nehmen Bb.-airgun-array a.D.				
1135	OBS 23	ausgelöst		45 50,7 N	124 10,3 W
1148	OBS 23	a.D.			
1245	OBS 24	ausgelöst		45 56,2 N	124 12,9 W
1257	OBS 24	a.D.			
1352	OBS 25	ausgelöst		46 03,0 N	24 16,6 W
1358	OBS 25	a.D.			
1444	OBH 52	ausgelöst		46 11,1 N	124 20,1 W
1455	OBH 52	a.D.			
1534	OBH 53	ausgelöst		46 17,8 N	124 23,5 W
1541	OBH 54	a.D.			
1627	OBH 54	ausgelöst		46 25,9 N	124 27,5 W
1635	OBH 54	a.D.			
1714	OBH 55	ausgelöst		46 32,9 N	124 30,9 W
1725	OBH 55	a.D.			
1802	OBH 56	ausgelöst			

1815	OBH	56	a.D.		46 38,9 N	125 33,9 W
1854	OBH	57	ausgelöst			
1904	OBH	57	a.D.		46 45,4 N	124 37,2 W
1938	OBH	58	ausgelöst			
1951	OBH	58	a.D.		46 51,3 N	124 40,0 W
2037	OBH	59	ausgelöst			
2045	OBH	59	a.D.		46 29,3 N	124 44,1 W
2122	OBH	60	ausgelöst			
2135	OBH	60	a.D.		47 05,7 N	124 47,5 W
2213	OBH	61	ausgelöst			
2225	OBH	61	a.D.		47 12,1 N	124 50,8 W
2259	OBH	62	ausgelöst			
2315	OBH	62	a.D.		47 18,5 N	124 53,6 W
2342	VA	12	ausgelöst			

08.05.1996

max. NW 6 ; See 5 ; später abnehmend auf NW 3 ; wolkig

0025	VA-Auftriebskörper a.D.				47 25,1 N	124 57,1 W
0028	VA	12	a.D.			
0100	OBH	63	ausgelöst			
0120	OBH	63	a.D.		47 30,6 N	125 00,0 W
0205	OBH	64	ausgelöst			
0225	OBH	64	a.D.		47 36,4 N	125 02,9 W
0320	OBS	26	ausgelöst			
0339	OBS	26	a.D.		47 42,4 N	125 06,0
0432	OBS	27	ausgelöst			
0451	OBS	27	a.D.		47 49,9 N	125 09,7 W
0536	OBS	28	ausgelöst			
0547	OBS	28	a.D.		47 56,4 N	125 13,0 W
0634	OBS	29	ausgelöst			
0642	OBS	29	a.D.		48 03,4 N	125 16,5 W
0952	OBS	30	z.W.	WT = 68 m	47 34,34 N	124 39,95 W
1021	OBS	31	z.W.	WT = 91 m	47 33,34 N	124 45,20 W
1044	OBS	32	z.W.	WT = 121 m	47 32,46 N	124 49,76 W
1118	OBS	33	z.W.	WT = 170 m	47 31,58 N	124 54,83 W
1155	OBH	65	z.W.	WT = 359 m	47 30,61 N	124 59,96 W
1225	OBH	66	z.W.	WT = 426 m	47 29,75 N	125 04,46 W
1259	OBH	67	z.W.	WT = 633 m	47 29,12 N	125 07,77 W
1329	OBH	68	z.W.	WT = 632 m	47 28,41 N	125 11,51 W
1350	OBH	69	z.W.	WT = 781 m	47 27,95 N	125 14,12 W
1415	OBH	70	z.W.	WT = 1405 m	47 27,07 N	125 18,65 W
1441	OBS	34	z.W.	WT = 1492 m	47 26,26 N	125 22,90 W
1513	OBS	35	z.W.	WT = 1485 m	47 25,27 N	125 28,29 W
1544	OBS	36	z.W.	WT = 1478 m	47 24,25 N	125 33,94 W
1617	OBH	71	z.W.	WT = 1361 m	47 23,02 N	125 40,19 W
1647	OBH	72	z.W.	WT = 1766 m	47 21,78 N	125 46,68 W
1725	OBH	73	z.W.	WT = 1828 m	47 20,26 N	125 54,76 W
1802	OBH	74	z.W.	WT = 1984 m	47 19,73 N	126 02,77 W
1837	OBH	75	z.W.	WT = 2496 m	47 17,35 N	126 10,55 W
1911 - 1917	VA	13	z.W.	WT = 2507 m	47 16,07 N	126 17,60 W
2000	OBH	76	z.W.	WT = 2536 m	47 14,52 N	126 25,42 W
2038 - 2106	OBH	77	z.W.	WT = 2563 m	47 12,77 N	126 33,73 W
	mit 2000m Leine zwischen OBH und Grundgewicht					
2318 - 2323	auslegen ministreamer					
2325 - 2338	aussetzen Stb.-airgun-array					
2340 - 2355	aussetzen Bb.-airgun-array					

09.05.1996

max. SW 3 ; 2 ; wolkig, keine Dünung

0008	1. Schuß		
0342	Beginn Profil 12 RF/HS/PS	47 07,6 N	127 01,4 W
1200		47 11,0 N	126 44,0 W
2400		47 18,8 N	126 02,6 W
		47 29,5 N	125 05,7 W

10.05.1996

max. SSE 4 ; 3 ; wolkig, flache SW`liche Dünung ;

0623	Ende Profil 13	47 35,4 N	124 34,0 W
0630 - 0637	holen mini-streamer ein		
0638 - 0650	holen Stb.-airgun-array ein		
0650 - 0700	holen Bb.-airgun-array ein		
0740	OBS 30 ausgelöst		
0753	OBS 30 a.D.	47 34,1 N	124 40,0 W
0823	OBS 31 ausgelöst		
0836	OBS 31 a.D.	47 33,0 N	124 45,3 W
0840 - 0912	Bootsmanöver mit Stb.-Boot		
0933	OBS 32 ausgelöst		
0943	OBS 32 a.D.	47 42,3 N	124 49,8 W
1008	OBS 33 ausgelöst		
1016	OBS 33 a.D.	47 31,5 N	124 54,8 W
1040	OBH 65 ausgelöst		
1047	OBH 65 aufgetaucht, nicht gesichtet		
1050 - 1120	Suchfahrt		
1126	OBH 65 a.D.	47 33,8 N	125 03,4 W
	3,9 sml NW`lich von Profil 13		
1144	OBH 66 ausgelöst		
1200	OBH 66 a.D.	47 29,7 N	125 04,5 W
1214	OBH 67 ausgelöst		
1236	OBH 67 a.D.	47 29,3 N	125 07,8 W
1244	OBH 68 ausgelöst		
1307	OBH 68 a.D.	47 28,4 N	125 11,6 W
1308	OBH 69 ausgelöst		
1325	OBH 69 a.D.	47 27,9 N	125 14,1 W
1327	OBH 70 ausgelöst		
1355	OBH 70 a.D.	47 27,1 N	125 18,6 W
1359	OBS 34 ausgelöst		
1426	OBS 34 a.D.	47 26,3 N	125 22,7 W
1432 und 1510	OBS 35 ausgelöst		
1541	OBS 35 a.D.	47 25,3 N	125 28,2 W
1606	OBS 36 ausgelöst		
1633	OBS 36 a.D.	47 24,4 N	125 33,8 W
1645	OBH 71 ausgelöst		
1711	OBH 71 a.D.	47 23,2 N	125 40,1 W
1720	OBH 72 ausgelöst		
1754	OBH 72 a.D.	47 22,0 N	125 46,6 W
1810	OBH 73 ausgelöst		
1836	OBH 73 a.D.	47 20,5 N	125 54,8 W
1856	OBH 74 ausgelöst		
1930	OBH 74 a.D.	47 18,9 N	126 02,8 W
1947	OBH 75 ausgelöst		
2018	OBH 75 a.D.	47 17,4 N	126 10,7 W
2019	VA 13 ausgelöst		
2107 - 2112	VA 13 a.D.	47 16,1 N	126 17,6 W
2130	OBH 76 ausgelöst		
2208	OBH 76 a.D.	47 14,5 N	126 25,4 W
2227	OBH 77 ausgelöst		
2258	OBH 77 a.D.	47 13,0 N	126 33,3 W

2317	Beginn Auslegen streamer, tailbouy z.W.	47 13,5 N	126 33,5 W

11.05.1996

max. SSE 6 ; bedeckt und regnerisch

0522	2400 m - Streamer ausgelegt und mit birds versehen	47 32,2 N	126 45,1 W
0657 - 0900	drehen über BB mit 3 Grad/Minute und v = 5 kn		
0900	erreichen Profilkurs von Profil 1o1	47 35,8 N	126 53,7 W
0958 - 1024	bringen Stb.-airgun-array aus		
1027 - 1043	bringen Bb.-airgun-array aus		
1118	Beginn Schießen	47 38,4 N	126 39,6 W
1125	Beginn Profil 101 RS/HS/PS	47 38,5 N	126 38,9 W
2400		47 52,8 N	125 15,0 W

12.05.1996

max. S 6 ; bedeckt und Regen ; twlg. 3 m-hohe Dünung aus WSW ;

0155	Ende Profil 101	47 55,0 N	125 02,0 W
0158	Ende Schießen		
0207 - 0218	holen Stb.-airguin-array ein		
0219 - 0248	drehen über Stb		
0248 - 0505	Anfahrt Profil 102		
0505 - 0635	drehen über Stb		
0635 - 0800	Reparatur am streamer	47 46,7 N	124 53,1 W
0800 - 1022	drehen über Stb		
1022	erreichen Profilkurs 102	47 43,5 N	124 50,9 W
1030 - 1044	setzen Stb.-airgun-array aus		
1050	Beginn Schießen		
1106	Beginn Profil 102 RS/HS/PS	47 42,5 N	124 55,6 W
2400		47 27,1 N	126 18,3 W

13.05.1996

max. WSW 4 ; wolkig, Nebel, Regen , Dünung aus WSW ca. 2-3 m hoch

0430	Ende Profil 102	47 21,4 N	126 47,7 W
0439 - 0453	holen Stb.-airgun-array ein		
0454 - 0504	holen Bb.-airgun-array ein		
0536 - 0920	holen streamer tlw. ein und reparieren		
0922 - 0940	bringen streamer aus	47 14,1 N	127 02,9 W
1142	Schiff auf Kurs von Profil 103	47 08,6 N	126 56,6 W
1240 - 1254	bringen Stb.-airgun-array aus		
1255 - 1308	bringen Bb.-airgun-array aus		
1310	Beginn Profil 103 RS/HS/PS	47 10,3 N	126 47,1 W
2400		47 23,7 N	125 36,3 W

14.05.1996

max. NW 4 ; 3 ; bedeckt ; NW`liche Dünung, 1-2 m hoch ;

0921	Ende Profil 103	47 35,4 N	124 34,4 W
0933 - 0941	hieven Stb.-airgun-array ein		
0942 - 1015	drehen über Stb.		
1015 - 1400	Anfahrt Profil 104		
1107 - 1205	und		
1220 - 1315	Einsatz Schlauchbott zur Klarierung und Kontrolle der Endboje		
1400 - 1435	drehen über Stb		
1436 - 1445	bringen Stb.-airgun-array aus		
1458	Beginn Profil 104 RS/HS/PS	47 15,6 N	124 45,2 W
2400		47 06,0 N	125 37,2 W

15.05.1996

max. SW 5 ; sonst 3 ; bedeckt, später wolkig ; Dünung aus NW-W 2 m ;

0815	Ende Profil 104	46 57,4 N	126 23,3 W

0822 - 0832	holen Stb.-airgun-array ein		
0833 - 0842	holen Bb.-airgun-array ein		
0858 - 1022	holen streamer ein zwecks Kontrolle und Entfernung der Bleigewichte der letzten beiden Längen		
1030 - 1200	Anfahrt Profil 105		
1231 - 1508	bringen streamer aus	46 32,3 N	126 29,6 W
1612 - 1622	bringen Stb.-airgun-array aus		
1625 - 1648	bringen Bb.-airguns aus		
1657	Beginn Profil 105 RS/HS/PS	46 45,7 N	126 09,0 W
2400		46 52,7 N	125 26,1 W

16.05.1996

max. SW 4, später drehend auf NW 4 ; wolkig, später bedeckt, flache W`liche Dünung

0636	Ende Profil 105	46 59,6 N	124 43,0 W
0645	Bb.-airgun-array aufgekürzt		
0646 - 0833	drehen über Bb		
0844	Bb.-airgun-array ausgesteckt		
0846	Beginn Profil 106 RS/HS/PS	47 00,4 N	124 44,4 W
1358	Ende Profil 106	46 36,9 N	124 32,9 W
1405	Bb.-airgun-array aufgekürzt		
1406 - 1556	drehen über Bb		
1600	Bb-airgun-array ausgesteckt		
1605	Beginn Profil 107	46 38,8 N	124 31,6 W
2400		46 39,0 N	125 23,4 W

17.05.1996

max. SSW 9 ; später abnehmend auf 7 ; hohe See ; bedeckt, Regen ;

0724	Ende Profil 107	46 39,0 N	126 12,0 W
0726 - 0731	kürzen Bb.-array auf		
0732 - 0804	drehen über Bb, schießen weiter mit Stb.-array		
0810	Beginn Profil 108 RS/HS/PS	46 37,0 N	126 15,0 W
0815 - 0823	holen Bb-array ein wegen Reparatur		
1010	Ende Profil 108	46 28,0 N	126 15,0 W
1011 - 1035	drehen über BB		
1045 - 1110	holen Stb.-array ein, Wetter wird zu schlecht Wind SSE-S 9 See langsam aufbauend		
1110 - 2400	wettern ab, Wind langsam abnehmend auf SW 7, jedoch hohe See		

18.05.1996

max. SW 5 ; bedeckt bis wolkig, Schauer, hohe SW`liche Dünung

0535 - 0552	bringen Stb.-airgun-array aus		
0555 - 0600	bringen Bb.-airgun-array aus		
0617	1. Schuß		
0630	Beginn Profil 109 RS/HS/PS	45 54,0 N	126 00,0 W
0636 - 0646	klarieren Schläuche Stb.-array		
1038 - 1055	dito		
1432 - 1448	dito, versehen SSchläuche mit Abholer	45 56,0 N	124 34,2 W
1939	Ende Profil 109		
1952 - 2000	holen Stb.-array ein		
2000 - 2032	drehen über Bb	45 57,9 N	124 30,0 W
2033	auf Profilkurs		
2315	Beginn Schießen mit Stb.-array	46 10,0 N	124 30,0 W
2320	Beginn Profil 110 RS/HS/PS		

19.05.1996

max. SW 6 ; wolkig, Schauer, hohe W´liche Dünung , 3-4 m ;

0247	Ende Profil 110	46 26,0 N	124 30,0 W
0250 - 0723	drehen Warteschleife über Bb		

0723	Schiff auf Profilkurs	46 28,2 N	124 23,9 W
0730 - 0740	setzen Bb.-airgun-array aus		
0742	1. Schuß	46 28,2 N	124 25,8 W
0805	Beginn Profil 111 RS/HS/PS	46 28,3 N	124 28,3 W
2042 - 2052	holen Stb.-airgun-array ein		
2336	Ende Profil 111	46 26.5 N	126 01,7 W
2340 - 2348	holen Bb.-airgun-array ein		

20.05.1996

max. SSW 6 ; wolkig bis bedeckt ; Schauer ; mittelhohe Dünung aus W - SW;

0000 - 0046	drehen über Bb		
0047 - 0400	Anfahrt Profil 112		
0400 - 0521	drehen über Bb		
0522	Beginn Profil 112 HS/PS	46 10,0 N	126 00,0 W
0830 - 0841	bringen Stb.-array aus		
0844 - 0850	bringen Bb.-array aus		
0859	Beginn RS	46 10,0 N	125 36,5 W
1203	Ende Profil 112	46 10,0 N	125 16,0 W
1204 - 1219	holen Stb.und Bb.-array ein		
1220 - 1256	drehen über Bb.		
1257 - 1305	bringen Stb. und Bb.-array aus		
1307	Beginn Profil 113 RS/HS/PS	46 12,6 N	125 13,2 W
2400		47 01,0 N	125 32,4 W

21.05.1996

max. WNW 4 ; bedeckt und Schauer, später aufgelockert ;

1500	Ende Profil 113	48 08,1 N	125 59,2 W
1506 - 1522	holen Stb.-airgun-array ein		
1523 - 1530	holen Bb.-airgun-array ein		
1540 - 1807	holen streamer ein		

Teststation 3 W 05 CTD/ROS

1904 - 2008	Teststation CTD/ROS mit W 5 WT = 1168 m	48 01,4 N	125 51,7 W

FAZ

Knall auf Fall

Von Haustieren abgesehen, sind die Säugetiere des Meeres des Menschen liebste Freunde in der Fauna. So war der Delphin „Flipper" jahrelang Liebling der Fernsehzuschauer. Der Schutz der Meeressäuger, die jahrhundertelang wegen Tran, Blubber, Fellen oder Elfenbein rücksichtslos gejagt wurden, ist notwendig und allgemein akzeptiert. Fragwürdig wird dieser Schutz aber, wenn die Tiere vor etwas behütet werden sollen, dessen Gefahrenpotential sich nicht einschätzen läßt. So mußten jene Ozeanographen, die Änderungen der Temperatur der Weltmeere mit Hilfe von Schall messen wollten, erhebliche Abstriche an ihren Versuchen hinnehmen. Der laute Infraschall gefährde Wale, hieß es ohne fundierte Begründung. Ähnlich geht es auch Geophysikern, die von Schiffen aus mit seismischen Verfahren den Aufbau der Erdkruste erkunden wollen. Tierschützer argumentieren, daß die knallenden „Luftpulser" die Meeressäuger störten. Sind solche Bedenken erst einmal in der Bürokratie verankert, hängt die Genehmigung lange geplanter, teurer Forschungsreisen oft bis zur letzten Minute in der Luft, wie auch jetzt beim deutschen Forschungsschiff „Sonne". Für seine morgen beginnende 108. Fahrt – sie führt im Nordostpazifik vor die Küsten Oregons und Washingtons – erhielt die Fahrtleitung erst vor wenigen Tagen von amerikanischen Behörden die mit erheblichen Auflagen versehene Forschungsgenehmigung. Wer je auf einem „seismischen" Forschungsschiff gefahren ist, wird die Argumente der Tierschützer kaum verstehen. Oft begleiten ganze Schulen von Delphinen das Schiff, während die Luftpulser ununterbrochen knallen. Die Schallwellen scheinen die Tiere überhaupt nicht zu stören, während die Schiffsbesatzung jenen Moment herbeisehnt, in dem die Preßluft einmal ausfällt und das „Knallen" für einige Minuten aufhört.

hra

FAZ 17.4.96

Anne Treht 7-2064

Thought you might want to pass this to the sci. crew on Sonne

— Fred

A6 News-Times, Newport, OR, Wednesday, May 1, 1996

Research vessel Sonne pays visit to Yaquina Bay

By Orna Izakson

When Toledo fisherman Richard Bolton caught a German seismic reader and brought it to shore on Tuesday, he unravelled a small mystery about a red research vessel that Yaquina Bay residents said they saw over the weekend.

Inquiries about the vessel early this week turned up no clues as to its identity, although U.S. Coast Guard Station Yaquina Bay did report radio contact with the Research Vessel Researcher on Monday.

Port of Newport officials also knew nothing of the reported ship in Yaquina Bay. But they did say a fisherman had brought a seismic reader up from the ocean floor Tuesday morning.

The German phone numbers on the instrument were the first clue presented to Fred Jones, the marine superintendent for the Oregon State University College of Oceanic and Atmospheric Science at the Hatfield Marine Science Center in Newport.

Contacted earlier on Tuesday, Jones said he knew nothing about the reported red research vessel. But after investigating Bolton's find, Jones discovered that the instrument belonged to the German research vessel Sonne.

The Sonne is on a geophysical cruise with scientists from the U.S. Geological Survey, based in Menlo Park, Calif. The ship is currently working off the Oregon coast, and is expected to reach Astoria soon. The researchers intend to continue north along the Washington coast.

The work, Jones explained, involves seismic instruments placed on the ocean bottom, known as seismometers. Other seismometers also have been placed on shore, including some in the Cascade Mountains, and involves OSU researchers in Corvallis.

P.S.: I gave them your name & number but guess that was too much exposure for a small town paper.

— Fred